ARTIFICIAL GRAVITATIONAL COMPACTION OF CLAYS

A Thesis submitted to the Faculty
of Science of the University of London
for the Degree of Doctor of Philosophy

By:
DEVAPRIYA CHITRAL WIJEYESEKERA
M.Sc., D.I.C.

Engineering Geology Division,
Imperial College,
London S.W.7.

6 January, 1975.

ABSTRACT

This work concerns the laboratory study of some of the processes involved in the process of gravitational compaction of clays: the dewatering of sediments as a result of progressive burial.

An unique high pressure temperature consolidation cell designed to simulate geological burial up to a depth of 10,000 feet and subsequent exhumation of sediments is described. Remoulded and undisturbed specimens of Kaolinitic clays have been tested to investigate the influence of the rate of loading and the effect of pore fluid chemistry on the high pressure consolidation of clay. The pore fluids expelled in the process of compaction have been chemically analysed and the results discussed in the light of the current theories of ionic filtration. Macro- and micro-fabric of the natural and artificial compacted clays are observed to shed further light on the aspects of development of preferred orientation of clay particles and the formation of fissures. The influence of heating on the low pressure consolidation of the remoulded clay has also been studied and results are discussed.

GENERAL INDEX

		Page
Abstract		I
General Index		II
List of Figures		V
List of Plates		XI
List of Tables		XIV
CHAPTER ONE	INTRODUCTION	1
1.1	Definitions	1
1.2	Focus of Study	3
1.3	Motive of Study	4
1.4	Specific Focus	5
1.5	Course of Study	6
1.6	Outline of Thesis	7
CHAPTER TWO	REVIEW OF LITERATURE PERTAINING TO GRAVITATIONAL COMPACTION OF CLAYS.	9
2.1	Introduction	10
2.2	Clay Sediments - Size and Composition	10
2.3	Clay-colloid Concept	15
2.4	Fabric	25
2.5	Sedimentation and Rates of Deposition	38
2.6	Effective Stress Concept	41
2.7	Historical Review of Gravitational Compaction	46
2.8	Laboratory Studies on Compaction of Clays	68
CHAPTER THREE	GEOTECHNICAL SIGNIFICANCES OF GEOLOGIC BURIAL AND EXHUMATION	84
3.1	Introduction and Definitions	85
3.2	Stress-induced Fabric Deformations	87
3.3	Chemical Changes in the Pore Fluid with Compaction	113
3.4	Clay Mineral Diagenesis	134
3.5	Abnormal Pore Fluid Pressures	141
3.6	Influence of Burial on Engineering Properties	152
CHAPTER FOUR	MECHANICS OF COMPACTION	160
4.1	Introduction	161
4.2	Mechanical Analogues for rheology of clays	162
4.3	Terzaghi Theory of one-dimensional consolidation	168
4.4	Critical review of Terzaghi Theory	173
4.5	Conventional Laboratory Consolidation	175
4.6	Constant rate of Strain Consolidation	180
4.7	Constant rate of Loading Consolidation	183
4.8	Computer Simulation of Geological Burial	192
CHAPTER FIVE	CONSOLIDATION EQUIPMENT AND TESTING PROCEDURE	199
5.1	Introduction	200
5.2	High Pressure Consolidation Cell	201
5.3	Constant rate of strain Consolidation Cell	233
5.4	Low pressure temperature Consolidation Cell	240

		Page
CHAPTER SIX	DESCRIPTION OF THE SOIL SAMPLES, SAMPLING SITES AND SAMPLING TECHNIQUE	245
6.1	Introduction	246
6.2	Recent Sediments from Falmouth Estuary	248
6.3	Ball Clay from Devon	268
6.4	Ball Clay No. 661	274
CHAPTER SEVEN	LABORATORY CONSOLIDATION TEST OBSERVATIONS AND RESULTS OF THEIR ANALYSIS	283
7.1	Introduction	284
7.2	High Pressure Consolidation Tests	285
7.3	Constant Rate of Strain Consolidation Tests	326
7.4	Influence of Temperature on Consolidation	331
CHAPTER EIGHT	CLAY MINERALOGY AND PORE FLUID CHEMISTRY	348
8.1	Introduction	349
8.2	Clay Mineralogy	349
8.3	Changes in Clay Mineralogy with Consolidation	367
8.4	Chemical Analysis of the Pore Fluids	372
CHAPTER NINE	FABRIC AND RELATED STUDIES	390
9.1	Introduction	391
9.2	Surface Features of the Final Specimen	393
9.3	Macrofractures observed in specimens	394
9.4	Slaking of air-dried Consolidated Clay	399
9.5	Details of Fabric Study Techniques used	404
9.6	Shrinkage of Clays	425
9.7	Representability of Micrographs	432
9.8	Localised Fabrics	437
9.9	Perfect preferred orientation	447
9.10	Fabric of Natural Samples	454
9.11	Development of Fabric with Consolidation	461
9.12	Fabrics produced in the Drained and Undrained Ends	469
9.13	Further Consolidation of Undisturbed Samples	474
9.14	Preferred Orientation Influenced by Organic Matter	481
9.15	Microscopic Study of Natural and Artificial Fissures	481
9.16	Observations of Mineralisation	489
9.17	P Wave Velocity Study	489
CHAPTER TEN	CONCLUDING DISCUSSION	496
10.1	Artificial Gravitational Compaction	497
10.2	Pore Fluid Chemistry Changes	499
10.3	Development of Fabric in Clays	503

		Page
APPENDIX A	Notations and Conversion Factors	507
A.1 Notations		507
A.2 Conversion Factors		509
APPENDIX B	Terzaghi Theory of one-dimensional Consolidation	510
APPENDIX C	Fourier Series Solution of the Diffusion Equation	512
APPENDIX D	Analytical Results from the High Pressure Consolidation Tests	514
APPENDIX E	Steady State Temperature Distribution within a test specimen	558
APPENDIX F	Results of the Chemical Analysis of the Pore Fluids	572
REFERENCES		583
ACKNOWLEDGEMENTS		602

LIST OF FIGURES

		Page
2.1	Crystal structure of Kaolinite	13
2.2	Desorbtion of adsorbed water on clays	18
2.3	Electrical double layer in clays	21
2.4	Force between adjacent clay particles	24
2.5	Clay particle association - terminology	26
2.6	Nomenclature for idealised clay fabrics	28
2.7	Salinity change with depth in the Pacific Ocean	32
2.8	Depositional fabrics in sediments	35
2.9	Influence of initial water content on clay compaction	37
2.10	Stress distribution in a normal sedimentary column	44
2.11	Differential compaction of clay	49
2.12	Athy's density-depth curve	52
2.13	Porosity-depth curve	53
2.14	Porosity and density variation with depth	56
2.15	Hedberg compaction model	58
2.16	Continuous porosity-depth curve	61
2.17	Compaction history of marine clay minerals	63
2.18	Burst compaction model	66
2.19	Interlayer water density variation with compaction	67
2.20	Influence of particle size on clay compaction	72
2.21	Influence of pore fluid electrolyte concentration on clay compaction	73
2.22	Influence of adsorbed cation on clay compaction	74
2.23	Influence of mineralogy on clay compaction	76
2.24	Laboratory and field compaction of clay	78
2.25	Sedimentation compression curves for normally consolidated clay	79
2.26	Liquidity index and its relation to effective overburden pressure	80
2.27	High pressure compaction curves	83
3.1	Normally and overconsolidated clay	86
3.2	Hypothetical two-dimensional fabrics	89
3.3	Effect of compaction on fabric	95
3.4	Development of fabric in consolidated Kaolinite	97
3.5	Application of microscopic techniques in study of clays	102
3.6	Principle of X-ray diffraction	108
3.7	Particle orientation model and Birefringence ratio	112
3.8	Solubility charts of some salts	115
3.9	Increase of salt concentration with depth in the field	119
3.10	Anticipated effects of shale compaction on pore fluid salinity, pore fluid pressure and porosity	120
3.11	Ionic concentrations in pore fluids expelled from sea water saturated montmorillonite	122

		Page
3.12	Composition changes in pore fluid expelled during compaction	123
3.13	Total dissolved content variation in pore fluids expelled during compaction montmorillonite saturated in sea water	126
3.14	Influence of temperature on the variation of ionic composition of expelled pore fluids	127
3.15	Characters of an electrolyte in a capillary	132
3.16	Statistical distribution of clay minerals in geological periods	135
3.17	Montmorillonite-illite transformation and the associated geothermal gradient	138
3.18	Destruction of Kaolinite during burial	140
3.19	Total dissolved solid content and the pore fluid pressure gradient	143
3.20	Reservoir fluid pressure variation with depth for Louisiana Gulf Coast well	145
3.21	Pore fluid pressure variation with depth and its relation to grain size of formation	146
3.22	Permeability and porosity relation for shale	148
3.23	Minimum permeabilities to achieve compaction equilibrium	150
3.24	Porosity depth curves for different pore fluid pressure ratios, .	151
3.25	Frequency distribution of fissures with varying angles of dip in deposits of different o.c. ratio	156
3.26	Coefficient of earth pressure as function of overconsolidation ratio and plasticity index	158
4.1	Load sharing in a two-phase solid-fluid system	163
4.2	Basic rheological models	165
4.3	Published rheological models of soil skeleton	166
4.4	Time deformation curve for a consolidating clay	167
4.5	Rheological models for deep burial of clay	169
4.6	Schematic diagram of sample and types of loading	171
4.7	Effect of load increment ratio on e-log p curve	177
4.8	e-log p curves for normal and long term incremental loading	178
4.9	Pore fluid pressure distributions in consolidating specimens	179
4.10	Pressure and velocity distributions of the pore fluids in a slowly loaded sample	184
4.11	Relationship between pore fluid pressure dissipation factor, for time factor and space parameter	187
4.12	Assumed variation of coefficient of consolidation	190
4.13	Schematic diagram for computer analysis of shale deposition	194

		Page
4.14	Results of computer simulation of geologic burial	197
4.15	Persistence of pore fluid pressure in shale after burial	198
5.1	Schematic diagram of the operational systems of the high pressure consolidation cell	204
5.2	Diagram of specimen cup, lower and upper plugs	207
5.3	Diagram of the pressure vessel	210
5.4	Cell extension calibration curve	211
5.5	Increase in axial pressure with number of balls	215
5.6	Servo system for the P_1 pressure control	216
5.7	Pressure pencil piston arrangement	217
5.8	Pressure pencil performance for P_1 pressure increase commands	219
5.9	Calibration of pressure transducers	220
5.10	Calibration of displacement transducer	226
5.11	Displacement transducer calibration of variation of error voltage with armature position	228
5.12	Flow chart showing main sections of computer programme	229
5.13	Diagram of constant rate of strain consolidation equipment	234
5.14	Load cell calibration	237
5.15	Diagram of the low pressure temperature consolidation cell	242
6.1	Simplified geological map of South West England	247
6.2	Geological map of the study area in the Falmouth Estuary	249
6.3	Map of area around Falmouth Estuary	255
6.4	Block diagram showing some sedimentological features in the estuary	257
6.5	Geometric interpretation of sedimentation at the seawater freshwater interface	260
6.6	Some geotechnical properties of the Falmouth clay	265
6.7	Details of the sampling equipment	266
6.8	Low pressure e-log p curves for Falmouth clay	269
6.9	Maps of Borey and Petrockstow Basins	271
6.10	e-log p curves for remoulded and undisturbed stoneware ball clay	275
6.11	Low pressure consolidation of remoulded Ball Clay no. 661	278
6.12	Particle size distribution of the clays tested	279
6.13	Philosophy of the choice of the samples for the testing programme	281

		Page
7.1	Distribution of the final moisture contents within the CHP test specimens	288
7.2	Summary of loading programmes used in the rapid consolidation tests	292
7.3	Retained moisture content - peak consolidation pressure variation	296
7.4	A graphical aid to estimate the duration of a CHP test	298
7.5	The variation of the observed parameters during a typical test	300
7.6	Influence of rate of loading on the pore fluid pressure difference across the specimen	302
7.7	Comparison of the e-log p plots of tests BC.CHP.12 and BC.CHP.14	303
7.8	Influence of rate of loading on the e-log p plots	305
7.9	Influence of rate of loading on the variation of M_v with pressure	306
7.10	Influence of rate of loading on the permeability -porosity variations	308
7.11	Influence of salinity of the pore fluid on the pore fluid pressure difference across specimen	312
7.12	Influence of pore fluid salinity on the e-log p character	313
7.13	Influence of pore fluid salinity on the permeability-porosity variation	315
7.14	Influence of remoulding technique in achieving complete saturation	317
7.15a	Percentage compaction variation with time	318
7.15b	Percentage compaction variation with pressure	318
7.16	The e-log p curves for the undisturbed normally consolidated clay at high pressures	322
7.17	The e-log p curves for the undisturbed normally consolidated and overconsolidated clay	324
7.18	K-$\emptyset$ variation for the normally consolidated and overconsolidated clay	325
7.19	Variation of observed parameters in a typical CRS test	328
7.20	e-log p curve for undisturbed ball clay as determined from CRS tests	329
7.21	Plot of constrained modulus with consolidating pressure	332
7.22	Heat flow patterns with progressive consolidation and different heating conditions	337
7.23	Experimental observation of temperature rise and decay in a specimen heated at one end	338
7.24	Temperature rise and system deformation on introduction of heat to a specimen	340
7.25	e-log p plot for elevated temperature consolidation tests	343

		Page
7.26	Void ratio-pressure plot for a typical low pressure temperature test	344
7.27	The relevance of viscosity change due to temperature rise on the primary consolidation	346
8.1	XRD trace of the whole rock of Falmouth clay	353
8.2	XRD trace of the whole rock of Petrockstow ball clay	354
8.3	XRD trace of the whole rock of Ball Clay 661	355
8.4	XRD traces of the oriented clay fraction of Falmouth clay	362
8.5	XRD traces of the oriented clay fraction of Petrockstow Ball Clay	363
8.6	XRD traces of the oriented clay fraction of Ball Clay 661	364
8.7	A general pattern of the observed variation of weight of dissolved solids in the expelled pore fluids with increasing total pressure	374
8.8	Schematic diagram of the modes of operation of atomic absorption spectrometer	379
8.9	General trend patterns for the variation of concentration of cations in the expelled pore fluids with increasing pressure	382
8.10	The observed variation of the percentage ionic concentration changes in the pore fluids expelled from two tests	387
8.11	The influence of rate of loading on the chemistry of the pore fluid expelled	389
9.1	The divisions of the final specimen for different investigations made in the study	392
9.2	Schematic diagram of the details of the optics used for Fraunhofer diffraction of micrographs	410
9.3	XRD traces of oriented clay with and without impregnation	421
9.4	XRD traces of carbowaxed, orthogonal sections from a consolidated specimen	422
9.5	Parameters of the XRD peaks used in the analysis of peak ratio	424
9.6	A photographic reproduction illustration of the effect of shrinkage	427
9.7	Shrinkage behaviour of Kaolinitic clay	430
9.8	Optical illumination rosettes at distinct points from the drained end	448
9.9	Variation of birefringence ratio and orientation ratio with increasing pressure	468
9.10	Illumination rosettes for Falmouth sediments before and after consolidation	478

		Page
9.11	Illumination rosettes for Petrockstow Ball Clay with and without consolidation	479
9.12	Result from P wave velocity study	493
9.13	Change in P wave velocity with moisture content on drying and as a result of consolidation	495

LIST OF PLATES

		Page
1.1	Natural gravitational compaction of clay	2
2.1	Fabric disturbance due to coarse particle	30
5.1	Layout of the high pressure temperature consolidation cell	206
5.2	Views of pressure vessel and specimen cup assembly	209
5.3	The equipment used for rapid consolidation and for preconsolidation	213
5.4	Close-up view of pressure balance piston	222
5.5	Displacement transducer calibration rig	224
5.6	View of the operation and observation console	225
5.7	View of the constant rate of strain consolidation equipment	236
5.8	View of the low pressure temperature consolidation equipment	241
6.1	Hand specimen of St. Austell granite	250
6.2	Kaolinised granite	252
6.3	Telescopic view of the Falmouth Estuary	253
6.4	Picturesque view of the Falmouth Estuary	256
6.5	Cross-sectional view of block sample of the clay from the estuary	263
6.6	Sampling equipment and sampling of the soft Falmouth clay	267
6.7	Bovey Whiteware ball clay beds at Preston Manor Clay Pit	273
7.1	View of the final condition of a sample drained only at one end and loaded and unloaded rapidly	287
8.1	A view of the Phillips X-ray diffractometer used in the study	351
8.2	A view of the atomic absorption spectrometer	376
8.3	A view of the nephelometer used in the analysis of sulphate ion concentration	385
9.1	Surface markings observed in test specimen BC.CHP.13	395
9.2	View of an impregnated vertical slice from test BC.CHP.21	396
9.3	Fissures produced in a final specimen	398
9.4	Magnified view of the fracture surface in Plate 9.3	400

		Page
9.5	Slaking of an air dried slice of specimen rapidly consolidated to high pressures (fissility test)	402
9.6	Fissility test results on vertical slices of different thicknesses	405
9.7	Fissility of equidimensional slices cut at different inclinations from the same specimen	406
9.8	View of the Cambridge Stereoscan 600	407
9.9	Layout of the optical microscope for quantitative fabric study	412
9.10	Optical micrographs of Carbowax 6000	414
9.11	Optical micrograph of a typical horizontal section of a consolidated ball clay impregnated in Carbowax	415
9.12	Optical micrograph of a vertical section of BC.CHP.17	417
9.13	A view of the XRD chart recorder and peak count indicator	423
9.14	The result of linear shrinkage of Falmouth and Ball Clay sediments	428
9.15	Electron micrographs of a vertical surface of a shrunk Ball Clay 661 specimen	431
9.16	Electron micrographs of different magnifications of the same area in the drained end of test BC.CHP.14	433
9.17	Example of electron micrographs that may be misinterpreted as a shear plane	435
9.18	Magnified view of a microfault in a specimen with oriented clay particles	436
9.19	Examples of flow structured fabrics	439
9.20	Optical micrographs showing shear structures due to rapid loading	441
9.21	Loading cap and ring effect on fabric during low pressure consolidation	443
9.22	Edge effects in high pressure consolidation tests	445
9.23	Fraunhofer diffraction pattern for fabric in Plate 9.22b	446
9.24	Optical micrographs of a vertical section from undrained end of BC.CHP.15	449
9.25	Stereo electron micrograph of specimen from drained end of BC.CHP.19	451
9.26	Optical micrographs of a shale-siltstone boundary	452
9.27	Electron micrograph of a shale	453
9.28	Packet structure of vermicullar Kaolinite	455
9.29	Optical micrograph of Falmouth sediment	456
9.30	Electron micrographs of Falmouth sediment	457
9.31	Optical micrographs of stoneware ball clay	459
9.32	Electron micrographs of stoneware ball clay	460

		Page
9.33	Comparison of the development of fissility on slaking of undisturbed Falmouth clay and Ball Clay	462
9.34	Electron microscope of Whiteware ball clay	467
9.35	Fabrics produced in the drained and undrained ends of test BC.CHP.12	471
9.36	Fabrics produced in the drained and undrained ends of test BC.CHP.18	472
9.37	Fabrics produced in the drained and undrained ends pf BC.CHP.17	473
9.38	Series of electron micrographs from the drained end of test BC.CHP.14	475
9.39	Electron micrographs of consolidated Falmouth clay	476
9.40	Results of fissility tests on vertical slices of undisturbed and consolidated samples	480
9.41	Electron micrographs of Whiteware ball clay with lignite seam and associated clay particle orientation	482
9.42	A view of a fissure in Whiteware ball clay	484
9.43	A developed view of the surfaces of a block of Whiteware clay included by a horizontal and an inclined fissure	485
9.44	Electron micrographs of fissures of different inclinations	487
9.45	Electron micrographs of the surface morphology of a natural fissure in a Whiteware ball clay	488
9.46	Electron micrographs showing calcite mineralization in the pore spaces of consolidated Falmouth clay sample	490
9.47	View of the ultrasonic materials tester used for P wave velocity determination	492

LIST OF TABLES

		Page
2.I	Basic properties of the common clay minerals	14
2.II	Salinity data from various seas	33
2.III	Thickness and rate of deposition of some argillaceous deposits	40
2.IV	Details of common laboratory compaction apparatus	70
3.I	References on the variation of preferred orientation with compaction	99
3.II	Anisotropic shrinkage in clays	101
3.III	X-ray diffraction intensity ratio in clay fabric study	110
3.IV	Stages of diagenesis	136
3.V	Some published anisotropy in clays	159
5.I	Basic system details of high pressure consolidation cell	203
6.I	Summary of details of spot samples from Falmouth Estuary	262
6.II	Summary of properties of the clay samples	276
7.I	High pressure consolidation tests	285
7.IIa	Details of extremely rapid loading tests	293
7.IIb	Details of controlled rate of loading CHP tests	294
7.IIIa	Composition of sea water (average)	310
7.IIIb	Composition of artificial sea water	310
7.IV	Summary of constant rate of strain compaction tests	327
7.V	The values determined for the preconsolidation stress of Ball Clay	333
7.VI	Thermal conductivity of relevant materials	336
7.VII	Summary of low pressure temperature tests	342
8.Ia	Qualitative interpretation of the X-ray traces of Falmouth clay	358
8.Ib	Qualitative interpretation of the X-ray traces of Petrockstow ball clay	359
8.Ic	Qualitative interpretation of the X-ray traces of Ball Clay 661	360
8.II	Summary of quantitative clay mineralogy	361
8.III	Summary of the Methylene Blue capacity data	371
8.IV	Summary of the settings used on the atomic absorption spectrophotometer	378
9.I	Results of the quantitative optical microscopy	463
9.II	Results of the XRD peak ratio for specimens at different rates of loading	464

		Page
9.III	Results of the XRD analysis for specimens with different salinity	465
9.IV	XRD analysis using single section technique	466

'HE hath made every THING
beautiful in His TIME;
Also He hath set the WORLD
in their heart, so that
no MAN can find out THE WORK
that GOD maketh from the
BEGINNING to the END.'

.....ECCLESIASTES; 3:II

CHAPTER ONE

INTRODUCTION

With progressive burial beneath younger sediments, clays expel their pore fluid and thereby acquire a more compact fabric. This is 'gravitational compaction' (Hedberg, 1936).

In soil mechanics, this process is called 'consolidation', the well known phenomenon which imparts an increase in strength and a decrease in deformability to the clay. To the geologist, however, gravitational compaction is but one of the many processes operative in geological consolidation; the evolution of rocks from argillaceous sediments. Thus these may lead to an apparent confusion in the use of the terms 'compaction' and 'consolidation'.

1.1 DEFINITIONS

The definitions of these terms by recognised professional bodies are quoted:

The American Society of Civil Engineers (1958) defines 'compaction' as the densification of a soil by means of a mechanical manipulation. The American Geological Institute's (1957 and 1962) definition of compaction is a decrease in volume of sediments as a result of compressive stress, usually resulting from continued deposition over them, but also from drying and other causes.

PLATE 1.1 Gravitational Compaction of Clays

Three examples from S.W. England of the Transition: Mud → Stiff clay → Shale.

a) Falmouth Estuary
Recent Deposit - Mud
Preconsolidation - very slight

a2) Block sample
Picture width = 15 cm.

a3) Electron micrograph
Picture width = 80μ

b) Preston Manor Clay Pit
Oligocene aged Ball Clay
Stiff fissured clay.
Preconsolidation ≃ 200 m

b2) Block sample
Picture width = 30 cm.

b3) Electron micrograph
Picture width = 80μ

c) Hartland Quay
Upper Carboniferous
Hartland Beds
Shale and Sandstone
Preconsolidation ≃ 5.1 - 13 Km
Temperature ≈ 440°C
(Photograph and sample received with thanks from Mr. M.H. de Freitas)

c2) Hand specimen
Picture width = 15 cm.

c3) Electron micrograph
Picture width = 80μ







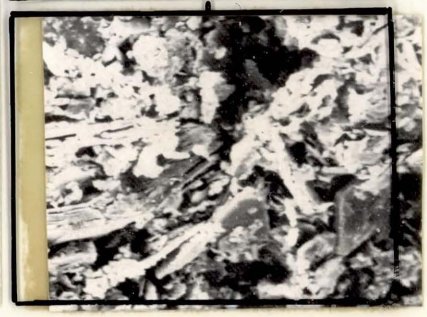




























Consolidation is defined in two ways: From an engineering view point, consolidation is the adjustment of a saturated soil in response to increased load, and involves the squeezing of water from the pores and decrease in void ratio. However, to a geologist, consolidation means more and is defined as any or all processes whereby loose, soft or liquid earth materials become firm and coherent (Americal Geological Institute, 1957 and 1962).

In this thesis, 'consolidation' is used in the soil mechanics sense;'compaction' when used refers to 'gravitational compaction'.

The progressive influence of compaction results in the transformation sequence: mud ⟶ soft clay ⟶ firm clay ⟶ stiff clay ⟶ clay-shale (Plate 1.1). This transition is accompanied by further inherent changes such as: clay mineral alteration, mineral intergrowth, variations in pore fluid chemistry and cementation. In order to investigate these burial induced phenomena, a feasible system to reconstruct the compaction history of a sediment at least from its time of deposition is doublessly desirable. Accordingly such an attempt is 'artificial gravitational compaction'.

1.2 FOCUS OF STUDY

This thesis therefore is focussed on the development and first research application of a special high pressure

temperature consolidation cell designed to achieve laboratory simulation of geological burial and exhumation.

The primary design capability of this consolidation cell is to impose upon either natural or artificial samples, a system of pressures (axial, lateral and back) comparable to that which are operative within a sedimentary column of a maximum depth of up to 10,000 feet. The system is further equipped to monitor the associated deformation of the specimen and collect pore fluids expelled.

1.3 MOTIVE OF STUDY

This study is motivated by the important role of clays and shales in the sphere of varied earth science disciplines. The civil engineer who encounters them as construction and load bearing material or as the cause of frequent havoc in the instability of earth slopes, may desire a knowledge of the process of acquisition of its characteristic geotechnical properties.

They are of interest to the Petroleum Geologist as caprocks, and source rocks of brines and petroleum. Moreover, instances of incomplete compaction can cause anomalous fluid pressures giving rise to drilling problems. In mining, geologists seek information on the migration of pore fluid from the clays and shale in the deposition of some epigenetic ores.

1.4 SPECIFIC FOCUS

The present research was restricted by the state of development of the apparatus and consequently all the high pressure consolidation tests were performed at ambient temperature.

The study was focussed on the following specific aspects:-

i) Influence of rate of loading.

ii) Influence of salinity of pore fluid on the high pressure consolidation of remoulded Kaolinitic clay.

iii) Pore fluid chemistry changes associated with high pressure consolidation.

iv) Development of macro- and micro-fabric in the clay with consolidation.

v) Estimation of the preconsolidation of heavily overconsolidated clay and comparison of the artificial gravitational compaction of recent sediment with that of the overconsolidated deposit.

vi) Influence of temperature on low pressure consolidation of remoulded clay.

1.5 COURSE OF STUDY

The specimens tested are dominantly Kaolinitic with illite as the second major mineral. Both remoulded and undisturbed specimens were tested. Undisturbed specimens were obtained from Falmouth Estuary, depicting recent sediments, and Oligocene aged ball clay ~~clay~~ deposits from Devonshire.

A mathematical analysis is proposed to analyse the observations of the laboratory consolidation of the specimens subjected to linear rate of increase of loading.

Remoulded slurries were tested at different rates of loading and with pore fluids of initially different chemistry. The chemistry of the expelled pore fluids were analysed using flame spectroscopy. The fabric of the specimens was observed using scanning electron miscoscopy, and optical microscopy, Further quantitative observations of fabric were made using X-ray diffraction techniques and the scanning electron micrographs were image analysed. The macro-fabrics produced in the specimen during this process of artificial gravitational compaction is compared with the fissures in the Bovey ball clay.

Undisturbed specimens were consolidated and their preconsolidation loads estimated. The consolidation character of the specimens are compared.

The conventional low pressure consolidation cells were modified to enable a study of the heating effects on the consolidation of the remoulded clay.

1.6 OUTLINE OF THESIS

This thesis forms a part of a series in an integrated research programme, centred round the use of the high pressure temperature consolidation cell designed to study the artificial gravitational compaction of clays.

Chapters Two and Three provide a comprehensive review of the process of gravitational compaction and its related geotechnical effects: Chapter Four outlines the mechanics of compaction and the proposed mathematical analysis is given.

The high pressure temperature consolidation cell is described in Chapter Five. The geotechnical details of the specimens, and their sampling sites are described in Chapter Six.

Analytical results of the consolidation parameters are given in Appendix D and are discussed in Chapter Seven. Imperial units have been used in the study and the respective conversion factors to the metric system are given in Appendix A.

Results of the chemical analysis are in Appendix F and they are discussed in Chapter Eight.

The fabric observations are presented in Chapter Nine.

CHAPTER TWO Review of Literature pertaining to Gravitational Compaction of Clays

2.1 Introduction 10

2.2 Clay sediments - size and composition 10

2.3 Clay colloid concepts 15

2.3.1 Adsorbed water 15
2.3.2 Diffuse double layer 19
2.3.3 Clay particle interaction 22

2.4 Fabric 25

2.4.1 Particle association 25
2.4.2 Factors influencing fabric of clays 27
2.4.2.1 Organic matter content 27
2.4.2.2 Particle size distribution of sediment 29
2.4.2.3 Chemistry of the suspension 31

2.5 Sedimentation and the rate of deposition 38

2.6 Concept of overburden stress 41

2.6.1 Effective overburden pressure 42
2.6.2 Compaction parameters 43

2.7 Historical review of theories of gravitational compaction 46

2.7.1 Sorby (1908) 46
2.7.2 Blackwelder (1920) 47
2.7.3 Teas (1923) 47
2.7.4 Terzaghi (1925) 48
2.7.5 Athy (1930) 51
2.7.5.1 Athy's compaction model 54
2.7.6 Hedberg (1926, 1936) 55
2.7.6.1 Hedberg's compaction model 57
2.7.7 Weller (1959) 60
2.7.7.1 Weller's compaction model 62
2.7.8 Powers (1967) compaction model 62
2.7.9 Teodorovich and Chernov (1968) compaction model 64
2.7.10 Burst (1969) 65
2.7.11 Beall's compaction model (1974) 65

2.8 Laboratory studies of compaction of clays 68

2.8.1 Low pressure consolidation 69
2.8.1.1 Influence of particle size 71
2.8.1.2 Influence of electrolyte concentration and adsorbed cation 71
2.8.1.3 Influence of mineralogy 75
2.8.2 Skempton (1943, 1953, 1970) 75
2.8.3 High Pressure Compaction 81

CHAPTER TWO

REVIEW OF LITERATURE PERTAINING TO GRAVITATIONAL COMPACTION OF CLAYS

2.1 INTRODUCTION

A clear understanding of the basic characteristics of a clayey sediment is imperative at the outset of this study. Therefore initial consideration will be given to the size, composition and fabric of clay sediments.

Particle interaction, resulting from the colloidal nature of the clay particles is more pertinent to the understanding of early compaction history than the gravitational forces associated with the particle mass. Accordingly clay-water and particle interaction is therefore discussed firstly and this will be followed by an insight into the factors controlling the fabric, particle association and orientation during compaction. The concept of effective stress, defining the steady state mechanics of load sharing between the particles and the pore water will then be discussed and followed by a review of literature on theoretical and practical aspects of gravitational compaction of clays in a chronological order.

2.2 CLAY SEDIMENTS - SIZE AND COMPOSITION

The term 'clay' has three different meanings (American Geological Institute, 1957):-

i) a natural material with plastic properties,

ii) to that size fraction of soils with particles less than 0.002 mm effective diameter as measured from their settling velocity in water, and

iii) also to crystalline fragments of minerals that are essentially hydrous aluminium silicates (or occasionally hydrous magnesium silicates).

Where a distinction between the latter two definitions is not obvious from the context, the terms 'clay size' and 'clay minerals' will be used in this study. The most common shape for clay size particles is platy; some clay minerals, however, have a characteristic rod or lath shape.

The clay minerals may be divided into five main groups - the Mica-like or Illite group, the Smectite or Montmorillonite group, the Kaolin group, the Chlorite group and the mixed layer group. The clay minerals are characterised by their atomic structure which may be simplified as an appropriate series of combinations (or stacks) of silicon-oxygen tetrahedra with aluminium-oxygen octahedra. The result of such combinations can be:-

i) Gibbsite,

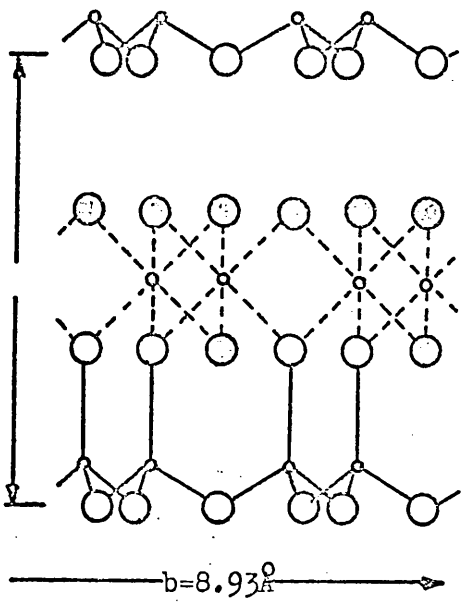
ii) Brucite, or

iii) Silicate sheet.

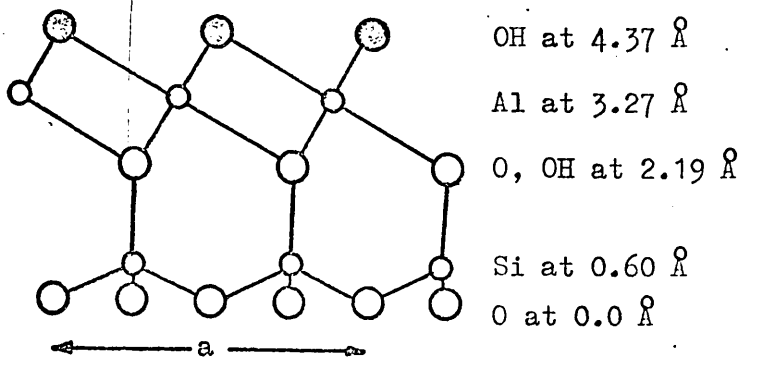
Figure 2.1 shows the atomic and symbolic structure for Kaolinite, the dominant clay mineral type, in the test materials used in this study.

Since each atom carries a small but finite electrical charge, the overall electrical stability of the clay mineral particle depends on the size, location, fit and electrical charge of the constituting atoms. Substitution of one ion for another in the clay crystal lattice and the imperfections in the atomic lattice at the surface of the particles cause different resultant electrical charge distributions in a given clay mineral. Accordingly the clay minerals carry negative charges on their flat surfaces and positive charges on their edges. Cations from the pore water are attracted to the surface of the particles to maintain electrical neutrality, and the number of the exchangeable cation is the cation exchange capacity, or the amount of negative charge per unit weight of the clay.

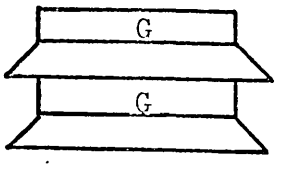
Inasmuch as the shape and thickness of clay minerals influences their behaviour during compaction, the more relevant physical properties of the four common clay minerals are presented in Table 2.I. The atomic structure of clay minerals in far greater detail and complexity than in the preceding summary outline is documented in Grim (1968).



(a)



(b)



(c)

FIGURE 2.1 (a) The ideal Kaolinite structure.
(b) The basal heights of atoms above the basal oxygen layer in Å units.
(c) Symbolic structure of kaolinite (Gibbsite and silicate units).

PROPERTY	CLAY MINERAL TYPE			
	Kaolinite	Illite	Chlorite	Montmorillonite
Structure Symbol				
Unit Cell Thickness (Å)	7*	10*	14.2*	9.6*
Surface Diameter (u)	0.3-4.0*	0.1-0.3*		0.01-0.1*
Clay Particle Thickness (Å)	500-20,000*	30*		10-80*
Surface Area (m^2/gm.)	10-20'	80-100'	5-50'	800'
Shape	Hexagonal	Hexagonal, Platy or Lath	Platy(?)	Platy (?)
Density (gm/cc.)	2.60-2.68*	2.64-2.69*		2.20-2.70
Cation Exchange Capacity (meq/100 g.)	3-15*	10-40*	20'	80-150*
Reciprocal of Average Surface Density of Charge ($Å^2$/unit charge)	83'	67'	700'	133'
Clay Mineral Compressibility	$2.5x10^{-6}$ cm^2/kg^+	$2.5x10^{-6}$ cm^2/kg^+	$2.5x10^{-6}$ cm^2/kg^+	2.5×10^{-6} cm^2/kg^+
Water Content (for 5 A layer) %	0.5	5		50

References

* - Warner (1964)
° - Brown (1961)
' - Lambe (1958)
+ - Skempton (1970)

TABLE 2.1

Average Values for some basic properties of the common clay mineral types

2.3 CLAY-COLLOID CONCEPT

The size range of colloids has been estimated at 1 to 2000 x 10^{-7} cm. and a specific surface area of 25 m^2/g. has also been suggested as a lower limit of the colloidal range. Thus because of the small size and the irregular shape, clay particles act as colloids in dilute suspensions. Therefore the behaviour of clay particles in suspension may be explained using the concepts of colloid chemistry.

2.3.1 Adsorbed water

Apart from aeolian deposits, most natural clays are deposited in water. As such the interaction between clay particles and water is a pertinent study prior to investigating the influence of overburden pressure on them. Clay particles in natural sediments are always hydrated, i.e., encompassed by layers of water molecules referred to as 'adsorbed water'. The plasticity, interparticle bonding, water movement and compaction are all influenced by this and the properties of this hydration cell will be investigated briefly.

The water molecules can be held to the clay surface by the following means. Being a dipolar molecule with a separation of centres of positive and negative charges the water molecules can be attracted by the resultant electrical charge distribution on the surface of clay particles, mentioned earlier. Furthermore,

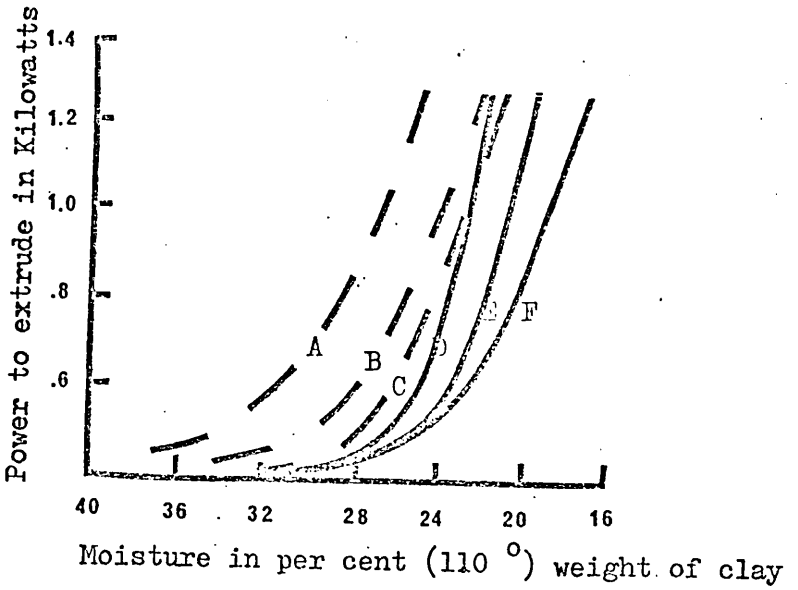
the hydrogen ions of water can lead to hydrogen bonding of water molecules with the exposed oxygen atoms on the clay mineral surface. The exchangeable ions are always hydrated in water and therefore when they are attracted to the negatively charged clay particle surface, the cations invariably carry with them water as water of hydration of the ions. The structure of this adsorbed water does not appear to conform to the simple model of a rod-like water molecule dipole as postulated by Terzaghi (1928). His model suggests an incorrect picture of the water molecule being aligned uniformly with positive ends at the clay surface and negative ends away from it. The surface density of the negative charges on the clay surface is too meagre for such an arrangement. Instead the Terzaghi model is superceded by that of Hendricks and Jefferson (1938) who proposed a V-shaped structure with each water molecule existing in tetrahedral co-ordination with the adsorbed water molecules, like in the structure of ice.

The adsorbed water has properties different from that of ordinary water, by virtue of the influence of the electric force field. The average density of adsorbed water is higher than that of free water. Values as high as 1.4 g/cc. have been measured for the first layer. It then decreases for the next few layers, dropping to 0.97 g/cc. at about four water layers, and then increases to 1.0 g/cc. for free water.

There is lack of agreement, in literature, as to the thickness of the adsorbed water layer. It is perhaps a variable as the resultant electrical charge on a clay surface is itself a variable. Approximate data on the amount of water that can be bound onto a surface of different clay minerals for a similar thickness of 5 Å (two molecular layers thick) is also given in table 2.I to illustrate the importance of this adsorbed water. Marked increase in permeability of the clays to saline water in contrast to fresh waters reflects an inverse relationship for the variation of the hydration of clays with the salinity of water (Amyx et al, 1960).

The power required to extrude clays, at different moisture contents, through an auger machine reflects the plastic properties of a clay which in turn is controlled by the thickness of the adsorbed water. An outstanding feature of such an observation by Grim and Cuthbert (1945) is that with more water than a certain minimum content, extrusion requires very little power (figure 2.2a). With water decreasing below this minimum amount, the power necessary to extrude increases rapidly to the point where extrusion is impossible.

Hypothetical observation of Powers (1967) shown in figure 2.2b illustrates the stages of expulsion of the adsorbed water layers with increasing depth of burial. Further experimental



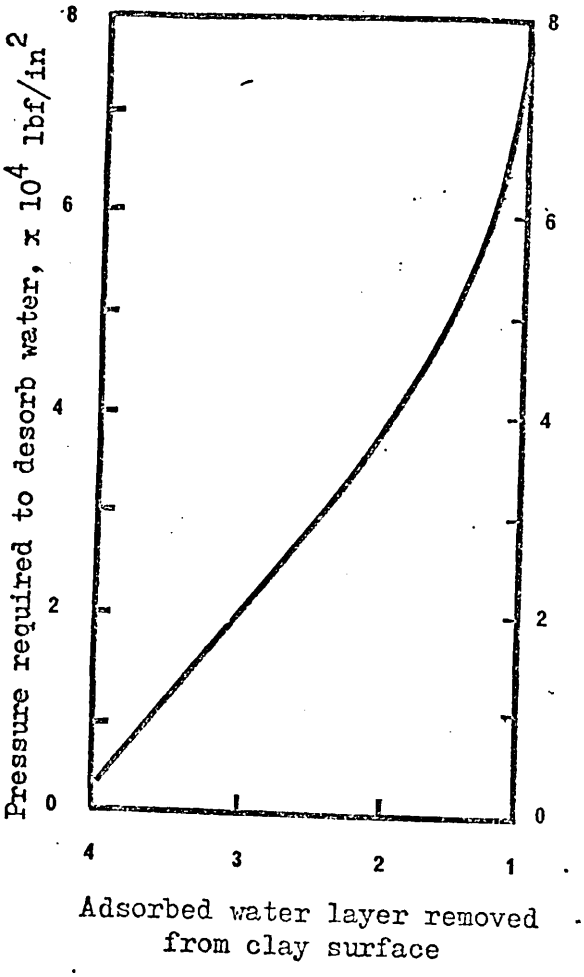


FIGURE 2.2 (a) Curves showing power required to extrude clays at different water contents through an auger machine. A: Kaolinite, B and C: Kaolinite and Illite, D, E and F: Illite. (After Grim and Cuthbert, 1945.)

(b) Pressure required to desorb the different molecular layers of adsorbed water from a clay surface (after Powers, 1967).

investigations of the bound water layer have been reviewed by Low (1961) and Martin (1962).

2.3.2 Diffuse double layer

The behaviour of clay-water mixtures can also be considered in terms of the forces that operate between adjacent particles. The theoretical concepts of colloidal suspensions (Verwey and Overbeek, 1948; Overbeek, 1952) has been introduced to soil mechanics by Jiminesz Salas and Serratosa (1953), Bell (1956) and Lambe (1958), and it aids in understanding the differences in behaviour that arise from variations in chemical and physical components of soils. However, Verwey and Overbeek's theory has been formulated for dilute colloidal suspensions and as such its application to compacted sediments is limited.

It is further assumed that the clay particle is a thin and a simple charged plate in an electrolyte medium of anions and cations. The electrical force between the negatively charged surface and the positively charged ions attract the cations to the surface, but they also desire to move away from each other because of their thermal energies. Thus the actual positions the cations occupy are a compromise between these two types of force. The balance between the coulomb electrical attraction and thermal diffusion results in a diffuse layer of cations, often known as

the 'diffuse double layer'. The fixed monolayer of cations attracted adjacent to the clay surface is referred to as the 'Stern layer'. The other cations in the diffuse double layer decrease in concentration towards the electrolyte with a higher density than that in the bulk of the electrolyte.

Electrical potential is a measure of the work required in displacing a unit charge from infinity to that particular point, and accordingly it is always negative for clay surfaces. Thus a variation in the electrical potential exists over a distance of the double layer thickness in clays. The terms Nernst potential, Stern potential and Zeta potential have been used to further define the potentials at the specific positions of:- the surface, the Stern layer and away from it respectively (see figure 2.3a). Figure 2.3b illustrates the fully developed double layers of the clay minerals, sodium montmorillonite and sodium kaolinite, when placed in pure water.

It is pertinent to discuss the three main factors that are known to influence the Zeta potential. An increase in the electrolyte concentration results in a 'crowding' of the cations in the Stern layer and it consequently reduces the Stern potential and the Zeta potential. The valency of the cation is a measure of the neutralising power. Hence a higher valency will effect a lowering of the Zeta potential. For similar conditions of

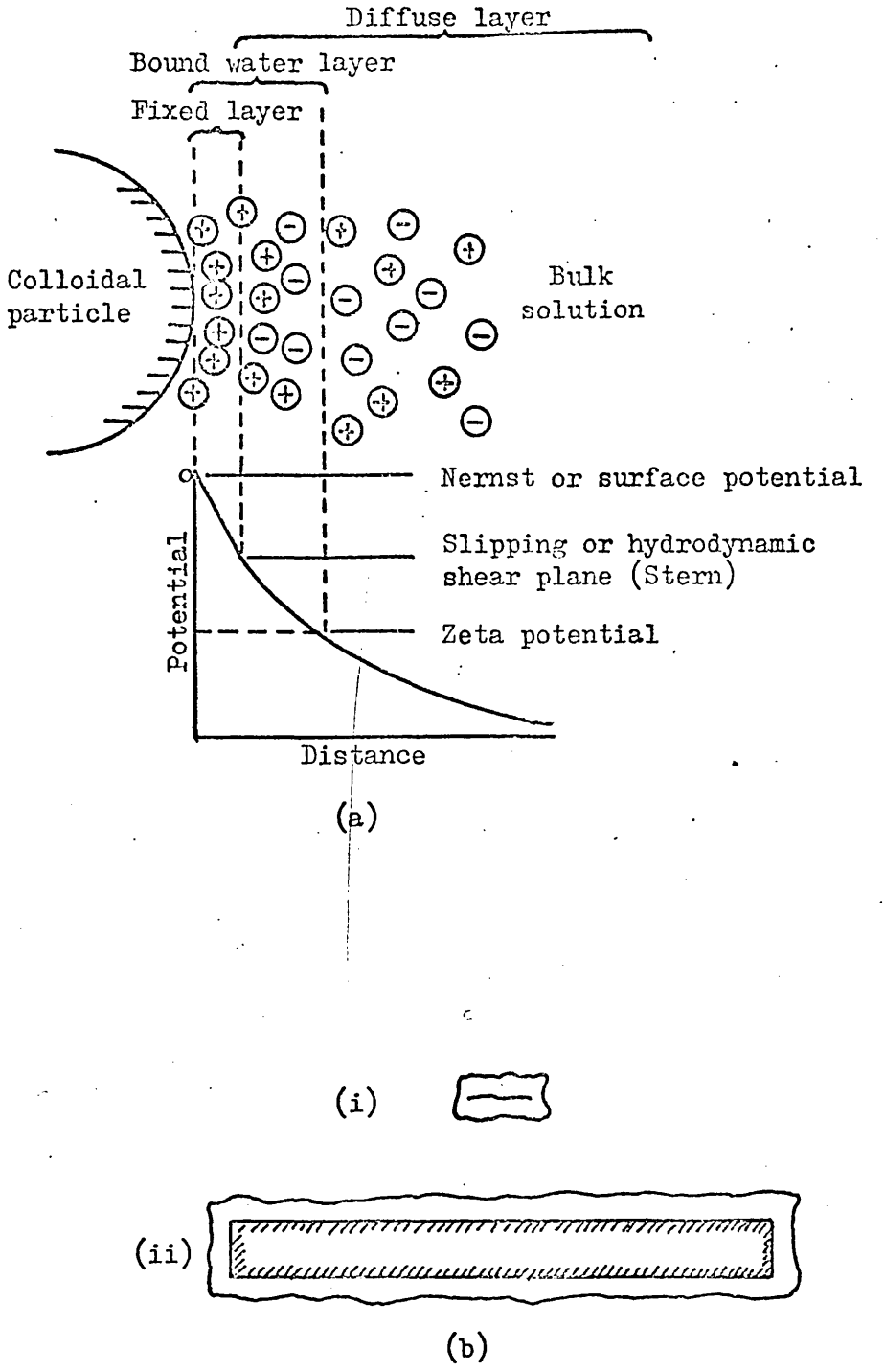


FIGURE 2.3 (a) Distribution of Electric Charge and Potential in the vicinity of a colloidal particle.
(b) Clay particles and the Adsorbed Water (i) Montmorillonite, (ii) Kaolinite (after Lambe, 1961).

electrolyte concentration, and valency of the cation, the crowding on the Stern layer will also be invariably dependent on the ionic size of the cations, because the number of cations accommodated in the layers depends on their physical size.

2.3.3 Clay-Particle interaction

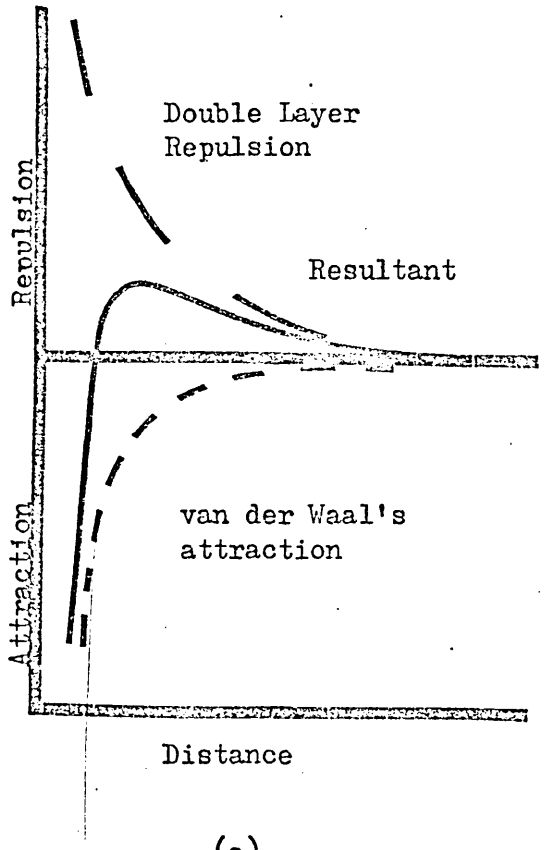
A study of the forces that operate between adjacent clay particles is relevant to a clearer understanding of the compaction behaviour of clays. The clay particles can interact through the adsorbed water layers, through the diffuse double layers and perhaps in some instances through direct contact.

The interaction of the adsorbed water layers may be conveniently visualised in terms of osmotic pressure. The function of clay particles in water to attract and hold cations, is the same as that in a semipermeable membrane in the classic osmosis experiment. The relative concentrations of the ions on the surface of the clay particles and in the rest of the clay water system, determines the magnitude and direction of the osmotic pressure. Accordingly if clay particles with ions attached to the surface are wet by water with a low electrolyte concentration, the osmotic pressure is great and causes an ingress of water between the particles, resulting in an overall swelling of the clay. On the other hand, in a high electrolyte concentration the repulsion between the particles will be less. The concent-

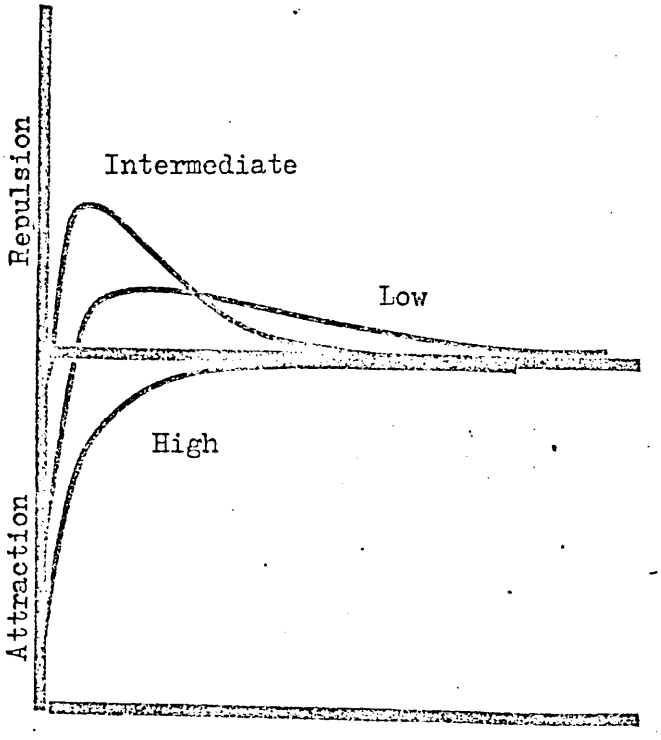
ration difference that leads to osmosis is dependent on the interparticle distance and the effective thickness of the diffuse double layer, which again is related to factors like valence as described in 2.3.2. Consequently interparticle repulsion will be greater with monovalent exchangeable ions and distilled water as the interparticle fluid.

It can be foreseen, from the above, that this osmotic pressure (or swelling pressure, as referred to in earth science texts) is one of the restraints that has to be overcome to effect compaction of the clays.

The preceding explanation has ignored the interparticle attractive forces which are effective when colloidal sized particles approach one another, over distances of separation of less than 15 Å. The intensity of these attractive Van der Waal's forces varies as an inverse function of a high power of the interparticle distance. Therefore, at a given interparticle distance the clay particles experience a resultant force of the combination of the attractive Van der Waal's forces and the repulsive double layer forces, Figure 2.4a shows this variation of the attractive and repulsive forces, and their resultant as a function of the interparticle distance. The influence of the electrolyte concentration on the resultant interparticle force is illustrated in figure 2.4b. The above variations have considered a parallel alignment of the clay particles. Other known modes of particle association and their respective terminology are cited in the following section.



(a)



(b)

FIGURE 2.4 Interparticle forces as functions of interparticle spacing (after Meade, 1964);

(a) effect of distance only,
(b) effect of electrolyte concentration.

2.4 FABRIC

There is an apparent looseness in the usage of the terms fabric and microstructure. Fabric in this study will be defined as 'the physical constitution of a sediment as expressed by the spatial arrangement of the solid particles and associated voids' (Brewer and Sleeman, 1960). Consequently fabric will be described in terms of the orientation and distribution patterns of the primary particles, compound particles and voids. As such, fabric will be considered as one element of the microstructure, the second element of which is the interparticle forces that were described in earlier sections. The fabric is a visible consequence of the interparticle forces of attraction and repulsion.

2.4.1 Particle Association

When a suspension of clay particles flocculate (or aggregate) three basic modes of particle association can result: face to face (FF), edge to face (EF) and edge to edge (EE). The interparticle forces differ for each of the above modes and the rate of diffusion in the three ways of mutual approach is also different. Consequently these types of associations need not necessarily occur simultaneously or to the same degree upon flocculation. Figure 2.5 illustrates some such possible combinations of particle association and their respective terminology.

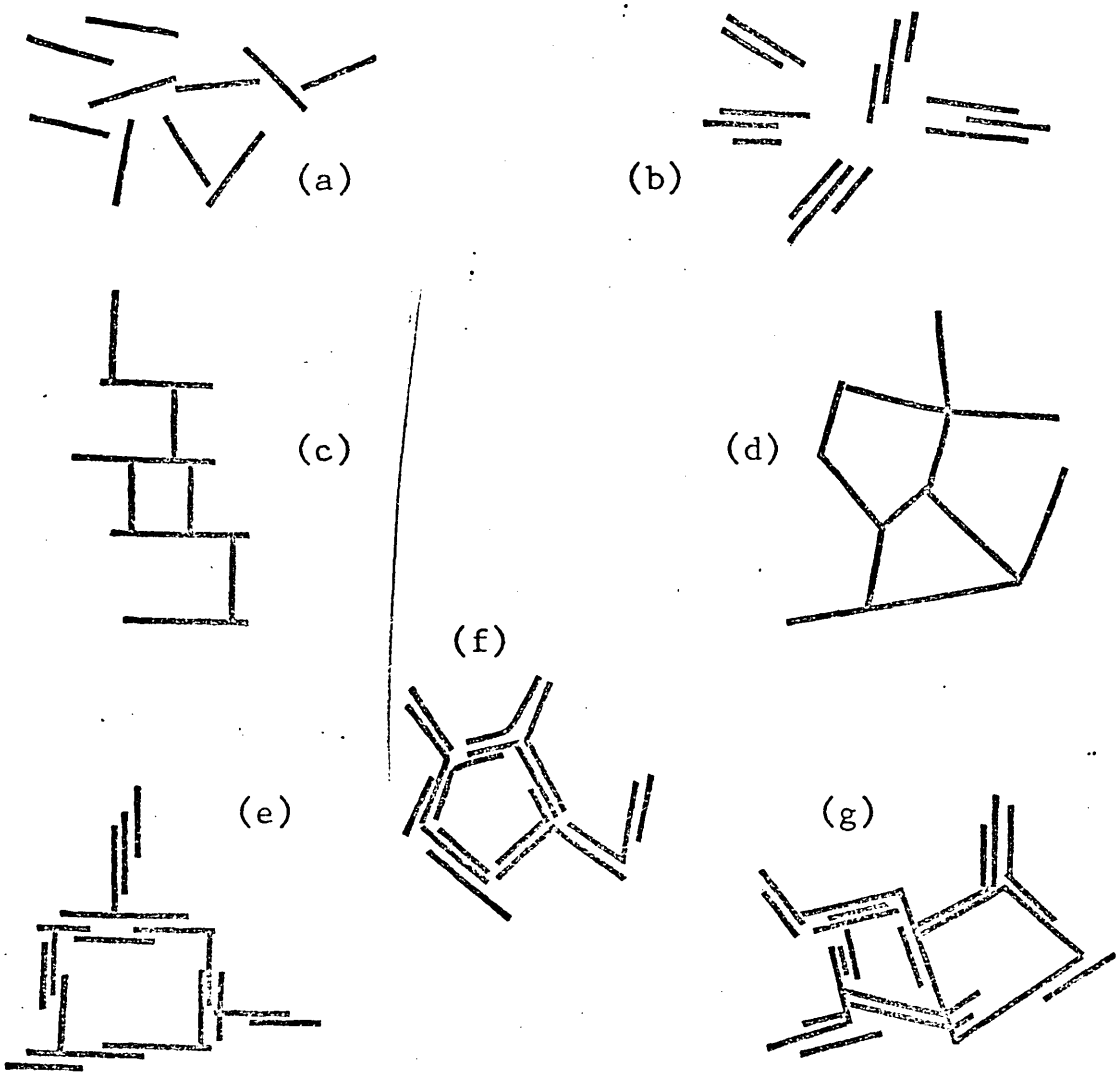


FIGURE 2.5 Terminology for possible modes of particle association in clay suspensions (after Van Olphen, 1965).

(a) 'Dispersed' and 'deflocculated'.
(b) 'Aggregated' but 'deflocculated' (face to face association, or parallel or oriented aggregation).
(c) Edge to Face 'flocculated' but 'dispersed'.
(d) Edge to Edge 'flocculated' but 'dispersed'.
(e) Edge to Face 'flocculated' and 'aggregated'.
(f) Edge to Edge 'flocculated' and 'aggregated'.
(g) Edge to Face and Edge to Edge 'flocculated' and 'aggregated'.

The term 'aggregated' has been used to refer to the FF associations. The dissociation of EE and EF modes is known as 'deflocculation' and the separation of the FF modes as 'dispersion'. Some of the common clay fabrics and their terminology as they appear in literature is presented in figure 2.6.

2.4.2 Factors influencing fabric of clays

Information available on those factors which influence clay fabric is limited. Most of the related published work has studied the separate individual influences, and very little work has been done on the combined effects. Factors influencing the depositional fabric will now be outlined and those associated with the subsequent burial will be discussed later in Chapter 3.

In reasonably calm depositional environments the fabric of the clay is susceptible to factors such as:-

Organic matter content,

Particle size distribution of the sediment, and

Chemistry of the suspension, viz. electrolyte concentration, pH, presence of ions.

2.4.2.1 Organic matter content

Apart from the observations of Ingram (1953), there does not appear to be any literature on this aspect. A direct

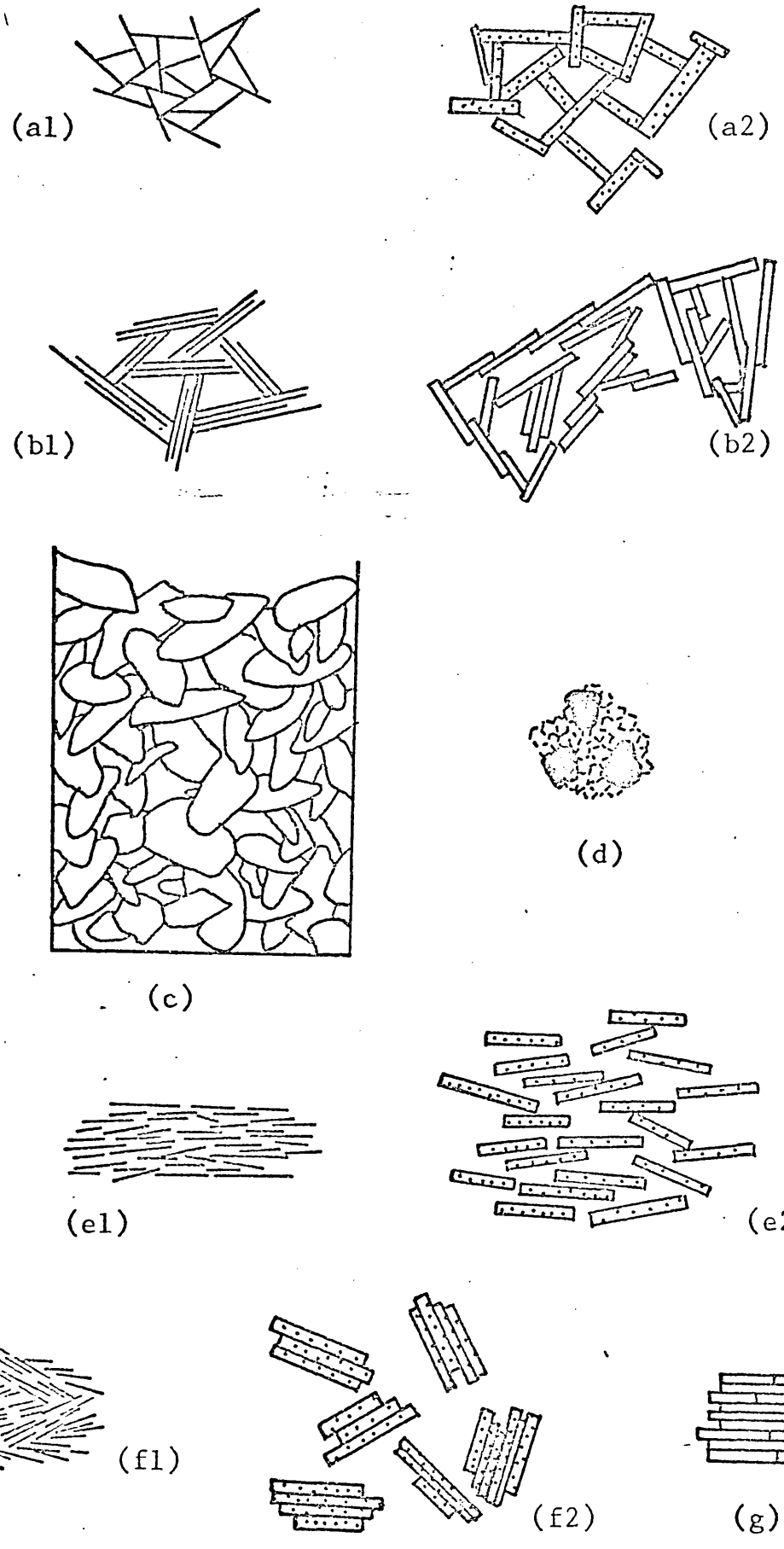


FIGURE 2.6 Idealised clay fabrics and their nomenclature.

a1; Cardhouse a2; Fresh water flocculated
b1; Bookhouse b2; Salt water flocculated
c; Flocculated edge to face (Tan, 1959)
d; Honeycomb (Casagrande, 1932)
e1,e2; Dispersed or preferentially oriented
f1,f2; Turbostratic (Aylmore & Quirk, 1960)
g; Stack

correlation between preferred orientation of clay minerals and the presence of organic materials has been observed (Ingram, 1953).

2.4.2.2 Particle Size distribution of Sediment

The presence of sand and silt sized particles has a marked influence on the fabric. Depending on the relative abundance of the coarse grained particles, three distinct kinds of fabrics can result (Brewer and Haldane, 1957):-

a) Coatings: clay sized material can occur as very distinct layers surrounding the coarse grains and filling the pore spaces of the soil skeleton formed by the coarse grains.

b) Clay sized material can occur as large uniform aggregates or flakes, having indistinct boundaries with coarse grained particles set to form a pseudo-porphyritic fabric. Plate 2.1 is an electromicrograph to illustrate dominant influence of coarse grained particles in distorting the local fabric.

c) Fine aggregations: clay sized material can itself aggregate to form equivalent silt size aggregates. Such aggregations cause distinctly different types of pore spaces in the fabric like interparticle porosity and intramicroblock porosity (Bochko, 1973).

PLATE 2.1 Distortion of preferred fabric by coarse particle:

a) Electron micrograph of the clay fabric distortion around a coarse quartz crystal.

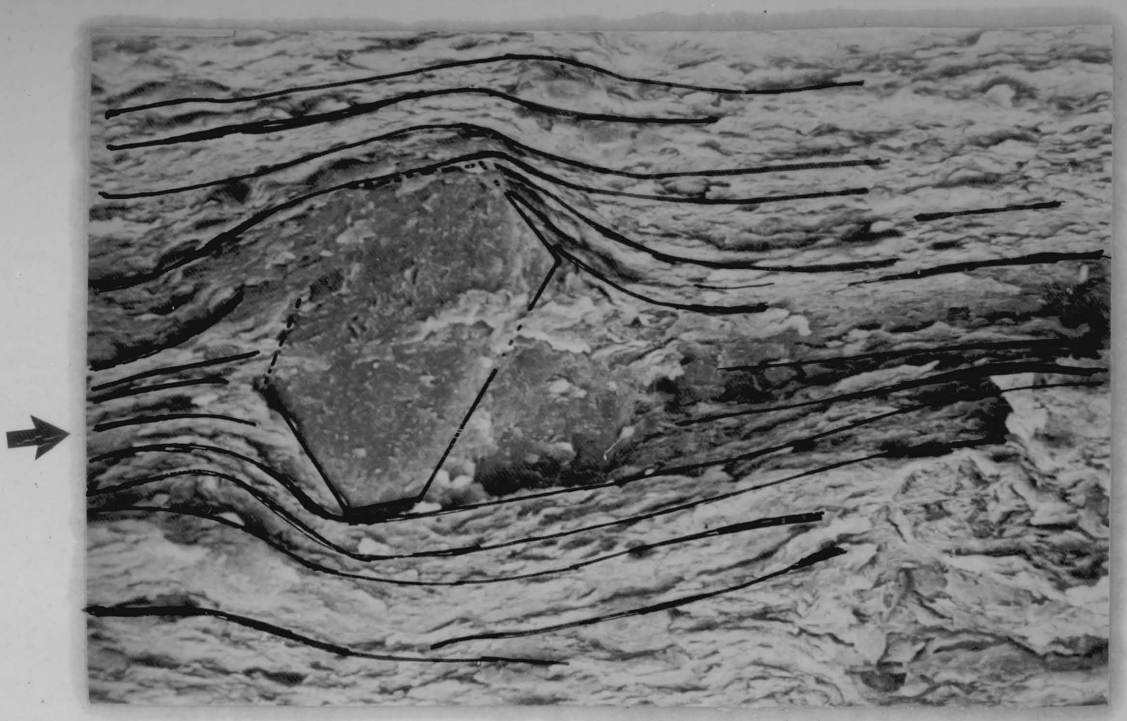
consolidation direction

magnification x 2000 x 2

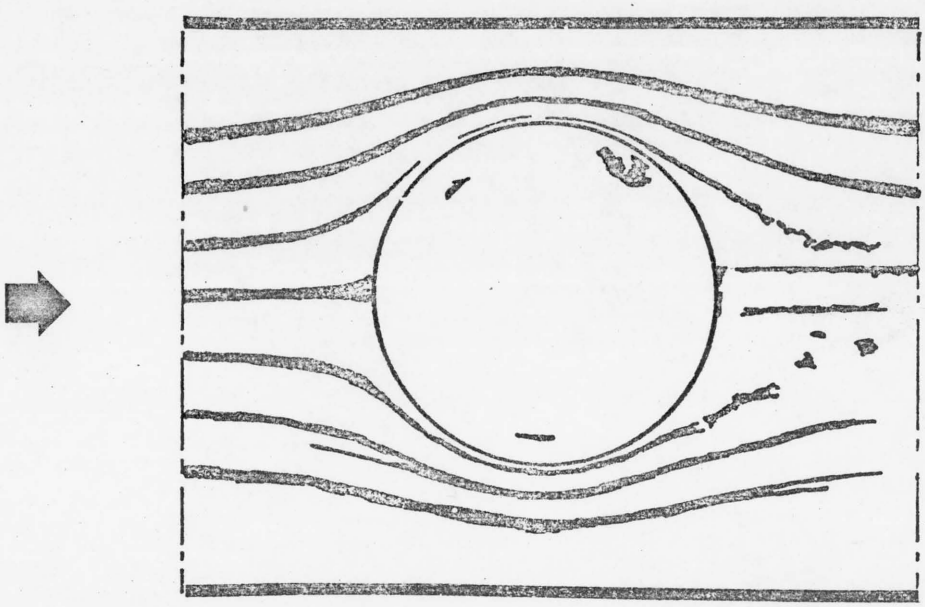
width of photograph ≡ 180 μ

b) Sketch of a smoke photograph of flow past a sphere showing the separation of turbulent boundary layer (after Harleman, 1966). Observe: similar flow structure pattern in the clay.

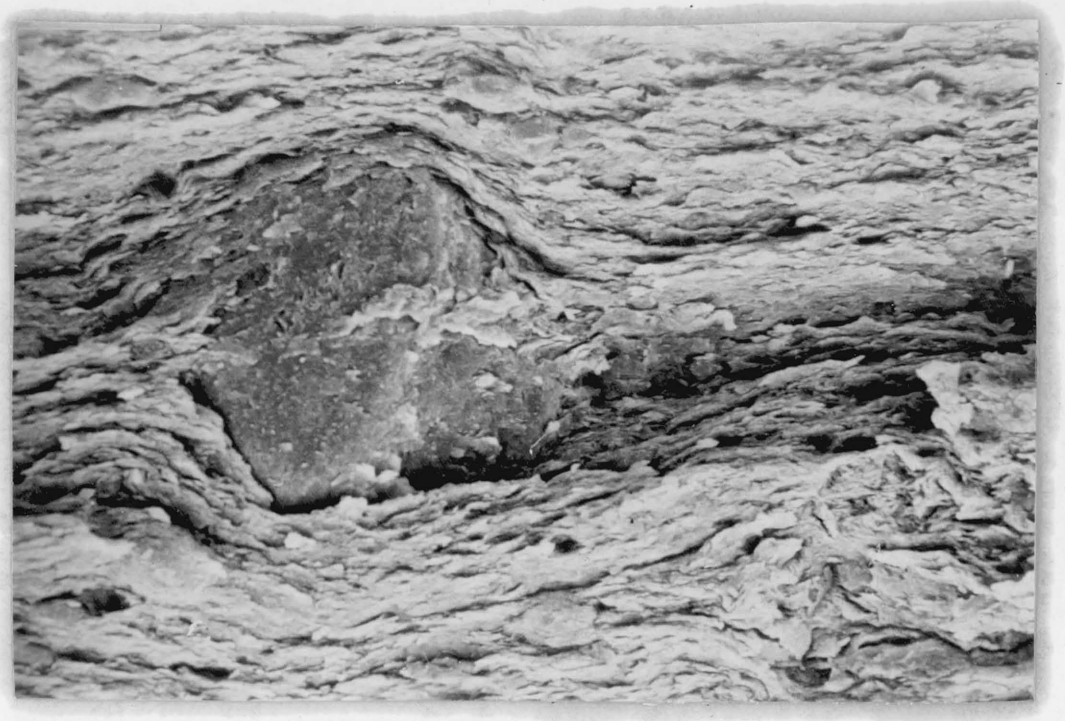
➡ indicates direction of fluid flow



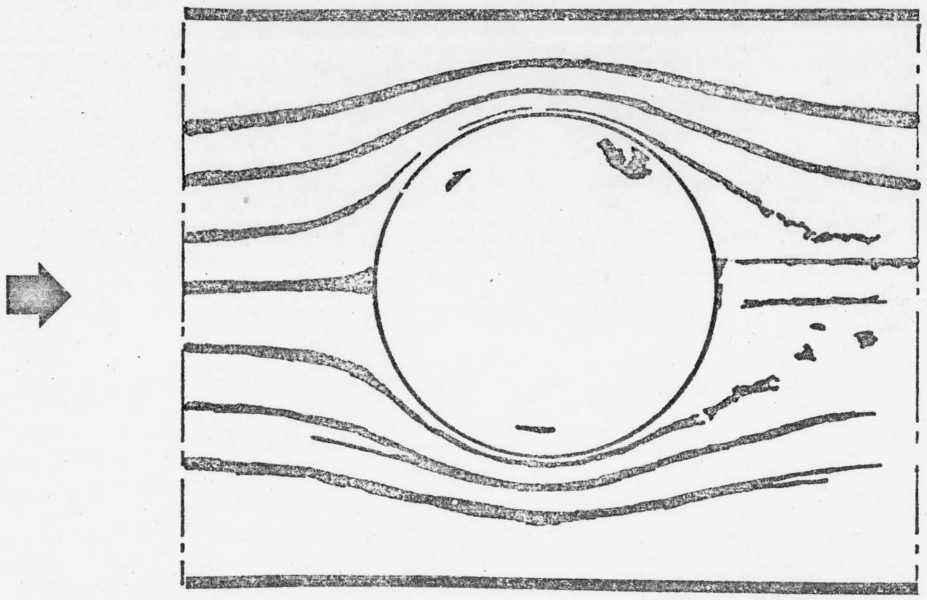
(a)



(b)



(a)



(b)

2.4.2.3 Chemistry of the suspension

The effect of the chemistry of the suspension on the fabric can be deduced from the clay colloid concepts discussed in the earlier sections.

Sedimentary clays can be deposited either in fresh water (rivers and lakes) or in a marine environment. The presence of dissolved solids is minimal in fresh water. The content of dissolved solids (salinity) in sea water may vary between 1-250 gms/litre (see table 2.II for values cited from texts). Furthermore the salinity can vary over the depth of the ocean or sedimentary basin (figure 2.7). In an estuarine environment there is a periodic change between a fresh water environment and a marine environment, where the period depends on the tide and the distance between the point of sedimentation and the river mouth.

The composition of saline water is a variable but is known to be a mixture of ions, with Na^{+}, K^{+}, Ca^{++}, Mg^{++}, Cl^{-}, SO_4^{--} being among the more dominant ions. Their presence depresses the development of the diffused ion layers and, as illustrated in figure 2.8, attractive forces become active participants in the formation of the fabric. Thus deposition in a marine environment yields a characteristic flocculated structure,

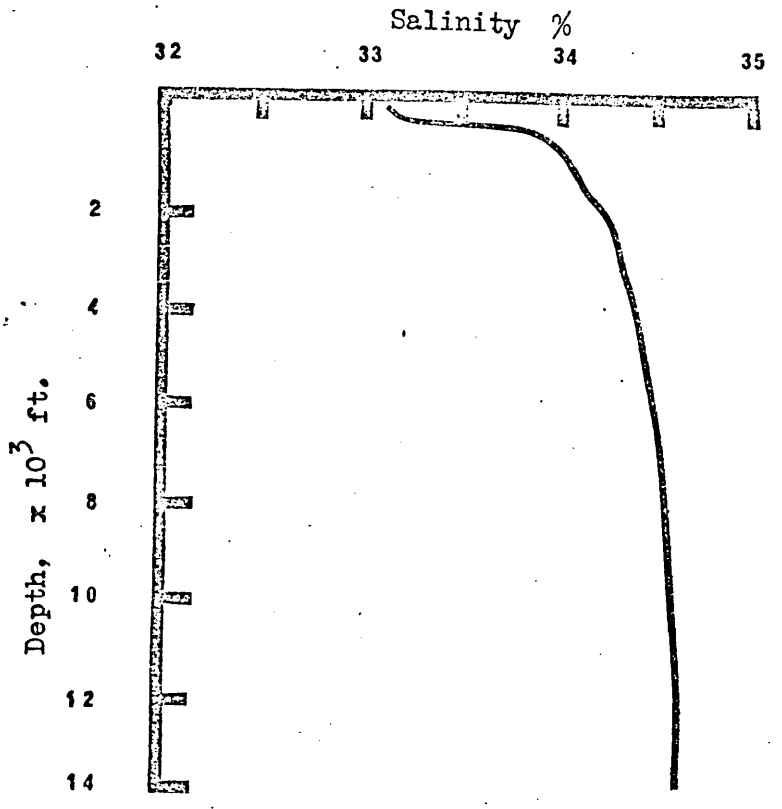


FIGURE 2.7 Variation of Salinity with Depth in the Pacific Ocean off South California (after Sahabad, 1962).

TABLE 2.II

Salinity data from various seas

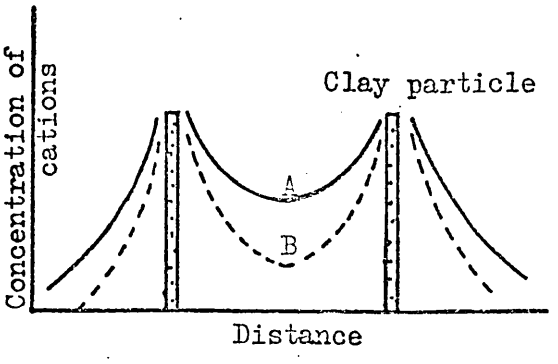
Type	Name	Salinity*	Reference
Large influx	Baltic	1	Lyman (1962)
	Black Sea	16	Lyman (1962)
	Yellow Sea	30	Lyman (1962)
	Bay of Bengal	34	Sverdrup et al (1962)
Open Ocean	Indian Ocean	36	Sverdrup et al (1962)
High evaporation areas	Persian Gulf	40	Lyman (1962)
	Red Sea	41	Lyman (1962)
Inland	Caspian Sea	13	Sahabad (1962)
	Dead Sea	250	Robertson & Anon (1962)

*Salinity is expressed in gms/litre dissolved solid content.

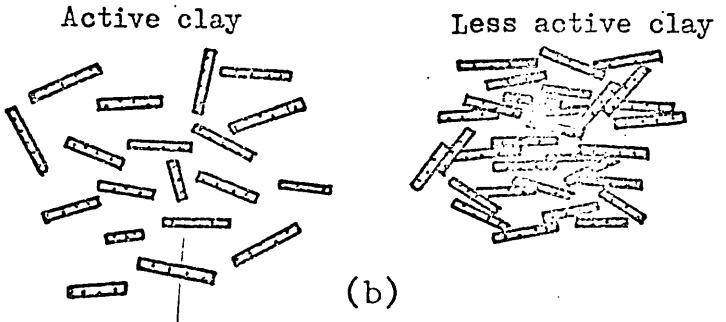
which is an open type of fabric with typical EF contacts. A reverse situation occurs with fresh water deposition where a dispersed fabric results on account of the enhanced development of the interparticle repulsive forces. These effects are further increased depending on the activity of the clay (i.e. more marked in montmorillonite than in kaolinite, figures 2.8b and 2.8c).

Schofield and Samson (1953) had investigated the influence of pH of the suspensions on fabric. Clay floccs result from the attraction between positive charged edges and negative charged particle faces. It has been observed that the positive edge charges are pH-dependent and eventually become negative with increasing pH values. However, Van Olphen (1965) has observed that addition of alkali to Sodium Montmorillonite results in the sediments showing slight tendency to flocculate instead of deflocculating.

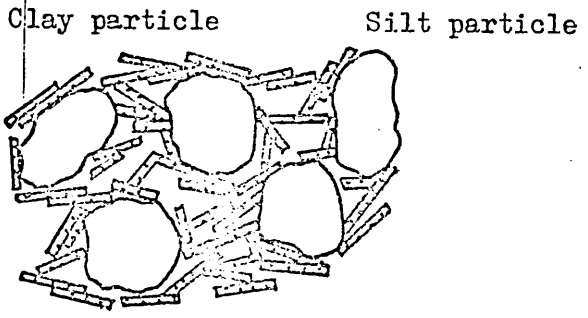
Contrary to the deductions in section 2.3.3, Hsi and Clifton (1962) suggested that the higher valence cations were associated with a more random particle arrangement. They have also observed that the nature of crystallinity of the sediments can also influence the formation of fabric. The settled volume of equal weights of sediments increased with the order of crystallinity (i.e. sediment volume in well crystallised kaolinite > meta halloysite > poorly crystallised kaolinite).



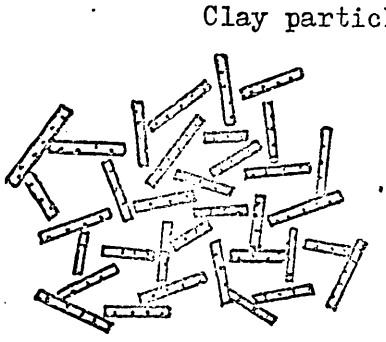
(a)



(b)



(c)



(d)

FIGURE 2.8 Deposition of sediments in fresh water and sea water. (after Yong & Warkentin, 1966)

(a) Interaction of the diffuse ion layers A; fresh water, B; sea water.
(b) Fabric of clay deposited in fresh water.
(c) Fabric of typical sediment deposited in fresh water.
(d) Fabric of clay deposited in sea water.

Existing literature on the effect of the concentration of the sediments in suspension on the formation of the fabric is conflicting and inconclusive. Meade (1964) reports the work of Raitburd (1958) whose experiments showed that kaolinite suspensions of 2 to 5 percent settled to form a preferentially oriented fabric whereas a 50 percent suspension settled to form a more or less random fabric. On the contrary, Olson and Mitronovas (1962) have shown that calcium illite sediments form a more flocculated arrangement of particles from dilute suspensions as compared with concentrated suspensions (see figure 2.9). No relevant inferences can be deduced from clay colloid concepts, as such concepts are strictly valid for dilute suspensions only.

Mechanisms such as the activity of burrowing organisms, viscous drag of turbidity currents, and early slumping is frequent in natural recent sediments. These induce a very marked but localised distortion of the fabric. The loose and open fabric of particularly the uppermost layers of the sediment makes them fragile and highly susceptible to such disturbances.

The initial water content of most argillaceous muds is about 50-80 percent corresponding to a porosity of 70-90 (Müller, 1967). However, average water contents of 150 percent have been observed in the upper two metres of the sediments of Lake Geneva (Serruya, 1969). Furthermore, the water content of

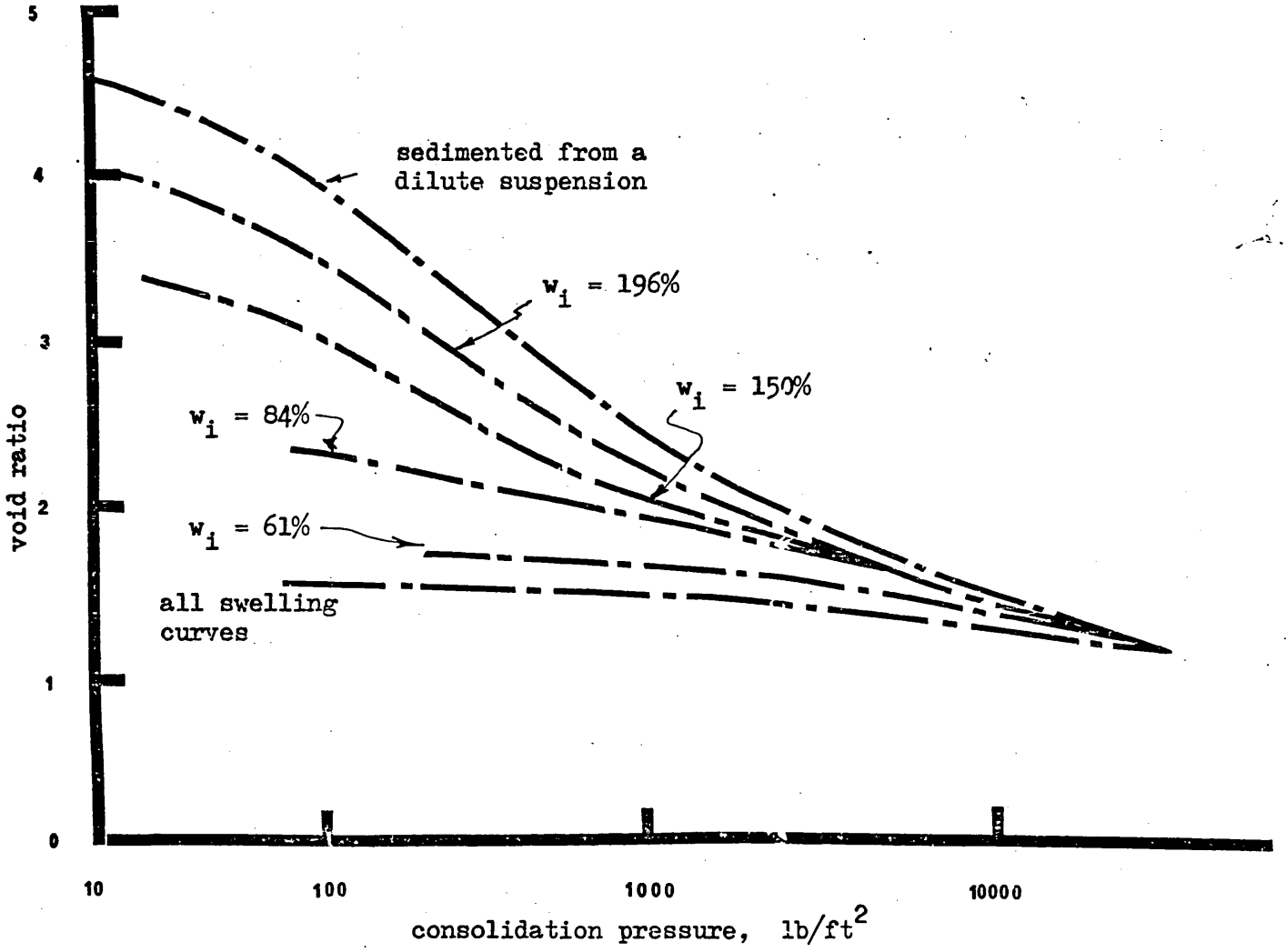


FIGURE 2.9 Influence of the initial water content (or 'concentration' of sediment) on the compaction behaviour of clay (Calcium Illite) (after Olson and Mitronovas, 1962).

the very first layers of these sediments, measured on undisturbed samples, has given values as high as 250 percent.

2.5 SEDIMENTATION AND RATES OF DEPOSITION

Most of the factors associated with the process of sedimentation have already been discussed, in the context of their influence on the fabric. A further pertinent aspect is the rate of deposition.

Assuming still water conditions, a soil particle or an association of particles (floc) will sediment when the gravitational forces on it exceed the viscous drag as defined by Stokes' theorem. The viscous drag is proportional to the viscosity of the suspension, the settling velocity, and the effective diameter of the particle or its associations. Hence the factors that aid flocculation will also enhance the rate of sediment deposition.

A review of the observed rates of sediment deposition in natural basins is not available in the literature (Dr. G. Evans - personal communication). In general, range of values of 1 to 10 mm in thousand years has been quoted for pelgaic sediments (Menard, 1964). While up to 50 metres in thousand years is a reasonable estimate for deltaic environments (Morgan, 1970). A very similar high rate of sediment deposition has been observed in the recent estuarine deposits of the Wash (Evans - personal communication).

Table 2.III is a brief collection of data from literature on the rates of deposition and thickness of deposits of some argillaceous sediments.

Introducing the terms 'honeycomb structure' and 'flocculent structure', Terzaghi (1925) considered the weight of the equivalent particle and the interparticle reaction to constitute a single force couple. The effect of any associated build-up of pressure in the fluid contained within the open structure was not considered. However, it is now known that excessive pore pressures will develop in sediments if they are deposited very rapidly or attain great thicknesses by continued sedimentation. This is a result of partial compaction. To achieve complete compaction the rate of sediment deposition must be theoretically infinitely slow. The consolidation theories of soil mechanics consider 95 percent consolidation as a fair approximation to equilibrium conditions. Developing the work of Gibson (1958), Skempton (1970) showed that to achieve a 95 percent consolidation in a sediment, 'h' metres thick and a uniform rate of deposition of 'r', the following condition must be satisfied:-

$$\frac{C_v}{rh} > 10$$

where C_v is the coefficient of consolidation defined later in Chapter Four.

Sedimentary Environment	Name of Basin	Stratigraphic System	Thickness of deposit m.	Rate of Deposition m/1000 yr.	Reference
Deltaic	Mississippi	Holocene	55	120	McClelland (1967)
	Rhone	Holocene	65	17	Lagaaij (in lit.)
	Orinoco	Holocene	40	8	Kidwell & Hunt (1958)
Estuarine	Avonmouth	Holocene	13	2.5	Skempton (1970)
	Tilbury	Holocene	16	2.0	Skempton (1970)
	Pisa	Holocene	10	2.5	Skempton (1970)
Pelagic	Caribbean	Pleistocene	-	0.03	Rosholt et al (1961)
	South Pacific	Holocene	-	0.001	Menard (1964)
	Baja California	Holocene	-	0.02	Menard (1964)
Marine shallow	Oslo Fjord	Holocene	-	0.80	Richards (1962)
	Po Valley	Pleistocene	2000	1.20	Skempton (1970)
	Po Valley	Pliocene	3000	1.00	Skempton (1970)
	Kambara	Pliocene	2600	0.90	Skempton (1970)
	North Sea	Pleistocene/ Holocene	300	0.05	Menard (1964)
	Gulf Coast	Lower Cretaceous to Pleistocene	8000	0.08	Menard (1964)

TABLE 2.III Thickness and Rates of Deposition of some Argillaceous Deposits.

Further aspects related to undercompacted zones are discussed in Chapter Three.

2.6 CONCEPT OF EFFECTIVE STRESS

The equation of effective stress was first proposed by Terzaghi (1923) defining the sharing of the total stress (σ) between the intergranular stress (or effective stress, σ') and the pore fluid pressure (u) as given in:

$$\sigma = \sigma' + u$$

In the original derivation of the above equation, Terzaghi considered the total stress to be shared proportionally to the active areas of interparticle contact in any horizontal surface through the soil. Accordingly the exact equation included a term f_b, the boundary porosity, multiplying the pore pressure, u. But subsequent experiments showed f_b to be very closely equal to unity (Terzaghi, 1936). Hubbert and Rubey (1959), on the other hand, assumed continuity of pores and derived the effective stress equation, independent of any correction for the area of contact of the particles.

It follows that the validity of the effective stress equation for clays and shales of low porosity is questionable, since discontinuity of pores can be highly probable. As much as it is difficult to ascertain the extent of continuity of

the pores, it is difficult to quantify a representative factor to be embodied in the equation. However, theoretical considerations have led to a more exact equation valid for a wide range of porosities, and was proposed by Skempton (1970) as:

$$\sigma = \sigma' + (1 - \frac{C_s}{C})u$$

where C_s and C are the compressibility of the clay particles and the clay structure respectively.

However, at porosities as low as 15 percent (when clays have become mudstones or shales), the ratio C_s/C can be as small as 1 percent and consequently the simple Terzaghi equation is not far from error.

The effective stress principle implies that volume changes and shear strength of soils are governed not by the total stress but by the effective stress.

2.6.1 Effective Overburden Pressure

In a sedimentary column, a change in effective stress at a point can occur as a result of either a change in total stress due to deposition or erosion of overlying sediments or as a result of change in pore fluid pressure subsequent to changes in ground water level. However, a simultaneous change of total stress and pore water pressure by the same amount (as in the

instance of the effect of change in sea level on a stratum below the sea bed) will not result in a change in the effective stress and consequently such a change will not induce any compaction on the stratum.

Figure 2.10 illustrates the application of the effective stress equation to a sedimentary column for both instances of the ground water level being within and outside the column. The total overburden pressure at any given depth Z is denoted by σ_v and is the vertical pressure resulting from the weight of all materials above it. The pore pressure u at the point is the equivalent of the head of water recorded on a piezometer placed there. As a result of capillary suction in the soil above the water table, negative pore pressures can develop and effective stresses of more than 1 Kg/cm^2 may be developed within this zone of dessication (figure 2.10b).

2.6.2 Compaction parameters

The state of 'compactness' of any porous body can be uniquely defined by any one of the quantitative parameters: void ratio, porosity, or solid grain proportion. Void ratio (e) is defined as the ratio of the volume of voids to that of the solid grains, while porosity (n) is the volume of voids expressed usually as a percentage of the total volume of the sample. Solid grain proportion (G) is a ratio of the proportion

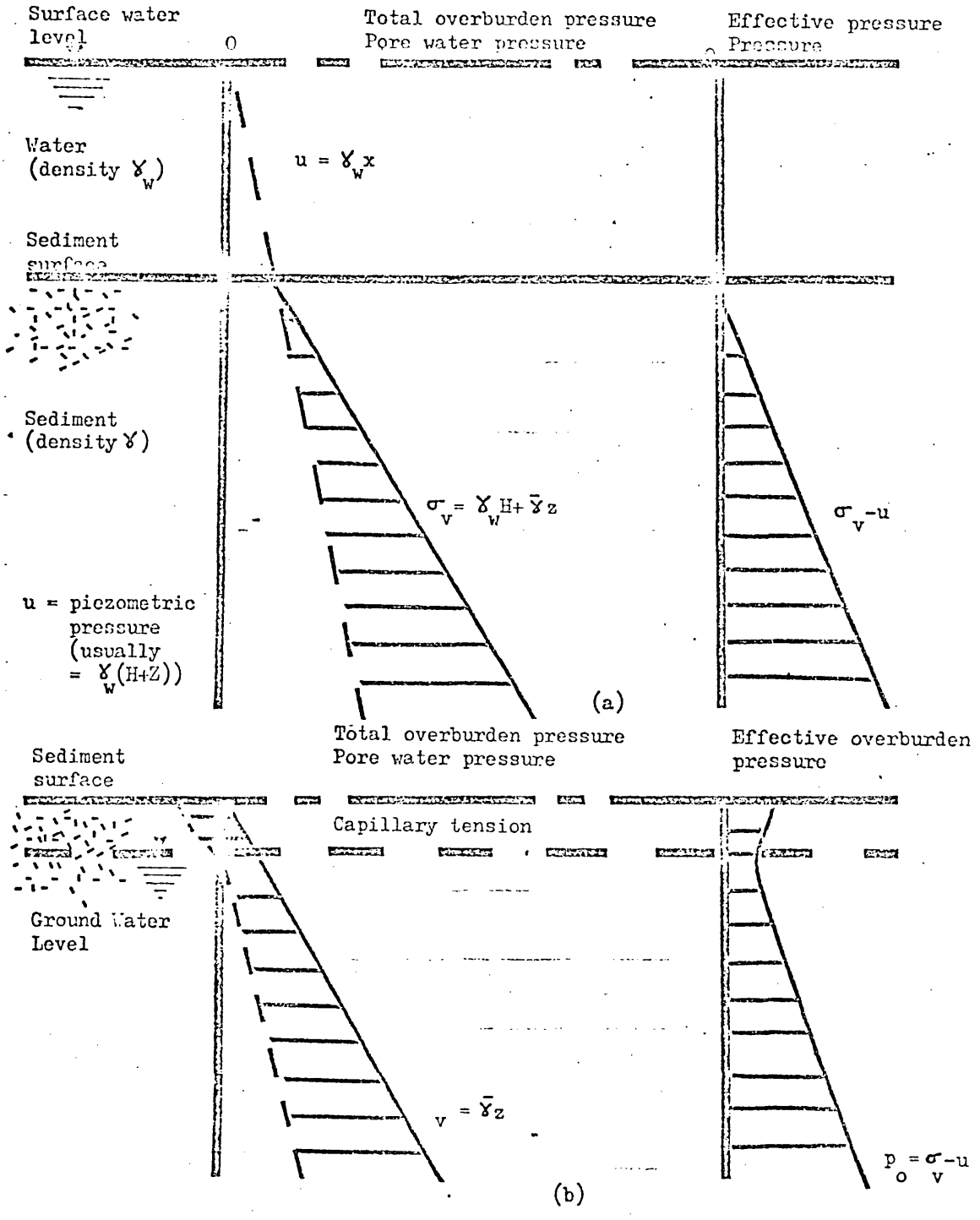


FIGURE 2.10 A normal distribution of total overburden pressure σ_v, pore water pressure u, and effective overburden pressure p_o, in a sedimentary column.

(a) Sediments completely submerged.
(b) Free water surface within the column.

of solids to the total volume (defined by Robertson (1967)). The above parameters are interrelated as in the equations;

$$n = \frac{e}{1 + e}, \quad G = 1 - n, \quad G = \frac{1}{1 + e}$$

It must, however, be noted that these parameters bear no indication of the particular sediment fabric. But for the hypothetical case of a perfectly oriented fabric, void ratio is directly proportional to the interparticle spacing.

The porosity of a sample can be measured using a porosimeter. The void ratio of a sample saturated with water is related to its water content (w) by the equation;

$$e = w \times \text{sp. gravity of solid grains}/100$$

and therefore can be computed. The solid grain proportion is computed as the ratio of the dry bulk density to the grain density.

It is apparent from the definitions that during the process of compaction, void ratio is an index of the volume change in the sediment while solid grain proportion is an index of the change in mass per unit volume. The parameter porosity is widely used by petroleum reservoir engineers as it is a convenient factor for computing storage.

In compaction studies, most of the results are presented usually as sediment compression curves which illustrate the

continuous variation of some of the above compaction parameters (often the void ratio) with effective pressure (usually plotted on a logarithmic scale).

2.7 HISTORICAL REVIEW OF THEORIES OF GRAVITATIONAL COMPACTION

This section reviews the development of theories of gravitational compaction of clays and shales and presents some of the major contributions. They are discussed in a chronological sequence.

2.7.1 Sorby (1908)

Sorby in 1908 pioneered the contributions to this field of study with his very informative paper entitled "The application of quantitative methods to the study of the structure and history of rocks".

His experiments with settling of clay suspension suggested the importance of the role played by the water in the compaction of fine sediments. Sorby suggested that 'the amount of interspaces varied in some way inversely as the pressure'.

Sorby presented original data on the porosity of natural sediments from which he discerned an inverse relationship between porosity and age, and recognised that compaction of sediments is essentially a change in porosity. The explanation

suggested for the reduction in pore space was that the solid clay particles deformed and filled the interspaces.

His work aroused little interest and no further research followed until the attention of the American petroleum geologists was directed to oil field structures, which gave this topic renewed momentum.

2.7.2 Blackwelder (1920)

Reviewing the oil domes of central Kansas, Blackwelder concentrated on the problem of lack of alignment of these domes.

Tangential compression or vertical readjustment to deep-seated rock flowage were among the explanations that had been suggested. Blackwelder supported the explanation of uneven 'condensation of deposits'. He suggested that domes were a result of the 'settling of sediments' quite uniformly, but over a hilly or mountainous foundation. It was further pointed out that as deposits of sand were less prone to settling than silt or mud, formations containing thick lenses of sand would be compacted unevenly in different parts.

2.7.3 Teas (1923)

Powers (1920, 1926) expanded the work of Blackwelder(1920) and Teas (1923) developed the influence of the sediment size on

differential compaction. He suggested the above phenomenon to explain the lack of consistency between the true bedding plane dips of Eocene clays and the underlying Cretaceous structure. Figure 2.11 illustrates the appropriate sketches used to support his theory where:

Fig. 2.11a Sand and clay is deposited in the same horizon but with an abrupt transition between them. Consequent differential compaction will produce dips up to 10° in the clay.

Fig. 2.11b Gentler dips of 1°-2° is produced in a deposit with a gradual transition between sand and clay.

Figs. 2.11c and d Differential compaction that can result in apparent synclinal and anticlinal dips.

2.7.4 Terzaghi (1925)

Terzaghi introduced a new dimension to the study of compaction when he presented a mathematical model for the theory of consolidation of clays. The mathematical analysis is presented in Chapter Four.

Terzaghi conducted experiments to measure the settlement of a clay slurry when subjected to increasing loads. In the apparatus used, a confining ring restrained any lateral

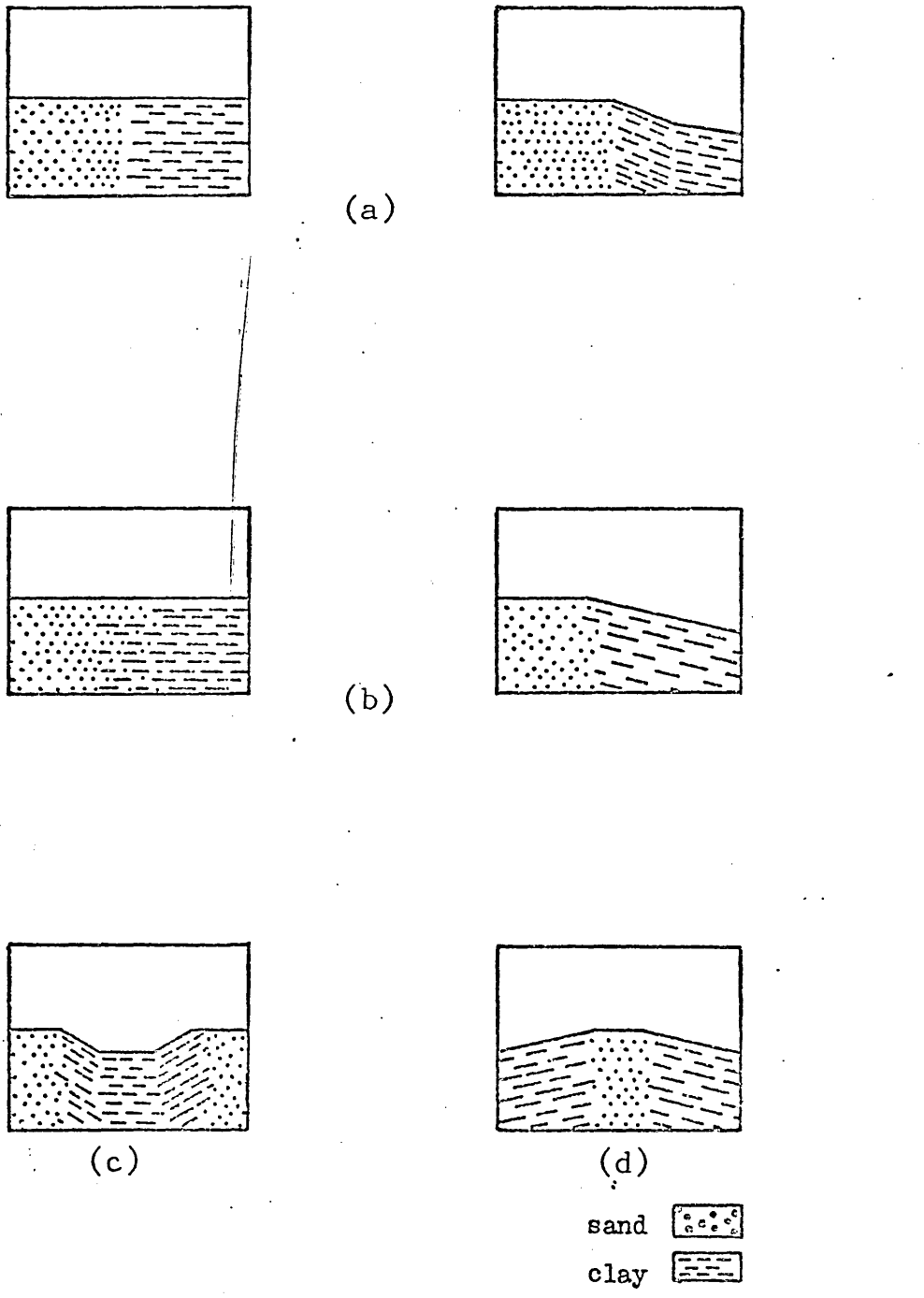


FIGURE 2.11 Differential Compaction of clays (after Teas, 1923).

(a) abrupt transition of sand and clay deposits
(b) gradual transition of sand and clay deposits
(c) formation of synclinal dips
(d) formation of anticlinal dips

deformation of the clay layer, which was always maintained saturated with water to exclude effects of surface tension of the pore water and those of drying. Such settlement observations, for constant loading, showed that the total settlement did not occur instantaneously but was characteristically time dependent. The application of the load must have produced a positive fluid pressure in the pore water within the clay layer but the pore water in the boundaries of the sample was always at zero hydrostatic pressure. This pore water pressure difference, which produces an outflow of pore water, is 'consumed' by the resistance of the clay fabric to such flow. The settlement (or compaction) of the clay layer is proportional to the volume of the pore water so drained. Consequently the process of compaction ceases only when this entire excess pore water pressure is dissipated.

Hedberg (1926) documented porosities of clays and shales from Kansas and also suggested an expression for its change with depth. A more comprehensive study was published subsequently in 1936 by him and to avoid duplication his observations are reviewed together later. However, it is noteworthy that in his early paper he visualises gravitational compaction as the following process:-

> 'The water content is determined by the equilibrium between the forces tending to hold it in the sediment

and the pressure due to weight of overlying strata. Assuming that these forces are in equilibrium at a certain moment, the further addition of sediment at the top of the column will disturb the equilibrium which can only be restored by the escape of water'.

2.7.5 Athy (1930)

Athy (1930, 1934) made density measurements of shale cores from wells sunk in Garber, Oklahoma. The relation between density and depth observed (figure 2.12) fit the curve of equation

$$D = B + A(1 - e^{-bx}),$$

where: D = density of shale,

B = density of surface clay - assumed to be 1.4, a representative value for muds of 48 percent porosity,

A = maximum density increase possible = 1.3,

b = constant,

x = depth of burial in feet.

The points through which the solid curve is drawn represent the measured densities and together with the dashed (theoretical) part, the entire curve represents the change in

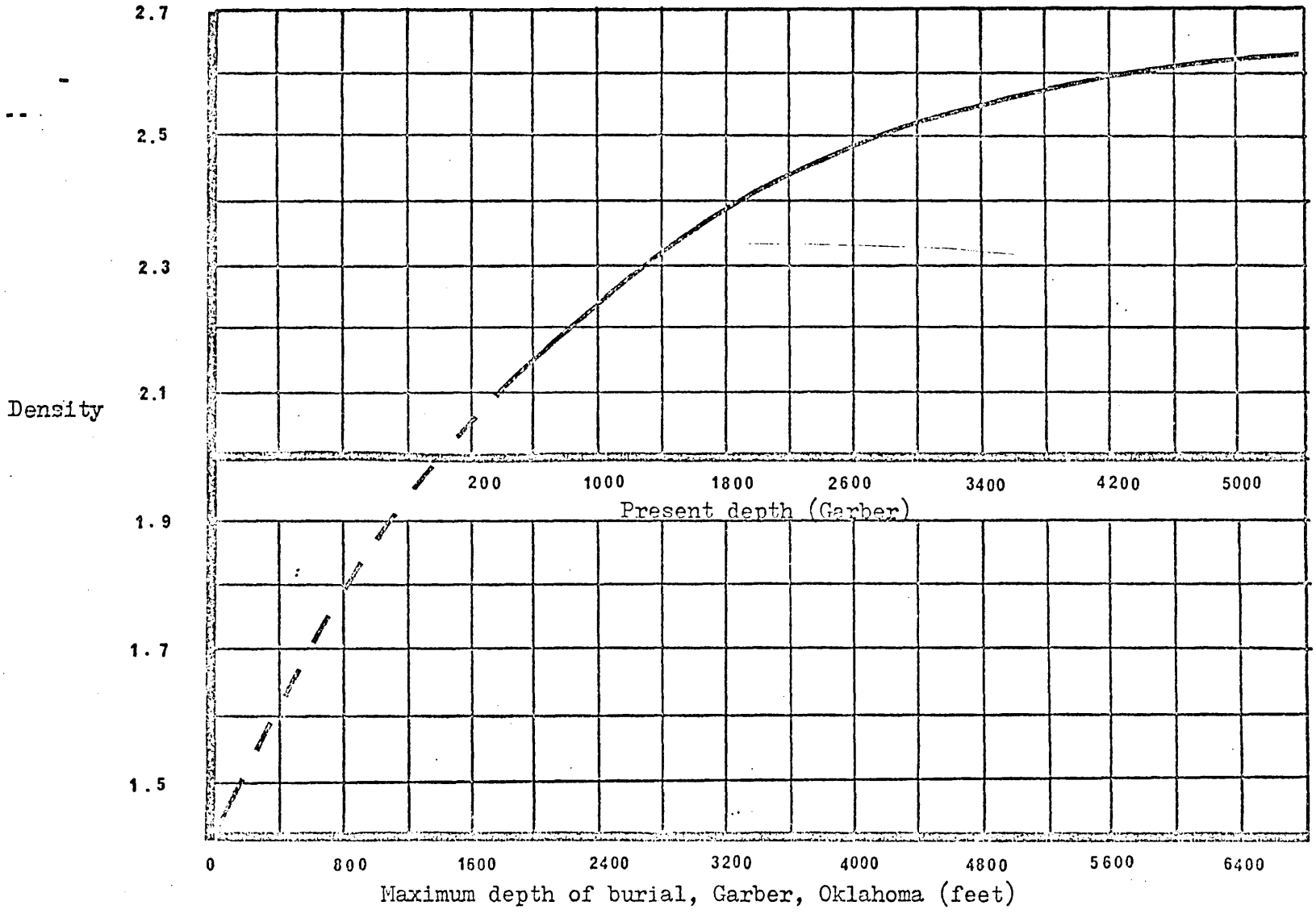
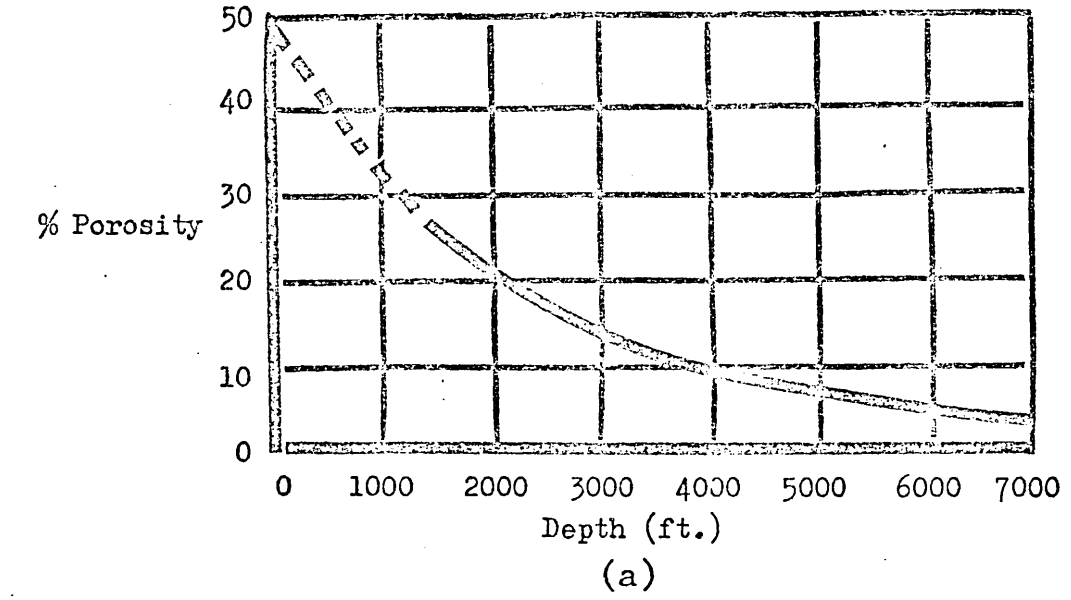
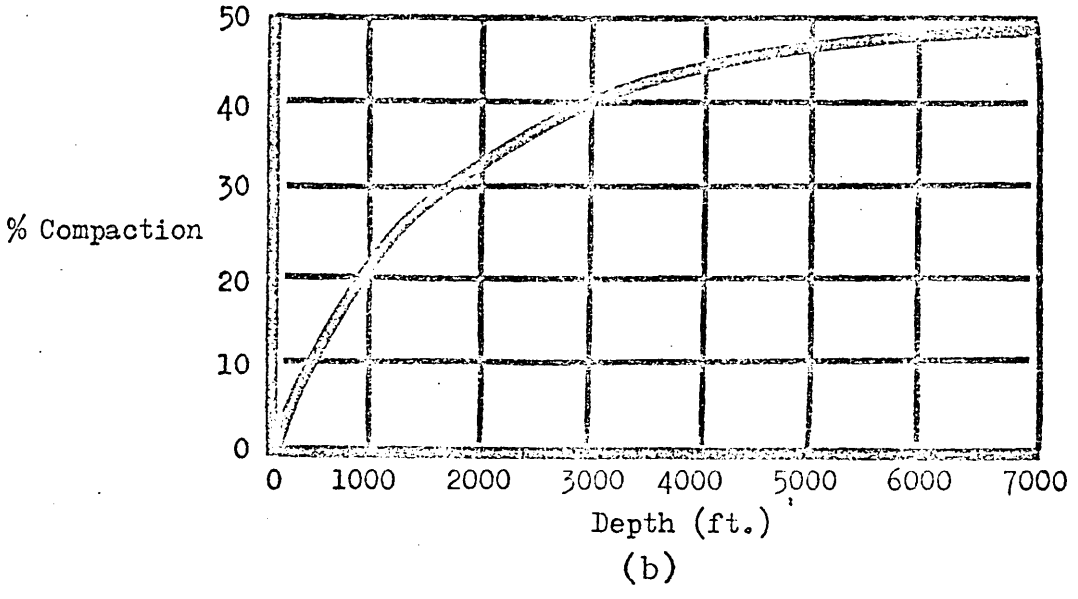


FIGURE 2.12 Density - depth curve (after Athy, 1930).



(a)



(b)

FIGURE 2.13 (a) Porosity - depth curve.
(b) Compaction - depth curve.
(after Athy, 1930)

density from 1.4 (which he assumed representative for surface muds) and up to maximum densities found at Garber. Comparing the densities at Garber with similar shales at similar depths in Oklahoma, the overburden eroded at Garber was estimated to be 1,500 ft (see figure 2.12).

Computing porosities from the measured densities, Athy also produced a corresponding porosity depth curve (figure 2.13a) fitting the equation

$$\phi = \phi_o e^{-bx}$$

where ϕ = porosity at depth x ft., and

ϕ_o = average porosity of surface muds.

Similarly, Athy published a compaction - depth curve (fig. 2.13b) which appears to conform to the equation

$$\text{Compaction (\% of original volume)} - C = \frac{B}{B+A(1-e^{-bx})}$$

2.7.5.1 Athy's Compaction model

Athy concluded from his curves that compaction is a simple process of squeezing one of the interstitial fluids, thereby reducing the porosity. The changes in porosity consequent to burial may be effected by the following stages:

1) deformation and granulation of the mineral grains,

2) cementation,

3) solution,

4) recrystallization,

5) squeezing together of the grains.

2.7.6 Hedberg (1926, 1936)

Hedberg devalued the experimental results of Terzaghi as applying only to low pressures and being only an approximation to natural phenomena. Athy's results were considered inaccurate due to his estimations of the thickness of previously eroded strata in order to obtain approximate depth values. Furthermore Athy's observations were from an area where forces other than gravitational compaction has affected the rocks.

Hedberg collected data from deep wells (depths of 291 to 6175 ft.) with excellent core records in Venezuela. The geology of the area is of essentially horizontal Tertiary strata, with thick shale formations, and far removed from areas of major tectonic disturbances or discontinuities. Variation of density and porosity with depth of overburden presented is shown in figure 2.14. The terms 'bulk density' and 'natural density' used by Hedberg (and in figure 2.14) are definable today as 'dry density' and 'saturated bulk density' respectively. As a result of the numerous processes involved in compaction, Hedberg considered it impossible to express satisfactorily pressure-porosity relationships for clays and shales throughout the entire depth range by any one equation.

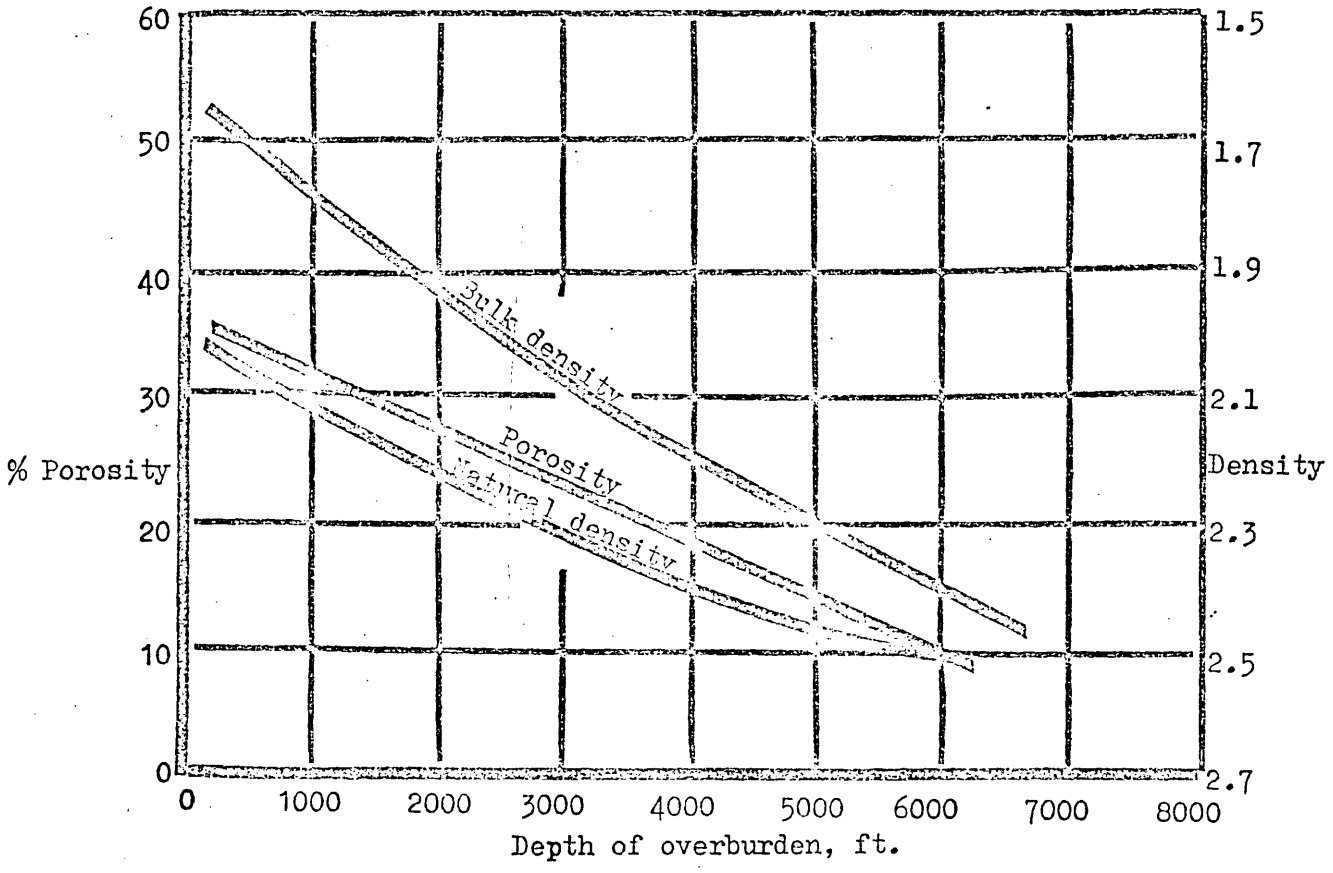


FIGURE 2.14 Porosity and Density variation with depth of overburden (after Hedberg, 1936).

2.7.6.1 Hedberg's compaction model

A compaction process consisting of four distinct stages (figure 2.15) was proposed.

i) Mechanical rearrangement stage:-

The fluid sediment, by virtue of the interparticle forces discussed earlier, seeks to form a fabric that is in equilibrium with such forces. This initial stage of compaction, extending from fluid sediment to roughly the liquid limit (range of porosity decrease from 90 to 75 percent) causes a rearrangement of the particles and expulsion of excess water.

ii) Dewatering stage:-

This stage of compaction results chiefly from the expulsion of free water from large cavities and adsorbed water from interparticle contacts. This can result from either evaporation or by pressures up to 800 lb/in^2. During this stage there is a rapid decrease in porosity for small increments of overburden pressure. At the end of this stage (porosity 35 percent), the solid grains mutually make contact over some parts of the surface and only a portion of the adsorbed water layer remains intact. The forces opposing this compaction are the interparticle repulsive forces over the surface area of the clay particles and the frictional resistance to the drainage of water.

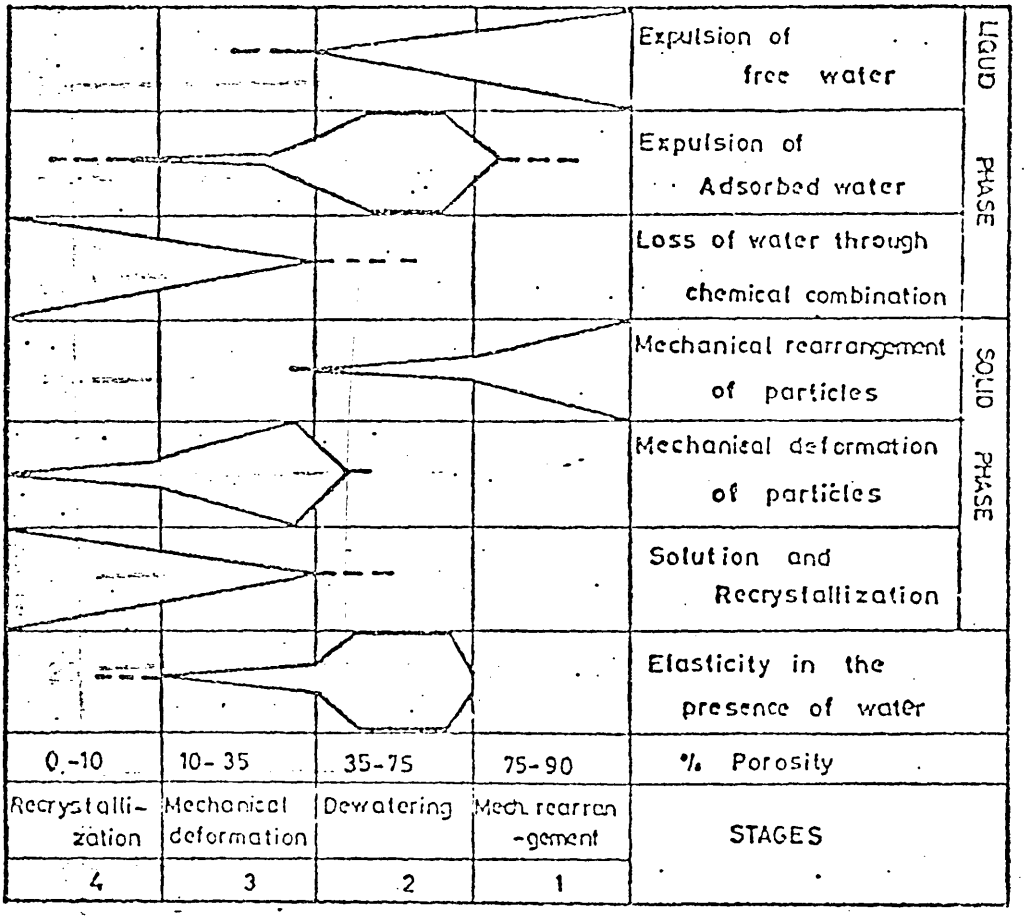


FIGURE 2.15 Hedberg compaction model.

iii) Mechanical deformation stage:-

In this stage the clay particles are in close proximity even as to make actual contact with each other; this results in greater resistance to further reduction in porosity. It is pertinent to note that according to Hamilton (1959), transition from clay to shale occurs at about 35 percent porosity, which is the upper bound value for porosity in this stage as defined by Hedberg.

Since individual particles have now acquired a stable configuration and adsorbed water has been removed from the points of contact, further compaction efforts up to 6000 lb. in^2 can result only with mechanical deformation of particles; the solid particles are crushed and deformed to fill more completely the pores remaining in the rock, and is accompanied by further expulsion of adsorbed water.

iv) Recrystallisation stage:-

In this final stage with porosities below 10 percent, temperature increase, that accompanies pressure, influences chemical readjustments. The reduction of pore volume resulting from drainage of pore water occurs slowly and only with large pressure increments.

Localised stress concentrations at the large number of points of interparticle contact tend to cause solid solution and subsequent redeposition in lower stress regions. Under further pressure, large crystals grow at the expense of the smaller and there is a gradual transition from shale to slate and from slate to phyllite.

At this stage, the pressure-porosity curve approaches asymptotically the zero porosity line.

Skempton (1944 and 1953) contributed the obvious and important link to the study of field compaction and laboratory consolidation. Skempton's work is reviewed more appropriately later with other attempts at laboratory studies of compaction.

2.7.7 Weller (1959)

Weller compiled Terzaghi's experimental results with Athy's and Hedberg's observations into a single continuous graph (figure 2.16). Conversions from one set of results to another required adjusting the factors which may have affected them. Estimated amount of erosion in Athy's work may have been erroneous while technical problems may have arisen with Hedberg's measurements in attempting to obtain undisturbed samples of high porosity. Terzaghi's results accounted for the hydrostatic uplift pressures while Hedberg had neglected them.

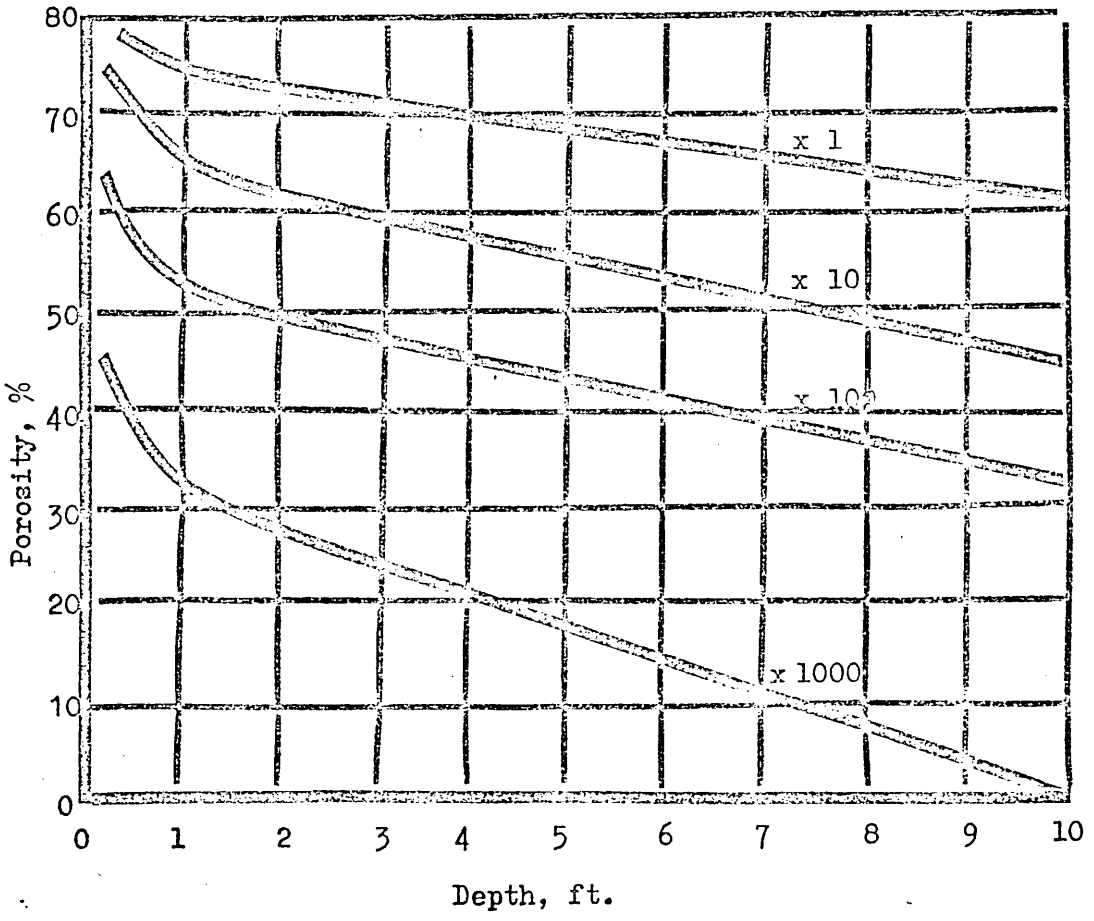


FIGURE 2.16 Continuous porosity depth curve (after Weller, 1959).

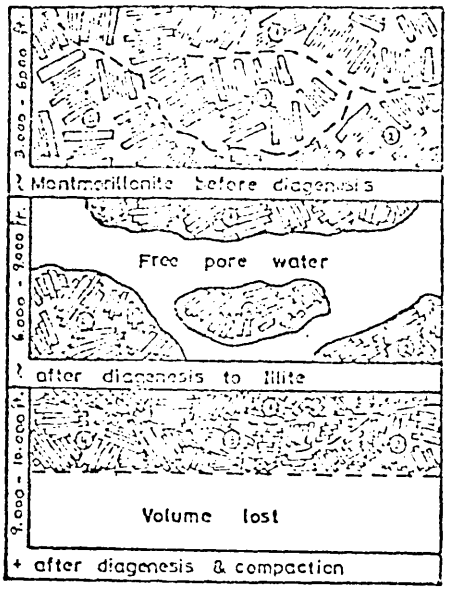
2.7.7.1 Weller's Compaction model

In the compaction process, Weller proposed, the initial stage is described from a surface mud having a porosity between 85 and 45 percent. With sedimentation, overburden pressure increases expelling pore fluids from the pore space in the porosity range from 45 to 10 percent. Weller theorised that at porosities of 10 percent, the non-clay minerals are in contact with each other and the clay particles are deformed and squeezed into the void spaces.

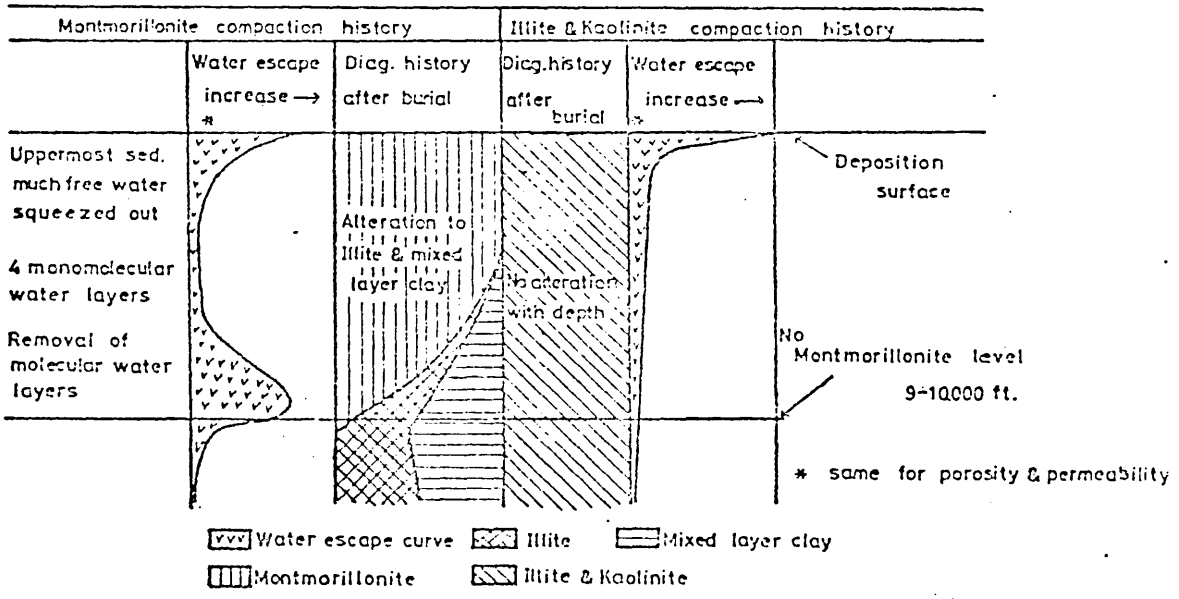
2.7.8 Powers (1967) - Compaction model

Powers theorised the fluid release mechanisms from shales to be based on burial induced changes in clay minerals and associated bulk properties. The mineralogical transformation of montmorillonite to illite with burial releases large volumes of bound water from montmorillonite surfaces to interparticle voids where it then behaves as interstitial water.

Powers deduced the relationships for expulsion of water, clay mineralogy, and depth of burial as shown in figure 2.17b. In the early stages of burial the marine montmorillonite sediments attain a balance between the water retained in the sediment and the water retaining properties of montmorillonite. Further burial results in less significant effects on expulsion



(a)



(b)

FIGURE 2.17 Compaction history of marine clay minerals (after Powers, 1967).

(a) Effect of clay diagenesis on removal of water from mudrocks.

(b) Clay mineral alteration.

of the remaining water. In the depth range of 1,500 - 3,000 ft. most of the water occurs as water of hydration of at least four monomolecular layers thick. This is further reduced to only a small amount of adsorbed water at depths up to 6,000 feet (see figure 2.2b). Associated with the clay mineral transformations from montmorillonite to illite, the adsorbed water is desorbed and behaves as free pore water at depth. This effects a marked change in the effective porosity, permeability and the available free pore water; and as a result the sediment attains a new balance with further burial at depths greater than 9,000 feet (see figure 2.17a).

2.7.9 Teodorovich and Chernov (1968)

Teodorovich and Chernov studied the compaction process in relation to the Apsheron horizons in Azerbayjan. They discerned three distinct stages in the process. Large amounts of water are squeezed out from the sediment in the first stage which is operative up to depths of 10 metres when the porosity of the muds decreases from 66 to 44 percent while in the case of sands and silts the porosity is reduced from 56 to 40 percent. The second stage is characterised by a rapid decrease in the compaction rate down to depths of 1,400 metres and the porosity of the sediments is reduced to 20-21 percent. The compaction in the final stage is very slow, and Teodorovich and Chermov

recorded porosities of 15 percent in sandstones and 7 percent in the shales at a depth of burial of 6,000 metres.

2.7.10 Burst (1969)

A three-stage compaction model was proposed by Burst. The relative proportions of the pore water, interlayer water and composition of the clay solids at each stage is shown in figure 2.18. The initial stage comprises essentially of a reduction in the interstitial water content to 30 percent from 70 percent and is operative in the first few thousand feet. The geothermal heat influences the second stage when the interlayer water is mobilised and discharged into the bulk system. In the third stage, with further increase in temperature the final water contained in the clay mineral lattice and the pores is expelled. Figure 2.19 describes the changes in the interlayer water density during compaction.

2.7.11 Beall's compaction model (cited in Chillinger & Rieke (1974))

Analysis of data from offshore well core samples, Louisiana, the JOIDES Deep Sea Drilling Project, and high pressure experiments on marine muds, Dr. J.A. Beall has proposed a compaction model with some quantitative fabric criteria. As in the earlier models, he defines the initial stages of compaction (up to depths of 3300 feet) to essentially involve the mechanical expulsion of large quantities of pore water

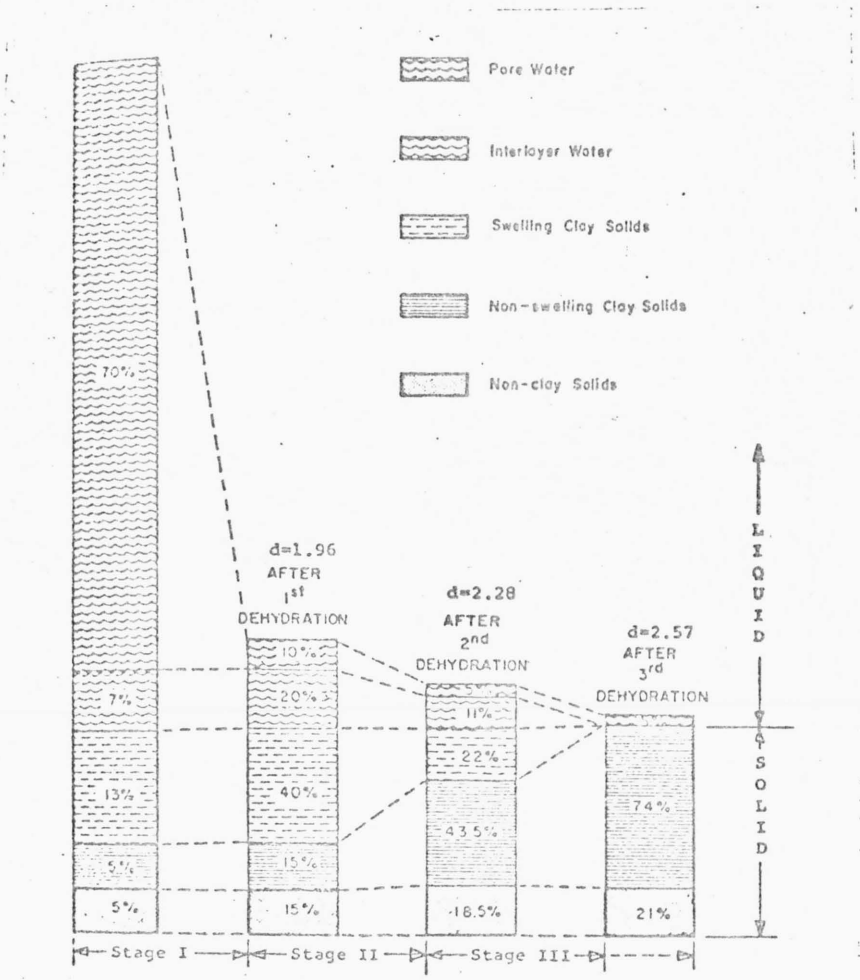


FIGURE 2.18 The compaction model of Burst (1969).

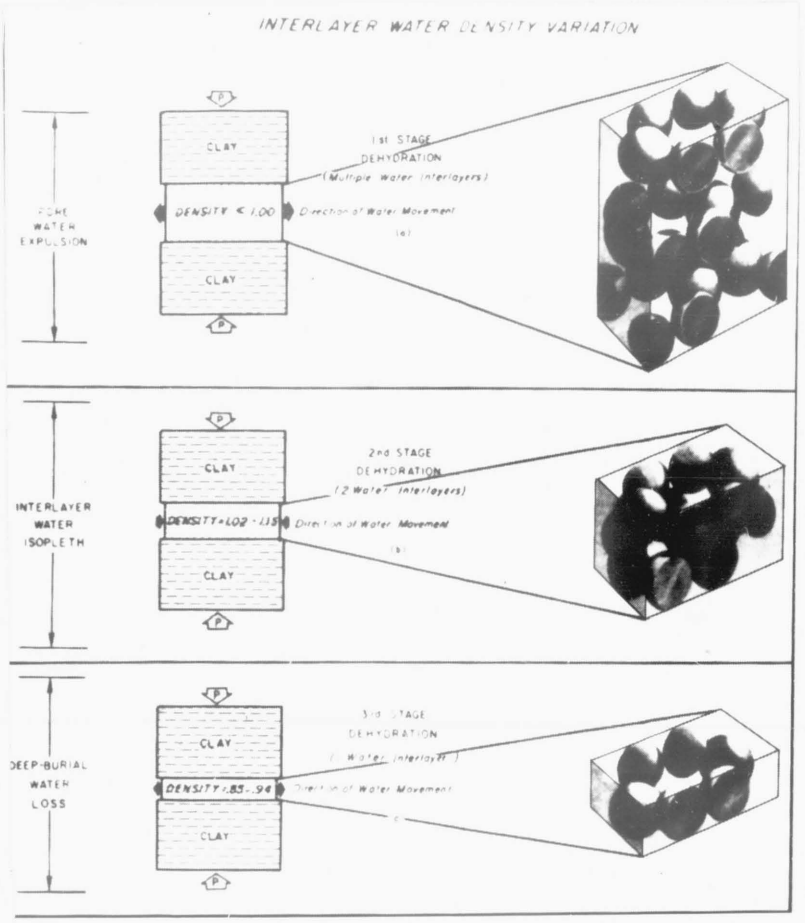


FIGURE 2.19 Variation of interlayer water density during the three stages of compaction (after Burst, 1969)

until 50 percent of the compaction is complete. The average pore throat diameters during this first stage is about 6 Å. About 75 percent of the compaction is completed during the second stage (depth range of 3,300 feet to 8,000 feet) and the pore throat diameters are reduced up to 1 Å. In the third stage the rate of decrease of porosity with depth is small and the pore throat diameters are less than 1 Å. Beall suggests that at this stage with pressure in the range of 8,000 and 12,500 lb/in^2 and small pore throat diameter, the initiation of sodium chloride filtration can result.

2.8 LABORATORY STUDIES OF COMPACTION OF CLAYS

The need to study the compaction behaviour of clays in the laboratory has been felt since the time of Terzaghi (1923). Unfortunately the studies are limited by the capabilities of the equipment used. Accordingly such investigations are of three broad types, viz.

a) Sedimentation studies - application of theories of colloidal chemistry to study the initial stage of compaction as discussed earlier (Schofield and Samson, 1953).

b) Low pressure consolidation - the use of soil mechanics theories of consolidation to evaluate properties of the soil that are pertinent in the range of loads usually encountered in engineering foundations (0 - 2,000 lbf/sq.in).

c) High pressure compaction - to investigate the compressibilities and diagenetic clanges in clays at high pressure (up to 200,000 lbf/sq.in).

Table 2.IV gives a summary of details pertaining to the common apparatus used up to now in such studies. It must be consequently appreciated that a single apparatus cannot therefore be designed to accurately study the entire process of gravitational compaction (that is, from fluid sediment to indurated rock).

The clay colloid concepts have been adequately discussed earlier and therefore observations from such will not be elaborated. The more pertinent results of low and high pressure compaction studies are reviewed.

2.8.1 Low pressure consolidation

Most of these tests have been conducted similar to the experiments of Terzaghi as outlined in Section 2.7.4. The results of such tests are usually presented in the form of pore spaces (void ratio or porosity), effective stress variations (e - log p).

Some of the factors that are known to influence the e - log p relationships for clays are briefly outlined.

Apparatus	Maximum applicable pressure lb/in^2	Investigator	Mode of application of pressure	Lateral constraint	Sample size (maximum)	Particular Features etc.
Consolidometer (Oedometer)	2000 on ($1\frac{1}{2}$" Ø) 500	Terzaghi (1925)	Free piston; load transferred through lever system	Fixed ring	$1\frac{1}{2}$", 3" or 4" diam. $\frac{3}{4}$" or 1" thick	Incremental loading Observations of settlement (and pore water pressure at undrained end if required)
Triaxial cell		Bishop (1962)	Axial pressure via loading ram; lateral pressure is hydraulic.	Fixed ring	$1\frac{1}{2}$" or 4" diameter.	Used mainly for strength tests but the consolidation characteristics may also be observed.
Rowe Cell	175	Rowe (1966)	Hydraulic application of pressure.	Fixed ring	2", 6", 10" or 20" dia 2.5" thick.	Observations of settlement and pore water pressure. Back pressure can be applied
Single stage Piston	20,000	Manheim (1966)	As in filter press.	Fixed ring		Chemical analysis of pore water squeezed from sediments
Dual Piston	500,000	Kryukov (1963) Chillingar (1960)	Mechanical compression machine	Fixed ring	$\frac{1}{2}$" diam. 2-3 cc. total vol.	Settlement and fluid extraction.
High Pressure Triaxial	40,000	Chillingar et al (1971)	Mechanical axial pressure & lateral hydraulic pressure	Floating membrane	$1\frac{7}{8}$" diam. 3" thick.	Settlement & fluid extraction Influence of temperatures. Studied by placing cell in oven.
High Pressure and Temperature consolidation cell	10,000	I.C. Engg. Geology Dept. London.	Hydraulic axial and lateral pressures and back pressure.	Floating membrane	4" diam. 4" thick.	Any preprogrammed loading effected compaction may be controlled by diff.criteria. Settlement & pore water press. measured (see Ch.5)

TABLE 2.IV Summary of details of some common apparatus used in compaction studies.

2.8.1.1 Particle size

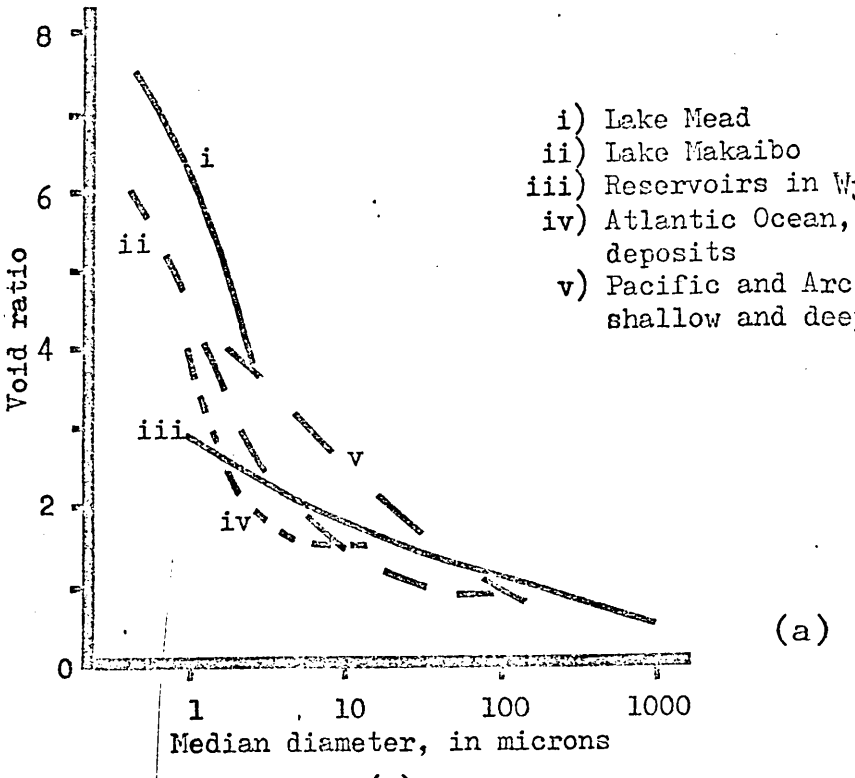
The particle size of the sediments influences the compaction behaviour by virtue of its colloidal effects. Figure 2.20a shows observations from recent sediments illustrating that larger void ratios result from finer sediments. As discussed earlier, the clays have water-retaining properties which characterise their plasticity. Skempton (1953) published a set of type e - log p curves for sediments of different particle size and consequently different plasticity indices (figure 2.20b).

2.8.1.2 Electrolyte concentration and adsorbed cation

Mitchell (1960) and Olson and Mitronovas (1962) investigated the influence of electrolyte concentration on the compaction behaviour of clays. Both their theoretical and experimental results are shown in figure 2.21. Their observations conform with the trends predicted from the double layer theory in that dilute electrolyte solutions yield a more flocculated structure.

Figure 2.22 illustrates the compaction behaviour of clays with cations of different valencies. As deduced in the study of clay colloid concept, the lower valency ions favour the formation of a flocculated fabric.

The above observations emphasise the dominant



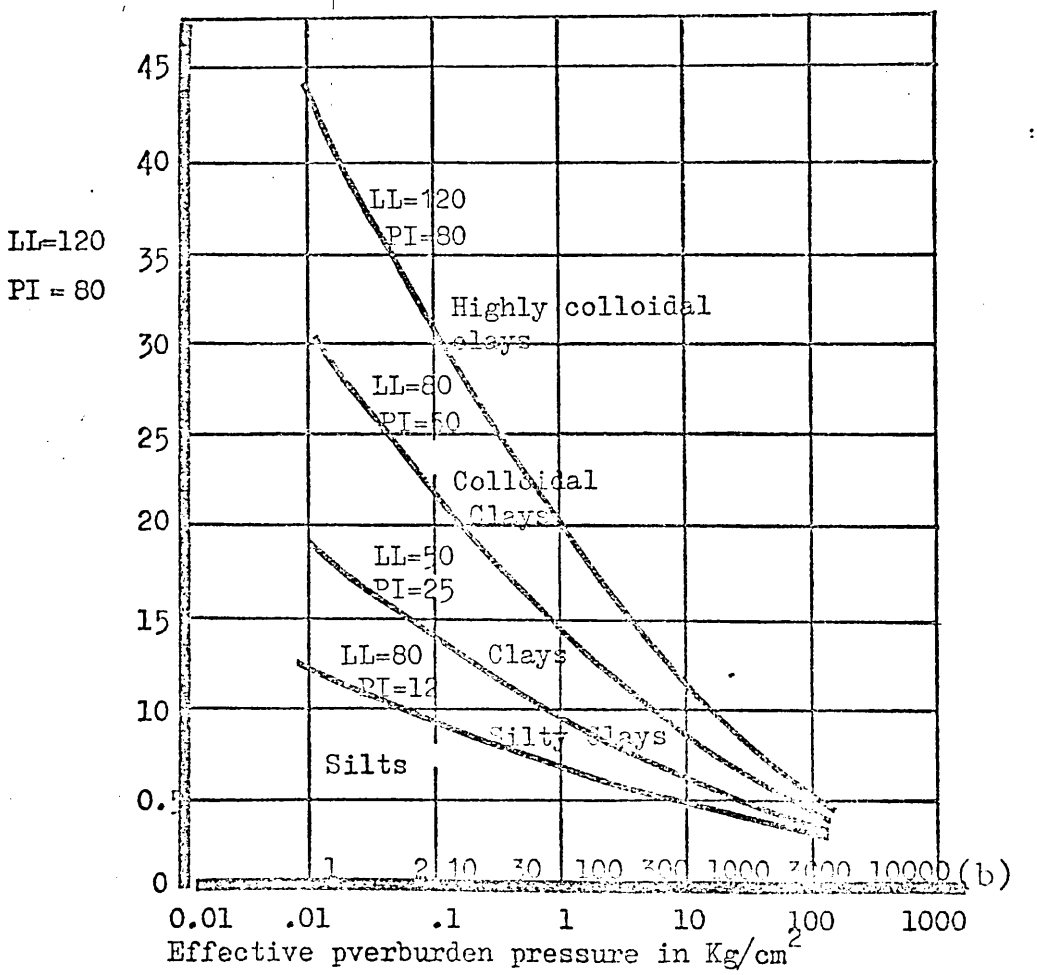


FIGURE 2.20 Influence of Particle Size on the compaction behaviour of clays:

(a) Unconsolidated sediments (Mead, 1964).
(b) After Skempton (1953).

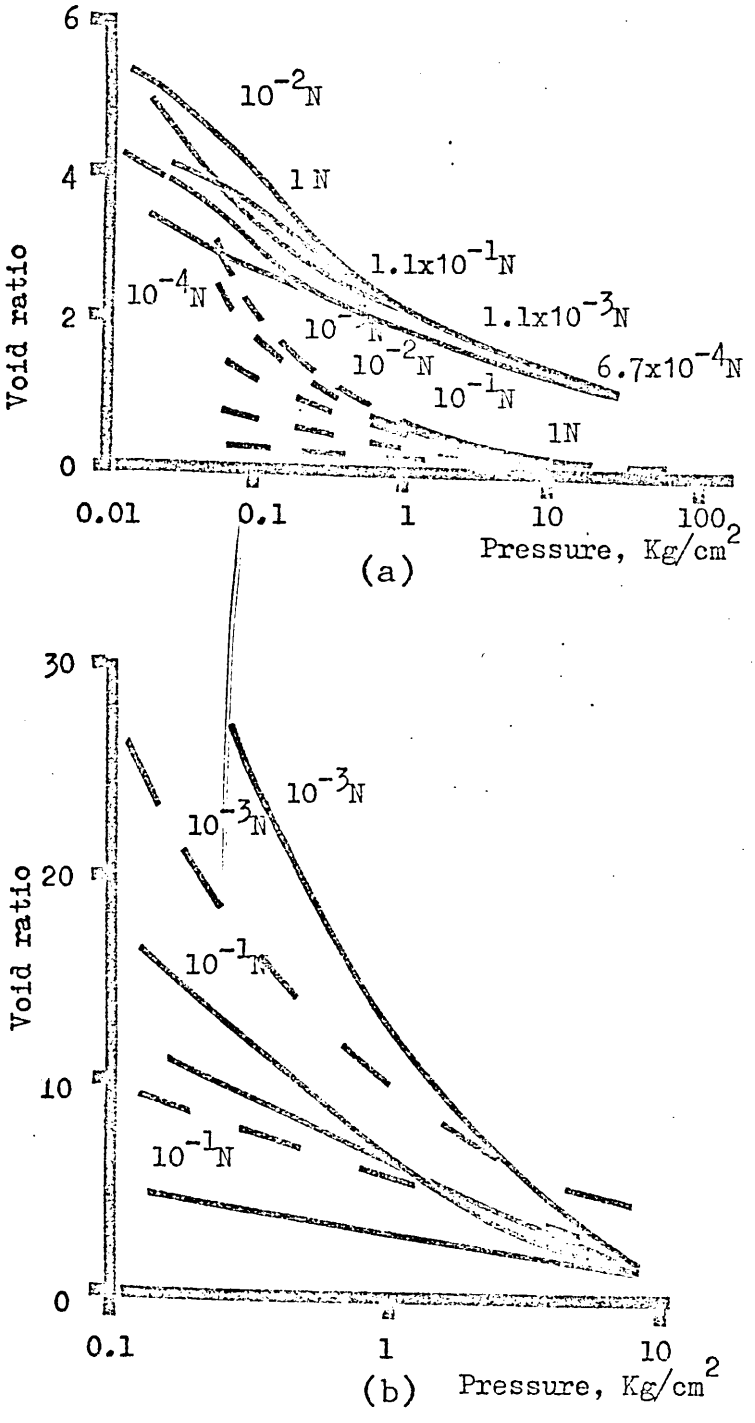


FIGURE 2.21 Influence of electrolyte concentration on the compaction of clays.
(solid lines are experimental results, dashed lines are theoretical predictions from double layer theory)

(a) Compaction of illite in $MgCl_2$, pore flu (after Olson and Mitronovas, 1962)

(b) Compaction of Montmorillonite in NaCl pore fluid (after Mitchell, 1960)

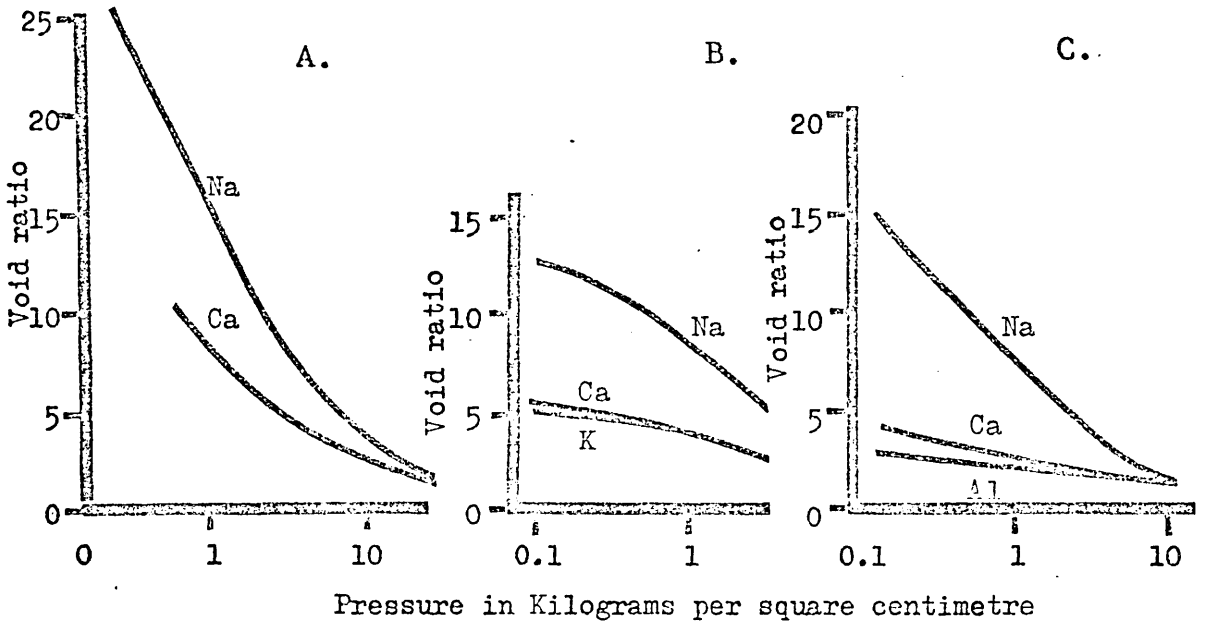


FIGURE 2.22 Influence of the adsorbed cation on the compaction behaviour of clays.

A. (after Bolt, 1956).
B. (after Jiminez Salas and Serratosa, 1953).
C. (after Samuels, 1950).

influence of the physico-chemical effects during the early stages of compaction up to effective stress levels of the order of 10 Kg/cm^2.

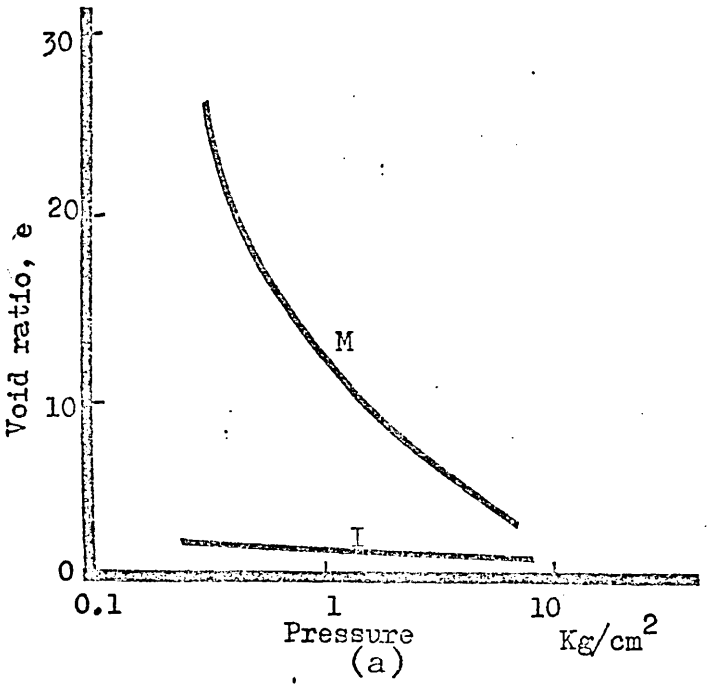
2.8.1.3 Mineralogy

As outlined in table 2.I, montmorillonite clays are distinctly 'more active' primarily as a result of their characteristic small size. The e - log p variation for montmorillonite and illite is compared in figure 2.23 (Mitchell, 1960). There is a marked variation in the compressibility of the montmorillonite compared with the more uniform behaviour of the illite. Such tests have been done on remoulded clays.

The consolidometers have been designed mainly for practical soil mechanics purposes but have also been used in simulating compaction to contrast artificial and natural processes. No representative stress path criteria have been adopted. The lateral expansion of the sample is minimised by a fixed confining ring, and it is assumed that in a sedimentary column, pressure of the surrounding sediment similarly confines the column.

2.8.2 Skempton (1944, 1953, 1970)

Skempton (1944 and 1953) presented observations from such experiments and compared them to natural compaction. He



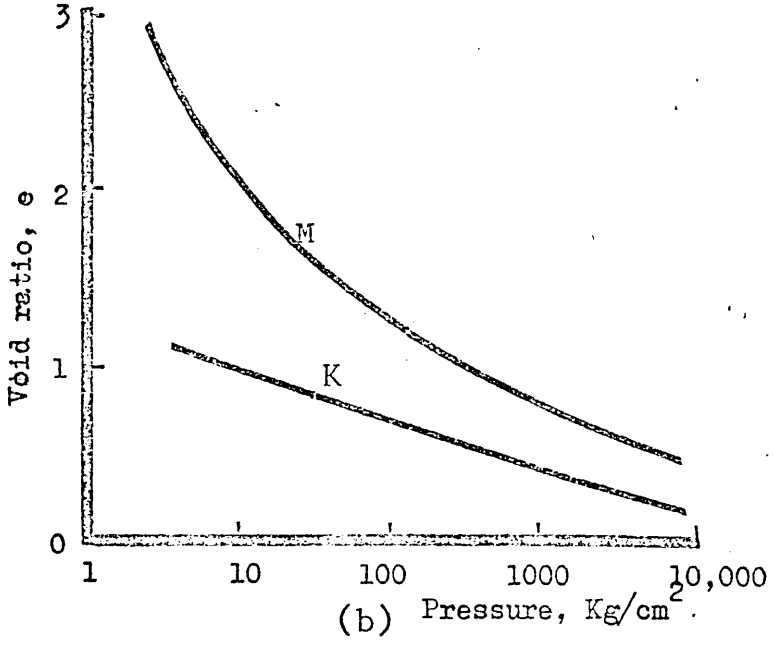


FIGURE 2.23 Influence of Mineralogy on Low and High Pressure compaction of clays.

M; Montmorillonite, I; Illite
K; Kaolinite

(a) after Mitchell (1960).

(b) after Kryukov and Komarova (1954).

confirmed Terzaghi's observations that recent sediments, being deposited, have natural water contents in the same order as liquid limit (L.L.).

For low pressures (0.5 - 10 Kg/cm^2) there was no agreement between natural compaction curves and results from his undisturbed laboratory consolidation. The laboratory curves fall below sedimentation curves. Such discrepancies were attributed to fabric differences in clay and the unrepresentative rapid loading in the laboratory. The large surges of mechanical energy in such tests break the physico-chemical bonds between grains. Thus the net effect is to attain smaller equilibrium void ratios. Skempton (1953) compiled data of variations of void ratio with effective overburden pressure for laboratory consolidated and natural compaction (figure 2.24). For overburdens in excess of 3,000 - 5,000 feet they lacked correspondence and the decrease in void ratio with increasing depth of burial was more rapid in nature. Skempton suggested that such differences are due to natural recrystallisation taking place over large geologic times.

Skempton (1970) published further studies of void ratio and effective overburden pressure (ranging to a maximum of 1,000 lb/in^2, commensurate with the stress exerted by a sedimentary column of approximately 1,000 feet depth) relations for recent sediments (figure 2.25). In this work he emphasised

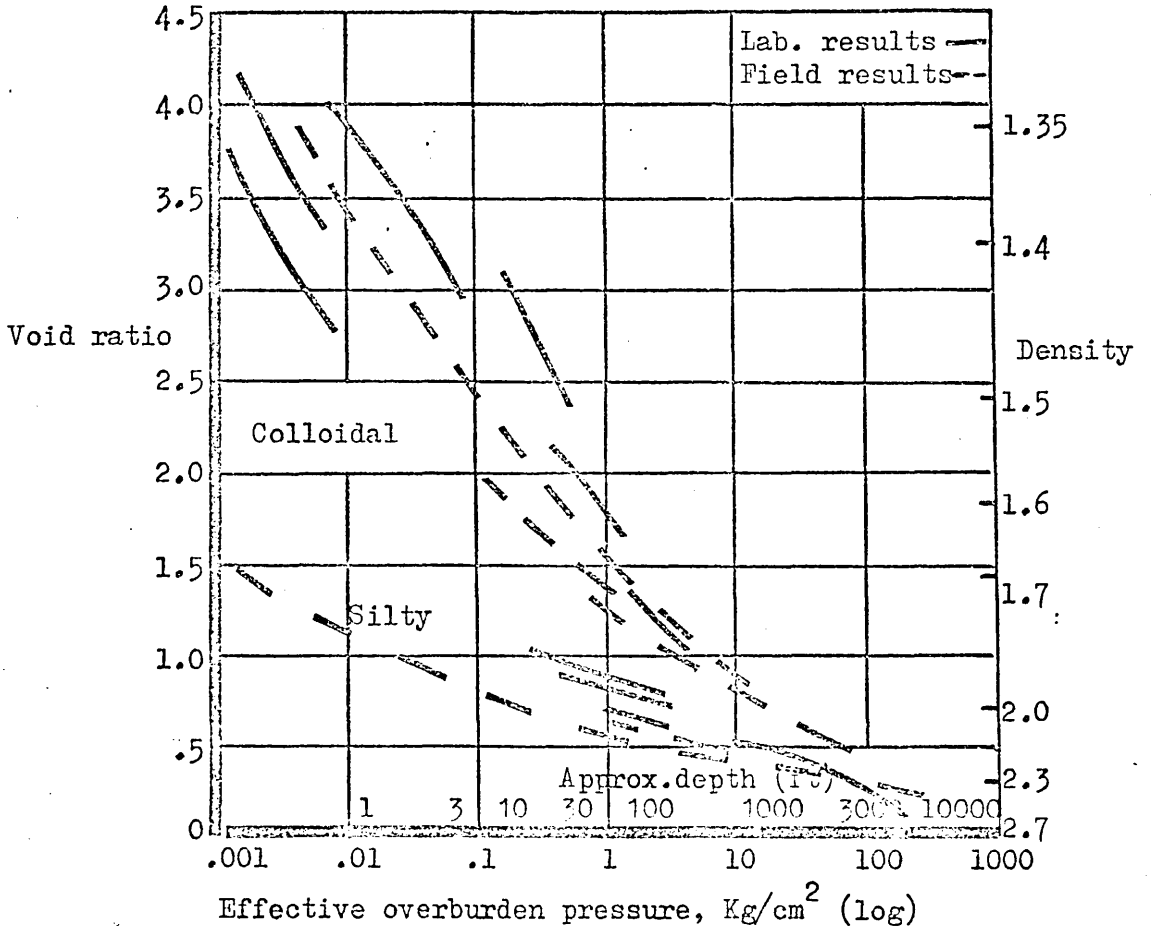


FIGURE 2.24 Laboratory and field compaction of clays (after Skempton, 1953).

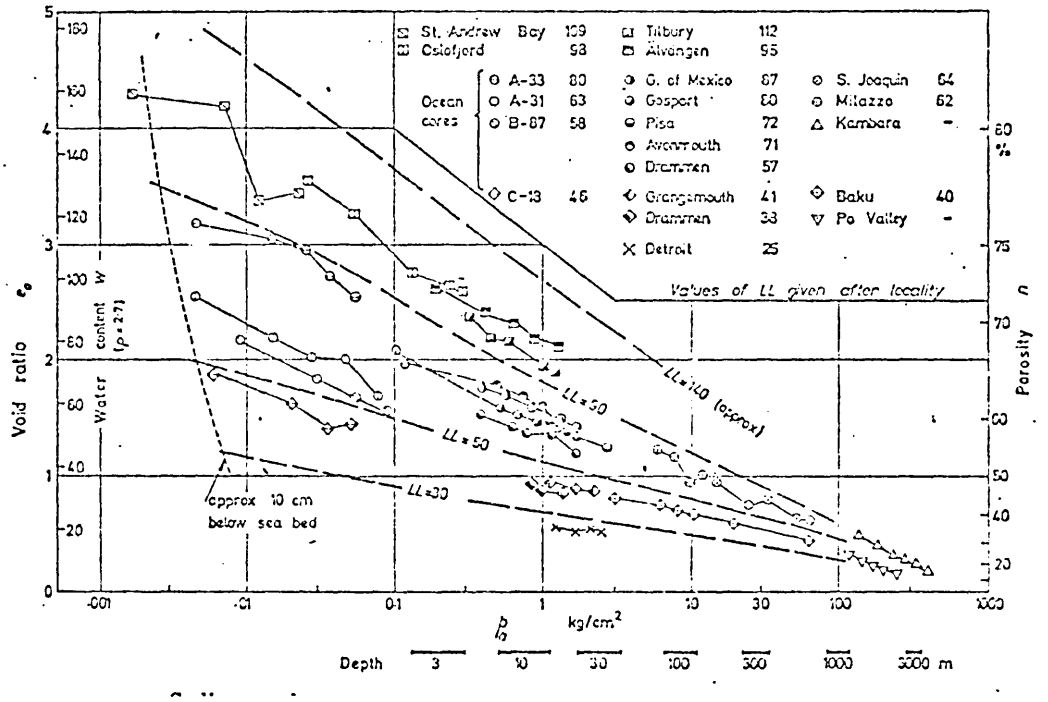


FIGURE 2.25 Sedimentation Compression curves for normally consolidated Argillaceous sediments (Skempton, 1970).

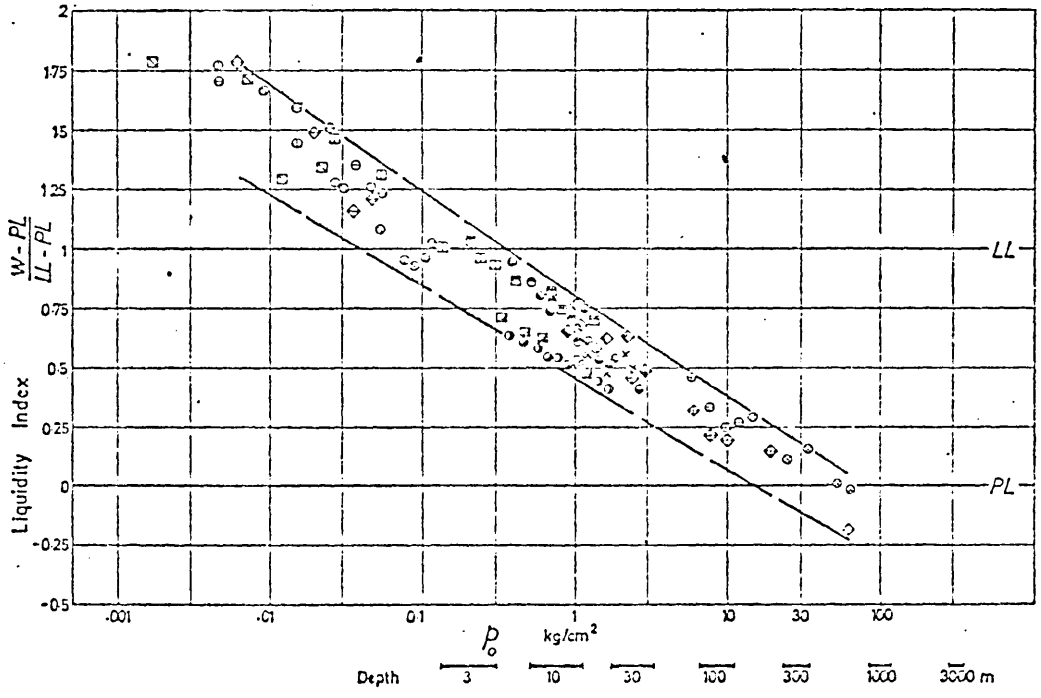


FIGURE 2.26 Relationship between the liquidity index and the effective overburden pressure for the clays shown in Figure 2.25 (after Skempton, 1970).

the relevance of the Atterberg limits of the clay on its compaction behaviour. He showed that (for a wide range of argillaceous sediments) the liquidity index bore a direct relationship to effective pressure, although the corresponding natural water content of the sediments varied widely (figure 2.26). Observations from deposits of recent sediments proved further that the liquidity index decreased linearly with depth. These deductions are somewhat a continuation of his observations (Skempton, 1944) when he suggested an empirical linear relationship between the compressibility (C_c) and the liquid limit (L.L.) as in

$$C_c = 0.009\ (L.L. - 10)$$

2.8.3 High pressure compaction (>1,000 up to 500,000 lbf/sq.in

Kryukov and Komarova (1954) conducted high pressure experiments on clays to obtain data on their basic chemical, physical and material properties. It was followed by a similar series of experiments by Chillingar (1960).

The main observations from the high pressure tests is that the Kaolinite and Illite clay show a uniform compressibility over the entire pressure range. Montmorillonite clays possess higher compressibilities in the low pressures, resembling slightly the corresponding behaviour of natural organic

colloidal gum tragacanth. He proposed from laboratory results the following straight line relationships to describe mathematically the separate compaction behaviour (see figure 2.27):

Montmorillonite	M = 104 - 18.06 log P (linear portion)
Illite	M = 50 - 8.7 log P
Kaolinite	M = 33.9 - 5.96 log P
Dickite	M = 26.7 - 5.04 log P
	M = retained moisture content.

These tests have, however, been conducted on very small samples and again no stress path criteria have been adopted to simulate geological burial.

The geotechnical significances of burial and sedimentation will be discussed in the following Chapter Three.

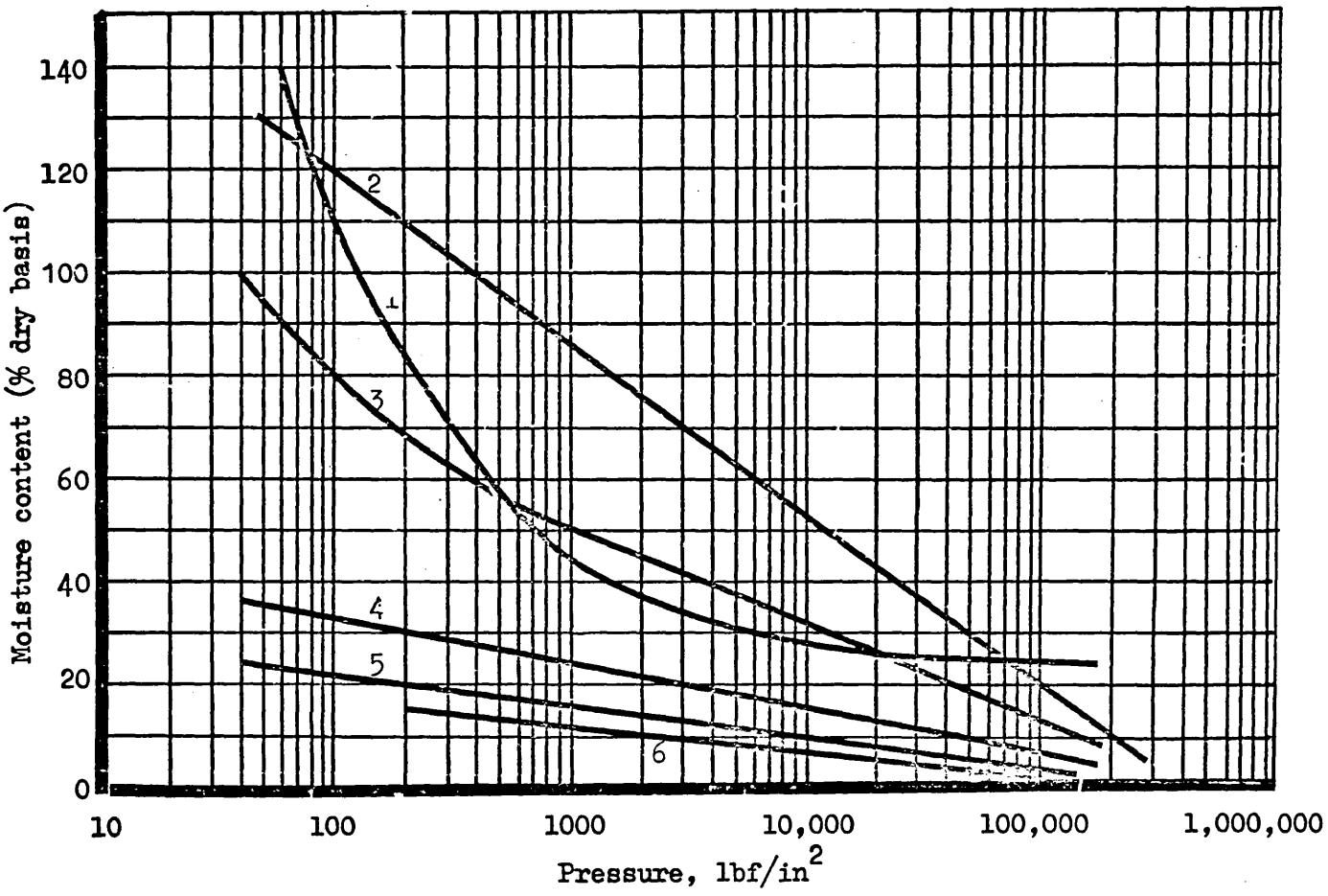


FIGURE 2.27 High Pressure Compaction behaviour (after Chillingar and Knight, 1960).

(1) gum tragacanth
(2) silicic acid
(3) Montmorillonite
(4) Illite
(5) Kaolinite
(6) Dickite

CHAPTER THREE Geotechnical significances of Geologic burial and exhumation

3.1 Introduction and Definitions 85

3.2 Stress-induced Fabric Deformations 87

3.2.1 Laboratory-produced fabric changes 90
3.2.2 Fabric of naturally compacted sediments 96
3.2.3 Techniques for determination of fabric 98

3.2.3.1 Electron microscopy 100
3.2.3.2 Optical microscopy 104
3.2.3.3 X-ray diffraction

3.2.4 Appraisal of the techniques of quantitative fabric analysis 109

3.3 Changes in Chemistry of Pore Fluid with Compaction 113

3.3.1 Solubility of various salts and mobility of ions 114
3.3.2 Some field observations of changes in the chemistry of pore fluid 116
3.3.3 Chemical changes observed in laboratory compacted clays 118
3.3.4 Influence of temperature on the chemistry of the pore fluid 125
3.3.5 Review of the current theories of diagenetic changes of pore water 125

3.4 Clay Mineral Diagenesis 134

3.4.1 Montmorillonite to illite transformation 134
3.4.2 Kaolinite diagenesis 137
3.4.3 Mixed layer mineral diagenesis 141

3.5 Abnormal pore fluid pressures 141

3.6 Influence of Burial on Engineering Properties 152

3.6.1 Permeability changes 152
3.6.2 Changes in strength properties 154
3.6.3 Directional properties 154

CHAPTER 3

GEOTECHNICAL SIGNIFICANCES OF GEOLOGIC BURIAL AND EXHUMATION

3.1 INTRODUCTION AND DEFINITIONS

In the preceding chapter the different theories of gravitational compaction were outlined but a notable void exists regarding the exhumation process.

A natural sediment retains a memory of its stress history. A rational interpretation of the e - log p curve for the sediment can describe the 'recent' stress history of the sediment. A sediment is defined as being 'normally consolidated' if during its geological history it had never been subjected to greater overburden pressure than that existing at the present. Another sediment may have been subjected in the past to an overburden pressure P_c, which is greater than the present pressure P_a, which has resulted from a stress relief-like erosion of some of the overburden. Such a sediment is said to be 'overconsolidated', and the overconsolidation ratio is P_c/P_a. These terms are further illustrated in figure 3.1. The pre-consolidation load, P_c, can be determined experimentally by an empirical graphical analysis of the region of marked change of slope (or compressibility) on the e - log p curve as described in Taylor (1948).

In this chapter, the geotechnical phenomena associated

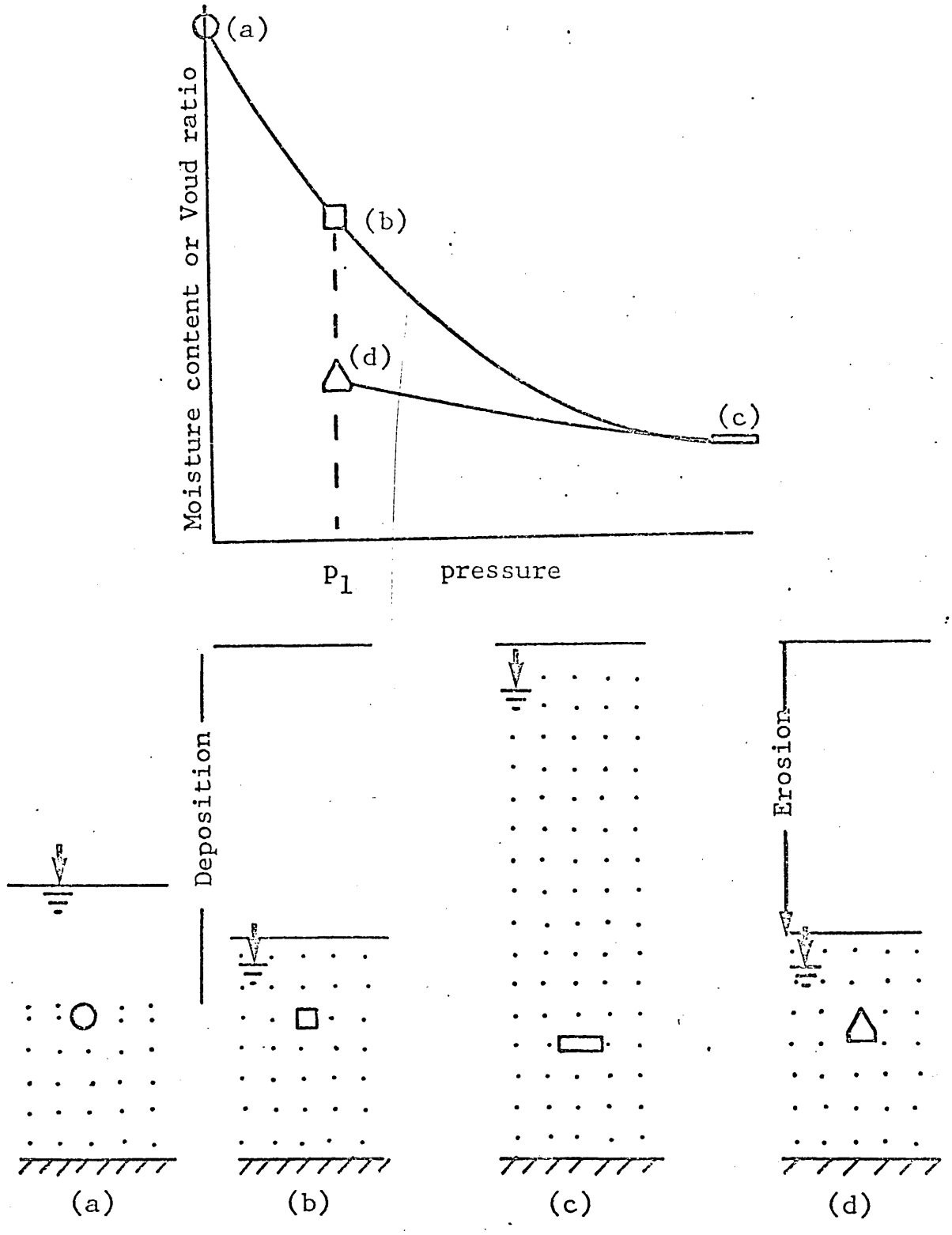


FIGURE 3.1 Normally and Overconsolidated Clay.

with the processes of geological burial and exhumation will be discussed. Changes in fabric, chemistry of the pore fluid, and the mineralogy of sediment, are the prime effects of burial and they occur in the above order with increasing depth of burial. The process involving such physical and chemical changes in sediments after deposition thereby converting it into a consolidated rock is defined as diagenesis (American Geological Institute, 1957). As a result of such diagenetic changes, the sediment can acquire characteristic macrostructural features such as fissility, fissures and changes in geotechnical properties like permeability, compressibility and anisotropy of strength. These are discussed individually in this chapter.

Furthermore the occurrence of abnormal geopressures are related, directly or indirectly, to the process of compaction. The current ideas on the origin of such abnormal pressures are also reviewed.

3.2 STRESS-INDUCED FABRIC DEFORMATIONS

The recognition of the belief that many mechanical properties of soils, like shear strength, are merely reactions of the fabric to certain external mechanical stimuli (Lambe, 1953, 1958a, 1958b), has necessitated microscopic analysis of fabric mechanisms. Accordingly the response of the clay fabric to loading has been investigated from both field and laboratory

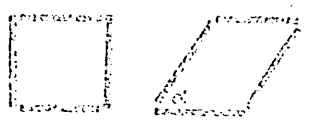
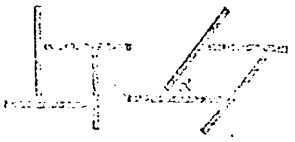
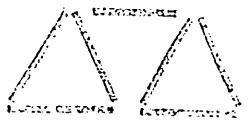
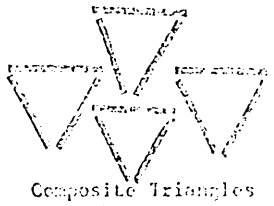
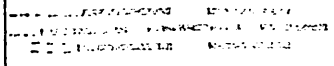
prepared samples, and these observations are discussed in sections 3.2.1 and 3.2.2.

A mechanistic approach to the study of the deformation of the clay fabric is to consider that the external loads and restraints applied to the soil system are transmitted within the system at the points of particle "contact". As such, the clay fabric can be visualised as a complex three-dimensional 'truss' with the points of contact functioning as the 'joints'. The forces at the contacts are the Van der Waal's forces of inter-particle attraction, the repulsive forces due to the interaction of the electric double layers on the clay surfaces, frictional torque due to cementation and a proportion of the externally applied forces.

Figure 3.2 is a series of such hypothetical two-dimensional clay fabrics. The clay particles are assumed to be platy and to have a length to thickness ratio of 'η'. The void ratio, e, for each type of fabric is expressed in terms of η. The fabrics are listed in the order of increasing structural stability and decreasing void ratio. Accordingly the parallel arrangement of particles or 'oriented fabric' corresponds to the arrangement of minimum free energy (Bolt, 1956).

Such a mechanism excludes the equally probable events of bending and crumpling of the clay plates (see plate 9.39)

Void Ratio Decrease
Stability of Structure Increases

Idealised two-dimensional Fabric	Void Ratio $e = f(\eta, \alpha)$	Typical Values		
		η = 2	10	100
 Parallelogram EE contacts	$e = (\eta^2 + 1)\ \mathrm{Sin}\alpha/2\eta$	1.25 - 0.625	5.05 - 2.52	50.0 - 50
 Z structure EE contacts	$e = \frac{1}{2}[\eta \mathrm{Sin}\alpha + \mathrm{Cos}\alpha - 1]$	0.5 - 0.4	4.50 - 2.40	49.5 - 24.5
 Composite parallelogram EF contacts	$e = \frac{1}{2}[\frac{\eta}{2}\mathrm{Sin}\alpha + \mathrm{Cos}\alpha - 1]$	0.2	2.00 - 1.15	24.5 - 12.4
 Triangle EE contacts	$e = (\eta^2 + 3)/2\sqrt{3}\eta$	1.01	3.00	25.0
 Composite Triangles EE and EF contacts	$e = [\sqrt{3}\eta^2 - 2\eta + 3\sqrt{3}]/6\eta$	0.50	2.50	16.2
 Brick wall or Oriented FF contacts	$e = \frac{d}{t} - 1$			

* e = Void Ratio η = ratio length/thickness α = acute angle included by particles

FIGURE 3.2

HYPOTHETICAL TWO-DIMENSIONAL FABRICS

and solid solution at the points of particle contact, which may occur at high stress regimes.

Means and Patterson (1966, p. 128) note that the theory of orientation of platelets in dense suspensions is complicated (cf. Mason and Mandy, 1956) and has not been thoroughly developed. This unfortunately is still true.

3.2.1 Laboratory-produced fabric changes

It is an intuitively established concept that the general effect of compaction on a sediment microstructure is to force the constituent particles together into an oriented ('preferred' or 'parallel') fabric (Mitchell, 1956; Kaanberg, 1959; Engelhardt and Garda, 1963) with a preferred orientation normal to the direction of compaction. The geometrical argument is clear in that when a sample is compressed the initial open type of fabric collapses, by breaking or rotating about its interparticle contacts, to orient parallel to each other as sketched in the hypothetical fabrics described in this study (section 3.2).

With very high water contents, the individual clay particles can begin to orient early in compaction when they are relatively free to move. On the contrary, with low water contents, the particle freedom is much more restricted and reorientation is inhibited.

The extent of lateral restraint on the clay sample during deformation bears a significant effect on the associated response of the clay fabric (cf; the influence of the support conditions on the orientation of the parallel members in the bridge truss analogue for clay fabric, section 3.20). As such distinctly different modes of fabric development can result from unconfined and confined compression of clays.

It has been observed that preferred orientation is rapidly produced during unconfined compression. Popov (1944) observed the development of preferred orientation in fluid montmorillonite pastes (water content 40 - 70 percent) by compressing the paste between two glass plates. Buessem and Nagy (1954) subjected aggregates of Georgia Kaolinite to uniaxial compressions of 0.22 and 0.55 Kg/cm^2 and demonstrated using X-ray powder photographs that the fabric in the uncompressed aggregates was random and that compression increased the orientation of the flakes normal to the direction of the applied load. A cylindrical sample of Kaolinite paste compressed to one-third its original thickness, between two plates, was observed by Raitburd (1958) to produce a clearly detectable (by X-ray diffraction technique) preferred orientation. Results from similar experiments by Clark (1970) have shown that a linear relationship exists between the deformation strain and the square root of the preferred orientation ratio (described later in section 3.2.3.3, and see table 3.III).

Williamson (1947) conducted somewhat different type of technique, in repeatedly dropping a ball of illite-kaolinite clay onto a glass plate from a height of about a foot. He observed, by means of optical microscopy, that the preferred orientation so produced was less marked than when a similar ball of clay was squeezed between parallel glass plates in a hand press. Becker (1904) calculated that a mass of mud containing randomly oriented mica flakes must be compressed to $\frac{1}{8}^{th}$ of its original thickness before the flakes could acquire an average inclination of 2° to the plane normal to the axis of compression. Such an average inclination implies a preferred orientation of a high order. Thin samples of clay having a high order of preferred orientation of clay minerals can be produced by either smearing a very wet clay on to a microscopic slide and allowing it to dry or by centrifuging a suspension on to a microscopic slide (or the suspension sucked onto a porous disc by evacuation) (Kittrick, 1961). It is pertinent to note that in the first technique the orientation is as a result of surface tension while in the latter it is due to the enhanced gravity forces.

Laterally confined deformation experiments represent the lateral restraint in natural compaction more closely than the unconfined but not quite. It has been observed by some that preferred orientation of the particles results under low pressures. Bowles, Bryant and Irwin (1969) observed that on normally loading

laterally confined marine cores from the Gulf of Mexico, predominantly random arrangement of particles existed over the greater portion of the void ratio range, and preferred orientation apparently developed at pressures in excess of a few Kg/cm^2. Mitchell (1956) studied the effects of uniaxial pressures of 2 Kg/cm^2 on marine and nonmarine clays from North America. The marine clays were dominantly illitic and compression caused an increase in the average order of preferred orientation over large areas and also within small domain-like aggregates. But the nonmarine clays, which contained montmorillonite, did not show such consistent results; the degree of preferred orientation was increased in some samples and decreased in others.

High magnification electron microscopy has made it possible to discern two distinct fabrics - preferred orientation and turbostratic fabric (see figure 2.~~10~~6). Such observations of microstructure of clays is often characterised by a dense packing of the particles which have been forced to form clumps (localised random arrangement of particles) and packets (groups of well ordered particles) (Aylmore and Quirk, 1960). In such an event, a compressive deformation of clay samples results in contacts occurring predominantly between adjacent clumps and packets rather than between individual particles. Smaller packets can be prevented from aligning themselves because of the presence of large packets. It is sometimes even probable that

certain packets can occur with an erratic particle orientation, parallel to the direction of compression supporting the belief that packets formed during, or prior to, remoulding continue to act as integral units during any form of subsequent mechanical testing. It is noteworthy that it is a usual habit for Kaolinite resulting from recent weathering to occur in such packets or stacks usually referred to in literature as vermicular Kaolinite (see plate 6.2).

Blackmore and Miller (1961) inferred from the sharpness of the X-ray reflections that when calcium montmorillonite is compressed, the number of 10 Å unit thick montmorillonite sheets per domain increased progressively with pressure, ranging from 5 unit sheets at 0.5 Kg/cm^2 to nearly 8 unit sheets at 90 Kg/cm^2. He further observed that this process was irreversible so that that the sheets in the domains did not dissociate with the release of pressure.

Sloane and Kell (1966) noted that packets are present whatever the compaction method. The extent of particle or packet orientation is dependent on the initial moulding water content. Below optimum water content, the packets are essentially arranged in a random fashion. At the optimum water content, impact and kneading compaction form trajectories of oriented packets, which are associated with zones of large shear strains. More oriented arrangements of packets result with water contents above the

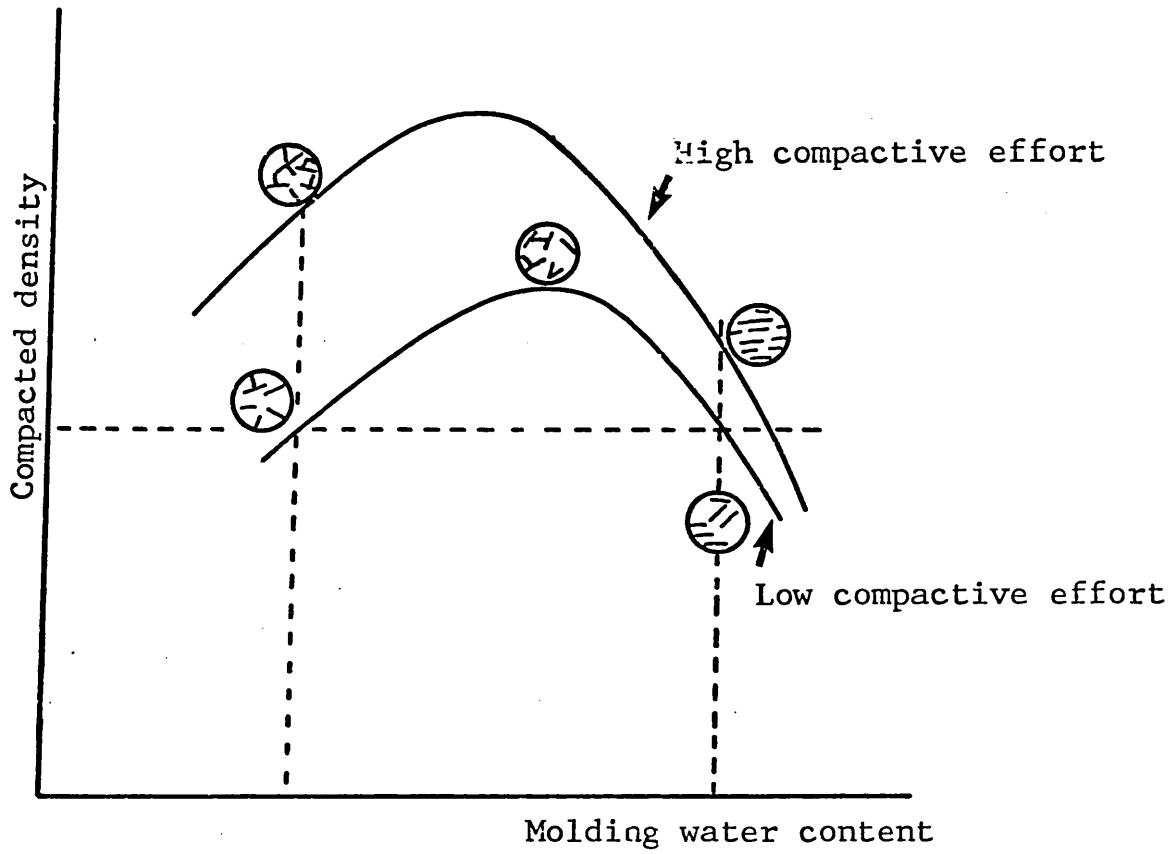


FIGURE 3.3 Effect of compaction on fabric
(after Lambe, 1962)

optimum and particularly with static compaction (see figure 3.3).

Tchalenko (1967) studied the consolidation of Kaolinite up to pressures of 25 tons/ft^2 with different initial moulding water contents and in both flocculated and deflocculated states. Optical microscopic investigations showed that a well oriented fabric was produced in all cases and the deflocculated suspension resulted in a superior preferred orientation. Such observations were presented diagrammatically as in figure 3.4.

Electron microscopic observations have shown that even a unidimensional stress of 2000 kN/m^2 is insufficient to produce a complete orientation of the particles in every region (Warkentin et al, 1957). Results from high pressure consolidometer tests by Laughton (1954) have consistently shown positive values for the ratio of decrease in volume per unit change in pressure, and this can sometimes be erroneously explained as a continuation of the orientation process. It may well be caused by the adsorbed water being squeezed out between all the orientated clay particles rather than by any fabric alteration.

3.2.2 Fabric of naturally compacted sediments

Contrary to the observations from laboratory studies conducted usually on monomineralic clays in special environments, fabric observations of naturally compacted sediment do not all show consistent trends towards preferred orientation.

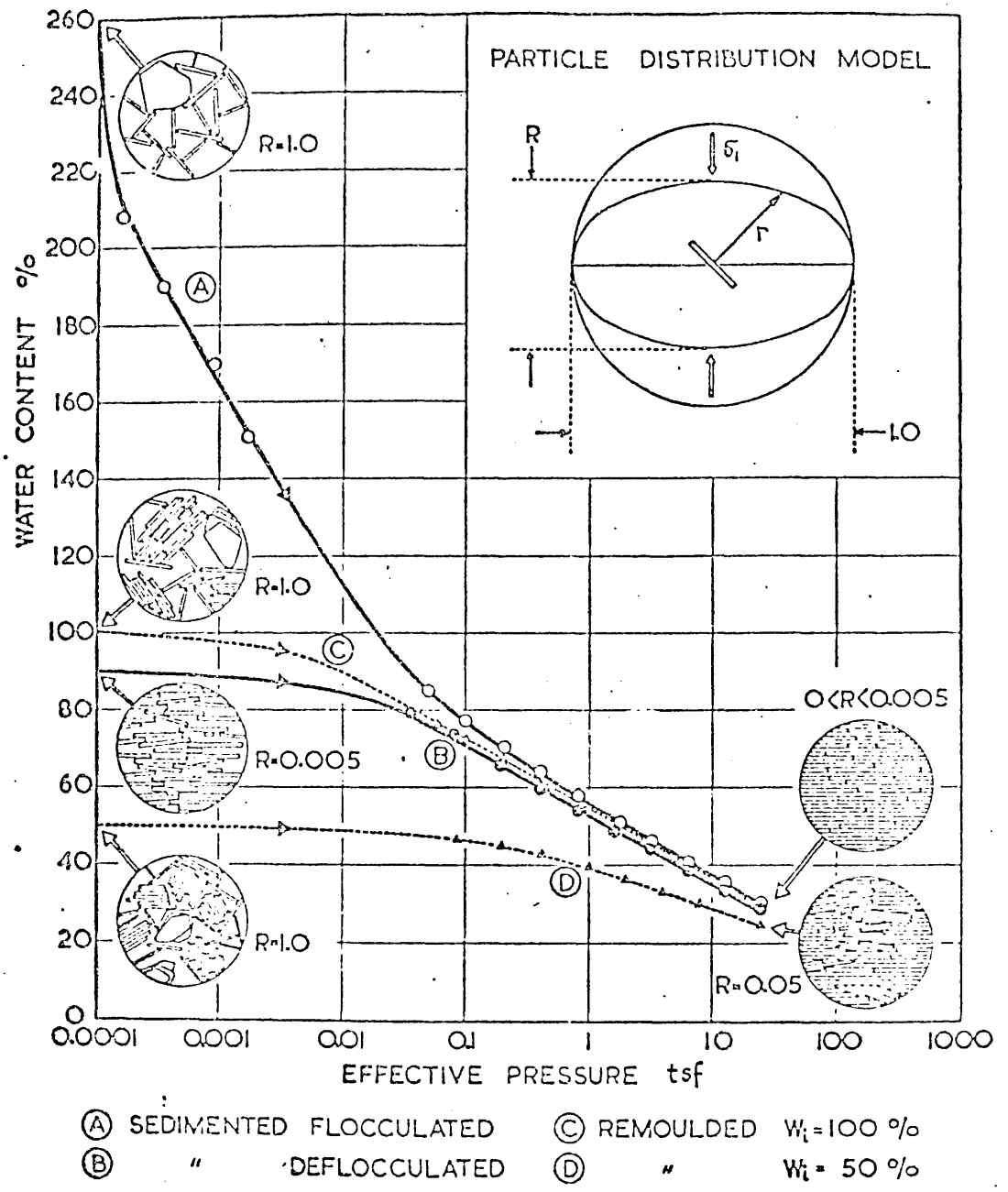


FIGURE 3.4 Development of fabric in consolidated Kaolinite.
(after Tchalenko, 1967)

A summary of the studies on this subject is given in table 3.I. These emphasise that the effect of overburden pressure is not the only process prevalent in geological burial.

For example, Grim and Allen (1938) note two significant features in underclays: a random orientation of clay particles and many small slickensided fracture surfaces. The geological history of these sediments must account for both these phenomena simultaneously. Schultz (1958) suggested 'slumping during compaction of a flocculated sediment' as a secondary process that occurred. Grim and Allen (1938) considered the slickensides to be the result of drying shrinkage that may have occurred in the sediment prior to burial, while O'Brien (1964) explained them as local shear deformations during compaction with a random matrix fabric being retained due to the stiffness of the clay.

3.2.3 Techniques for determination of fabric

The fabric can be determined using direct or indirect observations. The direct observation of clay particles is feasible only with electron microscopy. The indirect observations rely on the optical and the X-ray diffraction properties of the crystal structure. Furthermore, the anisotropy of certain physical and mechanical properties of the samples are considered to reflect its fabric. For instance, the shrinkage of a drying clay specimen is greater in the vertical direction than in the

TABLE 3.I

References on the variation of Preferred Orientation (P.O.) with compaction

Clay Type	Technique of fabric study	Observation	Reference
LABORATORY DEFORMED SAMPLES			
Remoulded Kaolinite	Optical Microscopy	P.O. increase with increasing normal load.	Mitchell (1956)
Remoulded Kaolinite	X-ray diffraction	P.O. increase with increasing normal load.	Martin (1962,1965)
Remoulded Montmorillonite Illite	X-ray diffraction	P.O. increase with increasing load.	Von Engelhardt and Gaida (1963)
Remoulded Kaolinite	X-ray diffraction	Increase of packet orientation with increasing moulding water content.	Sloane and Kell (1966)
Kaolinite Illite paste	X-ray diffraction	P.O. increase with increasing load.	O'Brien (1963)
Leda Clay	X-ray diffraction	P.O. increase with increasing load.	Quigley and Thompson(1966)
Remoulded Kaolin	Optical microscopy	P.O. increase with increasing load.	Tchalenko (1967)
Remoulded Kaolin	X-ray diffraction	Shear distortion and not compaction is a more significant cause for PO	Clarke (1970)
FIELD SAMPLES			
Illite Shales	X-ray diffraction	P.O. increase with depth	Kaarsberg (1959)
Non-marine montmorillonite	X-ray diffraction	No P.O. increase.	Meade (1961)
Paleozoic shale (Illinois)	Fissility study	No P.O. increase.	White (1961)
Cretaceous Mudstone (Texas)		No P.O. increase.	Beall (1964)
Pennsylvanian shales		No P.O. increase	Gipson (1966)

horizontal direction. Table 3.II is a summary of some such published results. Studies of anisotropic properties are reviewed later in the chapter.

3.2.3.1 Electron microscopy

An electron microscope is similar in function to an optical microscope, where the light rays are replaced by electron beams and electromagnetic coils perform the functions of the optical lenses and condensers. Figure 3.5 compares the relative performances of the optical, transmission electron and scanning electron microscopes for different lower limits of convenient resolution by the human eye. Electron microscopy was first developed to determine size and shape of crystals (Grim, 1953). Subsequent observation of fabrics of edge to face particle contacts in recent marine clays (Rosenquist, 1958, 1959, 1962) and extreme degree of particle parallelism in filter pressed Kaolins (West, 1964) have emphasised its usefulness.

The techniques of transmission electron microscopy and scanning electron microscopy are well described in Smart (1966) and Tovey (1967) respectively.

Clays cannot be observed directly in an electron microscope as the latter operates only under a vacuum. As a result any volatile liquids in the pores of the sample would cause it to distort the fabric. Therefore the pore fluid has to be either

Clay	Depositional Environment	Shrinkage %		Reference
		Vertical	Horizontal	
Halden		7.0	6.5	Rosenquist (1955)
Töyen	Quick Clay	5.5	6.8	Rosenquist (1955)
	Marine Clay	21.0	18.0	Warkentin & Bozozok (1961)
	Lacustrine Clay	23.0	9.0	Warkentin & Bozozok (1961)
Västeruk	Fresh Water	15.5	12.5	Pusch (1970)
Kungsbacka	Marine Quick Clay	8.4	8.5	Pusch (1970)
Morjärr	Organic Clay in brackish water	25.7	21.8	Pusch (1970)
Kaolinite	Laboratory	23.5	6.7 ovendrying	Tovey (1967)
	Consolidated	22.6	7.7 air drying quick	Tovey (1967)
	Remoulded	28.6	12.5 slow air drying	Tovey (1967)
		0.78	0.63 freeze drying	Tovey (1967)
		5.7	variable Carbowax	Tovey (1967)

TABLE 3.II

Anisotropic Shrinkage in Clays

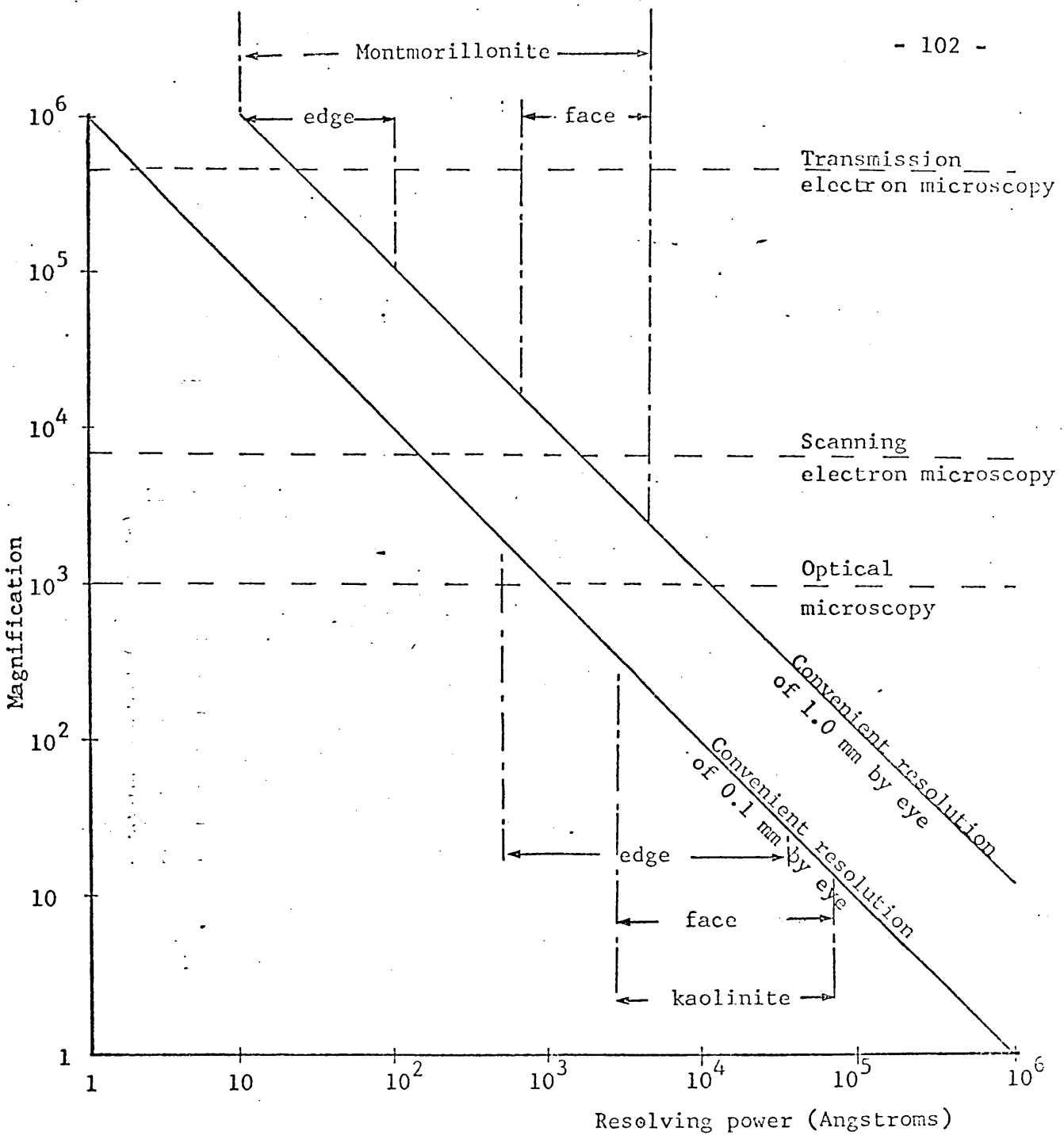


FIGURE 3.5 Application of microscopic techniques in study of clays

removed or replaced by a suitable non-volatile liquid. If the water content of the clay is beyond its shrinkage limit, air drying will result in excessive shrinkage and consequent distortion of fabric can occur. Freeze drying techniques have been adopted in such situations.

Ultra thin sections of 500-1000 Å thick or replicas are necessary for use with the transmission electron microscope. Such techniques are well documented in Bradley (1965).

In the scanning electron microscope, the observations made are from the reflections of a surface. The electron beam can be moved across the specimen by means of a scanning coil. Not all the incident electrons are reflected and as a result local charging on the surface occurs. These bright areas can mask any contrast and cause a loss in resolving power and make the micrograph of little value. Such effects are minimised by coating the surface using a suitable conductive medium (e.g. carbon, gold, or gold palladium).

A fresh fracture surface is usually chosen for observation. The loose debris of particles formed on the surface during fracture can obscure the fabric and yield an unrepresentative micrograph. Such sample disturbances can be got rid of by either directing an air jet on to the surface or by peeling the surface several times with an adhesive tape (Barden, 1972) or by

coating the surface with a silver dag solution and carefully peeling the dried dag (Tovey, 1967).

Procedures for quantitative measurements on scanning electron micrograph are of valuable importance especially in the field of material science and such have been reviewed in Hilliard (1971). The analyses are of two types: (a) mensuration; i.e. the determination of the properties of specific features such as lineal distances and the dihedral angle between planes, and (b) the estimation of bulk properties like volume fractions and boundary areas per unit volume. Smart (1966) analysed single transmission electron micrographs of ultra-thin sections using an area fraction technique. Such a technique is most conveniently effected using an automatic image analysing computer (Quantimet), described by Foster and Evans (1971).

3.2.3.2 Optical microscopy

Spotts McDowell (1926) first used the petrographic microscope to observe aggregates of clay particles. Urbain (1937) outlined a systematic technique for the application of polarised light microscopy in clay studies and he consequently distinguished the random and oriented clay fabrics.

Clay minerals possess different refractive indices along their crystallographic axes. In the case of Kaolin, in

particular, the optical axes coincide with the crystallographic axes. Its optical properties are biaxial negative and ranges of values of the refractive indices in the optical directions a, b, and c are 1.559-1.569, 1.560-1.570, and 1.553-1.563 respectively (Morgenstern and Tchalenko, 1967).

Most clay minerals are birefringent and when they are arranged with a preferred orientation birefringence continues to prevail in the clay 'en masse' and is referred to as the 'aggregate birefringence'. Such an aggregate of preferentially oriented clay particles transmit, under crossed polars, a minimum intensity (I_{min}) of the incident light intensity (I_o), when the trace of the plane of preferred orientation is parallel to either of the planes of polarisation of the polars, and a maximum intensity (I_{max}) occurs at 45° to these planes. As a result, when the microscope stage carrying the section is rotated through 360°, there are four stage settings (or two stage directions) for which the intensity of the transmitted light is a minimum and similarly four other settings for the maximum.

Smart (1966) adopted the term 'anisotropy index' (A) defined as the ratio

$$A = \frac{\sum I_{max} - \sum I_{min}}{\sum I_{max} + \sum I_{min}}$$

With the summation of the respective intensities used so as to overcome instrumental defects such as asymmetrical

positioning of the objective, condenser etc., 'A' can take values from 0 (random) to 1 (well oriented).

Morgenstern and Tchalenko (1967a) defined the term birefringence ratio (β) as the ratio I_{min}/I_{max} which can take values from 0 (well oriented) to 1 (random).

For such observations it is necessary to obtain sections cut with their planes in the direction of the maximum principal stress. The preparation of the thin section must neither cause any significant alteration of the original fabric nor effect any changes in the optical properties of the aggregates. As mentioned earlier, drying induces a shrinkage, and grinding in the process of preparing a thin section can drastically distort the fabric. Impregnation with the polyethylene glycol Carbowax 6000 (Mitchell, 1956) has been observed to provide a satisfactory solution to the above criteria. The consequent shrinkage is not entirely eliminated but is significantly reduced to as much as 7.2% in the horizontal and 8.8% in the vertical directions in undisturbed Leda clay, impregnated with carbowax (Quigley and Thompson, 1966). Other techniques of impregnating clays particularly with resins have been mentioned in literature (Sutherland and Singh, 1971; Foster and De, 1972).

Two further techniques of quantifying clay fabrics using optical microscopy have been described by Lafeber (1967).

The use of a Bereck compensator with the ordinary polarising microscope enables a three-dimensional study of the orientation. Another somewhat indirect technique is to observe the orientation of the pores. The introduction of a small quantity ($2\frac{1}{2}$ to 5%) of anthracene with the carbowax cause the infilled pores to fluoresce under ultraviolet light. The latter technique is not particularly beneficial in the study of clays.

3.2.3.3 X-ray diffraction

The first systematic study of clay particle orientation using an X-ray diffraction technique was by Martin (1962). The technique is based on the fact that the intensity of the diffracted X-radiation that enters the counter is a relative measure of the number of appropriate clay mineral lattice planes whose orientation satisfies the Bragg Law: $n\lambda = 2d \sin\theta$, (see figure 3.6), or in other words, is a measure of the number of appropriate lattice planes whose poles lie in the focussing plane of the goniometer and bisect the angle between the collimator and the goniometer.

The dimensions of the surfaces X-rayed by Martin (1962) were 1.4 mm x 12.0 mm (compared with 330 μ diameter field of view adopted in optical microscopy by Tchalenko (1967)). Hence results of such orientation studies represent averages over areas larger than many of the localised fabrics (like domains).

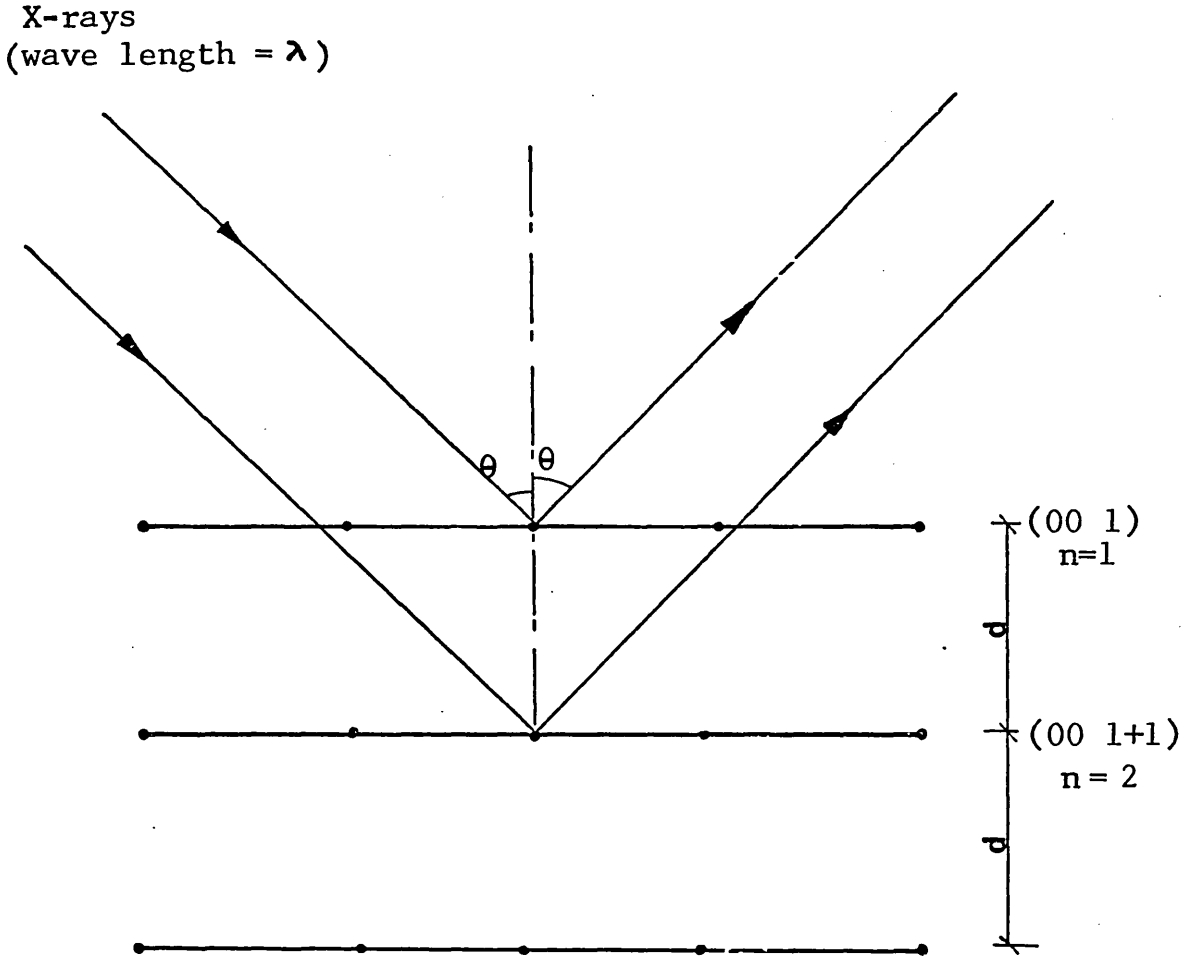


FIGURE 3.6 Bragg's Law Principle of X-ray diffraction

Quigley and Thompson (1966) presented similar data and they compared the absolute values of the intensities of the respective reflections. It must, however, be noted that the absolute intensity is not entirely dependent on the fabric alone but varies also with the mass density. Therefore the degree of orientation is best represented by analysing the ratio of intensities from either two adjacent crystallographic planes of the same section or the same crystallographic plane from two orthogonal sections (Meade, 1961; Martin, 1962). Table 3.III lists such ratios adopted in past literature.

Attewell and Taylor (1969) describe the use and principle of a texture goniometer which adopts the X-ray diffraction principles and produces a three-dimensional information of the orientation of the platy particles. The pole figure device permits three additional motions and at the same time maintains focussing geometry to satisfy the Bragg equation.

3.2.4 Appraisal of the techniques of quantitative fabric analysis

Apart from the stereoscopic analysis of scanning electron micrographs, the three-dimensional optical microscopy (Lafeber, 1967) and interpretation of texture goniometer results, all the other techniques described earlier do not give a direct quantitative estimate of the orientation of the particles. The three

TABLE 3.III

X-ray Diffraction Intensity Ratios used in study of clay fabrics.

Intensity Ratio	Equivalent Orientation Ratio	Reference
$\frac{(002)/(110)H}{(002)/(110)V}$	$\frac{1}{R^2}$	Bates (1947) Kaarsberg (1959)
$\frac{(001)\text{ and/or }(002)/(020)\text{ and/or }(110)H}{(001)\text{ and/or }(002)/(020)\text{ and/or }(110)V}$	$\frac{1}{R^2}$	O'Brien (1964)
$\frac{(002)/(020)H}{(002)/(020)V}$	$\frac{1}{R^2}$	Gipson (1966)
$\frac{(001)V}{(001)H+(001)V}$	$\frac{1}{R+1}$	Odom (1967)
$\frac{(002)/(020)V}{(002)/(020)H}$	R^2	Clark (1970)
$\frac{(001)V}{(001)H+(001)V}$	$\frac{R}{R+1}$	Jackson (1972)

R = Degree of orientation

H = Horizontal section

V = Vertical section

Figures in brackets are the Miller Indices.

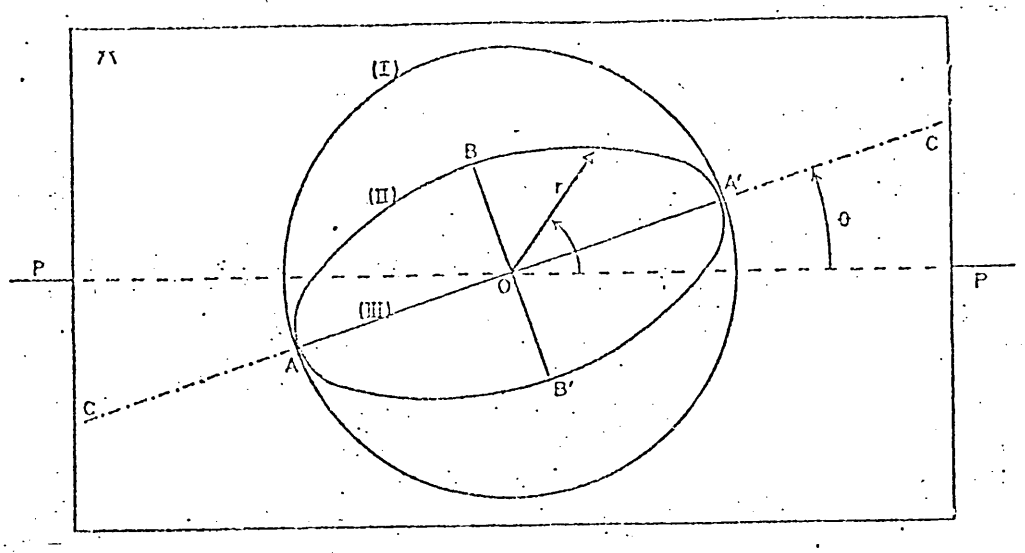
techniques mentioned above either adopt a tedious analysis or a special apparatus, whereas all other techniques define an indirect factor usually referred to as the 'anisotropy index'.

Morgenstern and Tchalenko (1967a) developed a quantitative relation between the degree of orientation and aggregate birefringence. This, however, necessitated an assumption of a representative particle distribution function. Tchalenko et al (1971) using the same particle distribution function obtained relationships between the various preferred orientation ratios (X-ray studies) and the degree of orientation (see table 3.III).

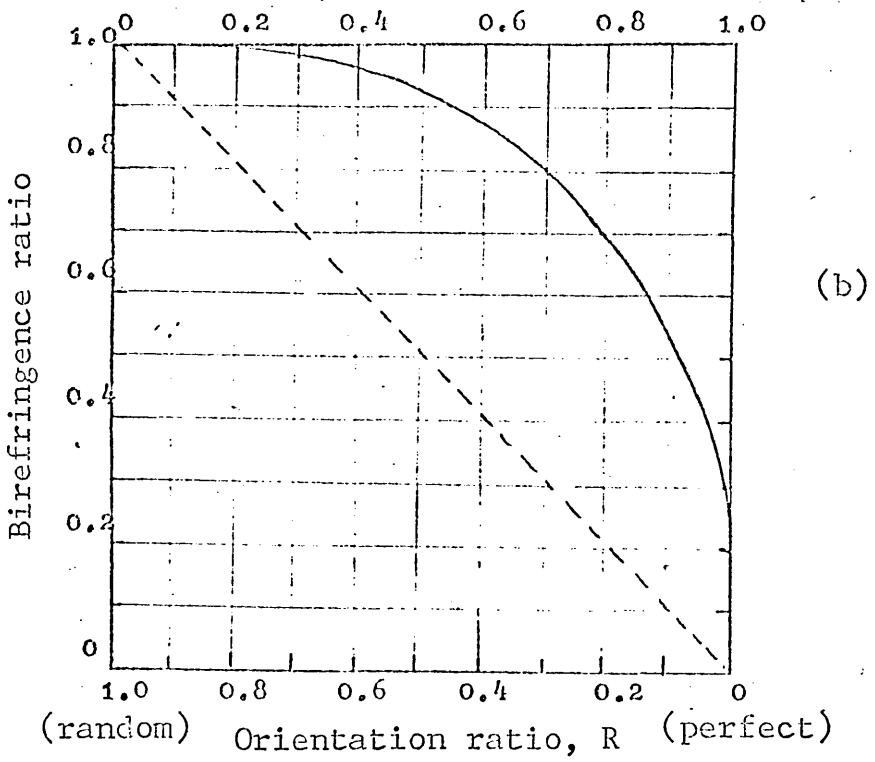
The distribution function so adopted was the length of the radius vector of a circle for the random case and the length of the radius of an ellipse for imtermediate degrees of orientation chosen such that there are unit crystals in the extinction position. Accordingly for perfect orientation the ellipse reduces to a straight line (see figure 3.7a). For an intermediate degree of orientation the particle distribution function takes the form

$$m(\alpha) = \frac{1}{\sqrt{\{1 - (1-R^2)\mathrm{Cos}^2\alpha\}}} \qquad \text{A.}$$

Morgenstern and Tchalenko (1967a) further showed that the birefringence ratio β, (ratio I_{max}/I_{min}) can also be expressed as



(a)



(b)

FIGURE 3.7 (a) Two-dimensional particle distribution function

π - Plane of the thin section
PP - Vibration direction of the polarised light
CC - Reference axis on the section
r - radius vectors
AA'- Major axis (= 2 units)
BB'- Minor axis (= 2R units)
I - random orientation,
major axis = minor axis = 2 units
II - intermediate orientation
III- perfect orientation, minor axis = 0

(b) Relation between birefringence ratio and orientation ratio,
(after Tchalenko, 1967).

$$\beta = \frac{\int_0^{\frac{1}{2}\pi} m(\alpha)\ \mathrm{Sin}^2 2\alpha\ d\alpha}{\int_0^{\pi/2} m(\alpha)\ \mathrm{Cos}^2 2\alpha\ d\alpha} \qquad \text{B.}$$

The integration of equations A and B gives a relationship between the birefringence ratio β, and the orientation ratio, R. This is shown graphically on figure 3.7b. It is noteworthy that the birefringence ratio β is independent of the section thickness and the wavelength. For monomineralic aggregates, β is also independent of effect of birefringence of embedding medium.

3.3 CHANGES IN CHEMISTRY OF PORE FLUID WITH COMPACTION

It is a well observed fact that in many sedimentary basins the salinity of the pore fluids from drill holes increases with increasing depth. Emery and Rittenberg (1952) note that even within spans of short sediment cores various measurable changes of the chemistry of the pore fluid can occur.

The compaction of the vast continental and marine sediments must lead to the expulsion of enormous amounts of pore fluids. Considering a value of 60% as a reasonable average for the porosity of a sediment at deposition, and using Athy's exponential porosity depth relationship outlined in chapter two, it appears that a volume of pore fluid equivalent to 1000' feet will be expelled during the deposition of 10,000 feet of sediment. The speed at which such a volume of pore fluid is expelled depends not only on the imposition of the overburden pressure but also

on factors such as fabric and mineral composition of the sediment and the physical and chemical properties of the fluid. Compaction proceeds more rapidly if the pore fluids contain an electrolyte. When the porosity of clays is high, the permeability is sufficiently large to allow water and dissolved salts to pass through without any appreciable change in the abundance of the various ions. During the process of further compaction, the pore fluid that is trapped within the sediment is prone to chemical alterations which are a function of time, pressure and temperature.

Posokhov (1966) discusses in detail the factors which affect the chemical composition of underground waters: (a) physiogeographic, (b) geologic, (c) hydrogeologic, (d) biologic, (e) physical, and (f) physico-chemical. The physico-chemical factor included processes such as; (1) oxidation-reduction conditions, (2) salt solubility, (3) diffusion, (4) osmosis, (5) gravitational differentiation, (6) mixing of different waters, and (7) base exchange.

3.3.1 Solubility of various salts and mobility of ions

Figure 3.8 illustrates the solubility characters of some varieties of salts. The solubility of NaCl is not appreciably changed with increasing temperature: 358.6 gms/litre at 18°C is 371 gms/litre at 60°C. The solubilities of Na_2SO_4 and Na_2CO_3 increase appreciably with temperature increase.

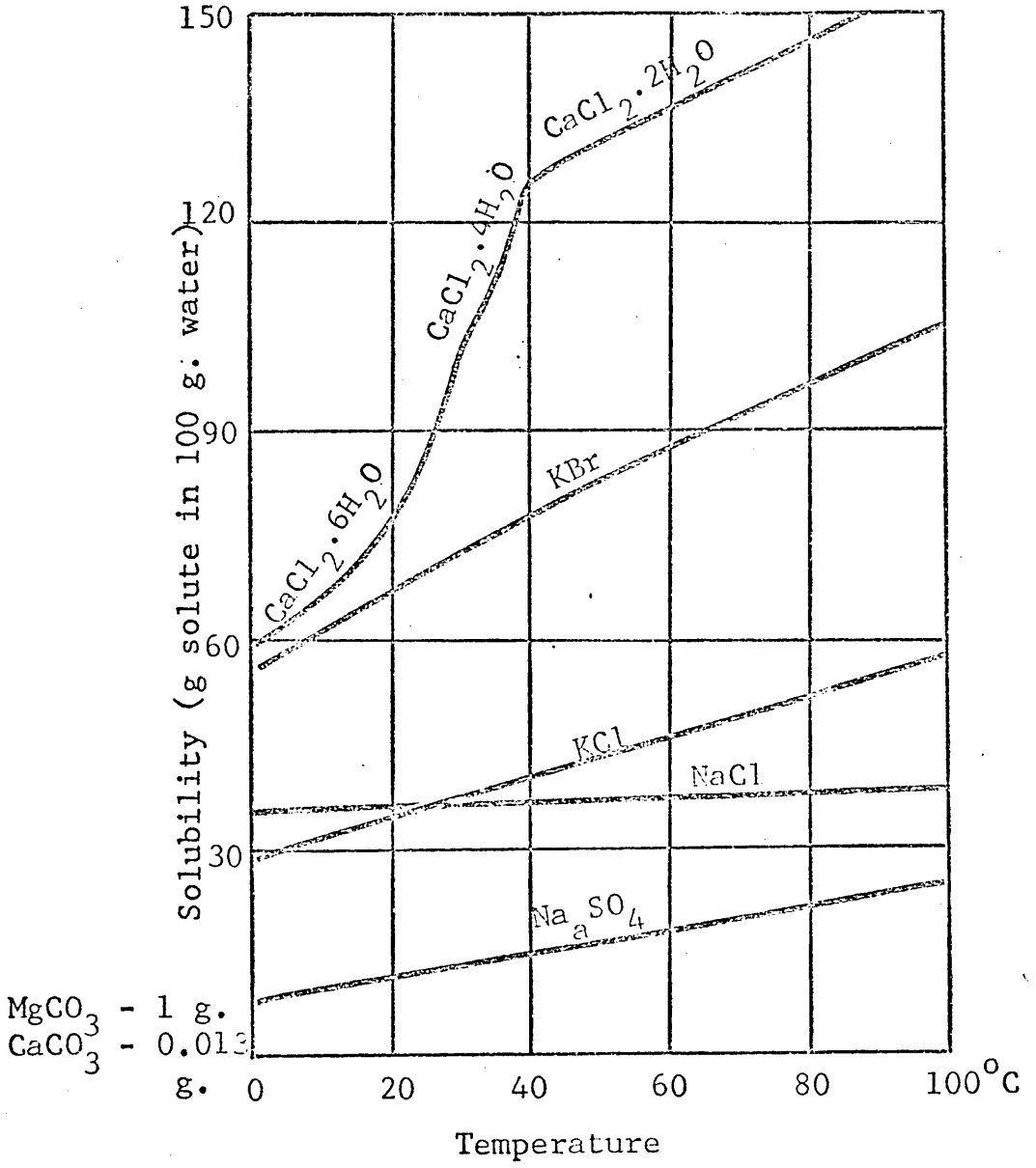


FIGURE 3.8 Influence of temperature on the solubility of various salts in water.

However, in mixtures of salts, the solubility of a particular salt decreases in the presence of other salts having an ion in common, while in the absence of the common ion effect the solubility increases.

The mobility of hydrated ions depends on their valence and ionic radius (Posokhov, 1966). Thus theoretically the mobility of anions must decrease in the order;

$$\text{highest } NO_3^- > Cl^- > SO_4^{--} > CO_3^{--} \text{ lowest,}$$

while in the case of cations;

$$\text{highest } K^+ > Na^+ > Ca^{++} > Mg^{++} \text{ lowest.}$$

However, the above orders are affected by factors such as pH of the medium, adsorption processes, etc.

3.3.2 Some field observations of changes in the chemistry of pore fluid

In the analysis of results from field samples, it is essential to assume that the salinity and ionic composition of the sea water has always been the same as that of today. Degens et al (1964) analysed the oxygen isotope composition of a number of pore fluids ranging in age from the Cambrian to the Tertiary and noted that the $\delta^{18}O$ values of the highly saline brines do not differ appreciably from those of present sea water.

Pore fluids have been sampled using either of two techniques: by flushing (or distilling) relatively permeable cores, or the core is pulverised and soluble salts are leached with distilled water. Contamination resulting in concentrating or diluting particular ions in the pore fluid during sampling can occur during drilling of the wells or dissolving the soluble minerals of the rock during leaching. Von Engelhardt and Gaida (1963) leached the interstitial salts from Jurassic claystone and shales. The leached solution was analysed for its chloride content which he reckoned was derived from the pore fluid only.

Friedman et al (1968) analysed the pore fluids in the sediments from the Atlantic Ocean off Long Island, New York. They reported that the concentration ratios Ca^{++}/Cl^{-}, K^{+}/Cl^{-}, and Rb^{+++}/Cl^{-} were higher in the pore fluids than in the overlying ocean water, while a converse relation was apparent with the Sr^{+++}/Cl^{-} ratio. The ratios Mg^{++}/Cl^{-} and Li^{++}/Cl^{-} were observed to be the same. They further noted that all the above ratios, excepting the Sr^{+++}/Cl^{-} ratio, increased with depth in the sediment.

Schmidt (1971) found the salinities of the waters of normally pressured sands increased with depth. This normal trend in basin salinities has also been noted by Fertl and Timko (1971), Dickey (1966), Bredehoeft et al (1963), De Sitter (1947), Cordell

(1972), and many others. Figure 3.9 illustrates the normal trend of increasing salinity with depth of burial as observed by observed by Dickey (1966).

Schmidt (1971, 1973) noted that pore fluids from shales were much less concentrated in dissolved solids than the adjacent sands. Figure 3.10 is a schematic diagram of some of the anticipated effects in the compaction of interbedded sand shale sequence (Magara, 1974). It must be noted that within a shale formation, the salinity of the pore water will increase in the direction of its drainage path.

3.3.3 Chemical changes observed in laboratory compacted clays

In laboratory investigations, the time scale adopted is highly unrepresentative of field compaction. The rate of expulsion of pore fluid must be an important factor that has to be considered. On squeezing saturated clays rapidly, the pore fluid near the drainage end is expelled at lower pressures while the pore fluids deeper inside the clay sample is expelled only after a fixed time or at higher pressures. Such a process can lead to unrepresentative sampling.

Rieke et al (1964) analysed the cold laboratory extruded pore water from montmorillonite clay (API no. 25) saturated with sea water. These results are presented in

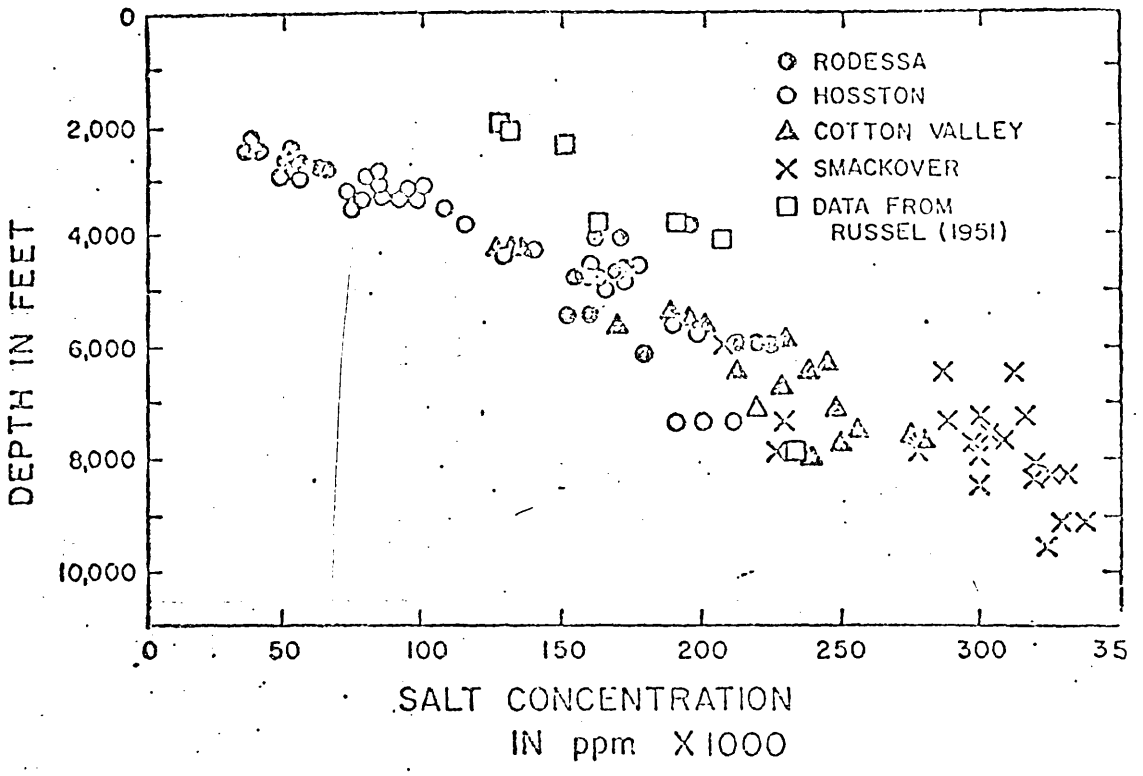


FIGURE 3.9 Increase of salt concentration with depth in:

Southern Arkansas and Northern Louisiana (after Dickey, 1969)

Paleozoic shales (after Russell, 1951)

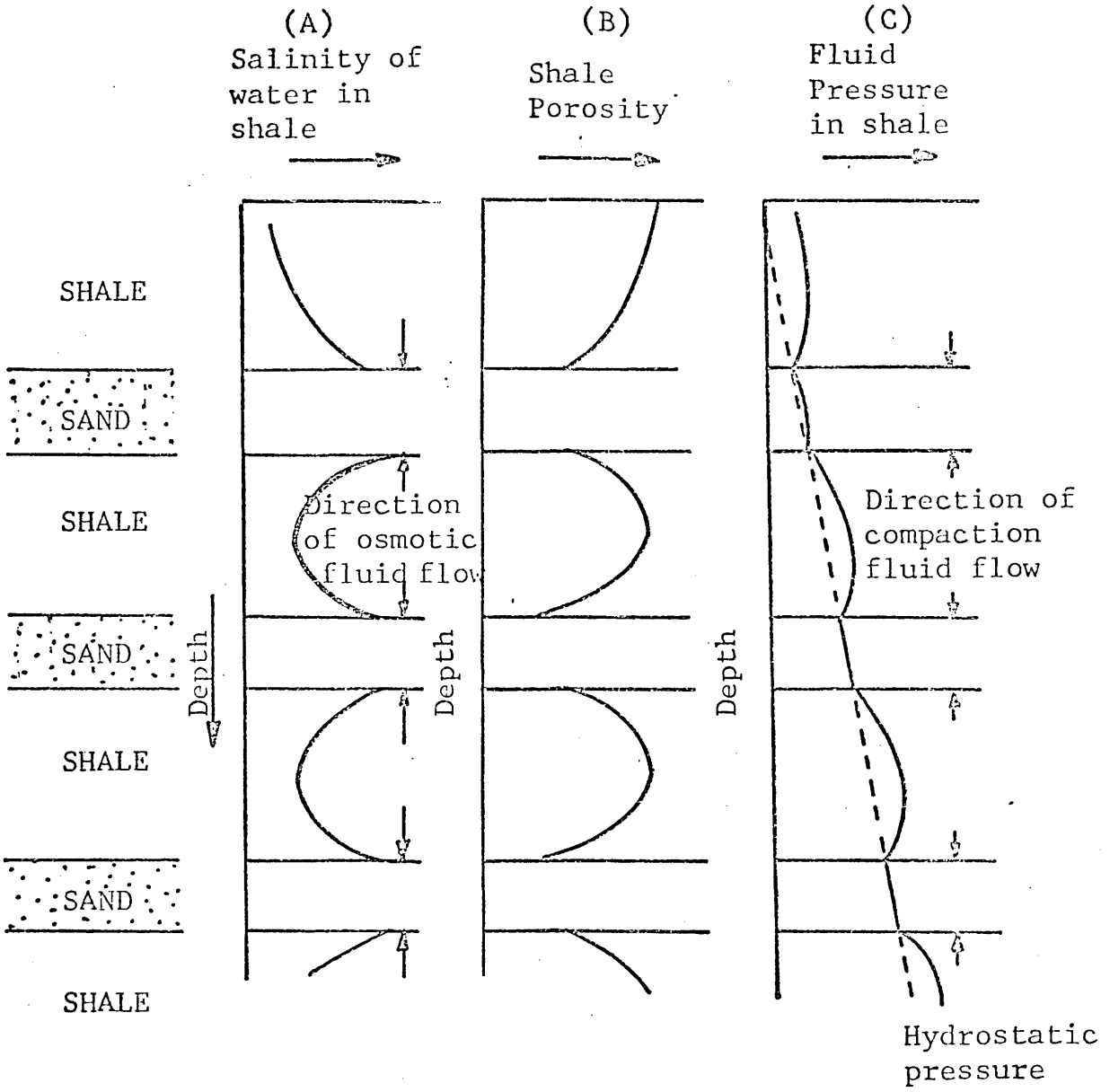


FIGURE 3.10 Schematic diagram showing the anticipated distributions of:-

A. Salinity of pore water
B. Shale porosity
C. Fluid pressure in an interbedded sand-shale sequence (after Magara, 1974)

figure 3.11, which shows that the mineralisation of the solutions squeezed out during different stages of compaction is a function of the overburden pressure. Similar results have also been reported by Kryukov et al (1962). Rieke et al (1964) further observed that in some experiments the percentage decrease in the concentration of the ions with pressure was nearly the same for all types of ions.

Warner (1964) observed no change in salinity of the pore waters expelled from Kaolinite. He argued that the packing of the platy Kaolinite particles probably never approached each other at a spacing equivalent to their combined double layer thickness (about 8 $\mathring{A}$ in 0.55 N NaCl). He further computed theoretically that even at pressures of 60,000 lb/in^2 the Kaolinite plates in 0.55 N NaCl solution will yet be separated by a distance of 90 A^o. Chillingarian and Rieke (1968) have observed, however, that the chemistry of squeezed-out solutions begin to change appreciably when the remaining moisture content is about 20-25% for Kaolinite and about 50-70% for montmorillonite clay. Similar results in Kaolinite observed by Kryukov and Zhuchkova (1963) shown in figure 3.12 demonstrate that the concentration of the solutions expelled at higher pressures is progressively less.

Sawabini et al (1972) also reported the effect of compaction on chemistry of pore fluid expelled from montmorillonite clay saturated in sea water. Their findings suggest that the

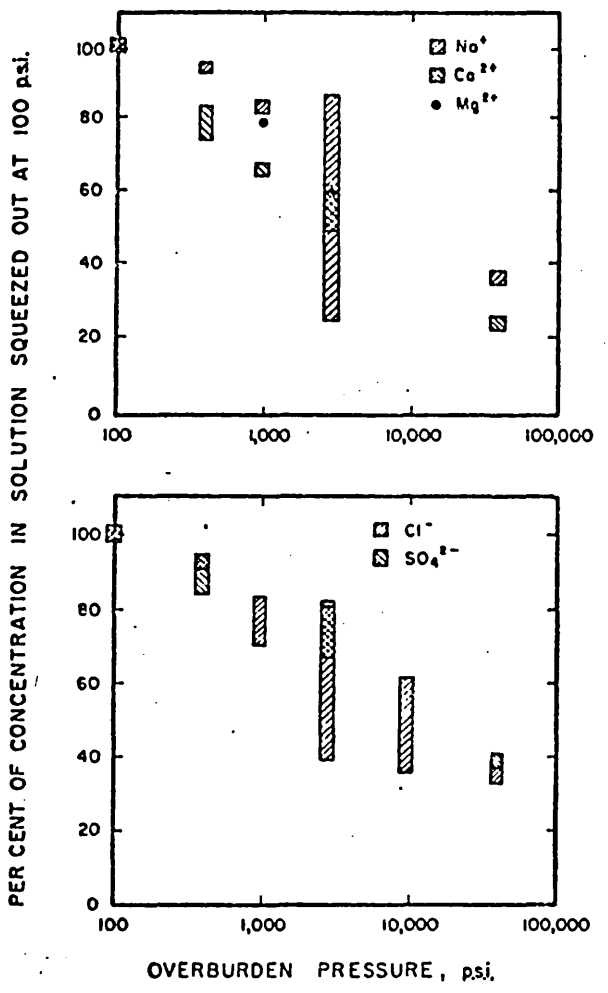


FIGURE 3.11 Concentration of ions in the pore waters expelled at different pressures from a sea water saturated montmorillonite. (after Rieke et al, 1964)

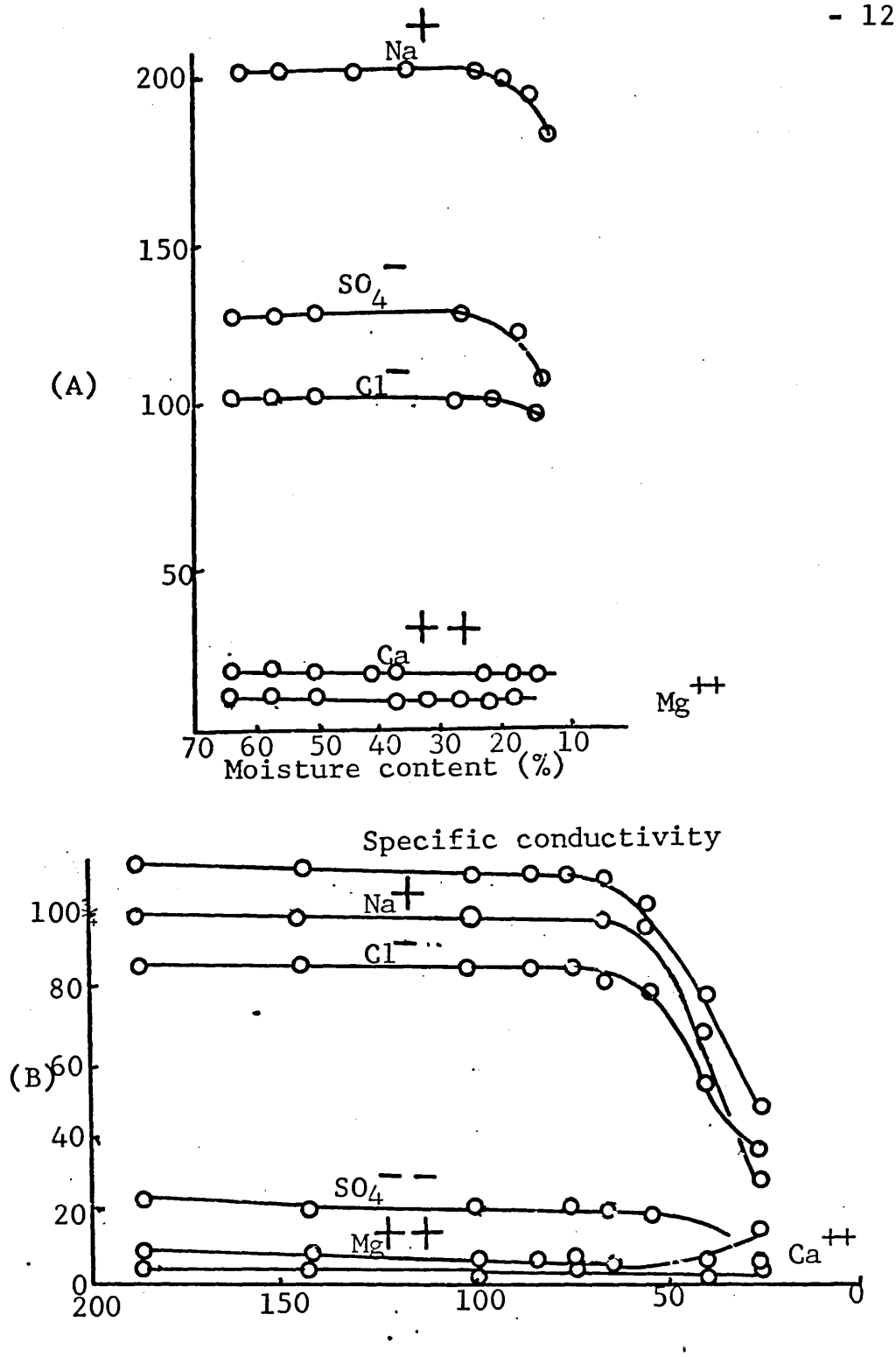


FIGURE 3.12 Changes in composition of solutions squeezed out of:-

A) Kaolinite
B) Bentonite

(after Kryukov and Zhuchkova, 1963)

concentration of the expelled solution passes through a maximum (peak) (or remains more or less the same) before decreasing with increasing overburden pressure (see figure 3.13).

3.3.4 Influence of temperature on the chemistry of the pore fluid

It is not feasible to single out the effect of temperature alone from the study of field samples. Such investigations can be made in the laboratory. Krasintseva (1968) observed the effect of temperature on the ionic concentrations in the pore fluids expressed during the compaction of a clay (Maykop clay). The observations illustrated in figure 3.14 show that heating the sample to $80^{o}C$ does not alter the trends for Na^{+} and Cl^{-} ion concentrations to decrease with increasing pressure. The influence of heating on the enhancement of Mg^{++} ion concentration with pressure is only to yield lower absolute values at high temperature. At high temperatures, the concentrations of K^{+}. Li^{+} and I^{+} were observed to be enhanced, while that of SO_4^{--} was lowered.

3.3.5 Review of the current theories of diagenetic changes of pore water

It is necessary to cite the fact that dissolved ions, like sediments, tend to settle out of a water column. Mangelsdorf et al (1970) calculated that gravitational settling of ions in an isothermal sediment column can produce increases of equilibrium

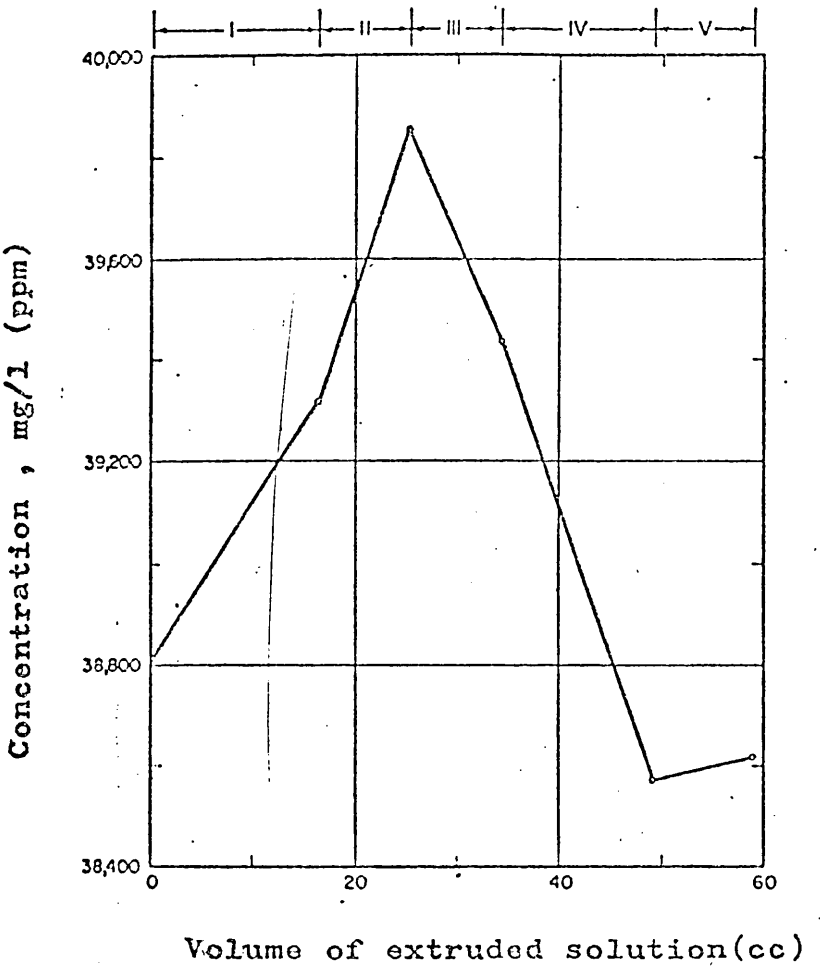
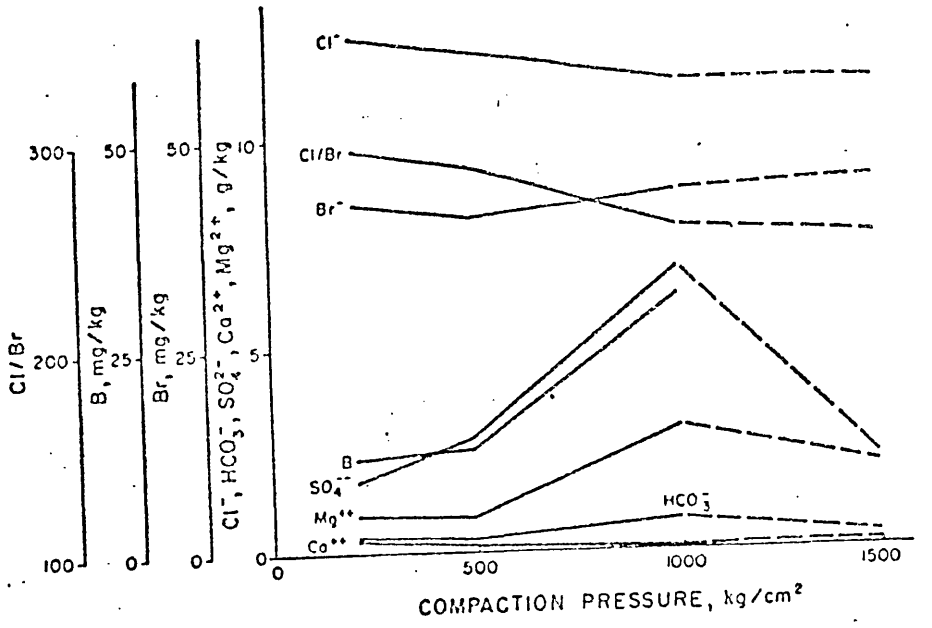
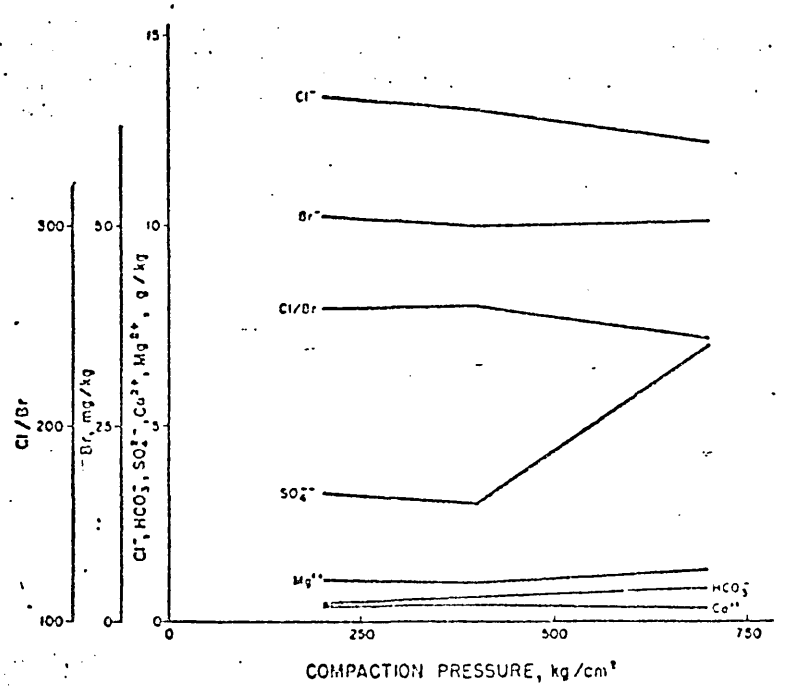


FIGURE 3.13 Variation of total dissolved solid content in pore solutions extruded from montmorillonite clay saturated in sea water with increasing compaction pressure.
(after Swabini et al., 1972).



A



B

FIGURE 3.14 Changes in compositions of solutions squeezed out of marine mud:

A) under room temperature,
B) at 80°C temperature.

(after Krasintseva and Korunova, 1968)

ionic concentrations in the pore water ranging from 1 percent per 100 metre depth for Cl^- ion to 4 percent per 100 metre depth for Sr^{+++}. They further reported that the migration of ions in a thermal gradient (Soret effect) would result in minor salt enrichment upwards towards the colder region, but the presence of cation exchanging clays reverses this tendency and causes pumping of salt downwards. Mangelsdorf et al (1970) calculated, assuming reasonable values for the geothermal gradients, that about 5% of enrichment in Cl^- ion per 100 metre depth can occur, under steady state conditions. Thus their calculations show that a thermal gradient imposed on a static sediment-water column can produce stronger ionic concentration gradients than could gravity, but such calculated concentration gradients fail to correspond to gradients observed in the field. Filatov (1955, 1958) proposed gravitational settling as the dominant mechanism to explain the increase of salinity of pore fluids with depth but was criticised by Ogilvy (1958a, 1958b) and Illarianov (1958).

Non-equilibrium mechanisms that can also influence salt distribution include chromatographic effects and membrane filtration through semipermeable media. De Sitter (1947) was the first to suggest the 'salt sieving' action of the clay sediments in forming concentrated salt solutions during compaction. He drew attention to the electrochemical behaviour of base exchanging clays in permitting preferential escape of water while retaining

some of the ions of the dissolved salts. White (1965) described fully this membrane filtration theory.

The effectiveness of clays as a semipermeable membrane filtering device has been demonstrated by several investigators Teorell, 1935; Davis, 1955; Hanshaw, 1962; McKelvey and Milne, 1962; and Hanshaw and Coplen, 1973). One of the properties of semipermeable membranes is to retard or prevent the passage of charged ionic species through the membrane pores, while allowing a relatively free flow of uncharged species. This phenomenon is termed salt filtering, reverse osmosis, or ultrafiltration (Hanshaw and Coplen, 1973).

Clay minerals exhibit a cation exchange phenomenon as a result of the net surface charge distribution on the clay particles discussed in chapter two. The cation exchange capacity varies with differing types of minerals (see table 2.I, chapter 2). Hanshaw and Coplen (1973) recasted the usual units of ion exchange capacity (meq. per 100 g) to $\bar{X}$, equivalents of negative sites per litre of pore volune as pore volume or porosity is pressure dependent. Accordingly $\bar{X}$ too is pressure dependent and is related to the ion exchange capacity as follows;

$$\bar{X} = \frac{\text{exchange capacity x grain density}}{\text{porosity}}$$

They observed that montmorillonites were more porous than illites under a compaction pressure of 330 bars. Consequently

though the exchange capacity of montmorillonites is over three times greater than that of illites, the corresponding $\bar{X}$ is less than twice as great in the montmorillonite at that pressure. $\bar{X}$ is a more representative quantity defining the salt sieving property of a clay.

White (1965) stated that the adsorbed cations can still move between adjacent exchange sites and through the membranes. An electrical streaming potential can thus be set up across the membrane. As a result of compaction the uncharged water molecules flow through the membrane in the direction of decreasing water pressure. Serruya et al (1967) report that movement of fluids as a result of compaction could create electrical potentials which, in turn, may be responsible for selective migration of ions (electrodiagenesis). McKelvey and Milne (1962) generally observed higher upstream to downstream salinity ratios (2/1 to 8/1) with compressed bentonite membranes. Kharaka and Berry (1973) have shown that the efficiency of the compacted clays as effective ion filters increases with the increase in cation exchange capacity of clays or increase in compaction pressure and decrease with increase in concentration of the input solution.

The size of the ions largely defines both the mobility of the ions through the clay membrane and its ion exchange capacity as discussed earlier. The experimental data of Larson (1967) suggest that the size of the hydrated ions influences the

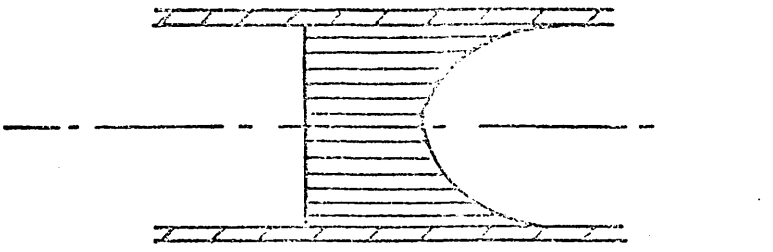
rate of ion rejection by a reverse osmosis process and in the order $Mg^{++} > Ca^{++} > SO_4^{--} > Na^{++} > Cl^{-}$. But such an order was not observed by Collins (1970).

Kotova and Pavlov (1968) adopted the term 'geostatic leaching' to describe the decrease in salt in clays with increasing overburden pressure. On the bases of their experimental and theoretical studies, these authors suggested an exponential rate of decrease of the mineralisation of the pore water (C) with increasing pressure, p, by the relation;

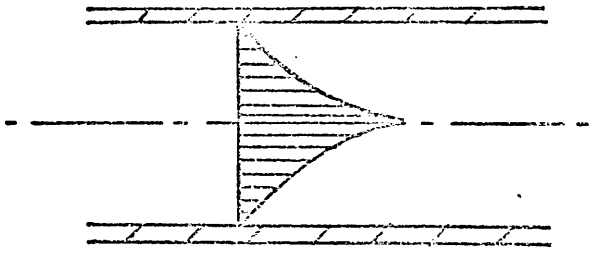
$$C = C_o \left[1 - \exp(-\lambda/p)^n \right],$$

where C_o is initial mineralisation of the pore water; λ and n are constants that depend on physicochemical, geological, structural and other variables.

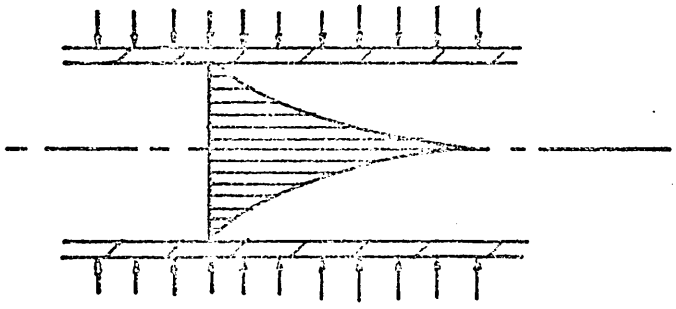
Kryukov and Zhuchkova (1963) also observed that the concentration of solutions squeezed out at higher pressures is lower and considered the last portions of water (probably the asorbed water) squeezed out of sediments are poor in electrolytes. This gradual decrease in the mineralisation of the squeezed-out solutions was explained by Pol'ster et al (1967), considering the characters of the absorbed water on the clay minerals. Figure 3.15 illustrates the behaviour of an electrolyte solution in a capillary radius 'r', which is smaller in cross-section than



(A)



(B)



(C)

FIGURE 3.15 Characters of an electrolyte solution in a capillary radius 'r':-

(A) Density variation

(B) Dissolving capacity of the electrolyte

(C) Effect of compacting the capillary is to expel the pore fluid with the maximum dissolving capacity

(after Pol'ster et al, 1967)

the pore space between two adjacent clay plates. The density of the water adjacent to the capillary walls is a maximum, while the density of the water at the centreline is the lowest and will approach the normal density if the radius of the capillary is large (figure 3.15A). The dissolving capacity of the water is inversely proportional to its density, and hence the variation of the dissolving capacity across the section of the capillary is as shown in figure 3.15B. With compaction, the radius of the capillary is decreased and the first pore water consequently squeezed out is the least bound water at the centre of the capillary (figure 3.15C). Thus the remaining adsorbed water is a less concentrated electrolyte which is expelled later. This explanation relies heavily on the density properties of the adsorbed water. The latter has not yet been investigated conclusively for some investigators even assign lower values to the density of the adsorbed water than to the free water (Anderson and Low, 1958; Grim, 1968).

The decrease in mineralisation of the pore water squeezed during compaction may also be a result of the fluid release mechanism associated with clay mineral diagenesis (Powers, 1967) and this is described separately in the next section.

3.4 CLAY MINERAL DIAGENESIS

The stages in the diagenetic evolution of clay minerals are too little understood to give them precise limits, but the terms early diagenesis, middle diagenesis, late diagenesis and anchizone have been proposed by Dunoyer De Segonzac (1970) and their limits of usage are as illustrated in table 3.IV. The absence of montmorillonite and the infrequent occurrence of Kaolinite is usual in ancient sediments. Numerous mineralogical data have been analysed statistically by Weaver (1967) resulting in a distribution of clay minerals as a function of stratigraphic age (figure 3.16).

3.4.1 Montmorillonite to Illite transformation

That montmorillonite becomes transformed to illite with burial, releasing interlayer water in the process, has become evident from the studies of a large number of workers: Burst (1959, 1969), Weaver (1959, 1961, 1967), Boswell (1961), Yaalon (1962), Keller (1963), Dunoyer de Segonzac (1964, 1970), Khitarov and Pugin (1966), Powers (1967), Steiner (1967), Perry and Haver (1970, 1972), Schmidt (1971), Van Moort (1971), Weaver and Beck (1971) and Cordell (1972).

In a study of the deep well sediments from the Texas Gulf Coast, Powers (1967) noted that the clay transformation commenced at about 6000 feet, and was fairly complete at a

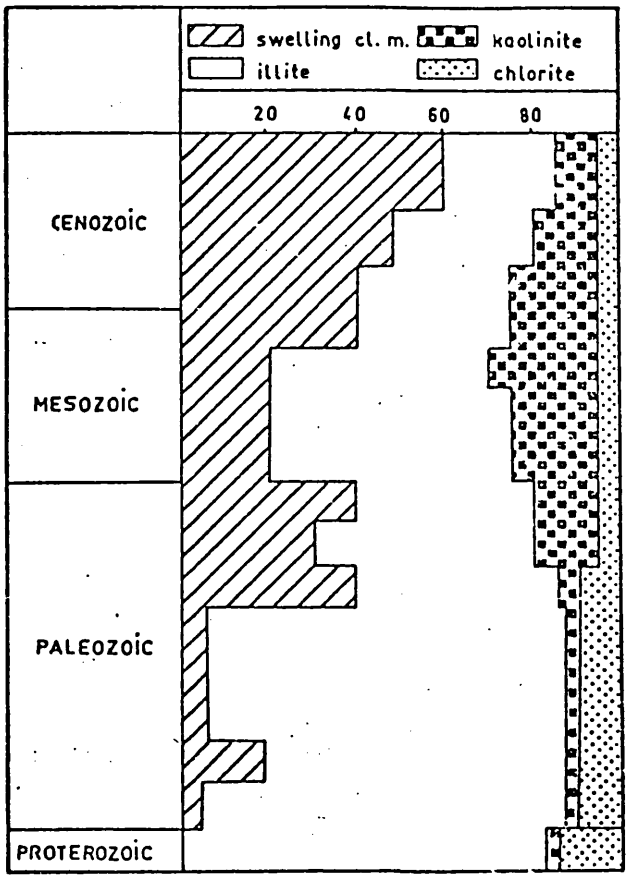


FIGURE 3.16 Statistical distribution of clay minerals in the geological periods. (after Weaver, 1967)

Terminology			Temperature	Porosity	Physicochemical effects	Clay Mineral alteration
After Dunoyer de Segonzac (1970)	Russian Authors	Müller (1967)				
Early Diagenesis	Diagenesis.	Shallow burial stage.		High	Aggradation by adsorption of Mg, K and Na.	All stable.
Middle Diagenesis	Early Catagenesis or Epigenesis	Deep burial stage.		Compaction has resulted in loss of excess of 50% pore water.	Replacement due to pore water, e.g. Kaolinite ⟶ Dickite, Montmorillonite ⟶ Illite.	All otherwise stable.
Late or Deep Diagenesis	Late Catagenesis or Epigenesis	-	Greater than 100°C.	Porosity weak.	-	Montmorillonite and irregular mixed layer disappear.
Anchizone	Metagenesis		200°C	Very low porosity.		Illite and chlorite are the only sheet silicates.

TABLE 3.IV

Stages of Diagenesis

depth of 2000 - 12000 feet. From the results of the high pressure tests of Van Olphen (1963a, 1963b), Powers ruled out pressure as the driving agent for the diagenesis. Weaver and Beck (1971) supported the suggestions of Powers that temperature and large electrostatic forces resulting from potassium and possibly aluminium adsorption are the controlling factors in the diagenesis. The change of montmorillonite to illite, caused by the adsorption of potassium, results in the release of large amounts of bound water from the interlayer surfaces to interparticle areas, when it becomes normal pore water. This is accompanied by a corresponding decrease in the clay particle size along with an increase in the effective porosity, permeability and free pore water content (see figure 2.18).

As illustrated in figure 3.17, Burst (1969) observed that in the deep sediments from the Texas Gulf Coast, the montmorillonite to illite diagenesis occurred in the depth interval 8,500 to 12,500 feet. His observation emphasised the temperature dependence for the diagenesis.

3.4.2 Kaolinite diagenesis

Millot (1964) has described many situations where the presence of Kaolinite has indicated Kaolinising climates. But Kaolinite can also indicate the proximity of shore lines since by virtue of its relatively large particle size, it is deposited closer to the source.

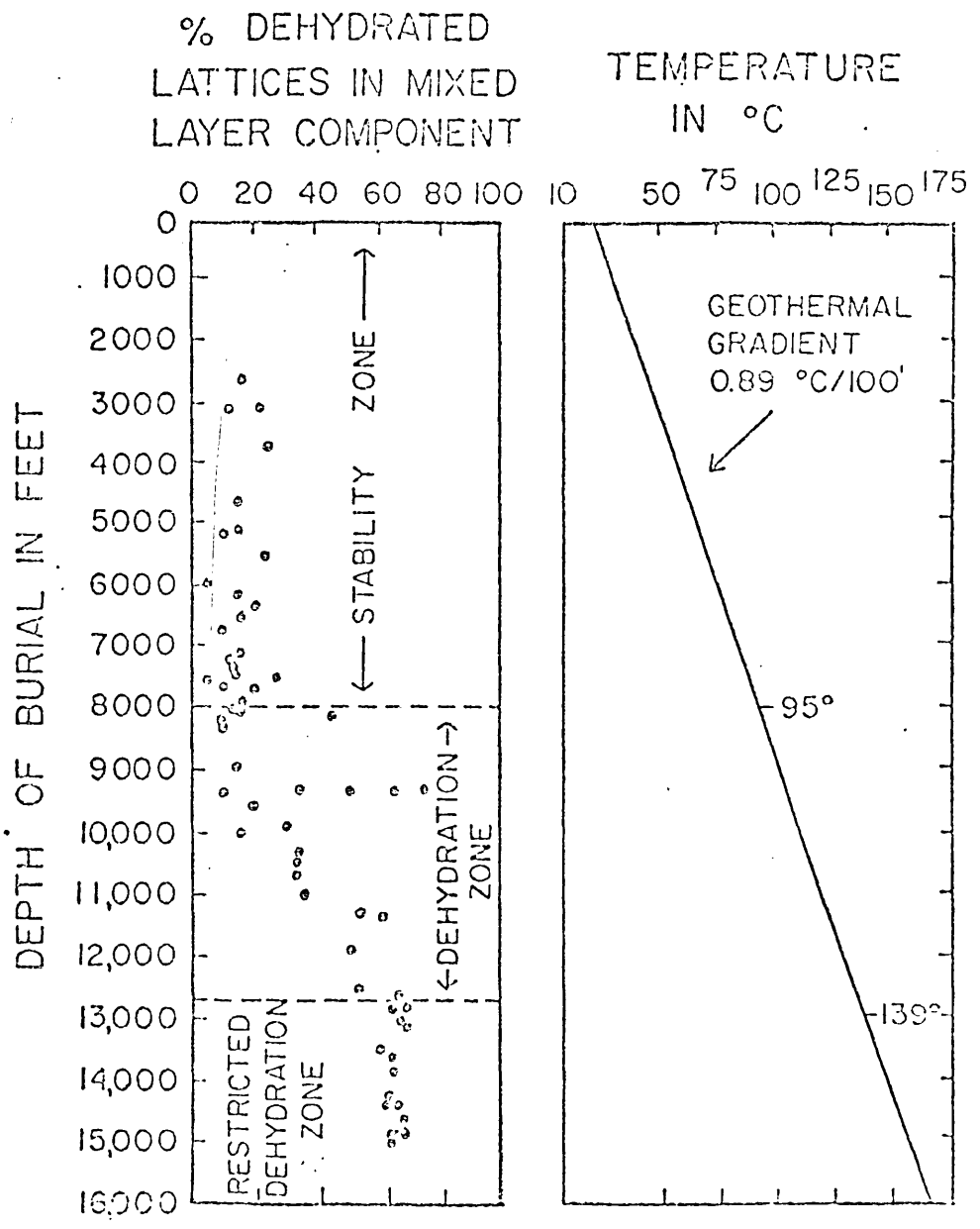


FIGURE 3.17 Dehydration of clays from Montmorillonite to Illite transformation and the associated geothermal gradient as observed in a Gulf coast well.
(after Burst, 1969)

Kaolinite is susceptible to changes in environment and can consequently be replaced. Dunoyer de Segonzac (1970) observed that in the Siluro-Devonian of the Sahara, the calcite of the fossils was replaced by Kaolinite, which was subsequently destroyed to give pyrophyllite. If interstitial waters are basic and concentrated, the Kaolinite cement of the sandstones can be altered to illite (Chepitov et al, 1959). Conversely, under dilute conditions, Millot (1964) and Keller (1968) describe the formation of Kaolinite during diagenesis.

Figure 3.18 illustrates the studies of Dunoyer de Segonzac (1970) on a large number of boreholes, which demonstrate the lower zone of stability for Kaolinite. It can be noted that the depths and temperatures of destruction are variable, but this is not surprising when the importance of the interstitial environment (pH, ionic strength) is itself non-depth related.

Weaver's statistical study (figure 3.16) demonstrates the destruction of Kaolinite with depth while Chlorite is enhanced. The decrease of Kaolinite/Chlorite ratio with depth has been reported by other workers too. Perry and Hower (1970, 1972), however, observed no gain or loss of Chlorite or Kaolinite with depth.

Thus it may be concluded that the instability of Kaolinite during burial is determined by the geochemical factors

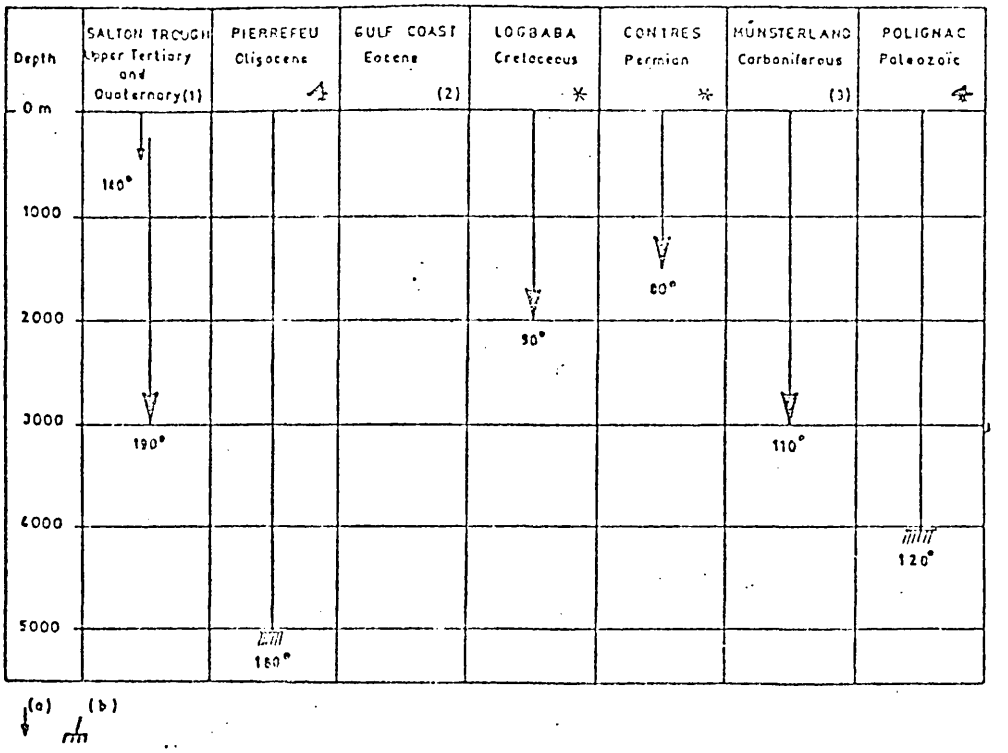


FIGURE 3.18 The destruction of kaolinite during burial:-

(a) disappearance of kaolinite
(b) persistence of kaolinite

(1) Muffler & White (1969)
(2) Burst (1959)
(3) Scherp (1953)
(4) Dunoyer de Segonzac (1969)

which are themselves not strictly related to regular gradients of temperature and pressure. Therefore unlike montmorillonite, Kaolinite is not a precise indicator of depth of burial.

3.4.3 Mixed Layer mineral diagenesis

Konyukhov and Teodorovich (1969) studied the Jurassic shales of eastern Ciscaucasia. They observed a gradual decrease of montmorillonite and disordered mixed layer clays with depth of burial. The transformation commenced at 2,300 - 4,000 feet with disappearance of discrete montmorillonite. With progressive burial the percentage of the expandable layers in the mixed layer clay decreased until at 12,000 - 13,000 feet the mixed layer ratio (montmorillonite:illite) has decreased to between 1:7 to 1:9.

3.5 ABNORMAL PORE FLUID PRESSURES

Abnormal or supranormal pressures are hydrostatic pressures found in sediments which are in excess of the pressures which could be expected usually from the weight of a simple water column. Occurrence of such abnormal pressures has been found in many basins all over the world, but the best known are from the Gulf Coast. The earliest example was published by Keep and Ward (1934) on the high pore fluid pressures in the steeply folded Tertiary sediments in the Khaur field of West Pakistan.

Abnormal pressures in the subsurfaces can be expressed conveniently in terms of a hydrostatic pressure gradient or as fluid pressure/overburden stress ratio (λ). Rieke and Chillingarian (1973) cite the data of Levorsen and observe a linear relationship between the hydrostatic pressure and the total dissolved solids in the pore fluid (figure 3.19). The above relationship clarifies an earlier definition of abnormal geopressures (hydrostatic fluid pressures) as any pressure which exceeds the hydrostatic pressure of a column of brine containing about 80,000 p.p.m. total solids (Dickinson, 1953; Fertl and Timko, 1970).

Various causes have been suggested for abnormal pressures:

1) Compaction:- Geologically rapid sedimentation inhibits complete escape of pore fluid from clays which give rise to high porosities and high fluid pressures.

2) Clay diagenesis:- Clays which have lost most of their porosity release interlayer water to impermeable sediments which dilutes the pore fluid and inhibits its escape (Powers, 1967).

3) Fossil pressures:- The particular formation may be uplifted whilst retaining the hydrostatic pressure it possessed at the greater depth. These pressures are consequently 'abnormally high' for the shallow depth (Reed, 1946).

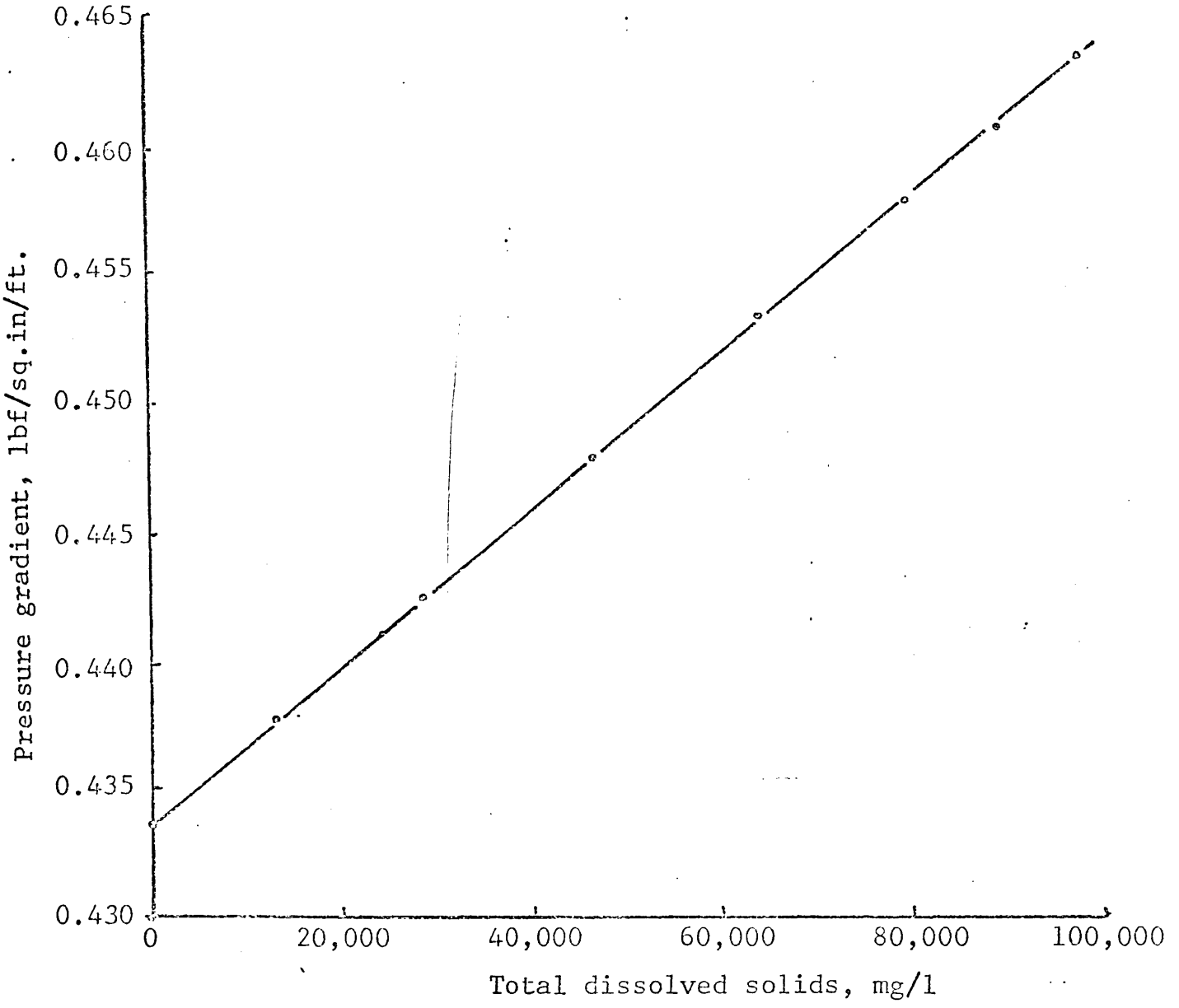


FIGURE 3.19 Relationship between total solid content and the fluid pressure gradient

(after Levorsen, In Rieke and Chillingarian, 1973)

4) Hydrocarbon maturation:- Lighter, less dense hydrocarbons can exert increasingly high pressures on the system (Chaney, 1950).

5) Tectonic activity:- Local tectonic forces accompanying structural growth have been considered to be a cause of the occurrence of abnormal pressures (Finch, 1969).

6) Osmosis:- When a low salinity solution is separated from a high salinity solution by a semipermeable membrane, the resultant osmotic flow can cause pressure to build up in the high salinity brine (Hanshaw, 1962).

In a study of the Louisiana Gulf Coast wells, Dickinson (1953) observed that abnormal pressures were apparent from depths between 6,000-8,000 feet (figure 3.20). Schmidt (1971) presented observations of abnormal pressure data superimposed on a plot of percent shale, percent sand with depth for a well also from the Gulf Coast. The pressures were estimated using electric-log data. From his observations in figure 3.21, it can be seen that abnormal pressures occurred at about 5,500 feet and below this depth abnormal pressures show a direct correlation to the percentage shale in the sediment. Thus, rises in abnormal pressures are associated with increases in the shale content and vice versa.

When continuous bulk density determinations were made on shale cuttings during drilling, Boatman (1962) observed some-

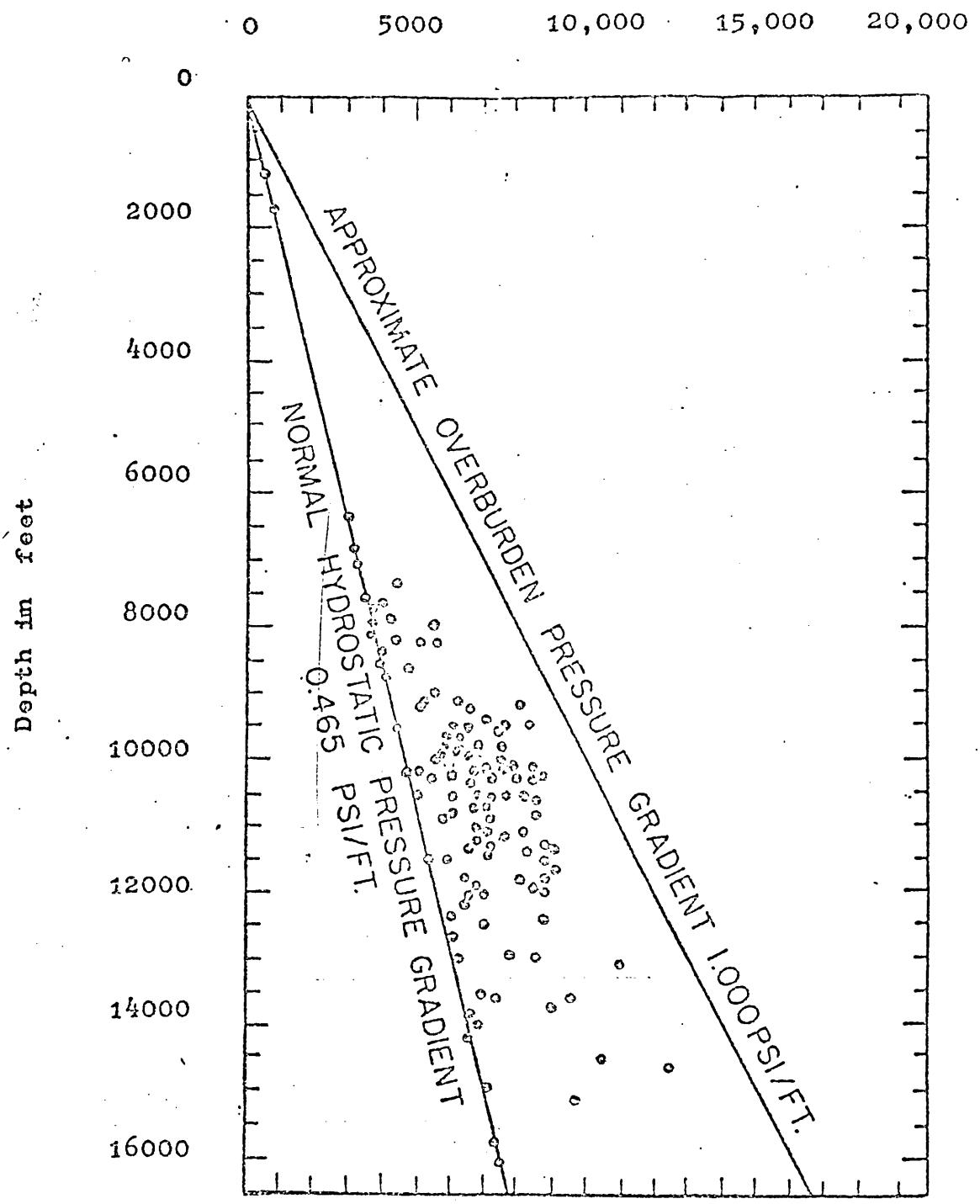


FIGURE 3.20 Reservoir fluid pressure versus depth for Louisiana Gulf Coast wells. (after Dickinson, 1953)

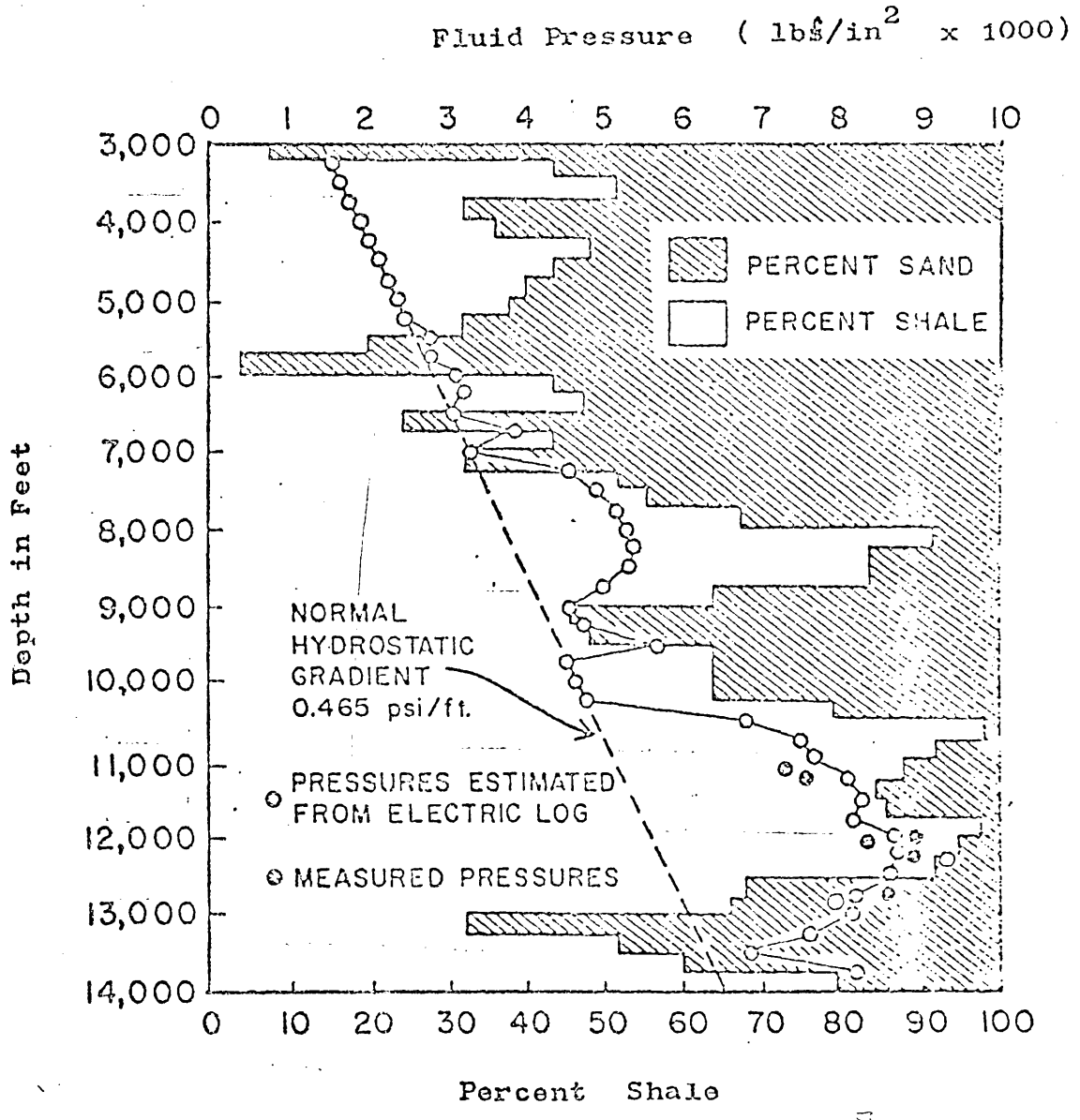


FIGURE 3.21 Percent shale - percent sand of the formation and pore fluid pressure versus depth for the well in Manchester Field, Louisiana.
(after Schmidt, 1973)

times reverse anomalies instead of normal increase in shale compaction. These reversals of normal density trends of shale indicated the entrance into abnormally high pore fluid pressured shales. Boatman indicated that a higher density, limy shale cap often overlies such high pressured, low density shales. He further drew attention to the fact that 'shales are more dense when close to sand bodies because more water has been squeezed out into the sand bodies'.

Magara (1973) used sonic and formation density logs to observe such zones of reverse porosity trends in the Cretaceous shales of Saskatchewan. Magara outlined the mathematics for the use of semigraphical analysis of the field porosity distribution to estimate the associated abnormal pressure distribution.

Fluid expulsion mechanisms associated with compaction of shales have been suggested as a probable cause for the occurrence of anomalous pore fluid pressures. If the relationships between permeability and porosity are known, the discussion of fluid movements in a shale column will become easier. Unfortunately there is very little literature available on such lines (Bredehoeff and Hanshaw, 1968). A collection of porosity permeability data for shales, siltstones and clays in Canada, U.S.A. and Japan was presented by Magara (1973) (figure 3.22). These data showed that permeability apparently increased less with increase in porosity, than what is expected from both the theoretical Kozeny

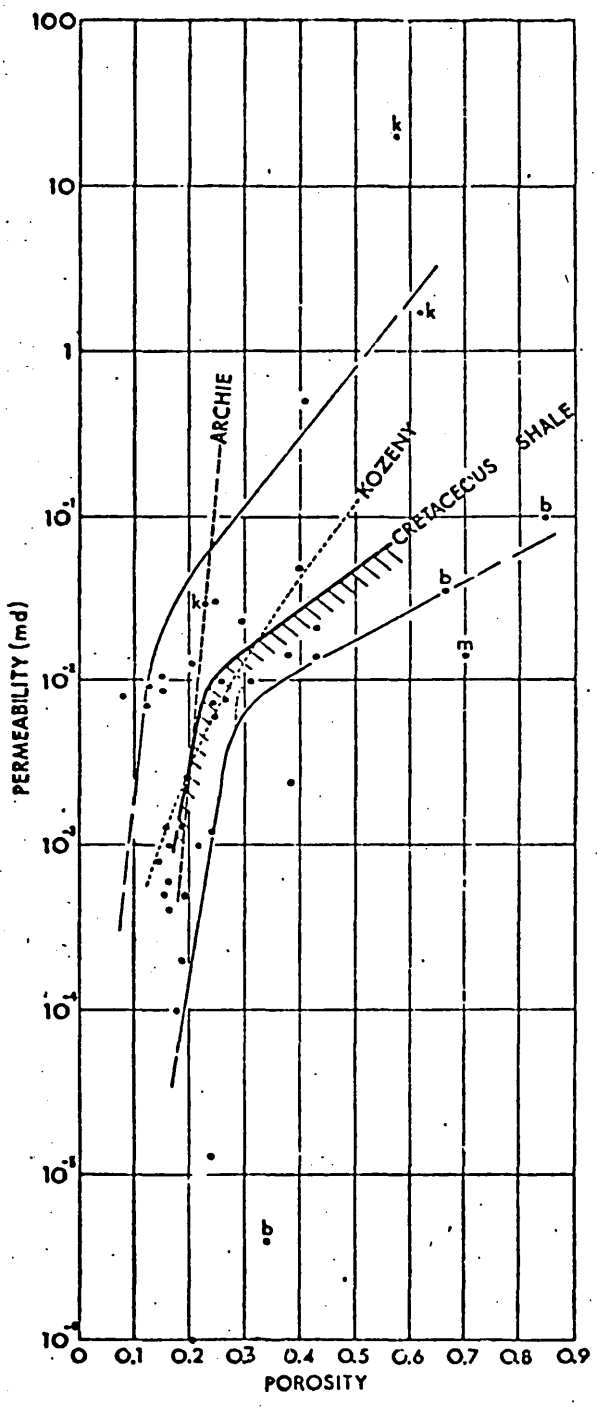


FIGURE 3.22 Relationship between permeability and porosity of shale

Laboratory measured porosity permeability data of shales, siltstones and clays in Canada, U.S.A. and Japan.

Kaolinite	k
Montmorillonite	m
Bentonite	b

(after Magara, 1973)

equation or Archie's relation which is based principally for sandstone and carbonate rocks.

At relatively shallow depths, the permeability of the formation is sufficiently high to effect an easy dissipation of the pore fluid pressure resulting from continuous deposition. For a given rate of sedimentation and a thickness of formation, its excess pore fluid pressures will be completely dissipated provided the permeability is in excess of a corresponding minimum value. Figure 3.23 illustrates the results of Magara's calculations for the relationships between minimum permeability for such 'compaction equilibrium' and the total thickness of the formation for a rate of sedimentation of 10^{-8} cm/sec.

If in deep formations, the actual permeability is less than the minimum for equilibrium, the trapped fluids will continue to build up excessive pressures. Rubey and Hubbert (1959) published a family of porosity depth curves for different values of λ (defined earlier, as ratio of fluid pressure to overburden pressure) (figure 3.24). Thus the porosity depth curve by Athy represents condition of compaction equilibrium where λ usually assumes a value of 0.465.

Abnormal pressures are therefore influenced by factors such as relative proportion of sand and shale, mean formation permeability, the time elapsed since deposition, the rate of

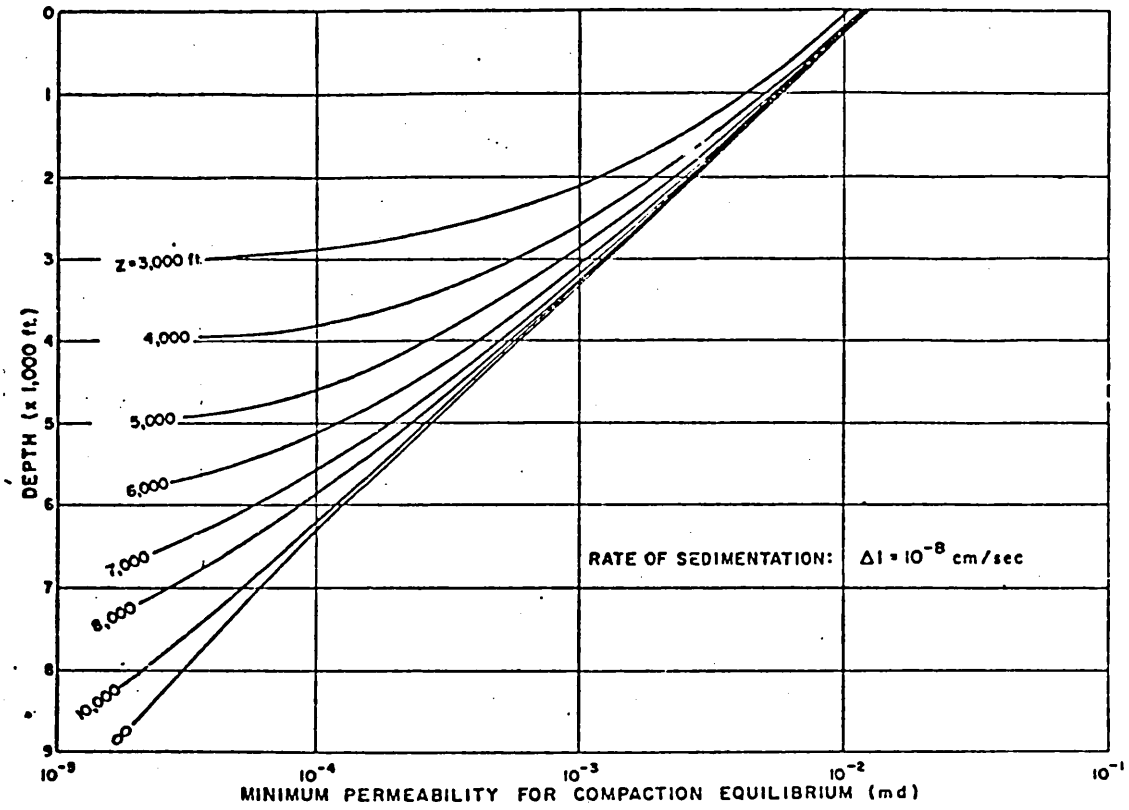


FIGURE 3.23 Relationship between minimum permeability for compaction equilibrium and total thickness of sedimentation of 10^{-8} cm/sec. (after Magara, 1973)

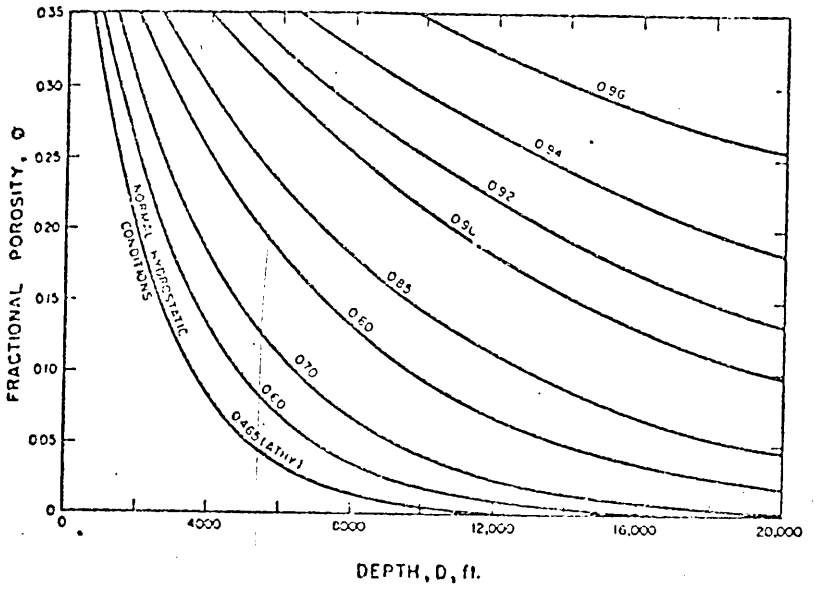


FIGURE 3.24 Family of porosity depth curves for various values of λ (ratio of fluid pressure/overburden pressure). (after Rubey and Hubbert, 1959)

deposition and the amount of overburden (Hoffman and Johnson, 1965; Smith, 1971). Hawkins and Baugher (1969) believe that abnormal pressures are likely to occur in shale formations that are over 200 feet thick and contain greater than 65 percent clay. A mathematical simulation of shale compaction was described by Smith (1971) and a brief outline is presented in Chapter 4.

3.6 INFLUENCE OF BURIAL ON ENGINEERING PROPERTIES

Cognisant of the various changes that occur in the fabric, pore fluid chemistry and mineralogy of the sediments due to burial, a resultant change in its engineering properties is to be expected.

The observation of Skempton (1970) that the liquidity index of a wide variety of normally consolidated argillaceous sediments lies within a narrow range of values for a given effective pressure has already been cited in Chapter 2 and figure

3.6.1 Permeability changes

A change in permeability occurs primarily as a result of the reduction in porosity subsequent to compaction. Some of the theoretical relationships that have been proposed are:-

i) Kozeny-Carmam equation, $K = \lambda \frac{\phi^3}{(1-\phi)^2 S^2}$

where ϕ = porosity

ii) Terzaghi (1925); $K = \lambda(e - 0.15)^3(1 + e)$.

iii) Nishida and Nakagawa (1969); $\log_{10}K=[e/(0101PI+0.05)] - 10$

where e is the void ratio,

K is the permeability,

λ is a constant,

PI is the plasticity index.

and S is the specific surface area.

Relationships (i) and (ii) are principally for spherical particles and therefore fall short when considering shales. Furthermore, the shale permeability is susceptible to changes in the concentration of the electrolyte of the permeant. Interstitial solutions having high salt concentrations have high permeabilities and vice versa.

Permeability is also directionally controlled by virtue of the anisotropic shape of the clay minerals. The development of an oriented fabric consequent to burial induces an anisotropy of permeability with the permeability in the horizontal direction being greater than the vertical permeability.

At any given void ratio the coefficient of permeability is progressively less from Kaolinite to Illite to Smectite and is the result of reduction in size of the individual flow channels

and an increase in the tortuosity of the flow path (Mesri and Olsen, 1971).

Fluid flow through compacted clay and shale does not generally obey Darcy's law (Olsen 1966). Apart from the hydraulic conductivity of the fluid, various electrokinetic pressures like electroosmosis, ion filtration are initiated upon the commencement of flow.

3.6.2 Changes in strength properties

The term 'strength' of a sediment or rock possesses different meanings depending on the context of its usage. The ultimate strength of a consolidated rock is defined as the stress (compressive or tensile, as the case may be) at the time of sudden failure. In unconsolidated sediments, the strength or 'bearing capacity' is governed by the permissible deformation. Shear strength, on the other hand, is directly dependent on the magnitude of the normal stress. These are further influenced by the pore water pressure. It is a rule rather than an exception that all such properties increase with increasing bulk density or in other words with increasing compaction. There is , however, a growing concern over the directionality of such soil properties.

3.6.3 Directional properties

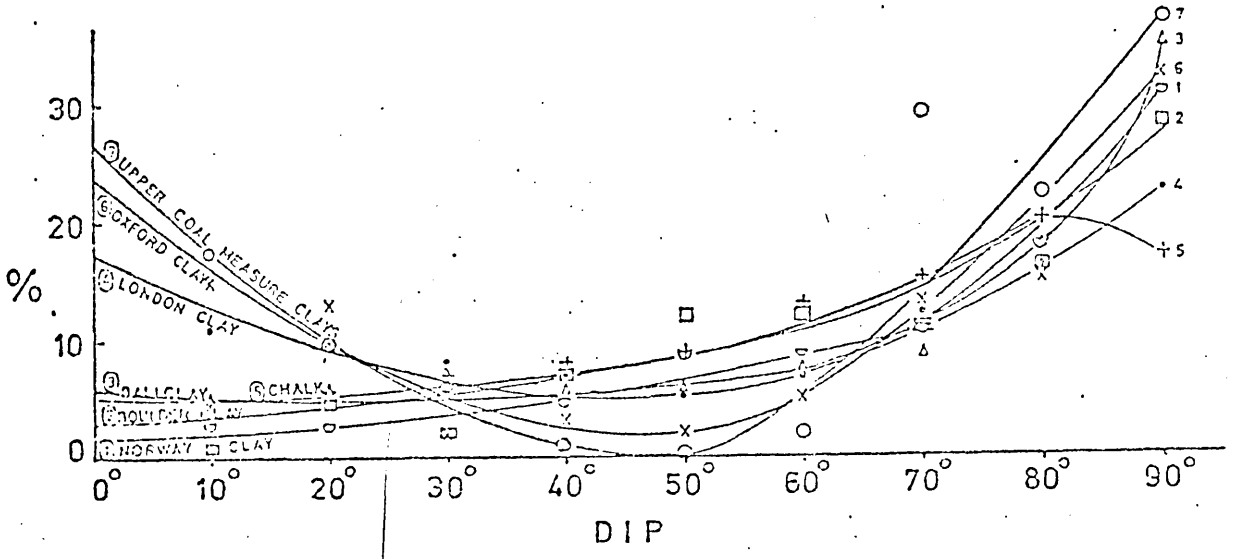
It has been customary to associate such directional variations with the anisotropic fabric. Mitchell (1970), however,

noticed anisotropy in the yield curve for Leda clay. Since Leda clay has been shown to be of a generally random particle orientation, he suspects that the anisotropy is due to a directional preference of cementation bonding.

Laboratory studies have shown that directional variation in velocity of wave propagation does occur in oriented clays (Franklin and Mattson, 1972). The anisotropy of seismic velocity is probably further accentuated by the presence of open joints, etc. The enhanced velocity in the horizontal direction over that of the vertical direction can be a result of horizontal open fractures that may result from a stress release process like erosion of overburden.

The statistical study of fissure distribution in sediment by Saldivar Sali (1973) adds fresh evidence to the relationship between macrofabric and burial-exhumation (overconsolidation)process. Figure 3.25 illustrates his observations of the dependence of the low angled fissures to the overconsolidation ratio, suggesting the influence of the microfabric on the origin of these fissures.

There appear to be two schools of thought as to the physical basis and extent of strength anisotropy in cohesive soils. Lafeber (1969), Ingles and Lee (1971), Barden (1971) have associated strength anisotropy with particle orientation.



Symbol	Sedimentary Deposit	Depth of eroded overburden (m)
o 1	Norway Clay	0
□ 2	Boulder Clay	?
△ 3	Bovey ballclay	32
• 4	London Clay	151
+ 5	Lower Chalk	126
× 6	Lower Oxford Clay	335
o 7	Upper Coal Measure Clays	>751

FIGURE 3.25 Frequency distribution of fissures with varying angles of dip for sediments of different overconsolidation ratio. (after Saldivar Sali, 1974)

Most of the geologic formations have anisotropic stress conditions in situ in as much as Ko - the coefficient of horizontal earth pressure at rest (defined as the ratio of horizontal stress to vertical stress - is generally not equal to unity. A typical variation of Ko with overconsolidation ratio and plasticity index is as shown in figure 3.26 (Lambe and Whitman, 1969). As such most clays not only exhibit anisotropy in fabric but also experience anisotropy in in situ stress conditions. Hansen and Gibson (1949), Schmertmann (1966), Bjerrum and Kenney (1967), and De Lory and Lai (1971) have associated strength anisotropy with anisotropy in in situ stress conditions.

Bishop (1966), Lo (1966), Duncan and Seed (1966) and Skempton and Hutchinson (1969) believe that both effects may contribute to measured anisotropy in in situ and one-dimensionally consolidated soils. Table 3.V is an attempt to collate some published values of anisotropy and relate them to burial.

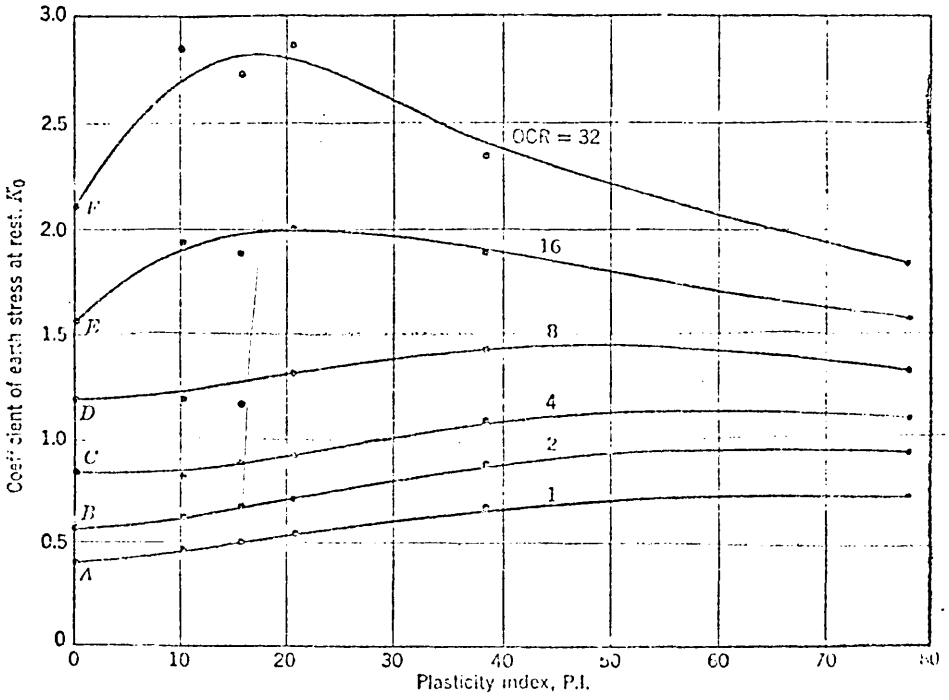


FIGURE 3.26 Coefficient of Earth Pressure at rest as function of overconsolidation ratio and plasticity index

(from Lambe and Whitman, 1969)

Property	Parameters in Anisotropy Ratio	Numerical Value	Clay Type	Reference
Preferred Orientation	Birefringence ratio	0.41 - 0.44	London Clay (Herne Bay)	Tchalenko et al (1972)
	Birefringence ratio	0.30 - 0.50	Oxford Clay	Jackson (1972)
	Birefringence ratio		Lias Clay	
	Birefringence ratio	$\leqslant$ 0.33	Kaolin (remoulded)	Tchalenko (1967)
	Xrd: (002)I/020(K+I)	0.36	London Clay	Tchalenko et al (1972)
	Xrd: $\frac{(001)V}{(001)V+(001)H}$	0.11 - 0.26	Oxford Clay	Jackson (1972)
Drained Shear Strength	$\frac{C'//}{C'l}$	$\leq$1.00	Blue London Clay o/c	Bishop Webb & Lewin (1965)
		$\leq$1.00	Kaolin	Duncan and Seed (1966)
	$\frac{\tan\phi'//}{\tan\phi'l}$	1.04	Blue London Clay n/c	Bishop Webb & Lewin (1965)
		1.00	Blue London Clay o/c	Bishop Webb & Lewin (1965)
		1.00	Kaolin	Duncan and Seed (1966)
Undrained Shear Strength	$\frac{Cv//}{Cvl}$	1.46	Blue London Clay o/c	Bishop (1966)
		0.89	Kaolin O.C.R. = 1	Sankaran & Bhaskaran (1972)
		0.90	Kaolin O.C.R. = 5	Sankaran & Bhaskaran (1972)
		0.92	Kaolin O.C.R. = 10	Sankaran & Bhaskaran (1972)
		1.03	Kaolin O.C.R. = 20	Sankaran & Bhaskaran (1972)
		1.12	Kaolin O.C.R.=heavy	Sankaran & Bhaskaran (1972)
One-dimensional Consolidation	$\frac{Cv//}{Cvl}$	1.0 to 4.5	London Clay	Ward, Samuels & Butler (1951)
		1.0 to 3.0	Kaolin	Tchalenko (1967)
Permeability	$\frac{K//}{Kl}$	2.0	London Clay	Webb (1966)
		1.3 - 1.7	Kaolin	Olsen (1967)
		0.9 - 4.0	Boston Blue Clay	Olsen (1962)
P Wave Velocity	$\frac{Vel//}{Vell}$	1.34	Kaolin (100 lb/in^2)	Franklin & Mattson (1972)
		1.71	Kaolin (240 lb/in^2)	Franklin & Mattson (1972)
		1.90	Kaolin (400 lb/in^2)	Franklin & Mattson (1972)

TABLE 3 V

Some published anisotropy in clays

CHAPTER FOUR Mechanics of Compaction

4.1	Introduction	161
4.2	Mechanical analogues for rheology of clay	162
4.3	Terzaghi theory of one-dimensional analysis	168
	4,3.1 One-dimensional consolidation equation	172
4.4	Critical review of Terzaghi theory	173
4.5	Conventional laboratory consolidation	175
4.6	Constant rate of strain consolidation	180
4.7	Constant rate of loading consolidation	183
	4.7.1 Slow rate of loading	183
	4.7.2 Rapid rate of loading	185
4.8	Computer simulation of geological burial	192

CHAPTER FOUR

MECHANICS OF CONSOLIDATION

4.1 INTRODUCTION

It is intended to outline in this chapter some of the relevant mechanics of the consolidation process. The different mechanical models, often referred to as rheological models, used in describing the deformation-time behaviour of sediments under stress, are outlined. Such models have been developed further to accommodate the effects of deep geological burial.

Terzaghi's theory of consolidation of a saturated clay is well established in soil mechanics. The geological application of this theory to the consolidation of fine grained clastic sediments was first elucidated by Hubbert and Rubey (1959). The Terzaghi theory is reviewed briefly in this chapter in the light of other current theories.

A simplified scheme of computation is proposed in order to obtain the compaction parameters from the analysis of observations made during the laboratory consolidation of a clay subjected to a linear rate of increase of axial loading.

The results of a computer simulation study of geological compaction (Smith, 1973) of shale is described briefly in context with the rest of the chapter.

4.2 MECHANICAL ANALOGUES FOR RHEOLOGY OF CLAYS

The simple spring water model of the Hookean type forms a basic analogy and a convenient method to describe the consolidation process. The elastic response of the clay structure is represented by a spring of the appropriate stiffness. The size of the flow ports simulate to an approximate degree the viscous retardation effects (figure 4.1a). With reference to the mechanical model in figure 4.1a, when the value V in the flow port is closed and an external pressure P is imposed on the piston, this entire pressure, P, is borne by an instantaneous build up of the fluid pressure to P, measurable on the gauge, M. When the valve V is open at time $t = t_o$, the load is gradually transferred from the water to the spring (figures 4.1a, 4.1a2, 4.1a3). Associated with the dissipation of the fluid pressure, a measurable settlement occurs in the system. The degree of consolidation, U, at a time, t, is defined as the ratio x_t/x_∞ where x_t is the current settlement and x_∞ is thus the ultimate settlement.

Figure 4.1b illustrates the equivalent effects in the consolidation process. The time lag in responding to consolidation of the edge and centre points in the clay is emphasised in figures 4.1b2 and 4.1b3.

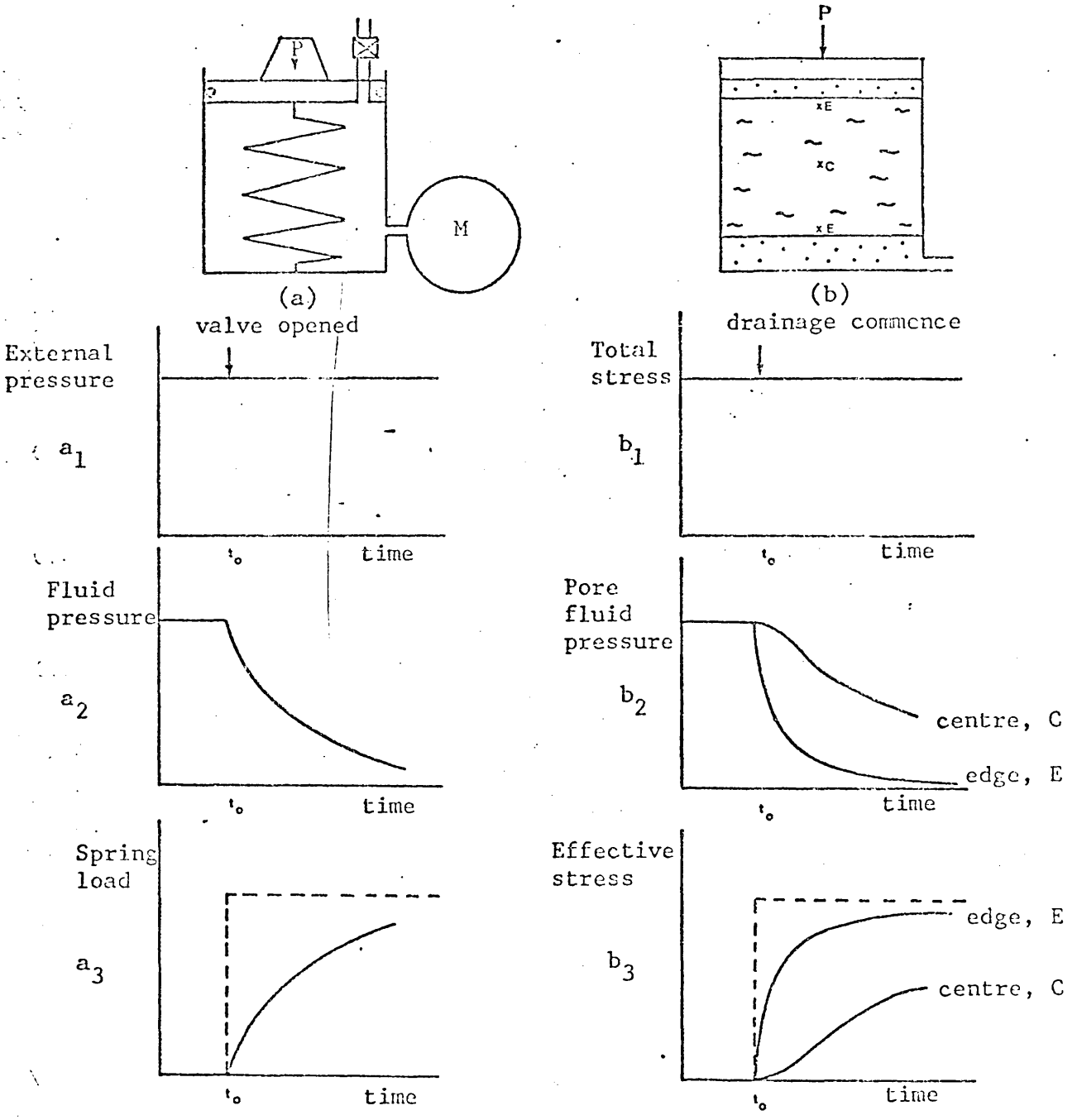


FIGURE 4.1 Load sharing between the soil and the pore fluid during the compaction process:

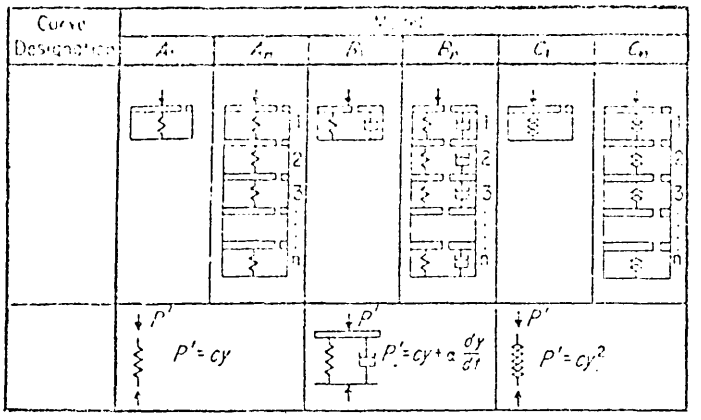
1a) The mechanical analogy.

1b) The soil compaction.

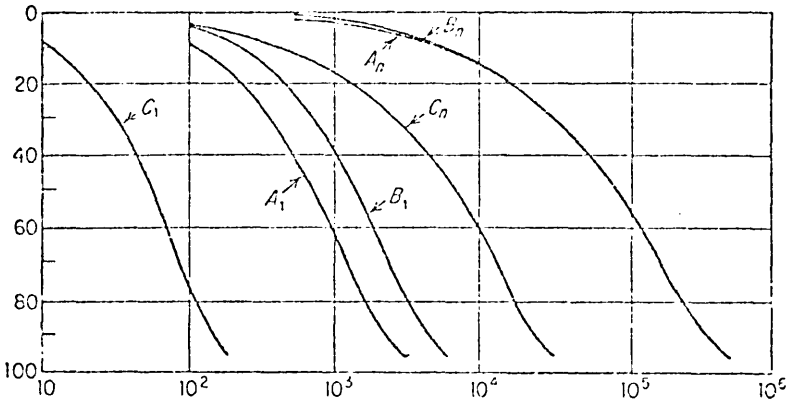
The viscous retardation of the fluid is better represented by means of a dashpot. Accordingly Taylor (1948) suggested a Kelvin type model with a parallel combination of a linear spring and a dashpot (see model B1 in figure 4.2).

Tan (1957), Murayama and Shibata (1959), Gibson and Lo (1961), and Lo (1961) have since modified the Taylor model to combinations of linear springs, dashpots and sliders (see figure 4.3). In all such models, when the fluid pressure is completely dissipated a cessation of the settlement is suggested. This corresponds to the concept of 'primary consolidation'. Figure 4.2 illustrates the comparison of pore fluid pressure dissipation rates expressed in terms of degree of consolidation for different rheological models (Leonards and Altschaeffl, 1964). It also shows the effect of sample thickness in comparing the pore pressure dissipation rates for single and multiple units of the basic model.

Soon after Terzaghi formulated his theory of consolidation various research workers observed that the clay soil skeleton exhibited the phenomenon of creep under constant effective stress - 'secondary consolidation' (see figure 4.4). Speculation followed on this matter as to the nature of this creep and it is considered to be a result of the increase in rigidity of the skeleton with time, which results in a change in its consistency.



(a)



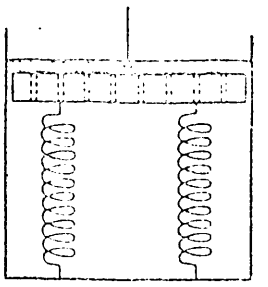
(b)

FIGURE 4.2 a) Some basic rheological models

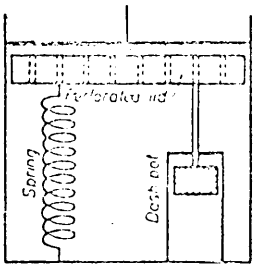
b) Degree of consolidation predicted from the rheological models

(after Leonards and Altschaeffl, 1964)

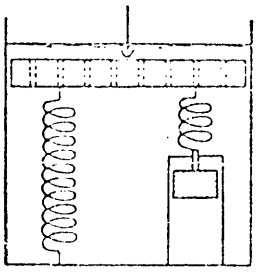
After Biot, 1935.



After Taylor, 1942.



After Tan, 1957.



After Murayama & Shibata, 1959

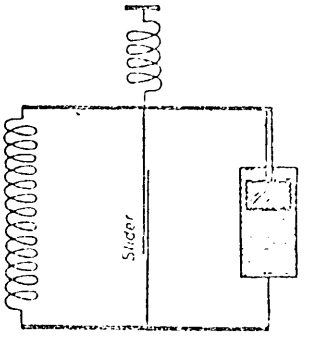


Figure 4.3 Rheological models of soil skeleton.

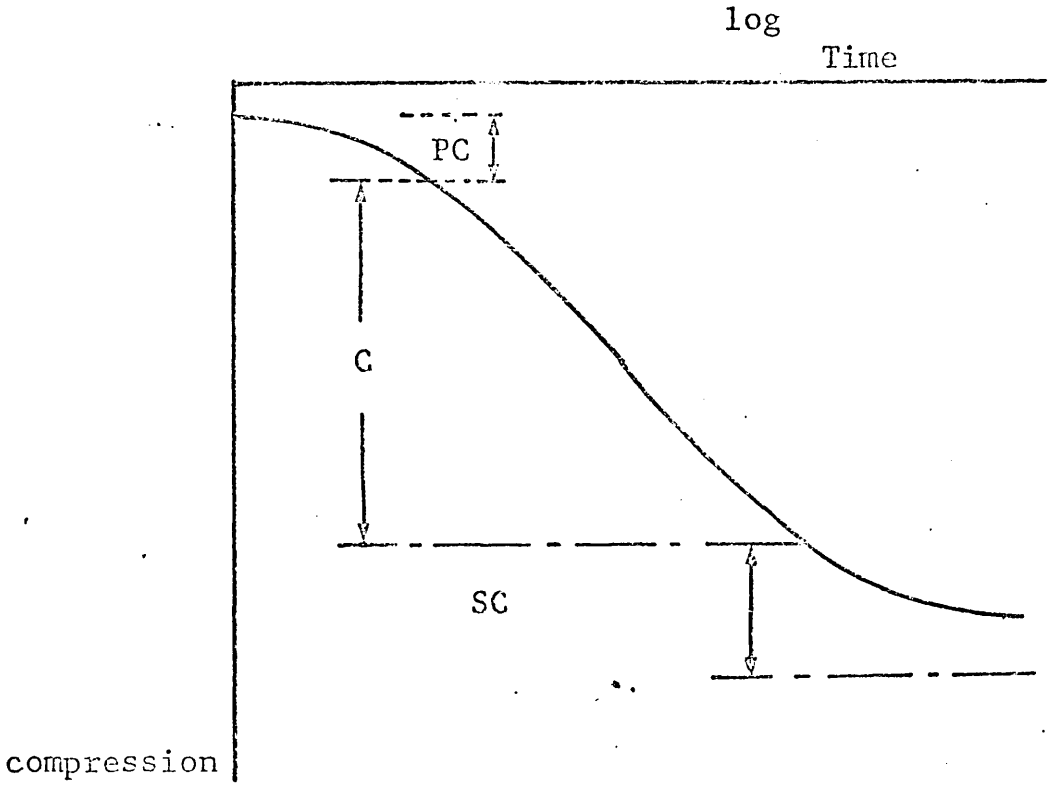


FIGURE 4.4 Time deformation curve for a clay;

Abbreviation	Process	Probable Cause
PC	Primary Consolidation	Particle readjustment and extrusion of air from soil voids of incompletely saturated soils
C	Consolidation	Extrusion of water in soil voids and particle reorientation
SC	Secondary Consolidation	Soil Creep (?)

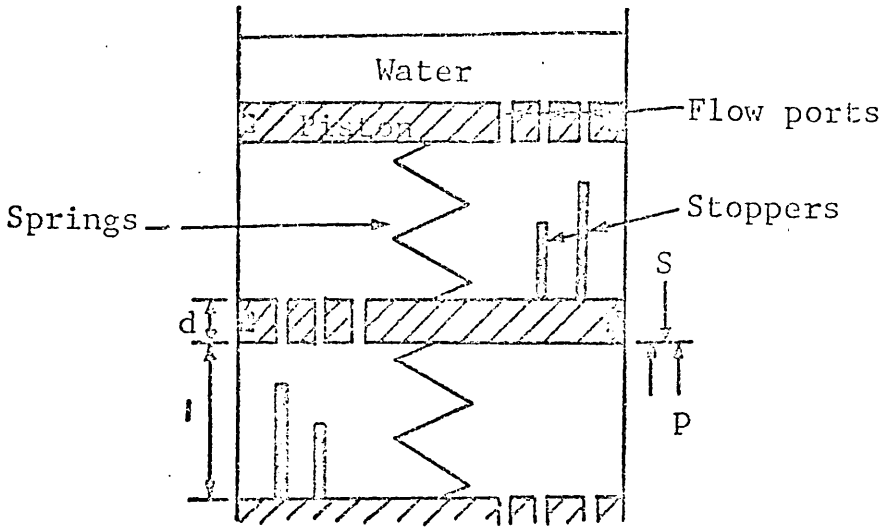
In all the hypothesised compaction models described earlier in Chapter Two, there is a unanimous reference to a distinct 'dewatering stage', and in the subsequent stages the expulsion of pore fluid is reduced. Smith (1971) proposed a mechanical model (figure 4.5a) in which he introduced to the Taylor's rheological model, a series of 'stoppers' which are made operative during the discrete stages of the process. This accounts for the changes in permeability of the clay soil with decrease in void ratio.

With deeper burial, the effects of a geothermal environment become significant. A temperature increase has the dual effect of both expanding the pore fluid and reducing its viscosity, which results in an enhanced permeability. Figure 4.5b is thus a mechanical model proposed to account for all possible stages of the process of geological burial.

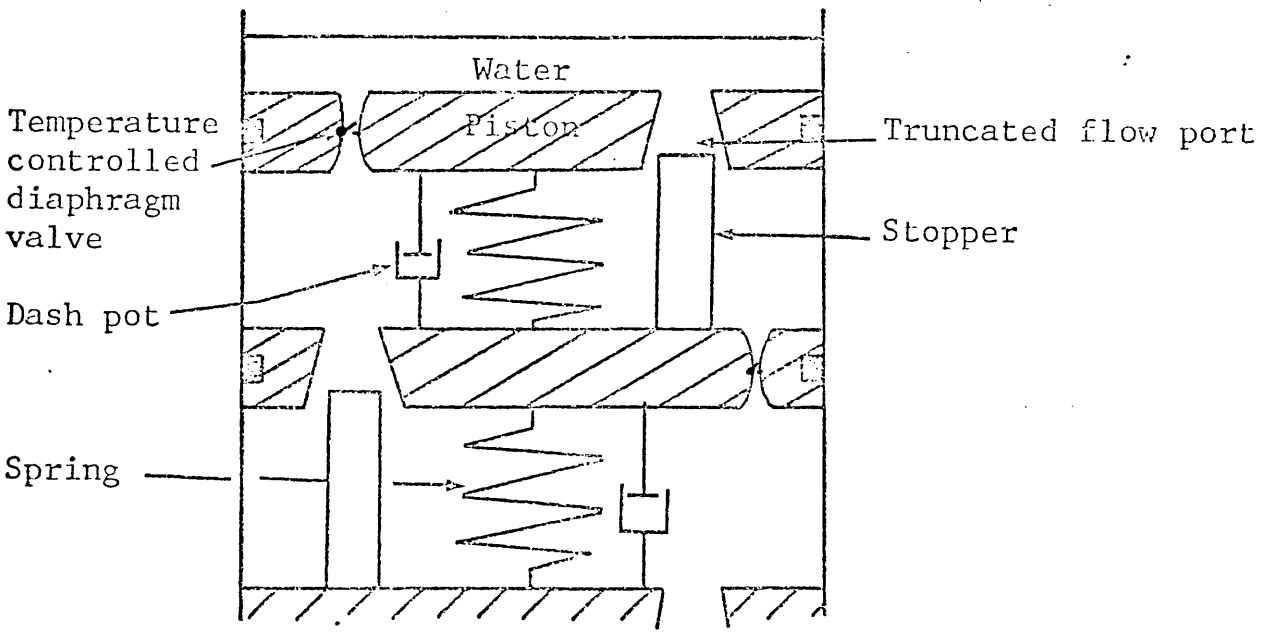
The truncated opening (P) of the flow ports suggests a more gradual change in permeability. The diaphragm valve (T) in the piston is a temperature-controlled flow port, and therefore an increase in temperature of the system will induce further compaction.

4.3 TERZAGHI THEORY OF ONE-DIMENSIONAL CONSOLIDATION

In the following analyses the reader is referred to figure 4.6a which shows a soil medium of thickness h_o. The



(a)



(b)

FIGURE 4.5 Rheological models for deep burial
a) After Smith, 1973.
b) Proposed model.

soil is allowed to drain from both ends so that the excess pore water pressure, Δu, is zero at its boundaries.

The mid plane, $x = 0$, of the medium is considered as the datum plane. The layer is subjected to a variable load $\sigma(t)$ and consolidation results.

Terzaghi (1923) in his simple theory of one-dimensional consolidation adopted the following assumptions:-

(a) the soil is homogeneous and isotropic;

$$K_x = K_y = K_z, \text{ etc.}$$

(b) the soil is completely saturated;

$$u_{air} = 0$$

$$e = m.G_s.$$

(c) the grains of soil and water are incompressible;

$$C_s = C_w = \infty.$$

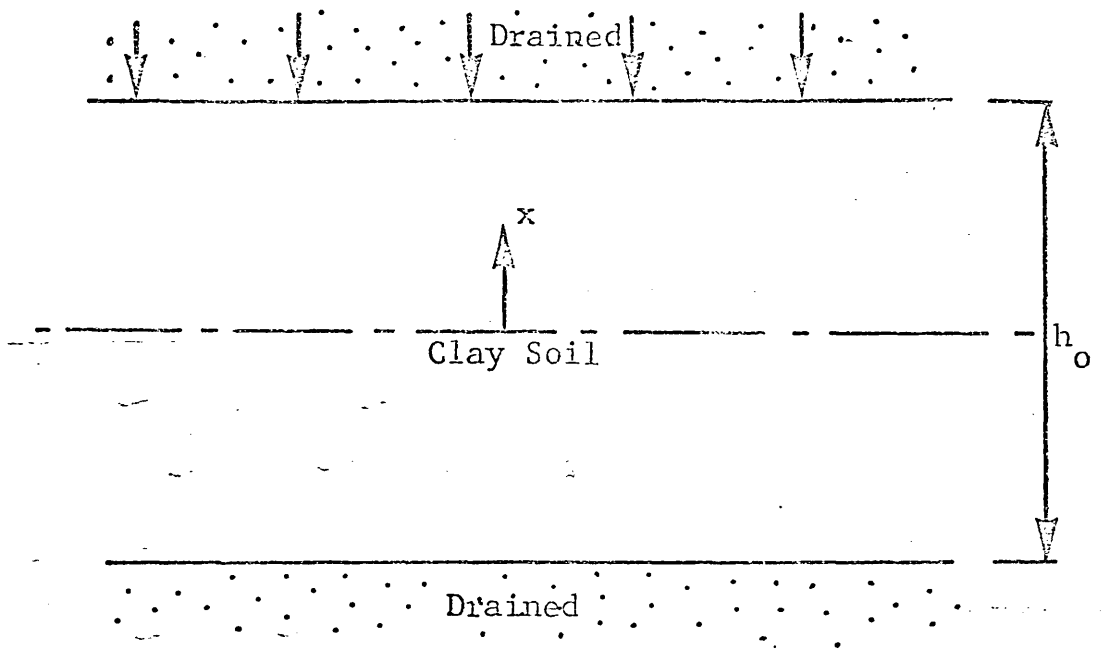
(d) the consolidation is unidirectional;

the flow of pore water and the strains occur in the vertical direction only.

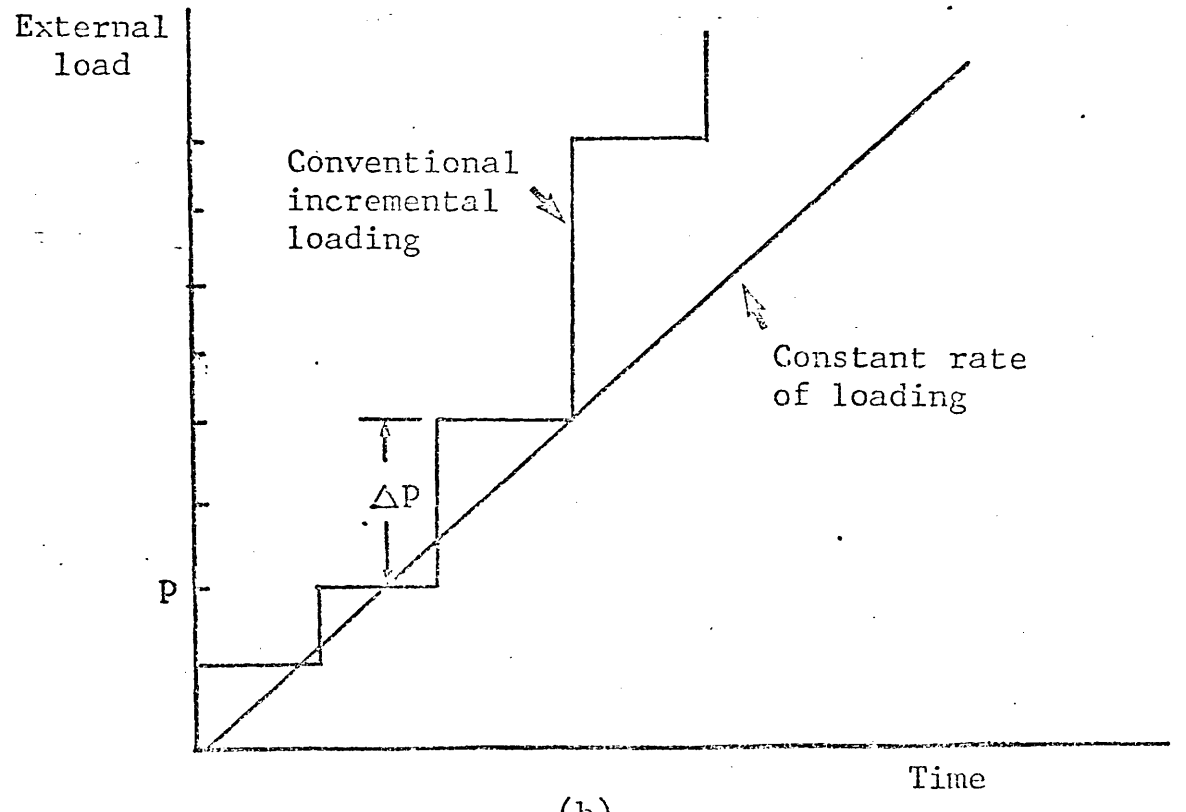
(e) the pore water flow is governed by Darcy's Law;

$$V = K. \frac{\partial u}{\partial x}.$$

(f) Some soil properties, which actually vary with the applied pressure, are assumed constant over the relevant range of effective stress.



(a)



(b)

FIGURE 4.6 a) Schematic diagram of sample drained at both ends.

b) Loading schemes.

e.g. coefficient of permeability, K.

(g) the action of infinitesimal masses can be extended to that of larger representative masses;

(h) the applied stresses are assumed large compared with the self weight stresses in the layer;

(i) the changes in void ratio are linearly dependent on the changes in vertical effective stress;

$$\Delta e = -a_v \Delta \sigma' \qquad (4.1)$$

4.3.1 One-dimensional Consolidation Equation

Appendix B gives the detailed mathematical derivations. The conditions of continuity of the pore fluid flow lead to the equation;

$$\frac{K}{\gamma_w} \frac{\partial^2 u}{\partial x^2} = \frac{1}{1 + e} \cdot \frac{\partial e}{\partial t} \qquad (4.2)$$

Using the assumption (i), equation 4.1 and the concept of effective stress,

$$\sigma' = \sigma - u \qquad (4.3)$$

we obtain $e \simeq -a_v \sigma' = -a_v(\sigma - u)$ (4.4)

Substituting 4.3, equation 4.2 becomes

$$\frac{K}{\gamma_w} \frac{\partial^2 u}{\partial x^2} = \frac{1}{1 + e} \cdot \left[-a_v \frac{\partial(\sigma - u)}{dt} \right]$$

Defining m_v, the coefficient of volume decrease, and C_v, the coefficient of consolidation by the following expressions

$$m_v = -\frac{a_v}{1 + e} \qquad (4.5)$$

and

$$C_v = \frac{K}{m_v \gamma_w} \qquad (4.6)$$

the consolidation equation thus becomes

$$C_v \cdot \frac{\partial^2 u}{\partial x^2} = \frac{\partial u}{\partial t} - \frac{d\sigma(t)}{dt} \qquad (4.7)$$

4.4 A CRITICAL REVIEW OF TERZAGHI THEORY

The most controversial of the assumptions adopted in Terzaghi theory is the validity of Darcy's Law at small hydraulic gradients. According to Hansbo (1960) the rate of dissipation of pore pressure at a given void ratio, would increase with increasing magnitude of consolidating pressure increments. This, however, is contrary to experimental observations; Davis and Raymond (1965) showed that large pressure increments produced slower rates of dissipation of pore pressure. But Matyas (1963) considered this departure was a result of incomplete saturation, while Olsen (1966) developed a technique minimising apparatus contamination and concluded that Darcy's Law was valid for all hydraulic gradients. The available evidence, however, is convincing that the load increment ratio has a marked influence on the consolidation (see figure 4.7, after Leonards, 1962).

When the applied incremental loads are small, the ability of the individual particles to readjust to positions of equilibrium must control to a great extent the resultant deformation.

Gibson et al (1967) adopted a more rigorous analysis in considering the relative velocity between the pore fluid and the soil skeleton to be proportional to the excess pore fluid pressure gradient (Darcy's Law).

Many of the other basic assumptions of Terzaghi, such as assuming a linear void ratio pressure relationship, have been modified by different workers in deriving theories to treat certain soils whose properties depart significantly from Terzaghi assumptions. The properties of a soil generally vary with depth and such effects of nonhomogeneity have been accounted for in the work of Schiffmann and Gibson (1964), and Raymond (1964). A theory for partially saturated clay and incorporating a compressible pore fluid and a decreasing permeability has been presented by Barden (1965).

Laboratory research has also often pointed to the existence of variations in the coefficients of permeability and compressibility during compaction. Theories for compressible normally consolidated clay, a decreasing coefficient of volume decrease and coefficient of permeability have been presented by

Davis and Raymond (1965), Barden and Berry (1965). Schiffmann (1958) suggested approximate techniques to obtain solutions in such events, and found that a variation of the permeability with changes in the excess pore water pressure led to a dependency of the coefficient of consolidation on the terminal permeabilities. This dependency was logarithmic in character and as a result it can lead to serious errors if mean permeabilities are used when large permeability changes do occur.

Mikasa (1965) and Gibson (1966) have considered the consolidation with large strains. All such considerations led to non-linear partial differential equations whose rigorous solutions are often tedious. Numerical methods of solution and the use of simplifying second order assumptions have often proved a suitable recourse.

4.5 CONVENTIONAL LABORATORY CONSOLIDATION (STEP LOADING)

In the conventional standard consolidation test adopted by engineers, a laterally confined clay specimen is loaded incrementally (see figure 4.6b), while observations of the change in thickness of the specimen with time are made after each increment of loading (ΔP). Figure 4.3 illustrated the three components of the characteristic compaction response of a clay specimen after such an instantaneous loading increment.

A load increment ratio ($\Delta P/P$) of 1 is recommended with a time interval of twenty-four hours between consecutive steps of loading (see figure 4.7). The significance of a standard choice of the time interval between loading increments is shown in figure 4.8. It also shows that it is possible to obtain different values for the preconsolidation load depending upon the choice of the time between the stages of loading.

The dissipation of the pore fluid pressure within the specimen, following any single loading stage, is also governed by the equation 4.7 with $\frac{\partial\sigma(t)}{dt}$ being zero, i.e.

$$C_v \frac{\partial^2 u}{\partial a^2} = \frac{\partial u}{\partial t}$$

and it is assumed that C_v remains a constant during this dissipation process.

A specimen, of thickness '2H', is loaded with drainage of pore fluid being permitted from one end only, the pore fluid pressure variation within the specimen is given by the expression

$$u = \sum_{n=1}^{n=\infty} \frac{2U_o}{n\pi} (1 - \text{Cos } n\pi)(\text{Sin } \frac{n\pi x}{2H})\ e^{-(n^2\pi^2/4)T} \qquad (4.8)$$

Figure 4.9 illustrates the expansion of the above expression diagrammatically, showing the variation of pore fluid pressure as a function of the space parameter x/H and time factor, T, defined as $C_v t/H^2$.

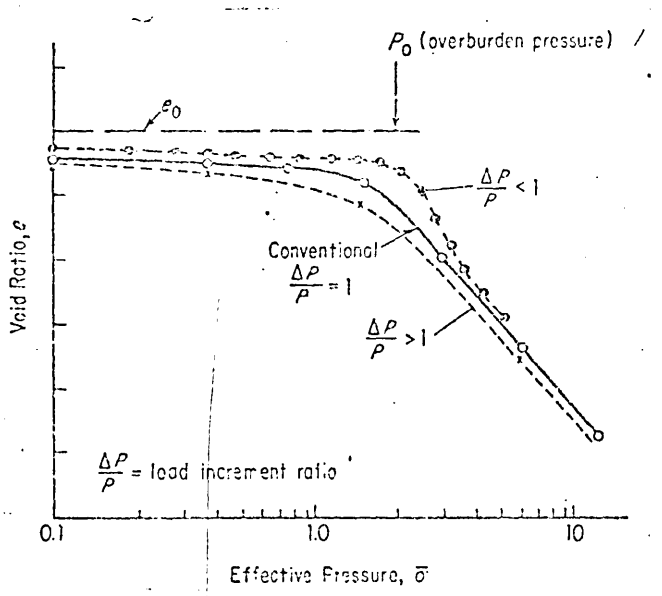


FIGURE 4.7 Effect of load increment ratio, (P/P) on e-log p curves

(after Leonards, 1962)

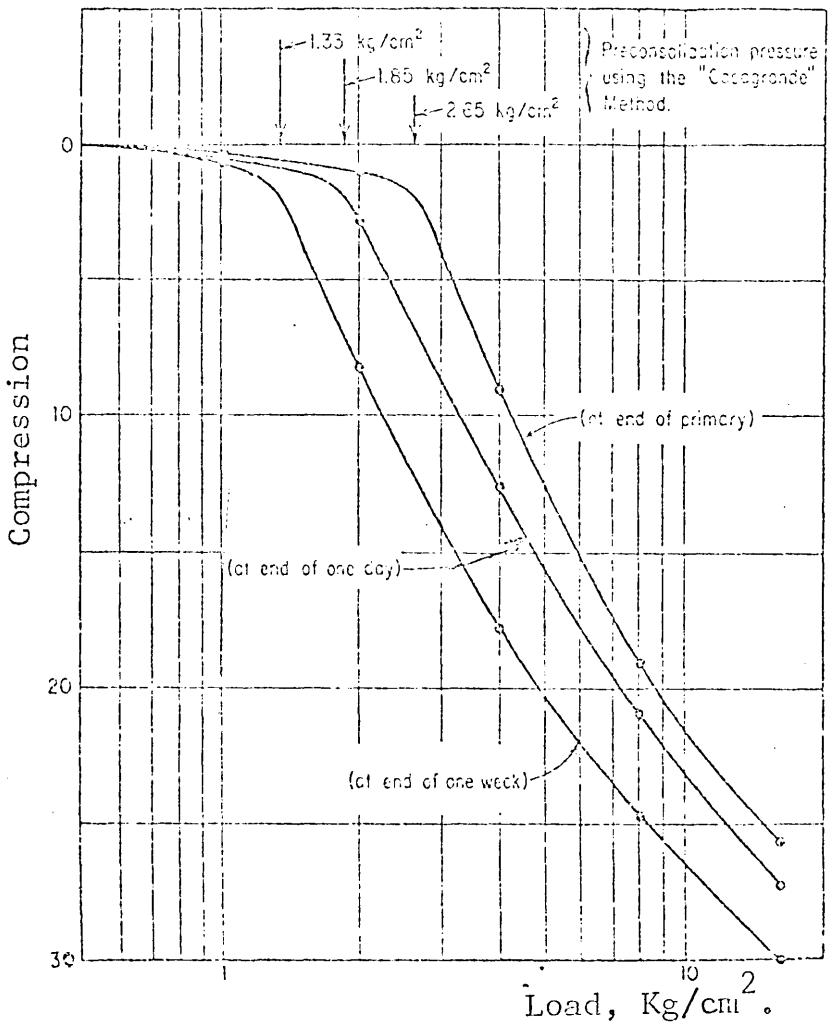


FIGURE 4.8 Compression-Log Pressure curves for normal and long term incremental loading

(after Crawford, 1964).

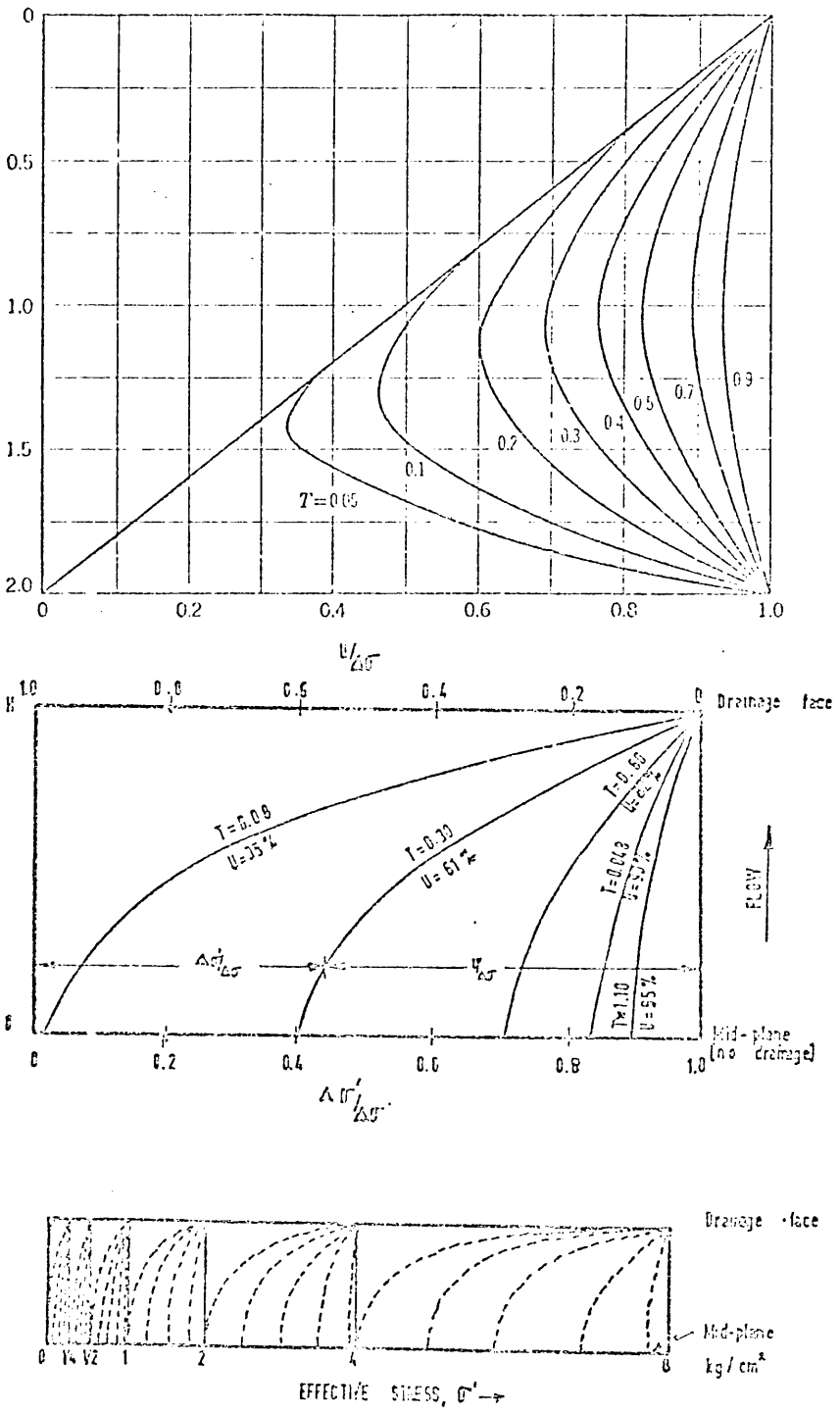


FIGURE 4.9 Pore fluid pressure variation within consolidating specimens:

a) 2H thick, one end drainage.
b) 2H thick, both ends drainage.
c) Variations with stress increments.

(after Lambe and Whitman, 1972)

4.6 CONSTANT RATE OF STRAIN CONSOLIDATION

Smith and Wahls (1969) introduced a more rapid technique of consolidation testing in consolidating cohesive soil at a constant rate of strain. The governing equation for the consolidation can be expressed most conveniently in terms of strains;

$$C_v \frac{\partial^2 \varepsilon}{\partial x^2} = \frac{\partial \varepsilon}{\partial t} \qquad (4.9)$$

Wissa et al (1971) recognised that one of the peculiarities of loading a specimen at a constant rate of strain is that immediately as the piston is set in motion, a transient condition is developed in the soil and steady state conditions are established only after this transient has ceased.

Smith and Wahls (1969) assumed the void ratio at any point and time to be restricted to a linear function of space and time of the form,

$$e(x,t) = e_o - rt\left[1 - \frac{b}{r}\left(\frac{x - 0.5H}{H}\right)\right]$$

where b is a constant depending on the variation in void ratio with depth and time, and r is the rate of decrease of the average void ratio. Thus the dimensionless ratio b/r indicates the variation of void ratio with depth and can assume any practicable value between 0 and 2.

Crawford (1964) conducted similar tests and observed that for slow rates of strain, the maximum excess pore pressure measured was only 5 percent of the applied load. It reached values of 15 percent with faster rates of strain of up to 0.133 percent per minute. Further observations by Wahls and Degodoy (1965) showed that with rates up to 0.23 percent per minute, a 75 percent response of the applied pressure was apparent.

In all such tests the properties of the clay are determined from plots of the effective pressure against void ratio. The average effective pressure was obtained by subtracting half the excess pore pressure at the base from the total vertical pressure (see equation 4.12 in section 4.7.1). Smith and Wahls (1969) drew attention to this oversimplifying assumption, which limited the use of this method to instances when the excess pore fluid pressure (ΔV) at the base of the specimen did not exceed 5 percent of the applied pressure.

From the analysis of the e-log p curves so produced, Crawford observed that the compressibility decreased with increasing rates of strain. Wahl and Degodoy, however, observed the reverse trend, viz., the compressibility increases with increasing rates of strain.

The data obtained from a constant rate of strain consolidation test are:

i) the average strain rate,

ii) pore pressure at the top and bottom of sample,

iii) total stress at the top of the sample.

Wissa et al (1971) showed that once the transients have been dissipated, the strain at a point in the specimen is given by:

$$\varepsilon(z,t) = rt + \frac{rH^2}{C_v}\left\{\frac{1}{6}\left[3\left(\frac{Z}{H}\right)^2 - 6\frac{Z}{H} + 2\right]\right\}$$

Both cases, cf. linear and non-linear soil, had been considered and the respective equations for each case are given below:

FUNCTION	EQUATION	
	LINEAR CASE	NON-LINEAR CASE
Average strain ε_{av}	rt	rt
Average effective stress, $\bar{\sigma}_v$	$\sigma_v - \frac{2}{3}\Delta u$	$(\sigma_v^3 - 2\sigma_v^2\Delta u + \sigma_v\Delta u^2)^{\frac{1}{3}}$
Coefficient of consolidation C_v	$\frac{rH^2}{2.\Delta u.m_v}$	$\frac{H^2 \log(\sigma v_2/\sigma v_1)}{2\Delta t \log(1-(\Delta u/\sigma v))}$
Coefficient of volume decrease M_v	$r(\Delta t/\Delta\sigma_v)$	$r(\Delta t/\Delta\sigma_v)$

4.7 CONSTANT RATE OF LOADING CONSOLIDATION

A stress controlled consolidation would require the solution of the consolidation equation with the appropriate boundary conditions. Geological burial mechanically corresponds to consolidation at a very slow rate of loading, dependent on the rate of deposition of the fresh sediment. In such an event the excess pore pressure developed at the base (Δu) is small and it is justifiable to assume a linear pore fluid pressure distribution across the specimen. The analysis in such a case is outlined next.

4.7.1 Case I - Slow rates of loading

With reference to figure 4.10, illustrating a specimen drained at one end only and being loaded very slowly, the pore fluid pressure at any point is a corresponding proportion of the pore fluid pressure at the undrained end (Δu) as in

$$U(x,t) = \Delta u(t).\frac{x}{H} \qquad (4.10)$$

Therefore the effective stress (p_1) at that point is

$$p_1 = P_1(t) - u(x,t)$$

Thus the average effective stress across the specimen is obtained from the expression

$$\bar{p}_1 = \frac{1}{H}\int_0^H p_1 \, dH \qquad (4.11)$$

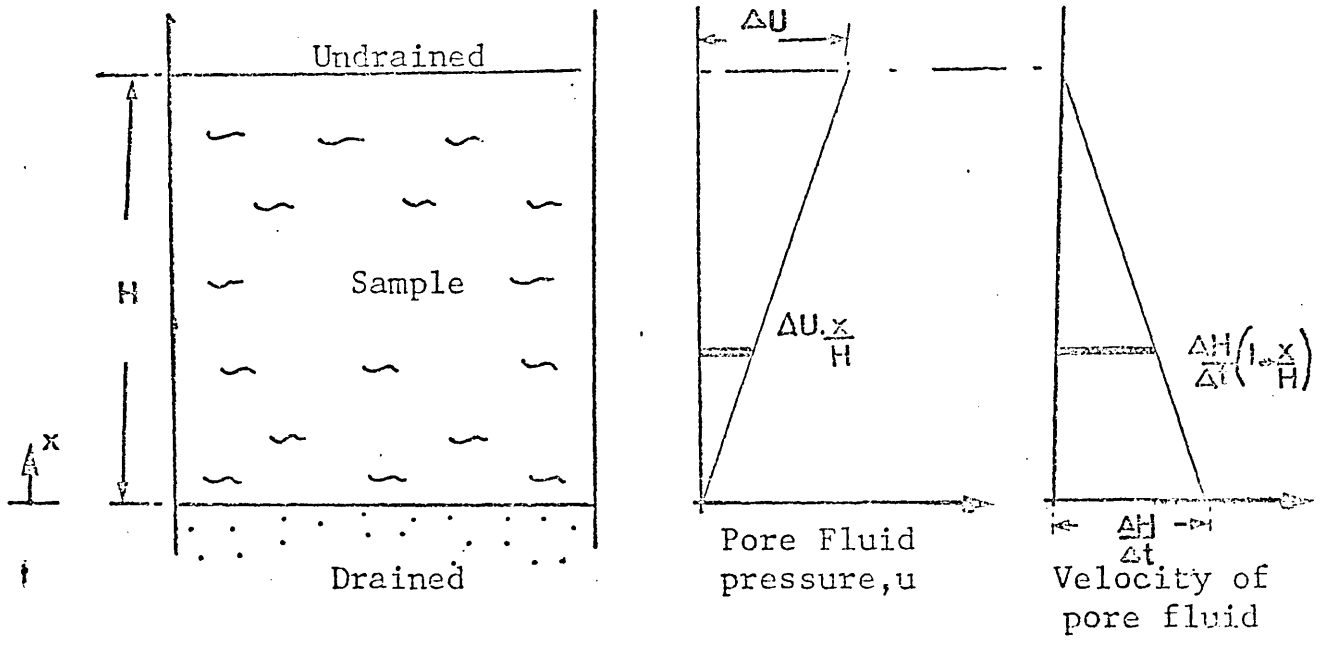


FIGURE 4.10 Pressure and velocity of pore fluid in specimens loaded slowly;

(a) Drainage conditions on sample

(b) Pore fluid pressure distribution assuming very slow rate of loading

(c) The distribution of the velocity of the pore fluid across the sample for elastic condition.

which reduces to

$$\bar{P}_1 = P_1(t) - \frac{\Delta u(t)}{2} \qquad (4.12)$$

If ΔH be the compaction of the specimen during a small interval of time Δt, the escaping pore fluid thereby has a terminal velocity of $\frac{\Delta H}{\Delta t}$ at the drained end and was at rest at the undrained end (see figure 4.10c).

Thus the velocity of fluid at the element = $(1 - \frac{x}{H}) \cdot \frac{\Delta H}{\Delta t}$.

Using Darcy's Law to the element

$$\frac{\Delta H}{\Delta t} \cdot (1 - \frac{x}{H}) = K \cdot \frac{du}{dx}$$

where K is the coefficient of permeability. Integrating the above equation, it reduces to the convenient form

$$K = \frac{1}{2} \cdot \frac{\Delta H}{\Delta t} \cdot \frac{H}{\Delta u(t)} \qquad (4.13)$$

4.7.2 Case II - Rapid rates of loading

Contrary to conditions in case I, when rapid rates of loading are used an associated build up of an excessive pore fluid pressure is inevitable. The corresponding distribution of the pore fluid pressure within the specimen is given by the solution of the partial differential equation

$$C_v \cdot \frac{\partial^2 u}{\partial x^2} + r = \frac{\partial u}{\partial t} \qquad (4.14)$$

where r = rate of loading.

and the boundary values for the above equation are

a) $u(0,t) = 0$; for zero pore fluid pressure at the drained end for all values of time t.

b) $u(H,t) = \Delta u$; the pore fluid pressure at the undrained end equivalent to that at midplane of a specimen 2H thick drained at both ends.

c) $u(2H,t) = 0$; the pore fluid pressure at the other drained end is zero.

The mathematical solution for the one- and three-dimensional consolidation with time-dependent loading has been outlined by Schiffmann (1958).

The Fourier series solution (see Appendix C) of equation 4.14 is

$$u(x,t) = \frac{16U_o}{\pi^3 T_o} \sum_{n=1,55}^{\infty} \frac{1}{n^3} \operatorname{Sin} \frac{n\pi x}{2H} \left\{1-\exp\left[-\left(\frac{n^2\pi^2}{4}\right)T\right]\right\} \quad (4.15)$$

U_o is the pore fluid pressure at an arbitrary time factor T_o on the loading curve. Thus the ratio U_o/T_o is the rate of loading. In order to obtain a simple solution it is assumed that the rate of the axial loading P_1/T, is equal to that of the pore fluid pressure.

Thus the equation 4.15 becomes

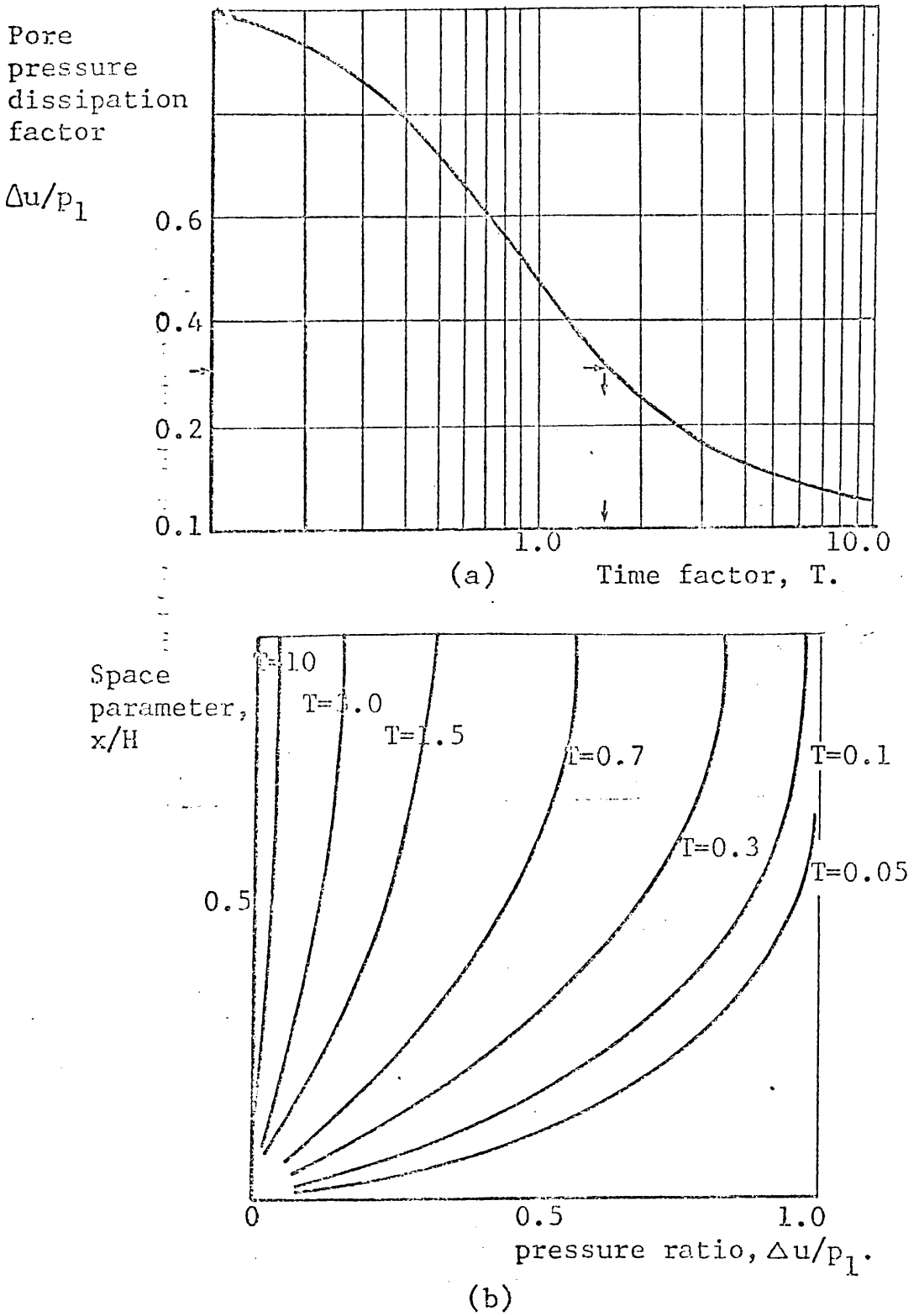


FIGURE 4.11 a) Theoretical relationship between pore pressure dissipation factor and time factor.

b) Pore fluid pressure distribution within the sample as a function of the space parameter and the time factor.

$$\frac{U(x,t)}{P_1(t)} = \frac{16}{\pi^3 T} \sum_{n=1,3,5}^{\infty} \frac{1}{n^3} \sin\frac{n\pi x}{2H} \left\{1 - \exp\left[-\left(\frac{n^2\pi^2}{4}\right)T\right]\right\} \quad (4.16)$$

During a consolidation test of a clay sample in the High Pressure Temperature Consolidation apparatus (described in Chapter Five), simultaneous observations of the following parameters are made periodically:-

i) Axial Pressure $P_1(t)$.

ii) Pore fluid pressure difference across the specimen (Δu).

iii) Change in thickness of specimen (ΔH).

Substitution of the conditions (b) in equation 4.16 gives an expression for "pore fluid pressure dissipation factor" which is defined as the ratio of the pore fluid pressure difference (Δu) across the specimen and the axial load (P_1):

$$\frac{\Delta u(t)}{P_1(t)} = \frac{16}{\pi^3 T} \sum_{m=1,3,5}^{\infty} \frac{1}{(2m+1)^3} \left[1 - \exp\left\{-\frac{(2m+1)^2}{4}.\pi^2.T\right\}\right] \quad (4.17)$$

In the above equation, the pore fluid pressure dissipation factor is clearly a function of the time factor T only. Thus at any stage of the test, for a measured value of $\frac{\Delta u}{P_1}$, the corresponding value of the time factor T can be conveniently determined using a semigraphical technique (see figure 4.11a). Figure 4.11b shows the distribution of the pore fluid pressure across the specimen as a function of the space parameter, $\frac{x}{H}$, and time factor, T.

The average effective stress across the specimen at any instant can now be computed as in case I (equation 4.11) and is

$$\bar{p}_1 = P_1 - \frac{32P_1}{\pi^4 T} \sum_{m=0}^{m=\infty} \frac{1}{(2m+1)^4} \left\{1 - \exp\left[-\frac{(2m+1)^2 \pi^2 T}{4}\right]\right\} \quad (4.18)$$

In order to allow for the variation of the coefficient of consolidation, C_v, with compaction, the technique suggested by Schiffmann (1958) was adopted.

With reference to figure 4.12, it is assumed that C_v varies in a stepwise form as shown. It is noteworthy that the choice of shorter time intervals of $t_i - t_{i-1}$ gives a more accurate and uniform variation. By definition, the time factor T_i is thus represented as a cumulative sum as in

$$T_i = \frac{C_{v1} t_1}{H_1^2} + \frac{C_{v2}(t_2 - t_1)}{H_2^2} + \frac{C_{v3}(t_3 - t_2)}{H_3^2} + \ldots + \frac{C_{vi}(t_i - t_{i-1})}{H_i^2} \quad (4.19)$$

The discrete values of C_v are then obtained systematically in a stepwise manner as

$$C_{v1} = \frac{T_1 \times H^2}{t_1}$$

$$C_{v2} = (T_2 - \frac{C_{v1} t_1}{H_1^2}) \times \frac{H_2^2}{(t_2 - t_1)}$$

$$C_{vi} = \left[T_i - \frac{C_{v1} t_1}{H_1^2} - \frac{C_{v2}(t_2 - t_1)}{H_2^2} \ldots \frac{C_{v(i-1)}(t_{i-2} - t_{i-1})}{H_{i-1}^2}\right] \times \frac{H_i^2}{(t_i - t_{i-1})} \quad (4.20)$$

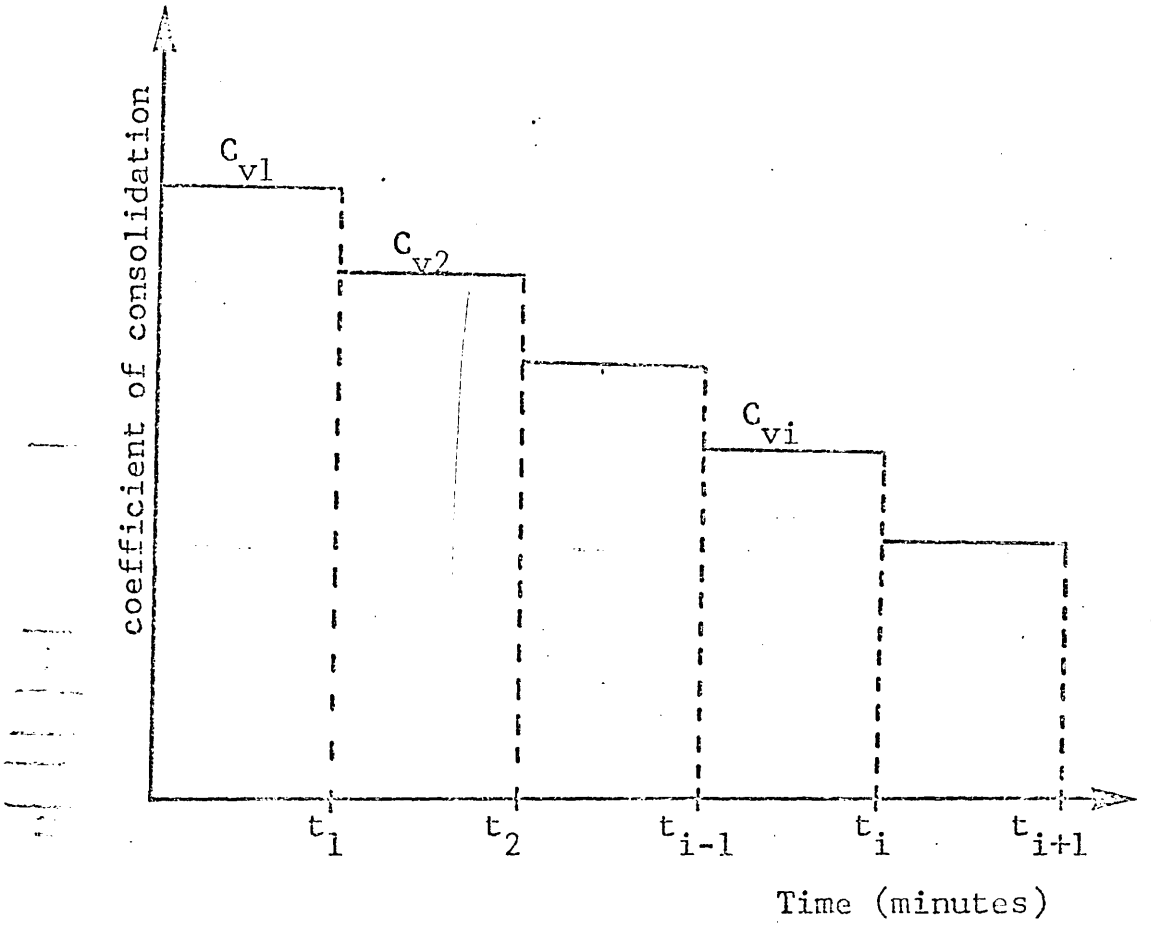


FIGURE 4.12 Assumed variation of the coefficient of consolidation with time.

As described in section 2.6.2, the void ratio at the end of consolidation, e_f, is determined by indirect means from the moisture content of the specimen using the equation,

$$e_f = \frac{\omega \quad G_s}{S} \tag{4.21}$$

where S is the degree of saturation which is determined from the equation:

$$S = \frac{w}{(\gamma_w/\gamma_B)(1+w) - 1/G_s} \tag{4.22}$$

γ_B in the above equation is the bulk density of the specimen at the end of consolidation. The specimens are fully saturated at the end of all consolidation tests and therefore S is invariably one hundred per cent.

The void ratio at any other instant of the test, e_i, is determined by the equation:

$$e_i = (1 + e_f) \frac{(H_i - H_f)}{H_f} + e_f \tag{4.23}$$

The coefficient of volume decrease, M_{vi}, at that instant may be then obtained from:

$$m_{vi} = \frac{1}{(1+e_i)} \frac{(e_i - e_{i+1})}{(p_{1i+1} - p_{1i})} \tag{4.24}$$

The coefficient of permeability, k_i, can therefore be computed as $k = \gamma \times m_{vi} \times C_v$, or using the corrected values of C_v, as:

$$k = \gamma \times m_{vi} \times C_{vi} \tag{4.25}$$

4.8 COMPUTER SIMULATION OF GEOLOGICAL BURIAL

It is considered pertinent to refer here to the work of Smith (1973); a computer study of the dynamics of shale compaction and the evolution of pore fluid pressure. The approach and aim of this study was the reverse of the laboratory study. Here the model assumed the following:

a) Porosity - depth relation Athy (1930)

$$\phi_N = \phi_T e^{-b(T-Z)}$$

adopting the values for the constants ϕ_T=0.48 and b=0.0014 /metre.

b) Permeability - porosity relation (Vasquez in Pirson, 1963)

$$K = h\phi^a/(1-\phi)^c$$

and the values for the constants a = 8, c = 0 and h = 3.99 millidarcy.

c) Dependence of water viscosity on salinity, temperature and pressure (Fabuss and Korosi, 1968).

d) Temperature at sediment water interface is 10°C and the geothermal gradient of 0.03°C/metre.

The equations outlined below are computer programmed to obtain the time dependence of porosity, pressure, water velocity, permeability and allied factors of similar interest within a compacting shale during

i) shale sedimentation,

ii) a time lapse following shale deposition,

iii) the deposition of normally pressures sediments over the shale, and

iv) a time lapse since the deposition of the normally pressured units.

The mathematical derivations of the equations governing shale compaction is somewhat more explicit than the Terzaghi theory, which by virtue of the incorrect derivation of its continuity equation and a misstatement of the Darcy's Law, assumes the rock matrix to be rigid.

Figure 4.13 illustrates the spatial relationships and the coordinate system used by Smith for the following equations. The continuity equations for the pore fluid and the solid matrix take the form

$$\frac{\partial \rho_w V_w \phi}{\partial Z} = - \frac{\partial \rho_w \phi}{\partial t} \qquad (4.21)$$

and

$$\frac{\partial \rho_r V_r (1 - \phi)}{\partial Z} = - \frac{\partial \rho_r (1 - \phi)}{\partial t} \qquad (4.22)$$

where ρ_w, ρ_r are the pore fluid density and the grain density, and

V_w, V_r are the velocities of the pore fluid and grain respectively.

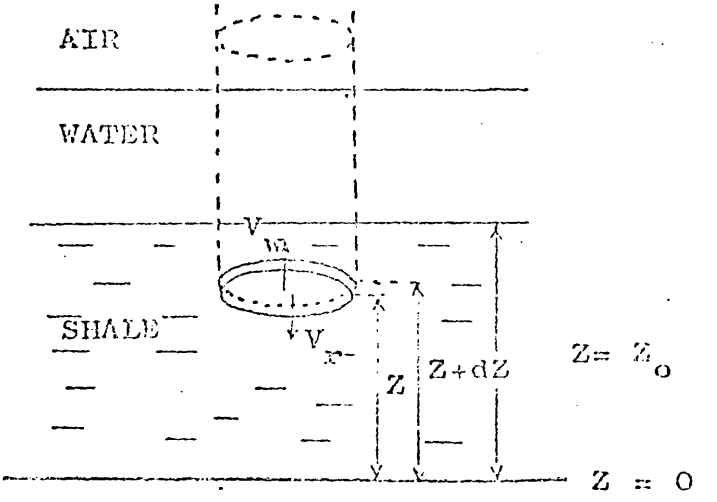


FIGURE 4.13 Schematic diagram for Shale deposition (after Smith, 1973)

Now applying Darcy's Law

$$(V_w - V_r)\phi = -\frac{K}{\mu}\frac{\partial \Psi}{\partial Z} \qquad (4.23)$$

where $(V_w - V_r)\phi$ is the instantaneous relative volume flow rate and Ψ is the fluid potential, which may be expressed as in

$$\Psi = u - g\int_{Z=-Z}^{Z_o} \rho_w \, dz - p_o \qquad (4.24)$$

where p_o is the fluid pressure at the top of the sedimentary column.

The total vertical stress (S) at the element is the sum of the weight of the sedimentary column and the fluid pressure at the sediment water interface, p_o.

$$S = g\int_{Z=-Z}^{Z_o} \rho_w \phi \, dZ + g\int_{Z=-Z}^{Z_o} \rho_r (1-\phi) dZ + p_o \qquad (4.25)$$

The normal hydrostatic pore fluid pressure, (P_N), at the element is

$$P_N = g\,\rho_w(Z_o - Z) + p_o \qquad (4.26)$$

The normal effective stress (σ_N; when $u = P_N$) is therefore $(S - P_N)$. Now substituting for ϕ in equation 4.25 from Athy's equation, and rearranging the terms, the expression for the normal effective stress is obtained as

$$N = \frac{g(\rho_r - \rho_w)}{b}\left[\ln \frac{\phi_o}{\phi} - (\phi_o - \phi)\right] \qquad (4.27)$$

However, by virtue of the consolidation process and the low permeability of shale, the effective stress at the point is S-u which will be less than P_N since the prevailing pore fluid pressure, u, is for a long time in excess of the normal hydrostatic fluid pressure, P_N.

Figures 4.14 and 4.15 illustrate some of the results of Smith's solutions of the above equations. The results in figure 4.14 show that the portion of the shale deposit next to a normally pressured sand tends to become more compacted as the overburden increases and a reduction in permeability occurs. Figure 4.15 aids in providing a time scale for the process of dissipation of the pore fluid pressure.

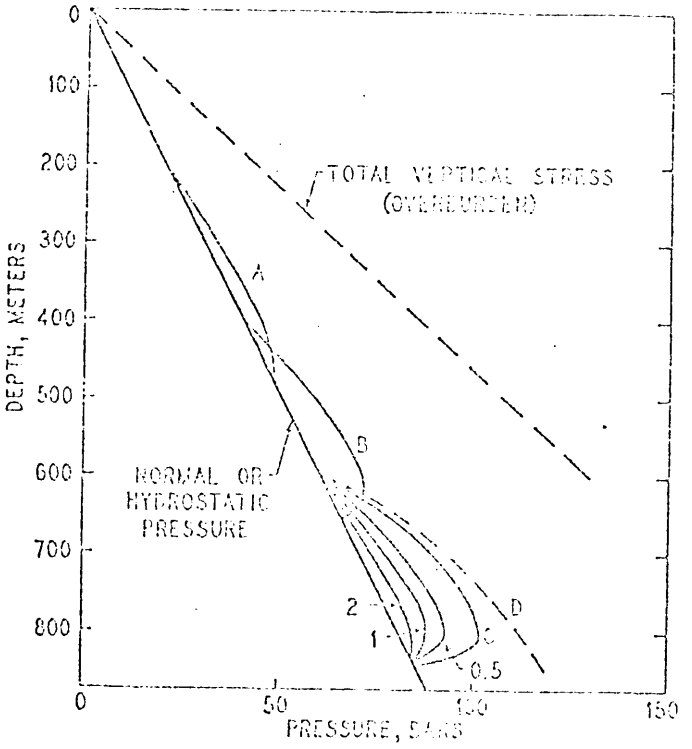


FIGURE 4.14 Stress history of a shale unit subjected to:-

A. - burial to depth of 200 m

B. - burial to depth of 400 m

C. - burial to depth of 600 m

- the corresponding change in stress after lapse of time of 0.5, 1.0 and 2.0 x 10^6 years

D. - burial with shale on an impermeable base

(after Smith, 1973).

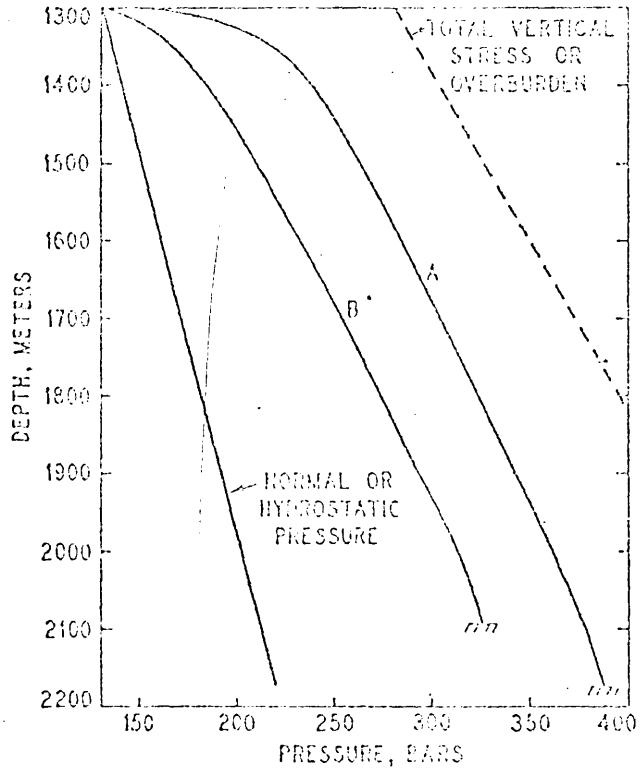


FIGURE 4.15 Persistence of pore fluid pressure in shale after burial:

A - immediately after deposition,
B - pore fluid pressure after 10^8 years

(after Smith, 1973).

CHAPTER FIVE Consolidation Equipment and Testing Procedure

5.1	Introduction		200
5.2	High pressure consolidation cell		201
	5.2.1	Specimen cup assembly and pressure vessel	202
	5.2.2	Pressure environment	205
	5.2.3	Specimen deformation	212
	5.2.4	Computer analysis	221
	5.2.5	Testing procedure	227
5.3	Constant rate of consolidation cell		233
	5.3.1	General description of the cell	233
	5.3.2	Measurement of axial pressure	235
	5.3.3	Measurement of the pore pressure	235
	5.3.4	Measurement of the axial compaction	238
	5.3.5	Testing procedure	238
5.4	Low pressure temperature consolidation cell		240
	5.4.1	Measurement of axial compaction	240
	5.4.2	Heat source	240
	5.4.3	Temperature measurement	243
	5.4.4	Test procedure	243

CHAPTER FIVE

THE CONSOLIDATION EQUIPMENT AND TESTING PROCEDURE

5.1 INTRODUCTION

Three different types of consolidation equipment were used during the course of this study. They are described in this chapter in the order of their relative pertinence to the study, viz.

a) High pressure consolidation cell (constant rate of loading).

b) Constant rate of strain consolidation cell.

c) Low pressure temperature consolidation cell.

In this study, the pressure was considered as 'high' if it was higher than the maximum pressure levels that are otherwise obtained from conventional dead load consolidation equipment (480 lb/sq.in), and up to a maximum value of 10,000 lb/sq.in.

The high pressure consolidation cell has been primarily designed and built to simulate the geological processes of deep burial and exhumation of sediments. Its basic design criteria, the present stage of development, its performance and the proposed near-future developments are described.

The constant rate of strain consolidation cell has

far more limited uses in the context of simulating geological burial. However, it was used in order to compare the void ratio - effective stress characters for the same clay as obtained from the independent use of the two consolidation cells.

The low pressure-temperature consolidation tests were performed on the test material so that a preliminary insight might be obtained into the influence of heat on the consolidation behaviour of the clay and the performance of the equipment parts.

Wherever applicable all measurements have been calibrated and their calibrations are also given under their respective headings. The mechanics of the analysis of the observations has already been outlined in Chapter Four. However, the computer programmes for the analysis of observations with their appropriate calibrations is given in this chapter.

5.2 HIGH PRESSURE CONSOLIDATION CELL

Some of the proposed aspects of the design of the cell have been outlined in Jackson (1972), Fookes and Jackson (in press), but a more complete description is contained in Osmaston et al (in press). The apparatus is a part of an integrated research programme in the Department of Geology at Imperial College, London to simulate geological burial of principally clayey sediments and to study the influence of burial and exhumation on the development of its geotechnical properties.

For the current research the apparatus was used in two distinct stages of development; Stage I and Stage II (see Table 5.I).

5.2.1 General Description of Apparatus

For all intents and purposes of this research programme, 'natural burial' is regarded as a process of smooth loading on the sample which responds to a perfectly uniaxial compaction. Table 5.I and Figure 5.1 outline the basic systems of the apparatus. The specimen is contained within the specimen chamber and the burial is simulated via an appropriate combination of time-dependent pressure systems.

The response of the specimen to the above constraints is to yield primarily:

a) a characteristic pore fluid pressure difference across the specimen (Δu)

b) a characteristic compaction behaviour, and

c) expel pore fluids with selective ionic chemistry.

These responses are monitored using a pore fluid pressure transducer, displacement transducer and pore fluid sampling systems respectively.

The complete simulation of deep burial of sediments can be further effected via a temperature control system which

DEVELOPMENT STAGE	SYSTEM	COMPONENTS	SPECIFICATIONS AND LIMITS	MATERIAL AND PROPERTIES
ONE	Consolidation Cell	Pressure Vessel	Weight of Outer Tube = 200 lb. Total Weight, assembled=400 lb.	Wrought Steel BS 970, 1955, EN26.
		Seals (Main) O,u and coaxial Seals		Du Pont Adiprene L100 Vitor Rubber
		Specimen Cup	Int. Diameter = 4.0" Max. Spec. Thickness = 4.0" Min. Spec. Thickness = 1.0"	Low Expansion 36% Nickel Steel.
		Cup Wall		ICI PTFE
TWO	Axial Pressure P'_1 System	Axial Pressure Pump	Range 0-10,000 lb/sq.in. Accuracy $\pm$ 0.02%	Low impurity Stainless Steel BS 970, 1955, EN58J.
		Pressure Control	Pencil Piston Travel = 0.75" Steel Ball Diam. = 0.75" Steel Ball Weight 0.062 lbs	Silver Steel Silver Steel
		Hydraulic Fluid		ICI Silicodyne "H"
	Pore Fluid Pressure	Transducer	Range 0-5,000 lb/sq.in.	
		Display	Accuracy $\pm$ 0.2%	
	Axial Compaction	Transducer	Range $\pm$ 0.3 inch. Accuracy 1%	
		Monitor	Resolution 1×10^{-5} inch. Accuracy 0.02%	
THREE	Heating	Heaters	Range 0-250°C	Spiral Wire Potted in Ceramic
		Temperature Control	Uniformity $\pm$ 5°C (within sample)	
		Temperature measurements	Accuracy $\pm$ ½°C	Platinum Resistance Thermometer

TABLE 5.I

Basic System Details of High Pressure Consolidation Cell

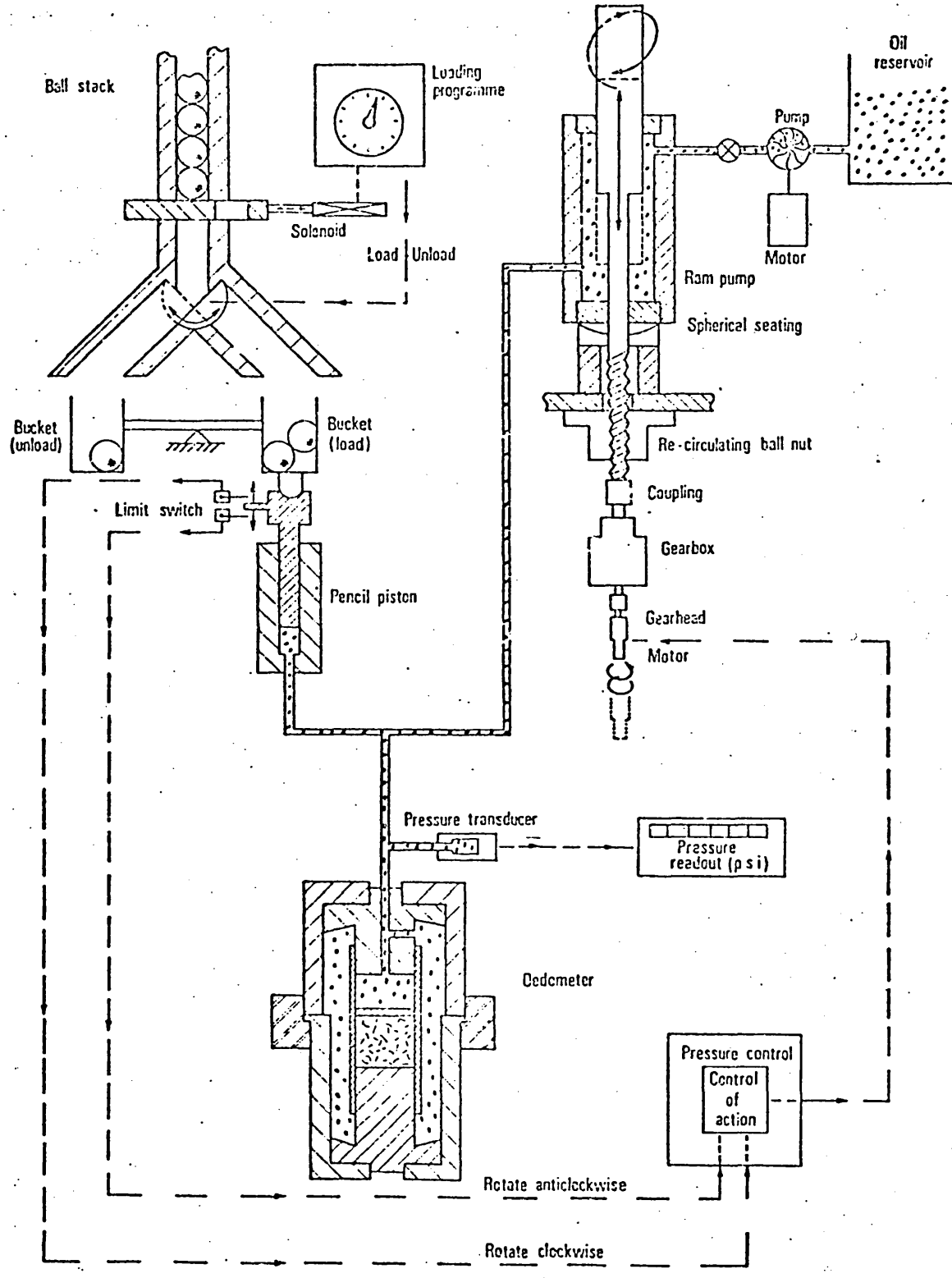


FIGURE 5.1 A schematic diagram of the operational systems of the high pressure consolidation cell.

simulates a geothermal gradient.

The entire apparatus is housed within a 8 ft. square space in the department laboratory which is itself 16 feet high and is maintained at a stabilised temperature of 20°C. A view of the apparatus in use is shown in Plate 5.1.

5.2.2 Specimen Cup Assembly and Pressure Vessel

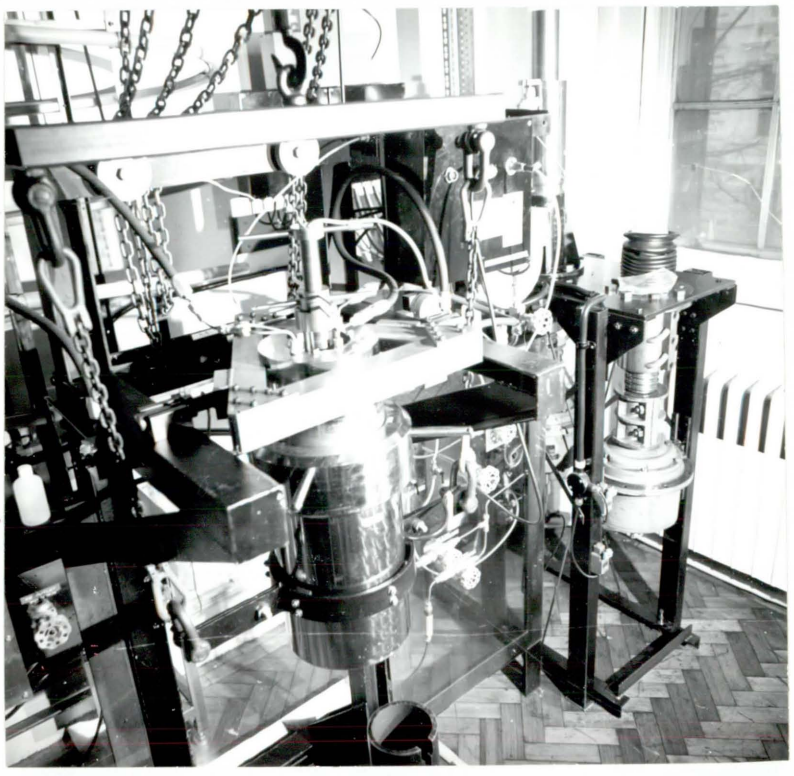
The specimen is contained within a cylindrical cup as shown in figure 5.2. During the compaction process the whole assembly moves downwards onto a rigid cylindrical plug as a result of the hydraulic axial compaction pressure (described later in Section 5.2.3). The ends of this assembly slide over seals on the upper and lower plugs. The choice of teflon surfaced seals and the use of teflon lining sleeves in the ends of the specimen cup assembly is to minimise the frictional effects on the seals which otherwise reduces the effective P_1 applied to the specimen.

0.062 inch thick, 4 inch diameter, sintered porous stainless steel discs at each end of the specimen facilitate the drainage of expressed pore fluid from either or both ends. The expressed pore fluid is transmitted to collection chambers and pressure transducers by means of 0.062" diameter stainless steel tubing. Discs of Whatman no. 1 filter paper are usually placed between the specimen and the porous discs to prevent their pores becoming blocked.

PLATE 5.1 Layout of the high pressure temperature consolidation cell:

a) A bird's eye view showing a general view. Note: the pressure pumps and the ball slack in the background.

b) The process of 'jacking down' of the pressure balance pistons.





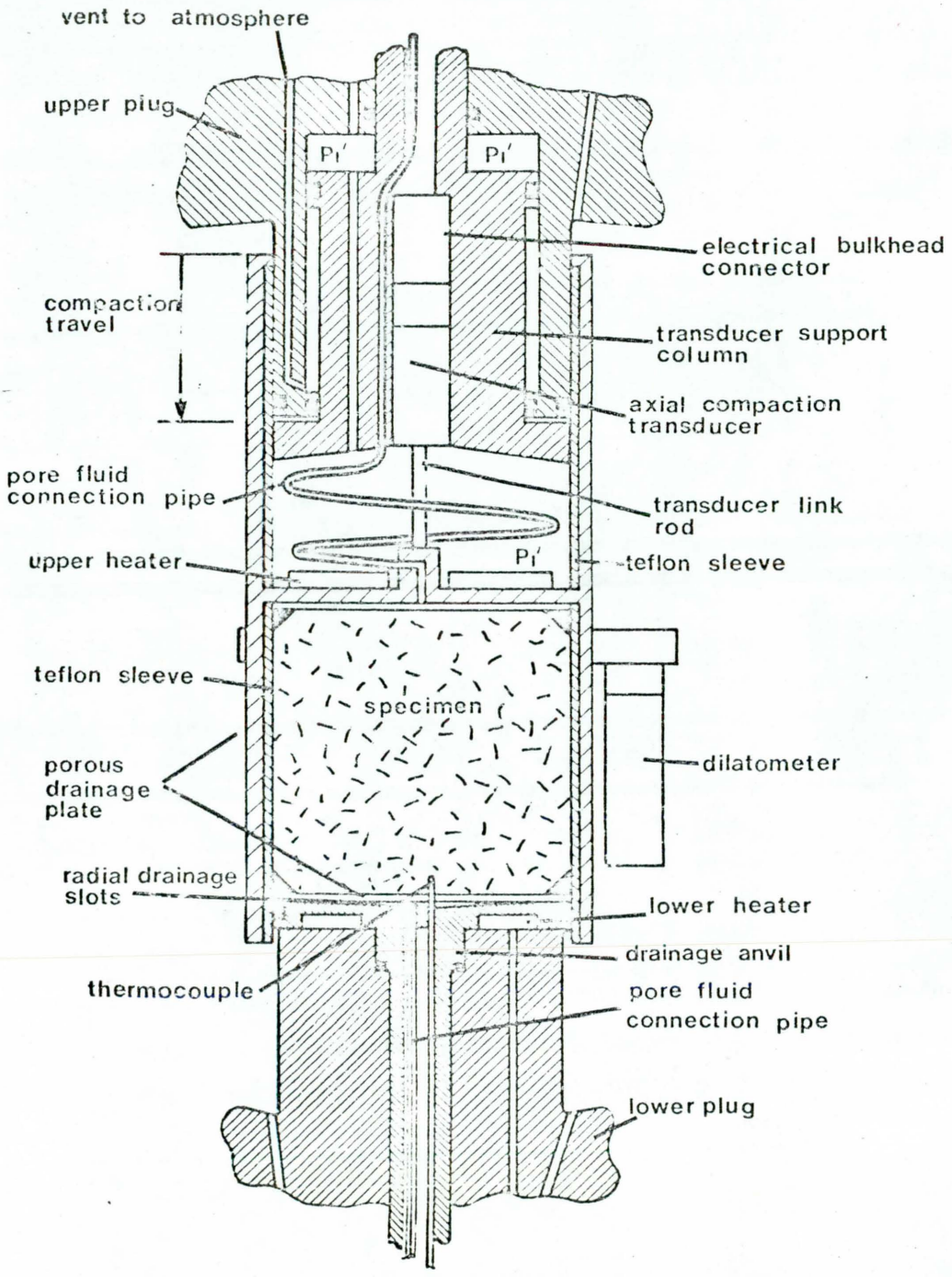


FIGURE 5.2 — A detailed diagram of the specimen cup, lower and upper plugs and their associated systems.

The apparatus is designed to accommodate 4" diameter specimens with a maximum thickness of 4". Thinner specimens may also be tested through the entire pressure range by suitably modifyin the present size of the specimen cup assembly (see Plate 5.2). Specim of very high consistency are usually preconsolidated within the same specimen cup.

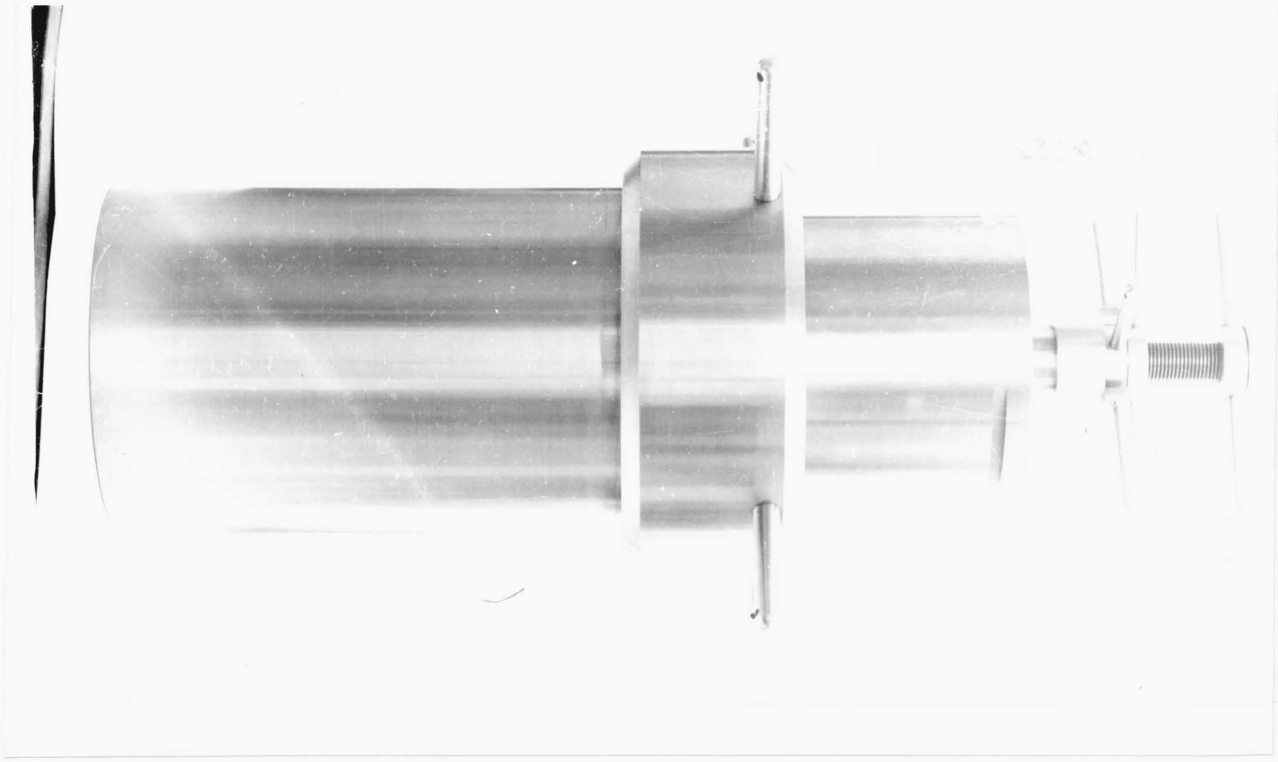
The specimen cup assembly is contained within the pressure vessel (fig. 5.3) which consists basically of an upper and a lower main tube, two end plugs, and a toggle ring, all machined from forged steel. This assembly is 60" long overall and weighs over 500 lbs complete with the hydraulic fluid (seen in Plate 5.1). To facilitate handling, the vessel is suspended from the top, in a gimbal mounted frame. For access to the specimen cup, the toggle ring is undone and the lower main tube and plug are lowered with a chain hoist until the plug rests on a support. The lower main tube is then lowered further to expose the specimen cup assembly for removal. The toggle ring method of joining the main tubes is not only more convenient than bolted flanges, but is also a saving in cost.

The pressure vessel extension with increasing pressure was observed by recording the compression of a standard steel block which took the place of a clay specimen. Figure 5.4 illustrates this observation which showed that the major part of the extension (.02") occurs below a pressure of 3000 lb/in^2, suggesting this extension to be a result of the closing up of the tolerances on the toggle ring.

PLATE 5.2 Views of pressure vessel and specimen cup assembly:

(a) A view of the pressure vessel showing the toggle ring that joins the main tubes of the pressure vessel.
(overall length = 60"
overall weight > 500 lbs.

(b) A view of the specimen cup assembly including the lower and upper plugs positioned in it corresponding to the maximum compaction travel position.





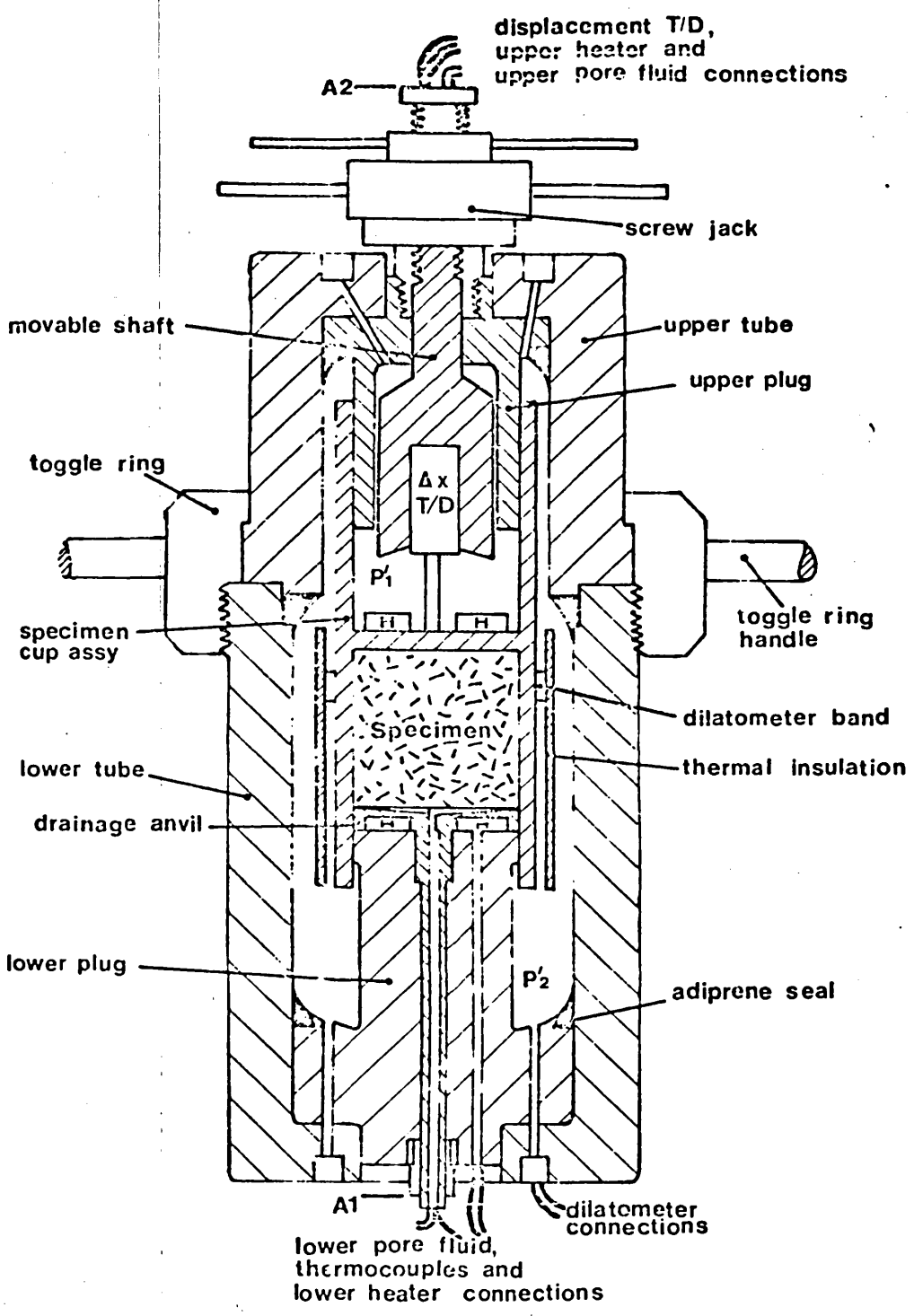


FIGURE 5.3 A detailed diagram of the pressure vessel.

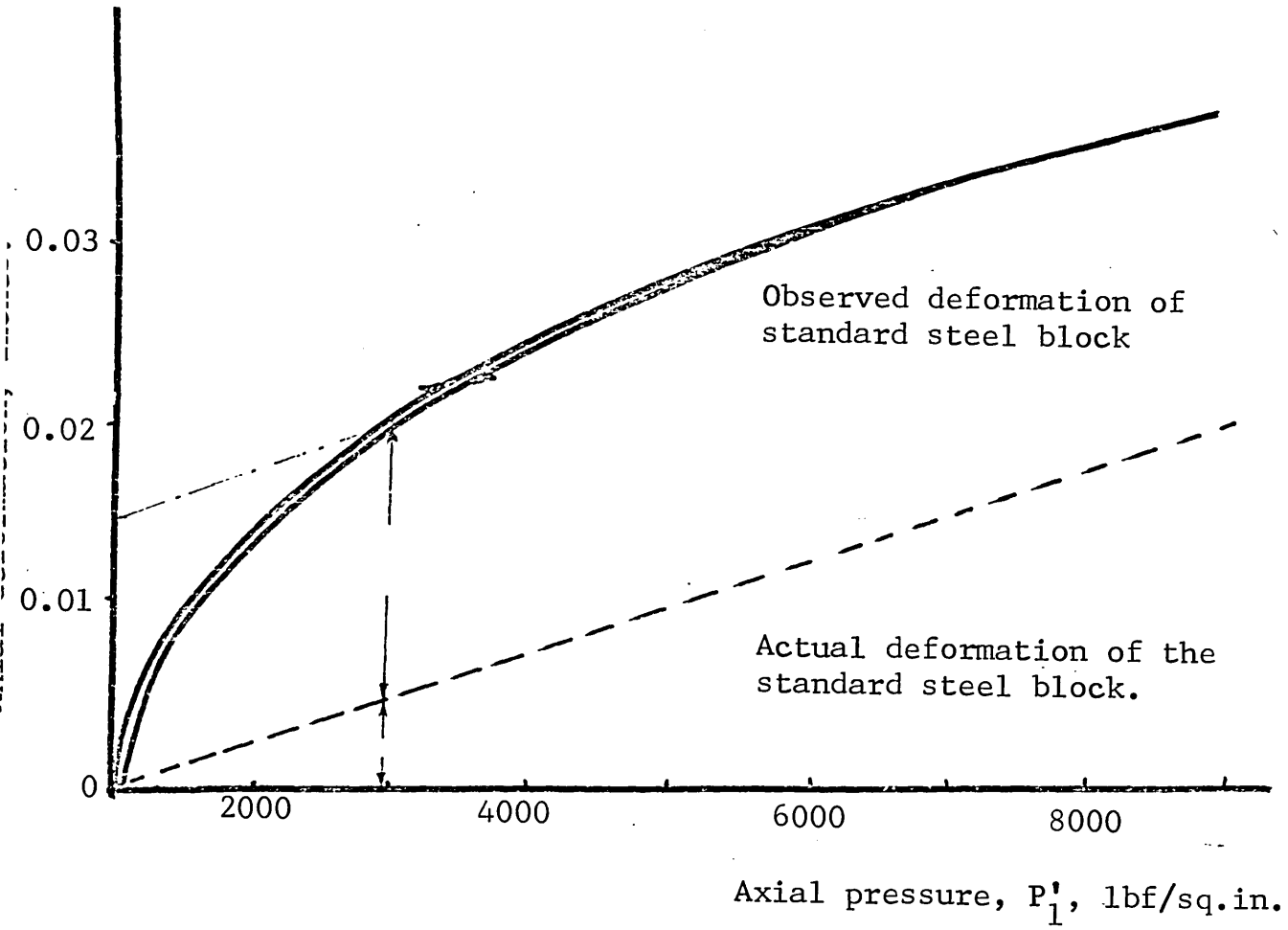


FIGURE 5.4 Cell extension calibration curve.

5.2.3 Pressure Environment

The three hydraulic pressures (viz. axial compaction pressure P_1', the radial constraint pressure P_2', and the back pressure U_z which opposes the pore fluid drainage), constitute the pressure environment for the specimen.

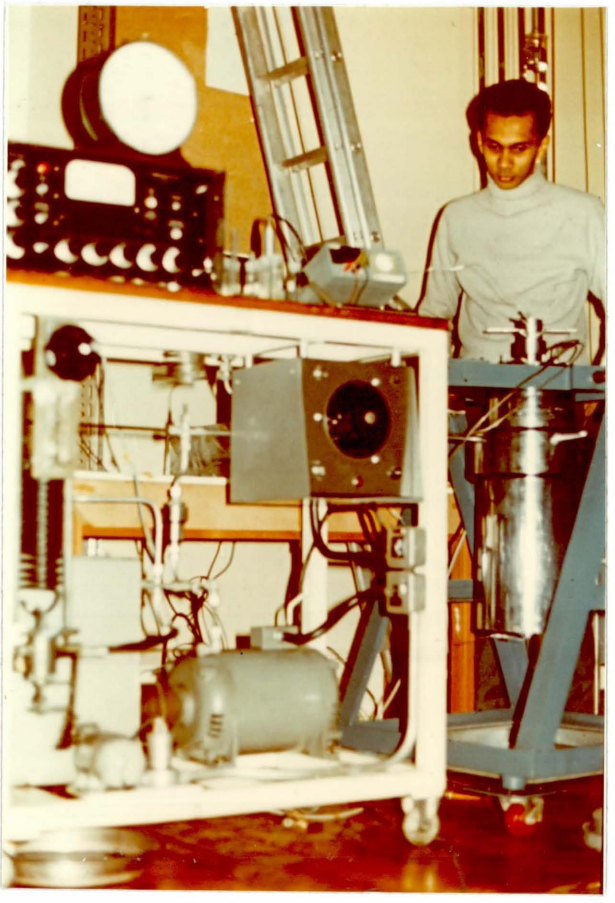
These hydraulic pressures are designed to be supplied by mechanical pumps. During the current research programme a separate P_2' source and a U_z source had not yet been developed, and as such the P_1' pressure was also used for radial constraint of the specimen. In Stage I of the development programme (see Table 5.I) the P_1' pressure was supplied by means of an Amsler valve pump as shown in Plate 5.3. The control of its pressure had to be done manually by increasing or decreasing the delivery rate of the pump. The tests so conducted were performed at very rapid rates of axial pressure loading, and the observations from such are reported in Chapter Seven.

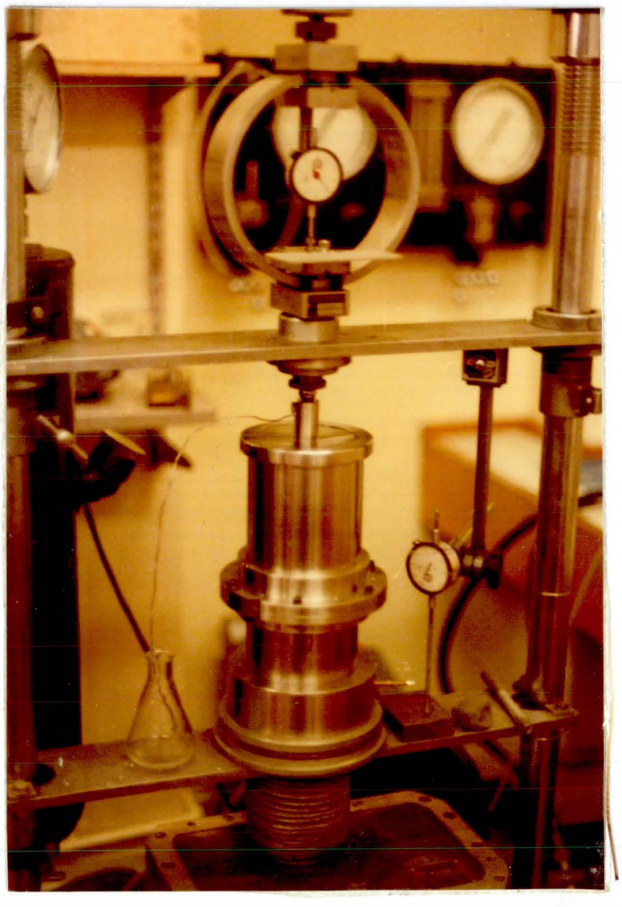
The actual pumps designed to supply P_1', P_2' and U_z are identical and of ram in cylinder type. Each has a swept volume of 40 cubic inches, and can absorb or deliver 9.2×10^{-4} cubic inches/second of hydraulic oil at pressures up to 10,000 lb/sq.in. This delivery rate corresponds to a compaction rate even as large as over an inch in a day. The P_1' pump was developed for Stage II and has subsequently been used in the testing programme.

The P_1 control system ensures that the required pressure is attained and maintained constant without pressure oscillation

PLATE 5.3 (a) Details of equipment used for rapid loading consolidation: pressure source is via the Amsler valve pump in the foreground, consolidation cell is to its right.

(b) Details of the preconsolidation stage of loading on the triaxial machine:
Proving ring measures total axial pressure induced by the constant rate of strain; pore fluid is drained from the top - the same end as in the main test.





or long term drift. The pressure is derived directly from the weight of an appropriate number of steel balls in a loading bucket, the effect of the weight of each ball is a pressure rise of about 5.1 lbf/sq.in. corresponding to a burial increment of about 5 feet. Figure 5.5 describes the observed pressure rise against the number of balls in the bucket, as observed during testing.

Thus P_1' can be varied according to an arbitrary time-based programme or be related automatically to strictly defined compaction conditions of the specimen. The demand for a rise or fall in P_1' is to release a ball into the loading or the unloading bucket as the case may be. Figure 5.6 shows the ball release gate and the solenoid arrangement which executes the above command.

Figure 5.7 illustrates the pressure pencil piston arrangement. The hardened steel pressure pencil piston, which is 0.125 inch in diameter, is maintained in a state of floating eqiulibrium to the opposing forces; the total weight of the loading bucket at its top and the P_1' pressure on the line at the bottom end. The execution of the command of a rise or fall in P_1' pressure is as follows: release of one extra ball into the loading bucket depresses the pencil piston which activates the 'pencil piston position sensor' to switch on the

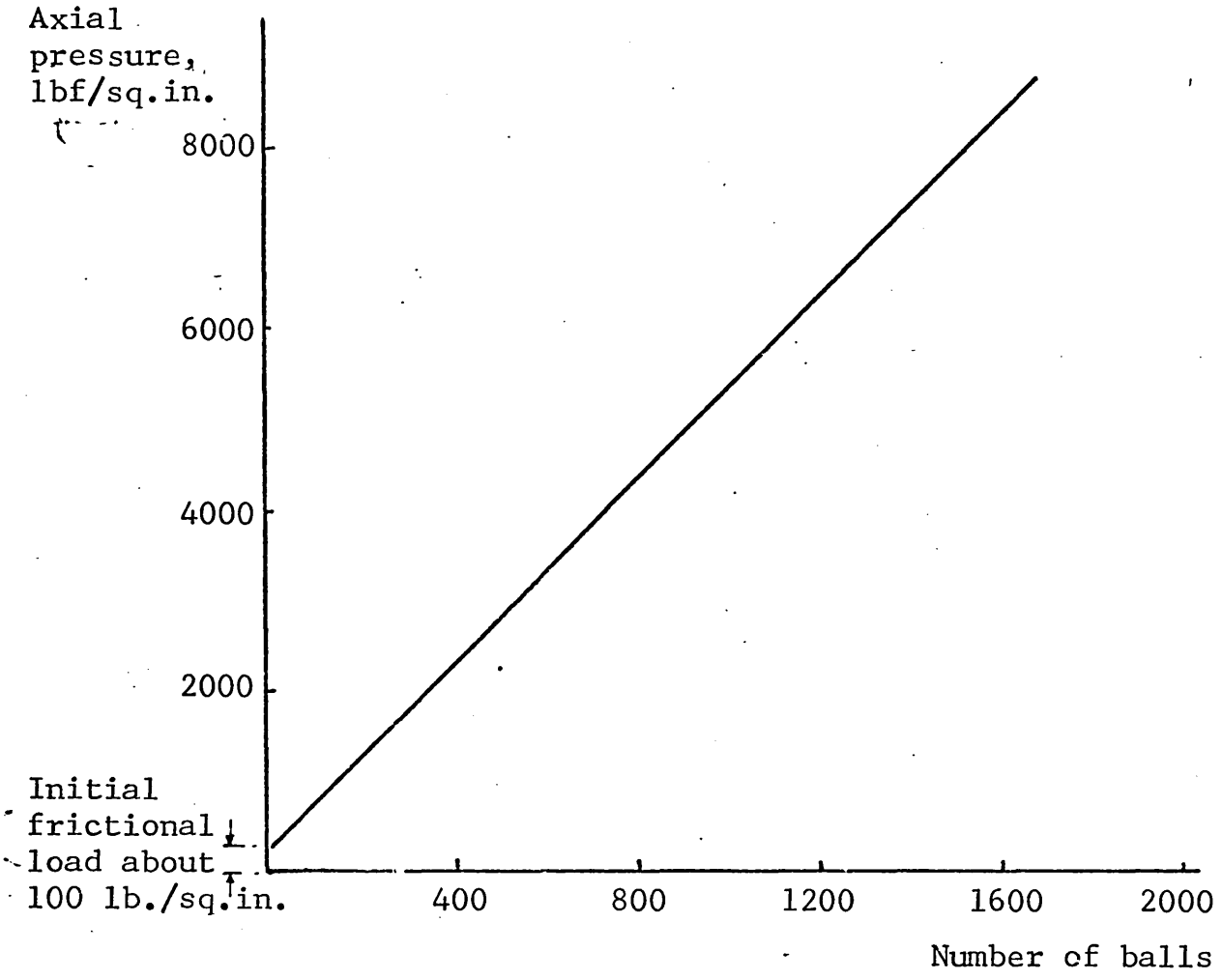
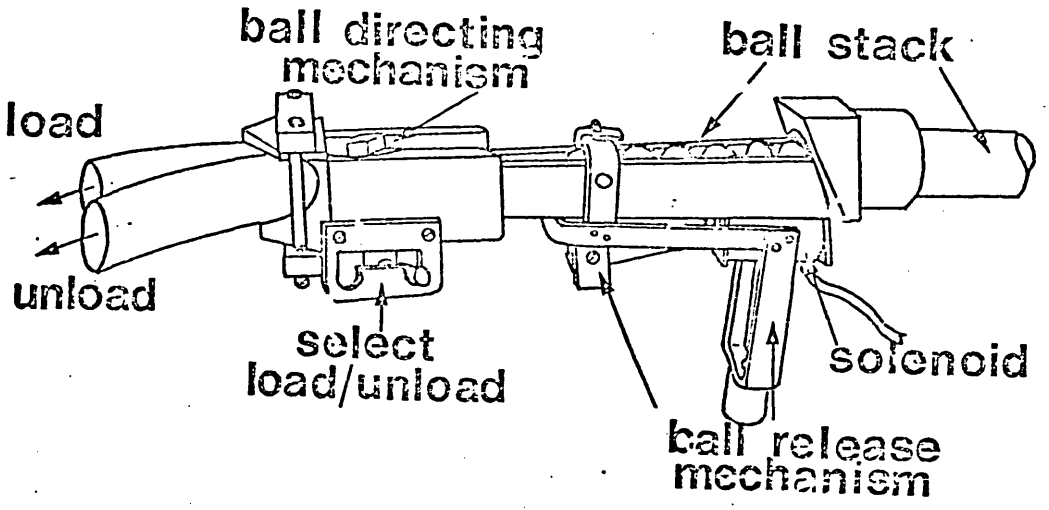


FIGURE 5.5 — The increase in axial pressure, P_1', with the number of balls.



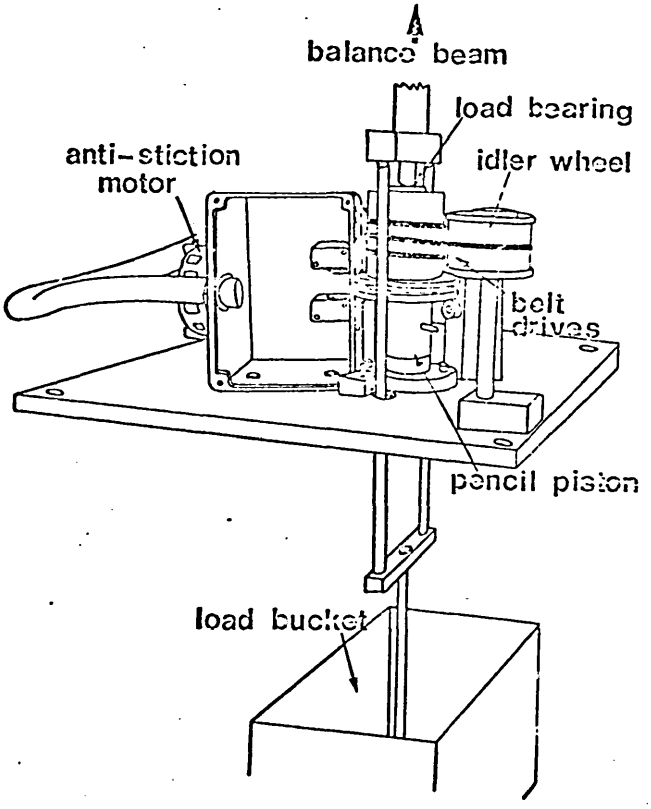


FIGURE 5.6 Details of the servo system for control of P_1 pressure:

a) Ball release gate.

b) Hydraulic pressure - deadweight balance.

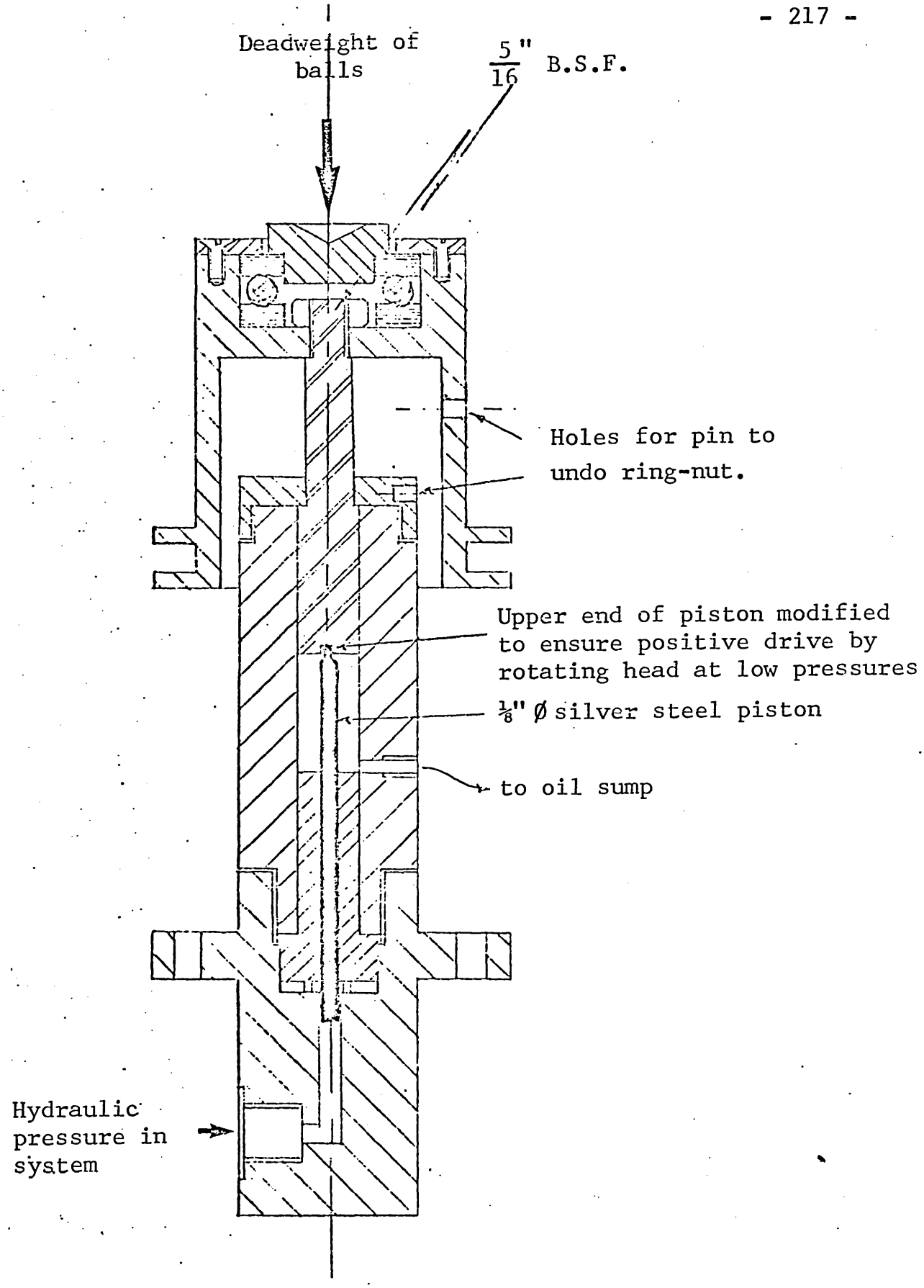


FIGURE 5.7 Pressure pencil piston arrangement.

P_1' ram pump which injects sufficient oil to restore the pencil into the original neutral position and as a result of this process the P_1' pressure is increased by 5.1 lbf/sq.in. A fall in P_1' pressure is executed in a similar way, with the pencil piston moving upwards with each ball released into the unloading bucket and the P_1' pump extracts sufficient oil from the system to restore equilibrium. The P_1' pressure is stabilised against the effect of compaction of the specimen similarly. For compaction increases the oil filled space within the pressure vessel, but the pressure is maintained at the desired level by the ball load on the pencil piston, which falls in consequence, until equilibrium is restored by the pump. Figure 5.8 shows a typical pressure pencil response characteristic.

P_1' and P_2' pressures are measured using zero deflection type pressure transducers. Their readings were calibrated using a Huggenberg pressure rig. Their calibration is shown in figure 5.9.

The pore fluid pressure difference (Δu) across the specimen is also measured using a similar type of pressure transducer but of the 0-5,000 lbf/sq.in. range. Its calibration is also given in figure 5.9. The Δu transducer is mechanically positioned between the u_z pressure line and the top of the specimen.

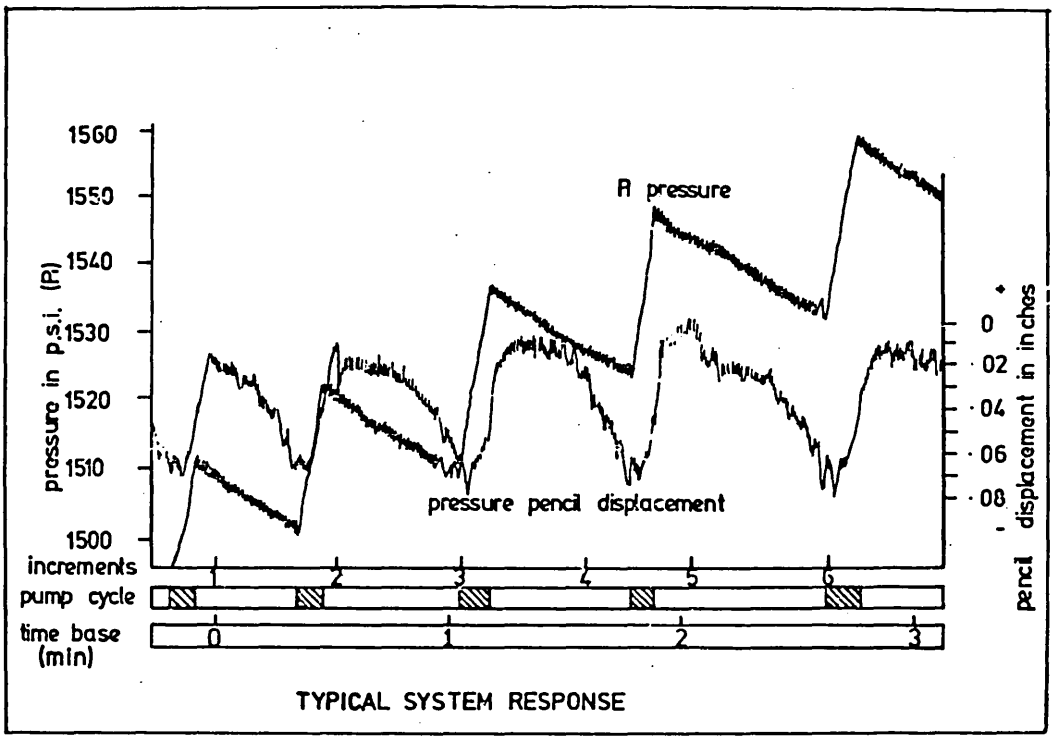


FIGURE 5.8 Graphs showing the performance of the pressure pencil to commands of increase of P_1 pressure.

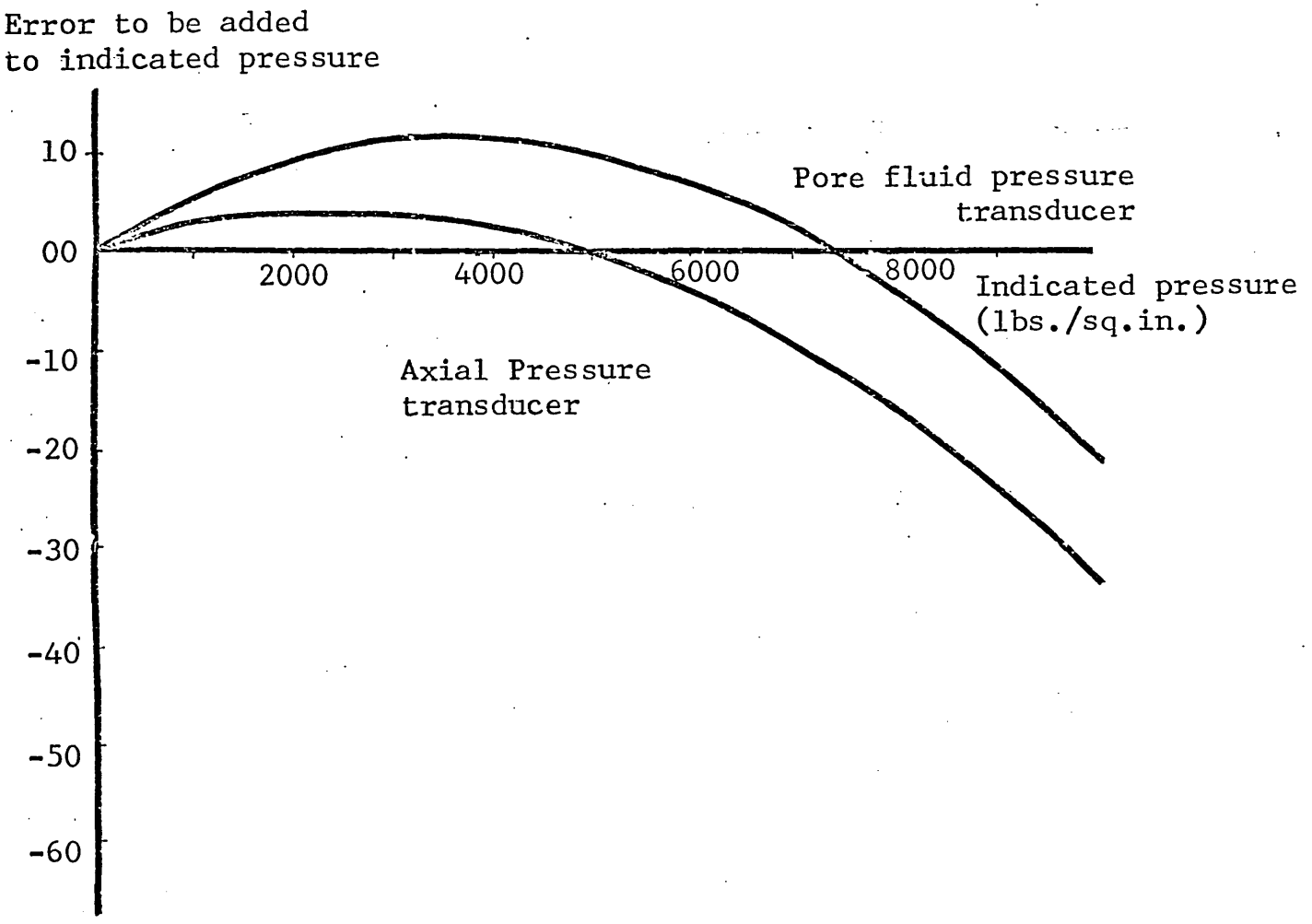


FIGURE 5.9 Calibration of the pressure transducers.

5.2.4 Specimen Deformation

By virtue of the axisymmetry in the shape of the specimen and also the application of the pressure, observations of the axial compaction (Δx) and the lateral dilation of the specimen is sufficient to define rigorously the state of deformation of the specimen. In the current research, it was assumed that the 0.315 inch thick walled specimen cup was sufficient to ensure rigid wall conditions.

The axial compaction (Δx) is measured using a displacement transducer of the bridge type with a working range of 0.50 inch. In the selection of a satisfactory transducer, the following aspects had to be considered:-

i) a suitable resolution of 1×10^{-5} inches,

ii) stability over temperature changes,

iii) a total compaction travel of 3.0 inches.

A linear differential transformer type of transducer developed by Boulton Paul Aircraft Ltd. for the Atomic Energy Authority seemed a suitable choice for purposes of resolution. To avoid wide ranges of temperature changes, convection baffles were designed to keep them within satisfactory limits. The working range of the transducer is, however, ± 0.3 inches.

Plate 5.4 and figure 5.3 show the movable shaft that

PLATE 5.4 Close-up view of the pressure balance piston. Shows:

one pore fluid outlet	= P.
precision thread used in jacking down	= T.
Lock nut	= L.
pressure seals	= S.
6" scale	= C.


P
L



houses this axial compaction transducer. As a result of the limited range of the transducer, the transducer supporting shaft has to be moved several times during compaction to observe the entire compaction of a specimen. Silicone rubber-energised teflon seals are used around this movable supporting shaft. The 'jacking' mechanism uses a coarse pitch differential thread and locking nut. The handles for operating these are seen in figure 5.3 (also see plate 5.1).

Plate 5.5 illustrates the rig used for calibrating the transducer. The bridge is balanced on the C61 type transducer meter shown in plate 5.6. Figure 5.10 shows the calibration curve (error versus observed reading) obtained for the transducer. It also illustrates the reason for the inapplicability of the transducer outside the range $\pm$0.30 inch. The influence of the change of inductance in the magnetic circuit on the calibration curve was observed by supporting the transducer in air and in different metallic environments. These results can also be seen in figure 5.10. Accordingly the most appropriate calibration was obtained with the transducer positioned in the top half of the cell. Change of the scale factor setting (seen in plate 5.6) has the effect of rotating the axes of the calibration curve. The scale factor 100/522 was found, by means of trial and error, to give the most suitable calibration curve.

PLATE 5.5 Displacement transducer calibration rig. Shows the micrometer screw, pressure balance piston and electrical connections.

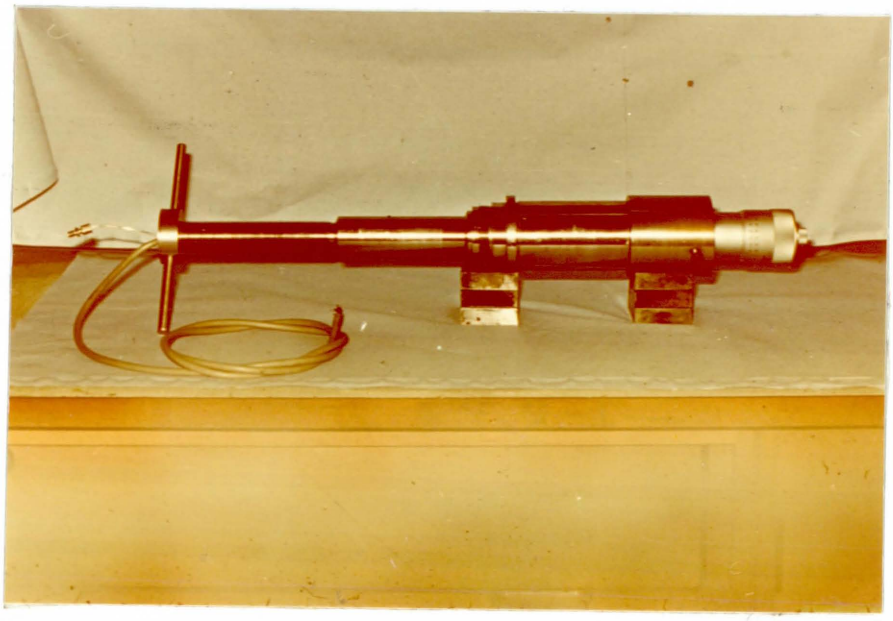


PLATE 5.6 View of the console housing the operational and observation systems of the cell.

1. Alarm unit
2. Priming pump control unit
3. Ram pump control unit
4. Hydraulic pressure source control
5. Power supply unit
6. Displacement transducer bridge
7. Displacement meter ± 0.5 inches
8. Bridge error voltage DPM
9. Main temperature DPM
10. PI' pressure DPM
11. Temperature DPM (auxilliary)
12. Printer control panel
13. U pressure DPM
14. Digital printer
15. P' signal conditioner
16. U signal conditioner
17. Four temperature measurement units
18. Temperature selector display unit
19. Temperature programme panel
20. Lower heater control unit
21. Upper heater control unit
22. Voltage reference unit
23. Back pressure pump control unit


5
4
3
2
1
15
16
17
18
19
20
22
21
7
ring
nstalled



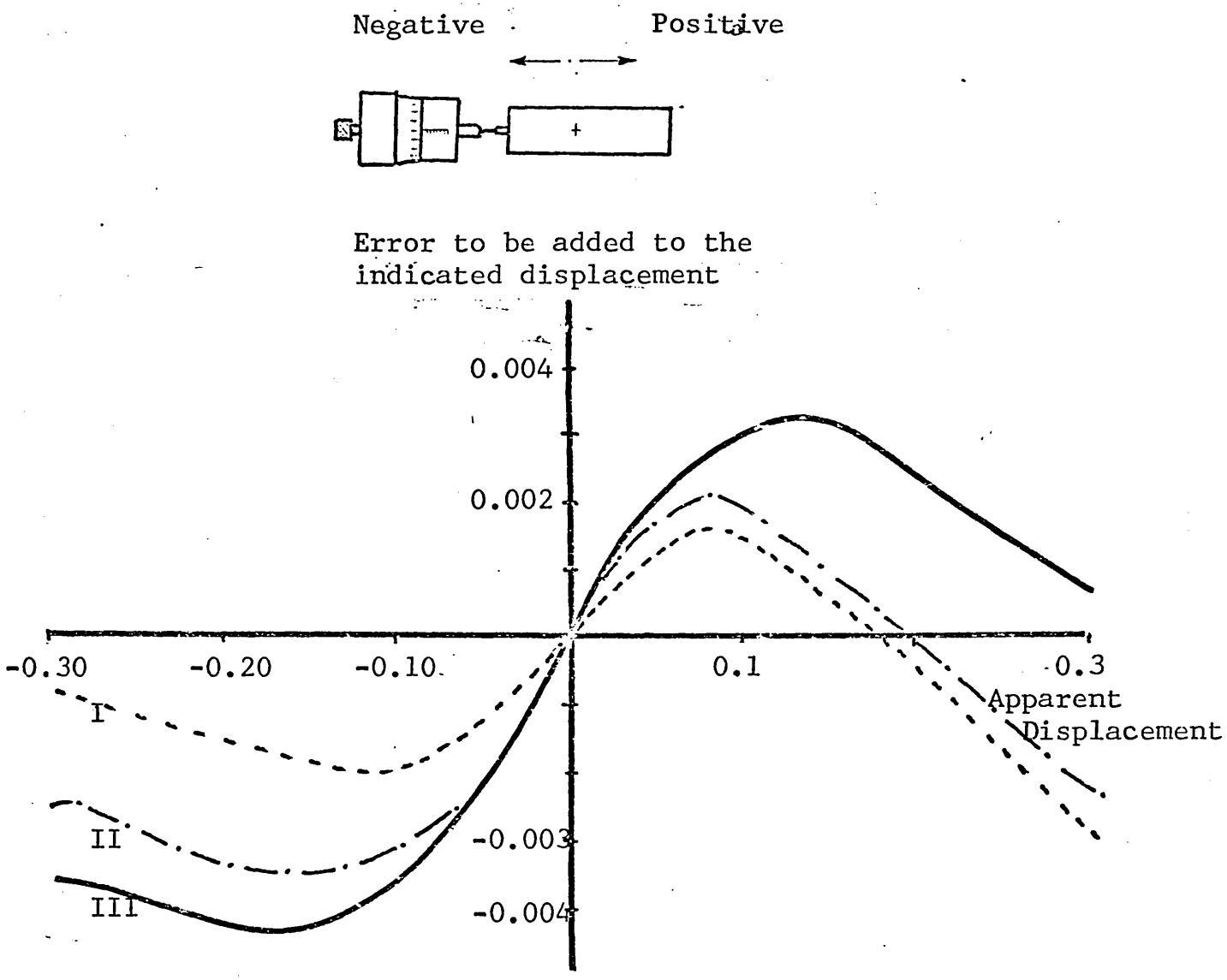


FIGURE 5.10 Calibration of the displacement transducer

I) Transducer in air

II) Transducer clamped in a metal jacket

III) Transducer housed in the pressure balance piston

In order to reduce the need for constant human supervision, over long durations, all data are digitised to four decimal digits and printed at appropriate intervals determined by the system clock. To cater for this need, the family of straight lines in the calibration curve (figure 5.11) supercedes the use of the earlier calibration curves which were obtained by nulling the galvanometer. Each curve gives a variation of the error voltage (voltage in error of being null on the galvanometer circuit of the potentiometer bridge) in millivolts with the position of the transducer lug (with the meter on low sensitivity) and the transducer meter on the appropriate decade switch setting.

Finally, to measure Δx accurately, the position of the body of the transducer has to be fixed accurately in relation to the bottom surface of the specimen. This is best done using an external reference frame which will be devoid of the effects of temperature and pressure within the cell. In the absence of such an arrangement, the cell extension calibration curve was used to correct the Δx observations. (Figure 5.4)

5.2.5 Computer programme for the analysis of observations

When a complete set of data for a test has been collected from the print out, they are punched on cards together with data such as number of tests, initial and final conditions of the specimen.

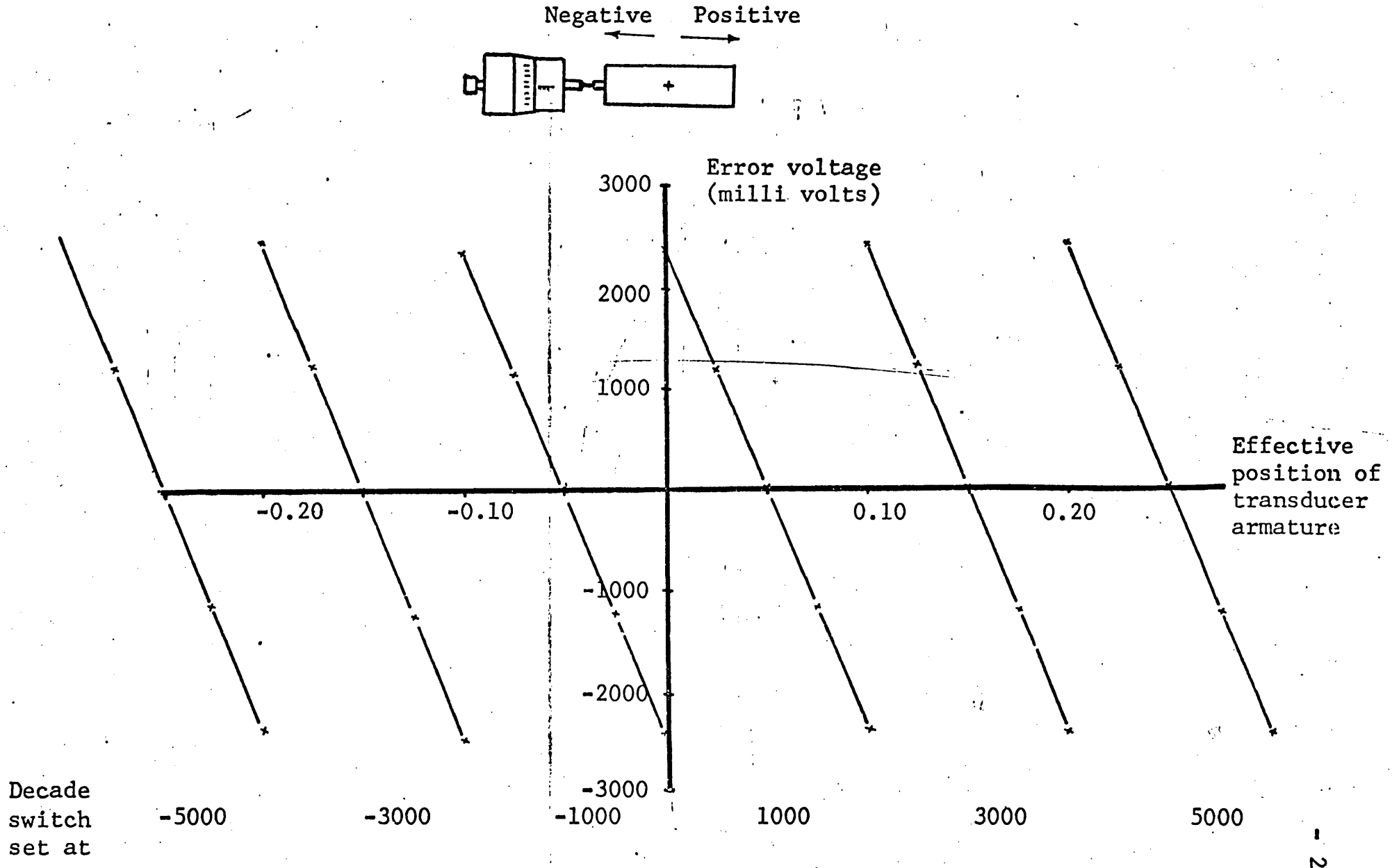


FIGURE 5.11 Displacement transducer calibration showing variation of error voltage with position of armature for different decade meter settings.

The corrections for these data using the appropriate calibration curves is done within the computer programme. The observed values of P_1, Δu, and Δx are both tabulated and also plotted.

In the second part of the programme the theoretical expression for the present ratio ($\Delta u/P_1$) derived in Section 4.7.2 of Chapter Four is used to generate a two-dimensional array of values for $\Delta u/P_1$ and time factor T. For each observed data set, the value of $\Delta u/P_1$ is computed and the corresponding value of time factor T is obtained from the array.

Therefore, the average effective pressure corresponding to that time factor can be determined. In the meantime, the voids ratio at each stage is computed from the knowledge of the final moisture content, final thickness and current thickness of the specimen. Thus, the coefficient of volume decrease and then the coefficient of permeability are obtained. The flow chart for the programme is shown in figure 5.12.

5.2.6 Testing Procedure

Clays, in both remoulded and undisturbed states, have been tested using the cell. These, however, require different testing procedures during the specimen preparation stage. Thus these are considered separately.

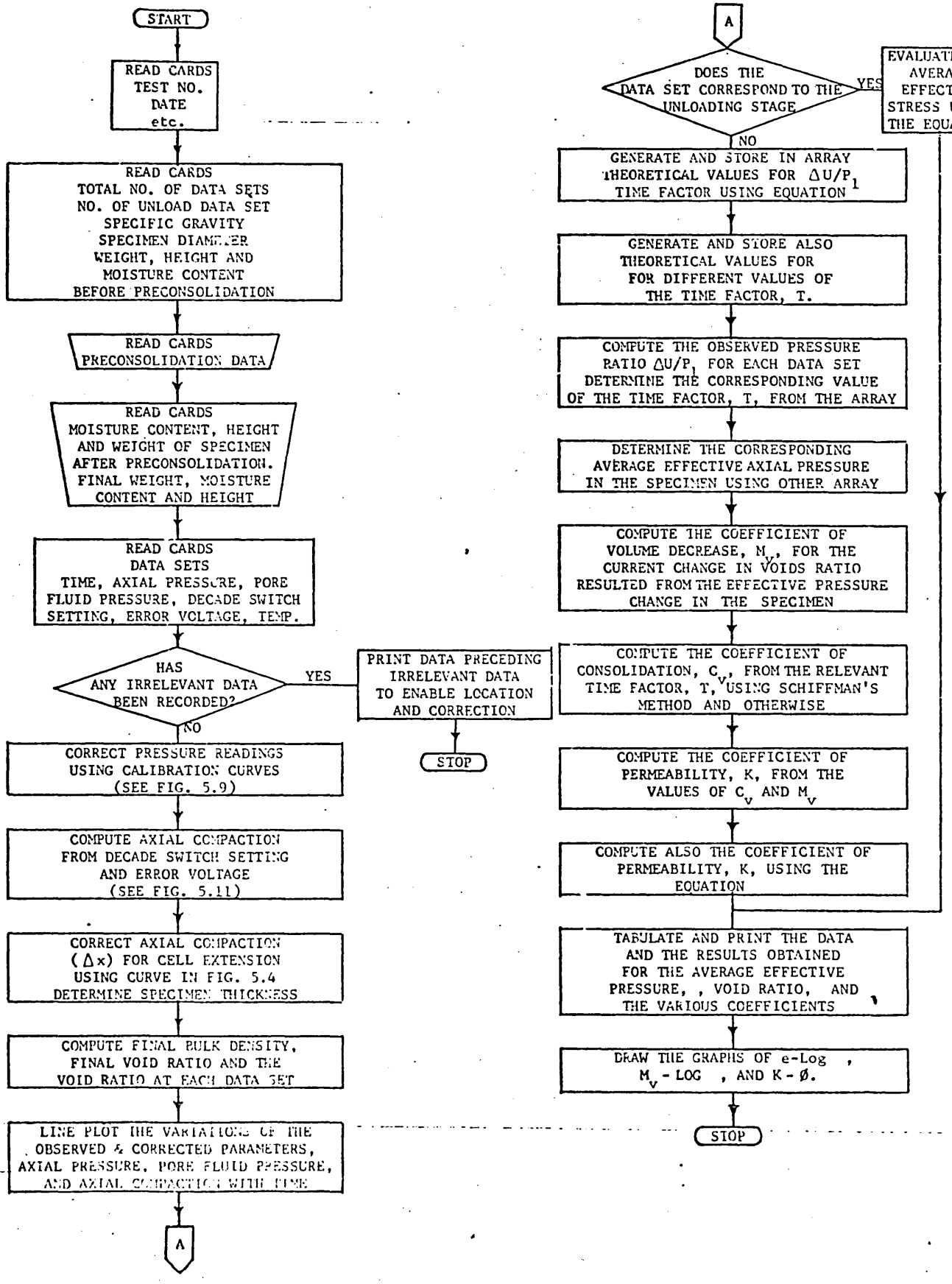


FIGURE 5.12 Flow Chart showing main sections of computer programme. .

a) Remoulded clay:

Remoulded samples were prepared by mixing the air-dried material thoroughly with the appropriate fluid in an electric mixer to a moisture content well above the liquid limit (in all the tests slightly more than 100 percent by weight of fluid was used). The clay thus mixed was kept covered in an humid environment for over forty-eight hours to ascertain that the clay particles have achieved complete hydration.

The slurry was then poured into the specimen chamber which had been previously prepared by flushing the porous plates and lubricating the teflon linings with a smearing of silicone grease. A Whatman no. 1 filter paper was used between the specimen and the porous plates to avoid the pores of the latter becoming clogged.

The first few tests showed that a specimen having one hundred percent moisture content was inconveniently soft for handling and in the subsequent tests the remoulded clay was preconsolidated within the same chamber to about 72 percent porosity. (See Plate 5.3b.)

As it was intended to observe the fabric of the final specimen, care was taken to ensure similar stress and displacement conditions. Thus the same end of the specimen was allowed to drain and a strain rate equal to the anticipated early rate

of strain was used. This preconsolidated specimen was now ready for assembly in the cell.

b) Undisturbed samples:

The undisturbed samples were collected in two different ways according to their consistency. The fresh estuarine muds were collected at once into a teflon sleeve (described later in Chapter Six). The overconsolidated clay specimen was carved out of a block sample. A 5" cube is cut out of the main block sample with wire cutters and spatulas. A 4" diameter cutting ring, with its inside greased, was then placed on the block, with the ring's cutting edge facing down and, using it as a guide, the clay was trimmed with a sharp knife until it was just over 4" in diameter. The ring was then gently and evenly pushed into the sample, the excess clay being automatically trimmed by the cutting edge. Finally, the specimen was cut on both sides of the ring to a thickness of slightly less than 4". Two filter papers are placed one on either side of the specimen. The exact weight and height of the specimen and moisture content of the cuttings are noted.

The lower plug of the cell now rests on a supporting stand (seen in plate 5.1). The specimen chamber containing the specimen, filter plates and the scraper blades in position is then inverted carefully onto the lower plug. The specimen cup has to be gently slid past the seals and

usually it settles under its own weight, driving the air trapped in the process. A perfect seating of the specimen is usually checked both by feeling the pressure on pushing the chamber and by checking the clearance between the top of the chamber and the lower plug. This plug and the chamber is positioned within the lower half of the cell body using the gimbal frame. Sufficient silicone oil is poured to fill the accessible parts of the P_1' and P_2' chambers and the two halves of the cell are brought together using the toggle ring.

The entire system is left to prime over a minimum period of forty-eight hours to ensure that no air is trapped in the system. Any compaction occurring during this stage is noted.

The first hundred lbs/sq.in of the selected loading programme is executed manually using the priming pump control (see figure 5.5). Once the pressure balance pencil commences to function, the ball feed is programmed and the system automatically executes the loading programme. The print-out takes readings of P_1', u_z, EV, and time at desired time intervals.

When the displacement transducer has run out of its working range, the pressure balance piston is gently jacked down until the displacement transducer is back within a reasonable area of its working range. Sets of observations are taken immediately before and after the jacking process.

The unloading is executed by correctly positioning the lever on the ball release mechanism. The specimen is recovered in a process reverse to that of assembly.

5.3 CONSTANT RATE OF STRAIN CONSOLIDATION

This technique of consolidation testing was first adopted by Smith and Wahls (1969) and a more versatile general purpose consolidometer was subsequently developed by Wissa et al (1971) at the M.I.T.

A constant rate of strain consolidation cell was also used by Som (1968) of the Department of Civil Engineering at Imperial College. The same equipment was used with slight modifications for long term testing.

5.3.1 General description of cell

A schematic drawing of the controlled rate of strain consolidation cell is shown in figure 5.13. It is built almost entirely of brass and is designed to withstand pressures of up to 10,000 lbf/sq.in. The sample dimensions are 3 inch diameter and 0.75 inch high. It is confined in a stainless steel ring also 0.75 inch thick, and rests on a brass base which contains an arrangement for measuring pore water pressure. The confining ring is secured to the base by means of a brass flange and six

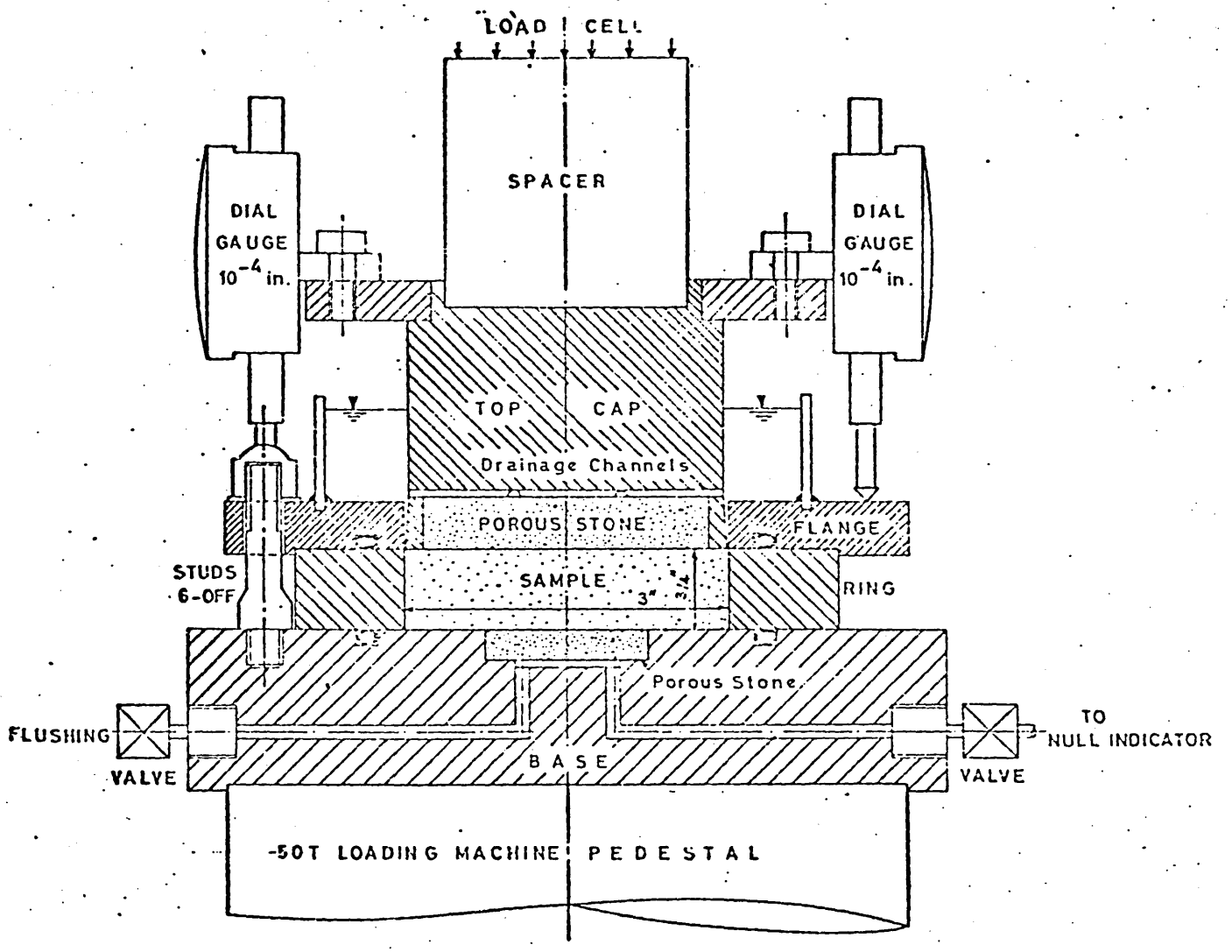


FIGURE 5.13 Constant rate of strain consolidation equipment

studs, and is also sealed at both top and bottom by O-rings. The axial load, P_1, is applied through a thick brass top cap, the base of which is recessed to include a 0.5 inch thick porous stone. The stored water in the porous stone is communicated through drainage channels to the outside water, thus ensuring the sample is submerged. Plate 5.7 illustrates these components further. The entire assembly sits on the pedestal of a 50 ton loading machine which can be geared to apply the load at a predetermined rate of strain.

5.3.2 Measurement of the axial pressure, P_1

The axial load applied externally to the top cap is monitored with a load cell. The load cell was an N.C.B./M.R.E. Type supplied by N.H. Mayes and Sons (Windsor) Ltd. The network of 16 electrical resistance strain gauges incorporated within the cell is connected to a signal conditioner module of the Sangame Weston data logger.

The load cell was calibrated in an universal testing machine. A number of loading and unloading cycles showed negligible zero shift and little hysteresis. Figure 5.14 is the linear relationship that was observed between the load and the meter readout.

5.3.3 Measurement of the pore water pressure, Δu

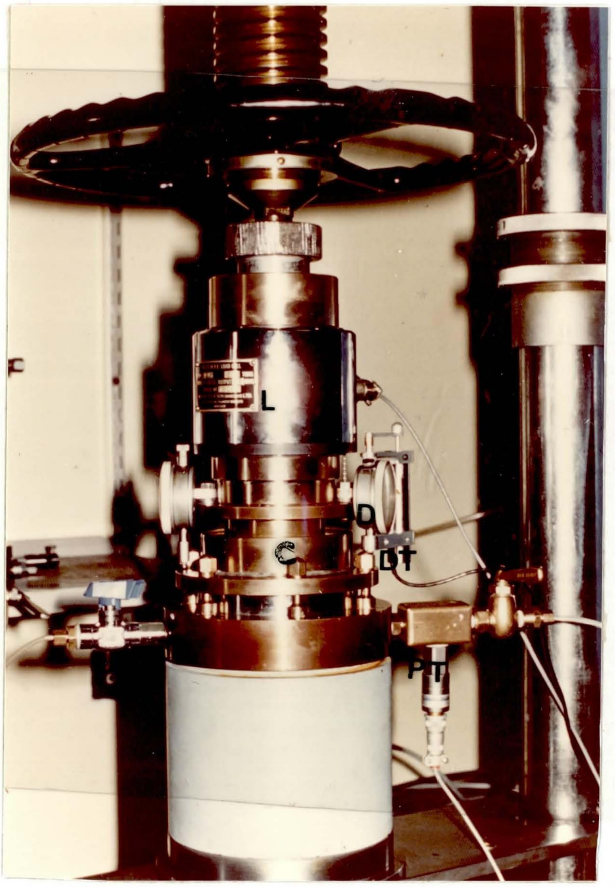
The pore pressure measuring system contained on the

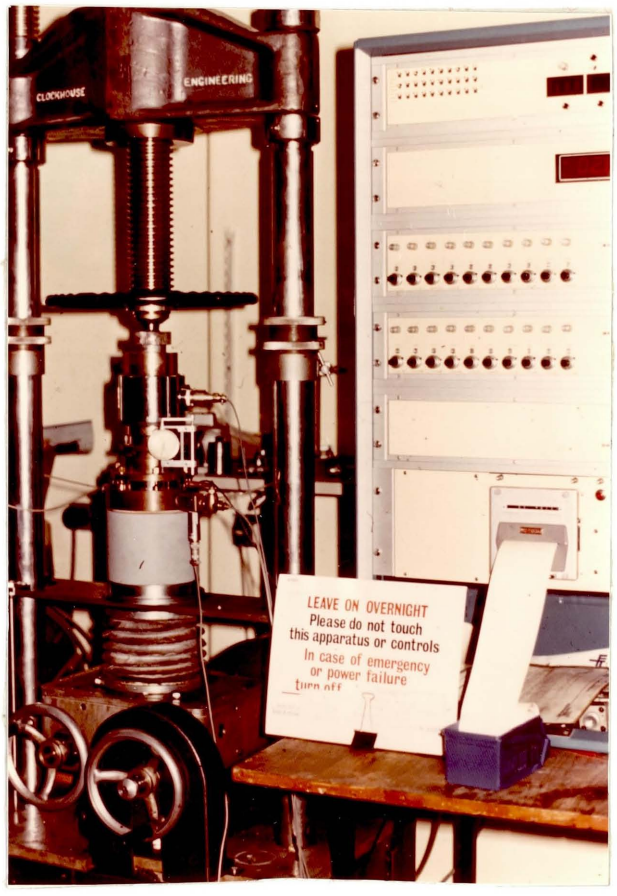
PLATE 5.7 Constant rate of strain consolidation equipment:

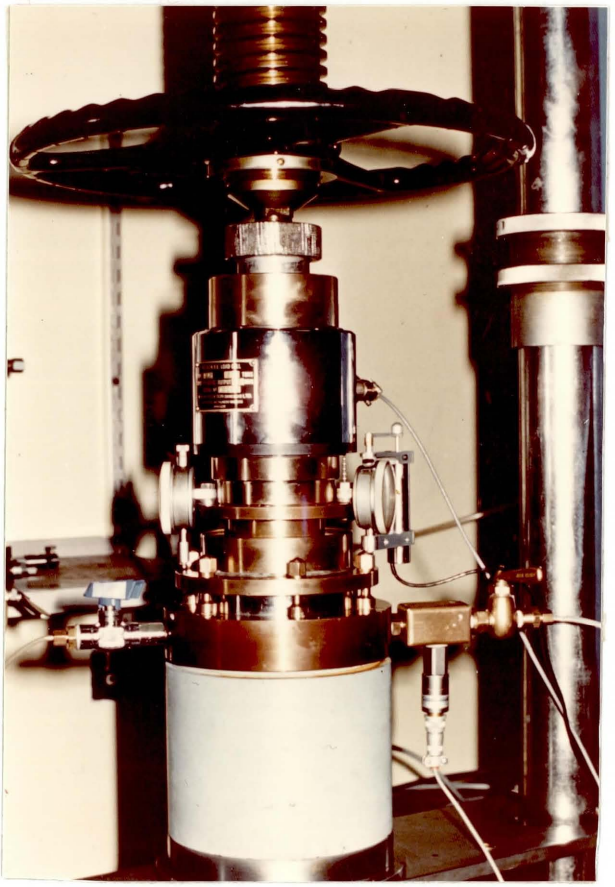
(a) View showing the cell positioned in the triaxial frame.

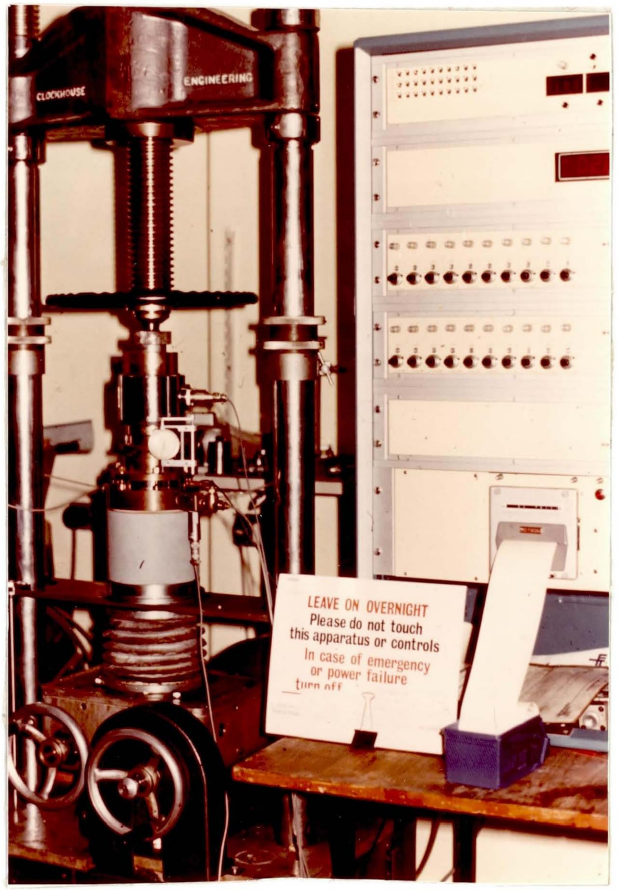
Load cell = L.
Consolidation cell = C.
Dial Gauge = D.
Displacement Transducer = DT.
Pore fluid pressure transducer = PT.

(b) View showing the electronic transducer measuring system linked to the automatic data logger for continuous record of time, axial pressure, specimen deformation and pore fluid pressure.


L
D
C
DT
PT


CLOCKHOUSE
ENGINEERING
LEAVE ON OVERNIGHT
Please do not touch
this apparatus or controls
In case of emergency
or power failure




CLOCKHOUSE
ENGINEERING
LEAVE ON OVERNIGHT
Please do not touch
this apparatus or controls
In case of emergency
or power failure

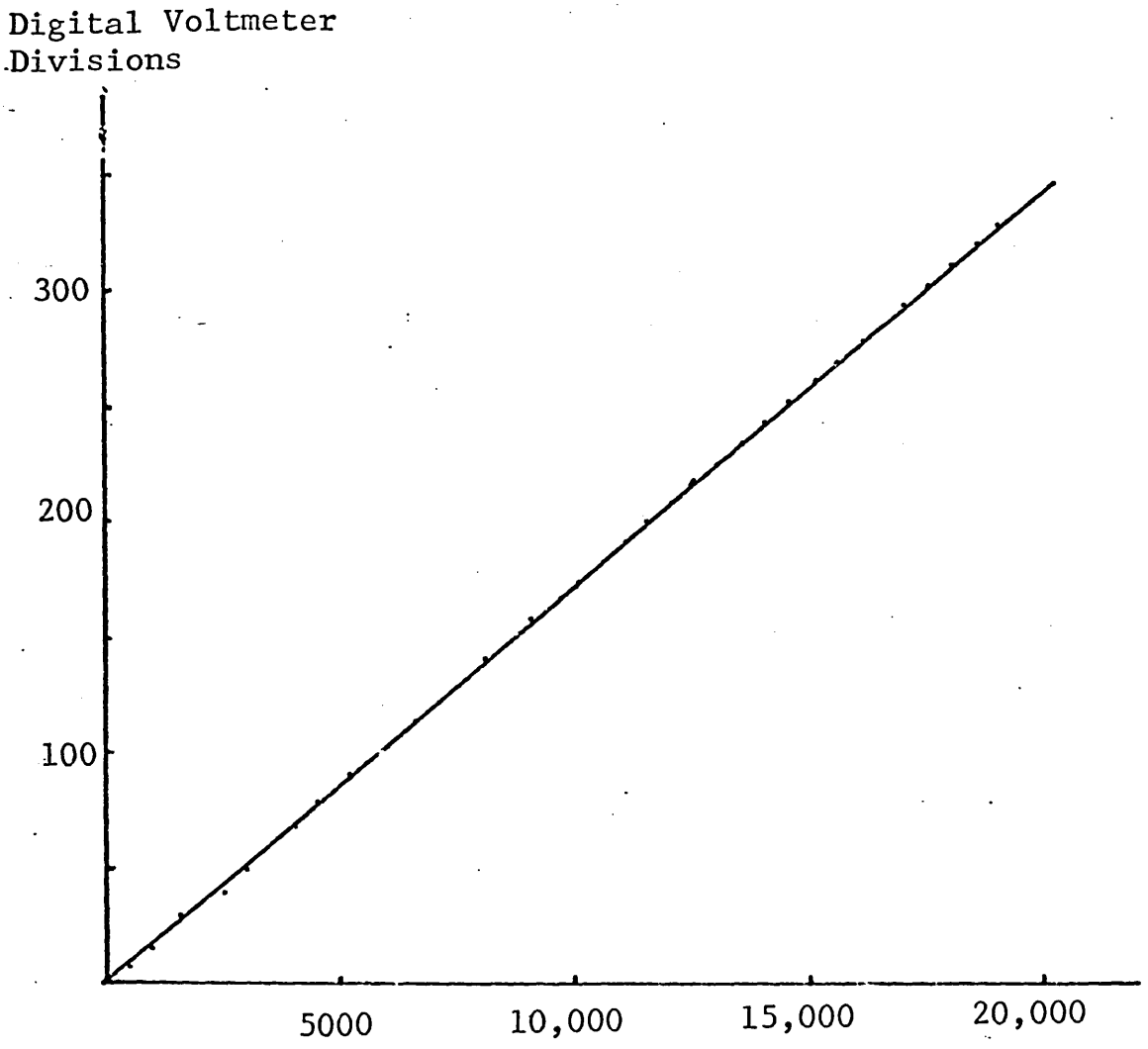


FIGURE 5.14 Load cell calibration.

base plate of the cell uses high air-entry ceramic porous stone, that fits into a recess in the centre of the plate. Two small boreholes connect the porous stone to a pressure transducer and an extra outlet. The pore pressure measuring system has been designed to have a very low system compressibility in order to minimise the hydrodynamic lag during the test. The signal conditioner on the readout is adjusted during the calibration to give a direct reading of the pore pressure.

5.3.4 Measurement of the axial compaction, (Δx)

Axial deformations (Δx) of the test specimen during loading are determined by measuring the movement of the top cap both with dial gauges and with an electrical displacement transducer. As shown in figure 5.13, the two dial gauges are screwed diametrically opposite to an annular plate sitting on the top cap. The electrical displacement transducer serves both as a check and also to aid in fully automating the test. Accordingly all necessary data are printed periodically during a test.

5.3.5 Test procedure

The pore water pressure transducer was connected to one of the outlets from the base of the cell using a Klinger valve. De-aired water was flushed through the system and after

closing the other flushing valve, a saturated porous stone 1.50 inch diameter and 0.25 inch thick was placed in the recess provided in the base.

The undisturbed specimens were prepared using a similar method to that adopted for the high pressure compaction tests. As usual, the specimen was first trimmed with a 3 inch internal diameter cutting ring and then pushed into the testing ring. Two saturated filter papers were placed on the top and bottom of the sample, which was then positioned accurately on the base and clamped with the flange and studs. Thus the centring of the sample was therefore automatically achieved. The top loading cap containing the larger saturated porous stone was lowered onto the sample and the annular plate with the dial gauges were positioned from the top. The spacers and the load cell were then positioned in place and the pedestal of the loading machine was raised to bring the assembly into contact with the head of the machine.

Then the gear box was adjusted to give the desired rate of strain. The rate of strain had to be chosen so as to produce only a negligible pore water pressure at the base. This was, however, achieved by trial and error. The rates of strain used for each test are given with their results in the relevant chapter.

5.4 LOW PRESSURE TEMPERATURE CONSOLIDATION CELL

For this phase of the research, to investigate the influence of temperature on the consolidation behaviour, the standard oedometers were modified. 4 inch diameter, 2 inch thick specimens were confined in a brass ring between two porous stones and the pressure was applied to the upper stone by placing dead weights on the hanger at the end of a lever arm (see plate 5.8).

The series of results of one-dimensional consolidation tests described in Chapter Six were also performed in these standard oedometers but on 3 inch diameter, 0.75 inch thick specimens.

5.4.1 Measurement of axial compaction, Δx

The axial compaction (Δx) is measured relative to the base of the cell using a dial gauge. Observations of the dial gauge are made at convenient $\sqrt{t}$ intervals.

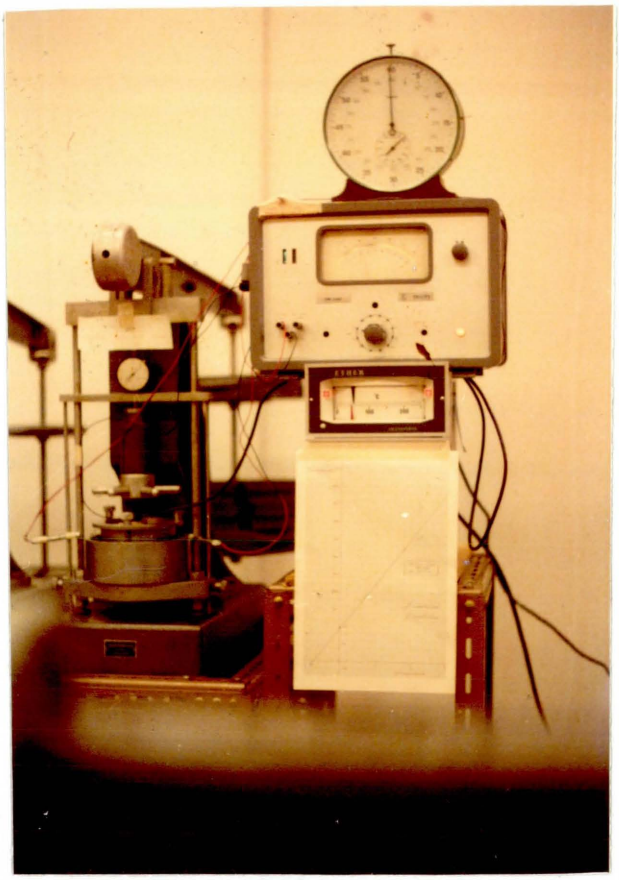
5.4.2 Heat source

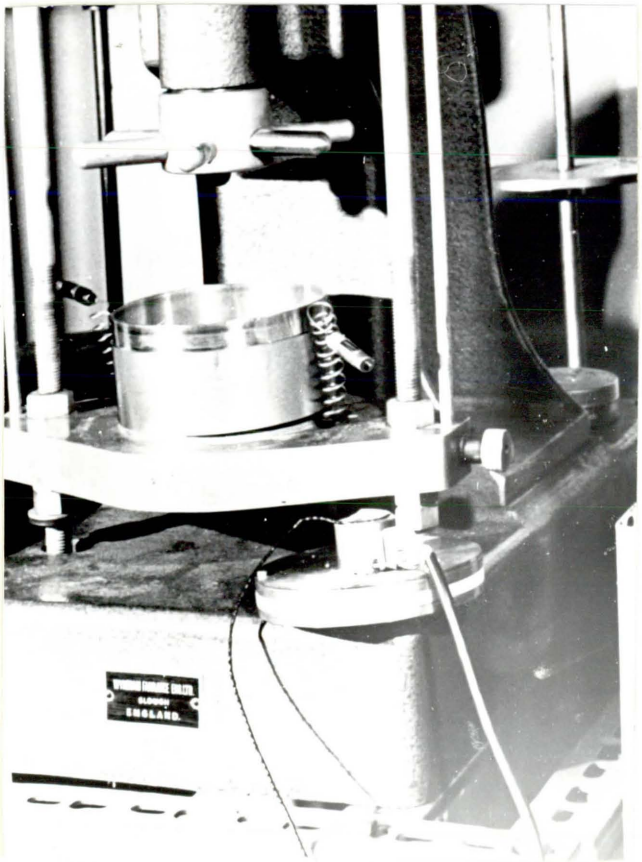
The loading cap is turned out of brass and is fitted with a PTFE coaxial seal to stop the drainage of water from the upper end of the sample. The heating element is located within the loading cap as shown in figure 5.15. The temperature of the surface of the heater is maintained by a thermocouple temperature

PLATE 5.8

(a) A view of the low pressure temperature consolidation equipment, showing temperature controlled, loading system.

(b) Detailed view of the modification to the standard Wykeham Farrance consolidation cell.




ENGLAND

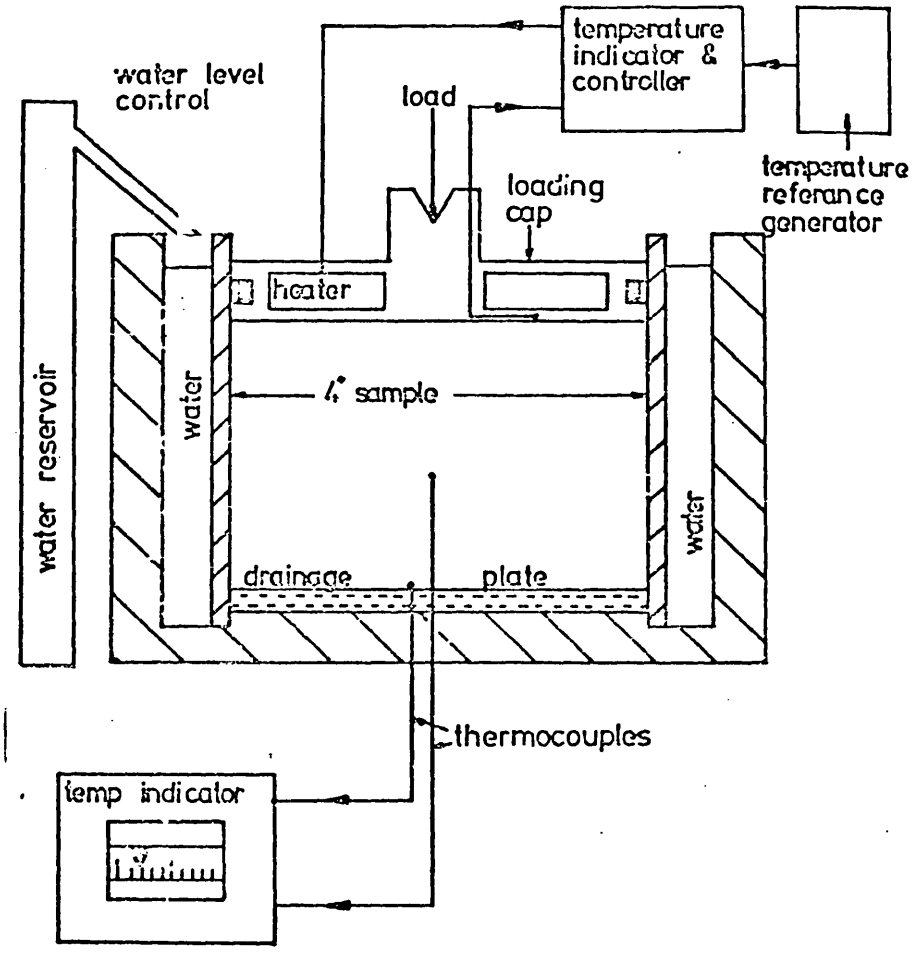


FIGURE 5.15 Low pressure temperature consolidation cell.

controller and a 250 Watt heater. The terminals and the body of the heater was insulated against shorting due to access of water.

5.4.3 Temperature measurement

The thermal gradient through the sample is measured from two fine thermocouples (head diameter < 0.01"). These were chosen as they were very flexible, and can also withstand ordinary testing procedures. The thermocouple voltage was observed on a potentiometer and the calibration of the thermocouples showed a linear variation between thermocouple voltage and temperature for the range $0^{o}C$-$100^{o}C$.

All other temperatures, such as the room temperature, temperature of the surrounding water, were observed using an electronic thermometer.

A second oedometer, identical except for the inclusion of heaters, was always used in conjunction to obtain comparative results.

5.4.4 Test procedure

In these tests, the specimens used were all remoulded at close to a hundred percent moisture content. With the fixed ring in place over the lower porous stone, the slurry was poured carefully avoiding trapping of air and damage to the thermocouples.

The upper surface of the clay is smoothed and the loading cap is placed gently on the slurry. This is then lowered carefully into the water bath and the entire cell arrangement is then positioned centrally on the loading device.

The desired temperature on the loading cap is set on the temperature controller and the system is left for twenty-four hours to achieve steady state conditions. Any associated deformations in the specimen are observed. An external water reservoir is used to augment the water in the water chamber to keep it from drying due to evapotranspiration.

The test is then continued in the usual way as for a conventional one-dimensional consolidation test using a load increment ratio ($\Delta P/P$) of one with twenty-four hour interval between any two increments.

CHAPTER SIX Description of the soil samples, sampling sites and sampling technique

6.1	Introduction		246
6.2	Recent sediments from Falmouth Estuary		248
	6.2.1	Source rock and catchment	248
	6.2.2	Falmouth Estuary	254
	6.2.3	Rate of sediment deposition	258
	6.2.4	Sampling technique	261
	6.2.5	Low pressure consolidation response	268
6.3	Ball Clays from Devon		268
	6.3.1	Source of sediment and depositional environment	270
	6.3.2	Ball clay type and their geotechnical properties	270
	6.3.3	Sampling technique	274
	6.3.4	Low pressure consolidation response	274
6.4	Ball Clay no. 661		274
	6.4.1	Low pressure consolidation of the remoulded ball clay	277

CHAPTER SIX

DESCRIPTION OF THE SOIL SAMPLES, SAMPLING SITES AND SAMPLING TECHNIQUE

6.1 INTRODUCTION

The sediments chosen for the laboratory consolidation studies were predominantly Kaolinitic and were obtained from sites in South-West England (Figure 6.1). The geological setting of these sampling sites and the sampling techniques adopted are described in this chapter. The geotechnical properties of these sediments and their response to low pressure laboratory consolidation will also be given here.

Undisturbed specimens were collected from deposits with two widely differing previous compaction stress histories; normally consolidated and over-consolidated; they were thus of different initial consistencies. Recent and soft estuarine sediments were obtained from the intertidal flats of the Falmouth Estuary in Cornwall, and stiff over-consolidated Ball Clay of Oligocene age was sampled from the open clay pits of South Devon.

Most of the studies, however, were made on samples remoulded in the laboratory, and as such a commercially available clay with a trade name, Ball Clay no. 661 produced by English China Clays Ltd., was used. Such remoulded samples were preferred for the preliminary series of comparative tests, as a strict control of the initial conditions of the sample was particularly desired.

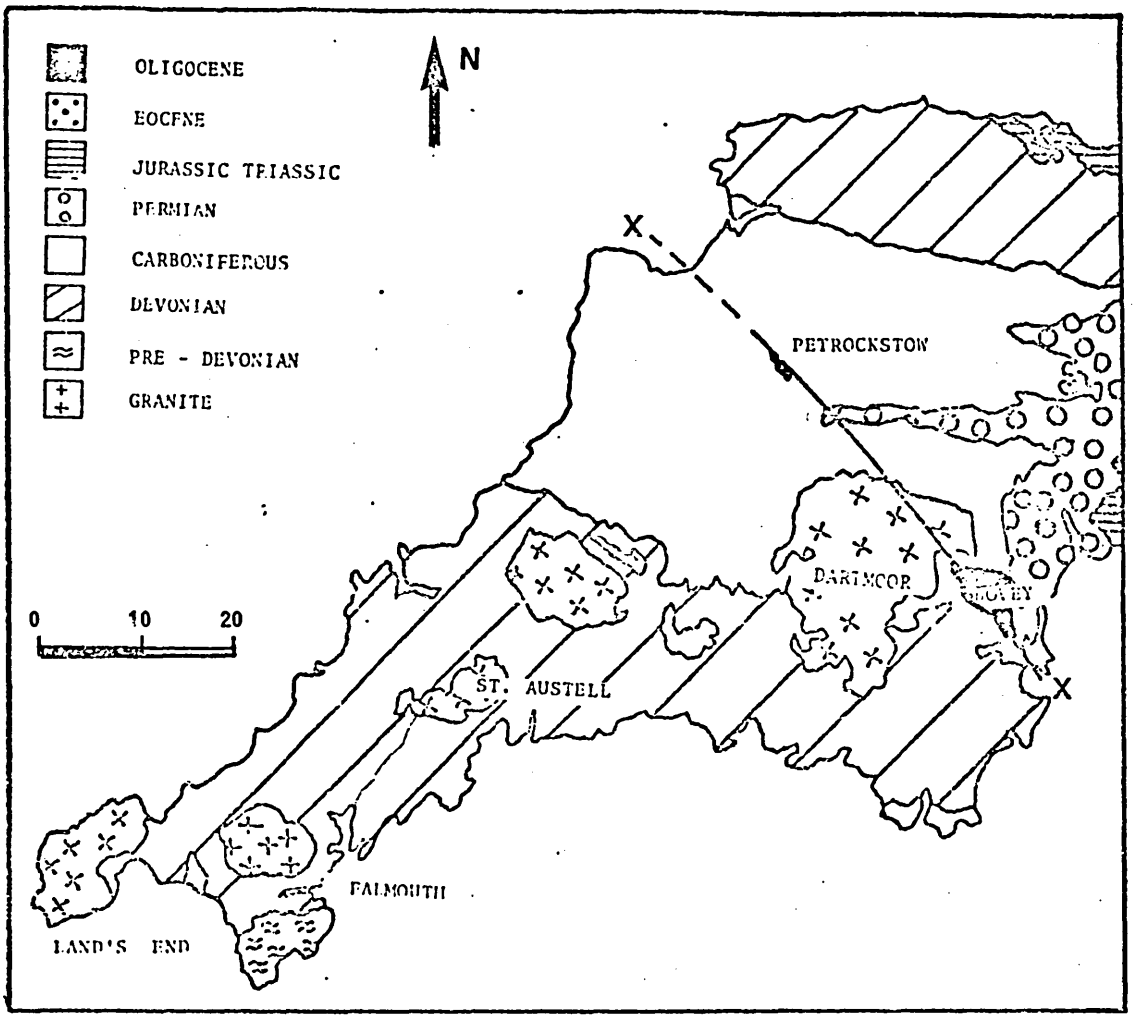


FIGURE 6.1 A SIMPLIFIED GEOLOGICAL MAP OF THE SOUTH WEST OF ENGLAND SHOWING THE SOURCE OF SEDIMENTS TESTED IN THIS STUDY

(after Geological Map of Great Britain, sheet 2, 1957)

6.2 RECENT SEDIMENTS FROM FALMOUTH ESTUARY

The sediments from the Falmouth estuary in Cornwall were known to be of relatively simple mineralogy and its accessibility was considered not difficult (Charmon, personal communication). Thus these formed an appropriate starting material in the task of laboratory simulation of geologic burial and exhumation. Accordingly during the summer of 1972, a field study was made of the Falmouth estuary, collecting a series of spot samples along the estuary in order to select a convenient and suitable site for the main sampling. The field area on the Falmouth estuary was located about 3 miles inland from the river mouth and extended over an area of about two miles square (Figure 6.2).

6.2.1 Source, rock and catchment

The Cornish china clays are considered to be the product of hydrothermal Kaolinisation of the orthogranites that have been intruded into the Devonian shales and slates. Despite the slight variations in composition of these granites from place to place, they are basically composed of feldspar, quartz and both biotite and muscovite with tourmaline as a common accessory mineral. These granites are generally porphyritic with large feldpsars being set in a fine ground mass. In particular the St. Austell granite exhibits large feldspar crystals sometimes as long as two or three inches (Plate 6.1).

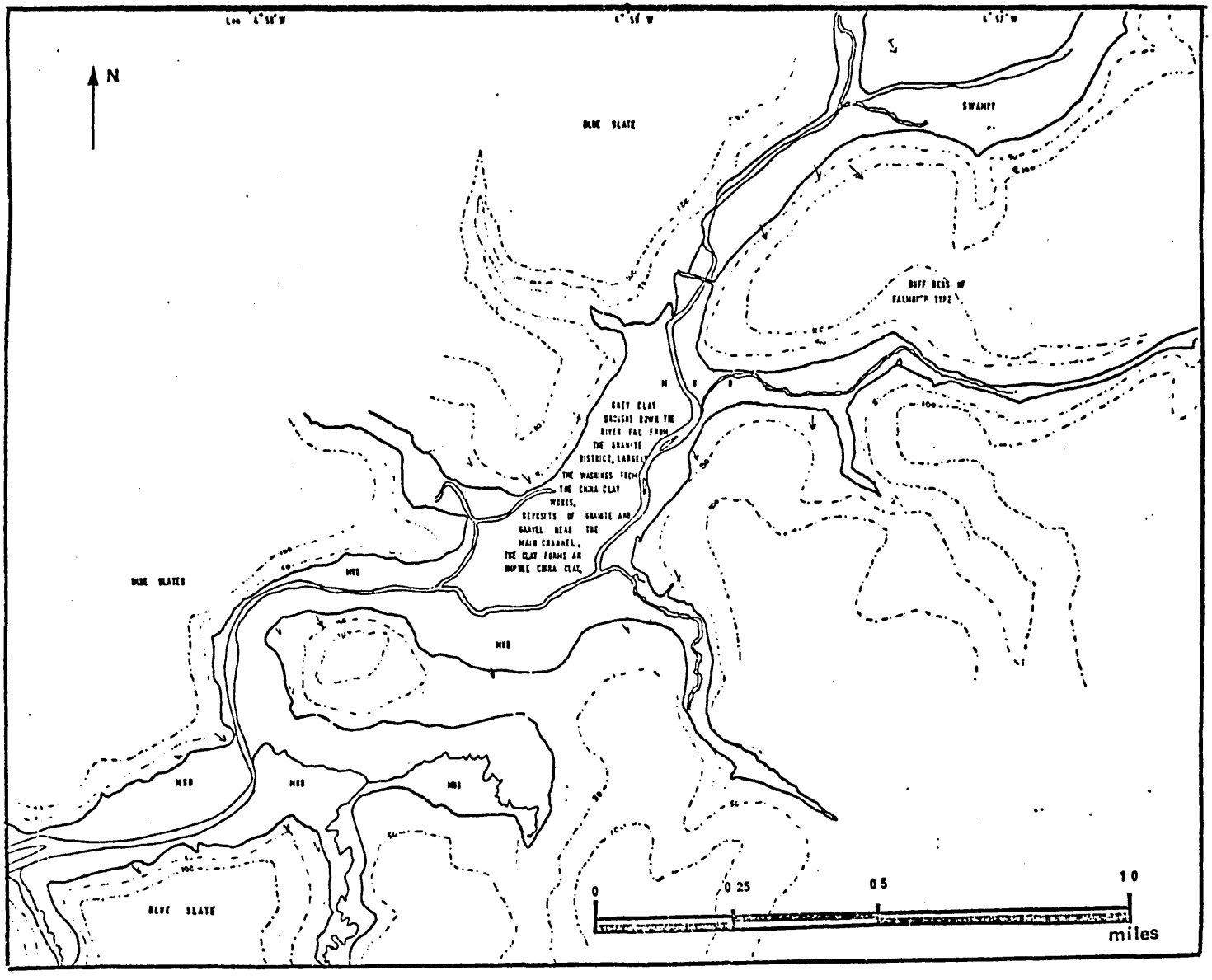


FIGURE 6.2 A geological map of the study area in the Falmouth Estuary.

PLATE 6.1 A hand specimen of St. Austell granite. Observe the characteristic elongated feldspars (F).

Scale: diameter of lens cap = 2.1 ins.


F
ASAHI
PENTAX

Complete kaolinisation has occurred on a large scale in the central and western portions of the St. Austell granite mass. However, in the area of about two square miles between Falmouth and St. Stephen's combe stream the kaolinisation is only partial and the granite is consequently being mined as 'china stone' (Barton, 1968) (see Plate 6.2a). In this material the orthoclase have been replaced while plagioclase have been unaffected. Plate 6.2b is an electron micrograph of this china stone showing in particular the occurrence of vermicullar kaolinite.

Associated with the extensive open cast mining of the china clay pits in St. Austell are the heaps of white quartz sand waste. These conical heaps form an outstanding feature of nearly every panoramic view of West Cornwall. Plate 6.3 is a telescopic view of the area as photographed from near Ardevora looking NNE and it shows the position of these quartz heaps of St. Austell (about forty miles away) in the background and the relevant Falmouth estuary in the foreground.

There would have been many repetitive elevatory movements associated with the several intermediate pauses and minor fluctuations of the sea level in the Pleistocene period. According to Barton, this discontinuous uplift is in excess of 430 feet and has resulted in repeated rejuvenation of the extending rivers and a rapid downcutting of the valleys. The river Fal has most of its catchment in the St. Austell granite

PLATE 6.2 Kaolinised granite.
Source St. Stephen's Coombe.

(a) View of a hand specimen of china stone showing the weathered white clay matrix.

(b) An electron micrograph of the china stone showing clusters or vermicullar kaolinite - natural habitat of the freshly altered Kaolinite.

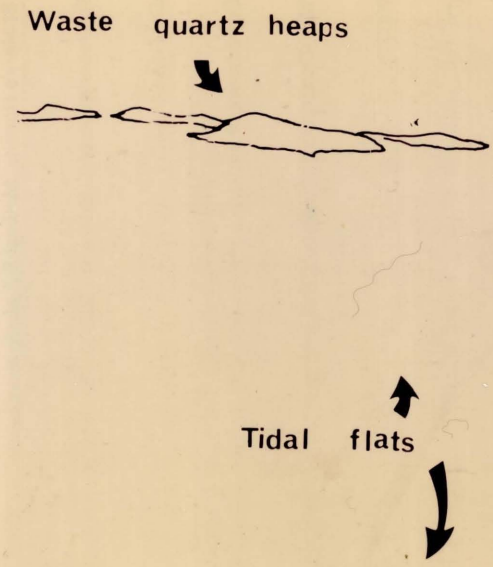

ASAHI
PENTAX


Vermicullar
kaolinite
2μ


ASAHI
PENTAX


2μ

PLATE 6.3 A telescopic view of the Falmouth Estuary, showing also the waste quartz heaps of the china clay workings in St. Austell (background).


Waste quartz heaps
Tidal flats


Waste quartz heaps
Tidal flats



and therefore wash down a considerable quantity of the clay. The river Fal was popularly known as the 'milky river' after the dense white colour of the waters that flowed. The water-borne sediment load was greatly reduced after the Cornish River Authority in 1968 took steps to ensure that the river was not polluted by the china clay workings.

6.2.2 Falmouth Estuary

These sediments have thus been deposited, not so long ago, under estuarine conditions and have formed vast areas of tidal flats. The portion of the river seawards from the bridge at Ruan Lanihorne (Figure 6.3) is highly silted and most of the flats are exposed at low tide when the light brown coloured tidal flats can appear picturesque in the west country setting (Plate 6.4). However, some parts of the estuary have apparently been abandoned and are now well below the mean high tide mark.

A block diagram illustrating the general features observed in the estuary is shown in Figure 6.4. Starting from the base, the sediments deposited in the channel bottom were characterised by the coarsest sediments of the tidal flats. Adjacent to the channel were the low mud flats across which many gullies passed. The sediments in them appeared laminated. Almost everywhere the sediments were infested with burrowing specimens.

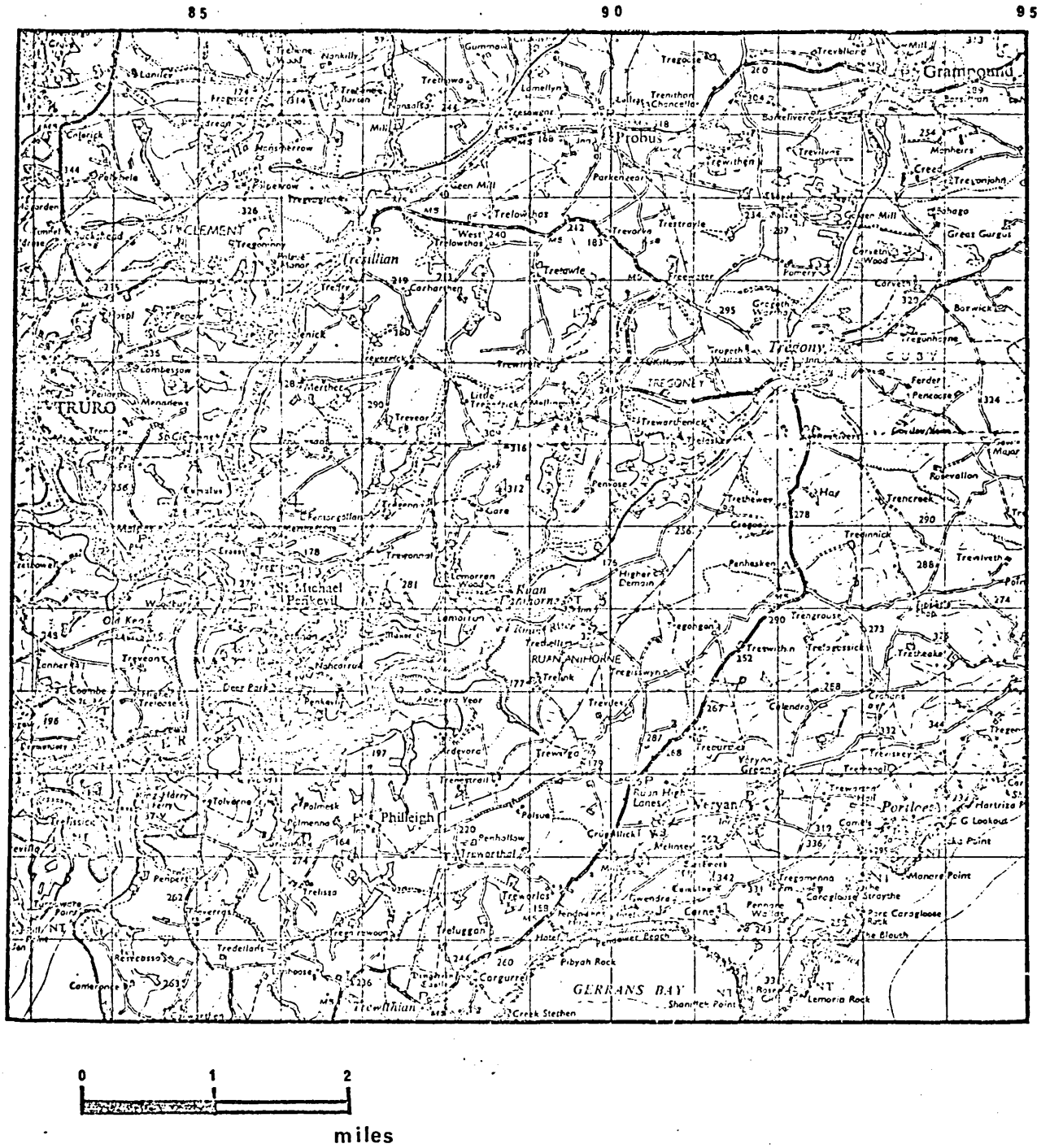
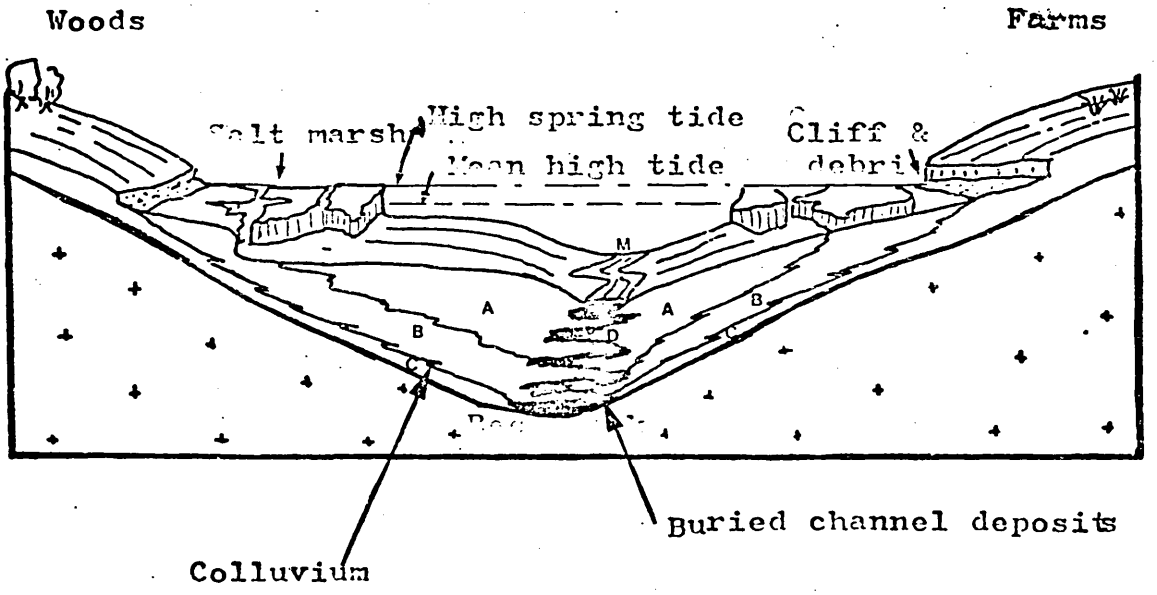


FIGURE 6.3 A map showing the area around the Falmouth Estuary.

PLATE 6.4 A picturesque view of the vast extent of the Falmouth Estuary in the West Country setting.





M : Main creek
A : Estuatine flats
B:: Salt marsh
C : Colluvium
D : Buried Channel deposits

FIGURE 6.4 A Block Diagram showing some of the sedimentological features observed in the Estuary.

Most of the tidal flats lay within the inter-tidal range and the actual river level lies below the mean tide level. The salt marshes on the abandoned flats lay above the mean high tide level and creeks with natural levels pass through these marshes.

6.2.3 Rate of sediment deposition

As discussed in Section 2.4.2.3, saline waters promote the aggregation of clay particles which subsequently suffer preferential gravitational settling due to their 'aggregated mass'. But, however, as a result of the continuous agitation caused by the mass of brackish water moving in and out of the estuary, most sediments are always kept in suspension. Most settling and deposition occur only during slack water when current velocities are low. At low tide, some of the flats are exposed and the consequent drainage of the pore fluids may cause negative pore water pressures in it that will temporarily fix the sediments. Much of these temporarily 'fixed' sediments will then become permanently fixed if the intensity of the following tidal current is not strong enough to resuspend these particles.

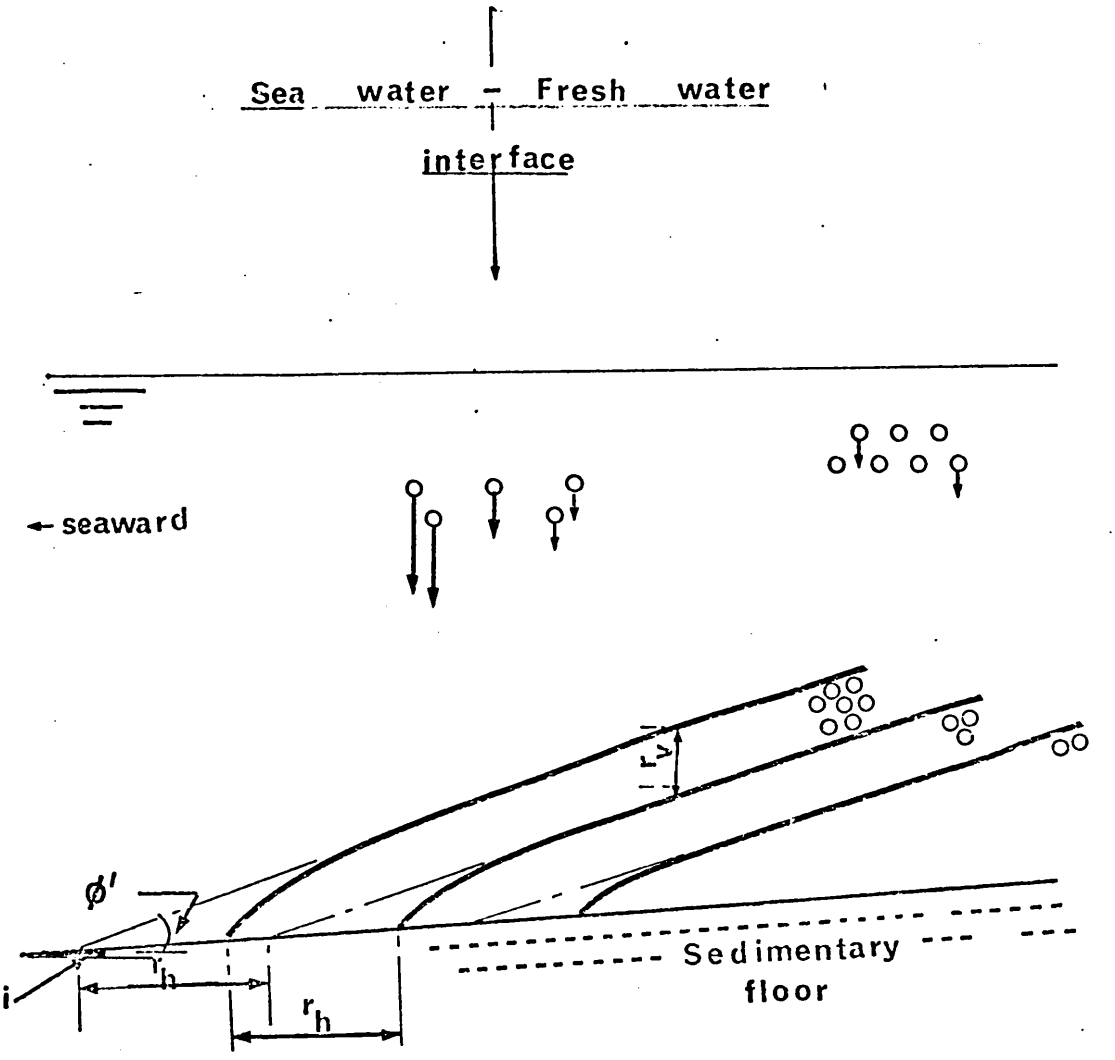
Barton (1968) has recorded the following information which amplifies the extent of siltation in the estuary:- Grampound was once "lapped by saline water" and till the year 1600, Tregoney had been a very active port but now both lie far away from tidal water (see Figure 6.3).

Figure 6.5 is an idealised representation of the sedimentation process in the vicinity of the sea water-fresh water interface in the estuary. The leading edge of the freshly deposited sediment will be inclined at an equivalent angle of repose to the horizontal to satisfy conditions of static equilibrium. The dynamic disturbances due to resuspension of sediments and turbidity currents, etc. are neglected. A relation between the lateral (r_h) and vertical (r_v) extent of siltation for any particular period may be sought in terms of the angle of repose ($\emptyset'$) and the slope angle of the sedimentation floor (i).

$$r_v = r_h(\tan\emptyset' - \tan i)$$

Submergence reduces the angle of repose and an average effective angle of repose of 8 is used as an approximate guide.

Applying the above equation to Barton's observations, a value for the rate of deposition is of the order of 1.2 metre/year. This appears very excessive in comparison with published data on other sedimentary basins (table 2.III). However, the Falmouth estuary has been more than a mere estuary in that it plays the role of a silting pond for the waste washings of the extensive china clay works of St. Austell. Furthermore this figure represents the maximum rate of sedimentation and at the seawater-fresh water interface, which itself is a non-stationary boundary moving with the tide.



$$r_v = r_h (\tan \phi' - \tan i)$$

FIGURE 6.5 An idealised geometric interpretation of the sedimentation at the sea water-fresh water interface in an estuary.

6.2.4 Sampling

A series of nine 1½" core samples were collected from various points along the tidal flats (figure 6.2). Results of certain preliminary investigations are summarised in table 6.I. The samples had an average void ratio of about 1.5. The particle size distribution depended on both the lateral and longitudinal location of the sampling point. The pore fluid chemistry showed that the pore fluids were less saline than common sea water.

The exposed flats between the Aredeveora Veor and Ardeveora farms proved to be the most conveniently accessible and suited site for collecting samples for the consolidation tests. These particular flats were about 300 yards away from the main river course and as such its sediments would have been deposited under relatively calm conditions and therefore they will also be uniformly fine.

Plate 6.5 shows a block sample of the sediments that was dug out of the flats. The surface of the flats is light brown in colour but immediately below the surface (about 1") it is of light to dark grey in colour, particularly when wet. On drying, the colour of the entire clay becomes muddy brown. Samples necessary for low pressure compaction studies were carved out of the block sample in the laboratory (see Section

Site No.	Grid Reference	Void Ratio	Concentrations of Ions in pore fluid (mg/L)					Remarks
			Na^{+}	K^{+}	Mg^{++}	Ca^{++}	SiO_2	
A	407881	1.501	83.8	18.0	62.0	143.7	1.0	Near main sampling site
B	406877	1.649	86.0	20.0	72.5	163.7	5.5	low tidal flat
C	404875	1.599	90.5	20.4	75.5	162.5	12.8	many burrow worms
D	403868	1.658	84.3	19.8	74.5	161.2	11.6	centre of river silty clay
E	410880	1.185	86.5	20.5	75.0	161.2	18.2	abandoned river terrace
F	412883	0.938	85.0	20.5	75.0	158.7	16.6	abandoned river terrace
G	408873	1.611	84.5	19.8	76.0	157.5	29.8	from a near creek
H	406889	1.523	85.8	19.5	76.2	156.2	20.4	Tuckingmill creek
I	419888	1.456	84.8	19.8	75.0	156.2	7.4	Ruar river salt marsh

TABLE 6.I

DETAILS OF SPOT SAMPLING SITES

PLATE 6.5 A cross-sectional view of a block sample of the clay from the Falmouth Estuary.


ASAHI
ENTAX

A series of careful observations were made on the variation of the index properties within the first few cms. of the sediment deposit and is presented in figure 6.6. The liquidity index is greater than one and falls with depth. The values for the colloidal activity for the grey clay appear somewhat constant and high (0.9), suggesting a relatively uniform and normally inactive sediment.

Fig. 6.7a illustrates the piston sampler that was designed and used for the collection of 4" diameter samples for the high pressure consolidation tests. The samples were collected within the PTFE sleeves to avoid contamination and to facilitate subsequent assembly into the apparatus. The piston on the sampler fits tightly on the sleeves and its position is fixed by attaching the rod on to the sampling frame via a chain. The body of the sampler is pushed into the sediment relative to the piston during the sampling process. The thick aluminium base on which the tripod frame is supported aids in distributing the bearing load on the soft sediments. It was at times necessary to loosen the sediments around the sampler so as to conveniently extract the sampler from the sediment deposit. Plate 6.6b shows the piston sampler in use. Figure 6.7b illustrates how the same sampler body was modified to serve as a pore water extracting press for chemical analysis of the pore fluid.

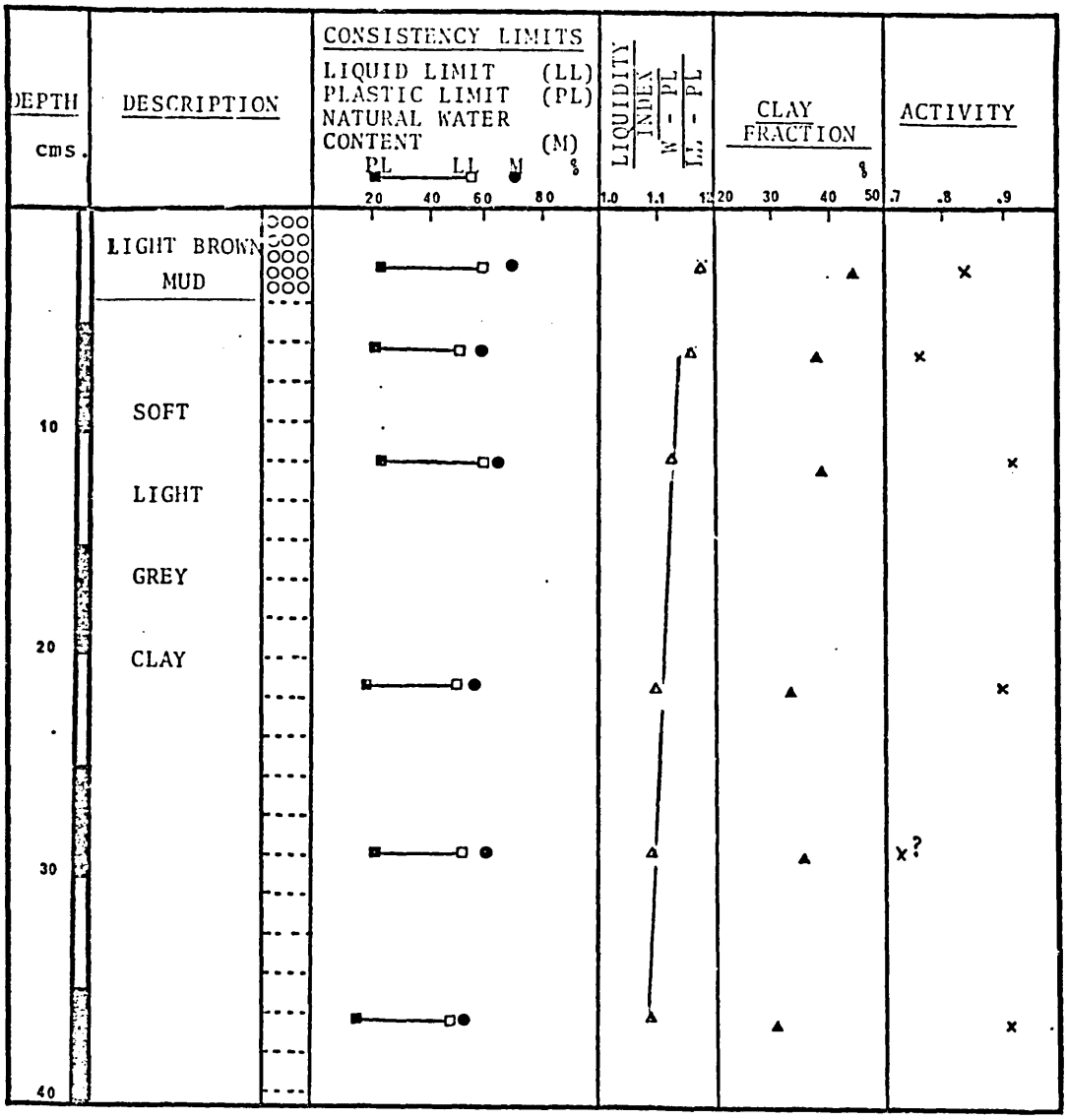
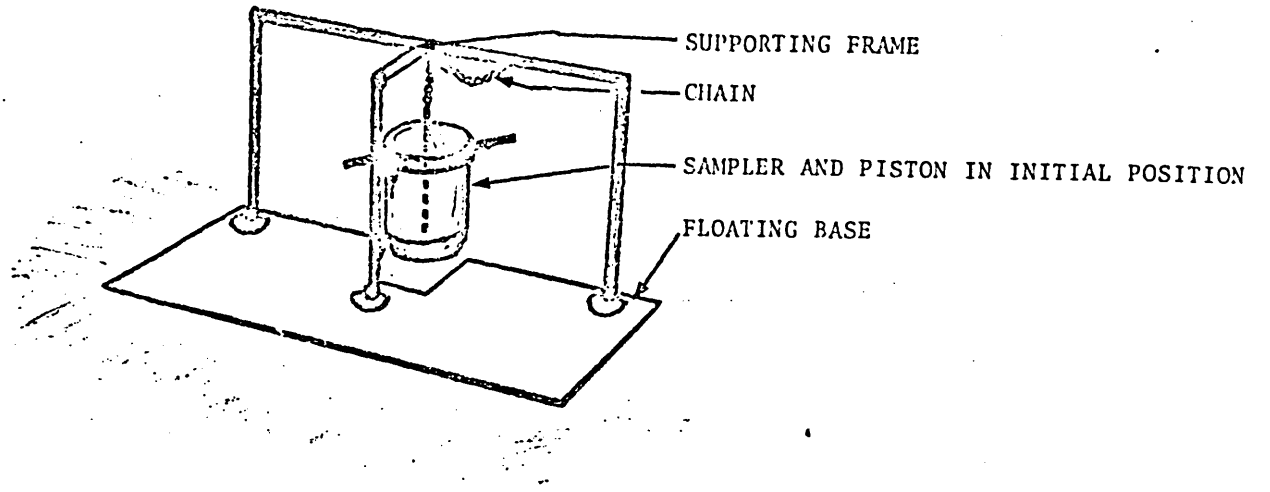
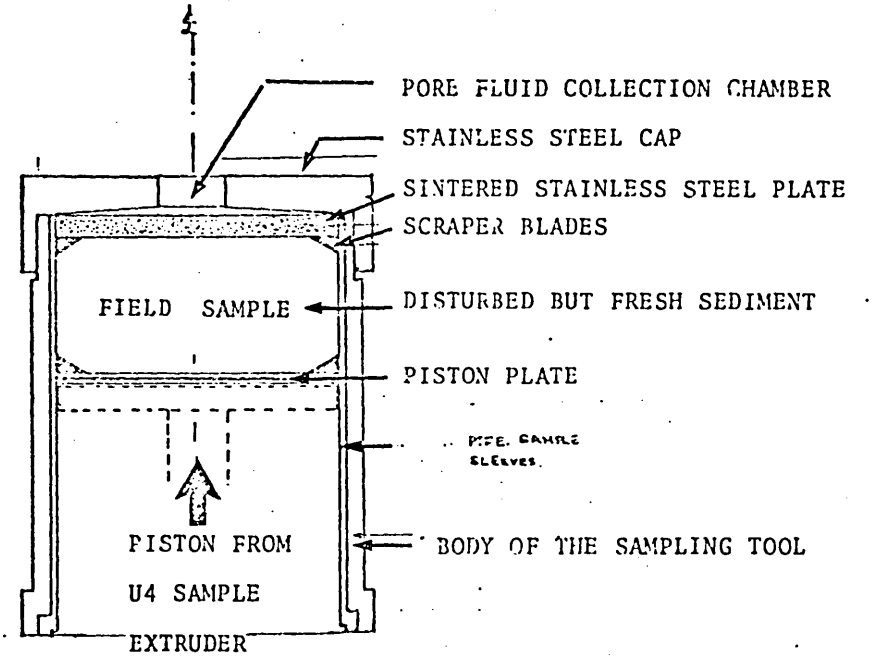


FIGURE 6.6 Some geotechnical properties of the recent sediments in the tidal flats of the Falmouth Estuary.



(a)



(b)

FIGURE 6.7 a. Details of the soft sediment sampling equipment.

b. Modifications to the sampler for its use as a pore fluid extractor in the field.

PLATE 6.6 Sampling equipment and sampling of the soft Falmouth Clay:

(a) A view of the sampling equipment showing:

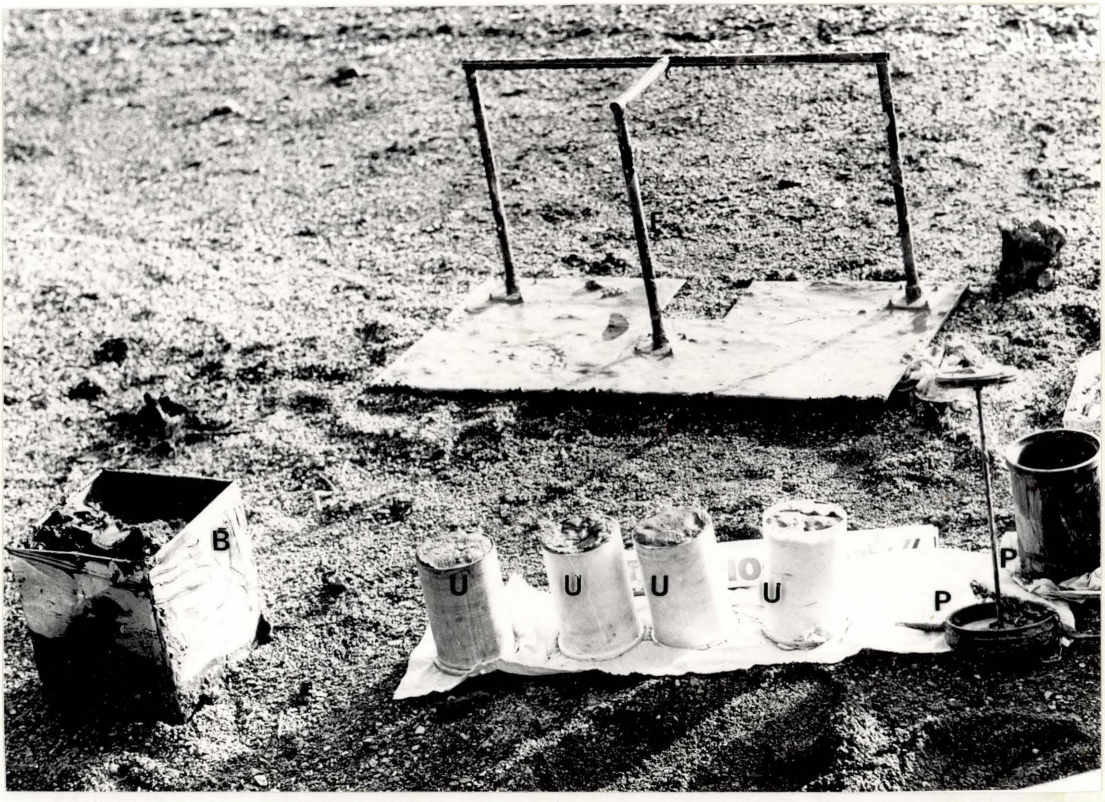
F - Frame and base of the equipment

P - Sample body and piston

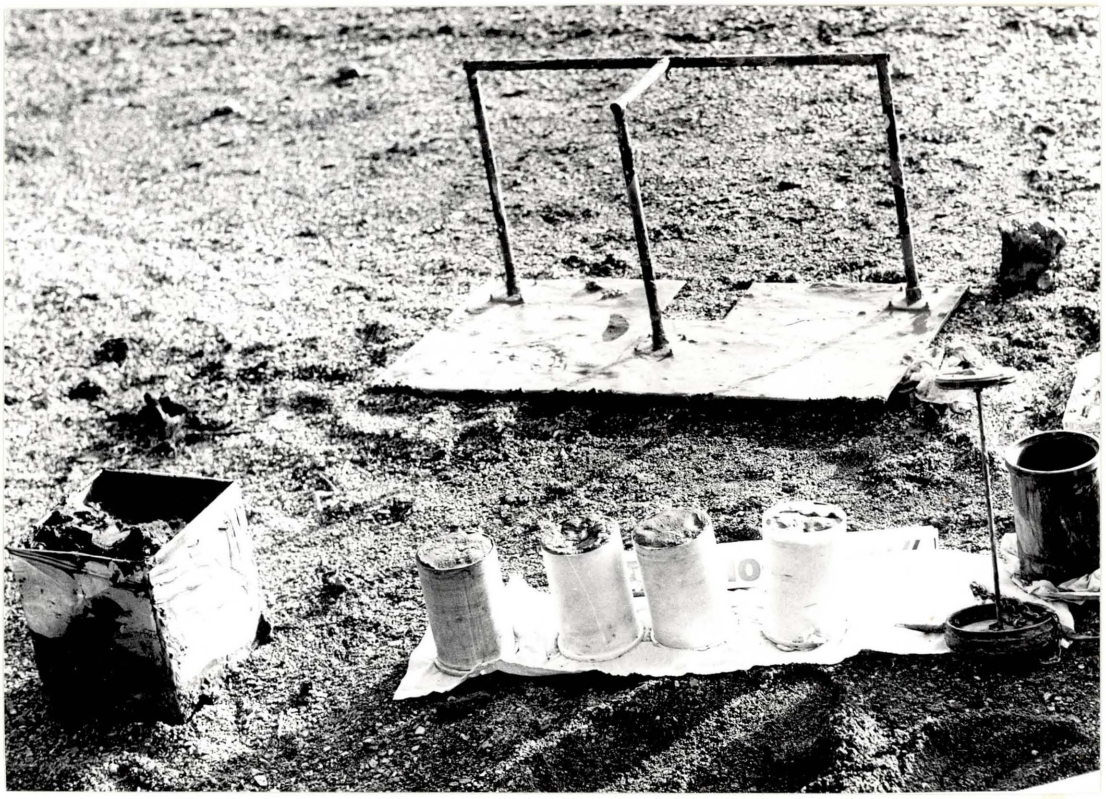
U - Undisturbed 4" core samples

B - Undisturbed block sample

(b) The piston sampler being used to extract an undisturbed sample. Spade is used to soften the sediment around the sampler body.


B
U
U
U
U
P
P







6.2.5 Low pressure consolidation responses

Figure 6.8 gives the results of the low pressure consolidation tests performed on a systematic series of horizontal specimens carved from a block sample. The results of N.FA.CLP.3 and N.FA.CLP.4 (for test coding see Section 7.1.1) are very closely similar and, as such, they represent the low pressure consolidation character for the grey Falmouth estuary clay. The e-log P curve for N.FA.CLP.1 differs from the above in showing a more porous structure which evidently results from its high clay fraction (see figure 6.6 and also compare figures

Unfortunately the test N.FA.CLP.2 did not yield representative results as it contained a dead bivalve mollusc which hindered consolidation.

6.3 BALL CLAYS FROM DEVON

The Bovey ball clays are an overconsolidated fluvio-lacustrine deposit. Some of their geotechnical and sedimentary aspects have been described by Best and Fookes (1970). They reported that their usual oedometer test results on samples of these deposits failed to give an estimate of its preconsolidation load (see figure 6.10). Thus, together with the studies of the effects of artificial burial of sediments, the high pressure consolidation cell was used to determine the magnitude of the preconsolidation load.

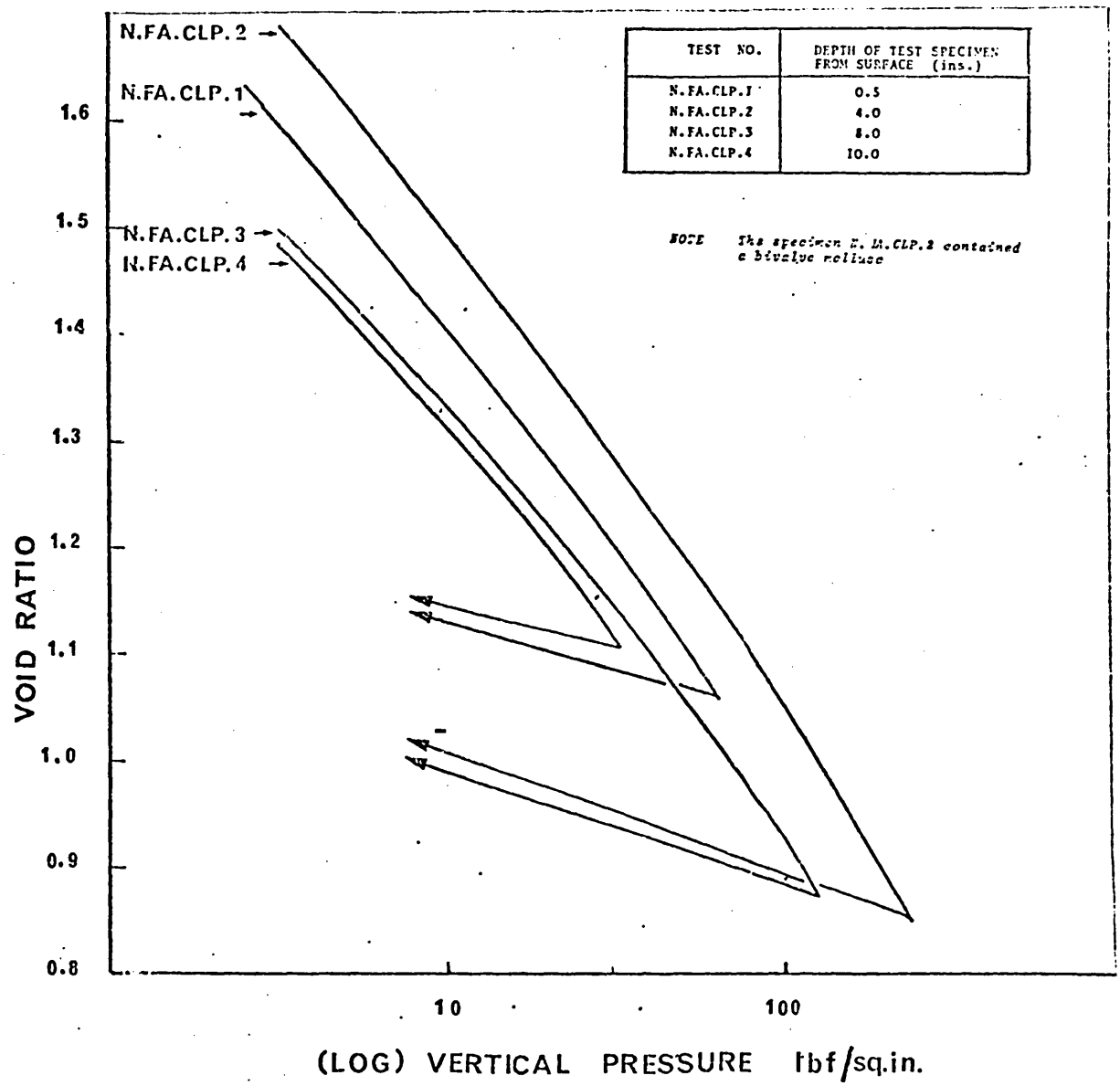


FIGURE 6.8 Low pressure e - log p curves for the undisturbed specimen of Falmouth Clay.

6.3.1 Source of sediment and depositional environment

The Bovey sediments underlie an approximately elliptical area of the low ground south east of Dartmoor (figure 6.9a). Reid (1898) believed these sediments to be derived from the kaolinised granite of the Dartmoor Massif, and deposited in a large freshwater lake within a rift valley. Bristow (1968) compared these sediments of the Bovey basin with those of similar lithology in the Petrockstow basin (figure 6.9b) and demonstrated them to be of basically similar mineralogy with kaolinite as the principal clay mineral. Bristow, however, has further demonstrated that the kaolinitic sediments of the Petrockstow basin were formed by erosion, transportation and deposition of a weathering mantle developed on Culm measure shales under humid sub-tropical or warm temperature climatic conditions in Oligocene times.

Gravity induced slump structures and small scale faulting are apparent in some vertical sections of the open cast clay workings of the Bovey basin. These typically result from the penecontemporaneous deformation of freshly deposited shallow water sediments and indicate rapid deposition by high speed sediment laden currents (Coleman et al, 1967).

6.3.2 Ball Clay types and their geotechnical properties

Scott (1929) described two principal types of ball clay with different ceramic properties - the stoneware and

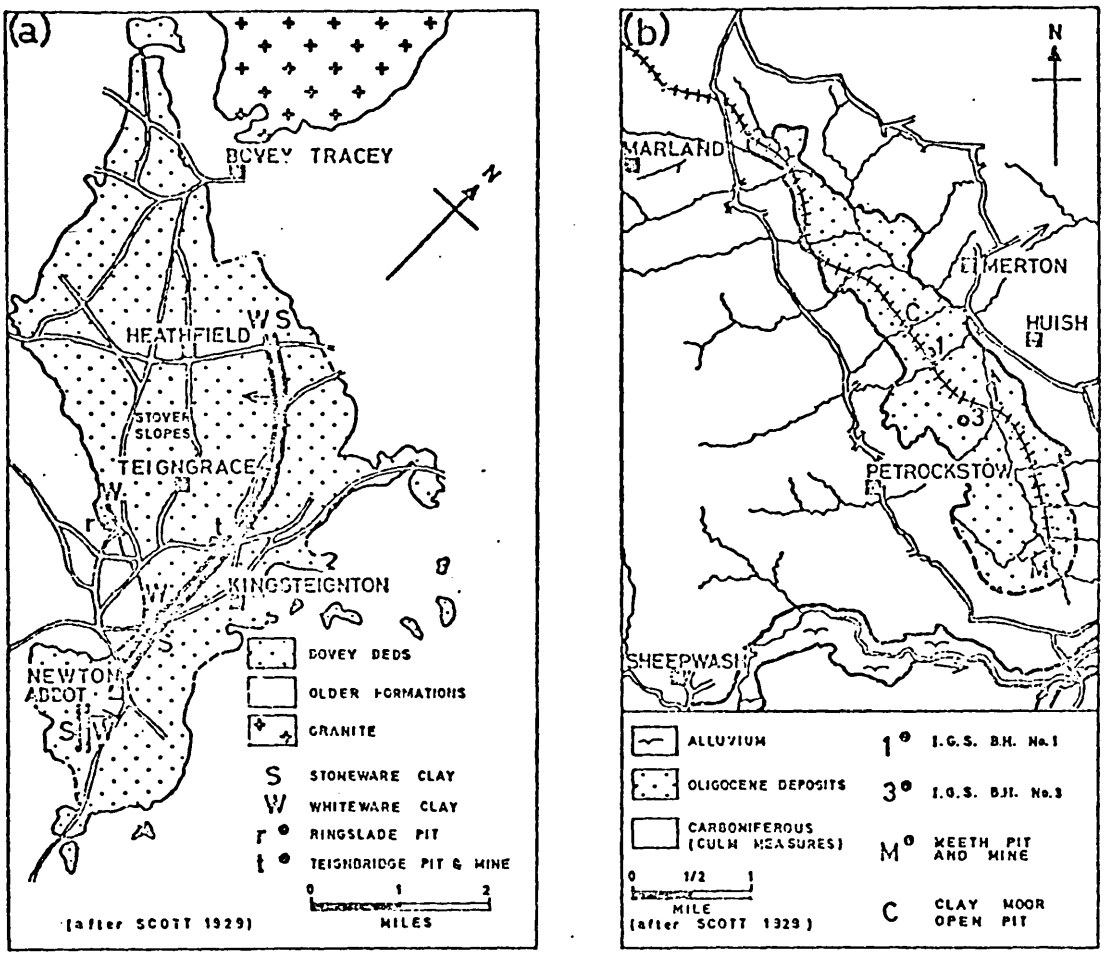


FIGURE 6.9 Sketch maps of the Bovey and Petrockstow Basins

(after Best and Fookes, 1970)

whiteware clays. The stoneware clays contain large amounts of silica ($< 2\mu$ typically 70-75 percent) and are non-carbonaceous. They are grey in colour but sometimes show red and brown mottling being interbedded with silts and sands; these are worked open cast at depths up to 60 feet. The stoneware clay is stiff to hard and is apparently intact and will have a consistently negative liquidity index implying an overconsolidated state.

The whiteware clays are slightly lignitic and are almost entirely free of sand or silt grains ($<2\mu$ about 90-98 percent). They are always found in association with lignite seams and are often worked underground. But they are also worked at lower levels in large open cast workings such as Preston Manor clay pit (Plate 6.7). These deposits are hard to very hard and are highly fissured. Their liquidity indices are lower than those of the stoneware clays, implying that they are apparently more overconsolidated.

It was the conclusion of Best and Fookes that the lowering of the water table during drying-up of the sedimentary basin caused the clays to be dessiccated, hence overconsolidated early in their depositional history. The degree of overconsolidation is dependent on the negative pore water pressures set up in the clay. Higher suctions are prone to be developed in the fine grained whiteware clays than the stoneware clays and this could account for the difference in the liquidity indices between the two groups.

PLATE 6.7

A view of the Bovey Ball Clay beds at Preston Manor Clay Pit. This shows the lignite seams in the matrix of whiteware Ball Clay.


Whiteware clay
Lignite seam



6.3.3 Sampling

Undisturbed block samples measuring approximately 10 x 10 x 9 inches were cut from freshly exposed bench levels in the open cast ball clay workings at Meeth pit in the Petrockstow basin. The block sample was trimmed carefully to fit inside a metal box whose lid was sealed on site in order to preserve the clay at its natural water content.

6.3.4 Low pressure consolidation response

Best and Fookes (1970) performed undisturbed low pressure oedometer tests on 3 inch diameter and ¾ inch specimens trimmed from the block samples. Owing to the difficulty of trimming accurately undisturbed specimens of whiteware clay, no tests had been performed. Their results of tests on stoneware clay and on remoulded specimens with initial water contents above the liquid limit are given in figure 6.10.

Further geotechnical properties of these clays are summarised in table 6.II.

6.4 BALL CLAY NO. 661

For the majority of the remoulded tests in this study, the above commercially available clay was used. They are produced from the ball clay areas of South Devon, North Devon and Dorset by the English China Clays.

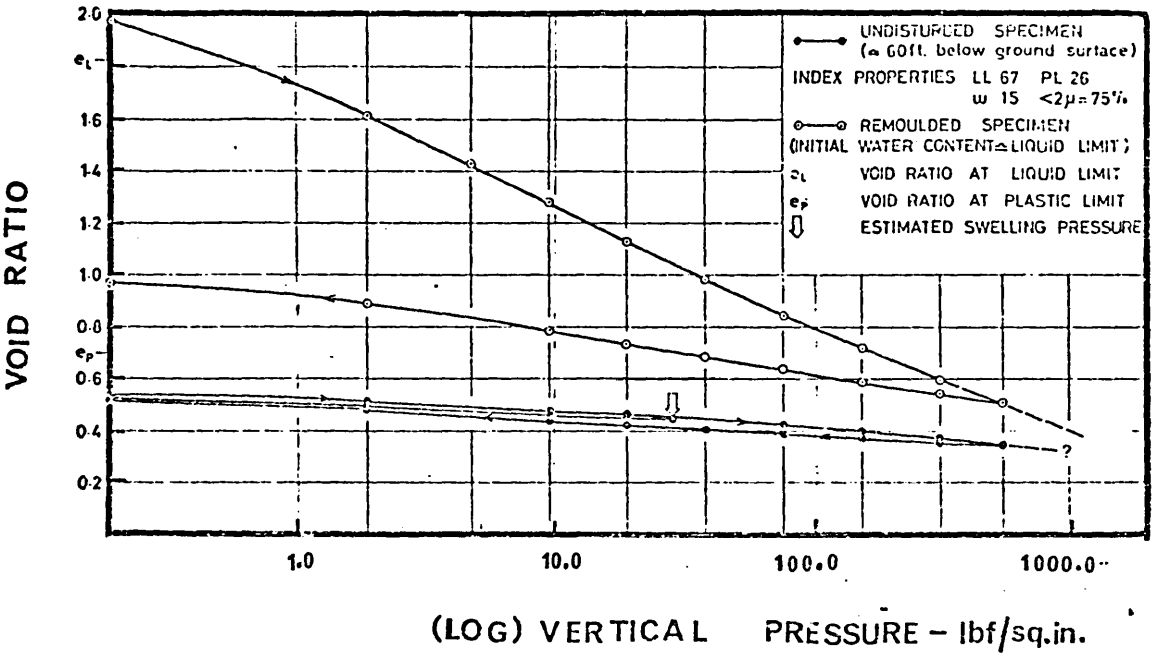


FIGURE 6.10 Typical e-log p curves for undisturbed and remoulded specimens of stoneware Ball Clay from the Meeth Mine in the Petrockstow Basin

(after Best and Fookes, 1970)

	Falmouth	Petrockstow	Ball Clay 661
Geological age	Recent	Oligocene	
Probable depositional environment	Estaurine	Rededimented non-marine	
Mineralogy (Kaolinite/ Illite/Quartz/other minerals)	35-25-25-15	55-25-15-10	58-12-17-13
Clay fraction $<2\mu$ %	38-26	73	82
Specific gravity	2.60	2.67	2.76
Organic content	3.8	7.0	
Natural water content %	65-58	22-25	
Liquid Limit %	58-56	68	66
Plastic Limit %	24-22	31	35
Liquidity Index	1.1-1.3	-0.16 to -0.24	
Activity	0.9	0.5	0.5

TABLE 6.II

SUMMARY OF PROPERTIES OF THE CLAY SAMPLES

Hand operated pneumatic spades are used to cut the selected clay from the seams exposed on the face of open pits, to a depth of above 100 feet. Below this level the seams are followed by inclined tunnels and are worked by mining techniques.

As further illustrated in figure 6.12 this ball clay is of very fine particle size and has a high plasticity (see also table 6.II). This and the other varieties of ball clay are usually dark in colour but all fire to give a satisfactory degree of whiteness. Accordingly its principal commercial use is in the manufacture of ceramic whitewares.

Referring to table 3.II, there is a notable difference in properties existing in the Falmouth clay from the others. The Falmouth clay is relatively more coarse grained and a major proportion of the "other minerals" is constituted by muscovite mica of the 'whole rock' (see plate 9.39, and also Section 8.2). On the other hand, the "other minerals" of the ball clays are mixed layer minerals and their presence is reflected in the relatively high activity of these clays.

6.4.1 Low pressure consolidation response

E-log P results of the low pressure consolidation tests on Ball Clay no. 661 remoulded at about 100% water content is shown in figure 6.11. Particular effort has been made to obtain the e-log p characteristic at lower effective pressure

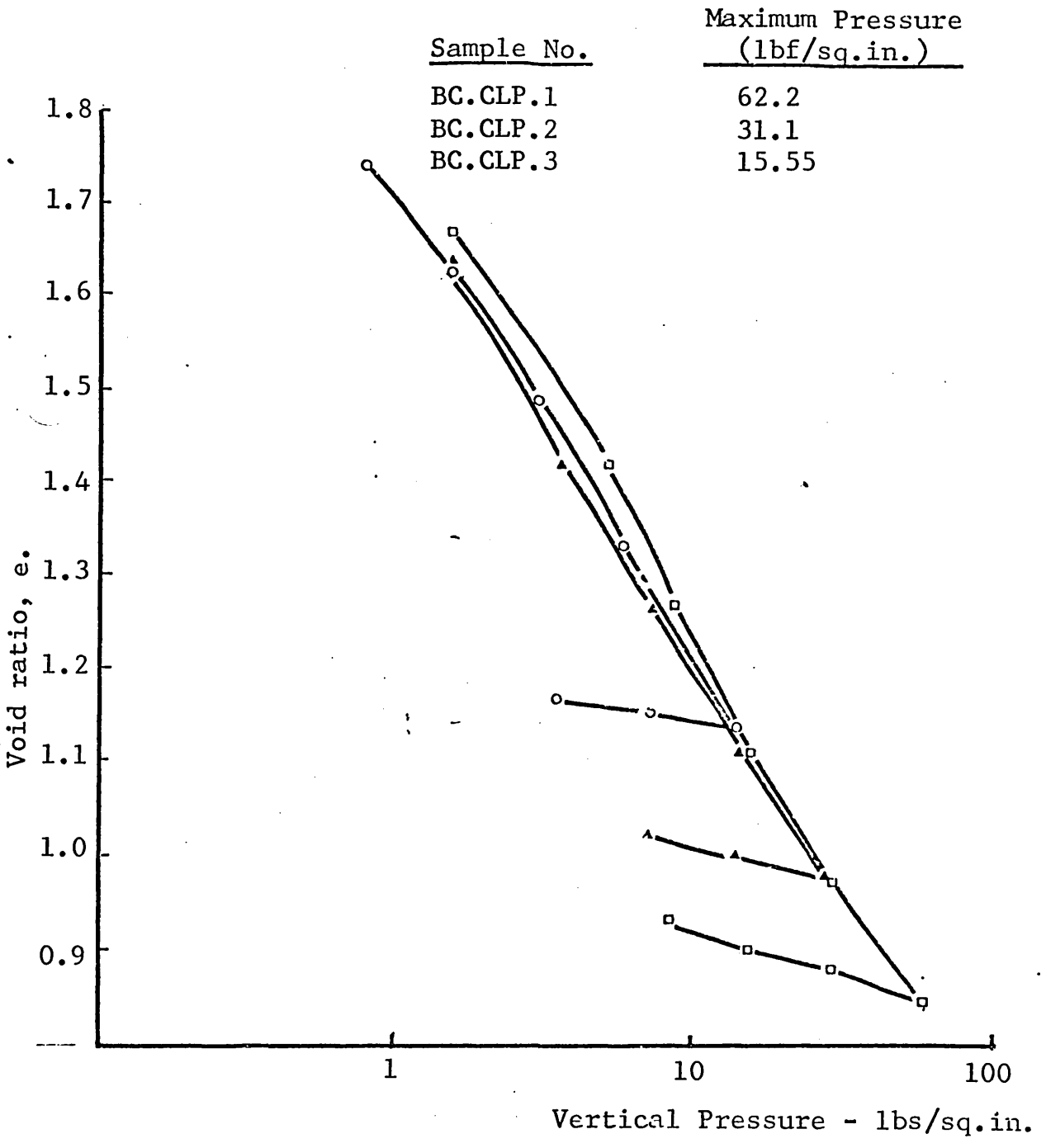


FIGURE 6.11 Low pressure consolidation response of remoulded Ball Clay no. 661.

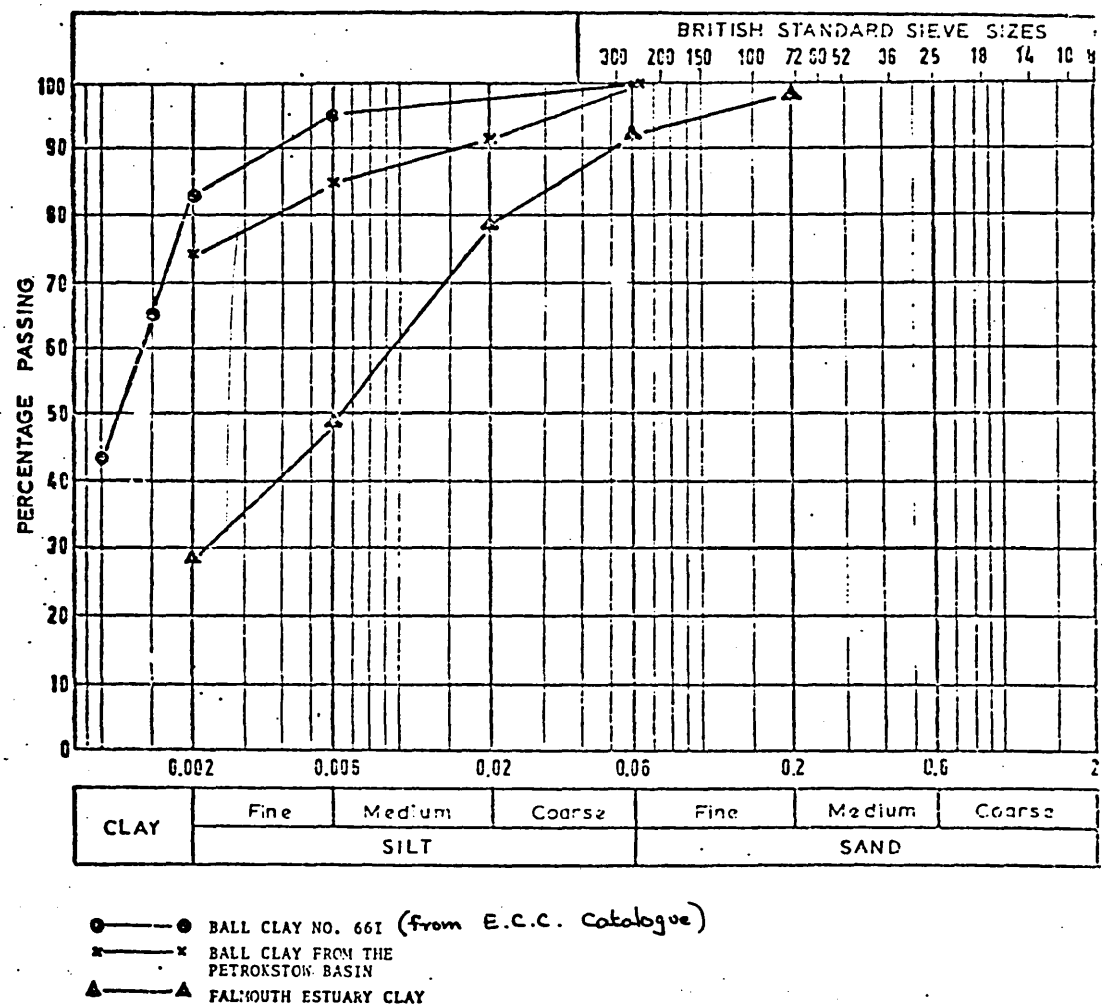


FIGURE 6.12 Particle size distribution of the sediment types tested.

levels than usual. The standard stress increment ratio of $\Delta P/P$ of one was used, but a lower starting consolidation pressure (P) was used.

The fundamental differences between the natural and artificial "gravitational compaction" is the inevitable influence of time scale. As described in the succeeding chapters, Ball Clay no. 661 has been remoulded to strict and similar initial conditions, and used in the study of the effects of different laboratory rates of axial loading, r_1, r_2 and 3_3 etc. (see figure 6.13). The two field undisturbed clays represent two separate points on the field curve of the variation of any particular geotechnical parameter under investigation with depth. The laboratory consolidation of these samples (rate of loading = r_ℓ) will also give results that invariably differ from those of the field curve, but in the light of the knowledge gained from earlier tests, the task of extrapolating the field behaviour from laboratory behaviour is less difficult. It is noteworthy to emphasise that the laboratory consolidation of more field samples with similar mineralogy, etc. but from different natural burial depths will shed more light on the processes involving the changes in geotechnical parameter of sediments with gravitational compaction.

Thus the three varieties of clays chosen for this research programme have basically similar mineralogy and very

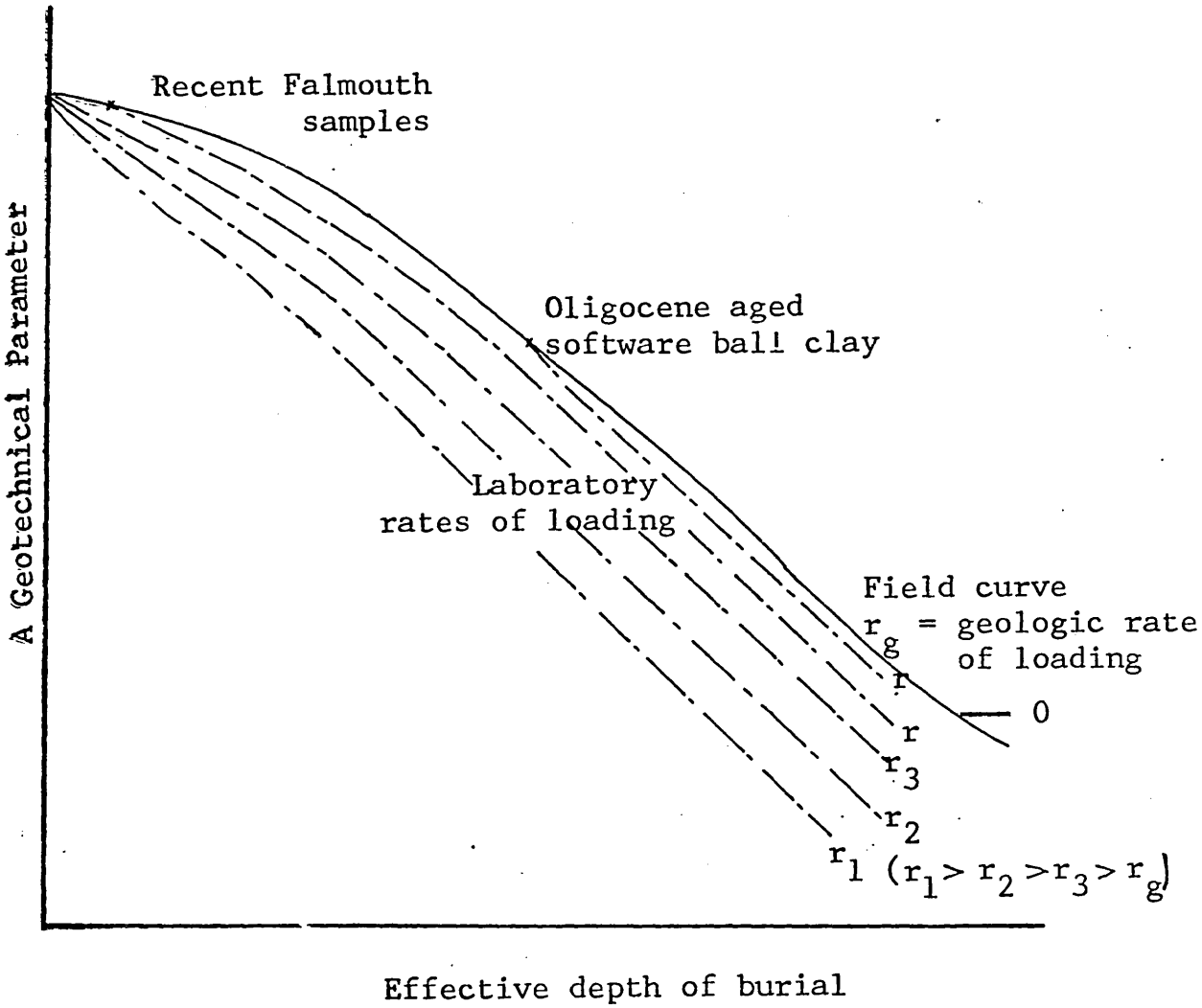


FIGURE 6.13 Philosophy of the choice of the samples for the testing programme

approximately similar particle size properties. Hence these fit in well to an initial overall programme of studying natural and artificial gravitational compaction and the allied processes.

CHAPTER SEVEN Laboratory Consolidation - Test Observations and Results of their Analysis

7.1 Introduction 284

7.1.1 Test Coding specification 284

7.2 High pressure consolidation tests 285

7.2.1 Final condition of the specimen 286

7.2.2 Consolidation with extremely rapid rate of loading 291

7.2.3 Consolidation with constant rate of loading 297

7.2.3.1 Influence of rate of loading 297

7.2.3.2 Influence of change in pore fluid chemistry 309

7.2.4 Review of BC.CHP tests 314

7.2.5 Consolidation of undisturbed samples 320

7.2.5.1 Falmouth samples 320

7.2.5.2 Undisturbed Ball Clay samples 321

7.3 Consolidation using constant rate of strain 326

7.4 Influence of temperature on consolidation 331

7.4.1 Temperature distribution within a test specimen 331

7.4.1.1 Experimental temperature distribution study 335

7.4.2 Low pressure/temperature consolidation test 339

7.4.2.1 Temperature induced strain 339

7.4.2.2 Low pressure consolidation at elevated temperature 341

LABORATORY CONSOLIDATION TESTS OBSERVATIONS AND RESULTS OF THEIR ANALYSIS

7.1 INTRODUCTION

The clay types described in the previous Chapter were tested in the three different types of consolidation apparatus (Chapter Five) in order to investigate in the laboratory some aspects of the process of gravitational compaction of clays. The observations and results of all these laboratory tests are given separately in Appendix D. Pertinent discussions are drawn from these results and are presented in this Chapter under three main sections (7.2, 7.3, and 7.4) in relation to the relevant type of test.

7.1.1 Test coding specification

Each test has been separately indexed with a set of four groups of symbols, such that the test type is made known from its index as illustrated below:

BC.CHP.2 or N.FAL.CRS.1

which denotes:

Ball Clay. Consolidation High Pressure. No. 2; and
Natural. Falmouth. Constant Rate of Strain. No. 1
respectively.

Thus the presence of the letter 'N' in the first of a set of four groups of symbols indicates that the specimen tested is natural (or undisturbed), and conversely the absence of 'N' indicates that the specimen is remoulded. The second group defines the type of test material (BC: Ball Clay; CC: China Clay; FAL: Falmouth Clay). The test type is known from the third group of letters (CHP: Consolidation High Pressure; CLP: Consolidation Low Pressure; CLPT: Consolidation Low Pressure with Heating; CRS: Consolidation constant Rate of Strain). The last group is a numeral indicating the particular test number of that series.

7.2 HIGH PRESSURE CONSOLIDATION TESTS (CHP SERIES)

Four broadly different investigations were made from the series of high pressure consolidation tests performed during this study. Thus the tests may be subdivided into four further subseries and their details are as shown in Table 7.I.

TABLE 7.I

High Pressure Consolidation Tests

Test Nos.	Investigation	Development Stage of the Apparatus (see Table 5.I)
BC.CHP.1 to BC.CHP.10	a) Extremely rapid rate of loading; specimen drained from both ends.	One
BC.CHP.12, 14,18,19.	b) Influence of rates of loading; specimen drained from one end only.	Two
BC.CHP.14, 15,17,20,21.	c) Influence of porefluid chemistry	Two
N.BC.CHP.1 N.FA.CHP.1 and 2.	d) Consolidation of undisturbed specimen and estimation of preconsolidation load.	Two

The specimen preparation and test procedure has already been described in Section 5.2.5. Further experimental details regarding these tests are given in Tables 7.IIa and 7.IIb.

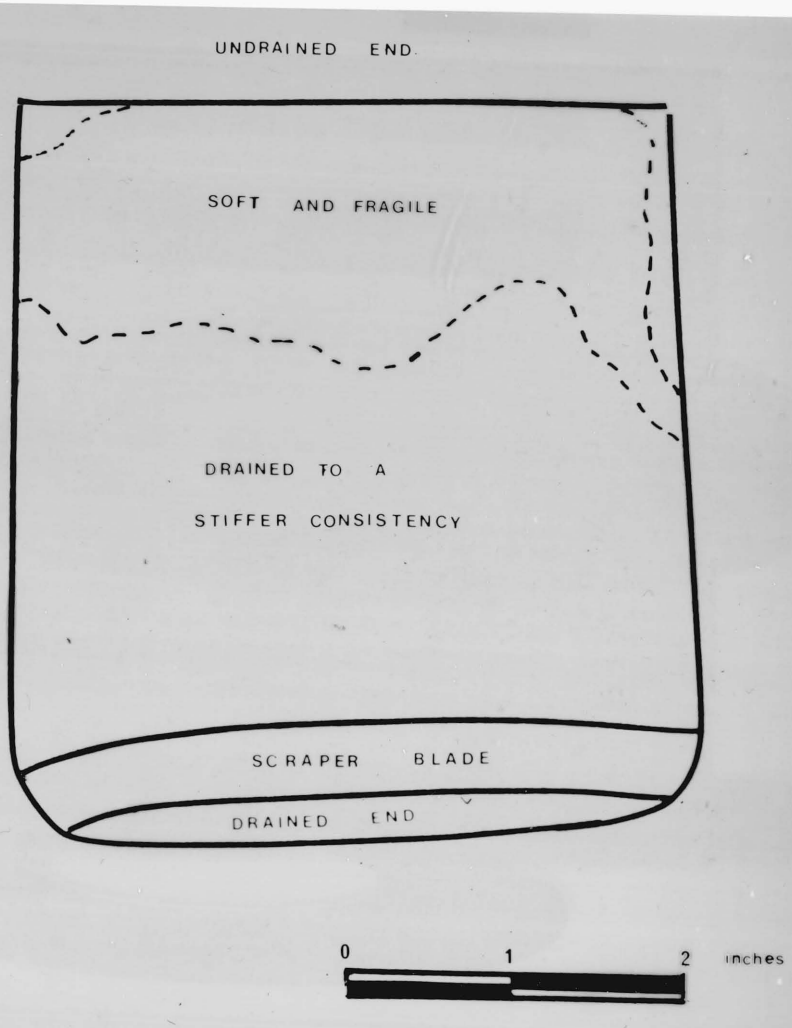
7.2.1 Final Condition of the Specimen

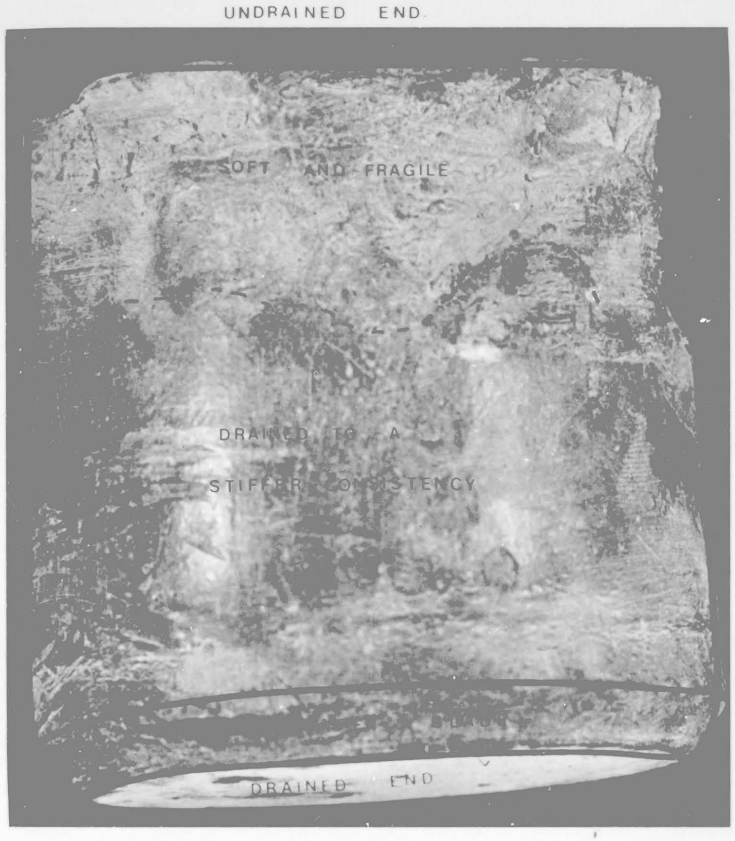
The state of the specimen at the end of a test is controlled primarily by its final moisture content which in turn is affected by factors such as the maximum pressure; rates of loading and unloading, and drainage conditions.

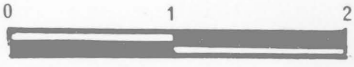
Plate 7.1 illustrates the wide variation in consistency apparent in a specimen which was very rapidly loaded for a short time and then instantly unloaded and the drainage of pore fluid being permitted only from one end of the specimen (test no. CC.CHP.1). The clay near the drained end had a stiffer consistency as a result of its lower moisture content. This emphasises the occurrence of non-uniform conditions in a specimen that is rapidly loaded and unloaded.

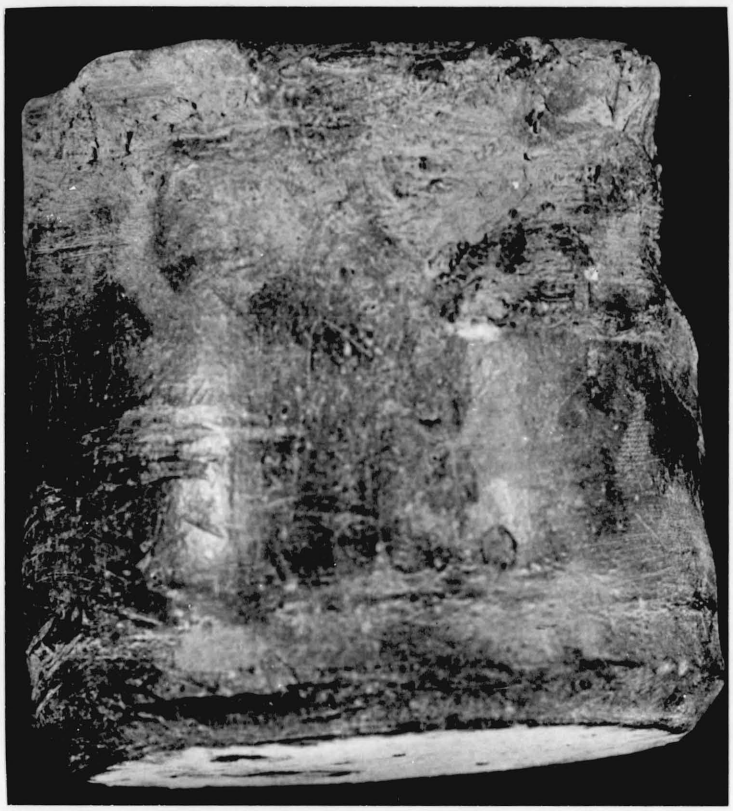
Figure 7.1 illustrates the observed moisture content distributions within the specimens at the end of some similar tests but consolidated relatively slower rates of loading. The moisture contents have been expressed as the percentage moisture, on a 105°C dry weight basis, and have been determined on spot cube samples (see Figure 9.1 and each weighed approximately 1 gram when moist) carved out of the final specimen from the

PLATE 7.1 The final condition of the sample from test CC.CHP.1 showing the result of non-uniformity consequent to rapid rates of loading and unloading with only one end drainage.


UNDRAINED END
SOFT AND FRAGILE
DRAINED TO A
STIFFER CONSISTENCY
SCRAPER BLADE
DRAINED END
0
1
2
inches


UNDRAINED END
SOFT AND FRAGILE
DRAINED END


0
1
2
inches



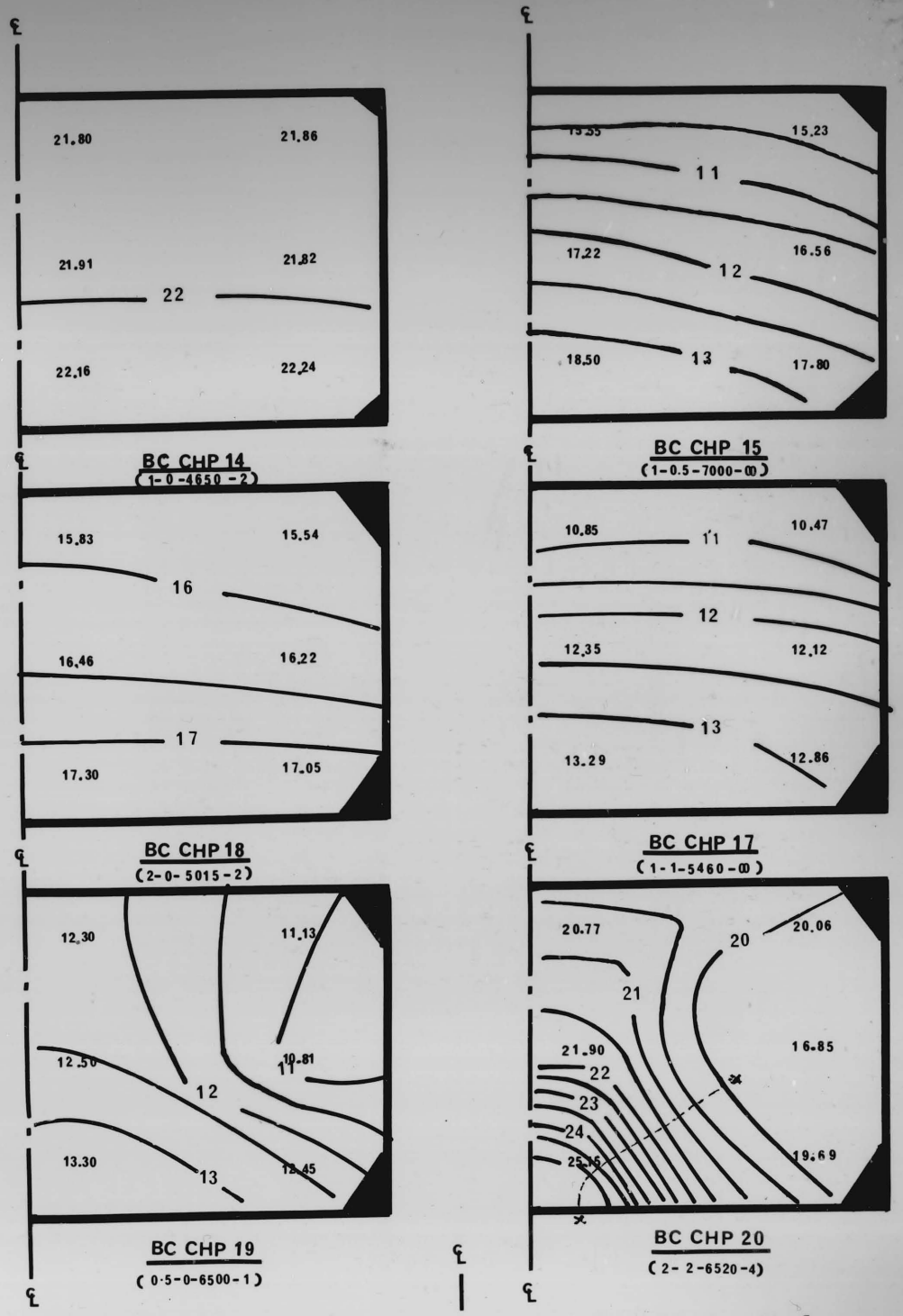
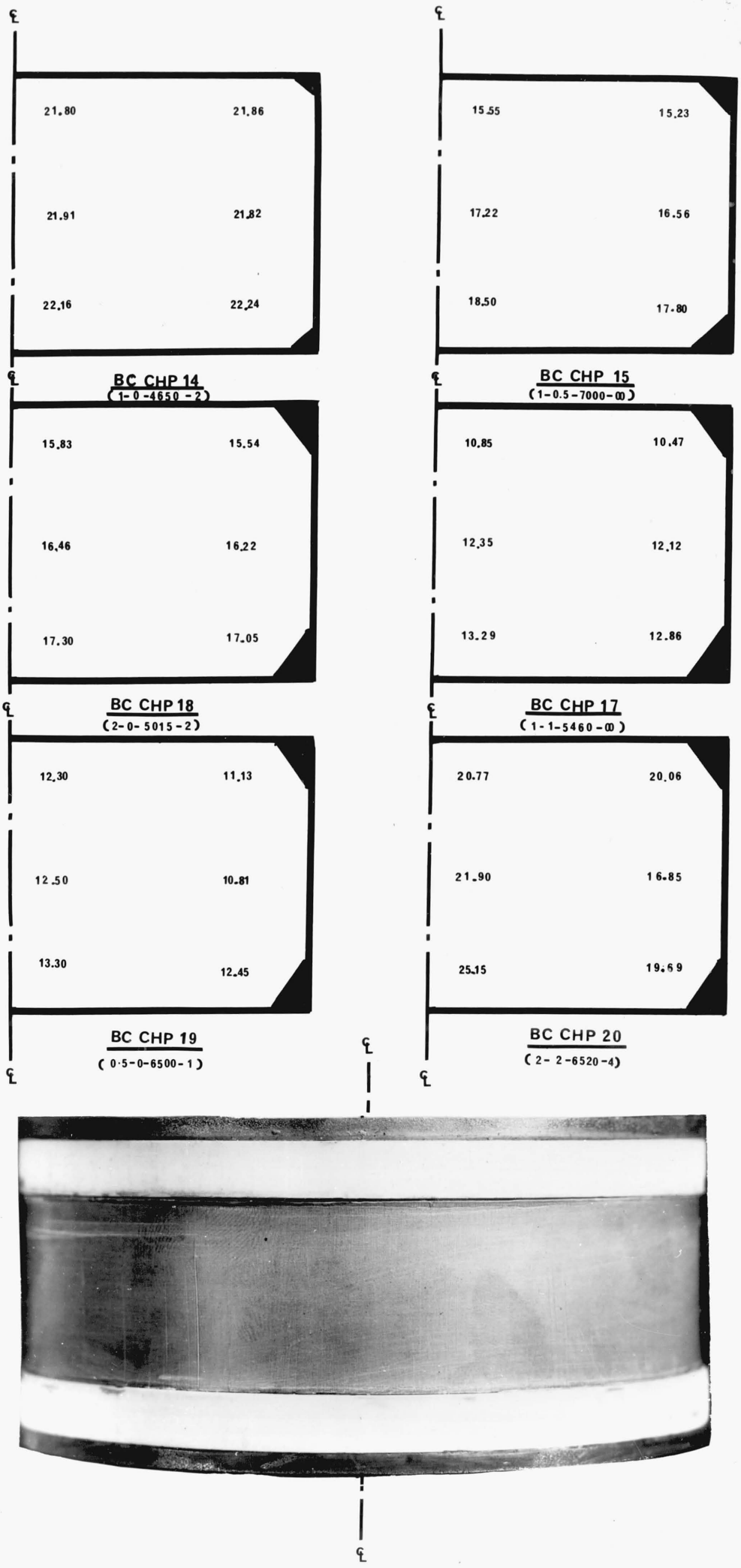


FIGURE 7.1 - Moisture content distributions observed in BC.CHP. test specimens


21.80
21.86
21.91
21.82
22.16
22.24
BC CHP 14
(1-0-4650-2)
15.55
15.23
17.22
16.56
18.50
17.80
BC CHP 15
(1-0.5-7000-00)
15.83
15.54
16.46
16.22
17.30
17.05
BC CHP 18
(2-0-5015-2)
10.85
10.47
12.35
12.12
13.29
12.86
BC CHP 17
(1-1-5460-00)
12.30
11.13
12.50
10.81
13.30
12.45
BC CHP 19
(0·5-0-6500-1)
20.77
20.06
21.90
16.85
25.15
19.69
BC CHP 20
(2-2-6520-4)

respective places. Figure 7.1a must be studied with simultaneous reference to Table 7.IIb which summarises the broad aspects of the particular tests cited. The figures shown within the brackets in the figure are a summary of the rate of loading (lbf/sq.in/min) - salinity 1 peak consolidation pressure (lbf/sq.in) - rate of unloading (lbf/sq.in/min) respectively for the particular test.

Figure 7.1b shows the physical appearance of a specimen at the end of such a slow test. The positioning of the drainage plates, filter paper and the scraper blades are also shown. The drainage of the pore fluid was permitted only from the lower end. Three different shapes of scraper blades were tried during the study to achieve one with efficient performance (described further on in Chapter Nine). However, their approximate shapes are reproduced in Figure 7.1a.

The boundary directions of the local pore fluid drainage within a specimen during a typical test is shown in Figure 7.1b. During unloading, when swelling of the specimen is permitted, these directions of pore fluid flow are reversed. Thus both outflow and inflow of the pore fluid from the specimen is primarily via the lower drainage plate and through the central 0.062" diameter stainless steel duct tube. The effect of the presence of this localised sink or source (as the case may be) is reflected by the striking concavity of

the isomoisture content lines around it as seen in all the distribution patterns.

Very similar moisture content distribution patterns were apparent in the final specimen of the tests BC.CHP.14,15, 17 and 18. The conspicuous difference in the density of the contours between them reflect the influence of the unloading rate. Rapid unloading gives higher moisture content gradients within the specimen. A similar effect can also result from a faster loading rate (see BC.CHP.18).

The distribution pattern in the specimen of test BC.CHP.19 is apparently different from the other two of its series (see Table 7.I). This specimen appears to be less permeable than the others to the backflow of the porefluid during the process of swelling. This, however, is consistent with the specimen acquiring a lower void ratio by virtue of its stress history of a slower rate of loading (0.5 lbf/sq.in/min) up to a higher peak consolidation pressure (6500 lbf/sq.in) and being subsequently unloaded at a faster rate (1.0 lbf/sq.in/min).

The specimen in test 20 had a hypersaline porefluid (salinity 2 - see Table 7.IIIb and Section 7.2.3.2) and was consolidated at a relatively rapid rate of loading (2 lbf/sq.in/min) and unloading was also rapid (4 lbf/sq.in/min). A prominent observation from a study of its moisture content

distribution pattern is that the normals (ex. xx) to the contours (the direction of pore fluid flow or maximum moisture contend gradient) tend to rapidly approach a 'horizontal' trajectory. The above effect probably demonstrates the establishment of anisotropy of permeability within the specimen, perhaps caused by an enhanced preferred orientation of clay particles.

7.2.2 Extremely rapid rate of loading consolidation tests

This particular series of tests was conducted during stage one (see Table 5.I) or the early stages of development of the high pressure consolidation equipment, when its effective function was that of a filter press in squeezing the wet sediments while the drainage of the expelled pore fluid was permitted from both ends of the specimen. The only observations recorded were the pressure, time and final moisture content of the specimen. This in effect corresponded similarly in function to the high pressure compaction apparatus used by Chillingar and Knight (1960) but in specimen size, the latter used specimens as small as only 3 c.c. in volume (the initial volume of the specimens tested in this series was in excess of 1000 c.c.).

Figure 7.2 illustrates the exponential type ($\Delta P_1/P_1 = 1$) loading programme adopted and Table 7.IIa is a summary of the test data and results. The swelling of the clay specimen during unloading was arrested in all but one test (BC.CHP.7).

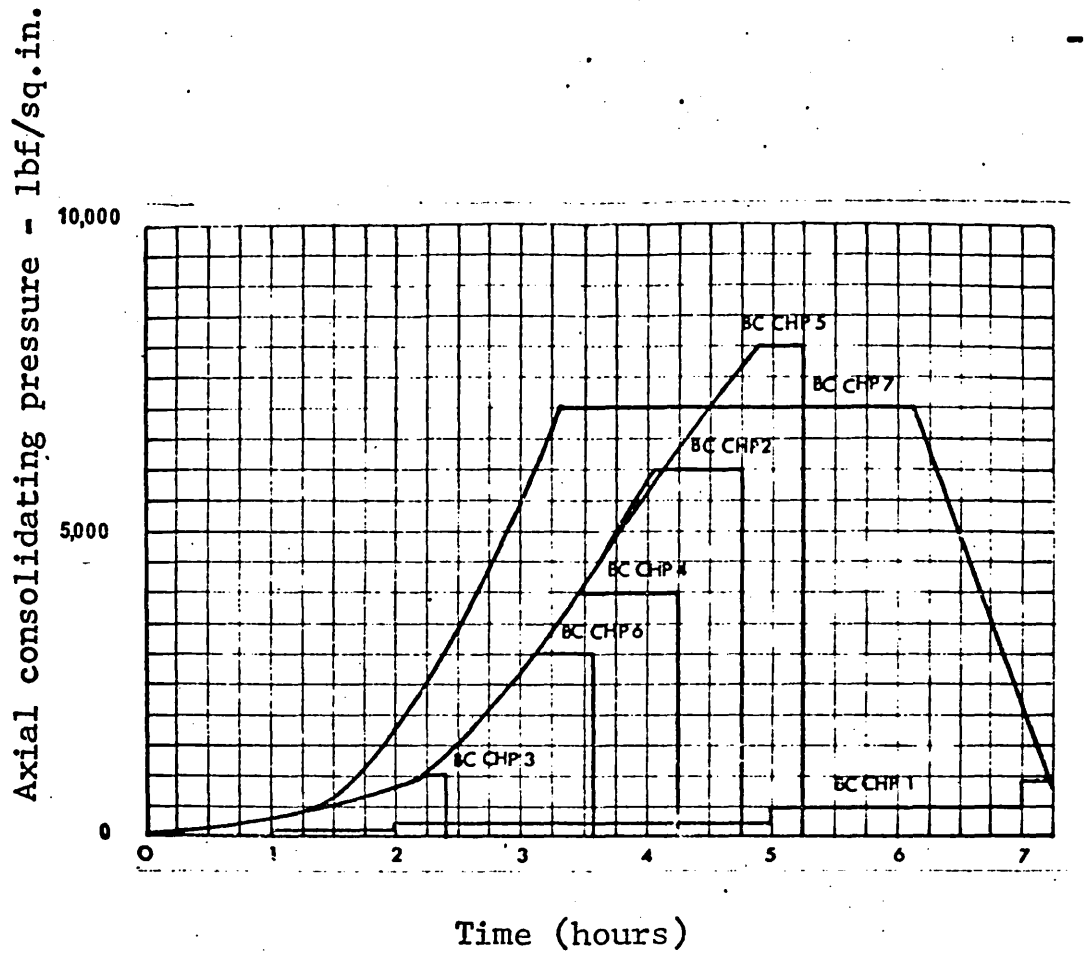


FIGURE 7.2 Summary of the loading programmes used in the rapid loading high pressure consolidation test series.

Test No.	Ball Clay Consolidation High Pressure No.							
	1	2	3	4	5	6	7	8
Date	5.9.71	7.9.71	8.9.71	9.9.71	10.9.71	8.1.72	2.3.72	10.4.72
Peak Pressure (lbf/sq.in.)	9,500	6,000	1,000	4,000	8,000	3,000	7,000	2,000
Total time of loading (hours)	3	4.5	2	4	5	4	4	20
Final Moisture Content (% dry basis)	13.65	14.20	22.40	16.35	14.70	16.20	26.50 (after swelling)	19.70

* In this series of tests, the specimens were remoulded in distilled water, and loaded manually using an Amster Valve Pump, with drainage being permitted from both ends of the sample.

TABLE 7.IIa

DETAILS OF EXTREMELY RAPID RATE OF LOADING TESTS*

TEST NUMBER	BC.CHP 12	14	15	17	18	19	20	21	N.BC.CHP. 1	N.FA.CHP. 2
Date of start of test	15.2.73	14.3.73	22.5.73	20.6.73	2.7.73	5.10.73	26.10.73	15.12.73		10.9.74
Total time for test (days)	7	11	11	8	8	16	10	20	15	15
Peak consolidation stress (lbf/sq.in.)	2500	4653	7000	5520	5015	6504	6800	8000		4320
Rate of loading (lbf/sq.in/min)	1	1	1	1	2	0.5	2	0.5	1	1
Salinity of pore fluid	0	0	0.5	1	0	0	2	2	Natural	Natural
Max. total precon. stress (lbf/sq.in.)	-	70	55	50	75	60	60	55		Natural?
Mode of P_1 increase	Auto.& Manual	Auto.& Manual	Manual	Manual	Auto	Auto	Auto	Auto	Auto	Auto
Mode and Frequency of Observations	Manual 15 mins	Manual 15 mins	Manual 15 mins	Manual 15 mins	Manual 15 mins	Auto 10 mins	Auto 10 mins	Auto 10 mins	Auto 10 mins	Auto 10 mins
Rate of Linear Deformation ($\times 10^{-3}$ ins/min)	1.38	1.12	1.56	1.25	1.25	0.925	1.20			
Peak Pore Fluid Pressure Difference (U lb/sq.in)	473	675	280	158	1104	363	900	Failure	159	122
Pressure Ratio at occurrence of Peak	0.69	0.71	0.66	0.39	0.68	0.74	0.90	Failure	0.25	0.6
Steady Pore Fluid Pressure Difference (lbf/sq.in)	215	425	155	90	550	120	600		131	56
Rate of unloading (lbf/sq.in/min)	2	2			1	1	2	1	2	2
Total rebound, inches	.179	.326								
Final Moisture Content	20.5	21.9	12.10	12.50	16.36	13.13	20.4	13.87	18.30	15.30
Final Thickness, inches	1.902	2.675	2.210	2.25	2.312	1.969	2.85	2.07	2.710	2.321
Final Bulk Density, gm/cc	2.24	2.25	2.10	2.19	2.15	2.21	1.91	2.13	2.23	2.20

TABLE 7.II b

DETAILS OF CONTROLLED RATE OF LOADING CHP TESTS

The influence of the swelling is reflected in an increase of moisture content of twelve percent from what would be otherwise expected (see Figure 7.3).

The average retained moisture content - peak compaction pressure variation observed for the Ball Clay (a Kaolinite illite clay; see Section 6.4 and Section 8.2.2.3) from this series of rapid tests is shown in Figure 7.3. The variation was apparently linear and the moisture content (M) - compaction pressure (P) are related mathematically by the equation

$$M = 52.4 - 10 \log_{10} P$$

The above results are further compared with those results of the type curves for the A.P.I. reference material by Chillingar (see Section 2.8.3. and overlay of Figure 7.3).

Cognisant of the observations of the previous section 7.2.1., and consequent upon the larger specimen thickness and short duration of tests, the test observations are an over-estimate of the final retained moisture content. The above explains the reason for the apparent discrepancy between the two sources of results. It is also noteworthy to refer to the moderately 'active' nature of the ball clay as a result of the pressure of the mixed layer minerals (Section 6.4). However, otherwise the general trend of this variation is compatible between the Chillingar curves for the Kaolinite and Illite reference models.

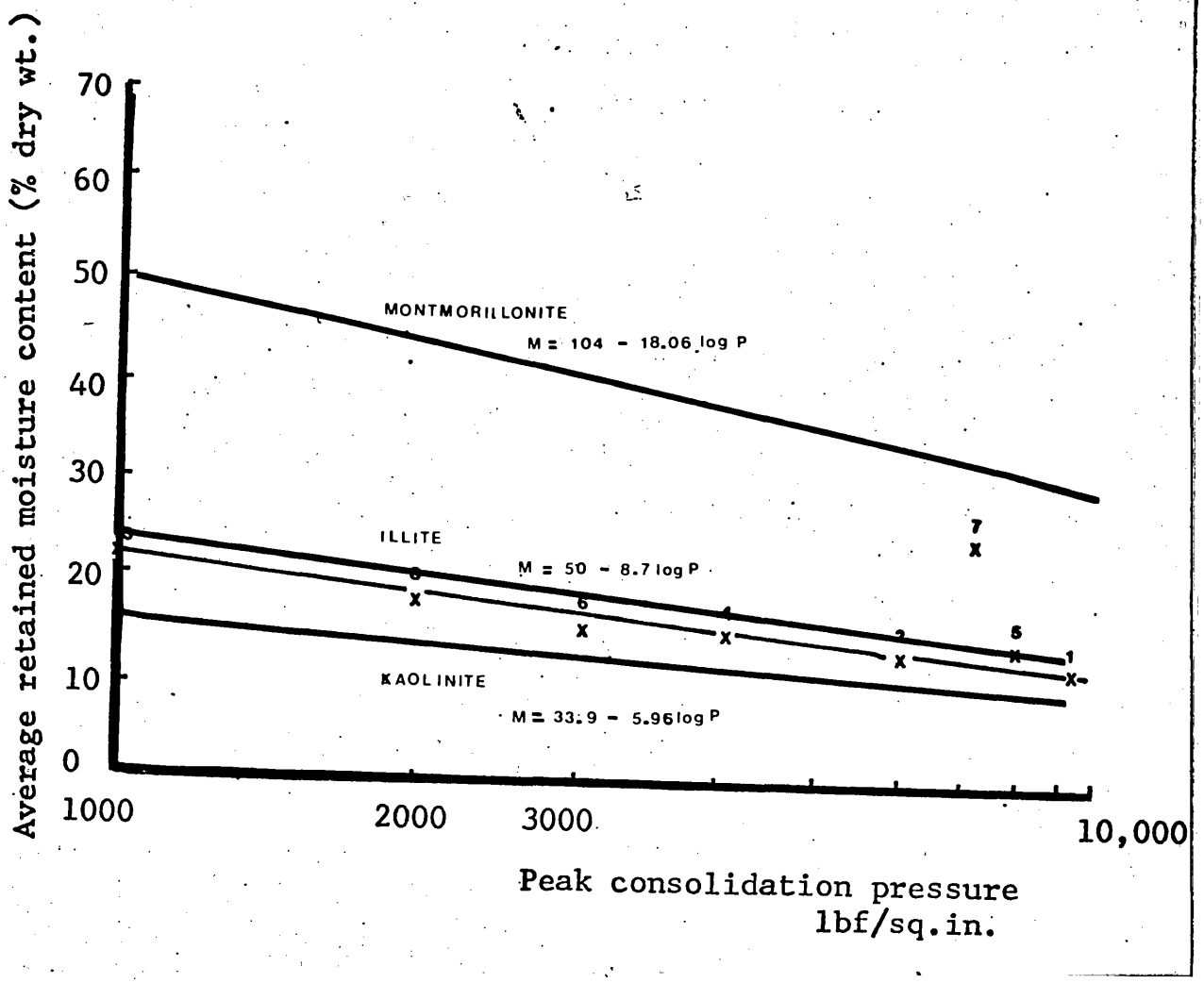


FIGURE 7.3 Retained moisture content - peak consolidation pressure variation for the rapid consolidation tests (numbers on the data points refer to the relevant test number).

The overlay gives the results of Chillingar (1960).

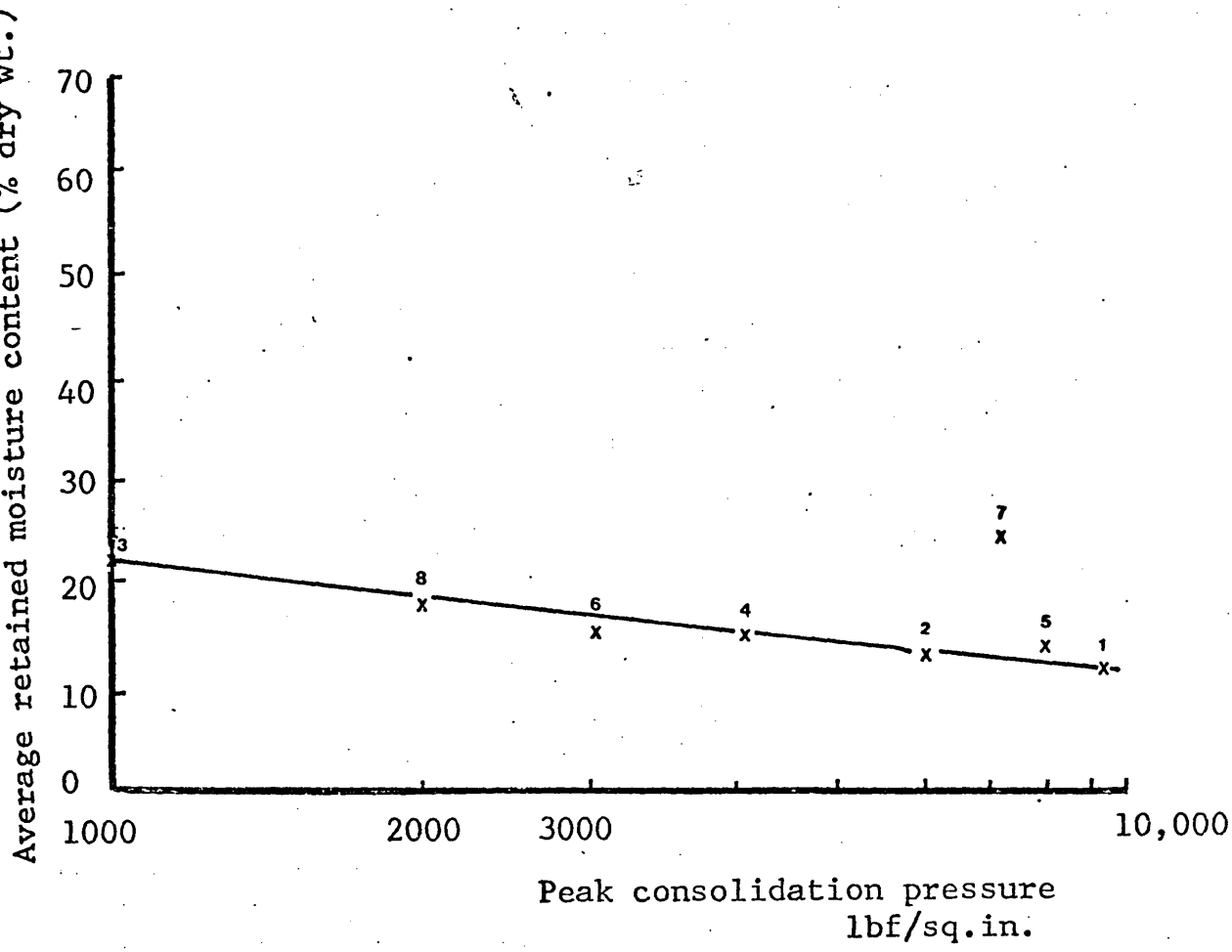


FIGURE 7.3 Retained moisture content - peak consolidation pressure variation for the rapid consolidation tests (numbers on the data points refer to the relevant test number).

The overlay gives the results of Chillingar (1960).

7.2.3. Constant Rate of Loading Consolidation tests

These tests were long term tests from one to four weeks duration. The duration of a test is dependent on the factors: time spent during preconsolidation stage, rate of loading, peak consolidation pressure and rate of unloading. Figure 7.4 is an aid to estimating the duration of such a test.

The early tests of the development stage two had to be manually observed and recorded which necessitated a full time (day and night) operator to attend the equipment during a test. Some of the early tests had to be abandoned due to equipment malfunctions associated with early familiarisation of same, and in most instances the major problems were due to hydraulic fluid pressure seals via unsatisfactory operation of high pressure seals. These were subsequently redesigned and manufactured to operate satisfactorily. Consequently, only the observations of the successful tests have been analysed. The observations and the results of their analysis are given separately in Appendix D.

7.2.3.1. Influence of rate of loading

The tests BC.CHP.12,14,18 and 19 formed a series to investigate the effects of different loading rates. Increased rates of loading gave undercompacted specimens as outlined earlier and illustrated in Plate 7.1. It was further apparent

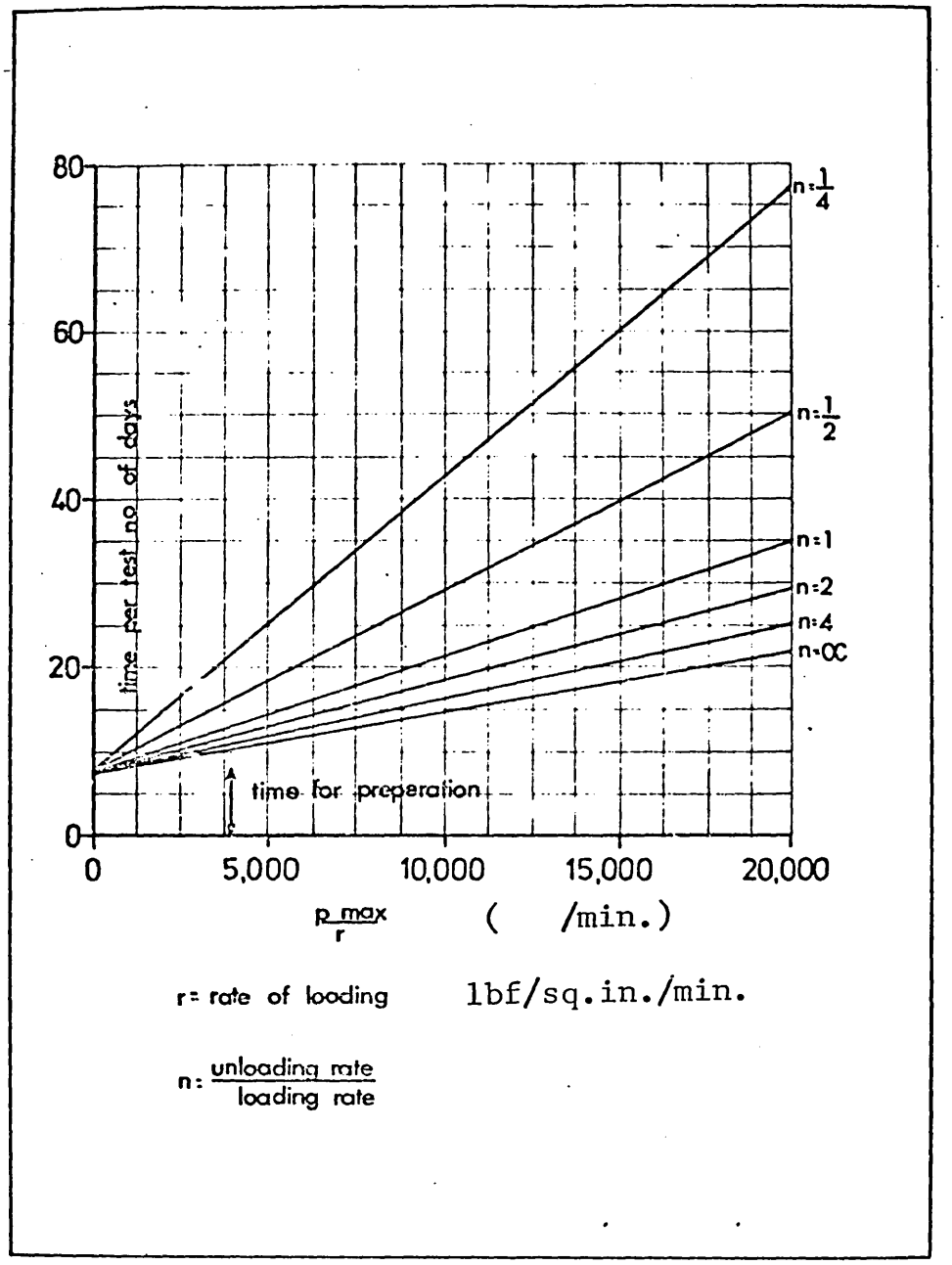


FIGURE 7.4 An aid to estimate the duration of a CHP test.

that the respective values of the pressure ratio ($\Delta u/P_1$) were susceptible to rate of loading.

Figure 7.5 is an illustration of a typical set of observations made during a usual controlled CHP test. The clay specimen compacts from the drained end, by virtue of the pore fluid pressure gradient induced by the process of compaction. It is apparent from Figure 7.5 that when the loading rate is constant, compaction proceeds at a constant rate until the specimen attains a porosity of the order of forty-two percent, and then the rate of compaction becomes very small. Relative orders of magnitude for the linear rates of compaction for the tests are given in Table 7.II.b.

The ceasing of the constant rate of compaction corresponds to the end of the visco-elastic deformation of the clay-fluid system, following the completion of the stages of the mechanical arrangement of the particles and dewatering of both the porefluid and a major part of the adsorbed fluid (see Hedberg compaction model, Section 2.7.6.1.).

The associated variation in the response of the pore-fluid at the undrained end of the specimen consists of three discrete stages, viz., a rise to a peak value and then a fall to an approximately steady porefluid pressure prior to its decay to zero during the unloading process. The magnitudes of

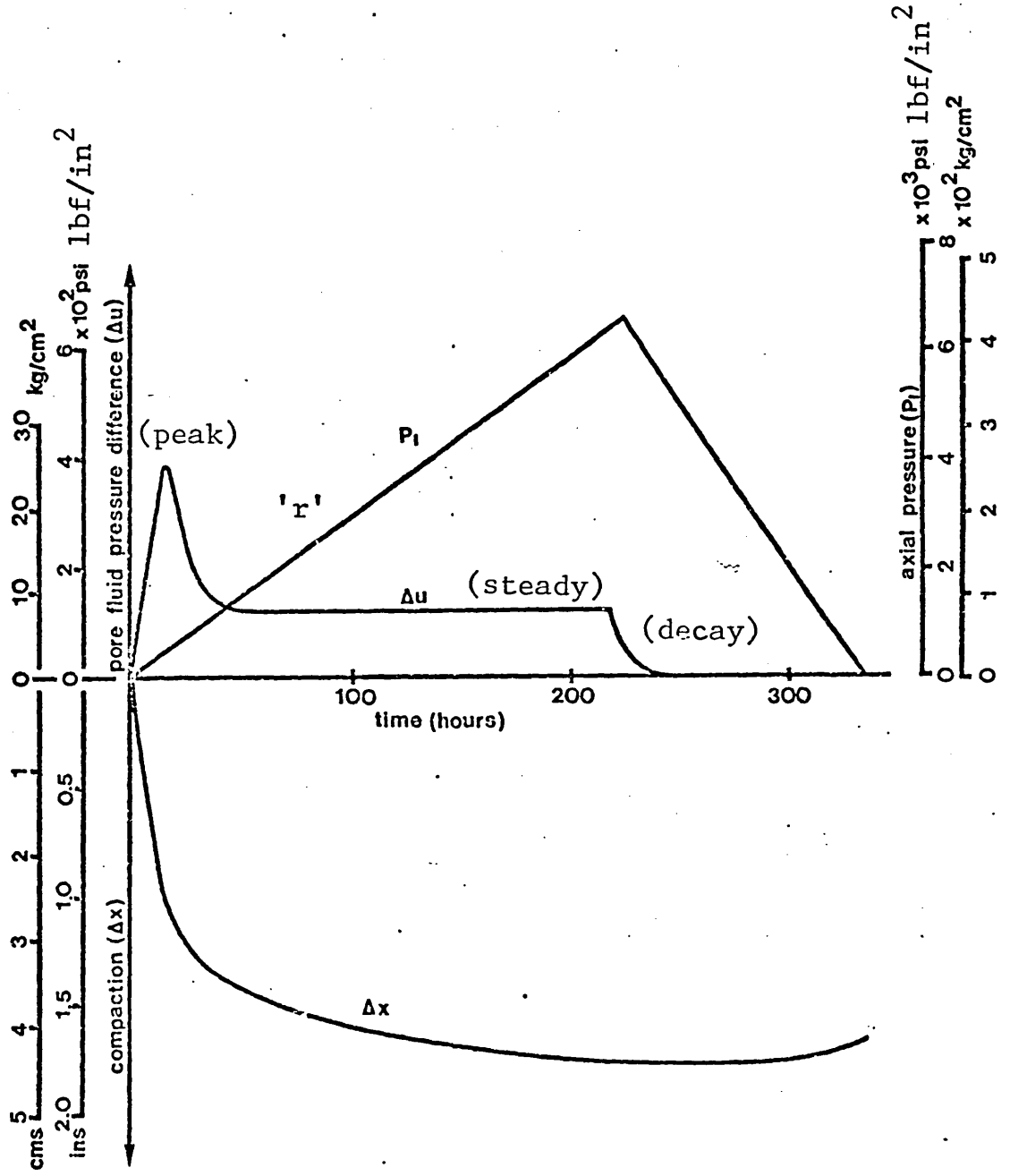


FIGURE 7.5 Variation with time of:-

axial pressure (p_1)

pore fluid pressure difference (Δu)

compaction (Δx)

observed during a typical high pressure consolidation (CHP) test.

this peak and steady porefluid pressures as observed during these tests are also given in Table 7.IIb. In some of the tests the 'steady value' is not clearly marked, and in such instances an average value is given.

Figure 7.6 is a plot of the variation of these 'peak' and 'steady' values of the pore fluid pressure difference observed in tests run at different rates of loading. Figure 7.6 aids in emphasising the primary effect of an increased rate of loading is to cause a corresponding increase in the pore fluid pressure difference. This particular enhancement is a result of the clay-fluid system achieving at each stage a higher equilibrium stress level between the pressure rise and the subsequent dissipation of the associated porefluid pressure over a shorter time.

The e-log p curves for the tests BC.CHP.12 and BC.CHP.14 are shown together in Figure 7.7. Though the same rate of testing was used in both these tests, the specimens were of two distinctly different initial consistencies (i.e. BC.CHP.14 was preconsolidated while BC.CHP.12 was not). The effect is similar to the difference in consolidation character for clays with different initial water contents (cf. Figure 2.9).

Another striking reproduced feature is seen in Figure 7.6: even though the absolute magnitude of the porefluid

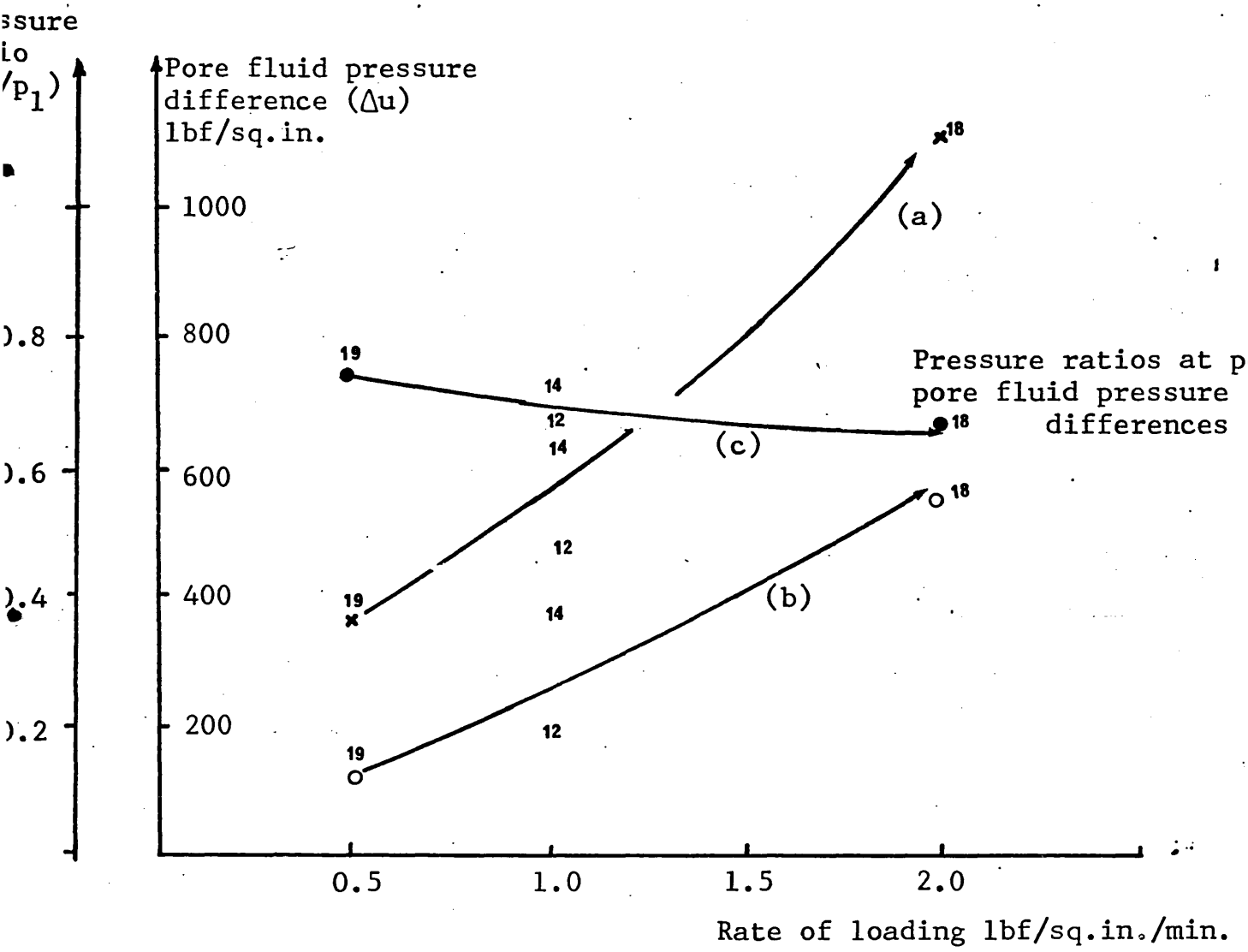


FIGURE 7.6 Variation of:-

a) Peak pore fluid pressure difference (Δu peak)

b) Steady pore fluid pressure difference (Δu steady)

and c) Pressure ratio at the peak pore fluid (Δu peak/p_1) pressure

with the rate of loading.

(Note: The numbers indicate the respective BC.CHP test numbers)

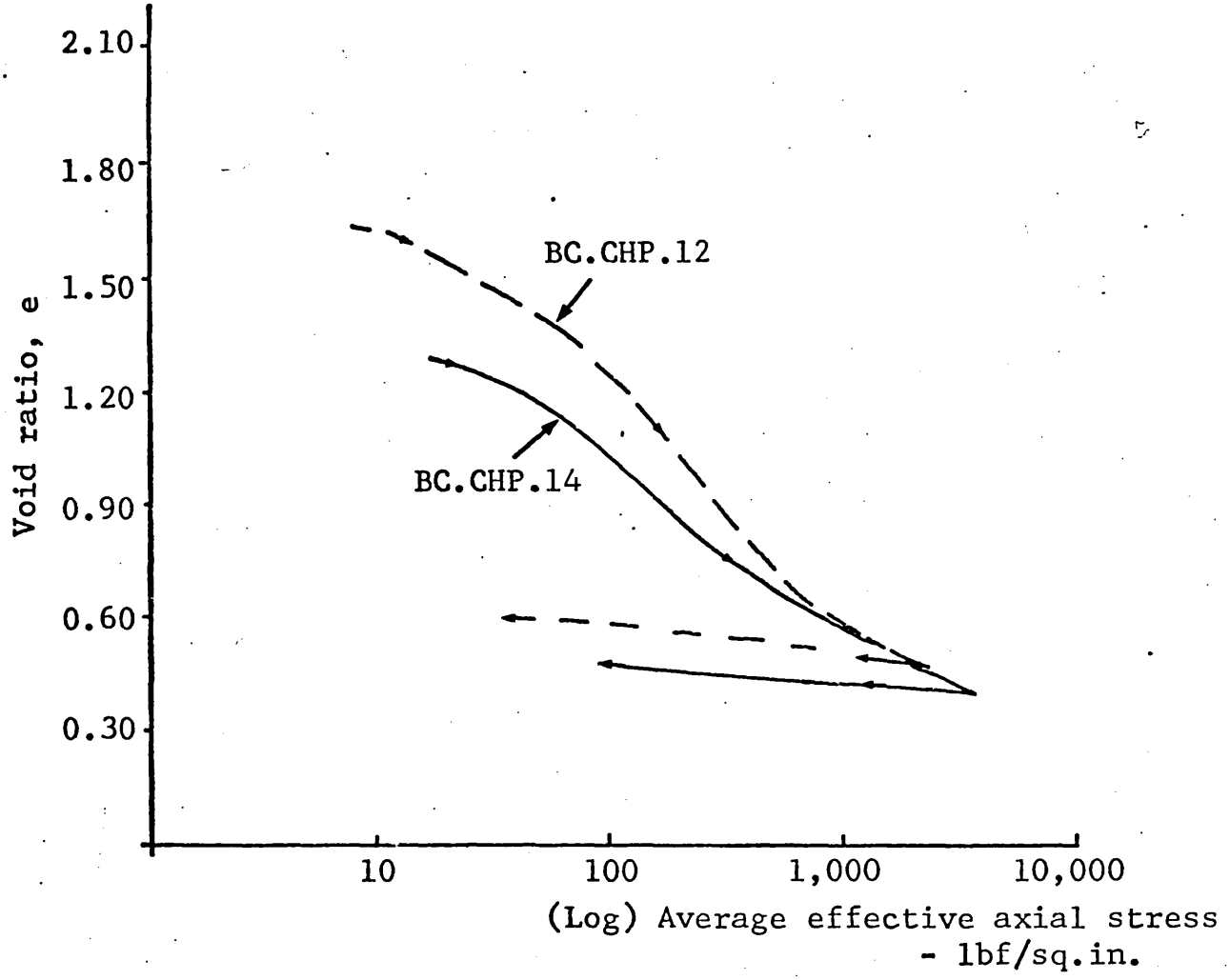


FIGURE 7.7 Comparison of the e-log p plots for two consolidation tests performed at the same loading rate, but on an initial 100% slurry (BC.CHP.12) and the other a preconsolidated specimen (BC.CHP.14).

pressure difference peaks in the above two tests is slightly different, the magnitude of the pressure ratio at its stage of occurrence is similar.

Figure 7.8 compares the e-log p curves for the tests BC.CHP.14,18 and 19 where different rates of loading had been used in each case. Its effect is comparable with that of Figure 4.8 . In both instances the effect of the differences is most manifested in the low pressure range. It is convenient to attribute this variation to the difference in the magnitudes of the porefluid pressures developed as described earlier in this section. The results from the conventional low pressure consolidation tests (BC.CLP. series) are also plotted for the purpose of comparison on the same figure (see curve d). It is clearly evident that rates of loading in excess of one lbf/sq.in/min. are far too rapid and unrepresentative for this type of material (Kaolinite sediments). Accordingly a loading rate of one lbf/sq.in/min. was used for the tests on the undisturbed specimens (described later).

The best fit curves for the coefficient of volume decreases ($M_v = \frac{1}{p} \times \frac{de}{dp}$) - effective pressure (log p) plots for the three tests are compared in Figure 7.9. All three plots are remarkably linear, suggesting a linear variation of the type

$$\log M_v = A - B \log p$$

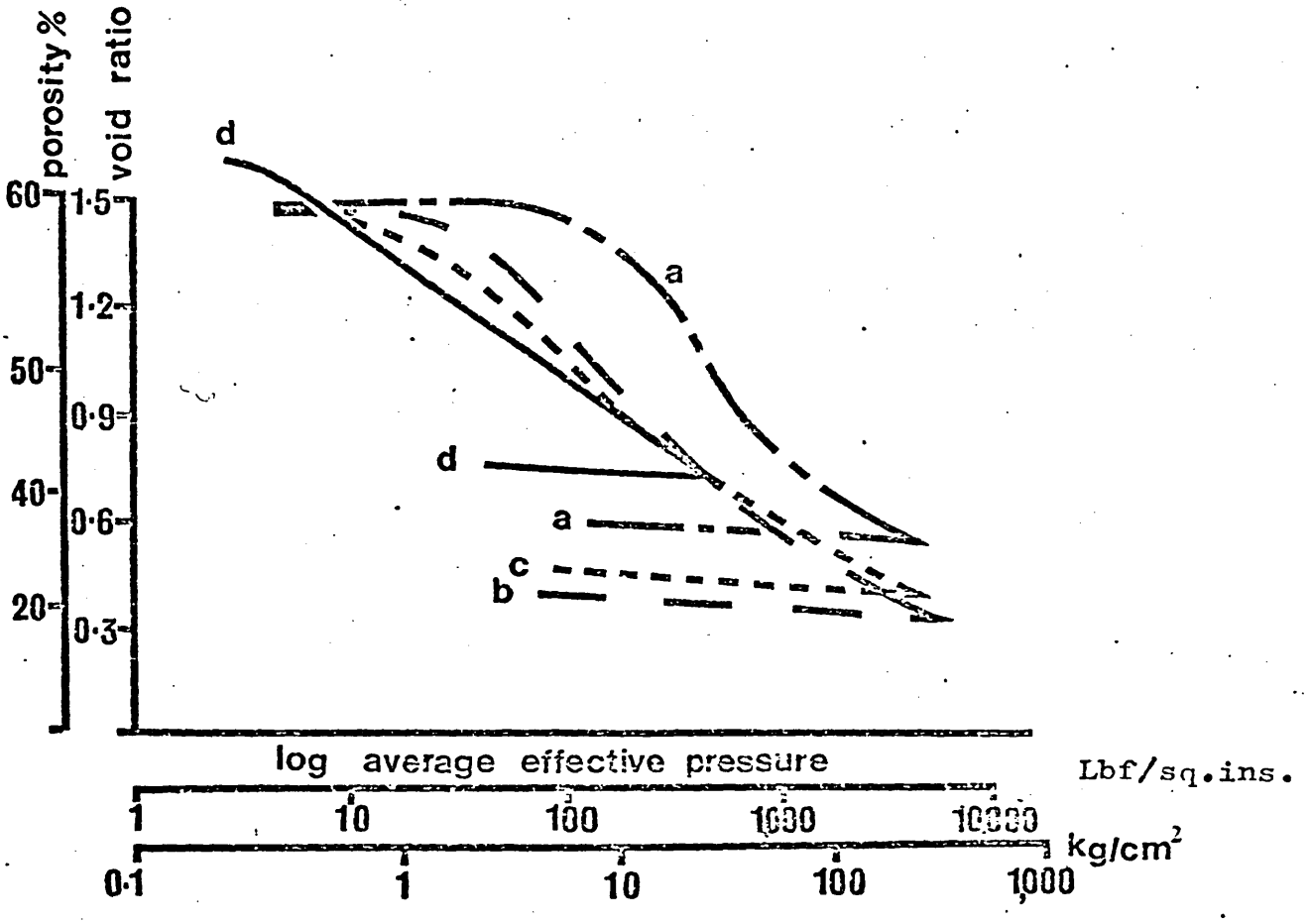


FIGURE 7.8 - Influence of the rate of loading on the void ratio - log pressure variations for remoulded Ball Clay no. 661

Curve	Test no.	loading rate
a	BC.CHP.18	2 lbf/sq. in. /min.
b	BC.CHP.14	1 lbf/sq.in. /min.
c	BC.CHP.19	0.5 lbf/sq.in./min.
d	BC.CLP. 1 - 5	$\Delta P/P = 1.0$

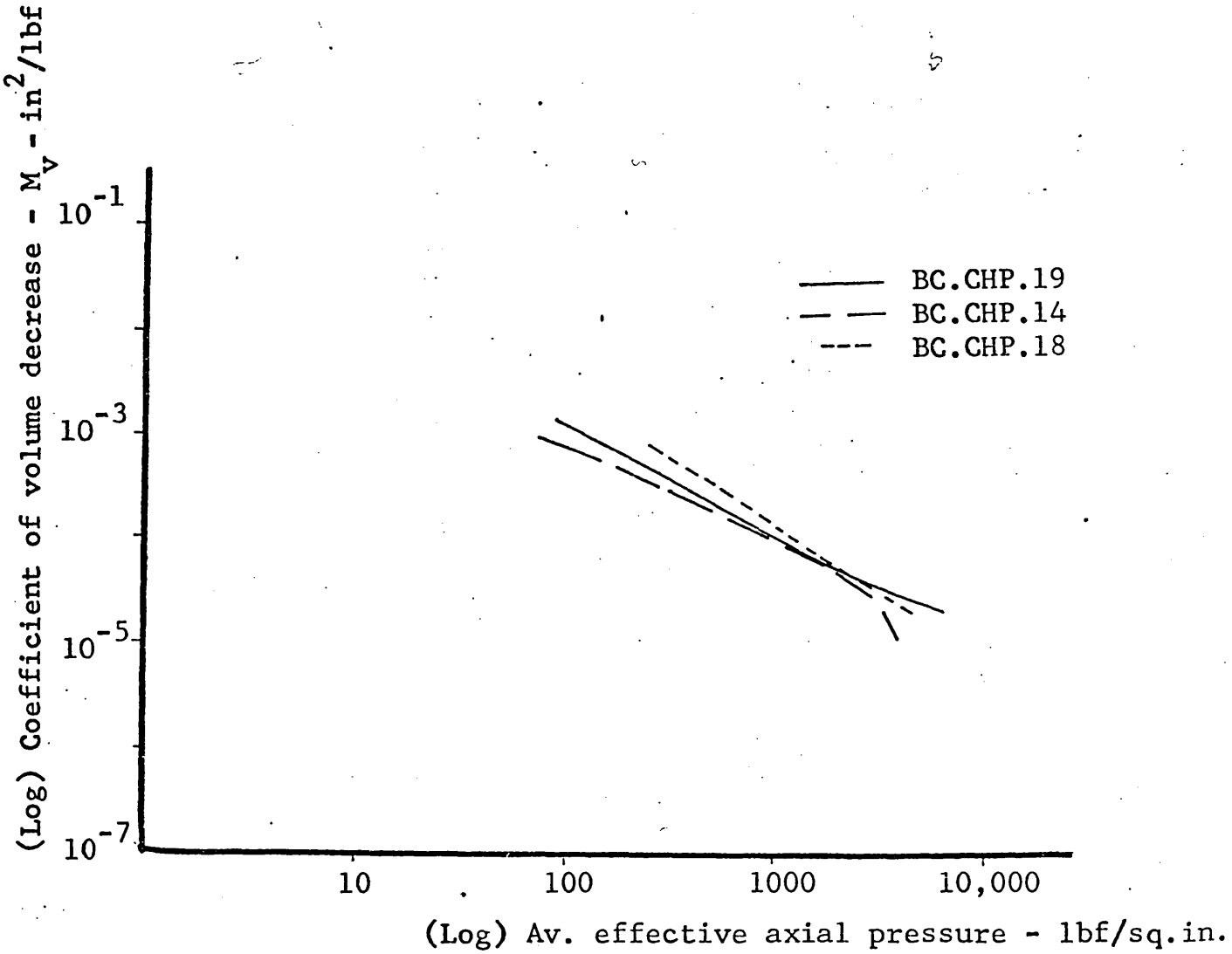


FIGURE 7.9 The variation of coefficient of volume decrease with average effective pressure as computed from observations of tests conducted at different rates of loading.

where A and B are constants.

It appears that the coefficient of volume decrease at a given effective pressure is approximately similar at high consolidation pressures ($>$ 1000 lbf/sq.in). At these pressures, the compressibility of the sediment is governed by a combination of the processes of expulsion of the adsorbed water, fabric compressibility, sediment compressibility, and to a lesser degree on the expulsion of free pore water.

However, at lower pressures the expulsion of free pore water is the chief process contributing to the coefficient of volume decrease of the specimen. And, as is evident from the figure at low pressures, rapid rates of loading give higher values of M_v, at similar effective pressure.

In the permeability-porosity plots for the tests that are given in the appendix, the values of the permeability have been computed in three different ways as described in Chapter Four. There is a difference between those computed using the assumption of a linear pore fluid pressure distribution and the rest. But this difference becomes less conspicuous in the tests with lower rates of loading which is again a direct consequence of the build up of a lower level of porefluid pressure. Figure 7.10 compares the permeability porosity variation as computed for the tests with the different rates of loading. A higher rate of loading apparently yields lower rates of permeability.

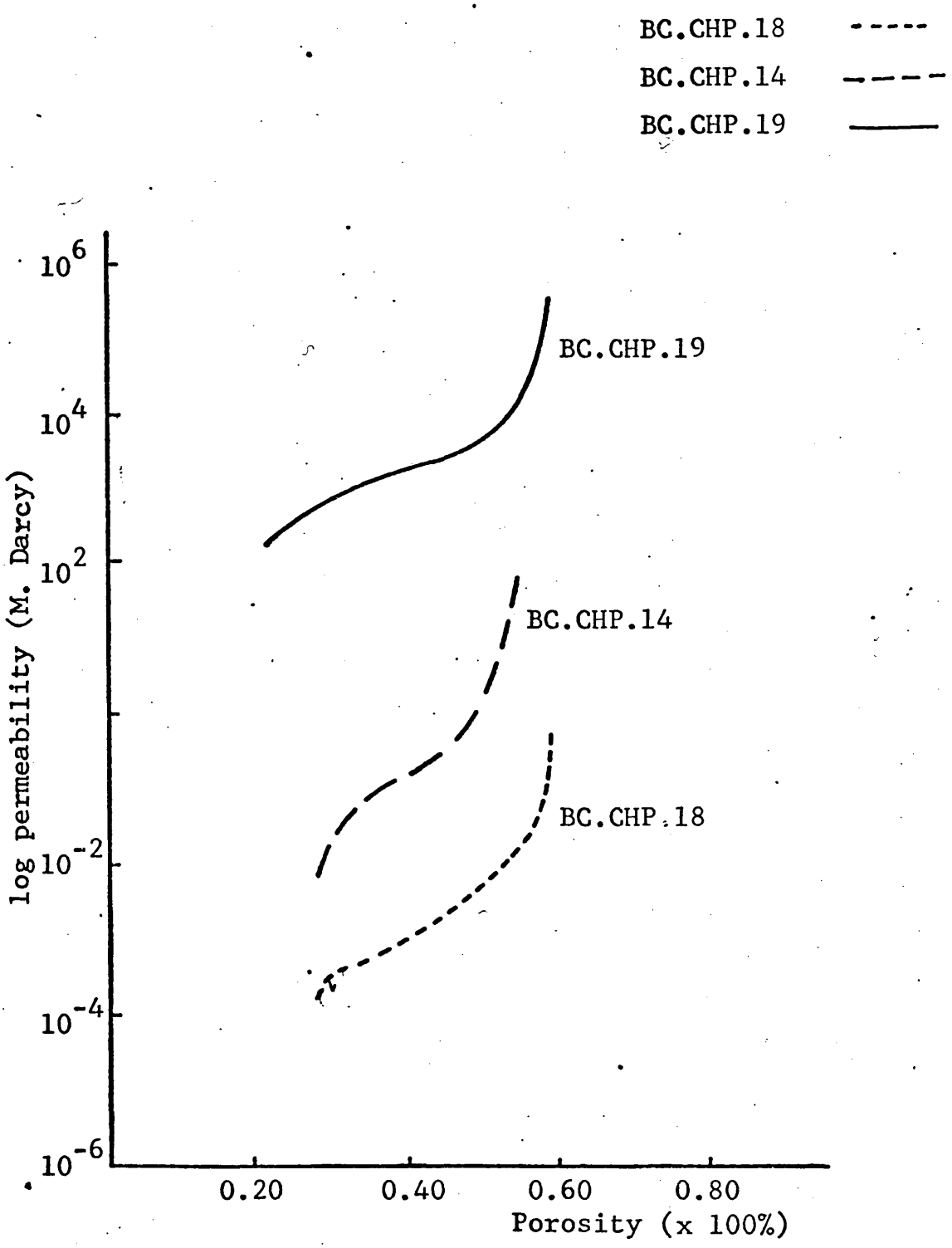


FIGURE 7.10 Effect of ratio of loading on the computed permeability-porosity variations.

This effect suggests an increased number of tortuous flow paths of the pore fluid to be prevalent in specimens consolidated at high rates of loading (discussed further in Chapter Nine).

7.2.3.2. Influence of a change in porefluid chemistry

BC.CHP.14,15,17 and 21 constituted a second series of tests conducted with the intention of investigating the influences of the initial porefluid salinity on the consolidation behaviour. Table 7.III gives the details pertaining to the definition of 'salinity' as used in the context of this study. A solution containing the six ions Na^{+}, K^{+}, Ca^{++}, Mg^{++}, Cl^{-} and SO_4^{--} in the approximate proportions of those given in Table 7.IIIa was considered to be of 'unit salinity'. Table 7.IIIb gives details of the approximate weights that were used in the preparation of a litre of artificial sea water of 'unit salinity'. Fractional and multiple proportions were used to prepare solutions of any other required 'salinity'.

The tests BC.CHP.14,15 and 17 were performed at the same rate of loading of a lbf/sq.in/minute but with increasing orders of salinity of the pore fluid of 0, ½ and 1. In these tests the porefluid pressure difference (ΔU) varied with consolidation in a very similar manner to that described in the previous section. However, as shown in Table 7.IIb, an increase in salinity of the porefluid had a reverse effect of diminishing

Reference			Mason (1956)	
Ion	Atomic Weight	Ionic Radius ^{o}A	Concentration g/L *	Per Cent %
Sodium Na^{+}	23.0	0.98	10.55	30.61
Potassium K^{+}	39.1	1.33	0.38	1.10
Calcium Ca^{++}	40.0	1.17	0.04	1.16
Magnesium Mg^{++}	24.3	0.89	1.272	3.69
Strontium Sr^{+++}	87.6		0.008	0.03
Chloride Cl^{-}	35.5	1.81	18.98	55.05
Bromide Br^{-}			0.065	0.19
Bicarbonate HCO_3^{-}			0.14	0.41
Sulphate SO_4^{--}			2.649	7.68
			34.47	

* Concentration of sea water of 19% chlorinity.

TABLE 7.IIIa

DETAILS AND APPROXIMATE PROPORTIONS OF THE IONS PRESENT IN NATURAL SEA WATER

SALT	Wt. per litre gm.	Concentration					
		Na^{++}	K^{+}	Ca^{++}	Mg^{++}	Cl^{-}	SO_4^{--}
NaCl	26.70	10.5	-	-	-	16.20	-
$CaCl_2$	0.805	-	-	0.29	-	0.515	-
$MgCl_2$	3.03	-	-	-	0.765	2.265	-
K_2SO_4	0.847	-	0.38	-	-	-	0.567
$MgSO_4$	2.54	-	-	-	0.502	-	2.038
	33.89	10.5	0.38	0.29	1.267	18.98	2.605

TABLE 7.IIIb

APPROXIMATE PROPORTIONS OF SALTS IN ONE LITRE OF ARTIFICIAL SEA WATER (UNIT SALINITY)

the respective values of the peak and steady porefluid pressure differences. This observation is further illustrated in Figure 7.11. An increase in salinity of the pore fluid has the double effect of both diminishing the size of the clay micelle as well as establishing a greater attractive force between the particles (see Sections 2.3.0 and 2.3.3.). The combined effect on the specimen is to make it more permeable to pore fluid, therefore resulting in a faster dissipation of pore fluid pressure and hence lower pore fluid pressure differences (ΔU) are observed.

Figure 7.12 compares the e-log $\bar{p}_1'$ plots for these three tests. It appears from the results that the curves differ in their early portions. The specimens have subsequent to the process of preconsolidation acquired decreasing void ratio with increasing pore fluid salinity. The curves converge towards each other and follow a common curve at higher pressures.

The permeability-porosity plot for the test BC.CHP.17 (Appendix D) shows a special feature in that the values of the permeability obtained from all three analytical methods give very closely similar results. The results from the low pore fluid pressure difference that is developed within the specimen and consequently the difference between an exponential and a linear pore fluid pressure distribution is small. The result strengthens the validity of the analytical technique developed in the study.

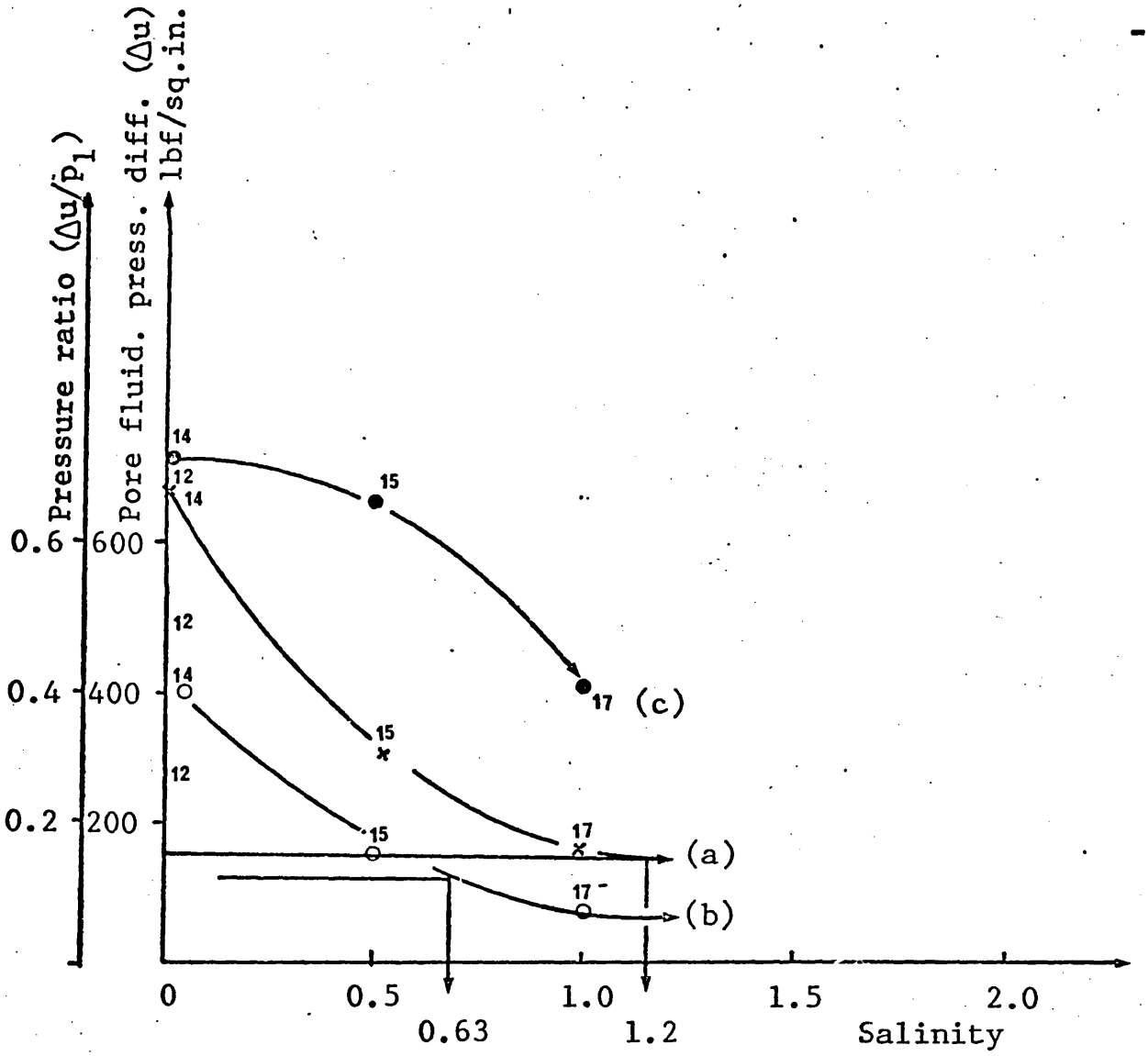


FIGURE 7.11 Variation of:

a) Peak pore fluid pressure difference (Δu peak)

b) Steady pore fluid pressure difference (Δu steady)

c) Pressure ratio (at the occurrence of the peak) (Δu peak/p_1)

with 'salinity' of the pore fluid.

(Note: the numbers indicate the respective BC.CHP test number)

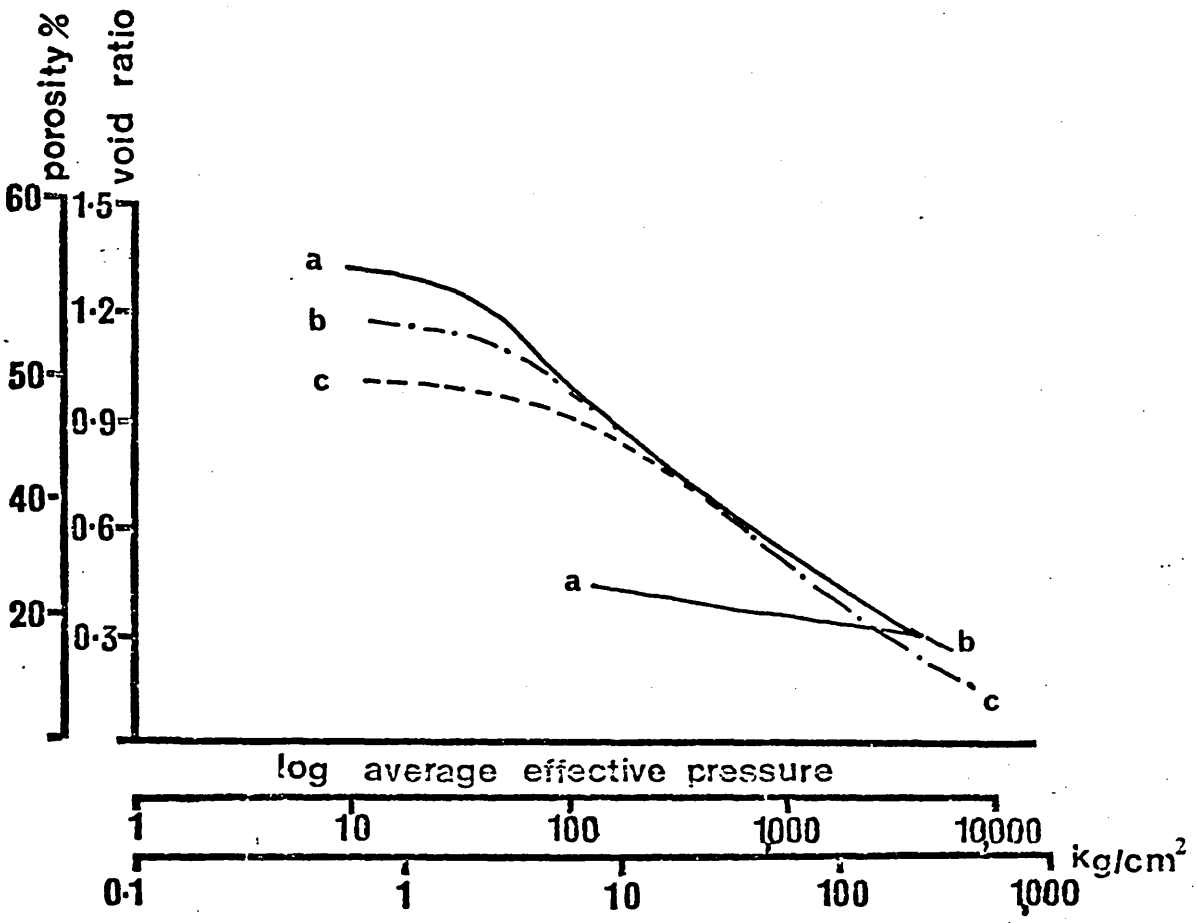


FIGURE 7.12 Influence of the salinity of pore fluid on the void ratio - log pressure characters of remoulded Ball Clay

Curve	Test No.	Salinity
(a)	BC.CHP.14	0
(b)	BC.CHP.15	0.5
(c)	BC.CHP.17	1.0

In Figure 7.13 a comparison is made of the 'best fit curves' for the permeability-porosity variation determined for these tests. In all the tests similar initial high values for the permeabilities are recorded (- 10^2 milliDarcy). The trend of the variations is somewhat similar in that every one of them comprises three distinct slopes. The first rapid decrease in permeability with decreasing porosity is arrested near a porosity of 40 percent. This probably suggests the end of the free pore water dewatering stage in gravitational compaction. Similarly the other two slopes may be characteristic of two further stages of the process.

7.2.4 Review of the BC.CHP tests

The controlled rate of loading BC.CHP tests are reviewed in entirety in this section.

7.2.4.1 Specimen preparation techniques

The original volume of the sediment slurries prior to preconsolidation is in excess of 1200 c.c. The process of remoulding of the sediments has to be effective to ensure complete saturation of the sediments. The specimens up to test BC.CHP.15 were remoulded manually using a pair of pallette knives. It was observed that such a technique sometimes produced lumps of unmixed clay (see Plate 9.1 showing such a lump from an abandoned test BC.CHP.13). The samples for the

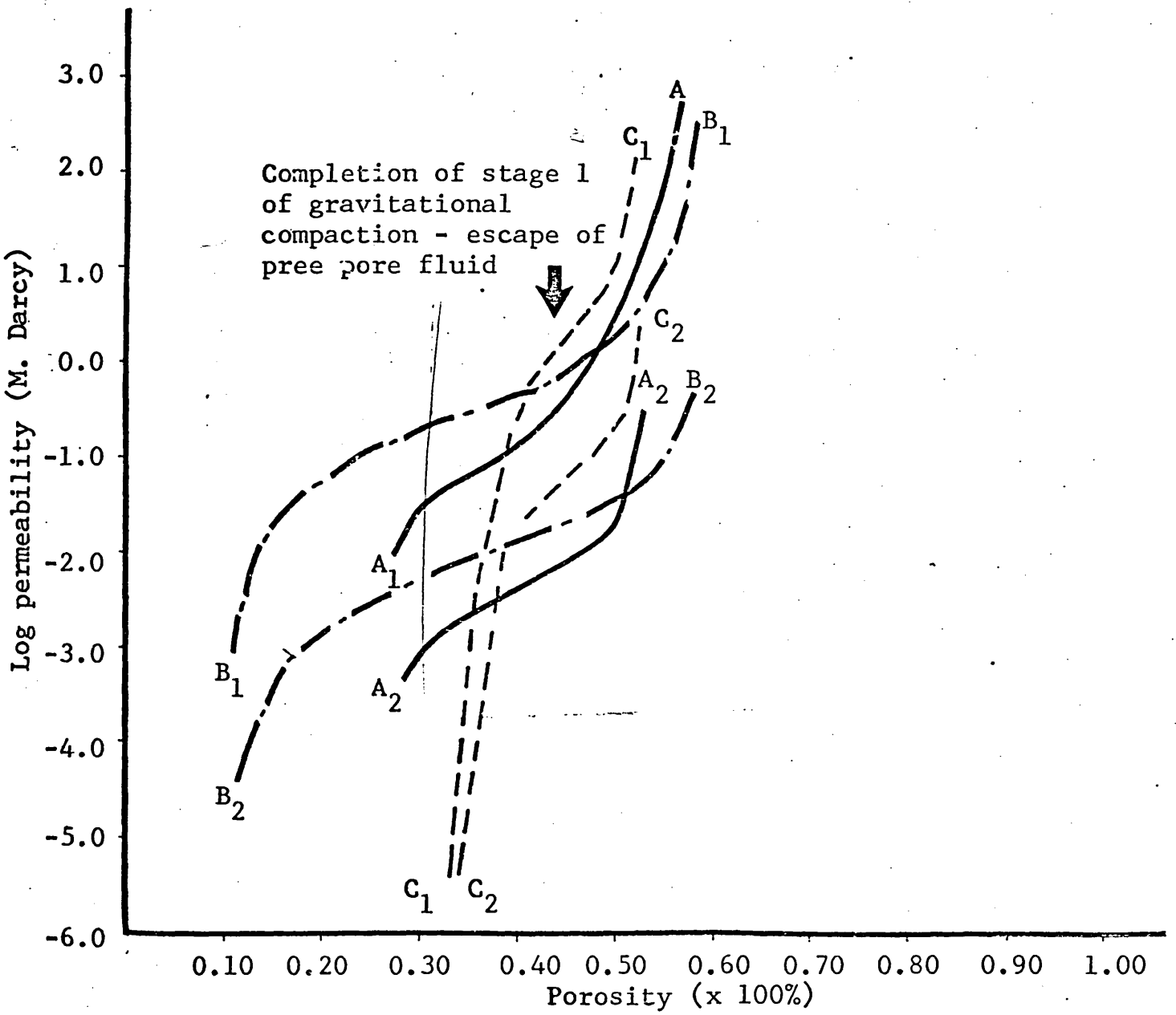


FIGURE 7.13 Influence of salinity on K-Ø characters

(1 denotes results using consolidation theory
2 denotes assuming a linear pore fluid pressure variation)

Curve	Test	Salinity
A-A	BC.CHP.14	0
B-B	BC.CHP.15	0.5
C-C	BC.CHP.17	1.0

subsequent tests were remoulded using an electric mixer.

Figure 7.14 is a plot of the voids ratio of the initial slurries (after correcting for the degree of saturation) against the initial moisture content. Strikingly the points appear to group separately dependent on the remoulding technique used.

The accuracy and representability of all the analyses of the tests cited in this chapter is dependent primarily on a reliable and an accurate determination of the final moisture content of the specimen. Figure 7.1 illustrated the moisture content distributions that were observed to occur in the final specimens. An average and representative value of the final moisture content was obtained from that of the remaining quarter of the specimen (Figure 9.1).

7.2.4.2 Compaction response

Here the term 'compaction' is used to describe the 'effect' of the uniaxial deformation of the specimen resulting from consolidation. Figure 7.15 is accordingly a collection of the compaction data from all the pertinent BC.CHP tests. The compaction is expressed as a percentage of the initial thickness (note specimen thickness after preconsolidation) and its corresponding variation with time and total axial pressure as shown in Figures 7.15a and 7.15b respectively.

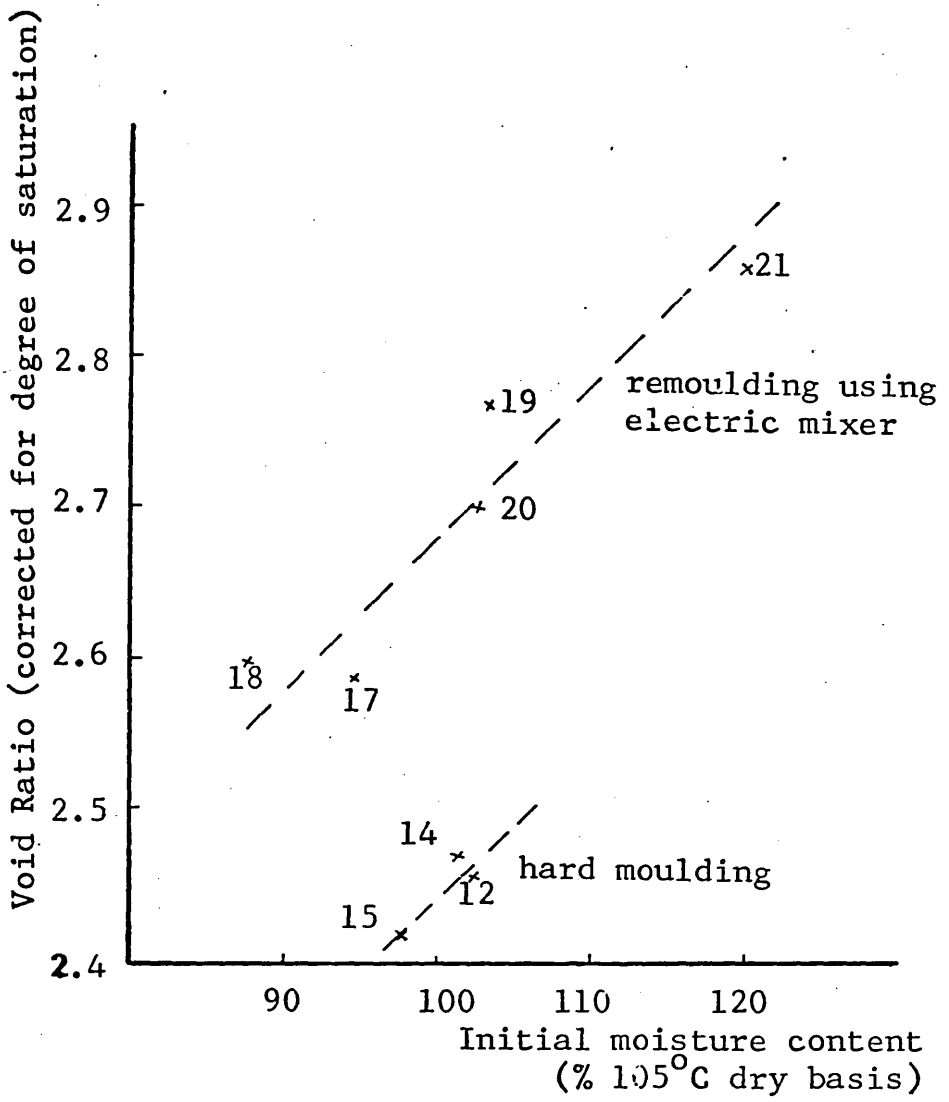


FIGURE 7.14 Influence of the technique of remoulding in achieving complete saturation.

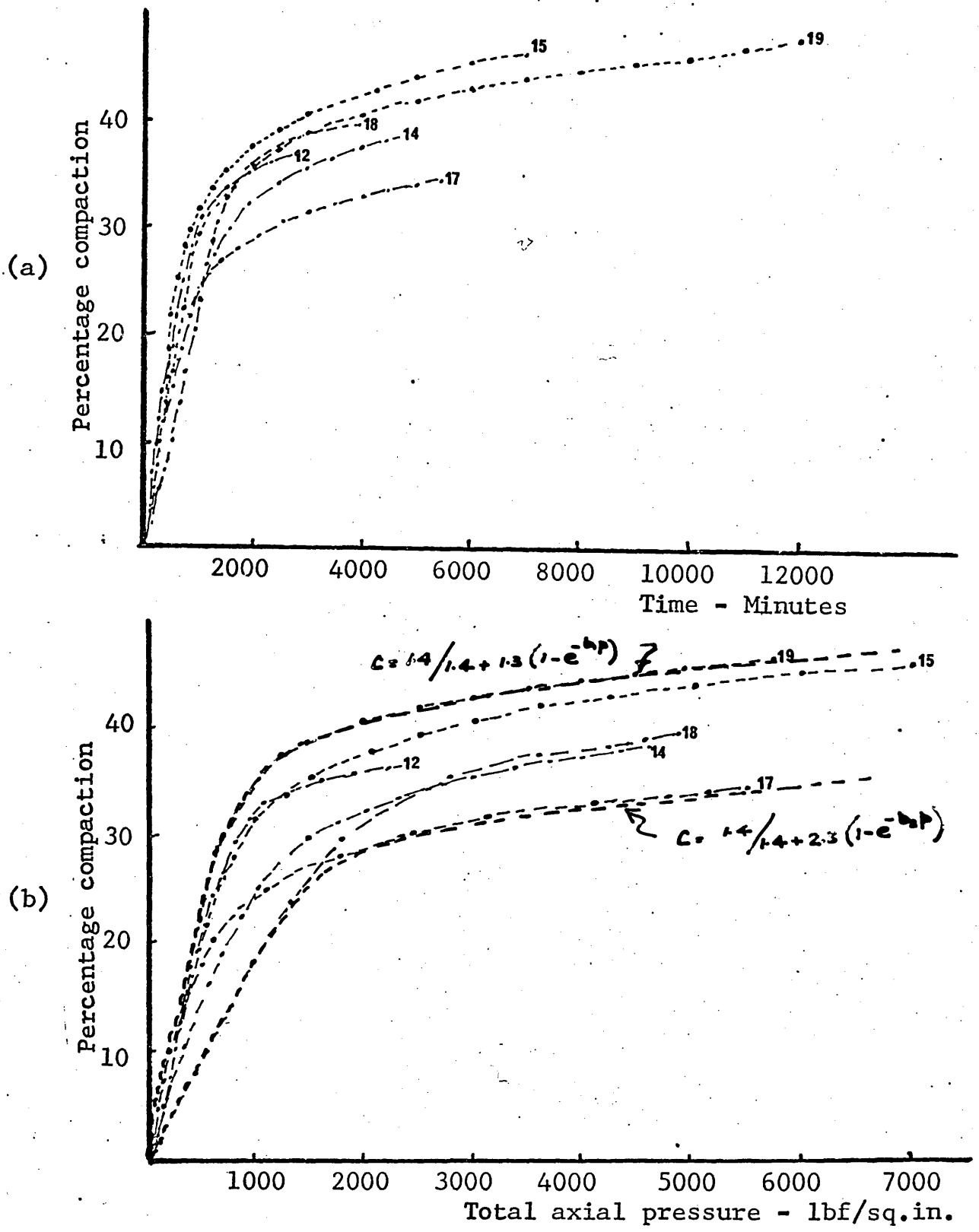


FIGURE 7.15 A summary of BC.CHP tests showing variation of percentage compaction with;

(a) time (b) total axial pressure

(number given indicates the test no.)

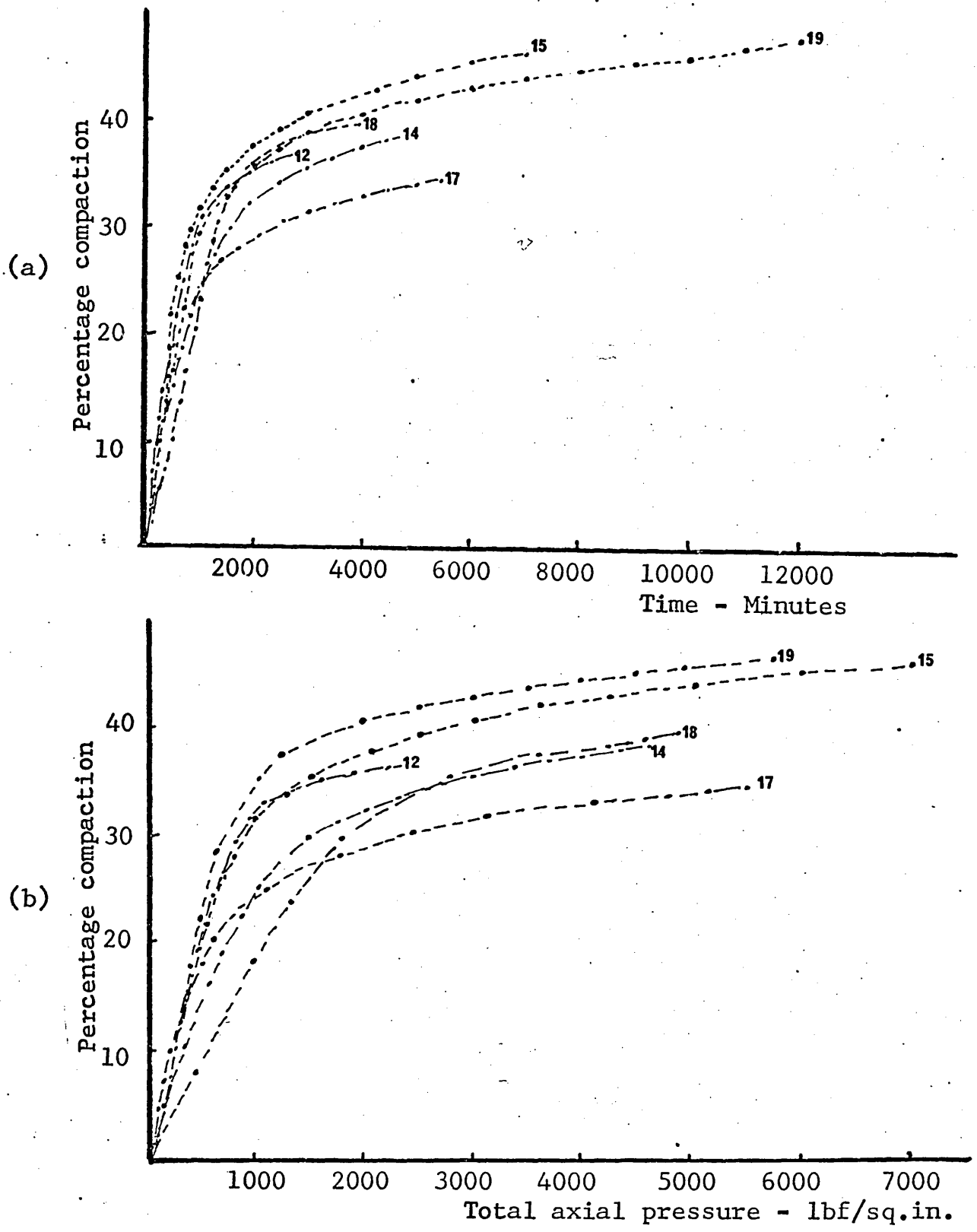


FIGURE 7.15 A summary of BC.CHP tests showing variation of percentage compaction with;

(a) time (b) total axial pressure

(number given indicates the test no.)

The compaction response curves for the tests BC.CHP.19 and 17 stand out from the rest in Figure 7.15a. The rate of early strain in the test BC.CHP.19 is less than those of the rest by virtue of the slower rate of loading that was imposed on the specimen. Pore fluid in the specimen of test BC.CHP.17 was of the greatest salinity and absolute values of the linear rates of these early strains have been given in Table 7.II.

There appears to be a much wider range of variations in Figure 7.15b where the dependence of % compaction on total axial pressure is illustrated. The envelopes to the curves (shown on overlay) can define a mathematical relationship between the two parameters following the suit of Athy's curves (see Section 2.7.5). However, it is noteworthy to emphasise that the pore fluid pressure in the specimen was not neutral but was in dynamic equilibrium with rate of loading and rate of compaction. Furthermore, this situation is apparent from the non-zero slopes of all the % compaction curves at the ends (peak pressures), thereby suggesting the existence of a state of incomplete pore fluid pressure dissipation, prior to unloading.

The test BC.CHP.21 was a solitary test in which the specimen was loaded extremely slowly (0.5 lbs/sq.in/minute) and in a hypersaline pore fluid (salinity 2) environment. The

'peculiar' variation of the pore fluid pressure difference was later found to be due to a leak in the pore fluid pressure line which was therefore open to a fraction of the hydraulic pressure - ~~a fraction~~

7.2.5 Consolidation of Undisturbed Samples

The preparation of undisturbed specimens for consolidation testing has already been described in 5.2.6 . The specimens, even those from Falmouth, were sufficiently stiff in consistency to allow the specimen chamber to be inverted and positioned in place on the lower plug of the apparatus in the usual manner. These tests were also conducted in the otherwise usual manner except for the preconsolidation stage which in this instance was not necessary. A loading rate of 1 lbf/sq.in/min. was used in all the tests.

7.2.5.1 Falmouth samples

The variation of the parameters observed in this test were similar to those observed earlier (see Figure D.24 in Appendix D). According to the variation of pore fluid pressure difference peak with salinity is observed and presented in Figure 7.11, the 'salinity' corresponding to a peak pore fluid pressure difference of 122 lbf/sq.in is 1.2. The actual salinity (as analysed from the early expelled pore fluid) corresponds approximately to a 'salinity' of 0.7 (c.f. Cl^- =

12.58 g/L, and Na^+ = 8.8 g/L but dissolved solids are less). The steady value of ΔU as observed is 55 psi which too corresponds to a 'salinity' of the order of 1.2.

Figure 7.16 illustrates the consolidation character of the Falmouth sample and is compared with that of the low pressure consolidation characters observed (see N.FA.CLP tests in Chapter Six). The correspondence between the low pressure and high pressure consolidation is satisfactory within experimental limits.

It is noteworthy that the variation of M_v with average effective pressure is outstandingly linear in the entire pressure range, characteristic of the "virgin" state of consolidation of this recent clay and is different from the rest of the CHP tests where the samples had some form of preconsolidation. (figure D.25)

7.2.5.2 Undisturbed Ball Clay samples

In this test (N.BC.CHP.1) too, a peak in the pore water pressure difference variation was apparent and was 195 lbf/sq.in. in magnitude. The results of the test are given in detail in Figures D.21 in Appendix D.

The preconsolidation stress of the ball clay as estimated using Casagrande method (Figure 7.20) amounts to the order of 200 lbf/sq.in. corresponding to 200 feet of burial. Attention must be drawn to the conclusions of Best and Fookes

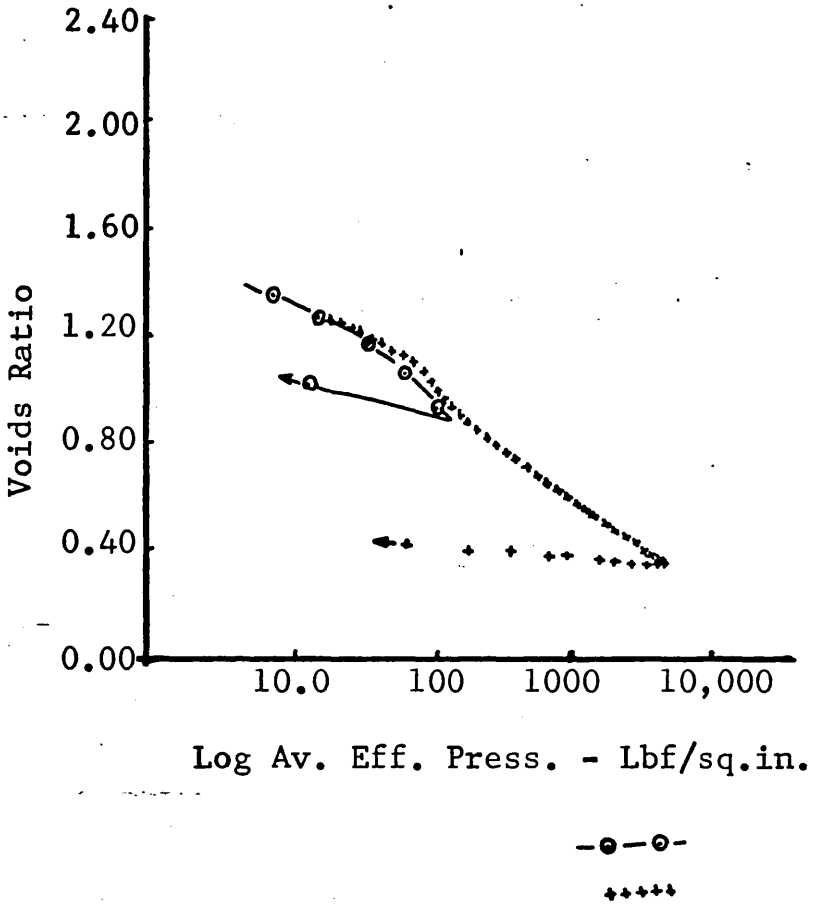


FIGURE 7.16 Consolidation character of undisturbed Falmouth Clay

(1970) who infer that the process of dessiccation after deposition has been responsible for the overconsolidation. Therefore a one to one correspondence may not exist between the preconsolidation stress and the 'depth' of overburden eroded.

The e-log p data for the undisturbed Falmouth and Ball Clays are plotted on the same axis and presented in Figure 7.17. Two distinct features of interest are apparent.

For effective pressures in excess of 2,000 lbf/sq.in., the Falmouth sample acquires a lower void ratio than the Bail Clay. In other words, the Falmouth sediments possess a higher compressibility at these pressures. It is also seen that the rebound curve for the ball clay is only as steep as that of the Falmouth clay even after consolidation to a higher maximum pressure.

Figure 7.18 is a further attempt made to study the extent to which the artificial gravitational compaction in the laboratory has been successful in making the Falmouth sediments achieve similar geotechnical characters. In this instance their respective permeability-porosity plots are compared. For similar porosities, the permeability variations show consistent trends. The N.BC.CHP.1 required a lesser permeability of the two and also showed a very marked decrease of the permeability early in consolidation. It must, however, be noted that the discrepancy between the

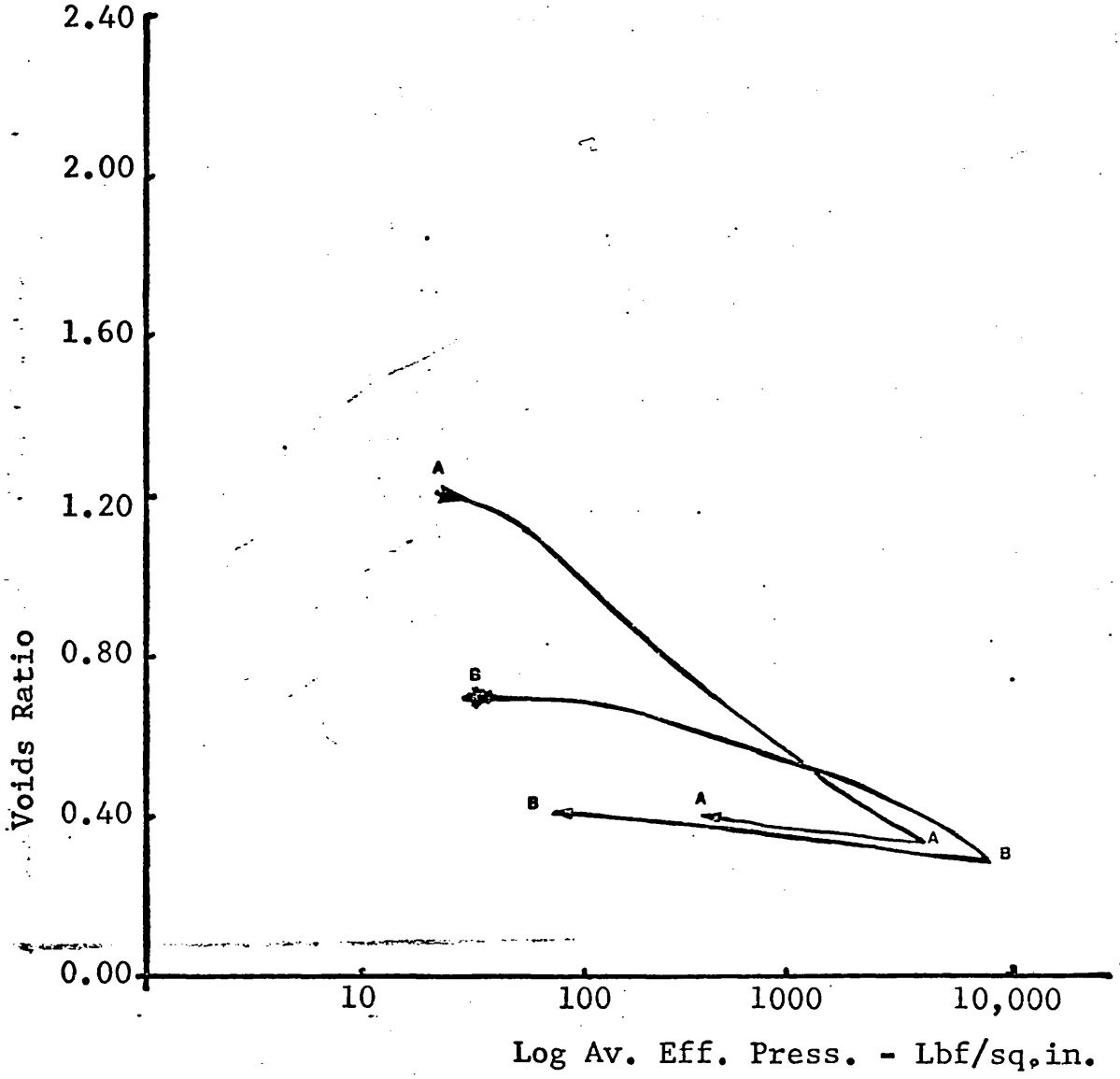


FIGURE 7.17 A comparison of the e-log p curve of the recent (Falmouth) and Oligocene aged (Ball Clay) undisturbed sediments.

Curve	Test No.
AAA	N.FA.CHP.2
BBB	N.BC.CHP.1

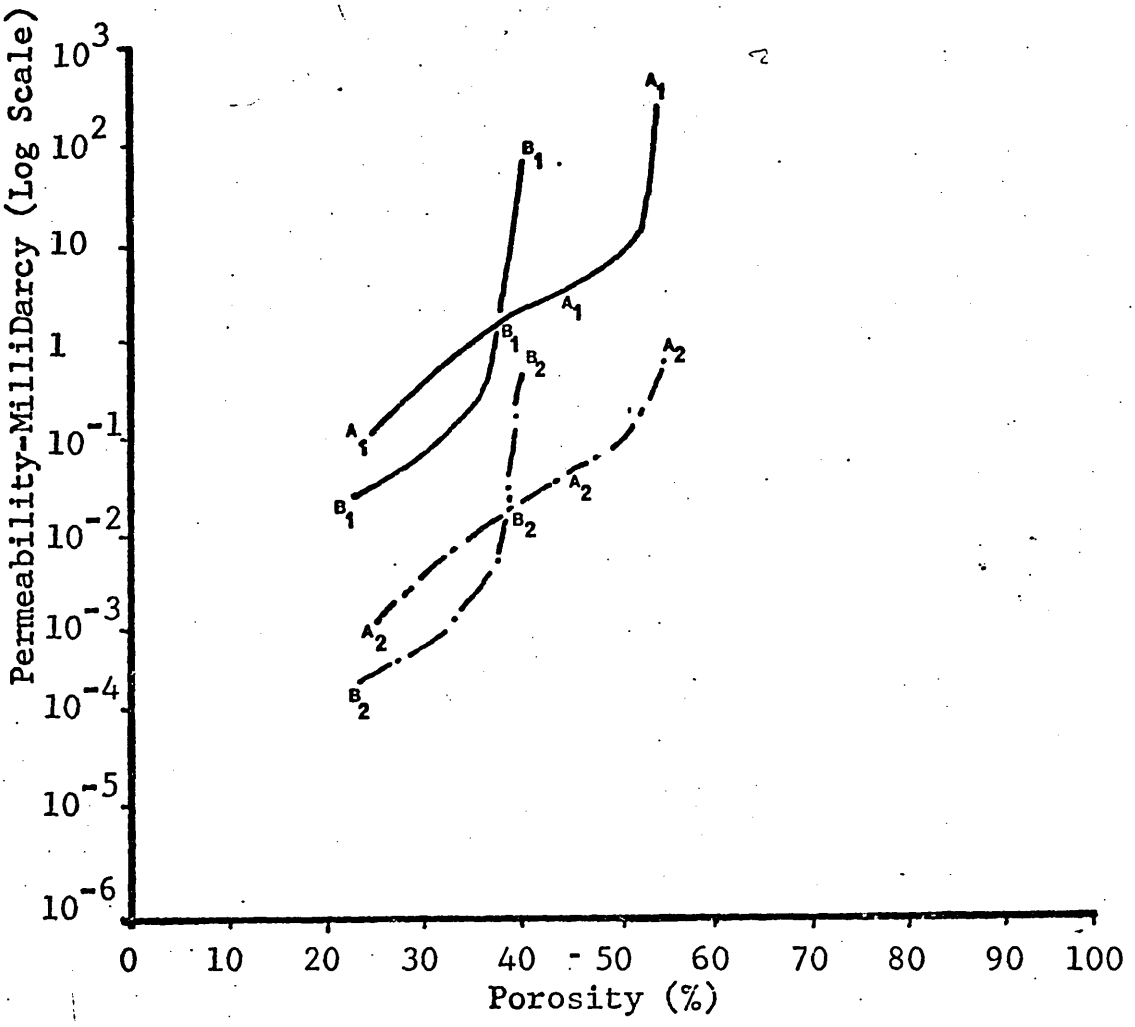


FIGURE 7.18 Comparison of the permeability-porosity plots for natural Falmouth and Ball Clay samples

AA - Falmouth
BB - Ball Clay
Suffix 1 - consolidation theory
Suffix 2 - assuming linear U variation

results cited for the two clays must be primarily a result of the differences in grain size of the sediments (see Figure 6.12).

7.3 CONSTANT RATE OF STRAIN CONSOLIDATION TEST (CRS TEST)

The constant rate of strain consolidation tests were conducted only on undisturbed ball clay specimens, and the experimental techniques have been described in Chapter Five. Details of the tests conducted are given in Table 7.IV. These tests were performed with the intent of comparing the results of the CRS tests with those of the associated CHP test. As a consequence of this study, it was possible to give an estimate of the preconsolidation stress of the Petrockstow Basin ball clay (see also Section 6.3.4).

Figure 7.19 is an illustration of the typical variation of the parameters observed during a CRS test (N.BC.CRS. Contrary to the CHP test series, in these tests a linear rate of strain was induced on the sample and its associated response to the build-up of the pore fluid pressure difference and the total axial pressure observed. In all other tests the build-up of pore fluid pressure difference was less due to the slower rates of strain used.

Figure 7.20 shows the e-log p character for the ball clay as computed from the observations of tests (N.BC.CRS.1

Test Number	BC.CRS			
	1	2	3	4
Date	4.1.74	21.1.74	13.2.74	1.3.74
Total No. of Days	8	8	4	8
Maximum Pressure psi	2380	814	failure	3450
Rate of Strain Inches/minute	0.0007	0.0049		0.0049
Final Moisture Content %	16.17	16.34		22.15

TABLE 7.IV

SUMMARY OF CONSTANT RATE OF STRAIN COMPACTION TESTS

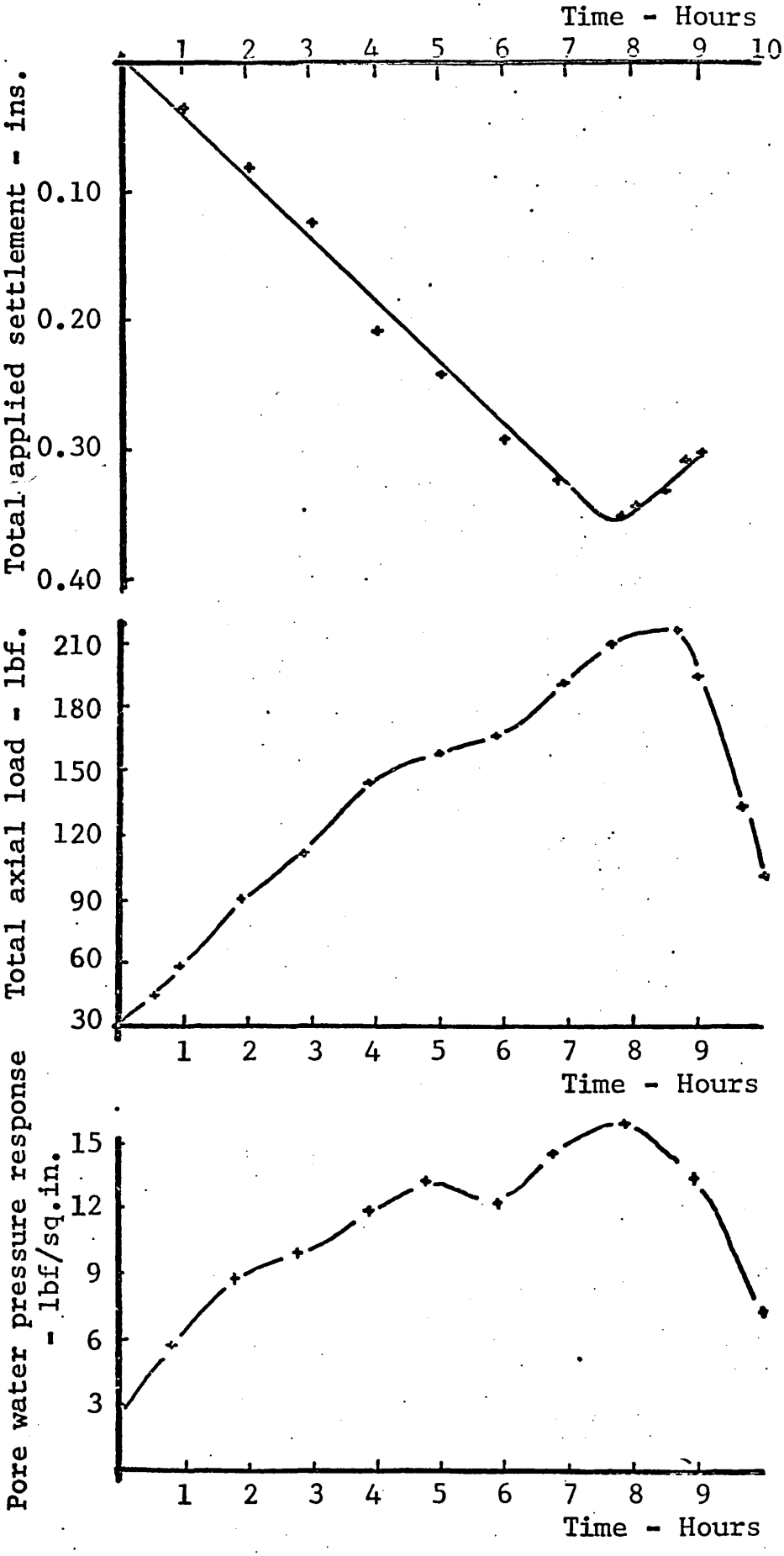


FIGURE 7.19 Typical variation of observed parameters (as per test N.BC.CRS.1) in the CRS tests; rate of strain 0.0007 in/min.

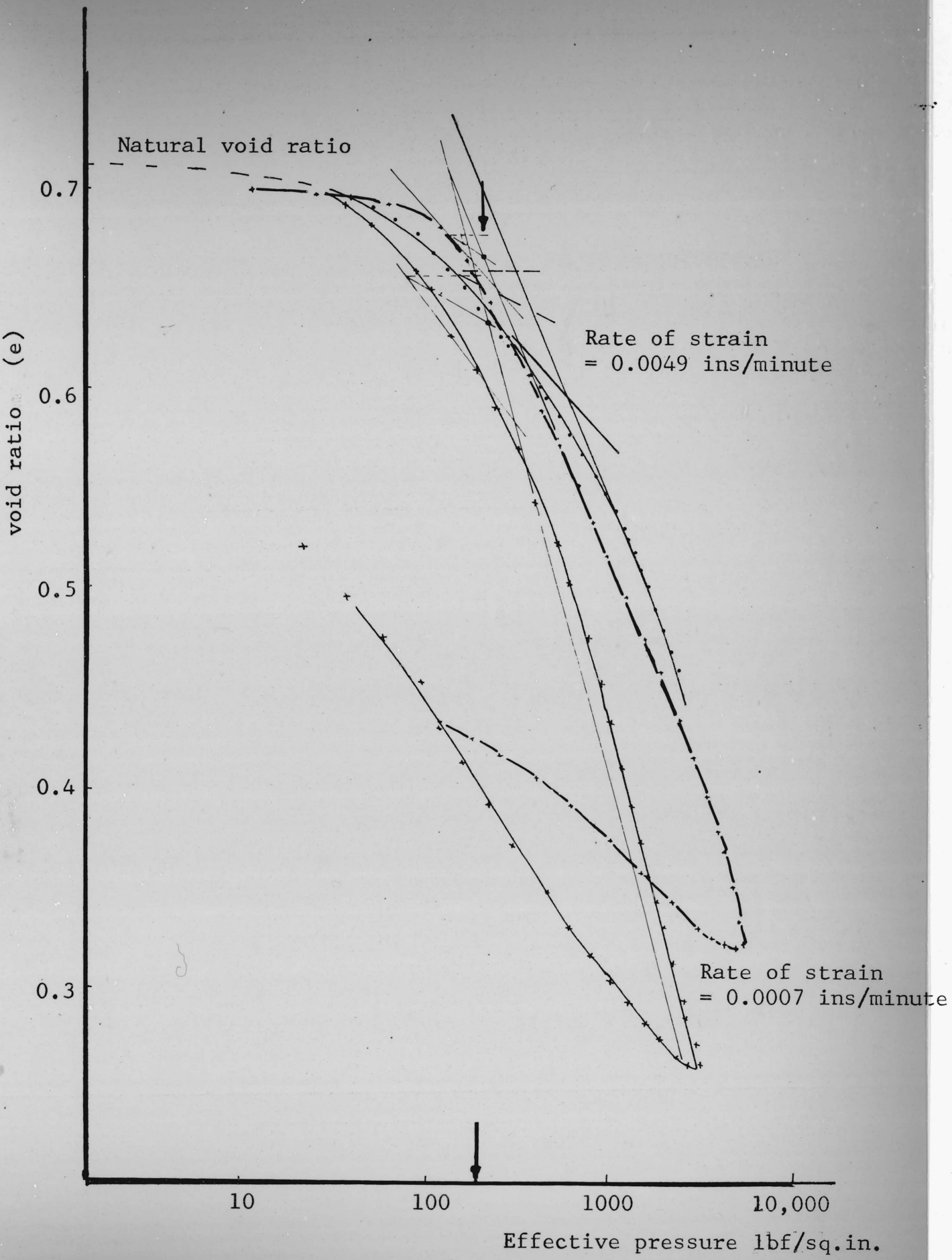


FIGURE 7.20 Void ratio log pressure plots for undisturbed ball clay as obtained per CRS tests.

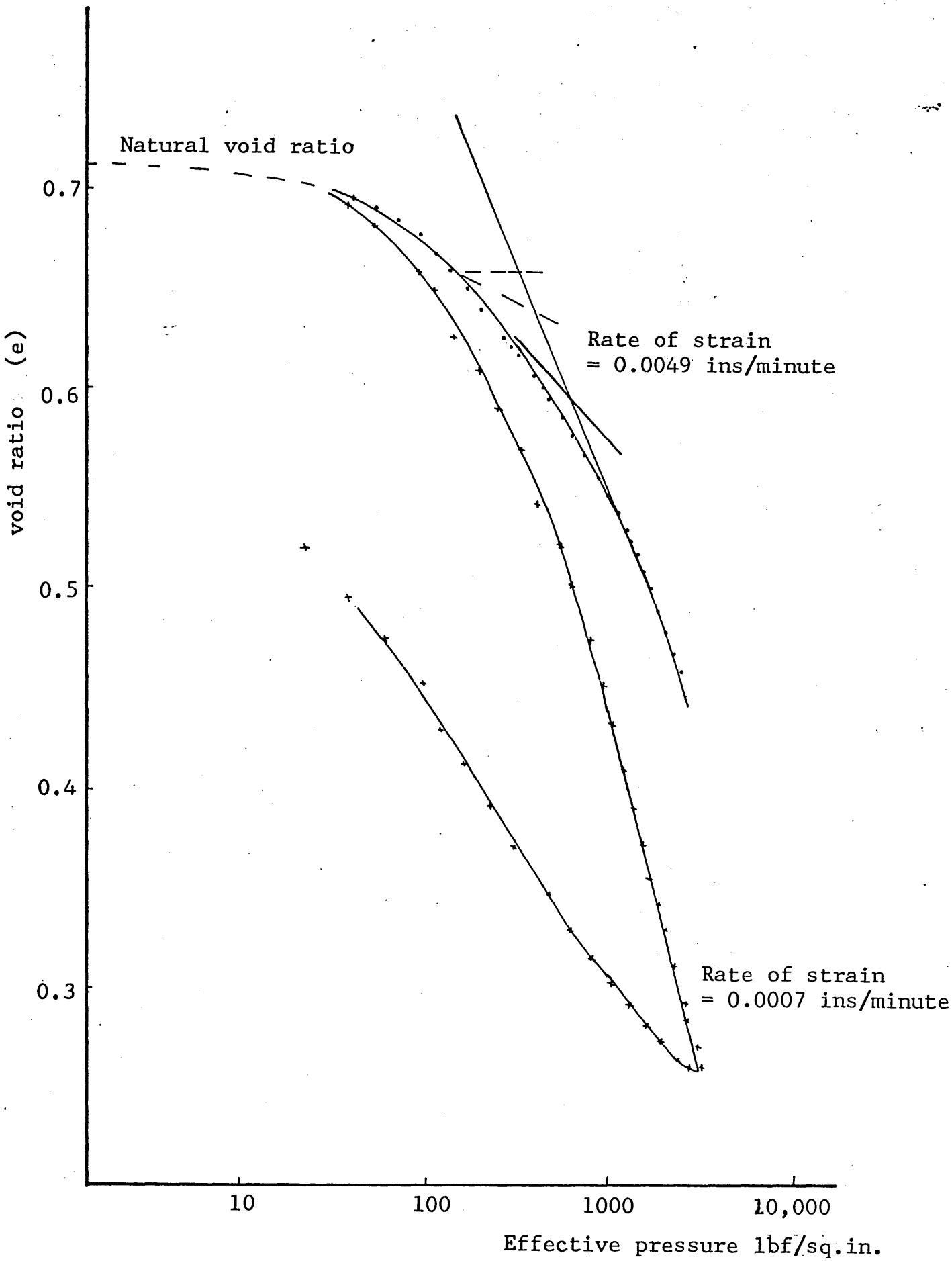


FIGURE 7.20 Void ratio log pressure plots for undisturbed ball clay as obtained per CRS tests.

and N.BC.CRS.4. Since the maximum pore fluid pressure difference developed was less than percent of the total stress, it was considered justifiable to assume the total stress to be equal to the effective stress (Smith and Wahls, 1969). Hereto it is evident that the e-log p character is susceptible to the rate of strain as it was observed to be effected by rate of loading (Figure 7.8).

The estimation of the preconsolidation stress is dependent on the shape of the e-log p curve which has now been shown to be dependent on the rate of strain. The overlay of the Figure 7.20 gives the e-log p plot for the clay as obtained from the CHP test and also illustrates the Casagrande construction (1936) used to determine the preconsolidation stress from it. The corresponding constructions for the BC.CRS.1 is also shown on the overlay.

It is clear from the figure that the N.BC.CHP.1 test results correspond closely to those of a CRS test conducted at a linear rate of deformation of 0.0049 in/minute. Their difference from the slower rate of strain is an overestimation of the effective pressure for a given void ratio. However, though the portions of the curve beyond the preconsolidation stress show widely different compressibilities, the application of the Casagrande construction gives very similar values for the preconsolidation stress.

Figure 7.21 is a plot of the constrained modulus, $D = 1/M_v$, as proposed by Janbu (1965) showing the difference in the compressibility below and above the preconsolidation stress as observed from the CHP and CRS tests. Table 7.V is a summary of the values obtained for the preconsolidation stress of the Petrockstow Basin ball clay.

7.4 INFLUENCE OF TEMPERATURE ON CONSOLIDATION

This phase of the research was conducted with the intent of clearing the ground for the proposed further development of the high pressure consolidation cell (stage 3, Table 5.T) where heating is to be introduced in order to simulate the effects of a geothermal gradient. Two particular aspects of the study made were:

a) the temperature distribution within a specimen when subjected to different forms of heating; and

b) the influence of heat on low pressure consolidation character of a remoulded clay.

7.4.1 Temperature distribution within a heat specimen

The sample being cylindrical in shape, it is practicable to heat the specimen in any one of the following methods:

i) all round heating, i.e. wall and end heating,

ii) uniform end heating only,

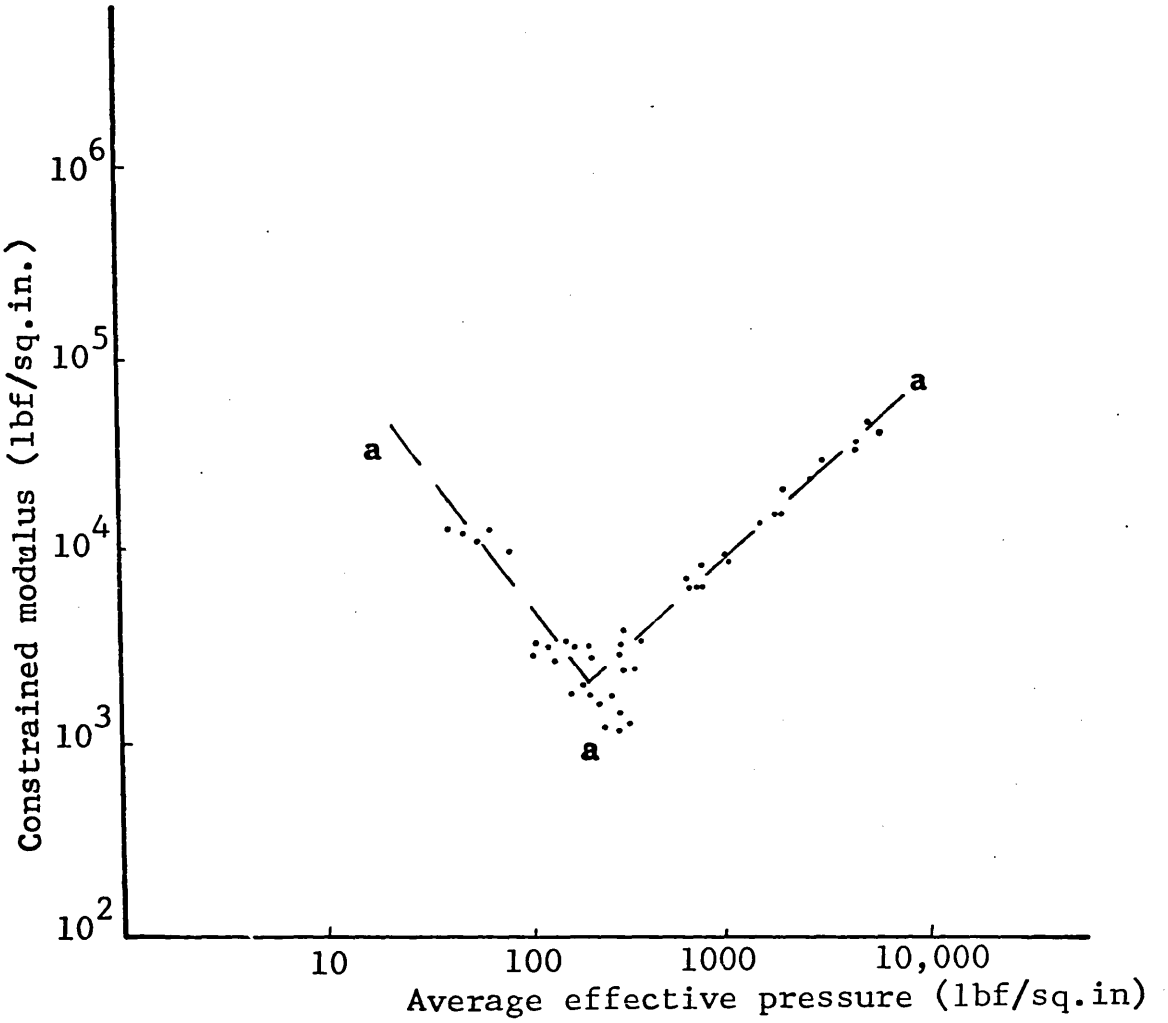


FIGURE 7.21 Constrained modulus, D, versus average effective pressure (log scale) for undisturbed Ball Clay

Curve	Test
aaa	N.BC.CHP.1

Test	From e-log p using Casagrande Const. lbf/sq.in.	From D-log p using Janbu Technique lbf/sq.in.
N.BC.CHP.1	228	185
N.BC.CRS.1	235	
N.BC.CRS.4	370	

TABLE 7.V

ESTIMATES OF PRECONSOLIDATION STRESS OF BALL CLAY FROM TESTS

iii) uniform wall heating only,

iv) wall heating with a linear temperature rise,

v) uniform wall heating and one end heating only,

A finite ~~difference~~ element technique was used to obtain theoretical temperature distribution patterns for each of the above cases of heating of the specimen. The relevant aspects of the analysis and the respective temperature distributions are given in Appendix E.

The thermal conductivity of a typical sample of consolidated ball clay was determined using a divided bar apparatus (Beck and Beck, 1958). It was determined to be

Conductivity of the non-porous rock $K_r = 8.4 \pm 0.7$ mCals/cm/sec/^oC

The conductivity at any desired porosity was determined by assuming the equation (Saas, J.H. et al, 1971):

$$K_{pr} = K_w\left(\frac{K_r}{K_w}\right)^{1-\phi_o}$$

ϕ_o = natural porosity.

K_w = thermal conductivity of liquid water at 25^oC,

= 1.46 mCals/cm/sec/^oC.

K_{pr} = thermal conductivity of porous rock.

The dependence of the thermal conductivity on factors such as mineralogy, temperature, pressure, pore fluid chemistry

etc. is appreciated (Akhmedora and Glymanov, 1970; Horai and Vyeda, 1960) but is not accounted for in the computations. However, the more important changes resulting from changes in porosity due to consolidation was taken into account and as such the values shown in Table 7.VI were used. The thermal conductivity values of all materials in the vicinity of the specimen are also given in the table.

Figure 7.22 illustrates the predicted change in the isotherm patterns with programme consolidation of the specimen.

7.4.1.1 Experimental temperature distribution study

The consolidated ball clay specimen from an abandoned BC.CHP test was used to verify the thecretical predictions. This specimen was placed in the specimen chamber of the High Pressure consolidation apparatus and the cell was filled with the hydraulic fluid too, so as to reproduce an exact thermal environment.

An annular heater was used to heat the specimen from one end only. Two thermocouples were positioned within the specimen, one at the base of the specimen and the other 1½" from the base of the 2½" thick specimen.

The graphs in Figure 7.23 indicate the observed temperature rise and decay curves, when the heater was energised

Component	Material	Thermal Conductivity mCals/cm/sec/^{o}C	Reference
Specimen chamber	Nilo Alloy 36	1541	B.S.C.
Specimen sleeve	PTFE	38	I.C.I.
Specimen:			
4" thick (100% m/c)	Ball Clay 661	5.91	Present study
consolidated to 2" thick		7.10	
consolidated to 1" thick		7.70	

TABLE 7.VI

THERMAL CONDUCTIVITY OF MATERIALS

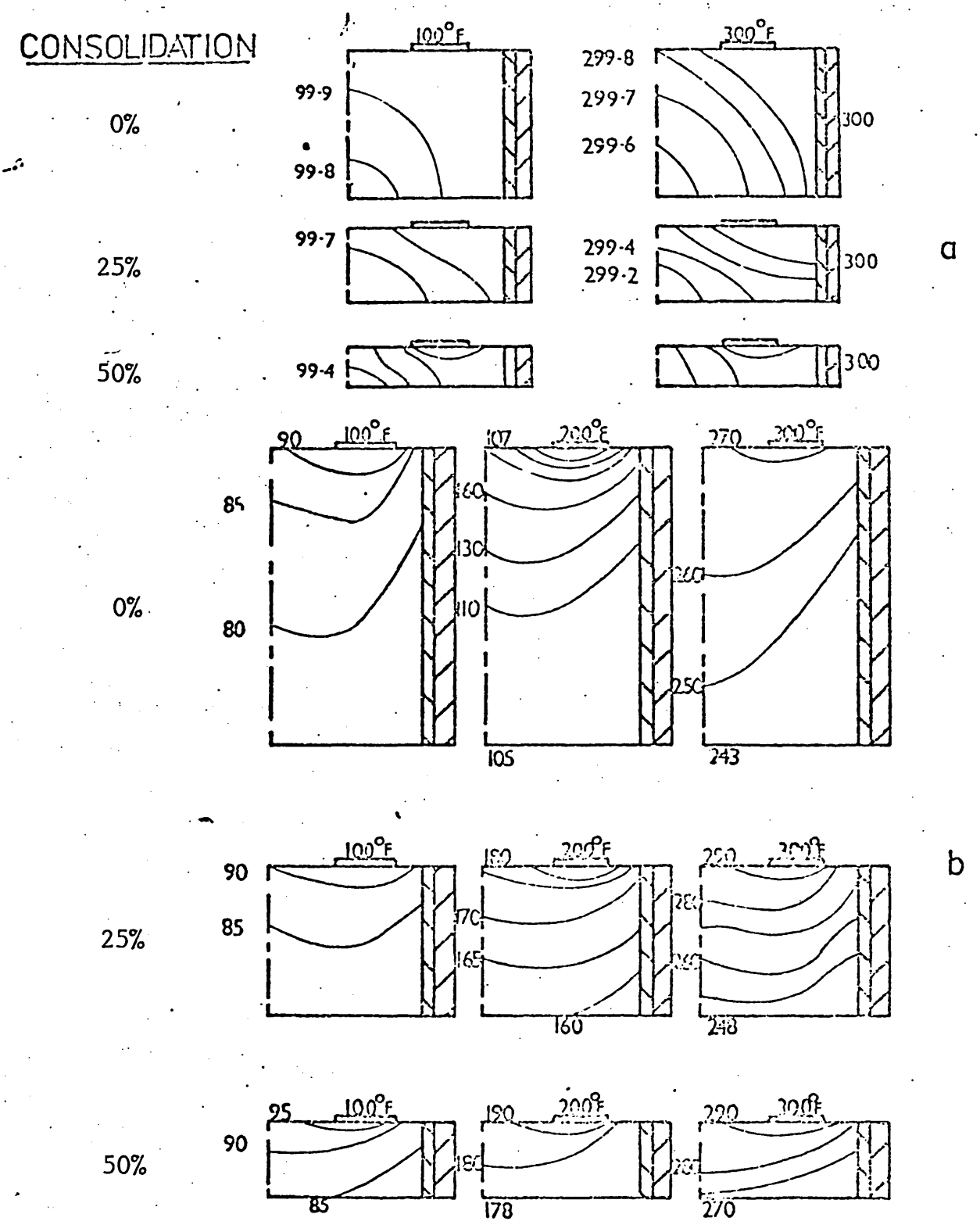
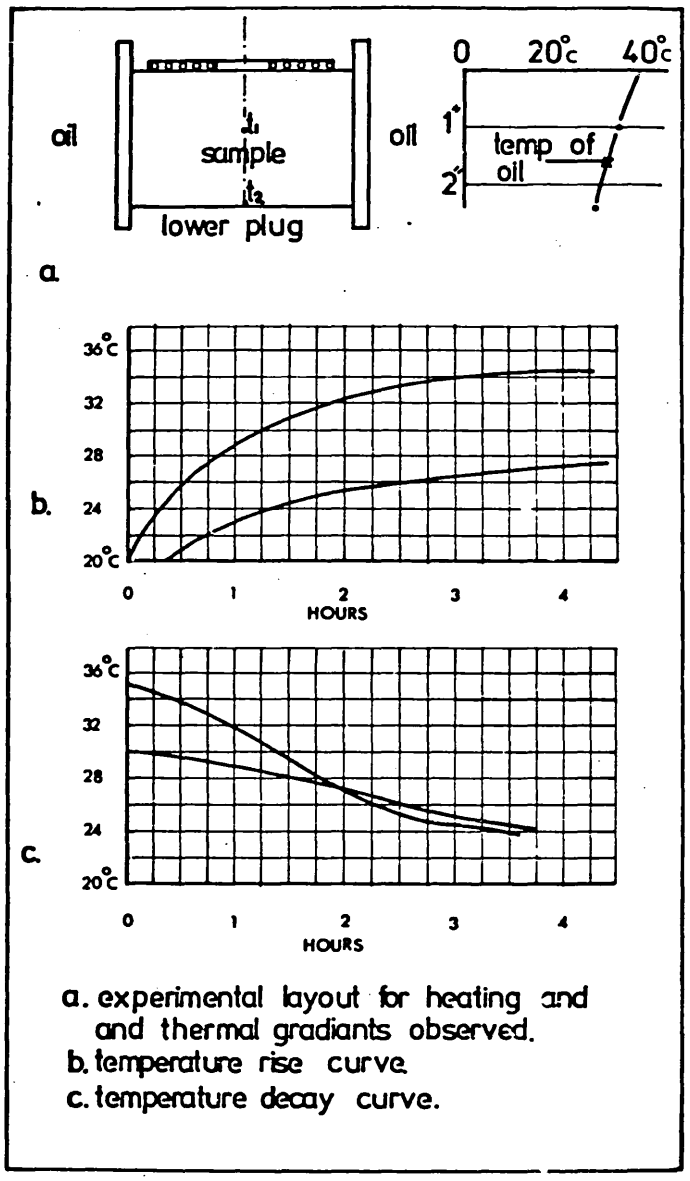


FIGURE 7.22 Heat Flow Patterns

a) wall and two end heaters
b) one end heater only



a. experimental layout for heating and and thermal gradiants observed.
b. temperature rise curve.
c. temperature decay curve.

FIGURE 7.23 Experimental observation of the heat conduction and subsequent temperature distribution within a consolidated ball clay specimen.

to a uniform temperature of 40°C. The steady state temperature in the oil was 32°C. The temperature gradient within the specimen is shown in the figure and it shows that the steady state temperature attained in the surrounding oil is equivalent to that at a point one-third the thickness away from the base of the specimen.

7.4.2 Low pressure temperature consolidation tests (CLPT series)

A series of four tests were conducted. Each set consisted of two tests run simultaneously under the same ambient conditions but only one was subjected to an elevated temperature (T) while the other was performed at room temperature (RT). In all the tests ball clay no. 661 was used remoulded to approximately one hundred moisture content. The equipment used has been described in Section.

7.4.2.1 Temperature induced strain

In all the tests, the heater was first energised to the required temperature level, with the specimen under no load. Observations were made of the thermocouples and the settlement dial gauge at frequent intervals. These observations are shown in Figure 7.24, which illustrates the temperature transients within the specimen and in Figure 7.24b,the associated deformation in the "system" is shown.

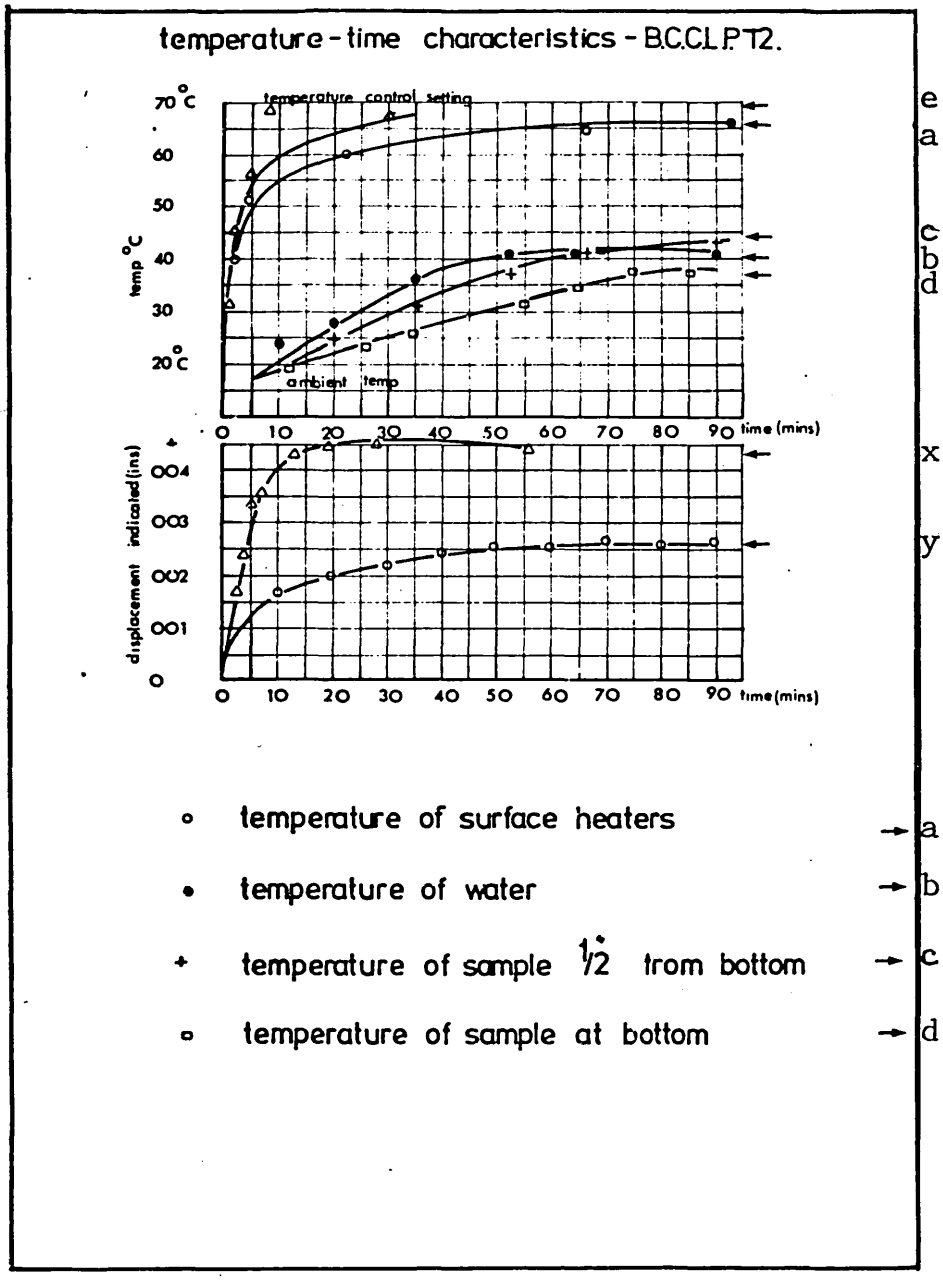


FIGURE 7.24 Temperature rise and system deformation observation when system temperature is raised to 70°C at no load.

e - temperature of loading platten as recorded.

x - temperature induced expansion of loading platten alone

y - deformation in the system

x - y - temperature induced consolidation

The expansion of the loading platten alone was observed separately but is shown on the same time base which helps to separate "temperature induced" consolidation within the specimen which amounted to 0.1% at 70°C. It is felt that this consolidation due to temperature alone is affected by the apparent volumetric expansion of the pore water which creates its own pore water pressure and dissipates it via a volume decrease.

7.4.2.2 Low pressure consolidation at different temperatures

Data pertinent to the tests are summarised in Table 7.VIII. The tests were conducted in the conventional manner using a stress increment value ($\Delta P/P$) of one and a time lapse of twenty-four hours between any two increments. Observations are analysed in the usual way too, and the resulting e-log p curves for all these tests are given in Figure 7.25 and it emphasises the influence of temperature in inducing the specimen to attain a more compact state. Figure 7.26 is an e-p plot for a single set which helps to show more clearly that most of the discrepancy in the void ratio between the two curves occurs at the low stress levels.

Analysis of the settlement time observation indicated a pronounced difference between the rates of early strain (primary consolidation stage) in the CLP.T and CLP.RT tests.

Test No.	BC.CLP.							
	RT1	T1	RT2	T2	RT3	T3	RT4	T4
Date of Test	22.7.73	22.7.73	4.9.73	4.9.73	29.9.73	29.9.73	14.10.73	14.10.73
Total No. of Days	14	14	14	14	14	14	9	9
Maximum consolidation pressure - psi	140	140	140	140	140	140	140	140
Temperature of Heater - ^{o}C	17	50	17	58	17	49	17	70
Temperature Gradient in Sample - oc/inch	0	6	0	5	0	5	0	5
Unloading	Stages	Stages	Instant	Instant	Stages	Stages	Stages	Stages
Final Moisture Content	42.50	42.10	41.70	41.50	42.45	40.60	40.00	37.70
Initial Thickness	1.6875	1.687	1.875	1.875	1.875	1.875	1.875	1.875

TABLE 7.VII SUMMARY OF LOW PRESSURE-TEMPERATURE CONSOLIDATION TESTS

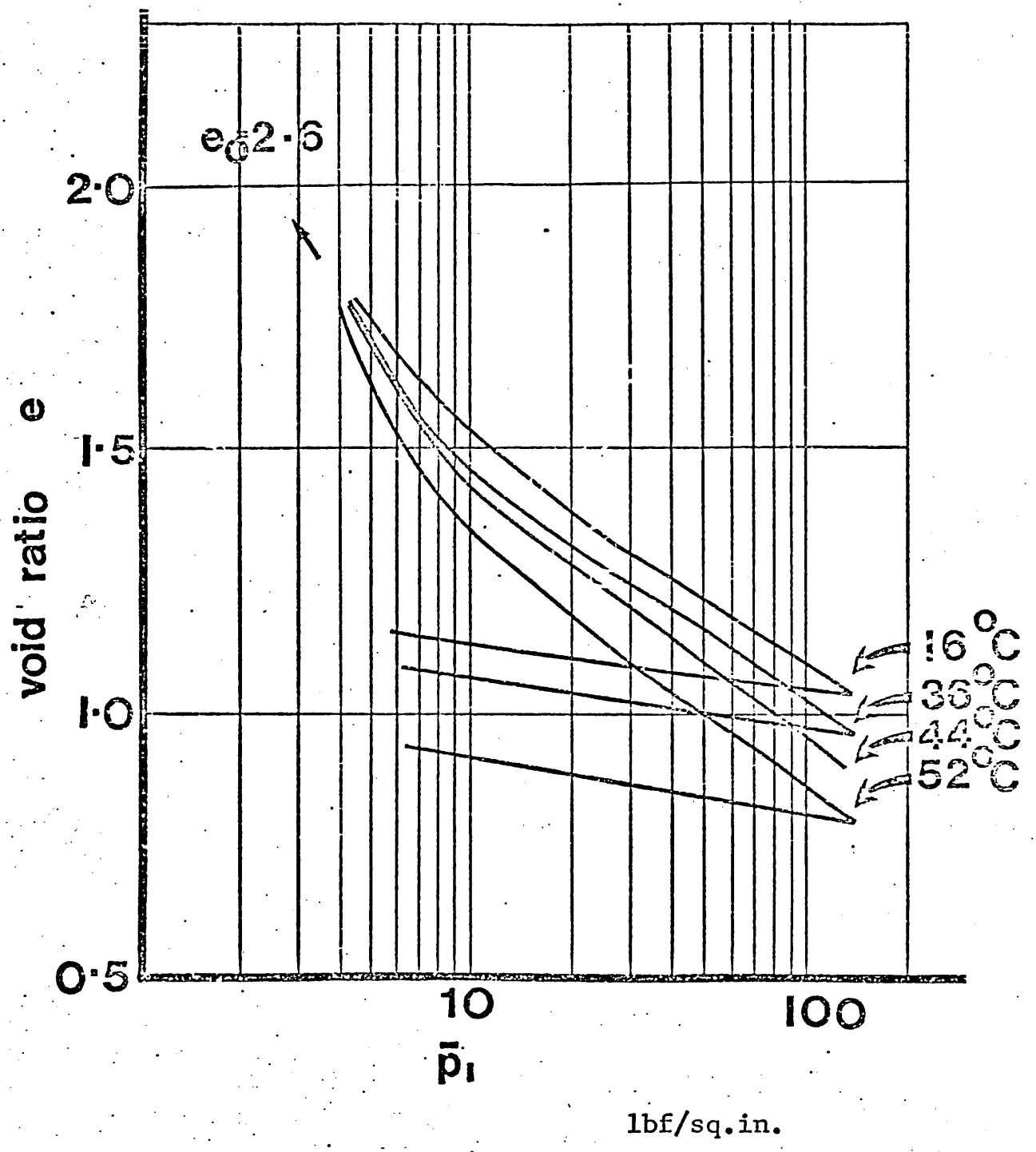


FIGURE 7.25 e-log p plots for elevated temperature consolidation tests.

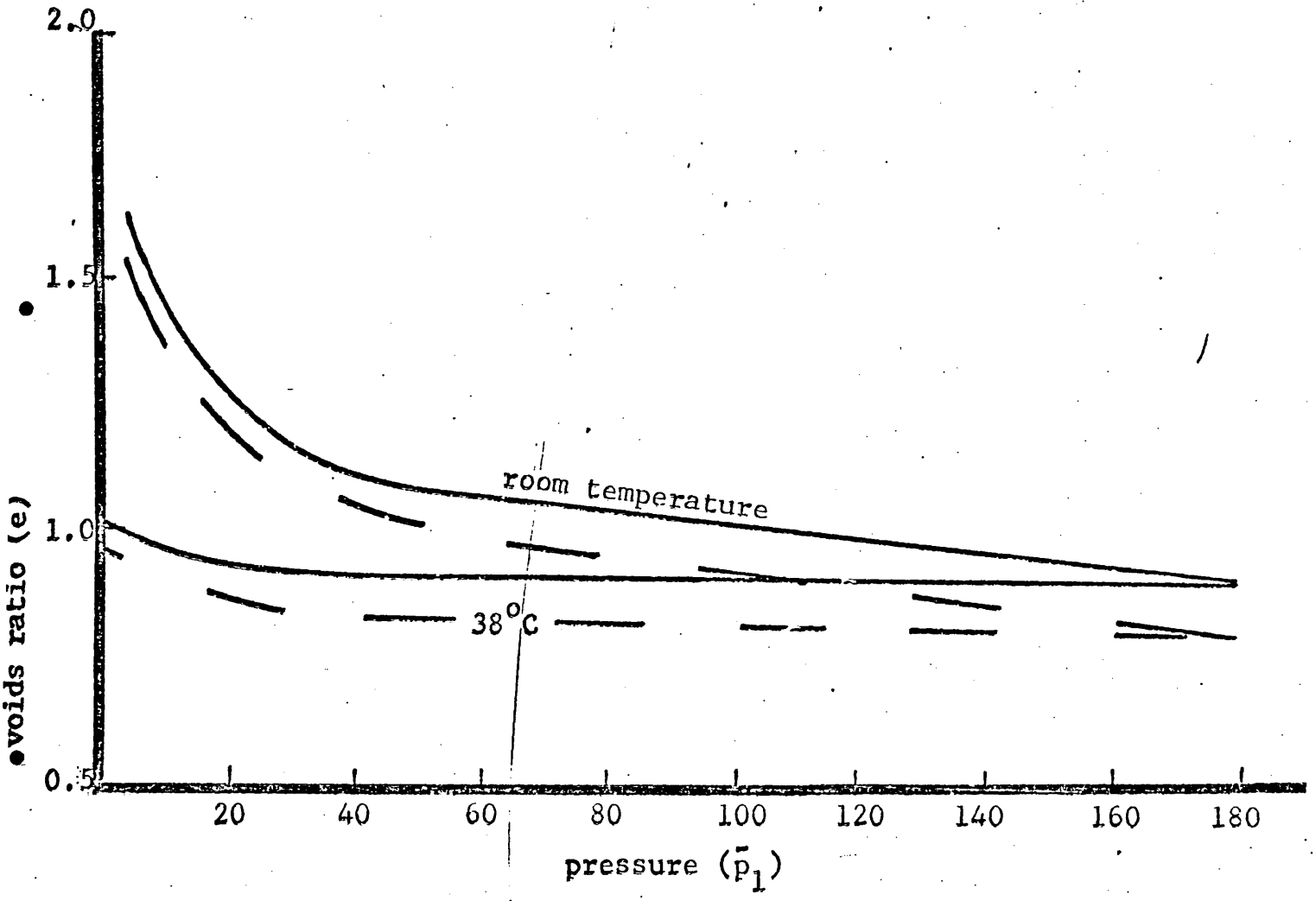


FIGURE 7.26 Void ratio-pressure plot for a BC.CLPT test.

This rate of strain is proportional to the permeability of the pore fluid. Figures 7.27a and 7.27b outline the variation of the viscosity of water with pressure and temperature respectively. Figure 7.27c is a study of the dependence of the rate of primary consolidation on the viscosity of fluid. The data are plotted separately for each step load increment, on a semilogarithmic plot of ratio of the strain of the sample, maintained at room temperature (RT) to that at the elevated temperature (T) against the ratio of the viscosity of water at the two temperature (log scale). It can be shown that the point (1,1) is a valid observation for all stages of loading (consider case of two room temperature tests).

From the graphs, which show nearly linear variations, the following relationship can be derived:

$$\frac{\partial \rho_{RT}}{\partial t} \Big/ \frac{\partial \rho_{T}}{\partial t} = A \log \frac{\eta_t}{\eta_{RT}} + 1$$

where:

ρ_T = settlement at temperature T,
η_T = viscosity of water at temperature T.

Furthermore, it is apparent that the slope of these linear variations flattens with increasing stress level from $A = 1.803$ at 0-5 lbf/sq.in. to $A = 1.037$ at 80-160 lbf/sq.in.

The immediate practical application of the above observations was to aid in designing the development stage

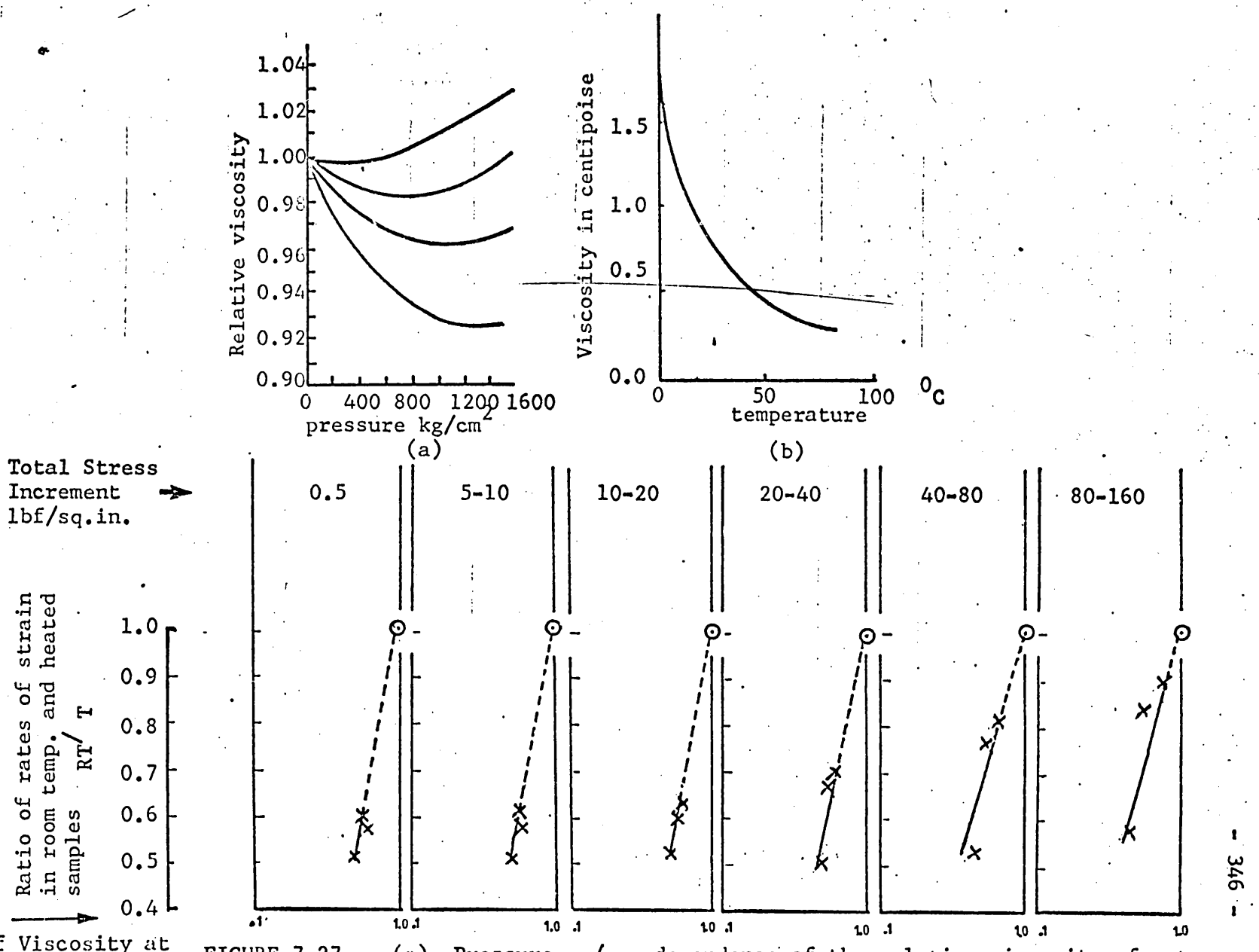


FIGURE 7.27 (a) Pressure $_{T/RT}$ dependence of the relative viscosity of water
(b) Temperature dependence of the viscosity of water.
(c) Separate plots of the rate of strain ratio of viscosity

three (Table 5.I) of the high pressure temperature consolidation cell. The most important observation was to ascertain that the delivery rate of the ram pumps was capable of catering for a further 50% enhancement over the rate of consolidation of a room temperature sample.

CHAPTER EIGHT Clay Mineralogy and Pore Fluid Chemistry

8.1 Introduction 349

8.2 Clay Mineralogy 349

8.2.1 Whole rock analysis 352
8.2.2 Clay fraction analysis 356

8.2.2.1 Falmouth clay 366
8.2.2.2 Petrockstow ball clay 366
8.2.2.3 Ball clay no. 661 367

8.3 Changes in clay mineralogy with consolidation 367

8.3.1 Methylene blue dye titration 369
8.3.2 C.E.C. values for field and laboratory samples 370

8.4 Chemical analysis of pore fluids 372

8.4.1 Weight of total dissolved solids 373
8.4.2 Determination of the concentration of cations 375

8.4.2.1 Atomic absorption spectrometry 375
8.4.2.2 Atomic emission spectrometry 377
8.4.2.3 Observed variation trends in concentration of cations 380

8.4.3 Determination of the concentration of the anions 383

8.4.3.1 Chloride ion concentration 384
8.4.3.2 Sulphate ion concentration 384
8.4.3.3 Observed variation trends in the anion concentrations 386

8.4.4 Review of the pore fluid chemistry changes observed with consolidation 386

CHAPTER EIGHT

CLAY MINERALOGY AND PORE FLUID CHEMISTRY

8.1 INTRODUCTION

This chapter consists of two basic sections both describing chemical aspects: one is concerned with the clays tested while the other deals with the pore fluid.

There are two principal objectives in carrying out this study. The first is to use X-ray diffraction techniques to analyse the composition of these clays to define a mineralogic basis for the respective tests. The second is to use geochemical techniques to study the 'early chemical composition changes' imposed on the pore fluid by virtue of the process of artificial gravitational compaction of the above sediments.

8.2 CLAY MINERALOGY

The X-ray diffraction analysis was made on both the 'whole rock' and 'clay fraction' of the three clays (Chapter Six). A Phillips PW 1060 diffractometer equipped with a linear recorder was used for this purpose. In all the X-ray diffraction studies, Cobalt ($K\alpha$) radiation was used with an iron filter being set before the receiving slit to eliminate any probable β radiation. A 38 KV and 24 mA supply was chosen with a 1 KW generator to obtain high intensity and a good peak to background ratio. The arm containing the Geiger counter was geared to scan

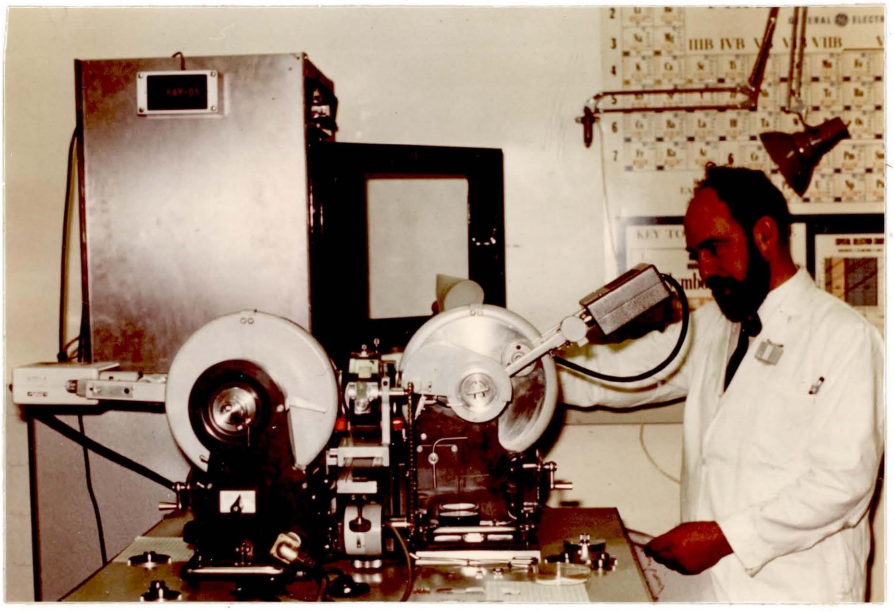
on a horizontal axis at a speed of 1° (2θ)/minute. $\frac{1}{2}^{o}$ divergence and scatter slits were used in the case of the diffraction of oriented specimens while 1° slits were used for the non-oriented specimen (whole rock analyses). In both instances the receiving slits used were 0.1 mm. Plate 8.1 is a further illustration of the equipment used.

A qualitative interpretation of the X-ray diffraction traces (XRD) were made with the aid of a standard tables (Brown, 1961). The technique proposed by Schultz (1964) for semi-quantitative mineralogical analysis of 'Pierre Shale' was adopted here too. However, it is desired to emphasise the absence of any technique to make rigid and reliable quantitative interpretations of the XRD traces. Existing techniques lack representability because of primary causes such as variable machine characteristics, non-standard specimen preparation techriques, difficulty of separating the interferences of some clay mineral types, and lack of representability in geologic sampling. Nevertheless, as the basic clay mineral suite was the same in all the three clays used in the study, the Schultz technique was adopted in order to obtain relative estimates of the abundance of the different clay minerals in them for the purpose of comparison.

The prime result drawn from these analyses was the marked dominance of Kaolinite in all the clays.

A summary of the results of the analysis has already

PLATE 8.1 A view of the Phillips X-ray diffractometer used in the study



been cited in Table 6.II. Further details are given in the following sections.

8.2.1 Whole Rock Analysis

'Whole rock' is used in this context to refer to the air dried, unfractionated and untreated sediments. These bulk samples were dried at 40°C and crushed in a teemar mill. Random samplings of the crushed samples were packed well and uniformly into special cavity mounts used for this purpose. A smooth flat surface of the packed sediments was exposed to the X-rays. The resulting diffraction traces for the three clays are given in Figures 8.1, 8.2 and 8.3. Identical machine settings were used for all three cases. A scanning speed of 1°/min. time constant of 2 and a rate meter setting of 400 counts for full scale deflection was used.

The general clay mineral peaks are apparent at 2θ values of 23°, 41° and 74°. Applying Schultz's intensity factors, the clay fractions for Falmouth, Petrockstow and ball clay 661 are estimated at 38, 80 and 75 respectively (compare the results from sedimentation, Table 6.II; 38-26, 82 and 73).

One of the striking differences between the traces is the presence of a sharp 10.4° and 30.8° (2θ) peaks in the

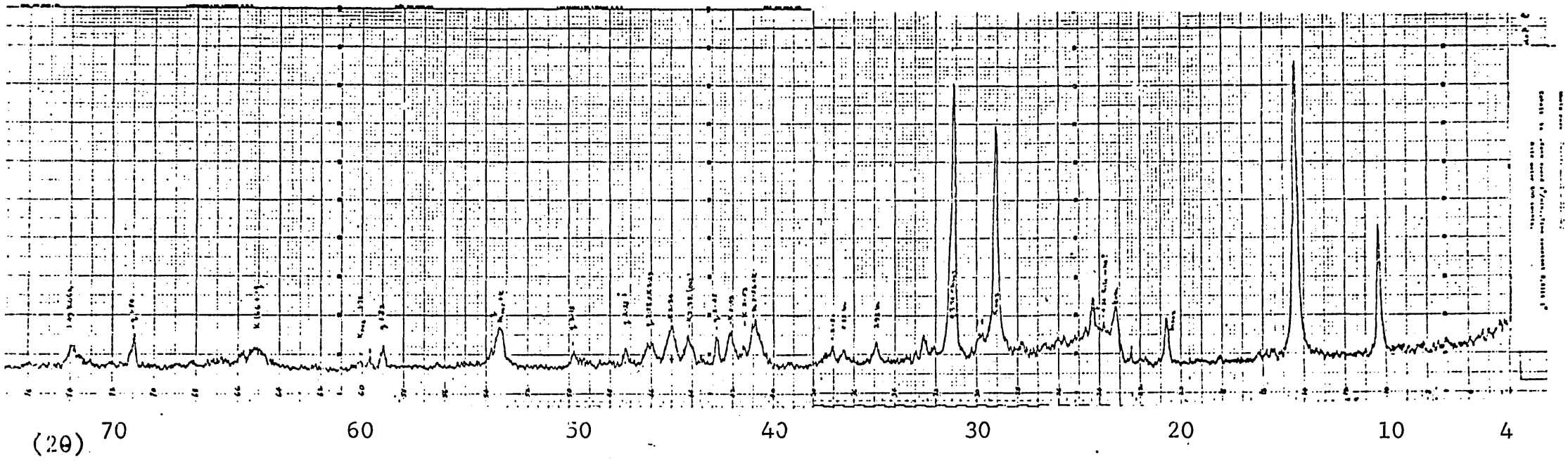


FIGURE 8.1 XRD trace of the whole rock of Falmouth Clay
Cavity Mount - Air Dry
Cobalt K radiation - Scan speed 1°/min, time constant = 2, Slit = 1°, Rate meter = 400 counts.

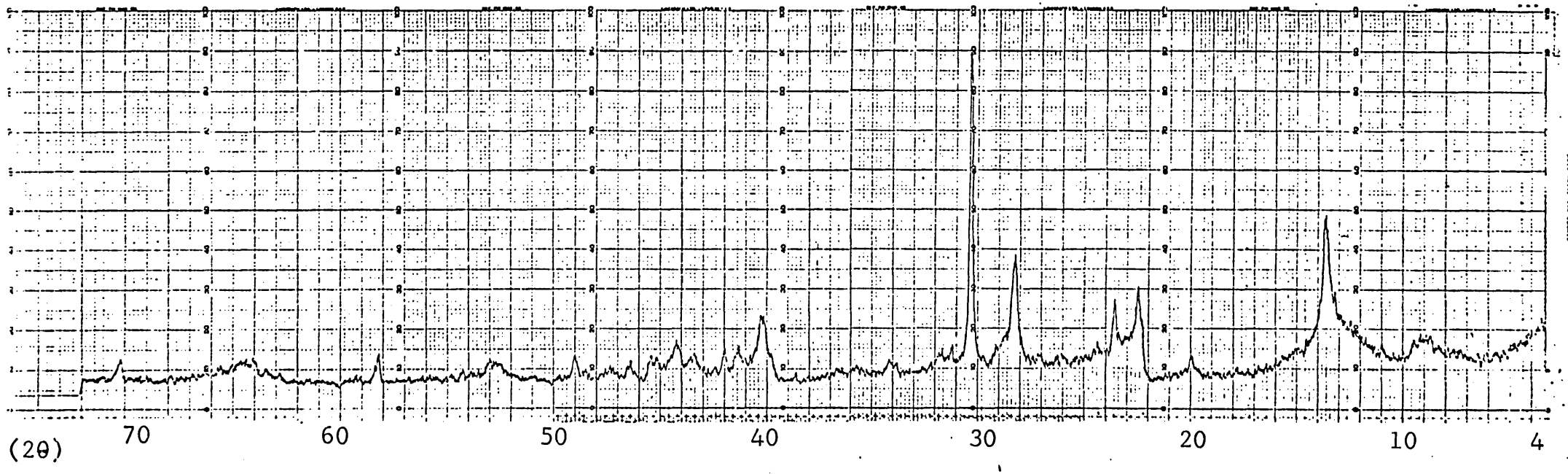


FIGURE 8.2 XRD trace of the whole rock of Petrockstow Ball Clay
Cavity Mount - Air Dry
Co K radiation - Scan Speed 1°/min., Time constant = 2,
Slit = 1°, Rate meter = 400 counts.

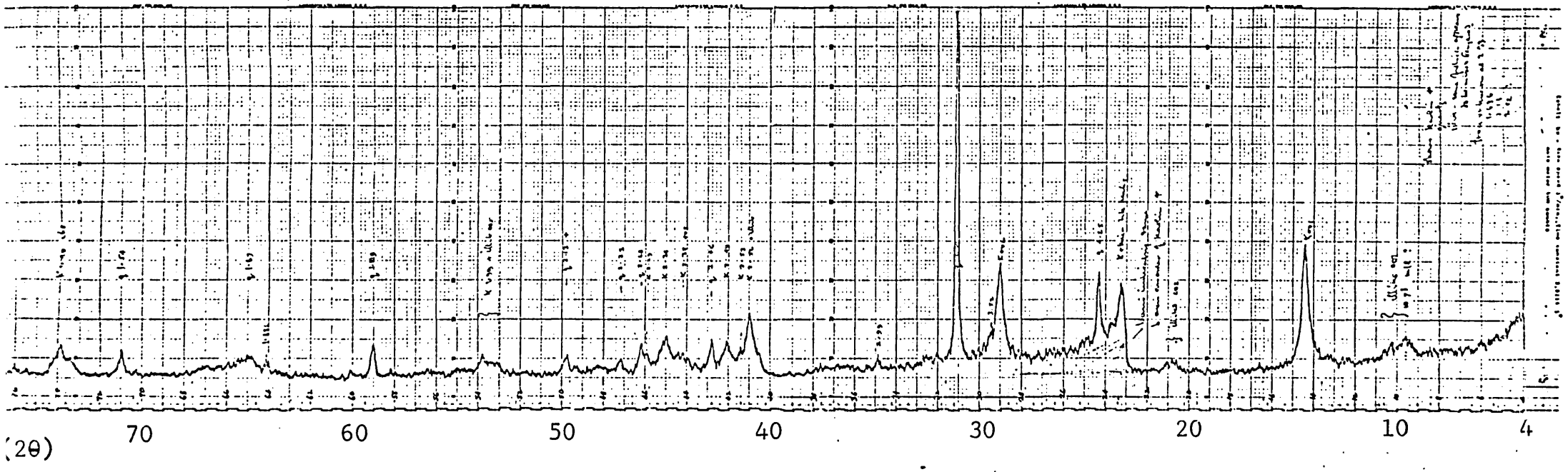


FIGURE 8.3 XRD trace of the whole rock of Ball Clay 661
Cavity Mount - Air Dry
Cobalt K radiation - Scan speed 1°/min.,
Time constant = 2, Slit = 1°, Rate meter = 400 counts.

Falmouth clay indicating a relative abundance of well crystallised muscovite mica but its (060) line is not too obvious. The other two traces show a broad peak at 9.8° (2θ) indicating illite of the muscovite type.

Fairly abundant presence of quartz is indicated by the peaks at 24.5°, 31.0° and 43.0° (2θ) values. Comparison of the peak intensities suggests an increased abundance of the quartz content from Falmouth ⟶ Petrockstow ⟶ Ball Clay. A quantitative estimate using Schultz factor gives values of 14, 16 and 18 percent respectively.

The 10-11 Å lines suggest the presence of mixed layer clay mineral while that of 2.58 in Falmouth suggests a trace of tourmaline with very weak lines at 4.56, 4.69,4.8.

8.2.2 Clay Fraction analysis

A sample weighing about 15 grams was dispersed in deionised water. The dispersion of the clay minerals was further ensured by placing it in an ultrasonic wave tank. The dispersed clay mineral suspension was centrifuged using specified times of centrifuging obtained from published nomographs (Tanner and Jackson, 1947).

The technique described by Shaw (1971) was adopted in the preparation of the oriented clay mineral specimens for

X-ray diffraction analysis. This method involved filtering the clay suspensions under suction through a stable ceramic medium so that the clay material was deposited on the ceramic.

In examining the clay fraction, the following experimental procedure was adopted:-

Run a) Air dried specimens mounted on a ceramic disc and scanned through 2θ values of 2°-54°.

Run b) Specimen glycerated by spreading a thin film of liquid glycerol over the dry specimen and allowing it to dry. A 2θ scan of 2°-20° was performed.

Run c) Specimen heated in a muffled furnace at $400^{o}C$ for half an hour and then scanned between 2θ values 2° and 15°.

Run d) Specimen heated in a muffled furnace to $550^{o}C$ for in excess of half an hour and then scanned over from 4° to 15° 2θ

Figures 8.4, 8.5 and 8.6 show the traces of the above runs for each of the three types of clay. The examination of the traces showed that the principal clay minerals present in all the samples are Kaolinite, illite with a little chlorite and mixed layer clay. A qualitative interpretation of the results is given in Table 8.I. Their relative abundance, evaluated using Schultz factor (1964) is given in Table 8.II. Identical

TABLE 8.Ia

QUALITATIVE INTERPRETATION OF XRD PEAKS IN THE TRACES FOR FALMOUTH CLAY

2θ	Whole Rock	Clay Fraction			
		Air Dry	Glycerated	Heated to 440°C	Heated to 550°C
7.3	cm	-	m	Sm	-
10.4	m	i	i	i	i
14.4	cm	K	K	K	-
20.8	m	i	i	i	-
22.6	T	-	-	-	-
23.2	cm	K+m	-	-	-
24.4	q	q	-	-	-
29.0	cm	K	-		
31.1	q+m	q+m			
32.2	m	m			
34.9	m	m			
37.0	T	-			
41.0	m+K	m+K			
42.0	K	K			
44.2	K	K			
45.0	K	K			
47.4	q				
49.8	q	q			
53.2	m+K	m+K			
59.0	q	q			
65.0	K+q	K			
71.0	q	-			
74.0	K	K			

cm - clay minerals Sm - swelling clays K - Kaolinite

m - muscovite T - tourmaline i - illite

q - quartz

TABLE 8.I b

QUALITATIVE INTERPRETATION OF XRD PEAKS IN THE TRACES FOR PETROCKSTOW BALL CLAY

$2\bar{\theta}$	Whole Rock	Clay Fraction			
		Air Dry	Glycerated	Heated to 400°C	Heated to 550°C
7.9	cm	Sm	Sm	-	-
10.4	i m	i	i	i	i
14.4	cm	K	K	K	-
20.8	i	i	i	i	i
23.4	cm	K+i			
24.8	q	q			
29.2	cm	K+i			
31.1	q	q			
41.0	cm	K+m			
42.0	K	K			
44.4	K	K			
45.2	K	-			
53.0	K+i	K+i			
59.2	q	q			
71.0	q	q			

Cm - clay minerals
Sm - swelling clays
m - mica
q - quartz
K - kaolinite
i - illite

TABLE 8.Ic

QUALITATIVE INTERPRETATION OF XRD PEAKS IN THE TRACES FOR BALL CLAY 661

2θ	Whole Rock	Clay Fraction			
		Air Dry	Glycerated	Heated to 440°C	Heated to 550°C
9.8	Cm	i Sm	i Sm	-	-
10.4	-	-	i	i	i
14.4	Cm	K	K	K	-
20.8	m i	i	i	i	-
23.2	Cm	K+m			
24.3	q	q	-	-	-
29.0	Cm	K			
31.2	q+i	q+i			
34.9	m	i			
41.0	K+i	K+i			
42.1	K	K			
42.8	q	-			
45.0	K	K			
46.2	q	-			
49.7	q	-			
59.0	q	q			
71.0	q	q			

Cm - clay minerals
Sm - swelling clays
m - mica
q - quartz
K - kaolinite
i - illite

Mineral	Falmouth %		Petrcckstow Ball Clay %		Ball Clay 661 %	
Quartz	14		16		17	
Clay Minerals	38		80		75	
Non-Clay Minerals	Mica) Tourmaline) Feldspar)	48		4		8
Kaolinite	$\frac{38}{100} \times 90$	34	$\frac{80}{100} \times 76$	61	$\frac{75}{100} \times 78$	58
Illite	$\frac{38}{100} \times 8$	3	$\frac{80}{100} \times 18$	14	$\frac{75}{100} \times 16$	12
Chlorite		-	$\frac{80}{100} \times 5$	4	$\frac{75}{100} \times 2$	1
Mixed layer Minerals		1		3		4

TABLE 8.II

SUMMARY OF QUANTITATIVE CLAY MINERALOGY

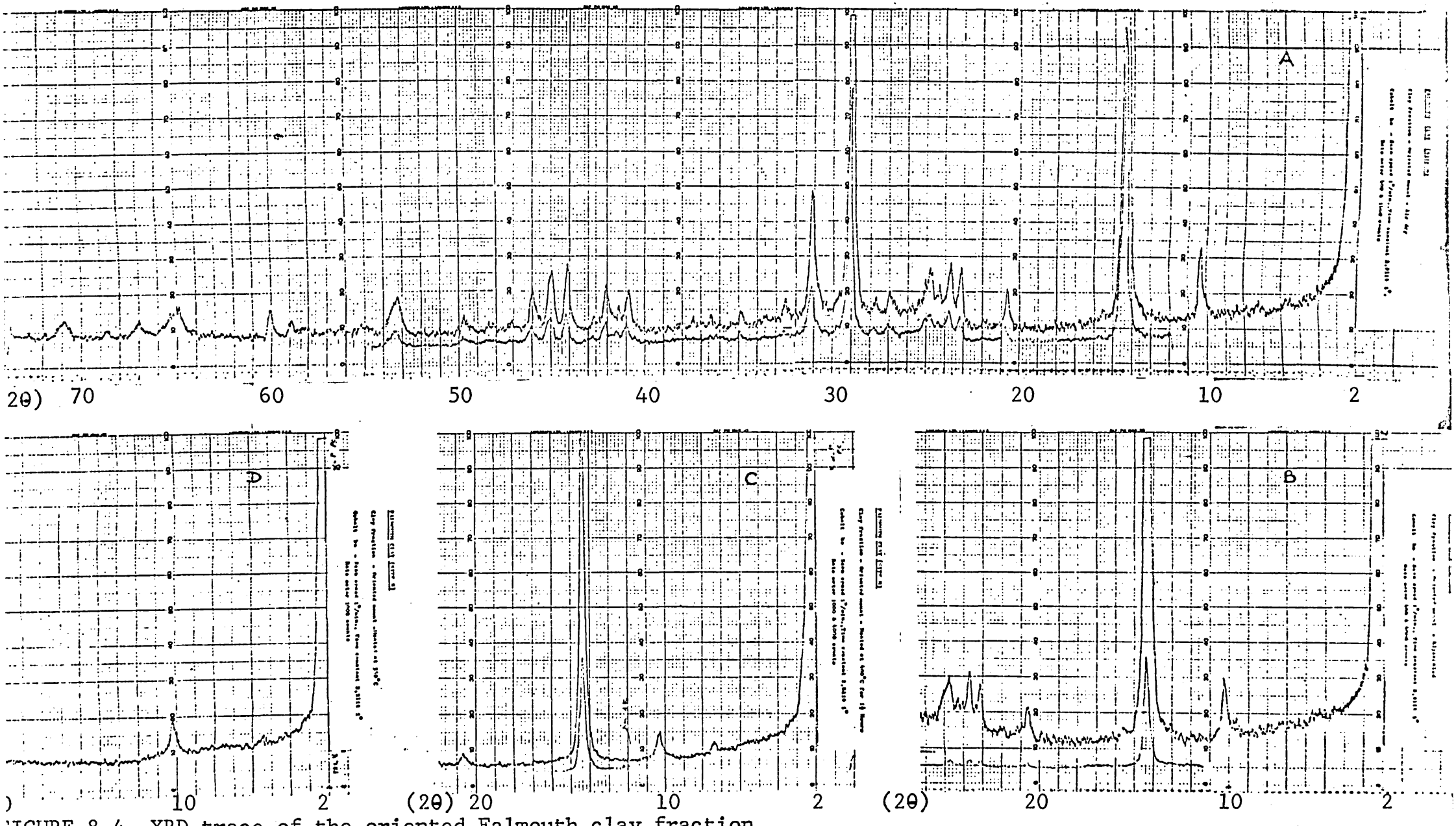


FIGURE 8.4 XRD trace of the oriented Falmouth clay fraction

Run A - Air dry rate meter 400 and 1000

Run B - Glycerated rate meter 400 and 4000

Run C - After heating at 400°C for 1½ hours.

Run D - After heating at 550°C.

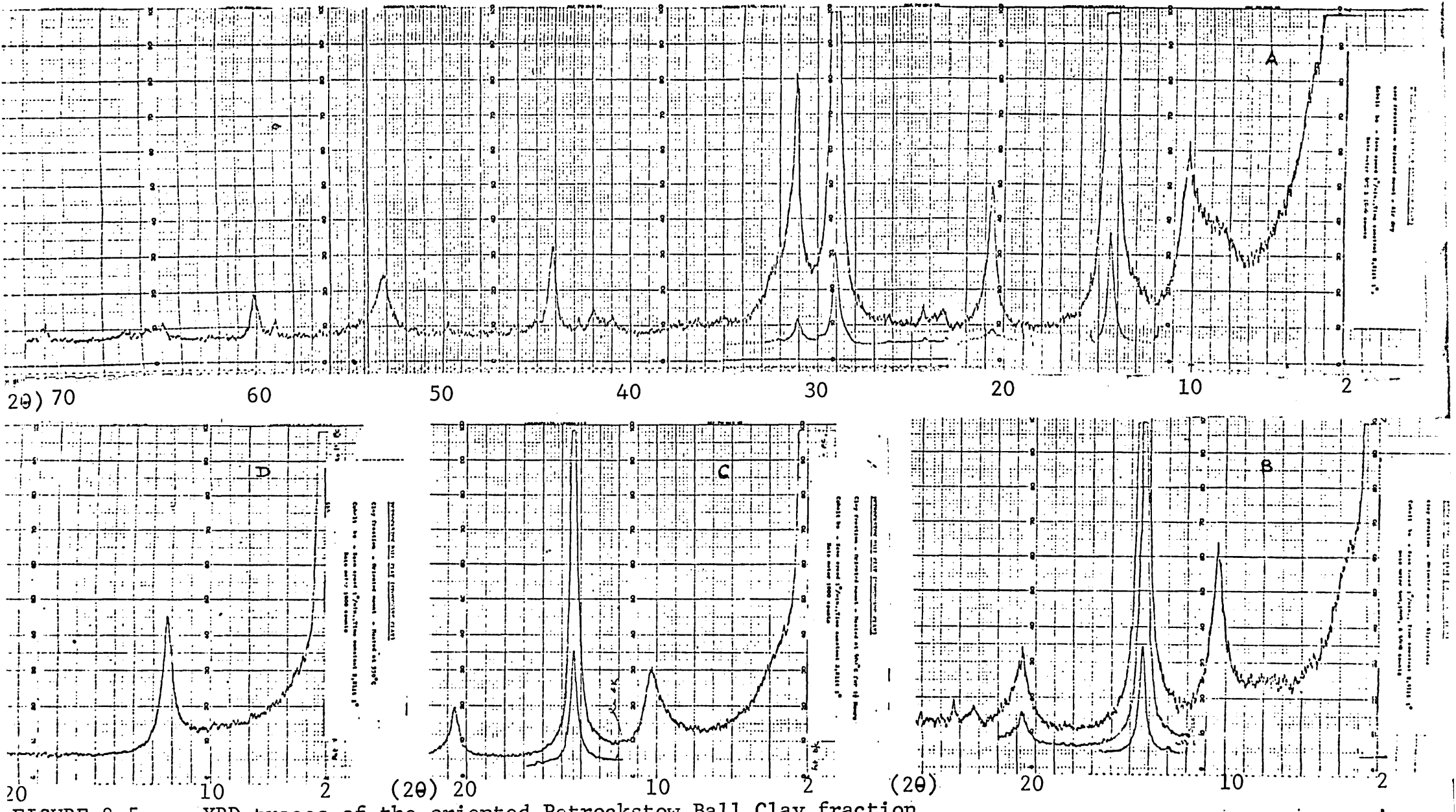


FIGURE 8.5 XRD traces of the oriented Petrockstow Ball Clay fraction

Run A - Air dry rate meter 400 and 1000.

Run B - Glycerated rate meter 400 and 4000.

Run C - After heating at 400°C for 1½ hours.

Run D - After heating at 550°C.

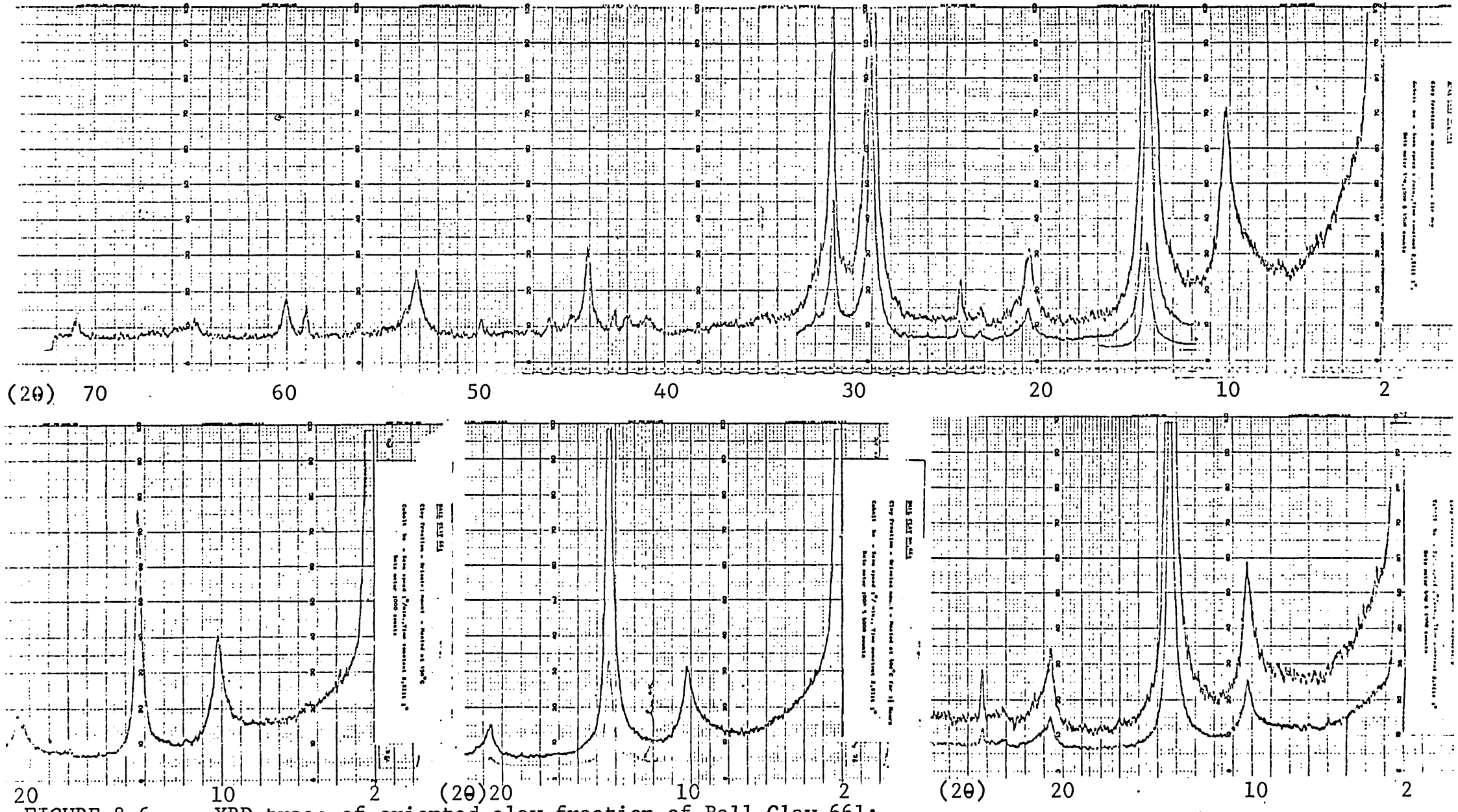


FIGURE 8.6 XRD trace of oriented clay fraction of Ball Clay 661;
Run A - Air dry rate meter 400 and 1000.
Run B - Glycerated rate meter 400 and 4000.
Run C - After heating at 400°C for 1½ hours.
Run D - After heating at 500°C.

machine settings were used and peak heights in excess of 400 counts were re-traced on a higher appropriate rate meter setting. In all these traces, a high background at 2-3° is conspicuous and it is a result of the X-rays reflecting off the sample due to the flat orientation of the clay particles.

Comparison of these traces with those of the whole rock helps to investigate the size fraction of the dominant minerals. It is seen that in the case of the Falmouth clay the intensity of the mica peaks and that of the mixed layer clay is reduced in trace of the clay fraction suggesting that much of the original muscovite mica and the mixed layer is coarse. The hk peaks of the Kaolinite appear to have enhanced in the clay fraction in spite of orientation, therefore much of the Kaolinite is fine. The quartz content in the clay fraction is apparently less.

On the contrary, in the clay fractions of the Petrockstow Ball Clay and Ball Clay 661, an enhanced muscovite illite peak is apparent, indicating the dominance of clay-sized illite.

In both whole rock and clay fraction traces of all three clay types a broad band of peaks in the range of 2θ values of 23°-27° is seen, implying appreciable b-axis disorder of the Kaolinite (Brown,1961, p. 67).

8.2.2.1 Falmouth clay

There is no apparent low-angled peak in the clay fraction indicative of swelling minerals (Figure 8.4). The slight shoulder on the 10 Å illite peak of the clay fraction shows tendency to swell to 18 Å, suggesting a trace of mixed layer clay of the possible illite montmorillonite type.

Thus the clay mineral assemblage is one of Kaolinite-muscovite illite - quartz with traces of feldspar and illite montmorillonite.

8.2.2.2 Petrockstow Ball Clay

The conspicuous right-handed shoulder on the illite peak (7° to 10° on run (a)) is due to the presence of a mixed layer clay mineral, composed of illite and an expanding clay mineral. The 10 Å illite peak is sharpened in run (b) (after glyceration) and the mixed layer minerals are expanded to a higher spacing of 14 Å. In the run (c) (on heating to 400°C) the above peak is collapsed to 10 Å with no further change on heating to 550°C (run (d)).

There are further slight peaks on run (a) at $5\frac{1}{2}^{o}$ and $7\frac{1}{2}^{o}$ (2θ) indicative of possible traces of free montmorillonite and chlorite. Run (b) shows that expansion to a 5° peak suggestive of montmorillonite. In run (d) a slight enhancement of the peak at 14 Å is possibly due to the trace of chlorite.

The hk reflection from the kaolinite is considerably less in run (a) when compared with that of the Falmouth Clay.

8.2.2.3 Ball Clay 661

Hereto the clay mineralogy suggests similar clay mineral suite except that the relative abundance of the constituents is different.

In run (a), there is only a very slight shoulder on the 10 Å peak and on glyceration these mixed layer minerals expand to a higher spacing as seen in the trace of run (b). The illite peak of the Ball Clay 661 shows a greater intensity than that of the other clays but on glyceration (run b) it notably reduces to an intensity less than that of the Petrockstow Ball Clay. Therefore a greater proportion of mixed layer illite montmorillonite is found in the Ball Clay 661.

8.3 CHANGES IN CLAY MINERALOGY WITH CONSOLIDATION

The current simulation of gravitational compaction in the laboratory was devoid of any form of simulation of a geothermal gradient. As reviewed in Section 3.4.2, Kaolinite is itself not very susceptible to mineralogic changes as a result of the burial depth. Thus, considering the above two points, no obvious mineralogic changes in Kaolinite were anticipated from the tests.

Even any probable changes, like crystallinity changes (e.g. the ordering of the b-axis of the Kaolinite), would have altered the diffraction traces only very slightly; and the separation of such differences from effects of variations in machine characteristics would have been arduous.

Accordingly it was decided to investigate only the gross changes of the nature of clay minerals.

The nature of the clay minerals present and their influence on the compaction process can be characterised by their cation exchange capacity (see Sections 2.3 and 3.3 and Grim, 1968).

The cation exchange capacity determination using the conventional ammonium acetate method is tedious and time consuming. An alternative technique of determining the adsorption of a basic dye by silicate clay minerals is conveniently rapid and simple.

Clays exhibit a strong adsorption to basic dyes while non-clay minerals, like mica and quartz, are virtually non-staining (Faust, 1940). Clays adsorbed methylene blue dye irreversibly from a dye solution with an equivalent release of exchangeable cations (Robertson and Plesch, 1948; Robertson and Ward, 1951).

8.3.1 Methylene blue dye titration

A 0.005 N methylene blye dye solution was prepared by dissolving 1.870 gms. Basic Blue 9, methylene blue dye powder ($C_{16}H_{18}N_3SCl.3H_2O$) per litre. This solution was titrated against aliquots of a dilute clay suspension (0.5 gms. of clay, 25 cc of deionised water, and 1 cc of 5 N sulphuric acid). The course of the titration to the end point was followed by periodically spotting a drop of the titrated slurry on a Whatman No. 1 filter paper. The titration was carried out systematically with increments of 1 cc of titrant until near end point, and then with 0.55 cc of titrant.

An end point was indicated when excess dye appeared as a sky blue coloration radiating from the normally darkly-dyed solids in the centre. This became confirmatory as a true end point if the titrated slurry would still show excess dye upon repeating the spot test after a two minute waiting period. The 'methylene blue capacity' was then computed simply as below:

$$\underset{\text{meq/100 g.Clay (105}^{\circ}\text{C)}}{\text{Methylene Blue Capacity (M.B.C.)}} = \frac{100}{\underset{\text{basis)}}{\text{sample wt. g.(105}^{\circ}\text{C}}} \times \underset{\text{ml.}}{\text{Vol. of titrant}} \times \underset{\text{meq/ml.}}{\text{Normality}}$$

Experimental results show a good one to one correspondence between Methylene Blue Capacity (M.B.C.) and Cation Exchange Capacity (C.E.C.) as determined by the ammonium acetate method (Nevins and Weintritt, 1967). Therefore the values of

C.E.C. referred to in this study were in fact obtained from determining the M.B.C.

8.3.2. C.E.C. values for field and laboratory samples

Table 8.III gives the results of the C.E.C. values for the three types of clay and for the final samples from most of the tests. The results are tabulated separately in four groups depending on the particular test type and investigation. Pertinent data on the conditions of the sample, etc, that may shed light on the cause of a variation in C.E.C. is also included in the table. The above C.E.C. values may be compared with the range of typical C.E.C. values for particular clay mineral types as cited in literature and given in Table 2.I.

A study of the C.E.C. values given in Table 8.III indicates a definite decrease in the C.E.C. values with consolidation. There is, however, insufficient data to shed light on the exact manner in which the consolidation process influences it. The observation of the gross reduction in C.E.C. is true of both the remoulded and the consolidation of field samples.

The specimens in the tests with saline pore fluids acquire even lesser C.E.C. A similar effect is observed with the influence of temperature. These reductions can probably be explained as a result of the absorption of ions from the pore fluids onto the clay particles surfaces, thereby reducing the

TYPE	Sample No.	Methylene Blue Capacity meg/100g.	Peak Pressure lbf/sq.in.	Rate of Loading $lbf/in^2/min$	Salinity	Peak Temperature °C	Void Ratio at Peak P
Original	Falmouth	22.3	0-5	?	1	-	
	Petrockstow	20.8	211	?	0	-	0.71
	B.C.	17.17					
	Ball Clay 661	17.64	-	-	-	-	
High Pressure Consol. Tests	BC.CHP.12	24.7	2500	1	0	-	0.408
	BC.CHP.14	20.95	4653	1	0	-	0.345
	BC.CHP.18	13.78	5015	2.0	0	-	0.491
	BC.CHP.19	16.07	6504	0.5	0	-	0.345
	BC.CHP.15	11.69	7000	1	0.5	-	0.45
	BC.CHP.17	8.64	5520	1	1.0	-	0.33
	BC.CHP.20	19.54	6800	2	1	-	
	BC.CHP.21	7.04	8000	2	2	-	
	N.FA.CHP.1	7.3		1	?		
	N.FA.CHP.2	6.4		1	?		
	N.BC.CHP.1	23.59		1	0		
Temp. Tests	BC.CLP.T1	17.4	140	-	0	17	
	BC.CLP.T2	10.91	140	-	0	58	
	BC.CLP.T3	23.6	140	-	0	49	
	BC.CLP.4	11.9	140	-	0	70	

TABLE 8.III

SUMMARY OF M.B.C. VALUES AND RELATED DATA

further available exchangeable ion sites. These effects are further described later in this chapter.

8.4 CHEMICAL ANALYSIS OF THE PORE FLUIDS

Intermittent sampling of the pore fluids expelled from the specimen during its consolidation favoured a study of the changes in its chemical composition in the context of the other continuous variables of the consclidation process.

It must be emphasised that analysis was made on the fluids expelled and it will invariably differ from the chemistry of the in situ pore fluid which can be analysed only by leaching the final specimen.

The results of the analyses for the tests have been presented in Appendix F. It is now clear (see also graph 1 of each of the sets of chemical analysis of the pore fluids for the tests), that the volume of pore fluid expelled falls rapidly with increasing pressure: even as much as only a couple of c.c. was expelled in the pressure range 7,000 - 8,000 lbf/sq.in. in the test BC.CHP.21. In this context it must be noted that this forms a very prominent advantage of testing such large diameter (4 inches) samples compared with the small diameter specimens tested in other types of high pressure equipment (see Table 2.III).

The pore fluids so collected were first filtered through membrane filters and the filtrates were contained in plastic bottles in a slightly acidified (1 drop of 0.5 N HNO_3 per 50 c.c. of filtrate) condition and preserved, refrigerated at less than $5^{o}C$, until used for testing.

The results of the chemical analyses of the pore fluids from the different tests (see Appendix F) show consistent trends in the variation of the different ionic concentrations with increasing pressure. These trends are described in the following sections.

8.4.1 Weight of total dissolved solids

A two c.c. portion of the pore fluid samples is oven dried at $105^{o}C$ and weighed to determine the dry weight of the dissolved solids.

A study of the results of the tests show a common trend in the variation of the concentration of dissolved solids in the pore fluids with axial pressure (Figure 8.7).

The initial depletion of the concentration of the dissolved solids may probably be due to an unavoidable dilution of the pore fluids by the deionised fluid present in the filter plate (volume of pores = 5 c,c.) and the pore fluid system. The steady increase in the concentration is in accordance with

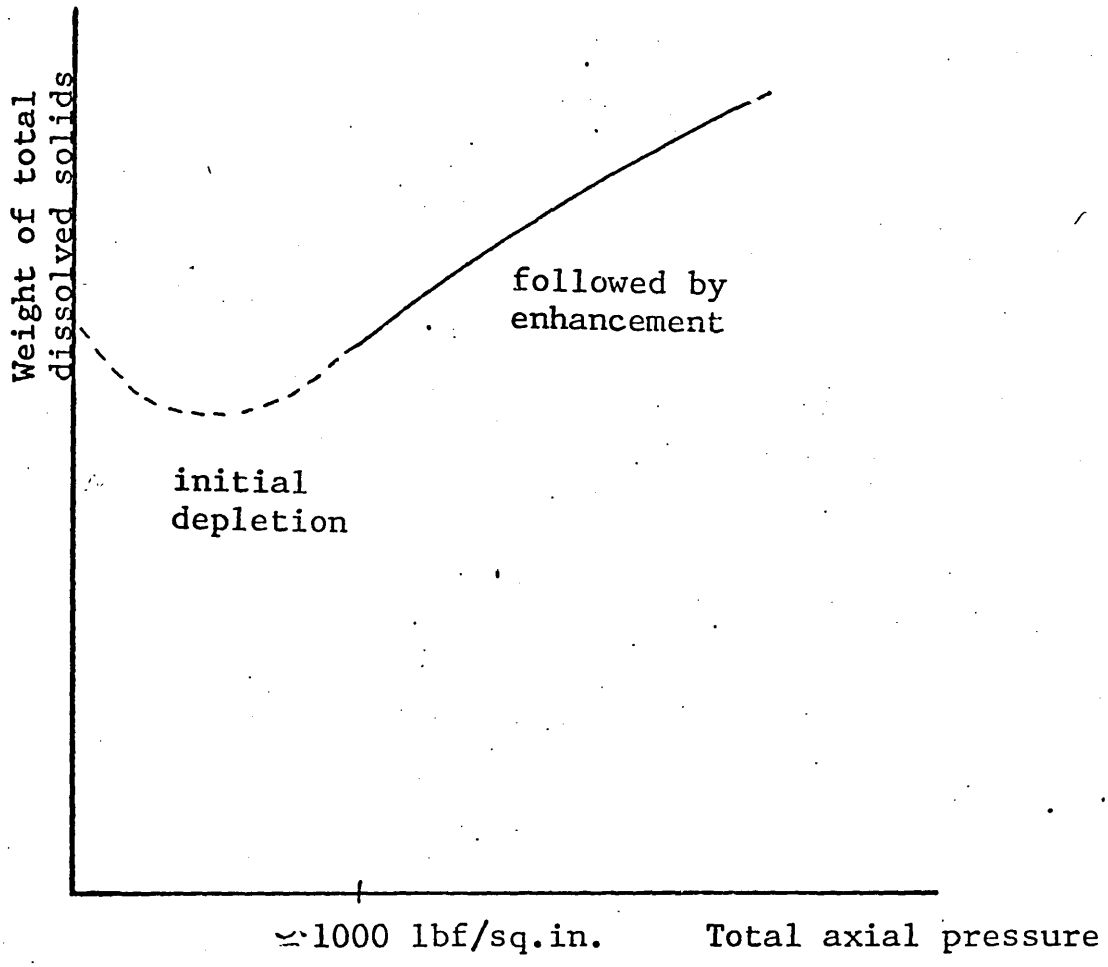


FIGURE 8.7 A general pattern of the observed variation of weight of dissolved solids in pore fluid expelled with increasing total pressure.

corresponding field observations (see Figures 3.9 and 3.13).

It must be pointed out that even in the tests BC.CHP.12,14,18 and 19 where the clay was initially remoulded in deionised water, the subsequent pore fluids expelled contained dissolved solids, resulting probably from the flushing out of some of the exchangeable ions on the clay minerals.

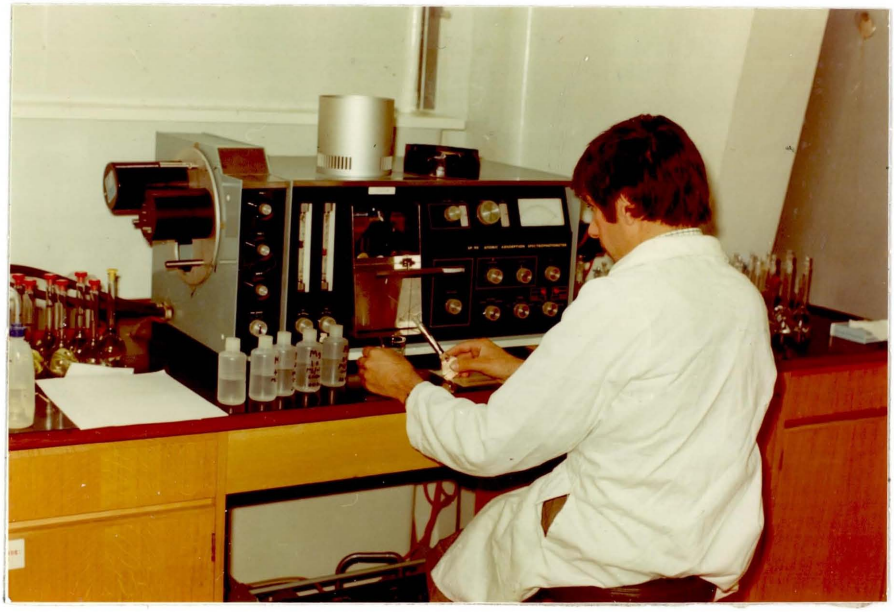
8.4.2 Determination of the concentration of cations

The cationic concentrations in the pore fluid sampled were analysed using a Pye Unicam SP 90 atomic absorption spectrophotometer (see Plate 8.2). The technique of measurement is based on the photoelectric measurement of the change in luminous flux emerging from a standard flame.

8.4.2.1 Atomic absorption Spectrometry

The light source (see Plate 8.2) is chosen so that it emits only the spectrum of the determinand. A separate standard lamp is therefore required for each element type. The light emitted from this lamp is modulated electrically and passes through a flame, into which is aspirated the solution to be analysed. The light from the lamp is partially absorbed by the atoms of the determinand, formed from the solution by its evaporation and thermal decomposition in the flame. The light emerging from the flame then passes through an optical monochromator, which is adjusted so that only light with the

PLATE 8.2 A view of the atomic absorption spectrometer.



wavelength at which maximum absorption (see Table 8.IV) in the flame occurs, falls onto a photoelectric detector and amplifier. The degree of absorption is proportional to the concentration of the determinand in the solution and is indicated on a meter. The calcium ion and magnesium ion concentration was determined with the spectrometer in its absorption mode of operation as described above. The instrument is calibrated against a series of standard solution and the calibration so obtained is always markedly linear.

8.4.2.2 Atomic emission spectrometry

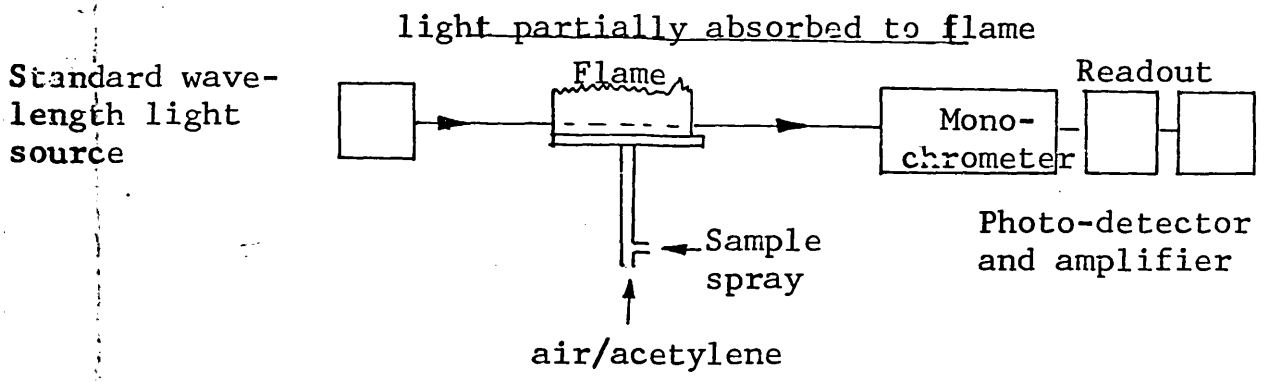
The same equipment described in the earlier section was used in its emission mode of operation to determine the sodium and potassium concentrations in the pore fluid samples. In this mode of operation, the sample is aspirated directly into a flame, when high temperature causes a fraction of the atoms of the determinand to emit light. The wavelength of this light is characteristic of the determinand and is isolated from the other wavelengths using the same monochromator system (serves the function of an optical filter) and the intensity of this characteristic wavelength is measured photo-electrically and is proportional to the concentration in the sample.

However, caution must be taken to allow for the masking effect by the relatively more brilliant sodium flame on the potassium flame. Figure 8.8(i)shows the experimental

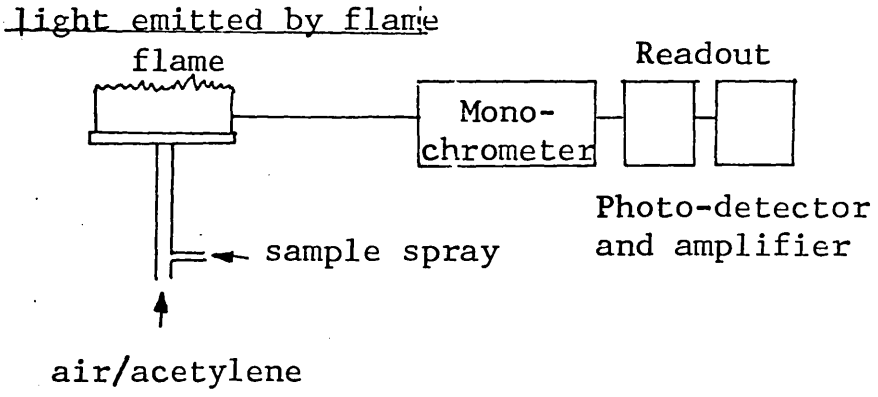
Cation Instrument analysed setting	Sodium Na^+	Potassium K^+	Calcium Ca^{++}	Magnesium Mg^{++}
Wave length m/	589.0	780.9	422.5	285,0
Burner Type	Emission	Emission	Absorption	Absorption
Burner Angle Height	- -1.8 cm	- -1.8 cm	5° -1.0	30° -1.0
Lamp Current mA	-	-	12	12
Slit, mm.	0.1	0.13	0.08	0.08
Gas (C_2H_2), l/min.	0.9	0.9	1.2	1.2
Air, l/min.	4.7	4.4	4.7	4.5
Detection limit, mg/litre	0.0006 to 0.002	0.004	0.002 to 0.008	0.0001 to 0.001

TABLE 8.IV

SUMMARY OF THE SETTINGS USED ON THE ATOMIC ABSORPTION SPECTROPHOTOMETER



(a)



(b)

FIGURE 8.8 Schematic diagram of the modes of operation of Atomic absorption spectrometer

(a) Absorption mode
(b) Emission mode

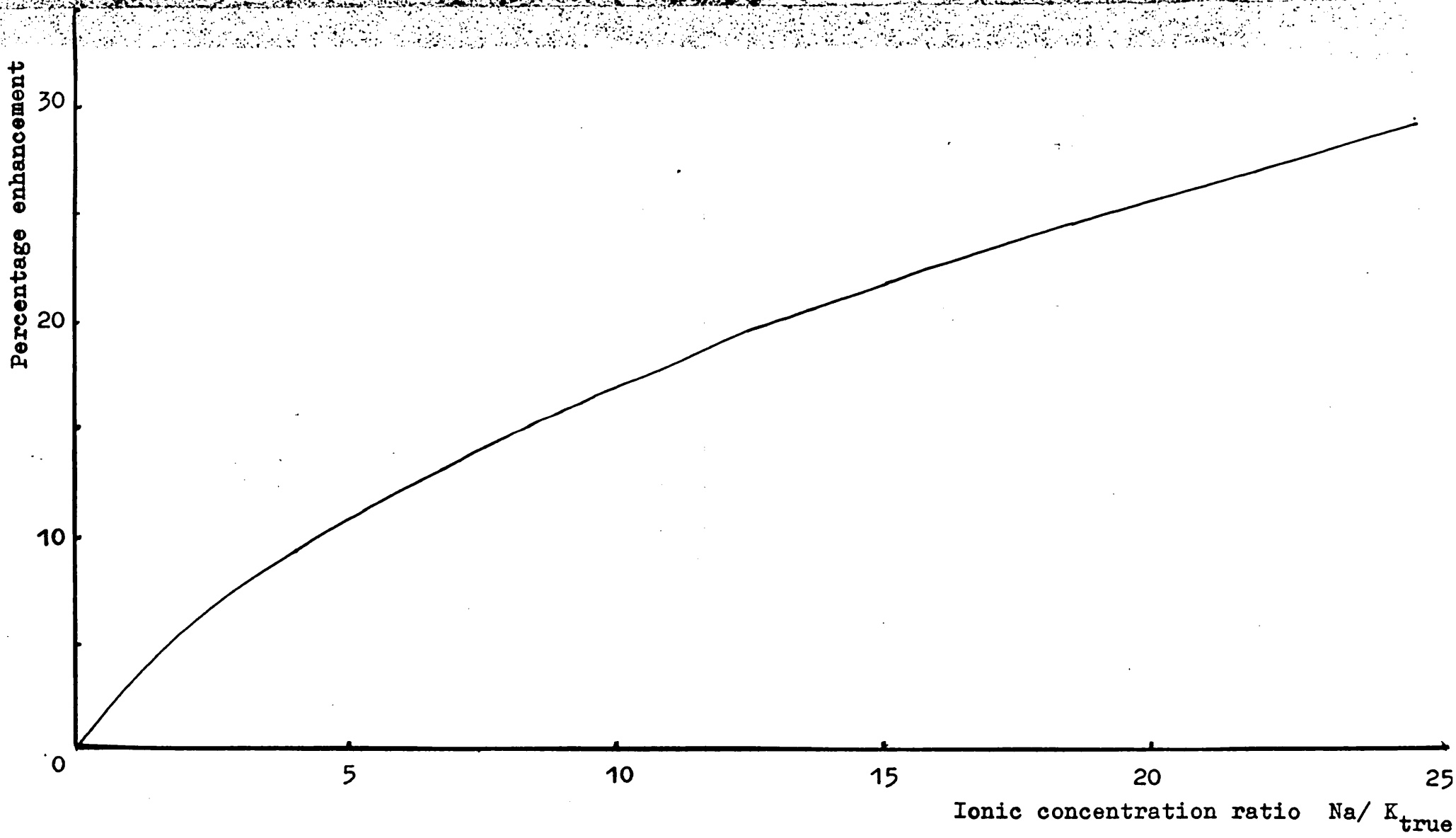


FIGURE 8.8 (1) Correction curve for the Sodium enhancement of Potassium

correction curve that was used to correct the potassium ion concentration determinations in samples containing fairly high concentration of sodium ions. Figure 8.8 is a schematic diagram illustrating the above two modes of operation. Table 8.IV describes the equipment settings adopted during the determination of the desired ionic concentration. A thorough description of the theoretical principles and instrument components can be found in literature (West, 1969; Kahn, 1968; and Reynolds, 1971).

The sensitivity of the apparatus is controlled by the adjustment of the gain on the amplifier. The incapability of the instrument to cater for extremes of concentrations must be appreciated. Too high a concentration of salts can cause an excessive precipitation of salts in the fluid ducts damaging to the equipment, leave alone the equally high inaccuracies of such observations. Thus permissible 'detection limits' have been proposed in 1969 to the second International Atomic Absorption Conference. The detection limit was defined as "that concentration in solution of an element which can be determined with a 95% certainty". The detection limits relevant to the four cations tested in this study are given in Table 8.IV. As such the pore fluids sampled had to be invariably diluted accurately to be within this detection limit.

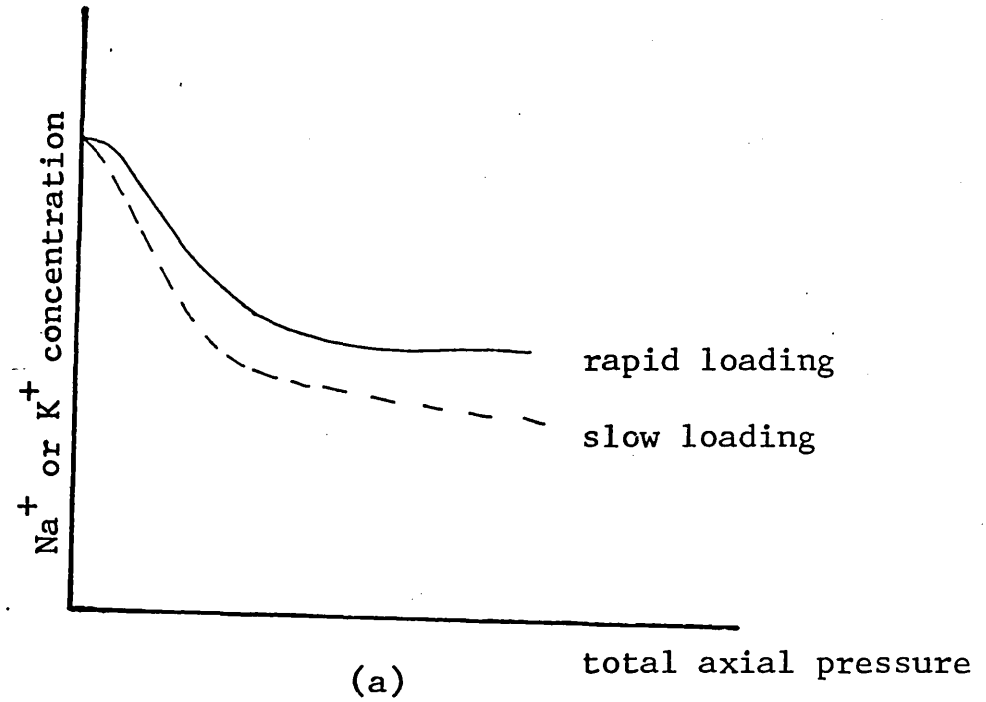
8.4.2.3 Observed trends

The observed pattern of changes in the concentration

of any particular cation with increasing pressure seems to be strikingly similar throughout all the tests. Two distinctly different trend patterns were observed dependent on the valency of the cation (Figure 8.9). The variation in the case of the monovalent $[Na^+]$ and $[K^+]$ is a fairly rapid depletion of the original concentration at low pressure levels (0-5,000 lbf/sq.in; or conversely in the higher porosity range 70% - 40%), after which the rate of depletion falls. It is interesting to point out an inverse pattern of trends, between the volume of pore fluid expelled and the $[Na^+]$ and $[K^+]$ depletion (in all the tests, see Appendix F) indicative of a probable dependence of the trend on the porosity of the specimen. But the persistence of this general pattern in the test of undisturbed overconsolidated Ball Clay (N.BC.CHP.1 - initial porosity of specimen $\simeq$ 42 %) suggests instead a pressure dependence.

The divalent calcium and magnesium ions show a different trend of variations but the general pattern was observed to be consistent in all the tests (see Figure 8.9b). As illustrated an initial depletion of their concentrations occurs up to low pressure levels. This is followed subsequently by a rapid enhancement of the concentration.

Such a pattern of variations may be explained as a result of two simultaneous mechanisms:



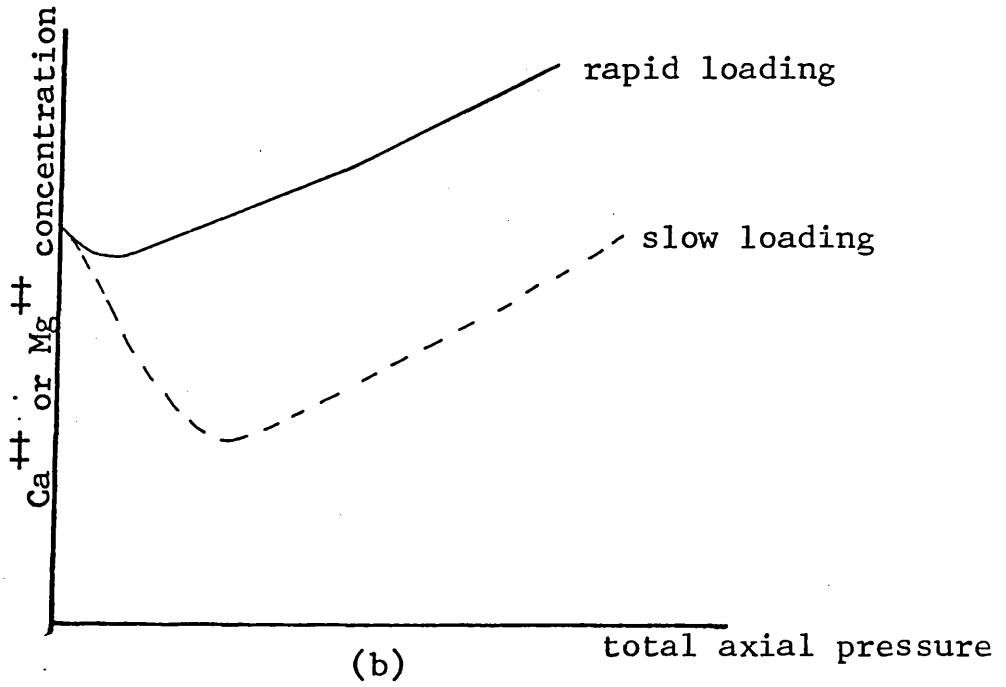


FIGURE 8.9 General trend patterns for the variation of concentration of cations in expelled pore fluid with pressure:

(a) Monovalent Na^+ or K^+

(b) Divalent Ca^{++} or Mg^{++}.

(a) Filtration of the ions by virtue of either electrostatic charged jet on the clay particles or due to their physical size, and

(b) The influence of a hydrodynamic force created as a result of the pore fluid pressure induced flow.

Mechanism (a) which depletes the concentration is operative at all stages of the consolidation process, but the reverse effect of mechanism (b) is operative only after the build up of a pore fluid pressure. Furthermore, the associated effect of flushing of the ions into the pore fluid escaping from the drained end is delayed due to its own drainage path across the sample (see also Figure 3.10 and Section 3.3 for a similar hypothetical situation in the field).

The absence of such a variation in the Na^+ and K^+ ions can be due to the larger affinity of monovalent bonds. The above arguments support the suggestion of Larsen (1967) (Section 3.3.3) in his observation that the rate of ion rejection is in the order:

$$Mg^{++} > Ca^{++} > SO_4^{--} > Na^+ > Cl^-.$$

8.4.3 Determination of the concentration of the anions

The concentration of the anions in the specimens with deionised water was often too low for detection. In other instances, their determinations were conducted in the manner described below.

8.4.3.1 Chloride ion concentration

The chloride ion concentration was determined in the usual manner adopted in analytical chemistry the volumetric titration of the following reaction:

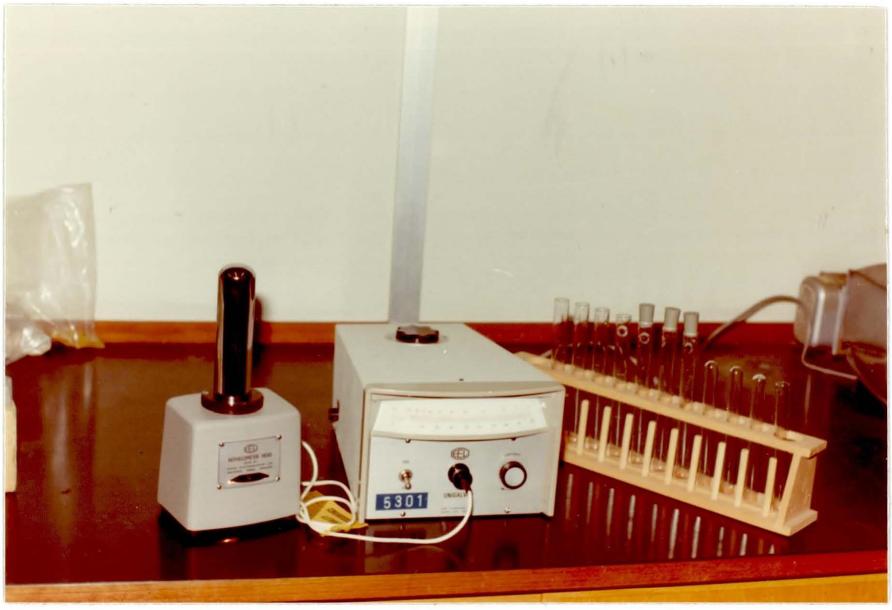
$$AgNO_3 + Cl^- \longrightarrow AgCl + NO_3^-$$

Potassium chromate was used as the indicator with the end point of the titration being the acquiring of a light pink shading on the precipitate.

8.4.3.2 Suplhate ion concentration

The conventional analytical chemistry techniques of gravimetric analysis could not be used here due to the low concentration of the sulphate ion. Instead a photochemical technique was used. The sulphate ion concentration was so low that the barium sulphate resulting from the reaction with a surplus of barium chloride, formed a colloidal suspension rather than a precipitate. The transmissivity of a standard source of light was proportional to the density of the colloidal barium sulphate and in turn to the sulphate ion concentration. A nephelometer (see Plate 8.3) was used to measure the transmissivity to light of the colloidal suspensions. A series of standard sulphate ion concentrations were first tested to obtain a calibration, which was always strongly linear.

PLATE 8.3 View of the nephelometer used in the analysis of sulphate ion concentration


5301

8.4.3.3 Observed variation trends in the anions

The general variation trend in the change of the concentration of anions is similar to that observed with the cations, but their order of variation is markedly less (see Figure 8.11). The difference in the proportion of these variations between the concentration changes for anions and cations, therefore, appear to be in concordance with the proportion of sites available on the clay particles for the respective ion exchange (viz., anions on the edges and the cations on the faces of the clay particles). The sulphate ion concentration changes like the divalent cations with an initial slight fall of the concentrations followed by an increase.

In the tests with high 'saline' waters, the order of variation of the changes was very small compared with that concentration and as such no marked changes were observed.

8.4.4 Review of the pore fluid chemistry changes observed with consolidation

An attempt is made in this section to have an overall study of the observed changes in pore fluid chemistry. In order to aid comparison and interpretation of the results in all the tests the respective ionic compositions are presented as percentages of the concentrations of the ions in the original solution. Accordingly Figure 8.10 compares the results from

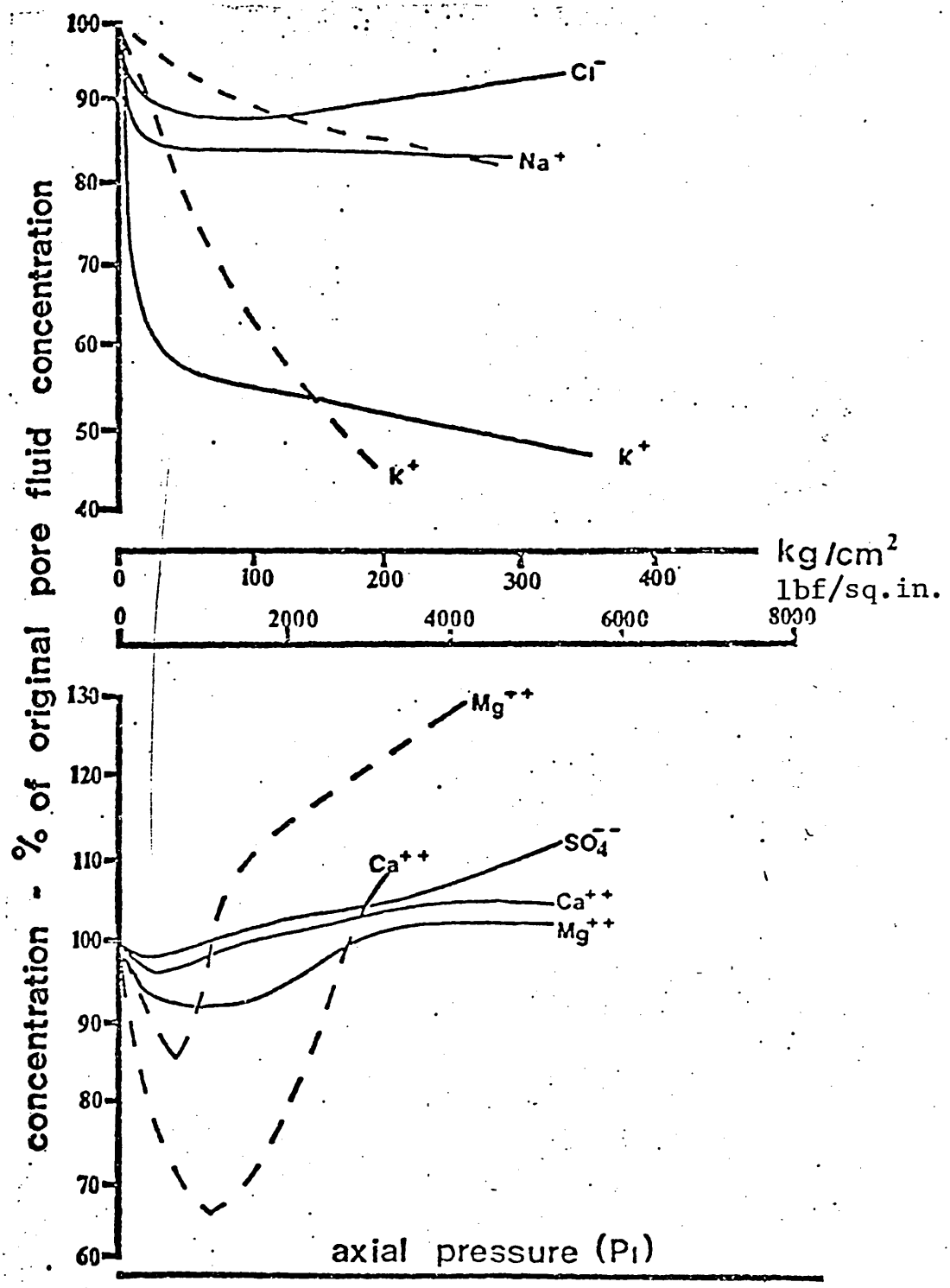


FIGURE 8.10 The observed variation of the percentage ionic concentration changes in the pore fluids expelled from two tests;

--------- BC.CHP.14 Distilled water

_____ BC.CHP.17 '1 saline' water

two tests (one of which was remoulded in 'saline' water and the other in distilled water) in order to investigate the influence of salinity. In the case of the distilled water test, the pore fluid samples obtained during preconsolidation were considered as the 'original solution' for the purpose of determining the concentration changes.

As illustrated in Figure 8.10, it is seen that a more conspicuous variation of the percentage concentration changes is apparent with the 'distilled water' test. This observation leads to the suggestion that the retention of a fixed (absolute) concentration of ions on the clay particles, and the value depends on the sites available for ion exchange on the clay particles.

Figure 8.11 is an illustrated diagram of the trend described already in Figure 8.9a and Section 8.4.2.3. Hereto the concentrations are expressed as percentage of that expelled during preconsolidation. This figure compares the results of the chemical analysis from three tests conducted at different rates of loading, and in all three, distilled water had been used for remoulding. A slow rate of loading favours further retention of ions as the pore fluid pressures developed will be too meagre to dislodge the ions from their absorption points.

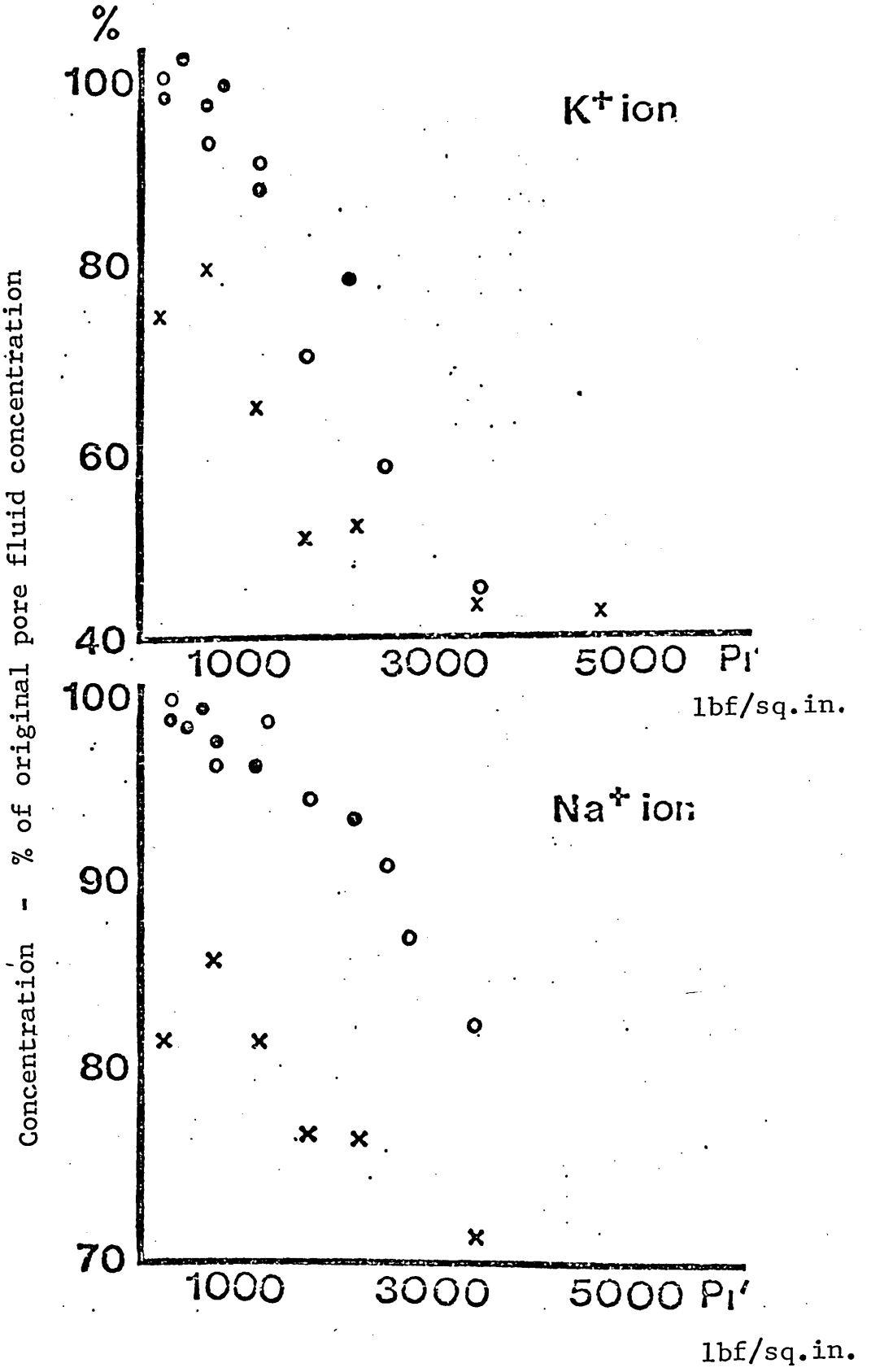


FIGURE 8.11 Influence of rate of loading on the chemistry of the pore fluid expelled:

xxxxx 0.5 lbf/sq.in/min

●●●● 1.0 lbf/sq.in/min

ooooo 2.0 lbf/sq.in/min

9.1	Introduction		391
9.2	Surface features of the final specimen		393
9.3	Macrofractures observed in the specimens		394
9.4	Slaking of air dry consolidated clay		399
9.5	Details of fabric study technique		404
	9.5.1	Scanning electron microscopy	404
		9.5.1.1 Presentation of the micrographs	404
		9.5.1.2 Quantitative image analysis	409
	9.5.2	Optical microscopy	411
		9.5.2.1 Thin section preparation	411
		9.5.2.2 Quantitative optical microscopy	416
	9.5.3	X-ray diffraction ratios	419
		9.5.3.1 Quantitative analysis	420
9.6	Shrinkage of clays		425
	9.6.1	Linear shrinkage of the sediments	826
9.7	Representability of micrographs		432
	9.7.1	Area of observation	432
	9.7.2	Interpretation of micrographs	434
9.8	Localised fabrics		437
	9.8.1	Flow structures	437
	9.8.2	Shear structures	438
	9.8.3	Edge structures	440
9.9	Perfect preferred orientation		447
	9.9.1	Laboratory samples	447
	9.9.2	Natural samples	450
9.10	Fabric of natural samples		454
	9.10.1	Falmouth sediments	454
	9.10.2	Ball Clays	458
	9.10.3	Comparison of natural fabrics with the fabric of artificially compacted clays	458
9.11	Development of fabric with consolidation		461
9.12	Fabrics produced in the drained and undrained ends		469
	9.12.1	Influence of rate of loading	470
	9.12.2	Influence of salinity	470
9.13	Further consolidation of undisturbed samples		474
9.14	Preferred orientation influenced by organic matter		481
9.15	Microscopic study of natural and artificial fissures		481
9.16	Observation of mineralisation		489

CHAPTER NINE

FABRIC AND RELATED STUDIES

9.1 INTRODUCTION

Different fabric observations made during this study are described in this chapter. Most of the observations are that of the fabrics produced in the specimens after laboratory consolidation. Figure 9.1 illustrates the manner in which the final specimen was divided for the purpose of the different types of observations.

As defined earlier in Section 2.4, 'fabric' is used here to refer essentially to the spatial arrangement of the particles and/or their associated voids. Different fabric study techniques were used and among them were X-ray diffraction, optical and scanning electron microscopy. Pertinent aspects associated with these techniques are also briefly outlined and a critical comparison is made of these techniques. Where certain observations were near consistent in most samples, only single illustrations are given to minimise the otherwise excessive and repetitive micrographs. Preferred orientation observed by these techniques have been quantified and a quick qualitative technique of fabric study is also described.

The influence of localised pore fluid pressures on the development of fabric in clays is emphasised with

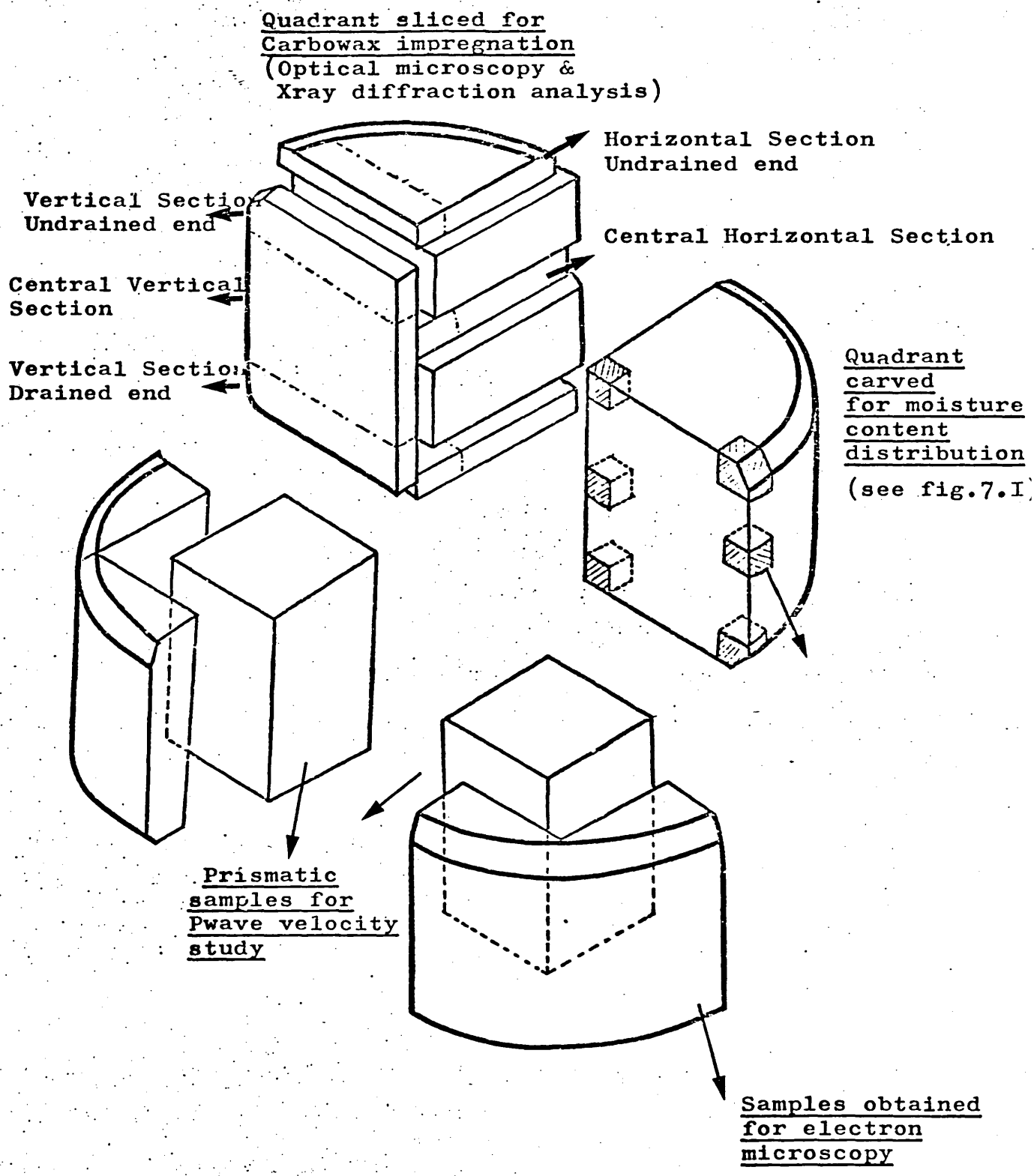


FIGURE 9.I Divisions of the final specimen for different investigations conducted in the study

illustrations. In particular, examples are given of the susceptibility of preferred orientation of clay particles to the localised direction of pore fluid pressure dissipation.

Fabric observations have also been made on natural examples with the particular intent of gaining an understanding of the micro-fabric patterns associated with natural fissures. These have been compared with similar observations on fissures generated in the samples after artificial gravitational compaction.

P-wave velocity measurements were made on the samples to use their observations as a non-destructive index test which also reflects to a certain extent the overall fabric within the sample.

9.2 SURFACE FEATURES OF THE FINAL SPECIMEN

The specimens consolidated on the high pressure consolidation cell were on the average about 1.50cms thick at the end of a test. In most tests, conducted at a relatively slow rate of loading and up to axial pressures in excess of 1,000 lbf/sq.in., the axial surface of the specimen had a polished appearance, caused by both the relative movement between specimen and the specimen cup wall and to a lesser extent due to the pore fluid drainage path between the specimen and the specimen cup wall (see figure 7.1). However, a

non-uniform appearance was clearly evident in the specimens from short term quick tests as already illustrated in Plate 7.1.

Plate 9.1 illustrates the final specimen from another test (BC.CHP.13) which was conducted at a slow loading rate of 1 lbf/sq.in./min. but had to be abandoned at a low axial stress level (418 lbf/sq.in.). Some interesting surface structures were apparent as illustrated.

A conspicuous feature of these markings is their increased curvilinearity towards the undrained end of the specimen which also happen to be the 'fixed end' during its consolidation. The specimen 'compacts' from the drained end where the particles possess finite grain velocities (see also figure 4.10). 'C' is a packet of partially saturated clay particles which has not suffered proper remoulding (cf. effects of remoulding by hand - figure 7.14). It is improbable that these curvilinear markings were influenced by the presence of 'C' being pushed into the soft specimen.

9.3 MACROFRACTURES OBSERVED IN THE SPECIMENS

Plate 9.2 is a photograph of a vertical section of a further specimen (BC.CHP.21) after it had been allowed to impregnate in carbowax 6000. The intrusion of the carbowax into the specimen had made its surface of weakness very

PLATE 9.1 Surface markings observed in the specimen of test BC.CHP.13.

Magnification of photograph x 1

Diameter of specimen : 4.0 inches

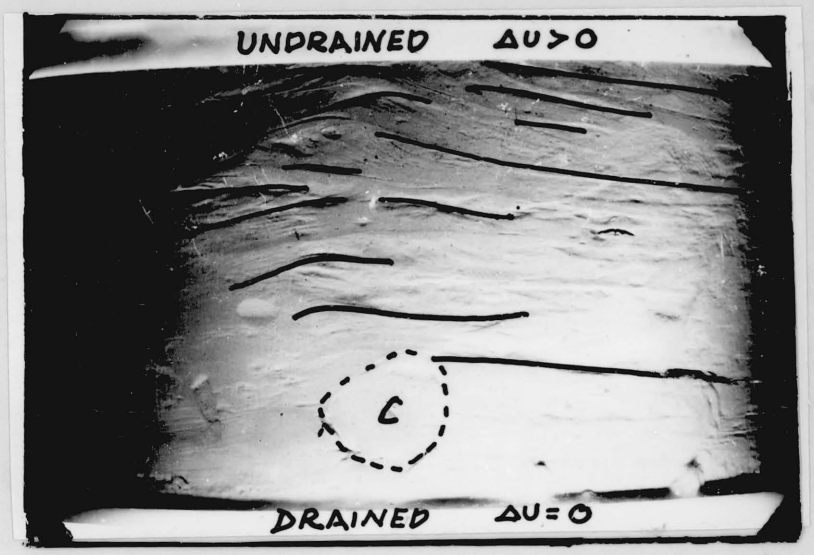
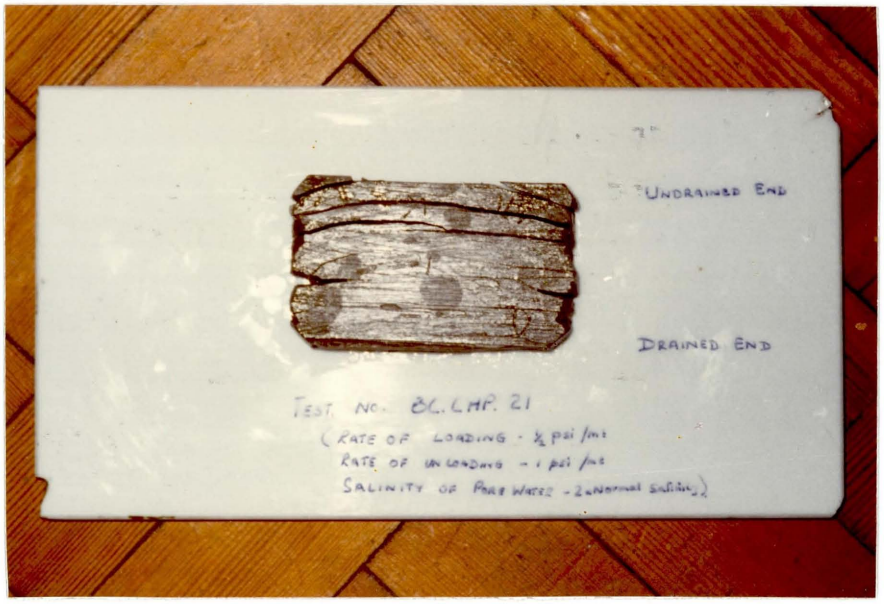

UNDRAINED ΔU>0
C
DRAINED ΔU=0



PLATE 9.2 A view of a vertical slice off the specimen from test no. BC.CHP.21 after partial impregnation with Carbowax.

(rate of loading = ½ lbf/sq.in/min
rate of unloading= 1 lbf/sq.in/min
salinity of porefluid = 2 x normally saline
scale of photograph : length of slice is 4.0 ins.


UNDRAINED END
DRAINED END
TEST NO: BC. LMP. 21
(RATE OF LOADING - ½ psi /min
RATE OF UNLOADING - 1 psi /min
SALINITY OF PORE WATER - 2 NORMAL SALINE)

prominent as seen in the plate. Hereto these surfaces of apparent weakness were more curvilinear towards the undrained end of the specimen. The persistence of this pattern even within the interior of the specimen suggests it to be caused by the local effects associated with the undrained end of the specimen. On the contrary Plate 9.2 also shows a feebly developed planar fracture near the drained end.

A genetically different type of macrofacture conforming to the definition of a 'fissure' is shown in Plate 9.3. Here the specimen was subjected to a rate of loading of 1 lbf/sq.in. up to a maximum consolidation pressure of 5,200 lbf/sq.in., which was subsequently rapidly unloaded (BC.CHP.17). A short while after the specimen was extracted from the specimen chamber, heavy fissuring was apparent at the drained end. The principal fissure, F_1, was planar and parallel to the ends of the specimen (cf. natural fissures parallel to bedding plane in nature). Such fissures were invariably apparent in test specimens which had been rapidly unloaded, suggesting a stress release mechanism for its origin.

The surface features on the above mentioned 'horizontal' fissure are shown in Table 9.3b. The absence of shearing and the distinct matt plumose structure on the face of the fissure is indicative of brittle tensile fracture

PLATE 9.3 (a) A view of the specimen no. BC.CHP.17 showing the orientation of the fissures with respect to the drainage boundary
(lower end = drained end).

(b) An half full size view of the surface features seen on the face of the fissure F_1 above.

BC CHP 17

MAXIMUM CONSOLIDATION PRESSURE - 5,200 PSI

RATE OF LOADING - 1PSI / MIN

RAPID UNLOADING

OBSERVATION:

HEAVY FISSURING AT DRAINED END OF THE SAMPLE



F_1

BC.CHP 17

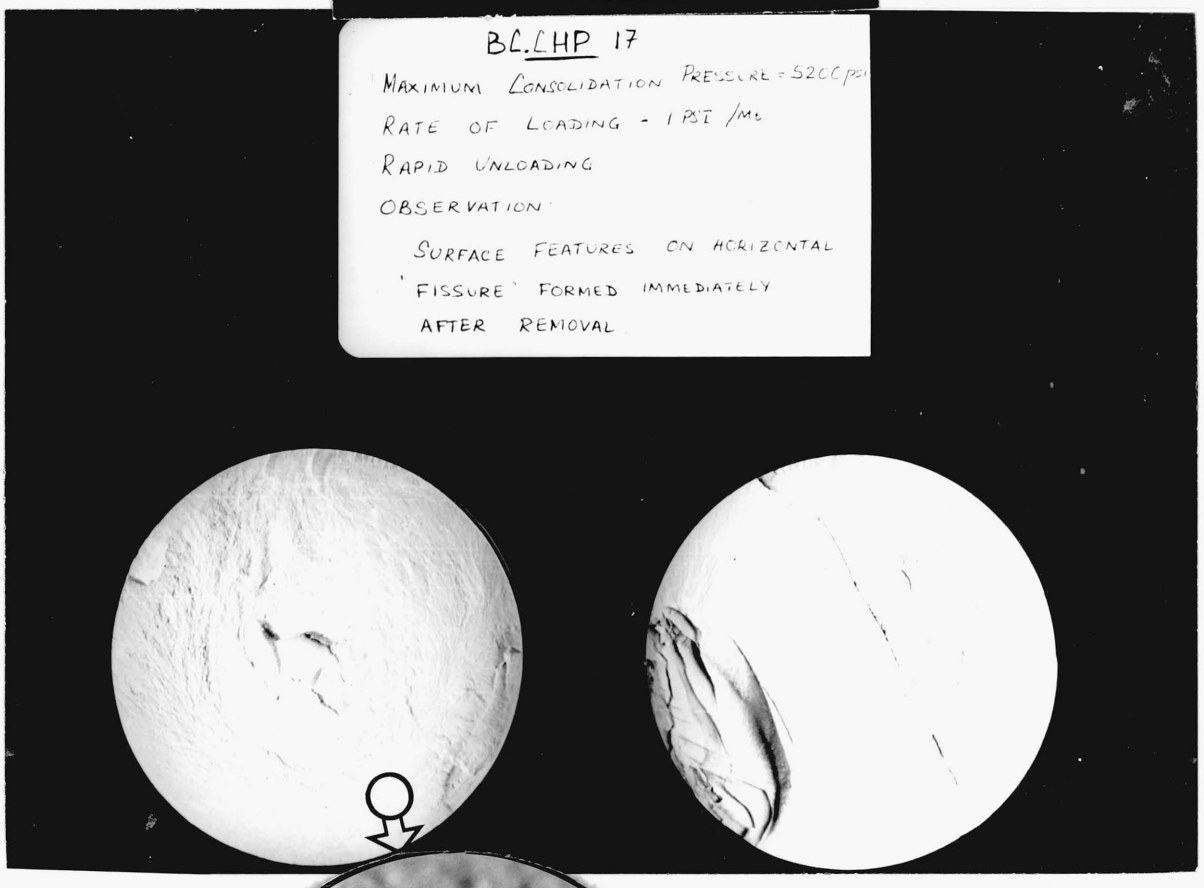
MAXIMUM CONSOLIDATION PRESSURE = 5200 PSI

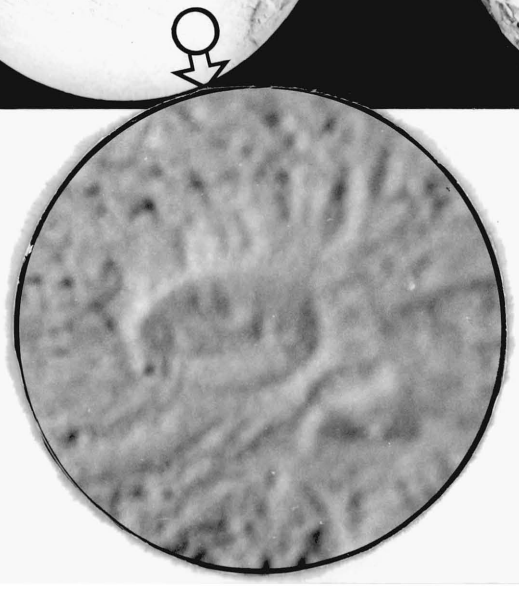
RATE OF LOADING - 1 PSI / MIN

RAPID UNLOADING

OBSERVATION:

SURFACE FEATURES ON HORIZONTAL FISSURE FORMED IMMEDIATELY AFTER REMOVAL





supporting that the stress relief was an important mechanism in its genesis.

The origin of the brittle fracture is also clearly marked in the photograph (Plate 9.3b). The eccentricity of its location suggest a localised stress concentration that may have been caused by a localised point of weakness such as air void.

Plate 9.4 is a series of electron micrographs showing magnified views of the above fracture surface. The wavy feathers (Plate 9.4(a)) of the plumose consist of partially dislodged blocks of clay particles. These dislodged particle packets lay in a bed of otherwise flat-lying clay particles (Plate 9.4(b)), and even within the dislodged packets the individual particles are aligned face to face in stacks (Plate 9.4 (c)).

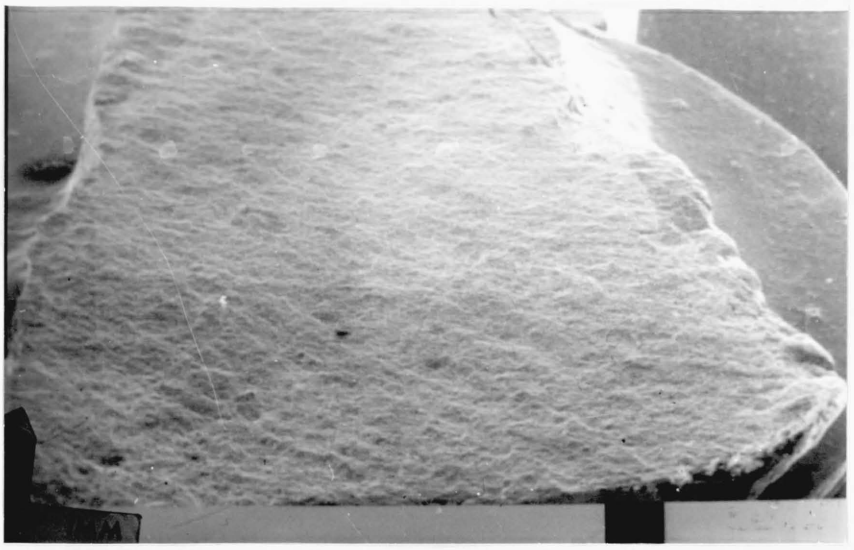
9.4 SLAKING OF AIR DRY CONSOLIDATED CLAY

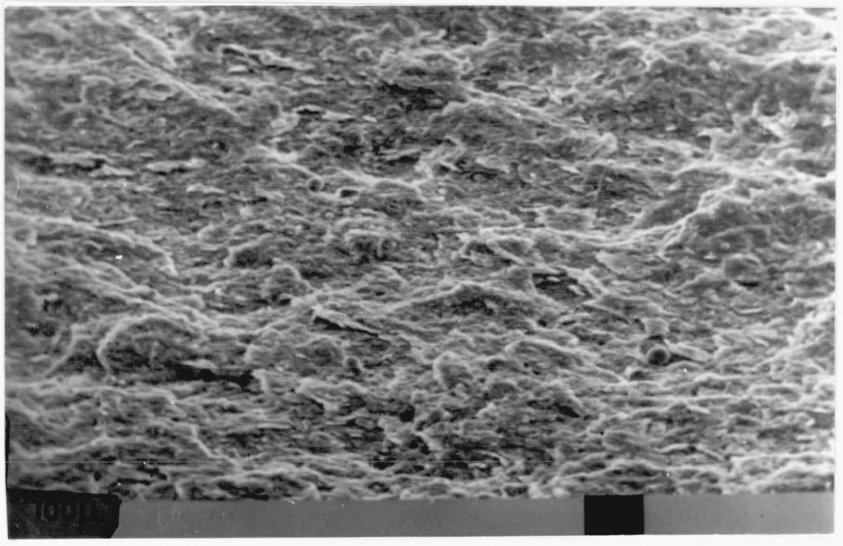
The reversibility of the consolidation process (viz. consolidated clay ⟶ clay slurry) was investigated. When vertical sections of a freshly consolidated specimen was placed gently in a dish of water, fractures similar to that illustrated in Plate 9.2 appeared.

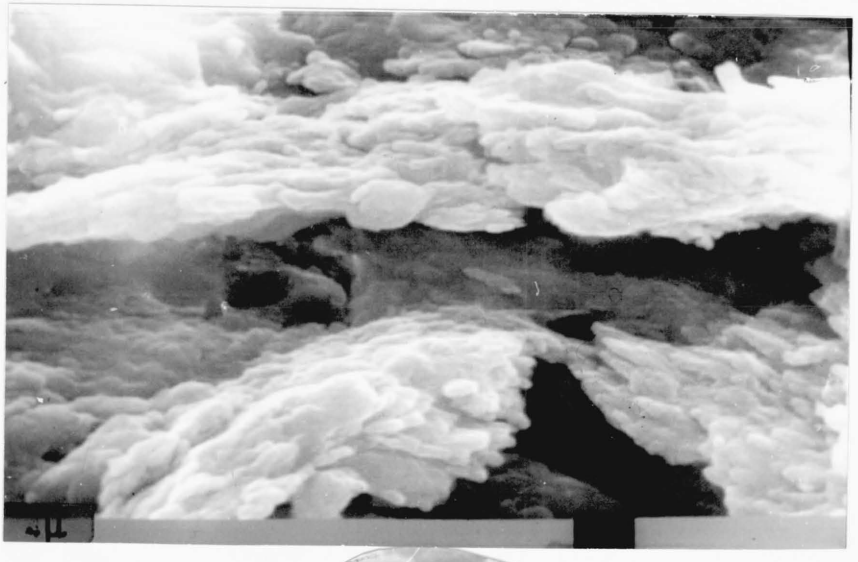
Thus when previously air dried sections of consolidated specimens were let to slake in quiet water a very

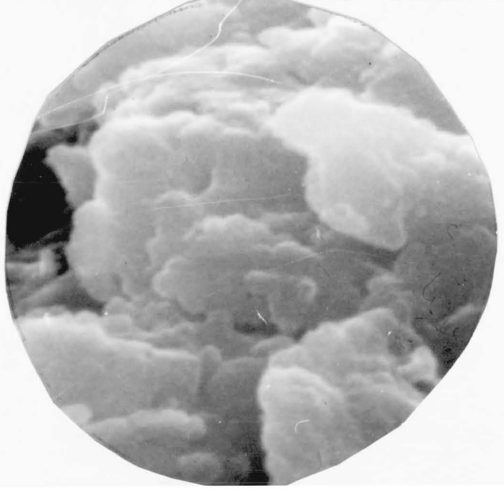
PLATE 9.4 Electron micrographs of the artificially formed fissure F_I of Plate 9.3

	Magnification	tilt
a) General view of the sample for electron microscopy	x I0	75°
b) Details of the plumose feather	x I00	75°
c) Clustered particles dislodged during the fracture	x 5,000	80°
d) Magnified view of the clusters showing localised preferred orientation of the particles	x I0,000	75°









rapid and explosive disintegration of the section occurred. This was more thoroughly examined.

Approximately an inch square orthogonal sections were cut from the air dried specimens along planes parallel (vertical sections) and perpendicular (horizontal section) to the direction of the axial consolidating pressure. These specimens were placed in a glass dish as shown in Plate 9.5a. The glass dishes were then gently filled with water. The short term and long term results of same are seen in the plates 9.5b and 9.5c and d respectively.

There is a stark contrast between the fissure patterns produced in the two types of sections which goes to suggest the process to be a result of orientation of the clay particles.

The violent fissuring occurs mainly as a result of the unsaturated state of the clay sections. The ingress of water into the clay sections is effected as a result of the cumulative effect of the processes of:

a) affinity of free water to clay particles

b) to supply the demand of unbalance of 'pore pressure'

c) surface tension affects

d) the interface repulsive forces of the clay particles

and e) the consequent escape of air from the pores

PLATE 9.5 Photographs illustrating the sequences observed in the process of slaking of thin sections of air-dried high pressure consolidated samples;

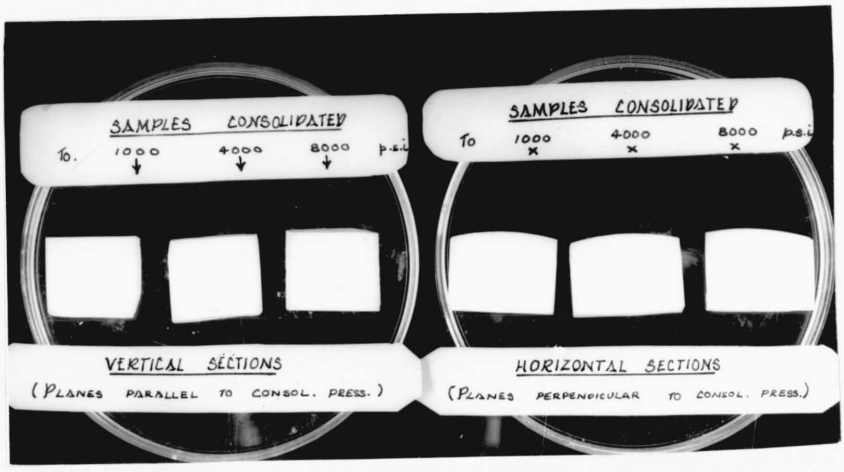
(a) vertical and horizontal sections before test;

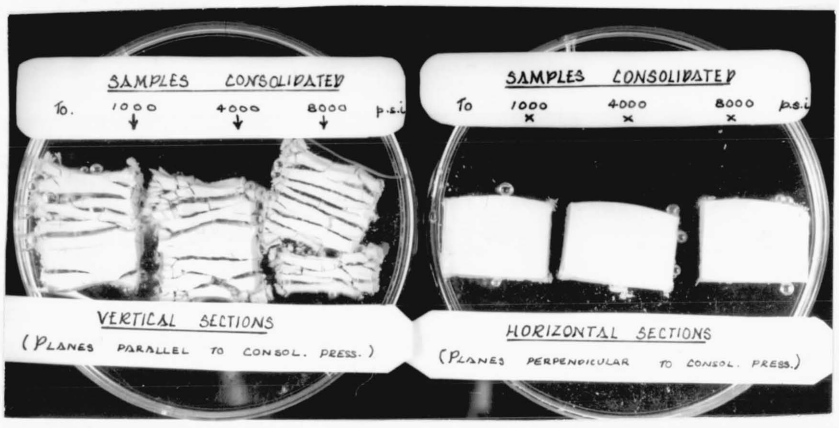
(b) 1 minute after adding water;

(c) 5 minutes after adding water;

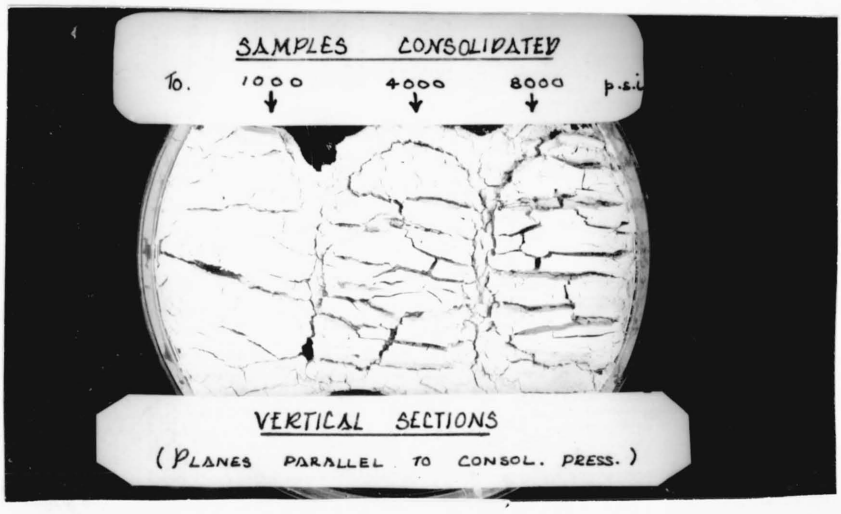
(d) long after adding water (vertical sections).

(Directions of influence of the consolidating pressures are shown by the arrows and the tails of the arrows.)


SAMPLES CONSOLIDATED
To. 1000 4000 8000 p.s.i.
VERTICAL SECTIONS
(PLANES PARALLEL TO CONSOL. PRESS.)
SAMPLES CONSOLIDATED
To 1000 4000 8000 p.s.i.
HORIZONTAL SECTIONS
(PLANES PERPENDICULAR TO CONSOL. PRESS.)


SAMPLES CONSOLIDATED
To. 1000 4000 8000 p.s.i.
VERTICAL SECTIONS
(PLANES PARALLEL TO CONSOL. PRESS.)
SAMPLES CONSOLIDATED
To 1000 4000 8000 p.s.i.
HORIZONTAL SECTIONS
(PLANES PERPENDICULAR TO CONSOL. PRESS.)


SAMPLES CONSOLIDATED
To. 1000 4000 8000 p.s.i.
VERTICAL SECTIONS
(PLANES PARALLEL TO CONSOL. PRESS.)
SAMPLES CONSOLIDATED
To 1000 4000 8000 p.s.i.
HORIZONTAL SECTIONS
(PLANES PERPENDICULAR TO CONSOL. PRESS.)


SAMPLES CONSOLIDATED
To. 1000 4000 8000 p.s.i.
VERTICAL SECTIONS
(PLANES PARALLEL TO CONSOL. PRESS.)

The path of the water is governed by the fabric of the clay and therefore the resulting fissure pattern reflects the fabric of the clay.

The sections shown in Plate 9.5 were obtained from tests in the series of rapid consolidation tests. The order of the increase of intensity of the fissure patterns seen in 9.5(b) corresponds well with the order of magnitude of the peak consolidation pressures. But the intensity of those that developed subsequently (Plates 9.5c and 9.5d) fail somehow to reflect the same order.

The short term fissure pattern is a reflection of the more dominant orientation direction of the particles whereas the subsidiary orientation directions are developed only later. Therefore it appears that there are increased secondary orientation directions with increasing pressures for specimens of this test series. A similar observation can also be drawn from a study of the long term fissure patterns developed in the horizontal sections.

The above observation suggests the occurrence of increased flow structures in the specimens compacted to the higher pressures. This is in accordance with the loading history of the samples (see figure 7.2) and the consequent build-up of higher order excessive pore fluid pressures in the samples compacted to higher total stress levels.

It was also considered necessary to study the effect of the thickness of the clay slices on the patterns produced. Accordingly Plate 9.6 shows the patterns observed for vertical slices of different thicknesses obtained from the test specimen, BC.CHP.19. A practicable minimum thickness was 3 mm. The above illustration advocates the use of 3 mm thick samples for comparative studies.

Plate 9.7 shows the fissure patterns produced in slices, which had been cut at different inclinations within the specimen. The direction of action of the component of the operating stress is shown in the overlay. The observations confirm an increased fissility (resulting from particle orientation) from zero for horizontal slices to a maximum for the vertical slices.

9.5 DETAILS OF FABRIC STUDY TECHNIQUES USED

The conventional methods of clay fabric analysis have already been described in Section 3.2.3. It is proposed to enlist here some of the more important aspects of the techniques used and also the personal experience with them.

9.5.1 Scanning electron microscopy

A Cambridge Stereoscan 600 (Plate 9.8) was used during this study. The samples obtained for the study were invariably air dried and the associated shrinkage effects are described later in this chapter.

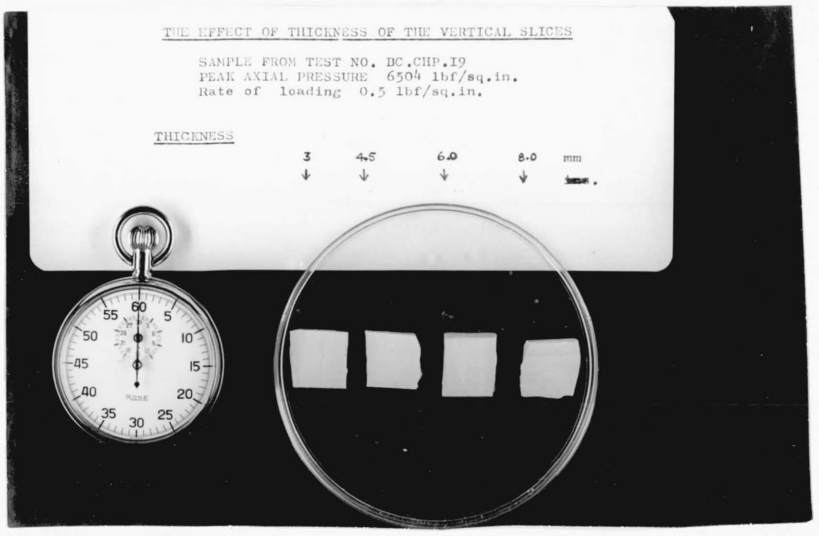
PLATE 9.6 Photographs showing the results of fissility tests on vertical sections of different thickness of the same specimen:

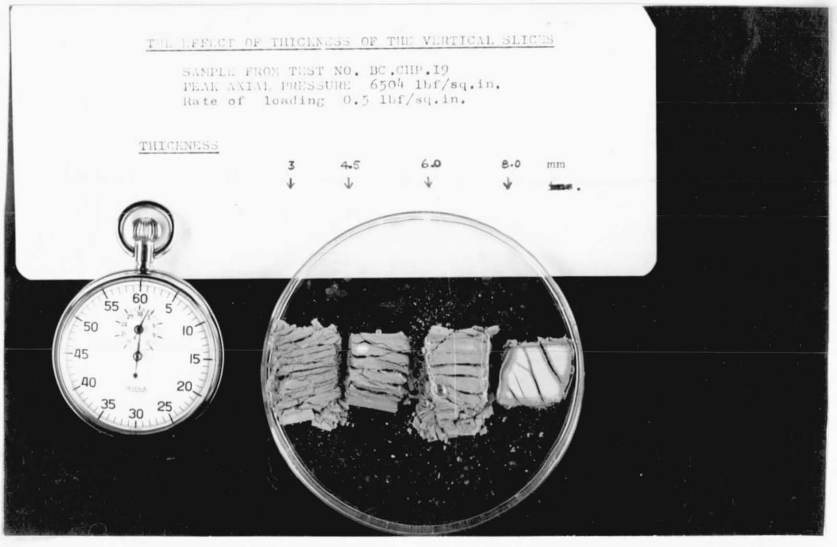
(a) Before test;

(b) 3 minutes after pouring water;

(c) Long after adding water.

(Direction of influence of the consolidation pressure is as shown by the arrows.)


THE EFFECT OF THICKNESS OF THE VERTICAL SLICES
SAMPLE FROM TEST NO. BC.CHP.19
PEAK AXIAL PRESSURE 6504 lbf/sq.in.
Rate of loading 0.5 lbf/sq.in.
THICKNESS
3 4.5 6.0 8.0 mm


THE EFFECT OF THICKNESS OF THE VERTICAL SLICES
SAMPLE FROM TEST NO. BC.CHP.19
PEAK AXIAL PRESSURE 6504 lbf/sq.in.
Rate of loading 0.5 lbf/sq.in.
THICKNESS
3 4.5 6.0 8.0 mm

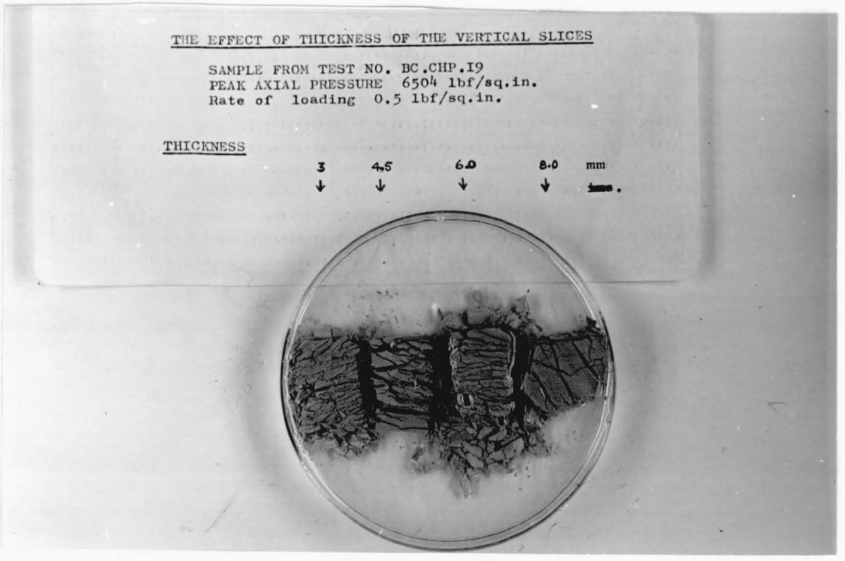

THE EFFECT OF THICKNESS OF THE VERTICAL SLICES
SAMPLE FROM TEST NO. BC.CHP.19
PEAK AXIAL PRESSURE 6504 lbf/sq.in.
Rate of loading 0.5 lbf/sq.in.
THICKNESS
3 4.5 6.0 8.0 mm

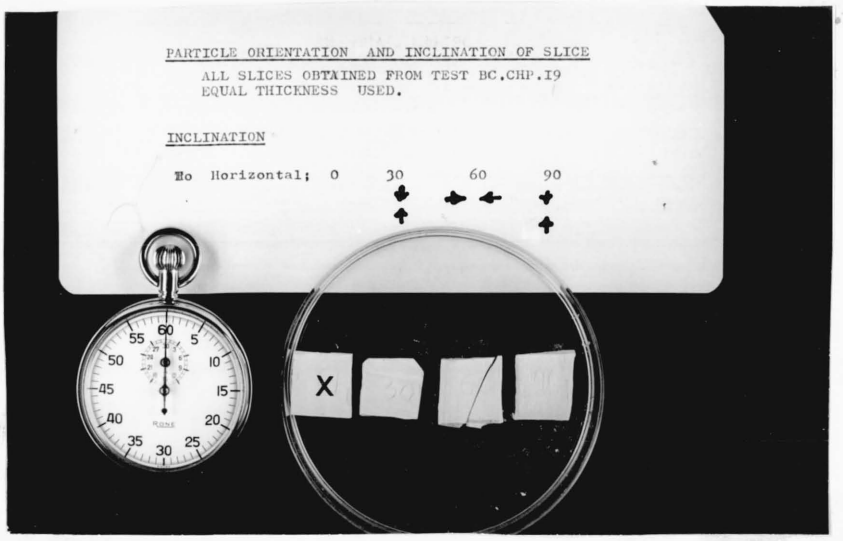
PLATE 9.7 Photographs showing the fissility of equidimensional slices cut at different inclinations from the same specimen:

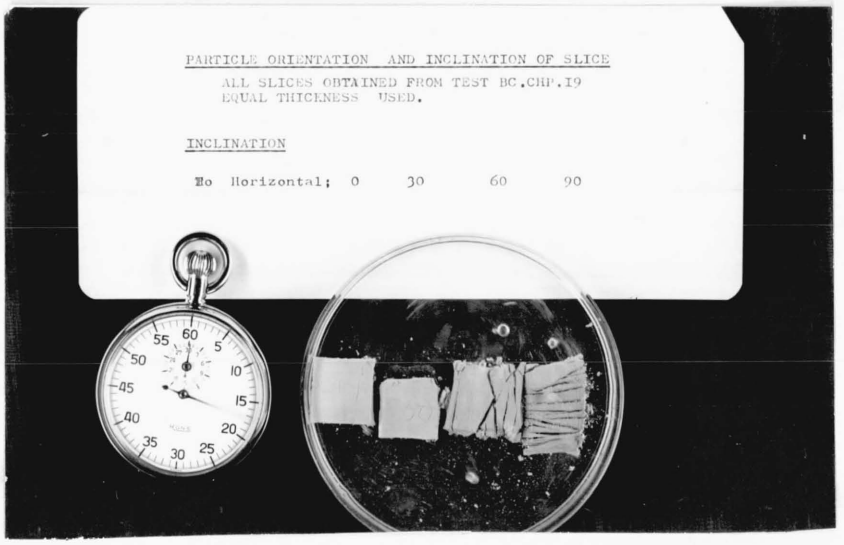
(a) Before test;

(b) 1 minute after start of test;

(c) long after pouring water.

(Direction of influence of the major component of the axial consolidation pressure is as shown on the overlay.)


PARTICLE ORIENTATION AND INCLINATION OF SLICE
ALL SLICES OBTAINED FROM TEST BC.CHP.I9
EQUAL THICKNESS USED.
INCLINATION
No Horizontal; 0 30 60 90
X


PARTICLE ORIENTATION AND INCLINATION OF SLICE
ALL SLICES OBTAINED FROM TEST BC.CHP.I9
EQUAL THICKNESS USED.
INCLINATION
No Horizontal; 0 30 60 90


PARTICLE ORIENTATION AND INCLINATION OF SLICE
ALL SLICES OBTAINED FROM TEST BC.CHP.I9
EQUAL THICKNESS USED.
INCLINATION
No Horizontal; 0 30 60 90

PLATE 9.8 View of the Cambridge Stercoscan 600

M = Microscope column.

S = Specimen stage.

I = Screen for receiving.

C = Camera.



Though different sample preparation techniques were used as described in Barden (1971), a combination of the processes in the following sequence was observed to give satisfactory results.

a) A 0.5 mm thick section perpendicular to and containing the particular surface of interest was sliced off the test specimen. A tensile fracture was effected at the point of interest. The sample containing the fresh fracture surface was fixed onto an aluminium stub using Durafix. A coating of aluminium paint was applied on the four sides of the sample and on the stub head to give a perfect electrically conducting surface.

b) The fracture surface was air jetted to remove all coarse dislodged particles that had remained as debris from the fracture.

c) The fracture surface was then peeled gently several times with an adhesive tape to remove all fine dislodged particles that still remained on the surface.

d) The fracture surface was then coated with about 200 $\overset{o}{A}$ thick film of gold under vacuum.

Most micrographs presented in this study are of natural or artificially consolidated clays in an air-dried state. Therefore the effect of shrinkage in disturbing the fabric is important and has been separately dealt with in Section 9.6.

9.5.1.1 Presentation of the micrographs

The majority of the micrographs presented in this chapter are monoscopic. Some of them are further illustrated with stereoscopic observations of particular features. It is pertinent to draw the attention of the reader to the fact that these stereo pairs are essentially of low depth. To the inexperienced reader, a vertical barrier between the pair may aid in obtaining the stereoscopic vision.

Magnifications of the micrographs are expressed as x 20,000 x 2 = 20,000, where x 20,000 represents the electronic magnification and the subsequent optical enlargement is x 2, resulting in a total magnification of 40,000. Where the optical magnification is unity, the quoted magnification is given as the electronic magnification.

Each micrograph is usually accompanied by a scale marker. In its absence an indication of the scale is given by the picture width, which is the width of the field of view in the micrograph as viewed from the direction of the title.

The tilt angle expressed represents the angle between the mean specimen surface and the beam. Stereo pairs have been obtained for two tilt positions of the specimen, differering by an angle in excess of 5°.

Details of the sample, specimen preparation, magnification and the like are given on the page facing each micrograph.

9.5.1.2 Quantitative image analysis

One object of the electron microscopy study is to investigate the development of preferred orientation of particles. The crude comparison of electron micrographs for the degree of preferred orientation invariably is prone to be biased by the human factor. Therefore it was important to use an image analysing technique to assist the subjective observer to a fuller comprehension of the preferred orientation by objective criteria.

A technique of study is the use of the two-dimensional Fourier transform of the electron micrograph applying coherent optics (Fraunhofer diffraction). This produces a qualitative record of the image details in the terms of dimensions and also enables a quantitative record to be made of the intensity pattern of the image (Nyberg et al, 1971).

Figure 9.2 is an illustration of the optical system developed in the Department of Physics, Imperial College.

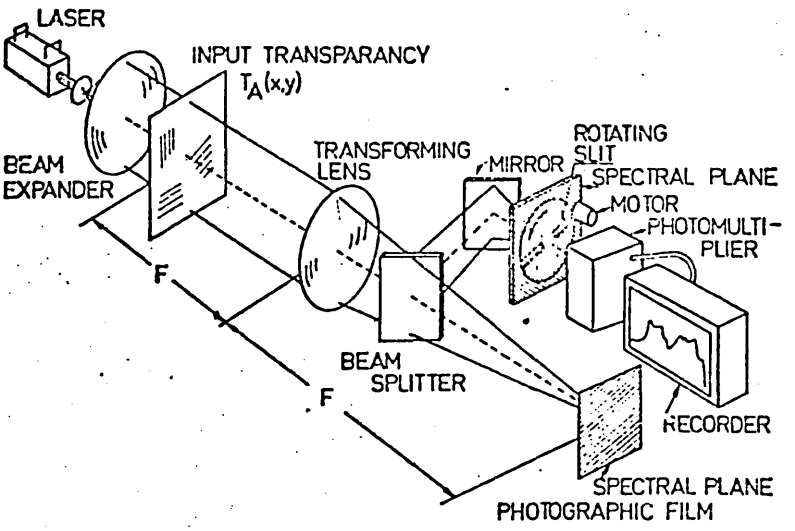


FIGURE 9.2 Schematic diagram of the details of the optics used for the diffraction pattern analysis of the electron micrograph.

Accordingly the Fourier transforms presented against their respective micrographs in this study have been obtained using the above apparatus.

A parallel coherent beam of light is passed through the transparency of a micrograph. Most of the micrographs in this study appear as a set of linear features which when Fourier transformed produces diffraction patterns in the form of a two-dimensional distribution which frequently approximates to an ellipse. In micrographs showing very high order preferred orientation the diffraction pattern is elongated in a direction perpendicular to the direction of particle orientation. Conversely, a circular diffraction pattern is the Fourier transform of a random oriented structure.

9.5.2 Optical microscopy

Plate 9.9 shows the optical microscope with its photometric attachments as developed by Tchalenko (1967). The same equipment was used in this study for both qualitative and quantitative microscopic study of thin sections of the specimen.

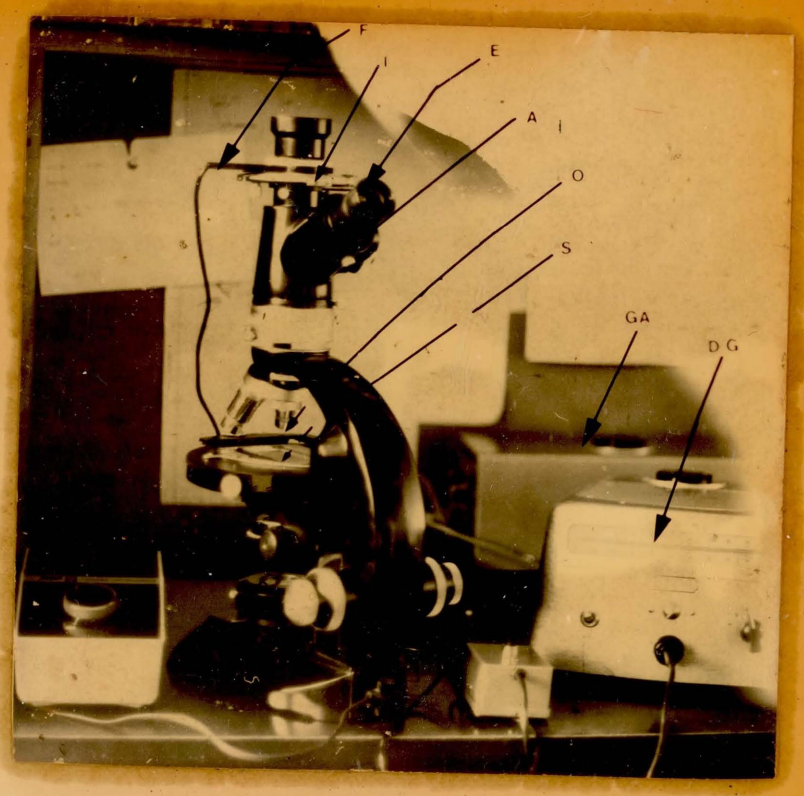
9.5.2.1 Thin section preparation

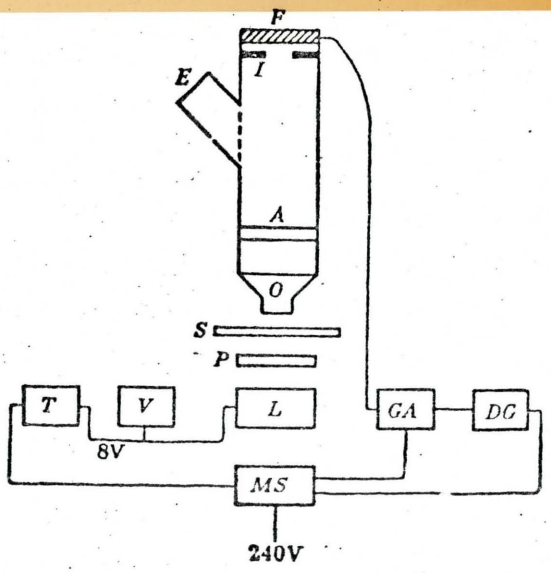
The appropriate slices of the clay specimen had to be first impregnated and Carbowax 6000 was used for this purpose. The optimum thickness of the initial slice was about 8 mm.

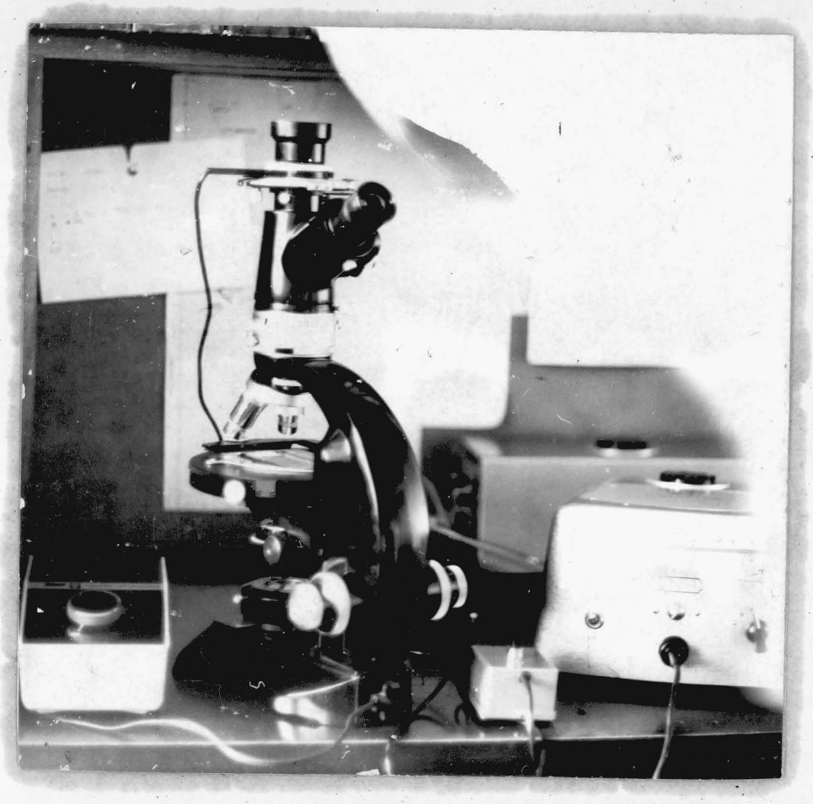
PLATE 9.9 (a) A view of the optical microscope and photometric attachment used in qualitative fabric study.

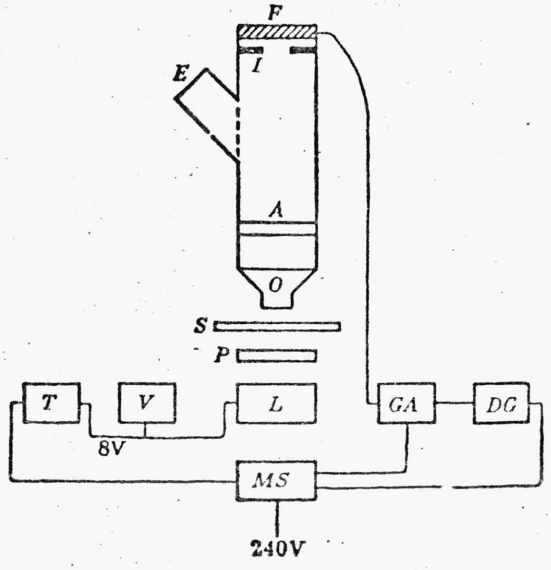
(b) A diagrammatic sketch of the microscope arrangement

A - Analyser
DG - Display galvanometer
E - Eyepiece
F - Selenium photocell
GA - Galvanometer amplifier
I - Iris diaphragm
L - Light source unit
O - Objective
P - Polariser
MS - Mains stabiliser
S - Thin section
T - Transformer
V - Voltmeter


F
I
E
A
O
S
GA
DG


F
I
E
A
O
S
P
T
V
L
GA
DG
8V
MS
240V




F
I
E
A
O
S
P
T
V
L
GA
DG
8V
MS
240V

Carbowax is completely miscible with water when liquid at 65°C, and is a solid with hardness on Mohr's scale of one at room temperature. Plate 9.10 is a series of micrographs of a thin section of carbowax alone at different magnifications. Carbowax sections showed no overall birefringence effect, confirming that the aggregate birefringence of impregnated Kaolin is unaffected by the presence of carbowax.

Replacing the liquid carbowax with fresh wax every two to three days hastened the diffusion exchange of the wax for water. The sections were kept immersed in liquid carbowax for a total period in excess of two weeks to ensure complete replacement of the pore water with carbowax.

The actual grinding of the sections was done with fine abrasive (carborundum No. 600) and in paraffin. The sections were mounted onto the glass slides using araldite. It was imperative to use cover slips to protect the fragile sections from damage and reaction with atmospheric moisture.

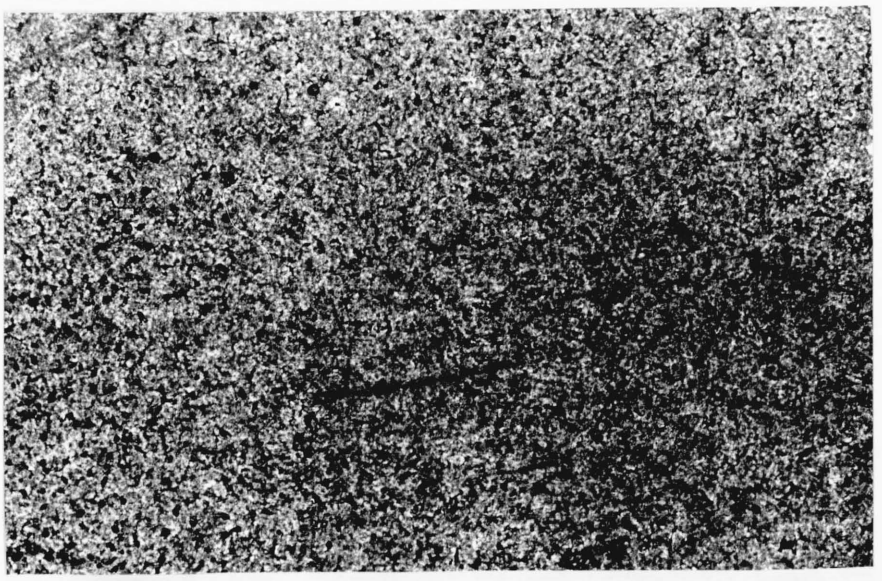
Plate 9.11 is an optical micrograph of a typical horizontal section of a remoulded Ball Clay 661 that has been consolidated. The flat lying coarse silt particles stand out of the mass of fine sized clay.

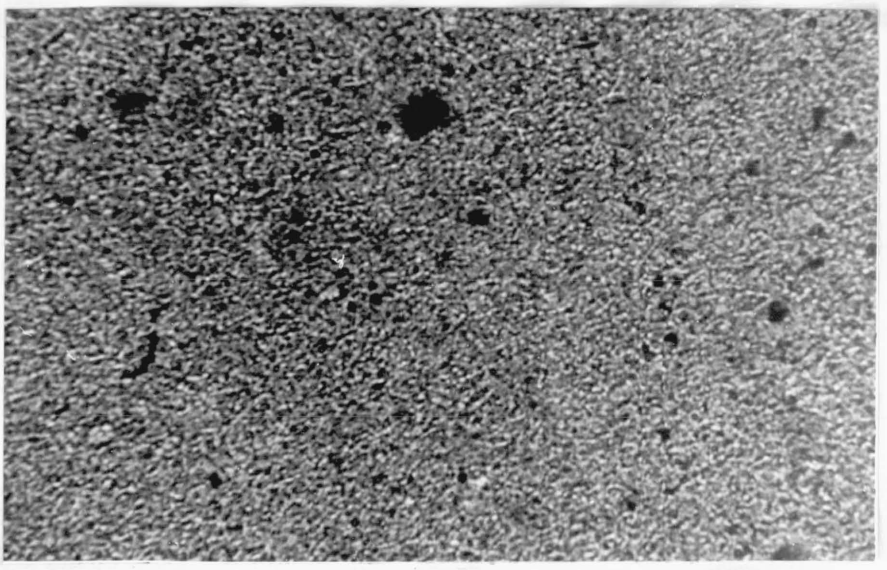
PLATE 9.10 Optical micrographs of Carbowax 6000

a) ordinary light - x10 magnification

b) crossed polars - x25 magnification

c) crossed polars - x150 magnification





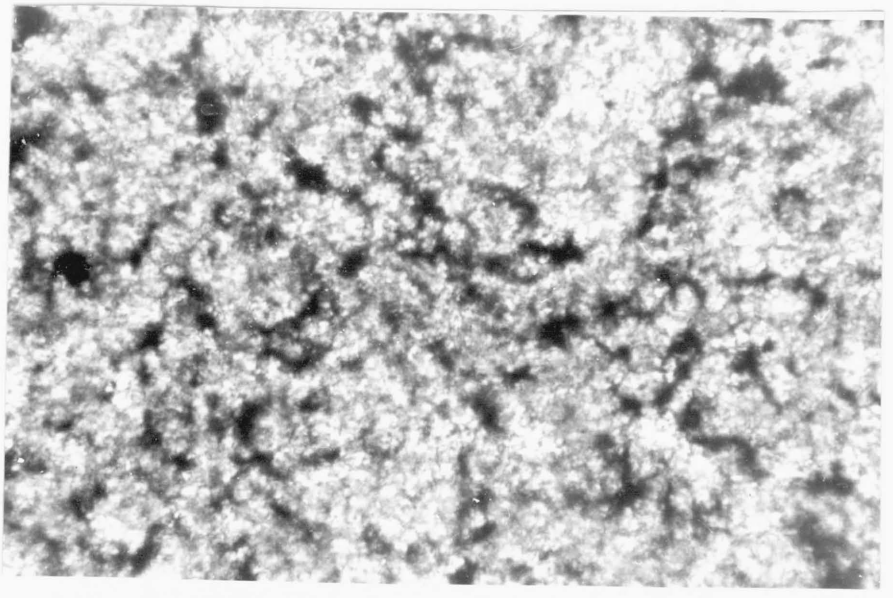


PLATE 9.11 Optical micrograph of a typical horizontal section of a consolidated Ball Clay specimen after being Carbowaxed
(crossed polars - magnification x 25)

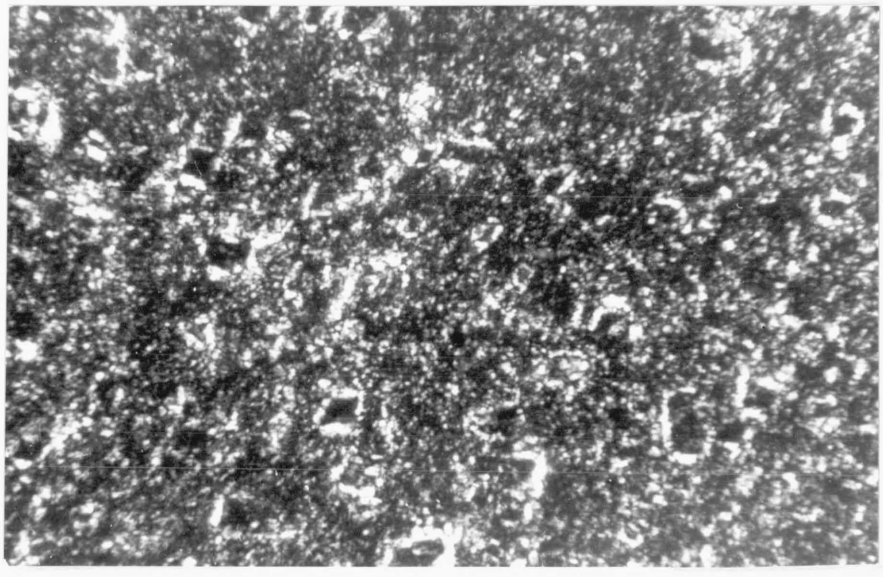
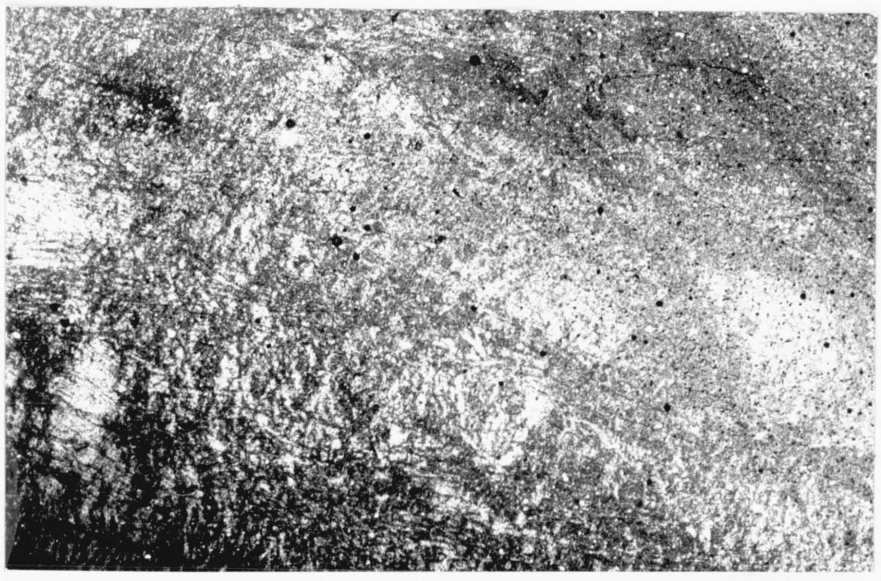
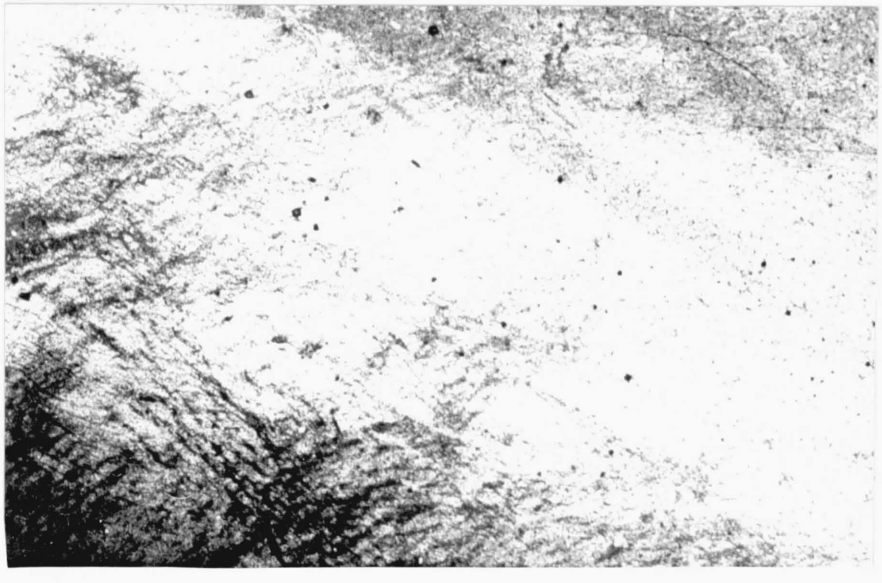


PLATE 9.12 An optical micrograph of a vertical section from test BC.CHP.17 showing the views of extinction (I_{min}) and illumination (I_{max}):

a) Crossed polars x 10 magnification.

b) crossed polars x 10 magnification.





9.5.2.2 Quantitative optical microscopy

To assess the degree of preferred orientation of the clay particles in a specimen, optical microscope observations had to be quantified. All thin sections used for such study were cut with their planes in the direction of the maximum compressive stress.

Observations were made of the intensity of light transmitted through crossed nicols for different stage angles. All intensity readings were made on areas of 0.33 mm diameter and at similar incident illuminations. The extreme values of the intensity of the transmitted light (I_{max}, I_{min}) and their respective stage angles were recorded. Accordingly both birefringent ratio ($\beta = \frac{I_{min}}{I_{max}}$), and the anisotropy index ($A = \frac{\sum I_{max} - \sum I_{min}}{\sum I_{max} + \sum I_{min}}$; Smart, 1967) were computed. A typical case of the positions of extinction (I_{min}) and illumination (I_{max}) is shown in Plate 9.12. Also it must be observed that zones or packets such as A and B appear out of phase with the rest of the section.

Rosettes of the variation of the transmitted light with stage angle was plotted for some particular cases. The range of birefringence ratios obtained for any one specimen is an indication of the homogeneity of the fabric. It follows that with high preferred orientations, the expected variations in β are small and that this variation increases with increasing

disorder. There are two primary causes for this variation. The first is associated with the choice of field area of investigation. Large field areas encompass a more representative fabric while small areas can miss or include only localised fabrics such as clay packets or stacks.

A second cause for the variation of β is the influence of boundary effects in the consolidation apparatus. Therefore such is evident only in laboratory consolidated specimens and are further described in section 9.8.3.

Accordingly, the sharp narrow cross-shaped rosettes are indicative of homogeneous and high degree of preferred orientation. Therefore, an 'overall orientation factor' can be represented by the ratio of the area of a circle of radius, I_{max}, and that of the area of rosette:

$$\text{Overall orientation factor} = \frac{I_{max}^2}{\text{Area of rosette}}$$

Overall orientation factor can take values from 1.0 (random) to infinity (perfect orientation). Such a factor has been used in the comparison of some of the natural fabrics and is described in section 9.13.

9.5.3 X-ray diffraction ratios

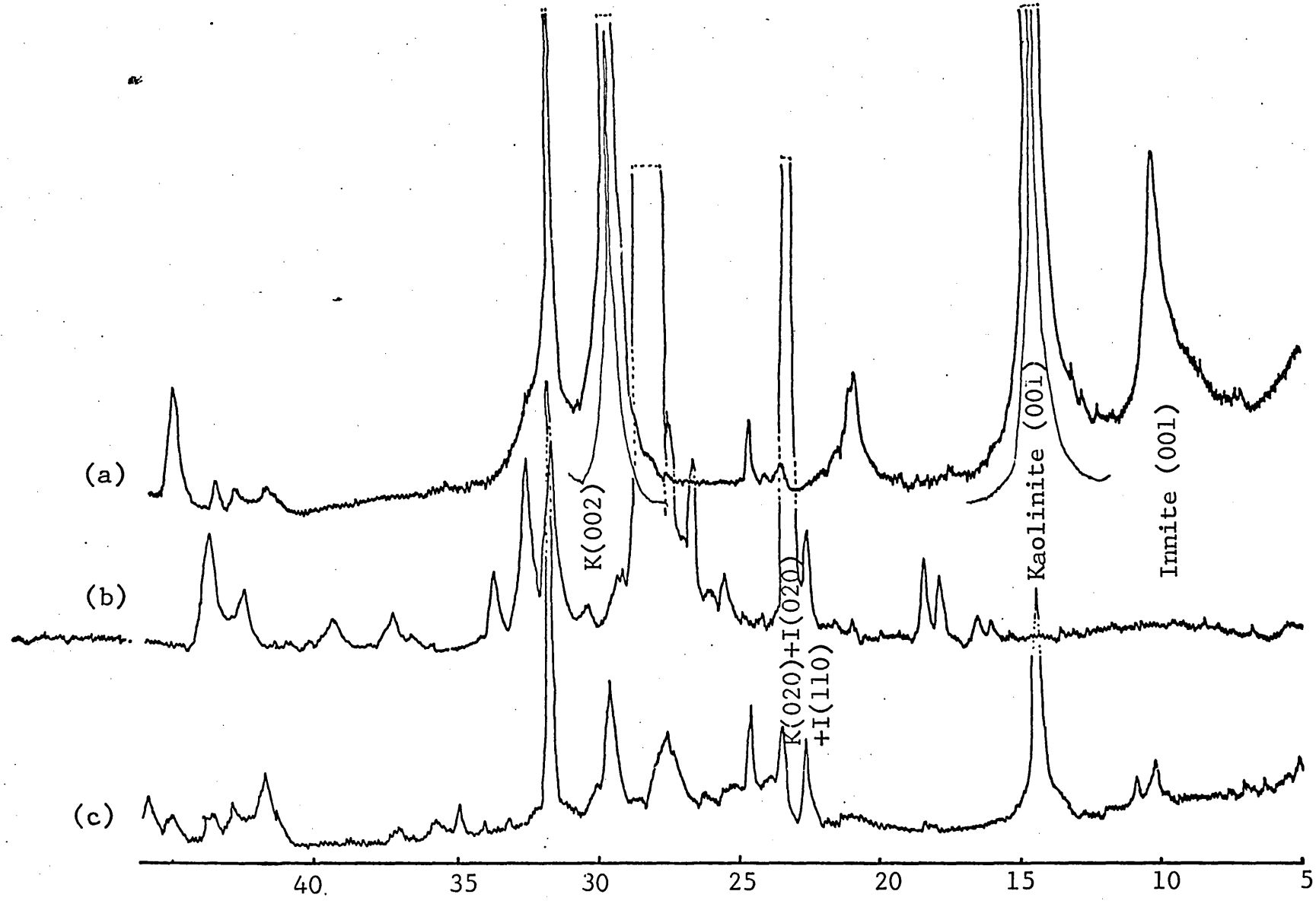
The X-ray diffraction apparatus described in section 8.2 was used. In all quantitative studies ratios of peak

intensities (peak ratio) were used so that the data are then automatically corrected for variations in crystallite concentrations. The specimens were prepared in the same way as for optical microscopy but were not ground to a thin section.

Figure 9.3 shows a series of X-ray diffraction traces presented for the purpose of investigating the interference of the carbowax trace. Figure 9.3a is a X-ray diffraction trace of perfectly oriented disc-mounted Ball clay 661 performed in the air-dried state. The diffraction trace for carbowax alone is shown in figure 9.3b. Figure 9.3c is a trace of a carbowax impregnated horizontal section of a consolidated Ball clay 661 specimen. The clay mineral peaks analysed in the study were 001, 002, 110, 020 and 060 peaks of Kaolinite and Illite. It is clear from the figure that these peaks are unaffected by the peaks of the carbowax.

9.5.3.1 Quantitative analysis

X-ray diffraction traces for analysis were obtained by using iron filtered cobalt ($K\alpha$) radiation at a scanning speed of 1° (2θ) per minute. The area of the specimen radiated was 2.0 cm x 1.0 cm. Figure 9.4 compares the XRD traces from two orthogonal sections and the peaks analysed are shown. The diffraction radiation was detected by a scintillation counter (Plate 9.13). The intensity of any peak was evaluated by five different methods. They are illustrated in figure 9.5. Two



CoK radiation - (2θ)

FIGURE 9.3 XRD traces of (a) Disc mounted oriented BC 661 clay fraction (b) Carbowax only, (c) Typical carbowaxed horizontal slice of a consolidated specimen.

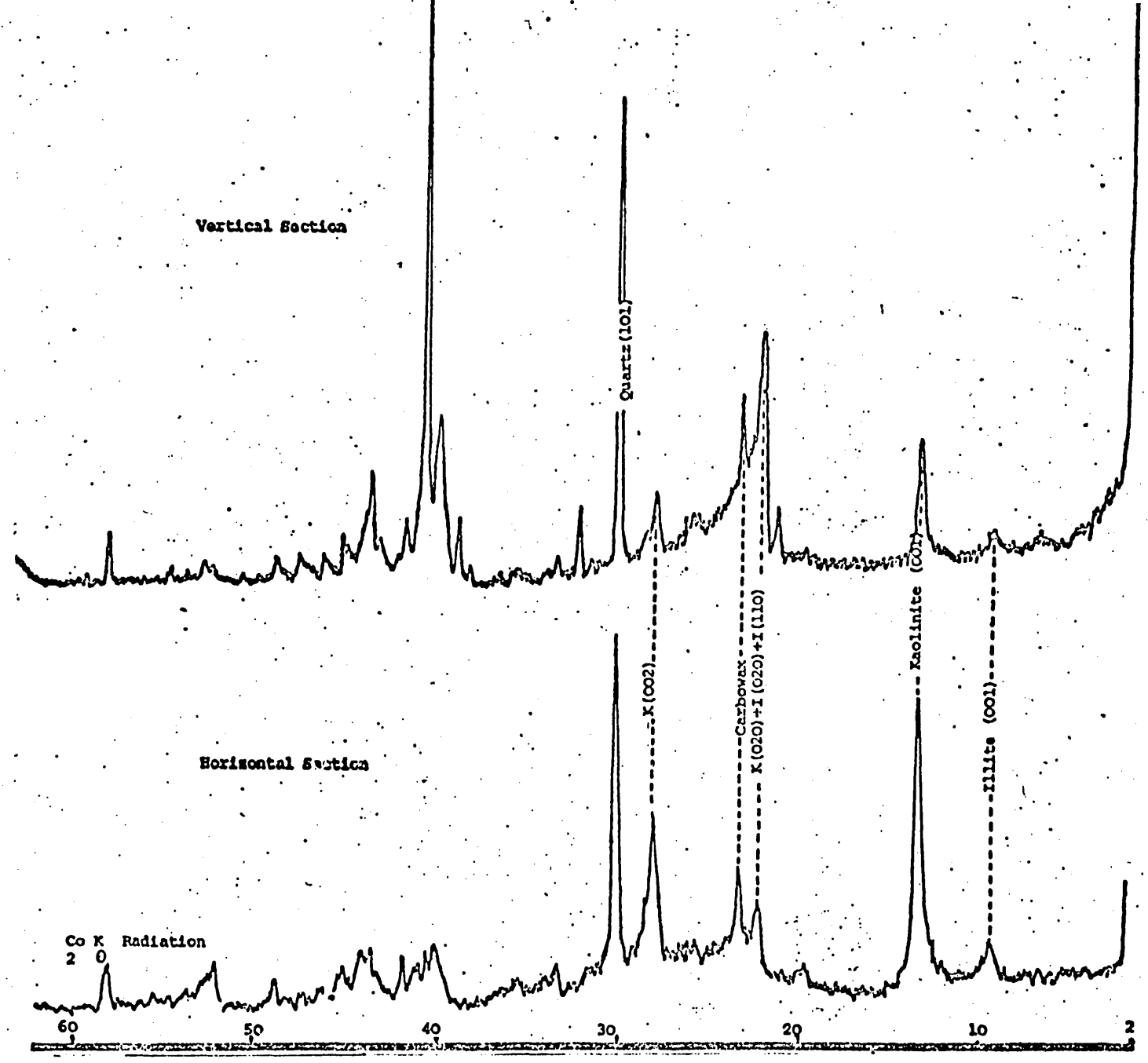
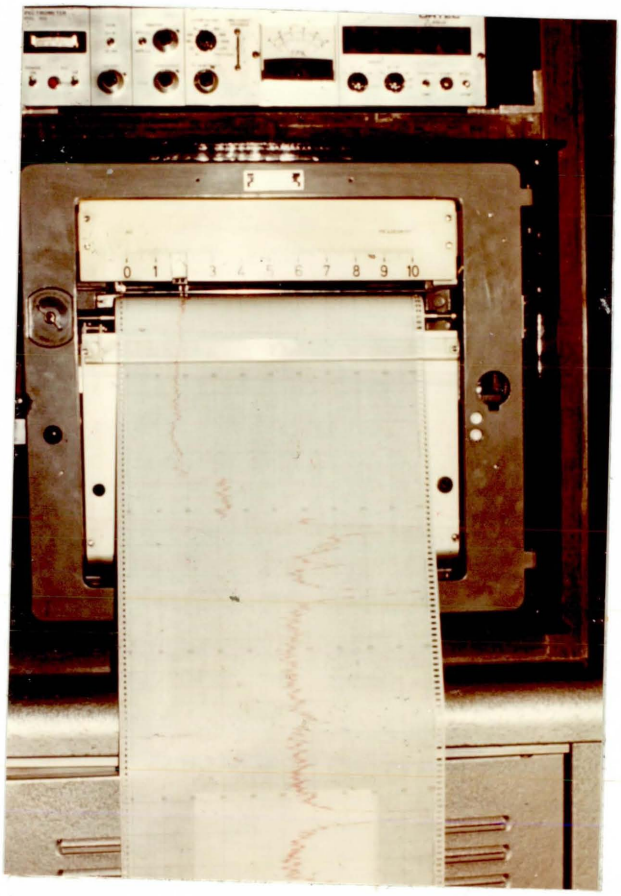
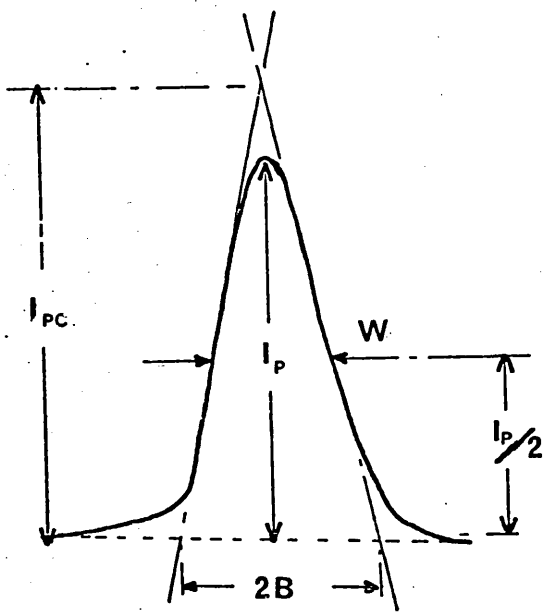


FIGURE 9.4 XRD traces of two carbowaxed orthogonal sections from a consolidation test (BC.CHP.18)

PLATE 9.13 A view of the XRD Chart recorder and peak count indicator.


0 1 2 3 4 5 6 7 8 9 10

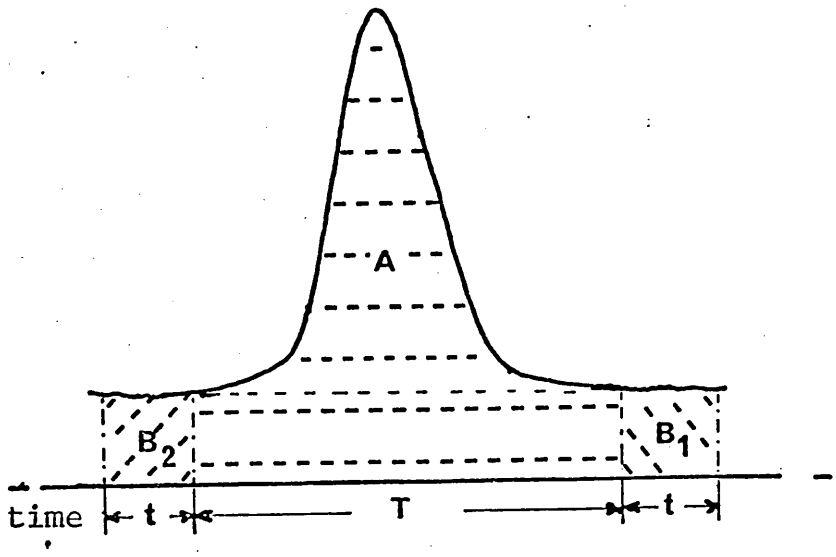


I_P - Observed peak intensity

$I_P \cdot W$ - Observed area of peak

I_{PC} - Corrected peak intensity

$I_{PC} \cdot B$ - Corrected peak area



$A = (B_1 + B_2)\frac{T}{2t}$ = Total no. of counts in peak

B_1 and B_2 = measure of background

FIGURE 9.5 Parameters used in the determination of peak ratios in X-ray fabris analysis

of them use the plotted intensity and the peak area which are dependent on the factors such as scan speed and chart speed. Two others smoothed the peaks as shown in figure 9.4a and give corrected values. The fifth technique used the visual readout of the counter (shown in Plate 9.12) to obtain the peak counts A, B_1 and B_2 over the preset times of T and t.

The degree of particle orientation was inferred from diffraction ratios using both orthogonal and single section techniques of fabric analysis. Section 3.2.4 has already described some of the peak ratios cited in literature. In most cases a diffraction ratio of 1 represents random distribution of particles while a diffraction ratio of 0 is that for perfect orientation of particles.

9.6 SHRINKAGE OF CLAYS

As mentioned earlier, this aspect of shrinkage in clays resulting from the drying of a moist specimen is very critical in the study of fabric.

Furthermore, it is noteworthy that the American Geological Institute definition of 'compaction' includes also the process of decrease in volume of the sediments resulting from drying too (see section 1.1 and American Geological Institute, 1957). Therefore the following study was made.

Figure 9.6 illustrates the results of an attempt of a photographic reproduction test to describe the affects of increasing order of shrinkage in distorting the fabric. With progressive drying, shrinkage causes a definite reduction of the volume of the pores, but the dimensions of the clay particles are not much affected. This results in physical deformation processes of rotation or bending of the particles from their original position. By virtue of the infinite degrees of freedom of the particles, many fabric deformation mechanisms are possible but only one of them is shown in the figure. Accordingly, oriented fabrics can suffer disturbance of the preferred orientation and random fabrics can attain fabrics unrepresentative of their initial fabrics; their effects being marked with increasing shrinkage.

9.6.1 Linear shrinkage of the sediments

A series of tests were conducted to determine the linear shrinkage behaviour of the sediments. One hundred percent moist clays were packed into the linear shrinkage apparatus and the resulting shrinkage observed as described in B.S. 1377.

Plate 9.14 shows a view of the final shrunk specimen of ball clay 661 and Falmouth clay in their respective standard moulds.

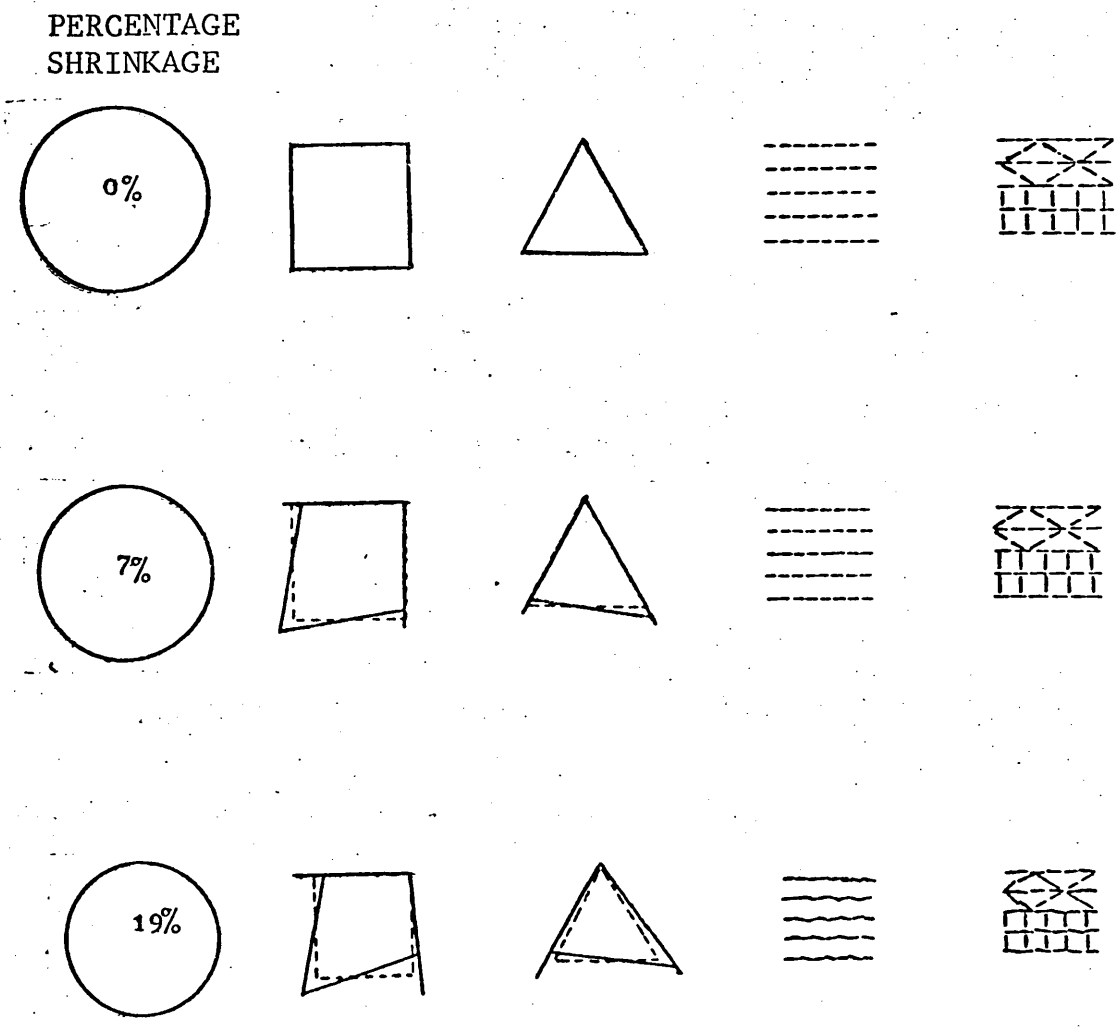


FIGURE 9.6 A photographic reproduction illustration of the effects of shrinkage.

PLATE 9.14 The result of linear shrinkage of Falmouth and Ball Clay sediments.

Total shrinkage on oven drying from 100% moisture content;

Ball Clay = 15.5%

Falmouth Clay = 10.3%

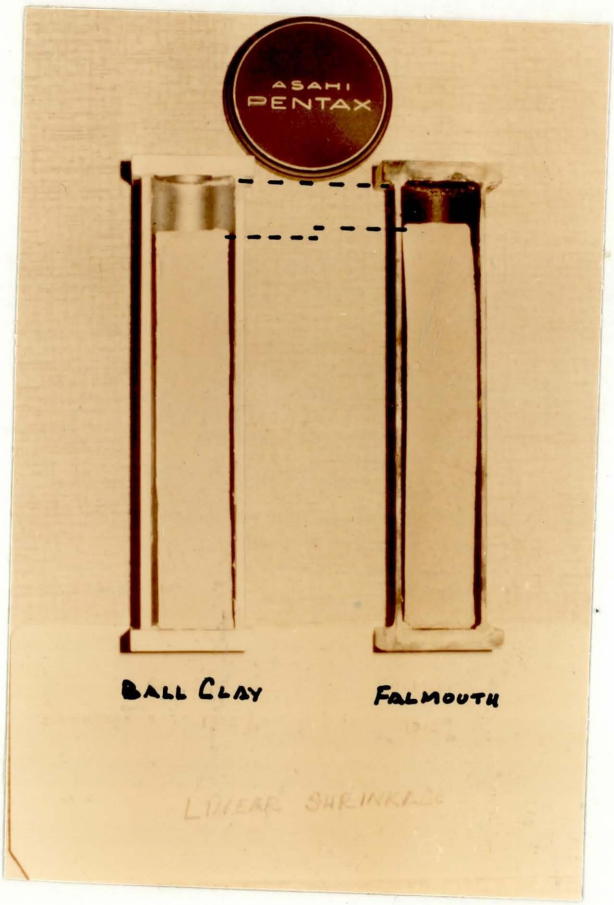
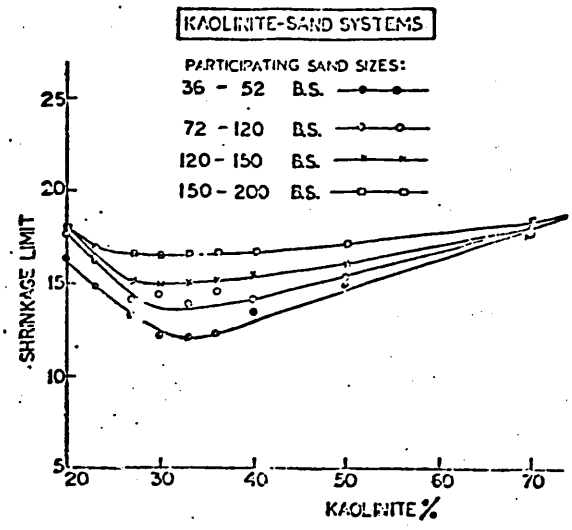

ASAHI
PENTAX
BALL CLAY
FALMOUTH

Figure 9.7a describes the results of Das et al (1969) on the shrinkage behaviour of sand clay systems. It can be concluded from his results that the shrinkage limit of a kaolinite-sand system is dependent on both particle size of the sand and the clay content. Finer the quartz grains, the higher is the shrinkage limit. The minimum shrinkage limit corresponds to a critical state of packing, wherein all the available void spaces are completely filled by the clay particles. Figure 9.7b shows the manner in which Ball Clay 661 and Falmouth clay shrank with decreasing moisture content. The greater shrinkage in the more fine-grained Ball Clay 661 is in accordance with the observations of Das et al.

Plate 9.15 shows a series of magnified views of a vertical surface of the shrunk Ball Clay 661. Several interesting observations arise from same. Even with one hundred percent moisture content, the slurry is sufficiently stiff to trap air bubbles. The shape of these air voids conforms to the deformation process induced by the weight of the sediments above it (note the definition of 'fabric' includes the distribution pattern of the voids too). Magnified view in Plate 9.15b shows the preferred orientation of the clay particles around the circumference of the air voids, and 9.15c shows the orientation of the clay particles that have resulted due to the effect of the two pneumatic pressures within the voids. It is possible to observe the thinning-out of the wall, with

(a)



(b)

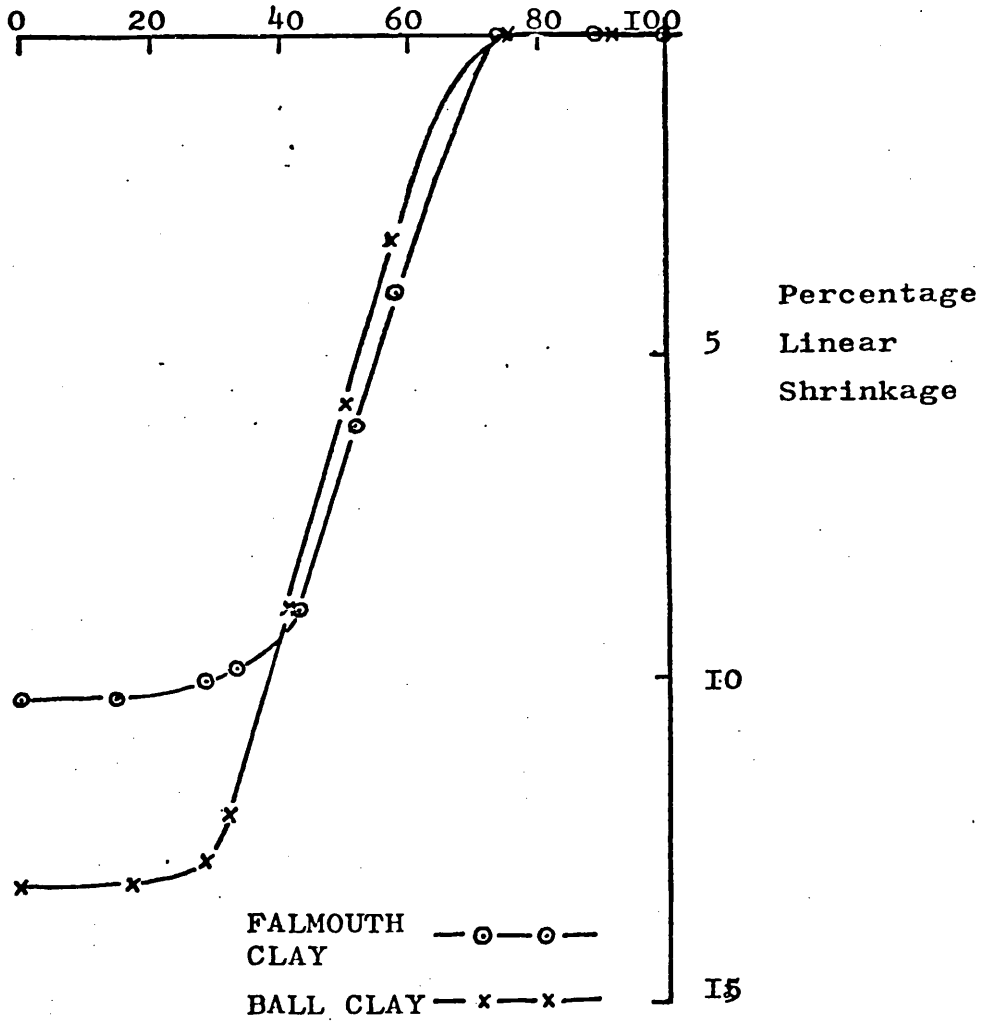


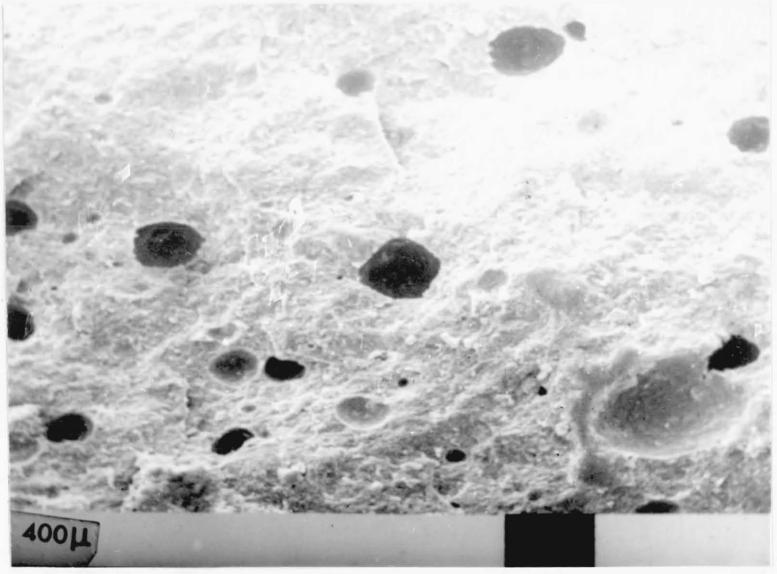
FIGURE 9.7 Shrinkage behaviour of Kaolinitic clays

(a) Shrinkage limit at different clay content (after Das et al, I969)
(b) Linear shrinkage for Falmouth and Ball clay

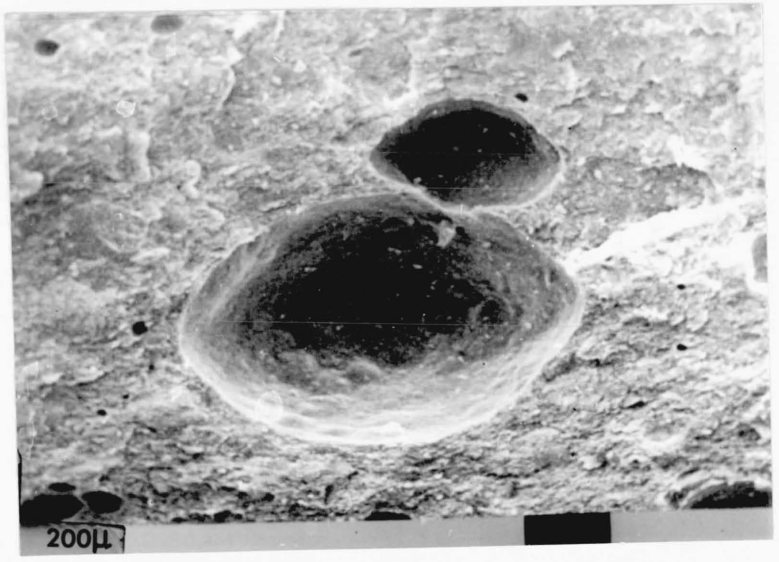
PLATE 9.15 Electron micrographs of a vertical surface of a shrunk Ball Clay 661 showing:

		Magnification	tilt
a)	general vertical surface	x 20	85°
b)	view of interaction of air voids	x 50	85°
c)	wall between voids	x 5,000	85°

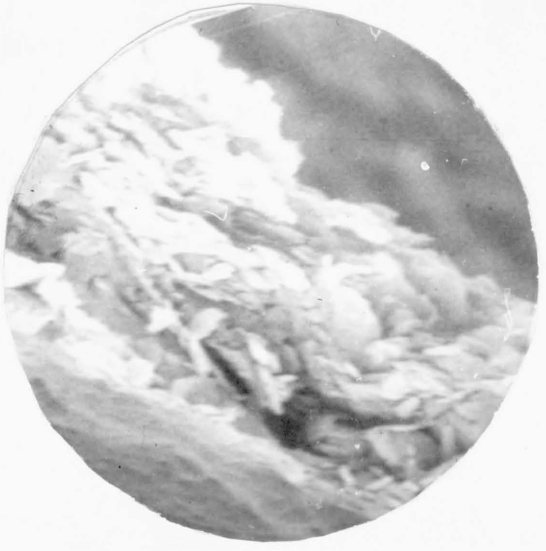
a



b



c



in this case preferred orientation being enhanced by virtue of the freedom for such lateral deformation (cf. unconfined consolidation, if such is possible).

9.7 REPRESENTABILITY OF MICROGRAPHS

One of the prime difficulties of fabric interpretation from micrographs is to assess its representability over the rest of the specimen. Especially in areas of fabric inhomogeneity it is wrong to represent the fabric by one single micrograph of high magnification.

9.7.1 Area of observations

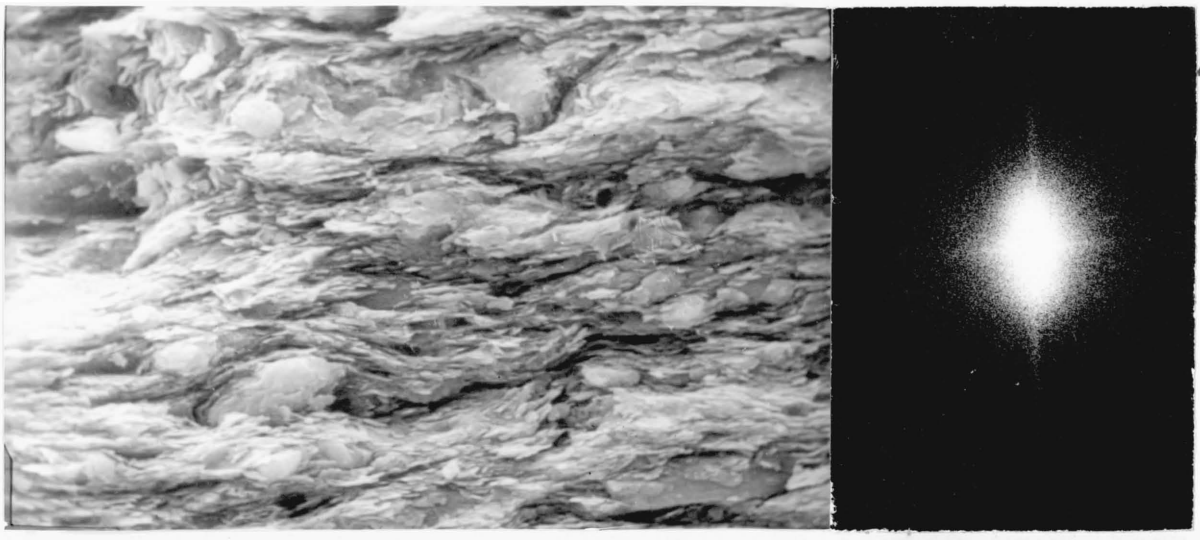
Particularly in high magnification electron microscopy the field area of observation is very small and can be highly unrepresentative.

Plate 9.16 is a series of electron micrographs obtained from the same specimen under similar conditions of instrument settings but at different magnifications. This particular surface is of fairly homogeneous fabric, but yet serves to emphasise aspects of sample representability. The above micrographs have been image analysed and their results are also shown in Plate 9.16. These diffraction patterns help to compare the degree of orientation as interpreted from the micrographs. The highest magnification micrograph shows a less oriented fabric, as shown by the diffraction pattern.

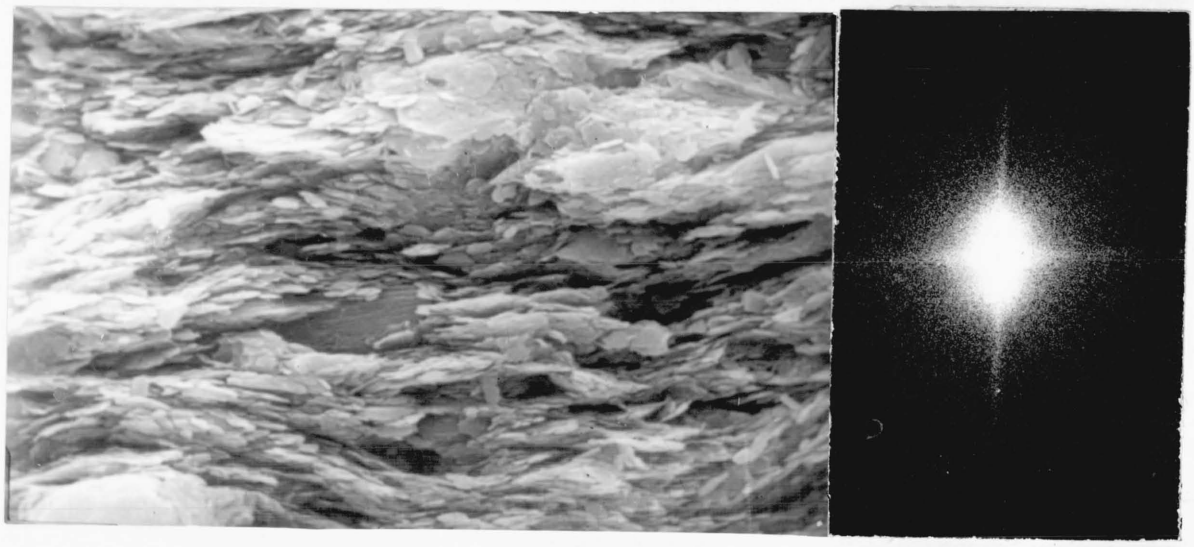
PLATE 9.16 Electron micrographs of the drained end of test BC.CHP.14 showing the views at different magnifications and their associated diffraction patterns:

	Magnification	Tilt	Picture width
a)	x 2,000	87°	75μ
b)	x 5,000	87°	58μ
c)	x 10,000	87°	13μ
d)	x 20,000	87°	6.5μ

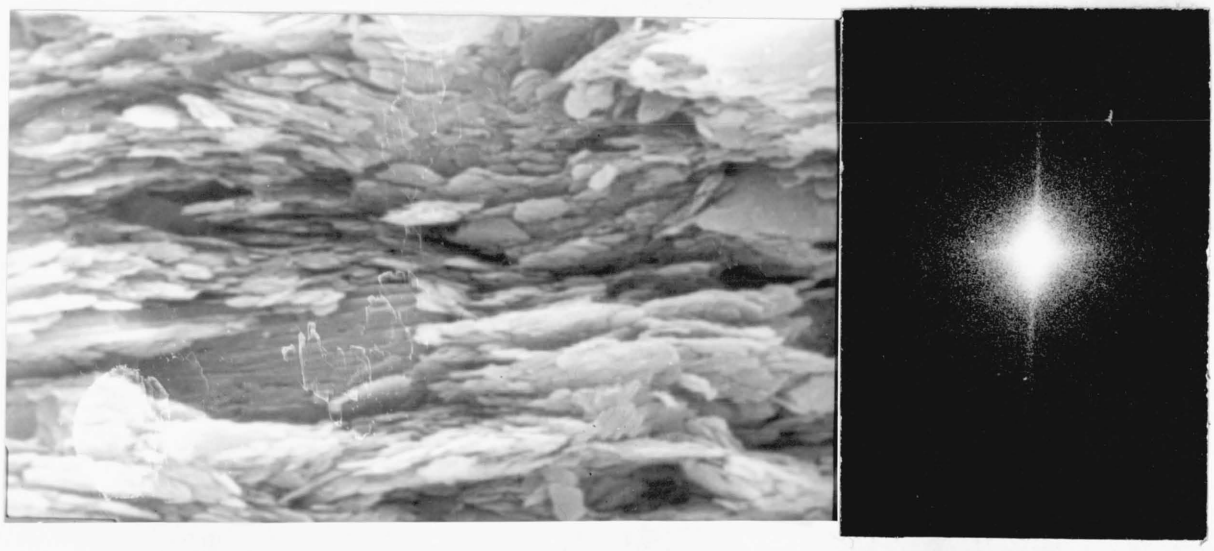
a



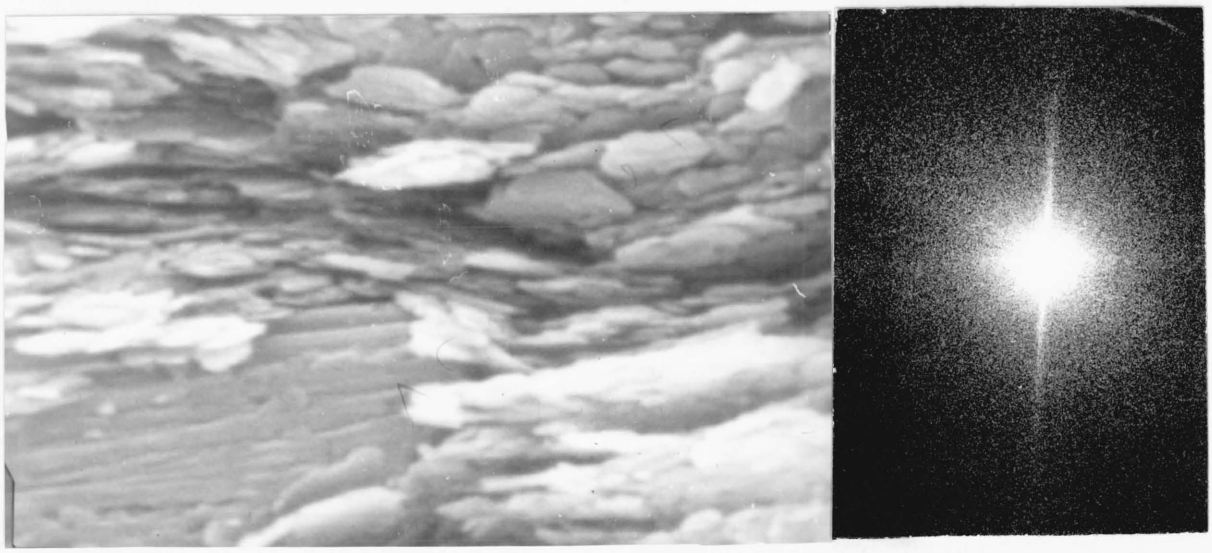
b



c



d



Thus, in this study, whenever fabrics are compared a standard electronic magnification x 5,000, was used, and wherever possible the micrographs are accompanied by their respective image analysis pattern.

9.7.2 Interpretation of micrographs

It is not difficult to misinterpret micrographs and an interesting example is presented here.

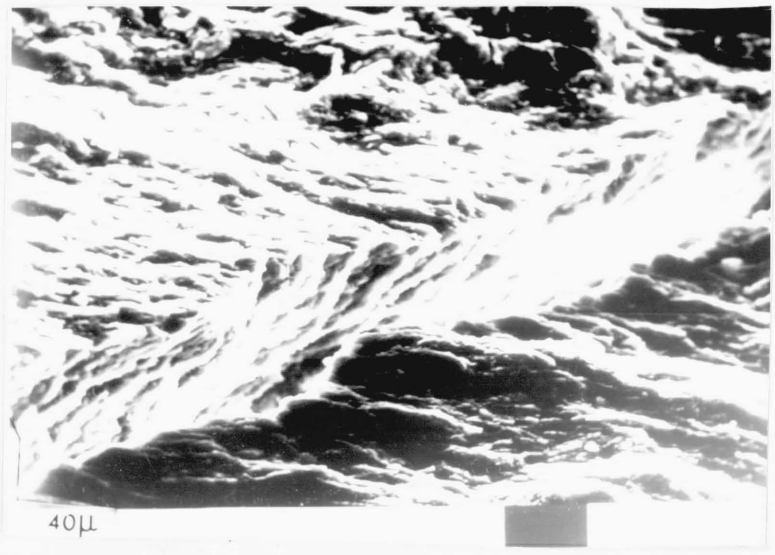
Plates 9.17a and 9.17b are micrographs at two different magnifications of the same area and they show a structure comparable to that which one will expect from a shear zone - a kink band fabric. A stereo pair of the same surface is also given in Plate 9.17. As one may infer from the stereographic vision, the area is not representative at all of such a shear zone.

The above observations have been made on a spot in the sample shown in figure 9.18a, and the area is of a 'micro fault' in the specimen of an otherwise perfectly oriented fabric (Plate 9.18b). The upthrow of the microfault is on the right hand side of the micrograph and the surface of the fault plane is crudely visible. Due to improper coating of gold on this surface, the features appear blurred due to excessive accumulation of electric charge. Plate 9.18c shows two views of a model attempting to illustrate the significance of the

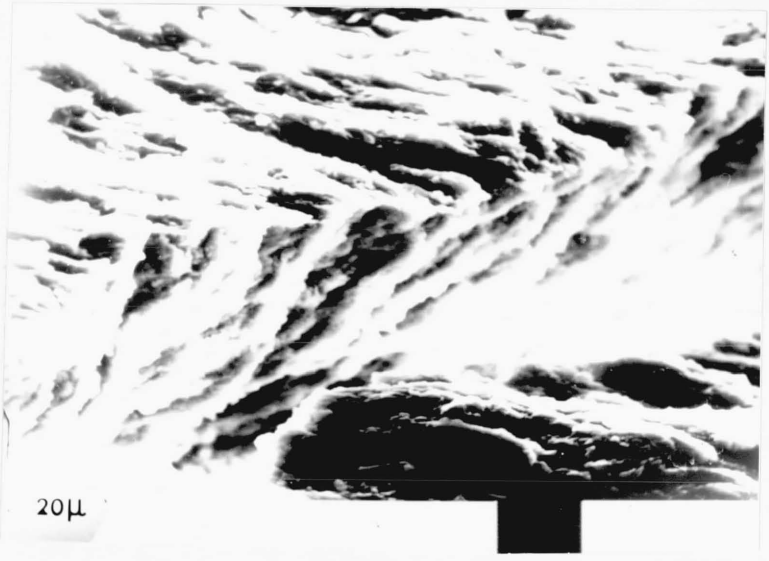
PLATE 9.17 Micrographs suggesting a shear structure by the kink band fabric as shown

	Magnification	Tilt
(a)	x 50	35°
(b)	x 500	35°
(c)	Stereo of the (a) and (b) tile angle difference 7° magnification x 50.	

a



b



c

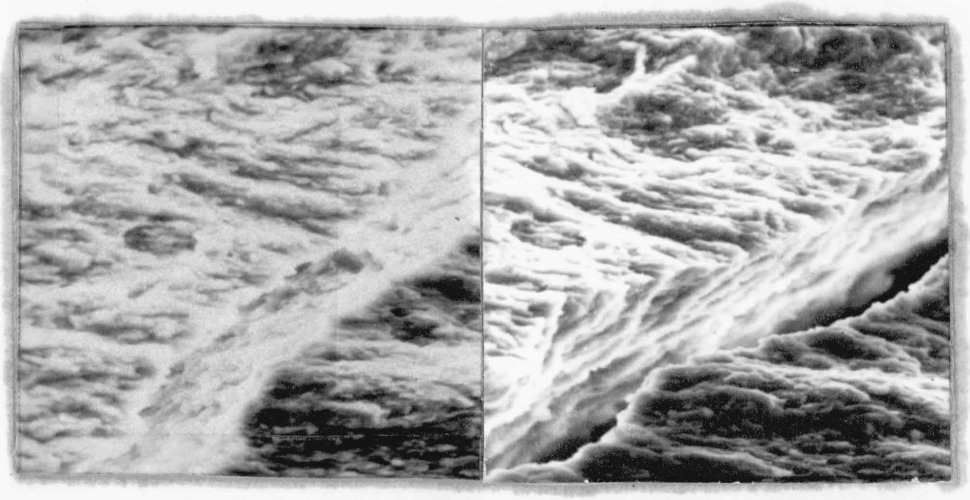
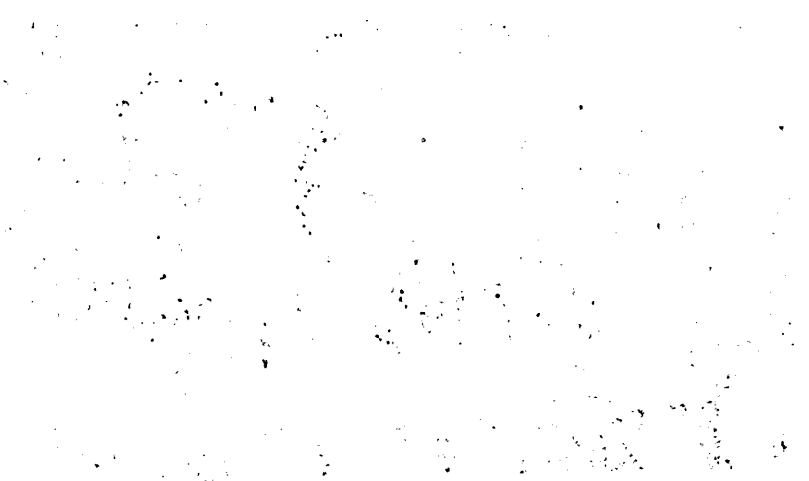


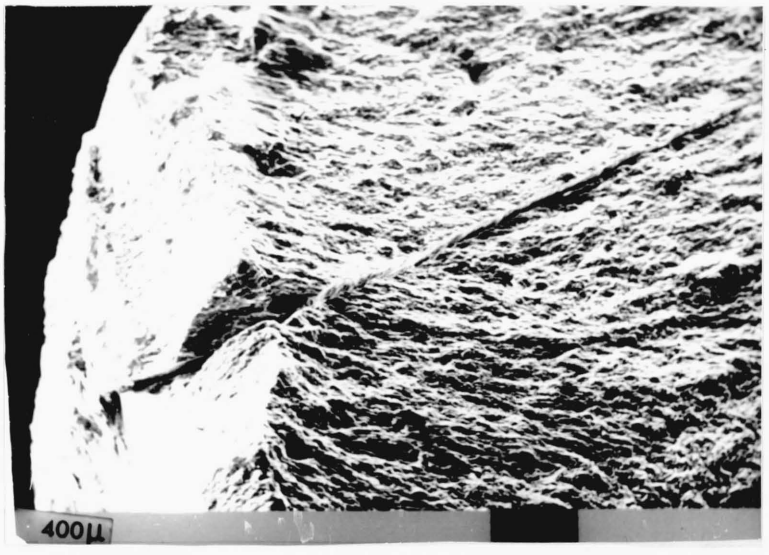
PLATE 9.18 Views of a microfault in a specimen with oriented clay particles:

	Magnification	Tilt
a)	x 20	87
b)	x 200	87

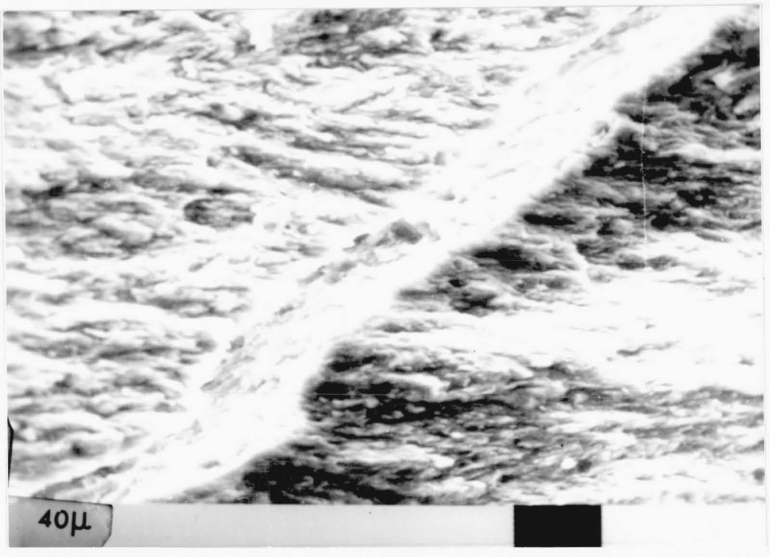
c) A woodwork model illustrating the anomalous effect of an unrepresentative tilt.



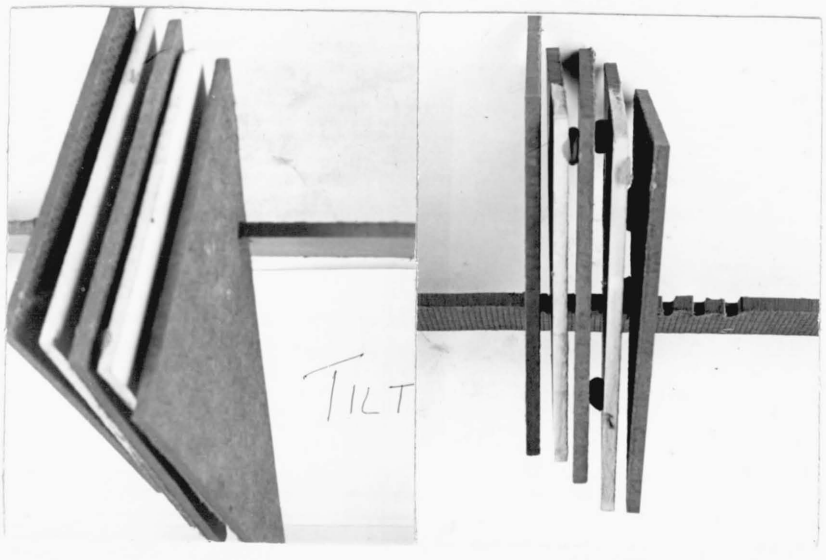
a



b



c



use of a correct tilt angle in observing the fabric so as to avoid obtaining misrepresentative micrographs.

9.8 LOCALISED FABRICS

In fluid sediments of very high moisture content, the discrete sediment particles achieve a preferential orientation direction parallel to the direction of fluid flow. Fine grained clays are more susceptible to the flow than coarse grained particles. With decreasing moisture content the degree of freedom for such orientation is reduced. Such a situation exists in the case of laboratory consolidated sediments.

9.8.1 Flow structures

However, a slightly different process occurs when a consolidated specimen is further loaded. The instantaneous build-up of pore fluid pressure induces pore fluid flow paths which by themselves seek to follow more permeable routes. Clay particles in the vicinity orient themselves along this flow path and thus form flow structures in the fabric of the sediment. Examples of such structures are shown in the following micrographs.

A striking example of flow structuring has already been presented in Plate 2.1. In the micrograph it is clear how the clay particles have followed the path of the water

around the obstacle of a coarser piece of quartz. The fabric is so well affected that even the exact flow direction can be deduced by comparing same with 3.1b, showing a smoke photograph of the classical fluid flow around a spherical obstacle.

Plate 9.19a is a further example of another mode of flow-structuring. The flow here is analogous to a fluid flow around a stagnation point. The clay particles have thus achieved multiple equilibrium directions.

The stereo pairs of Plate 9.19b are an example of contorted pore fluid path. One prime observation is the consistent clay particle orientation at all points along the pore water channel. At each point the particles lay tangential to the contorted pore water channel. It is conceivable that such pore water channels eventually form a fissure. This aspect is discussed in detail later.

9.8.2 Shear structures

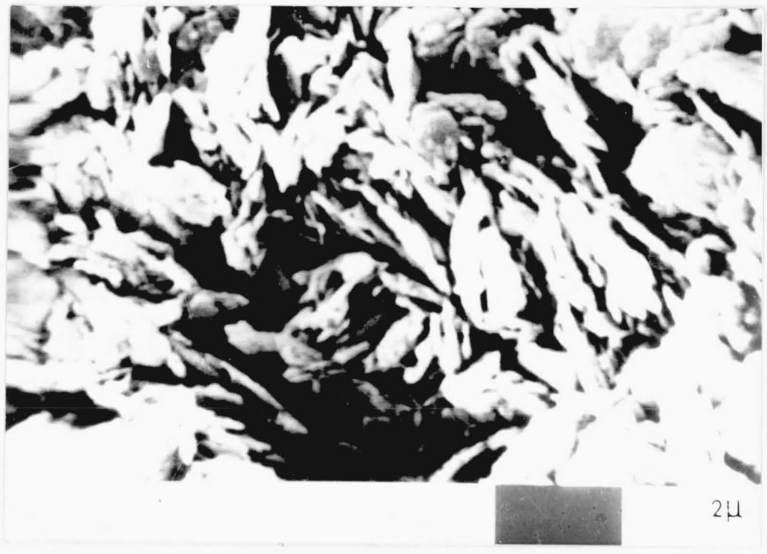
Plate 9.20 shows the optical micrographs obtained from a vertical section of test specimen BC.CHP.18. In this particular test the rate of loading was excessive and amounted to 2.0 lbf/sq.in./min.

Such rapid loading has caused a pattern of penetrative shear structures at the drained end of the specimen (Plate 9.20a).

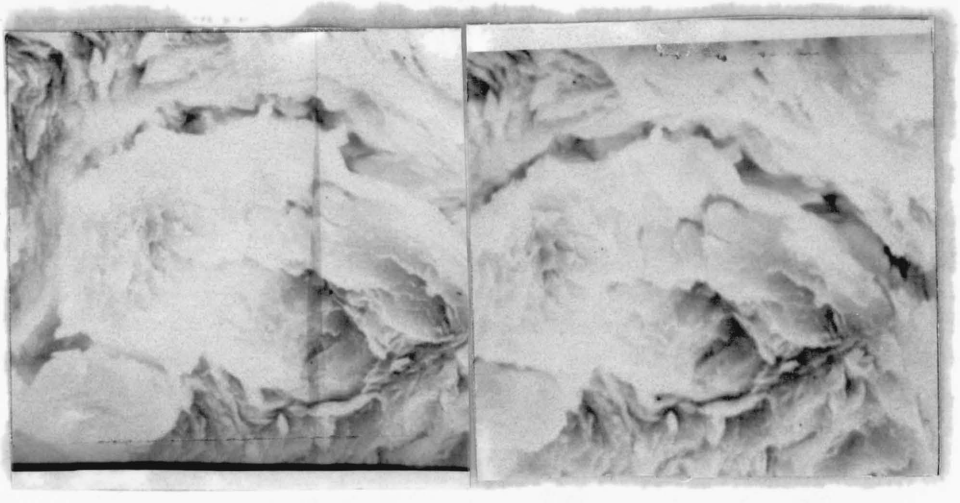
PLATE 9.19 Examples of flow structures

	Sample	Magnification	Tilt
(a)	Test BC.CHP.18	x 10,000	88°
(b)	Test BC.CHP.20	x 2,000	86° & 80°

a



b



The conjugate shear directions are less marked as the section is that near the edge of the specimen. However, its direction may be picked up from the slight toning of the section under crossed nicols (Plate 9.20b and 9.20c).

The dominant preferred orientation of the particles near the drained end of the sample is demonstrated by the strong birefringence in that area (Plate 9.20b and 9.20c).

Similar shear structures have also been observed by Tchalenko (1967) in consolidated specimens of clays remoulded below its liquid limit. In either case it can be argued that these are developed as a result of the progressive growth of pore fluid pressure induced pore water channels described in section 9.8.1. In the current instant rapid loading causes high pore fluid pressures and in the latter, the relative impermeability gives rise also to high pore fluid pressures which initiate the growth of the micro pore water channels.

9.8.3 Edge structures

One chief drawback of the laboratory testing of materials is the indeterminacy of the stress conditions at the edges of the specimens. A similar effect is reflected in the unpredictability of the fabric at these areas.

Plate 9.21 is a series of optical micrographs of a vertical section from a low pressure consolidation test

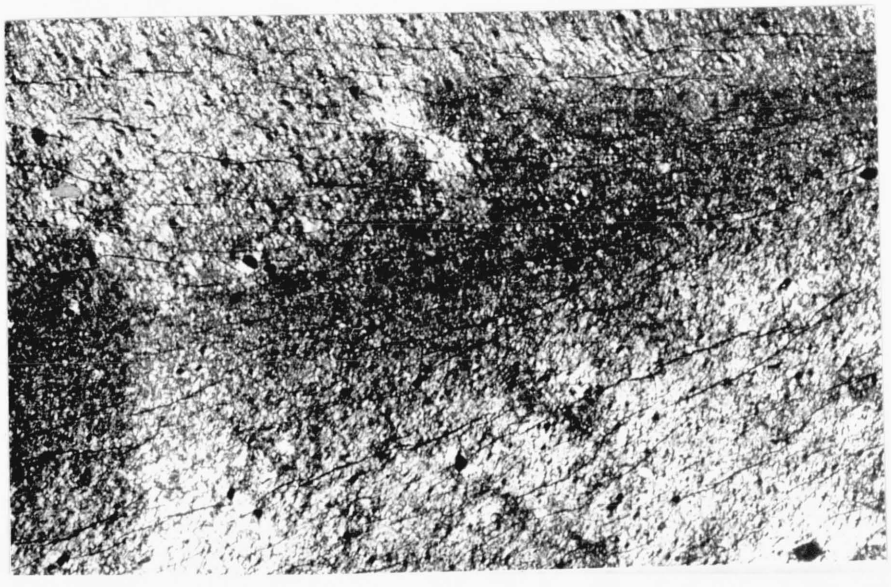
PLATE 9.20 Optical micrographs of a vertical section of test BC.CHP.18 showing shear structures at drained end:

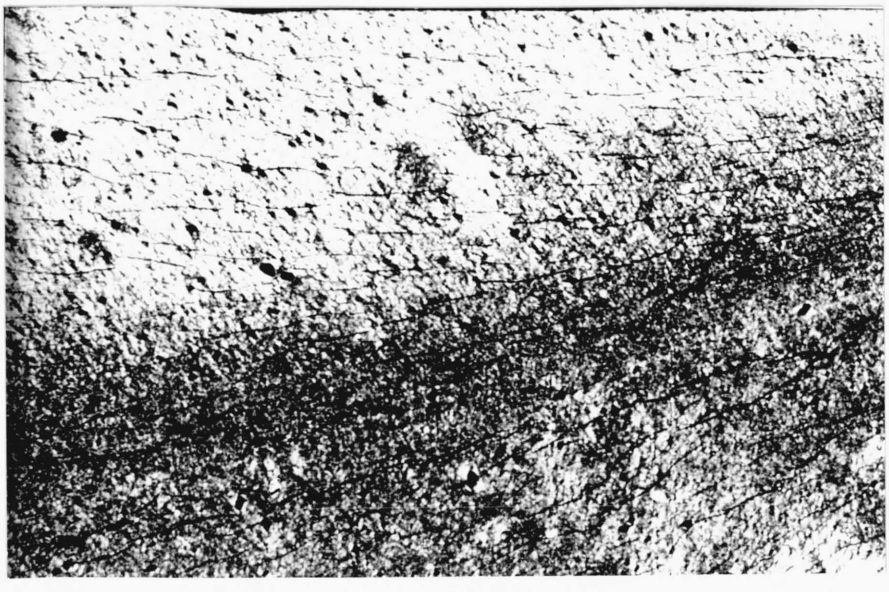
a) ordinary light - x10 magnification

b) crossed polars - x10 magnification extinction

c) crossed polars - x10 magnification illumination







(BC.CLP.4), showing in particular the features near the consolidation ring and the upper porous stone.

The loose fit of the upper porous stone with the ring causes a slight extrusion of the material around the porous stone. This is associated with the development of a series of shear structures (Plate 9.21a).

From plates 9.21b and 9.21c, a characteristic preferred orientation near the ring and the drainage plate is evident. The 'skin friction' between the ring and the clay is the cause for both the preferred orientation near the vicinity of the ring and also the set of slip lines observed as a result of same. The direction of preferred orientation near the ring is in a direction parallel to the ring (or viz. axial). This conforms again with a 'realistic' boundary condition of the drainage direction of the pore fluid in this area. Observations have shown this zone of 'fabric disturbance' is about 10 mm.

Hereto the orientation of the particle near the drainage end is clearly marked.

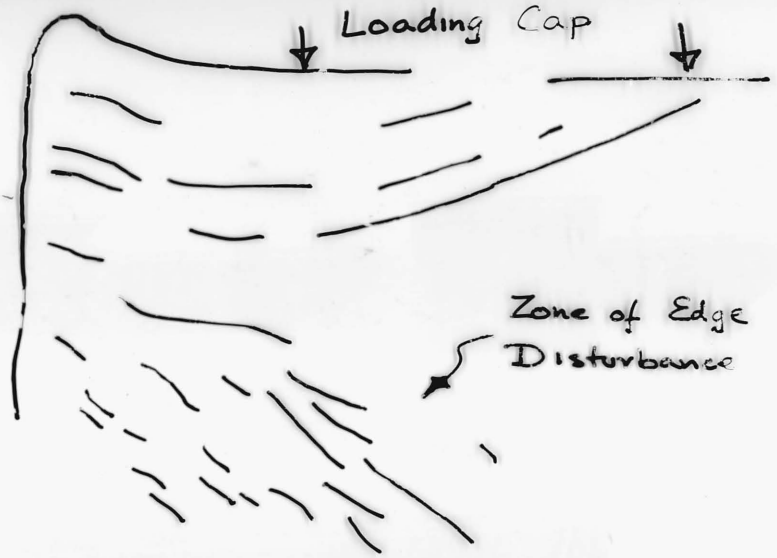
In the high pressure consolidation tests the above effect of sample extrusion at the edges was avoided by the use of scraper blades (see figure 7.2), and it was logical to investigate its influence on the fabric.

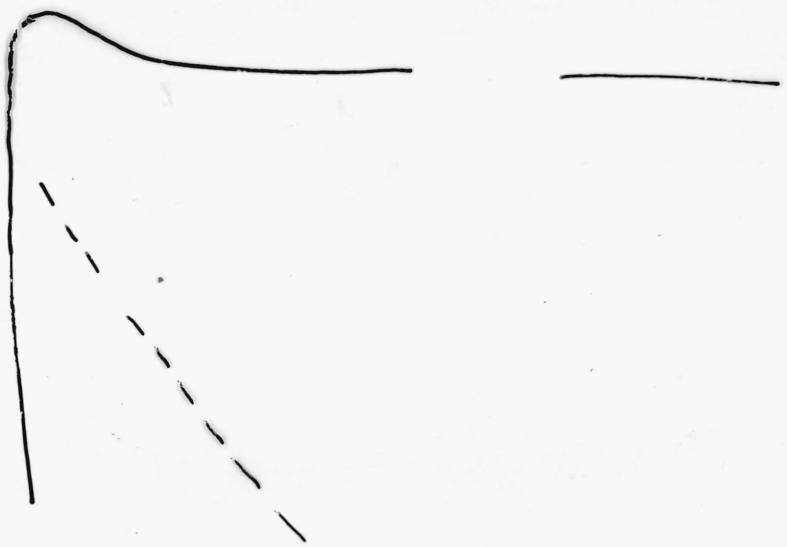
PLATE 9.21 Loading cap and ring effect on fabric during low pressure consolidation (BC.CLP.4):

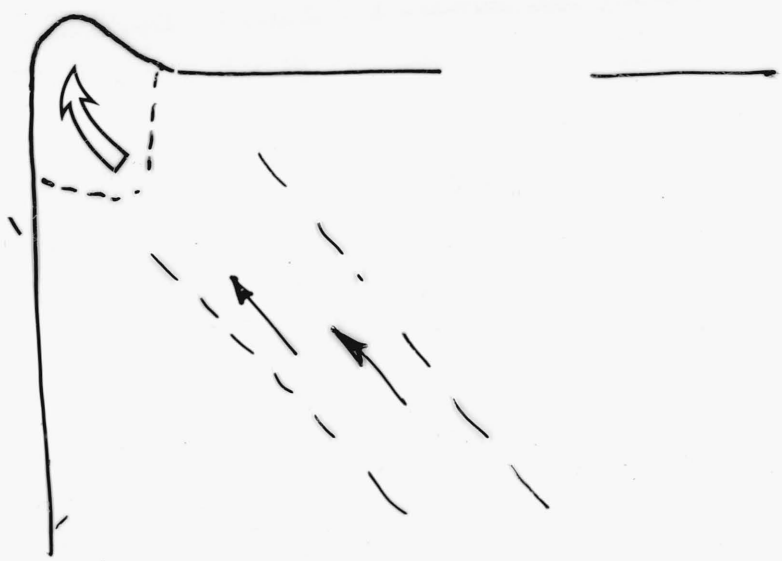
a) Ordinary light x 10 magnification.

b) Crossed polars x 10 extinction.

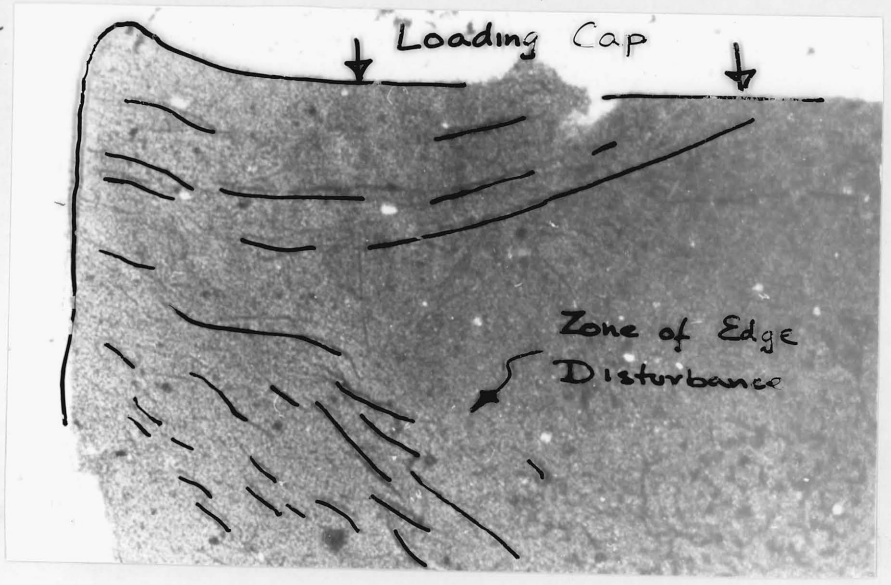
c) Crossed polars x 10 illumination.


Loading Cap
Zone of Edge
Disturbance

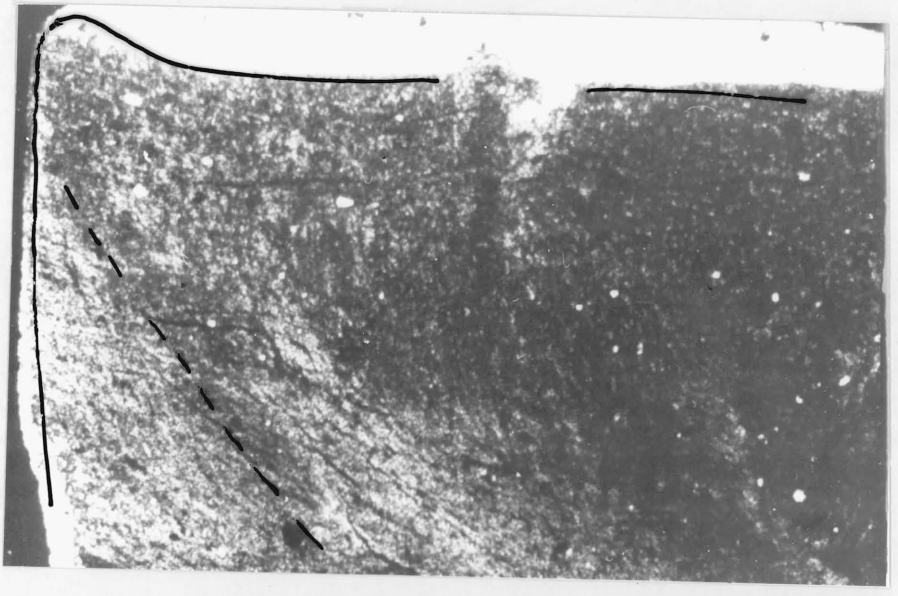




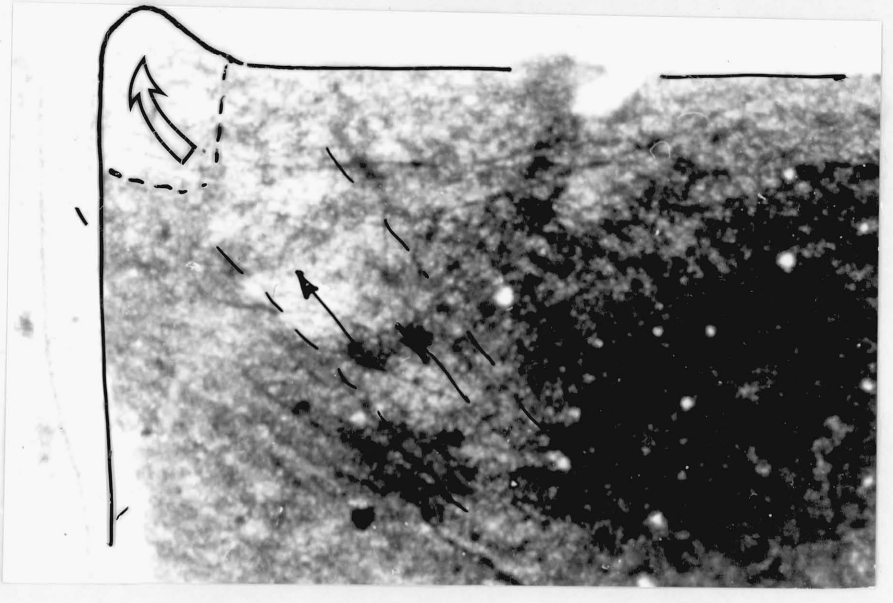
a



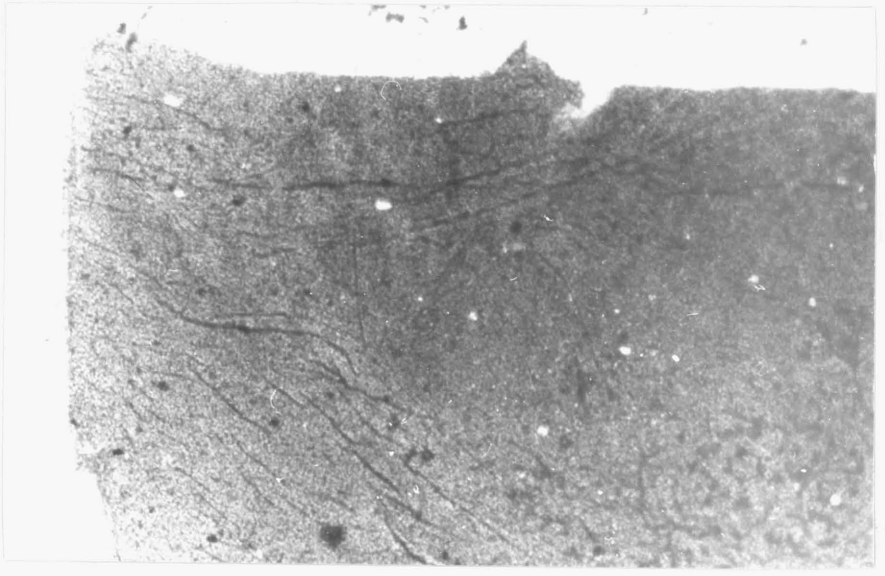
b



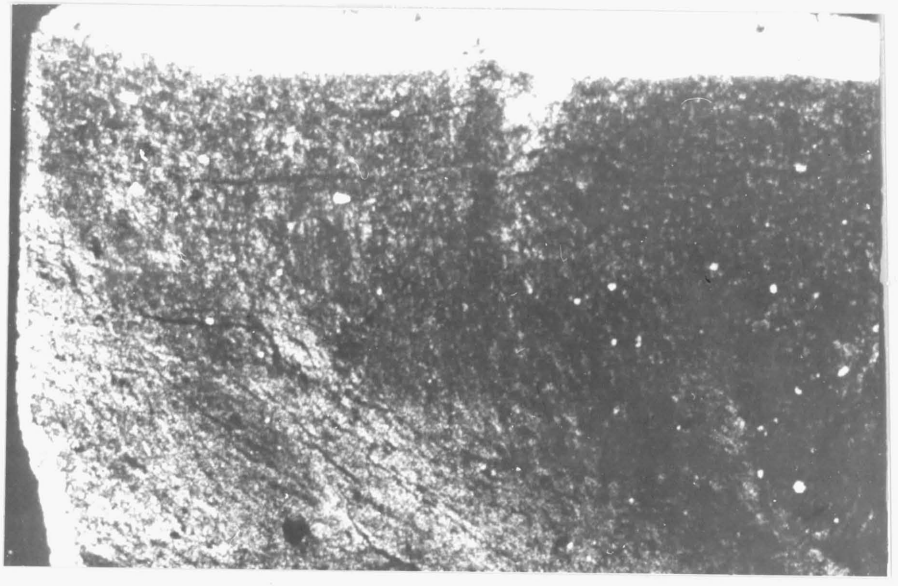
c



a



b



c

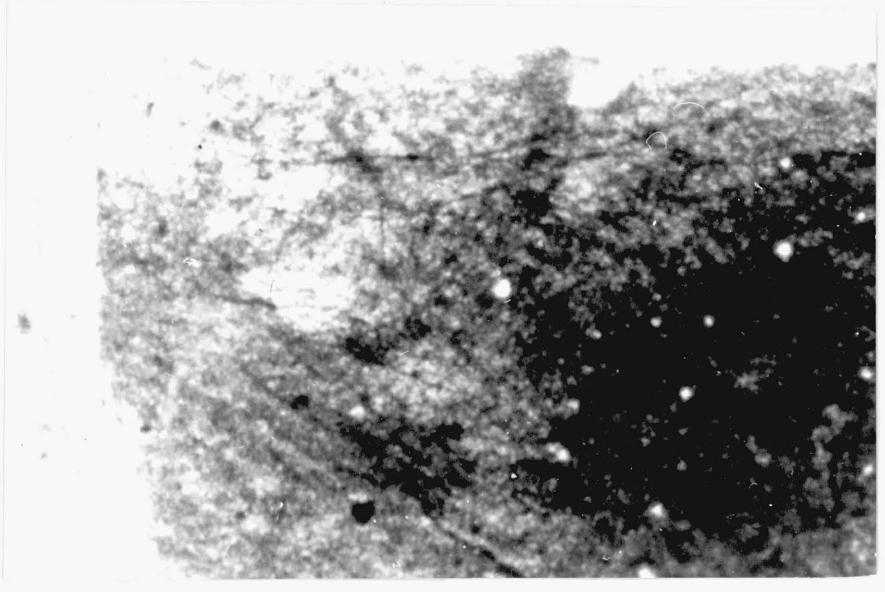


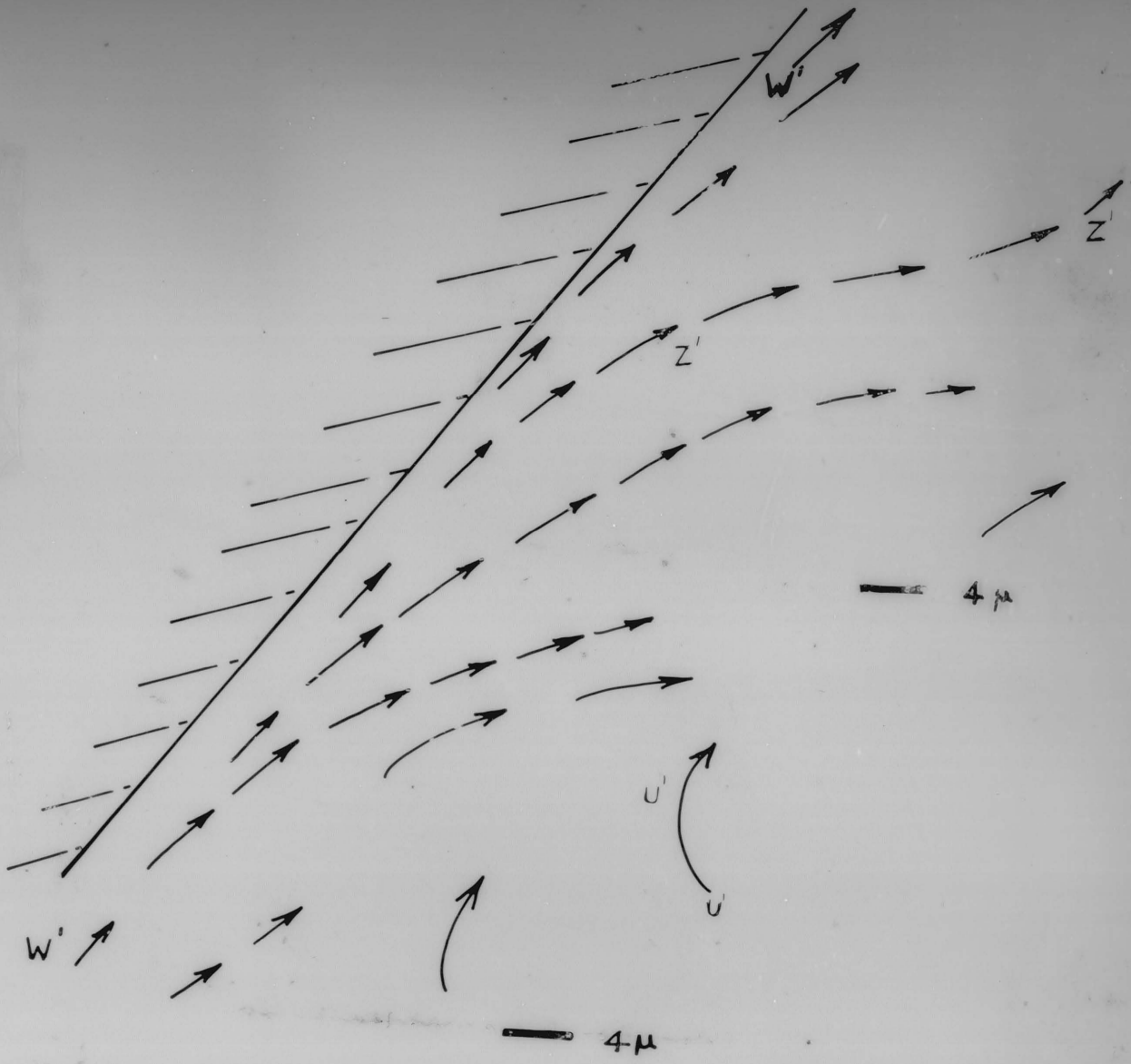
Plate 9.22 illustrates the electron microscope observation of such an area. Plate 9.22b shows a general area at a low magnification but the details near the scraper blade clay interface is blurred due to excessive charging of electrons on the edges of the clay particles. Therefore a mosaic of higher magnification micrographs are presented in Plate 9.22a. Details of the fabric in it very clearly indicates an orientation of the particles in a direction parallel to the surface of the scraper blade. This observation is further confirmed by the Fourier diffraction pattern (Plate 9.23) of the micrograph in Plate 9.22b.

This direction of preferred orientation is to be expected considering that the flow of the pore water at this point will also be parallel to the surface of the scraper blade (direction w'w') (see figure 7.2b). Deviations of particle orientations from above is also governed by the path of the pore fluid flow towards the drainage end. It is very clear that on the background of weak horizontal orientation of particles (shown by the diffraction line ZZ), there are many other fairly strong orientation directions superimposed. One of them (ww) represents the orientation of particles parallel to the wiper blade (direction w'w') whereas the other minor diffraction line represents other flows structured particle orientation direction such as u-u.

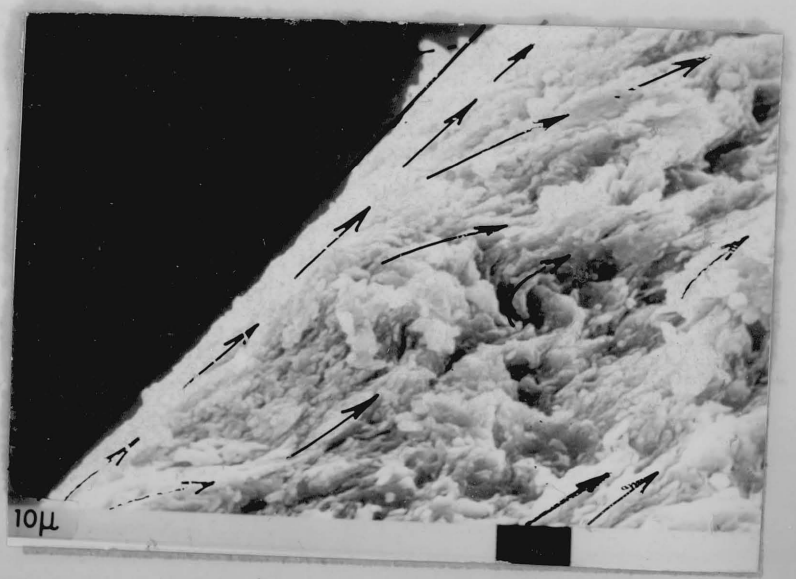
PLATE 9.22 Edge effects in high pressure consolidation tests:

a) mosaic of photograph magnification 5,000; tilt 80°

b) a general view magnification 2,000; tilt 80°


W'
Z'
Z'
4 μ
U'
U'
W'
4μ


W'
Z'
4 μ
W'
4-μ


10μ



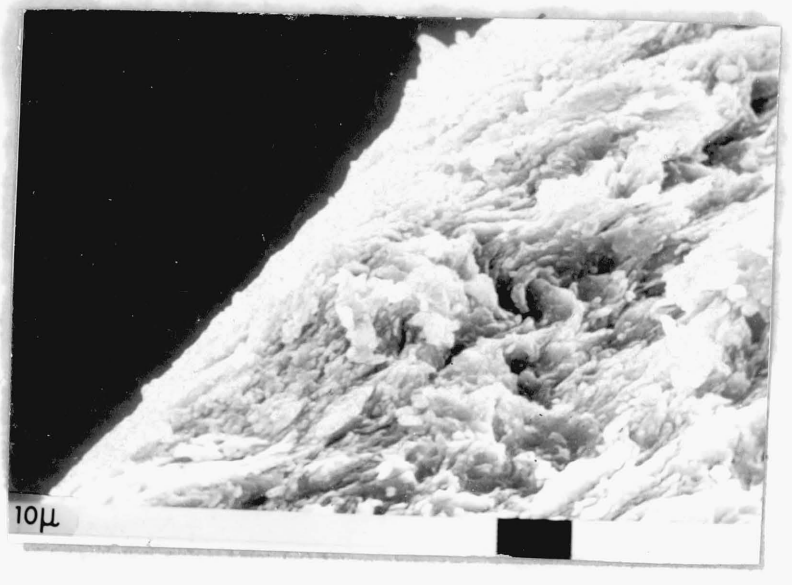
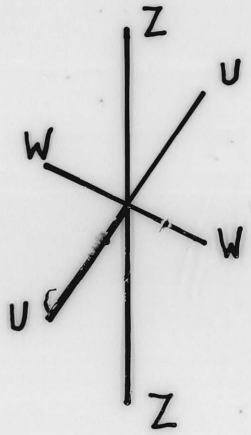

10μ

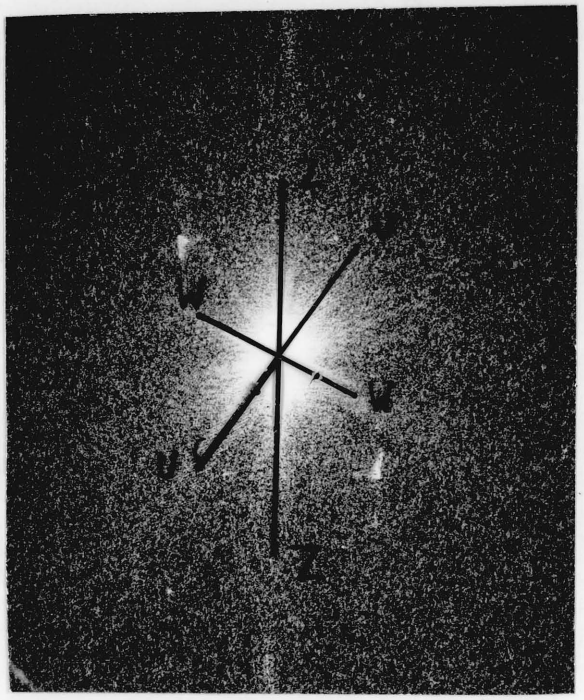
PLATE 9.23 Fraunhofer diffraction pattern of Plate 9.22(b):

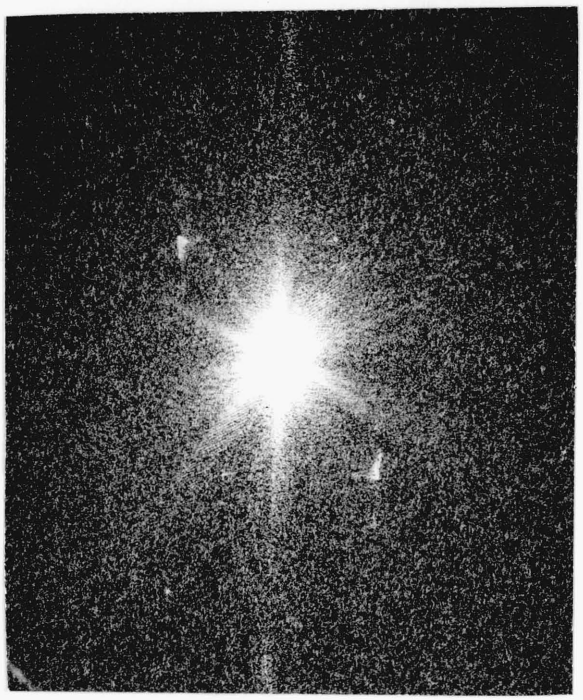
ZZ diffraction line for horizontal orientation of particles

WW diffraction line for orientation parallel to wiper blade surface

UU lesser order flow structure


Z
U
W
W
U
Z


X
W
W
W
Z



The above particle orientations are further detected from the optical micrographs of Plate 9.24. This is a clear example of fabric inhomogeneity (section 9.5.2.2). Figure 9.8 is a series of rosettes of the intensity of transmitted light as observed at a sequence of points within the specimen from the drainage end as indicated. It is also made clear that the expected symmetry of the intensity rosette improves away from this zone of fabric disturbance.

It is noteworthy to reemphasise that all the fabrics described in section 9.8 showed dependence on the pore fluid drainage path.

9.9 PERFECT PREFERRED ORIENTATION

It is now easy to deduce from the observations cited earlier, the conditions that promote the development of preferred orientation. Prime consideration must be given to suppressing the build-up of excessive pore fluid pressures, which can be affected by the consolidation of thin samples at a very slow rate of loading.

9.9.1 Laboratory samples

It was fortuitous in this study to have inadvertently obtained a specimen consolidated under such conditions. In the test BC.CHP.19, a very small amount of clay (about 5 grams) had

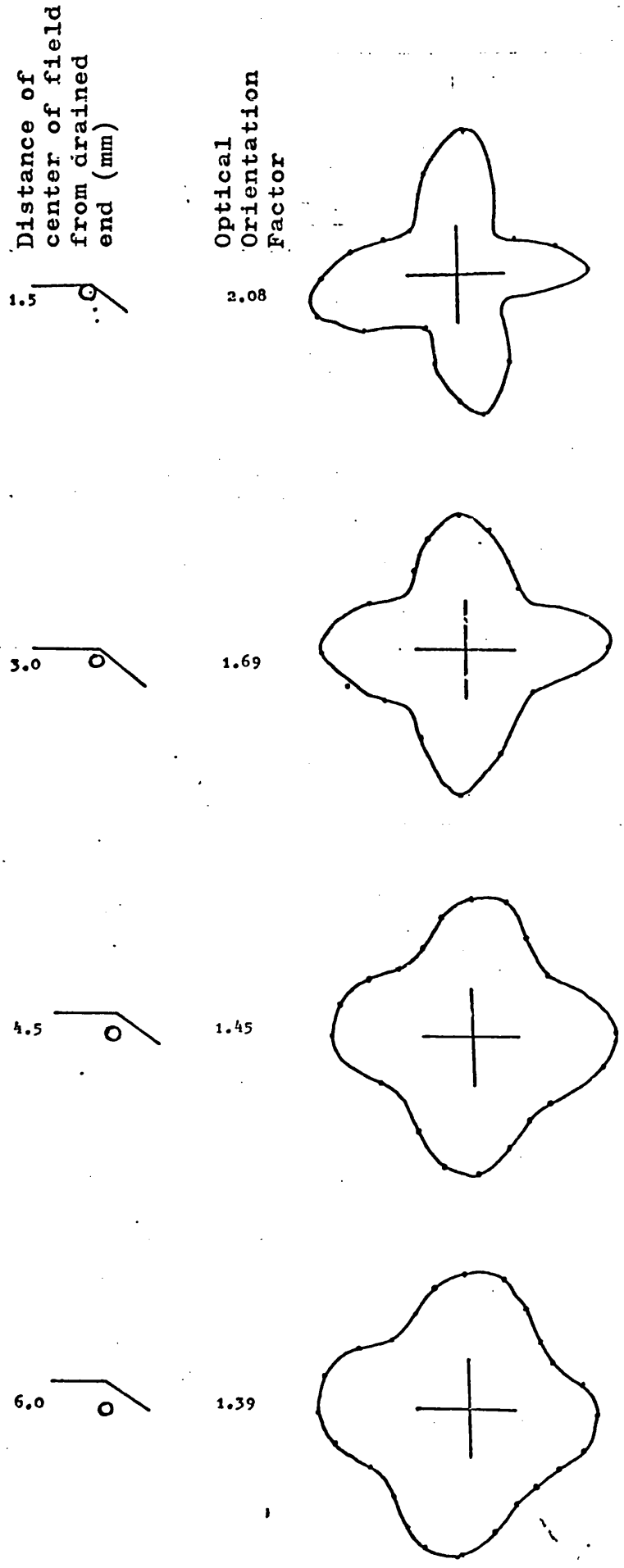
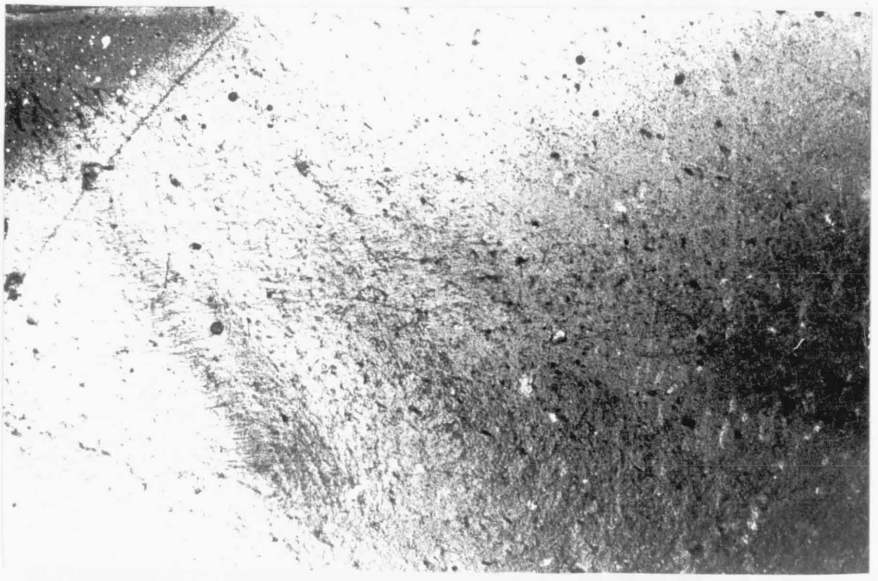


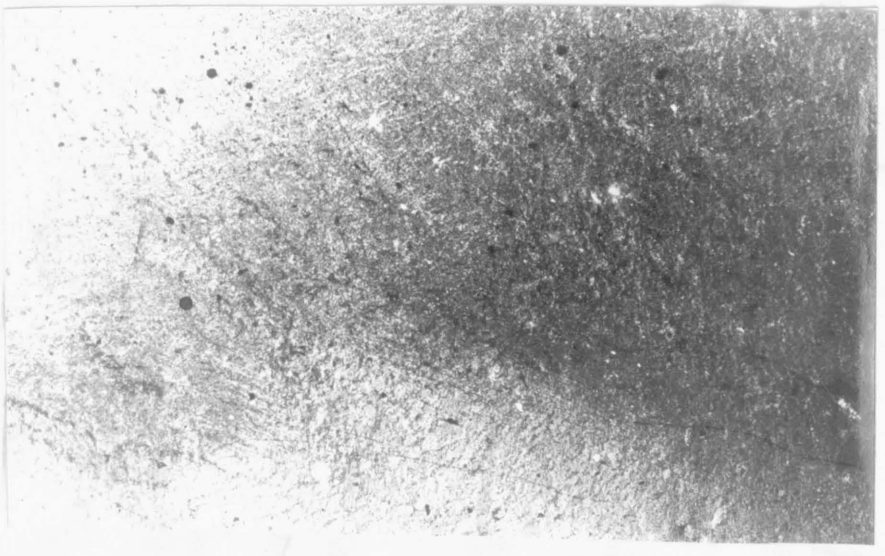
FIGURE 9.8 Optical Illumination rosettes at distinct points away from the drained end of a consolidated specimen

PLATE 9.24 Optical micrographs of a vertical section from the undrained end of a test BC.CHP.15 showing orientation near wiper blade:

(a) crossed polars - x 10 magnification
- illumination

(b) crossed polars - x 10 magnification
- extinction





remained between the filter paper and the porous plate of the drained end. Accordingly the specimen was thin (2 mm in thickness), was loaded very slowly (0.5 lbf/sq.in./min.) and drained from both ends. A series of electron micrographs of the specimen at different magnification has already been shown in Plate 9.16. Plate 9.25 is a stereo pair of the high magnification. There is a slight disturbance in fabric off the orientation direction which may be the result of shrinkage.

9.9.2 Natural samples

Plate 9.26 is an optical micrograph of a thin section of the shale specimen shown in the frontispiece (Plate 1.1). This plate highlights a typical geological drainage boundary. By virtue of the difference in grain size of the silt stone and the shale, the silt stone is more permeable to pore fluids and accordingly acts as an efficient drainage surface. It is clear that the original sedimentation has been in small increments. Thus the sedimentation is favourable for the development of a preferred orientation. Plate 9.27 is an electron micrograph of the shale, showing the constituting coarse grained illite particles aligned preferentially parallel to the drainage surface.

There exists no better example of preferred orientation than the natural habitat of freshly altered Kaolinite

PLATE 9.25 Stereo electron micrograph of specimen from drained end of BC.CHP.19.

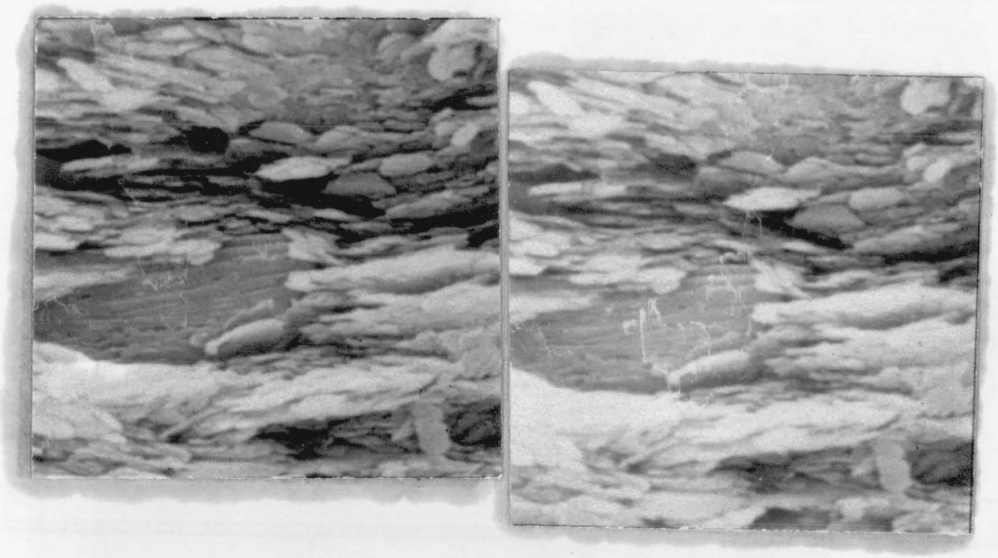


PLATE 9.26 Optical micrograph of shale specimen (Plate 1.1) showing a geological drainage boundary.

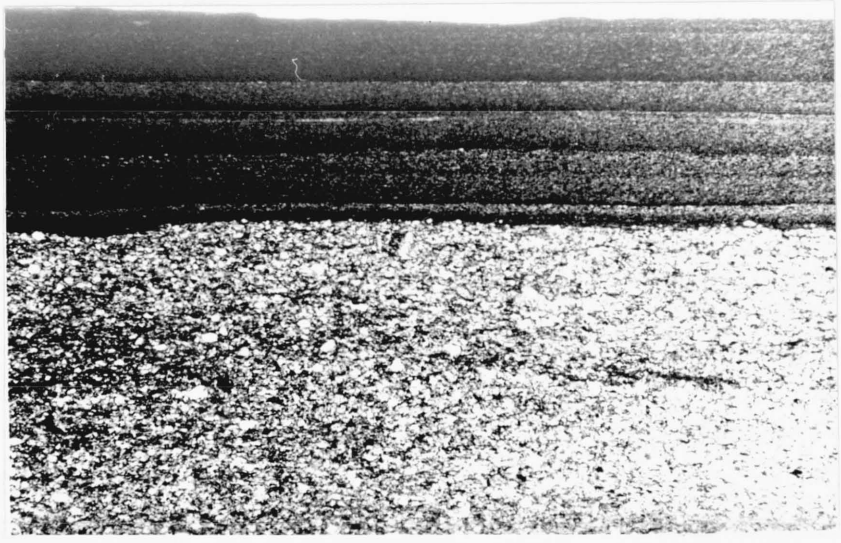
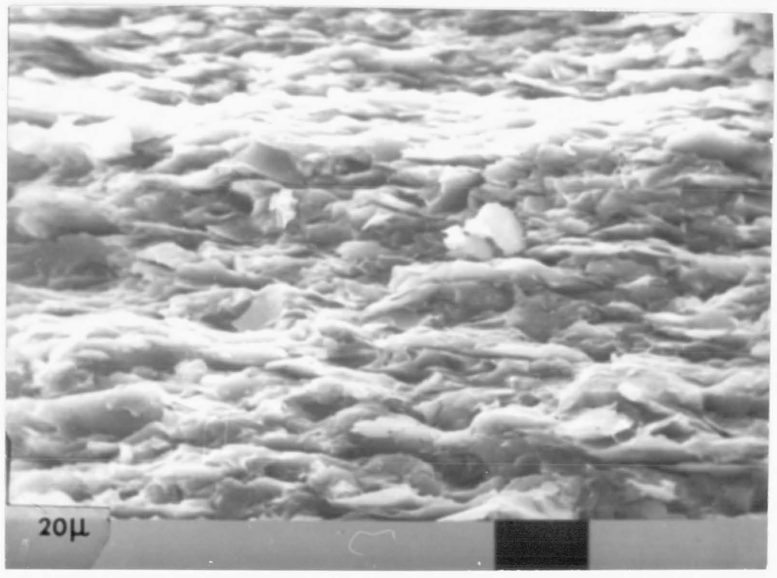


PLATE 9.27 Electron micrograph of the Shale in Plate 9.26:
magnification x 1,000
tilt 86°.


20μ

in its native form of vermicullar Kaolinite. Plate 9.28a shows one such stack of perfectly oriented clay particles. Plate 9.28b is the respective diffraction pattern for same, confirming other regular order of orientation in the 'stack'.

9.10 FABRIC OF NATURAL SAMPLES

In this section fabric observations of the undisturbed field samples of the Falmouth sediments, Petrockstow (stoneware) and Borey (whiteware) ball clays are described.

9.10.1 Falmouth sediments

Plate 9.29 is an optical micrograph of the Falmouth sediments and it shows a somewhat coarse texture with elongated mica particles set in the matrix of finer silts and clays.

The Plate 9.30b is a more detailed electron microscopic view of the sediments and serve to show the silt and clay sized particles with mica particles and stacks of vermicullar Kaolinite. Plate 9.30a is a stereo pair with more details of the vermicullar structure of the kaolinite, while the stereo pair of Plate 9.30c shows the details of flocculated fabric with edge to face contacts in the unconsolidated sediments.

The X-ray diffraction peak ratio of 0.27 and the birefringence ratio of 0.987 is further confirmation of the

PLATE 9.28

a) Electron micrograph of a vermicullar Kaolinite - an example of the 'stack' structure.

b) Fraunhofer diffraction pattern of 9.28(a).

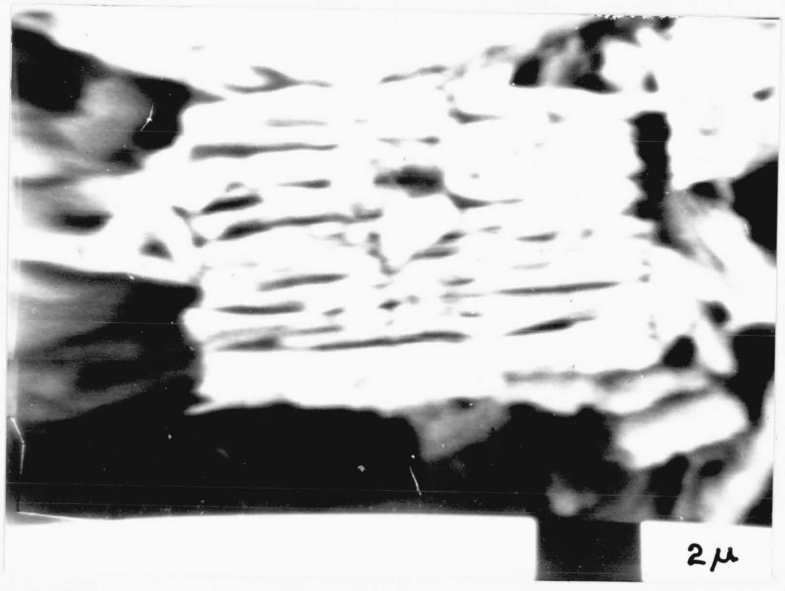

2μ



PLATE 9.29 Optical micrograph of Falmouth sediment; magnification x 10.

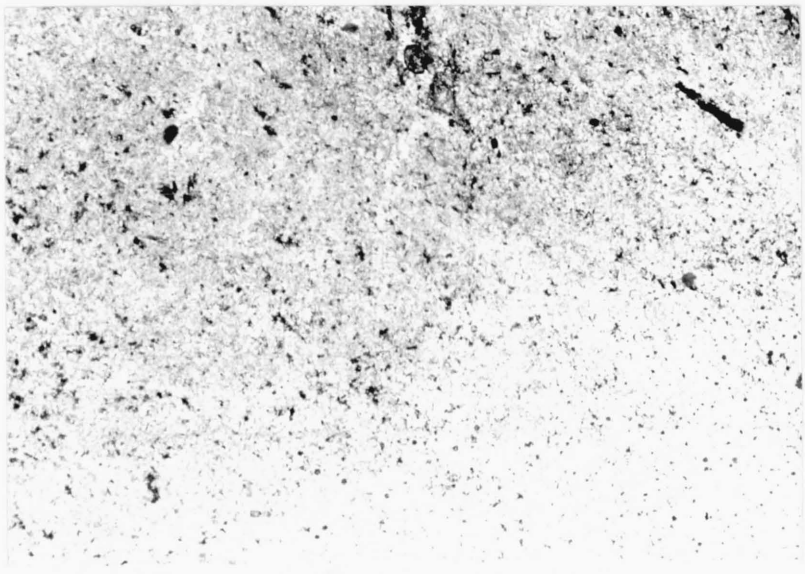


PLATE 9.30 Electron micrographs of undisturbed Falmouth clay:

(a) Stereo pair of vermicullar Kaolinite

Magnification 5,000 x 2
Picture width 12μ
Tilt angle difference 6°

(b) General monoscopic view of sediment

Magnification 2,000 Tilt 75°

and its corresponding Fraunhofer diffraction trace.

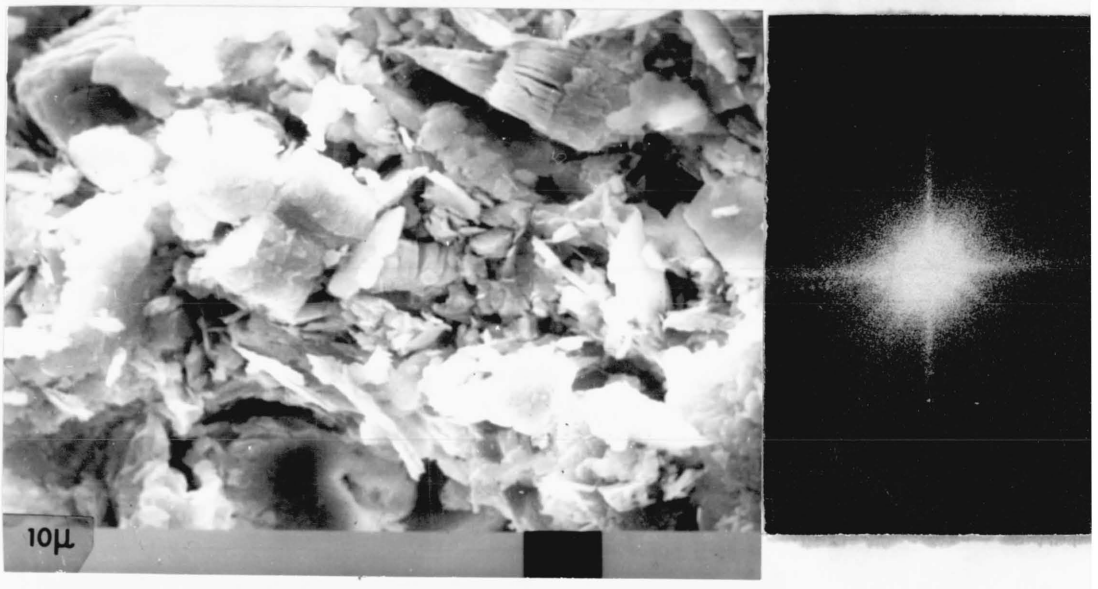
(c) Stereo pair of particle contacts in flocculated structure,

Magnification 5,000 x 2
Picture width 12μ

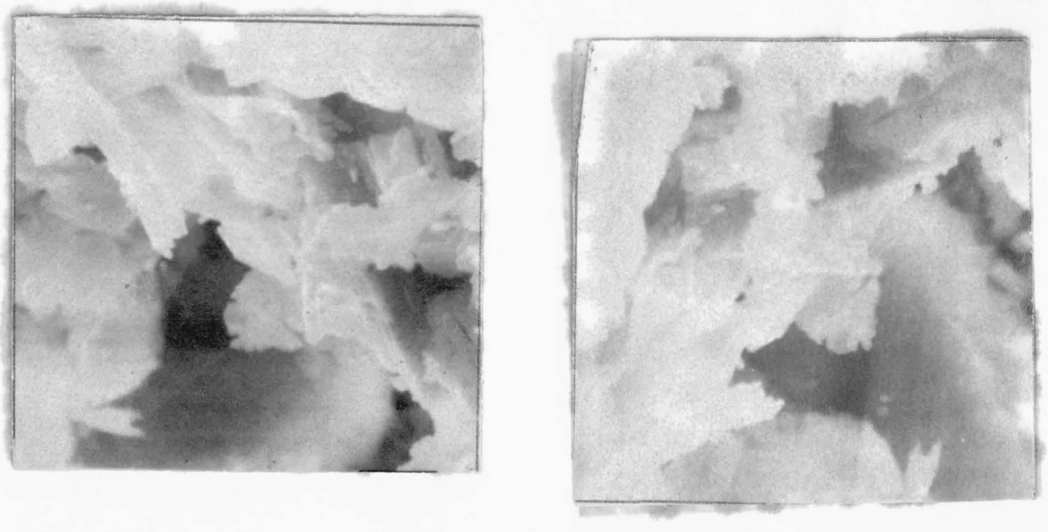
a



b



c



random fabric seen in the micrographs. The Fraunhofer diffraction trace of the micrograph is also shown in Plate 9.30 and it indicates a random fabric.

9.10.2 Ball clays

Plate 9.31 compares the optical micrographs of the two varieties of Ball Clay - stoneware and whiteware clay. A distinct difference is the presence of lignite in the whiteware clays. It is difficult to specify a single orientation direction even for the lignite seams.

The electron micrographs in Plate 9.32 fail to show any preferred orientation in the clays too. But instead, they show a heavily flow structured fabric.

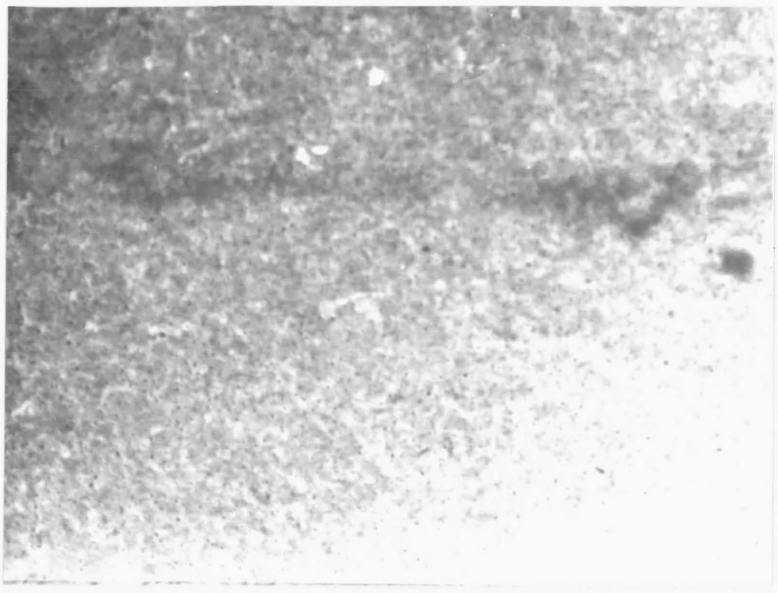
9.10.3 Comparison of the natural fabric with the fabric of artificial compacted sample

The lack of orientation in the ball clay was of concern, as it was popularly considered to be "overconsolidated". A relatively low preconsolidation stress of the order of 290 lbf/sq.in. (section 7.3) and the quantitative fabric contradict this popular belief. It must, however, be pointed out that the block sample of the clay analysed was obtained from the surface and may have been subjected to some degree of softening. Higher degrees of orientation may be found at depth.

PLATE 9.31 Optical micrographs of Stoneware and Whiteware Ball Clays:

a) Stoneware Ball Clay
Ordinary light x 10 magnification.

b) Whiteware Ball Clay
Ordinary light x 10 magnification.



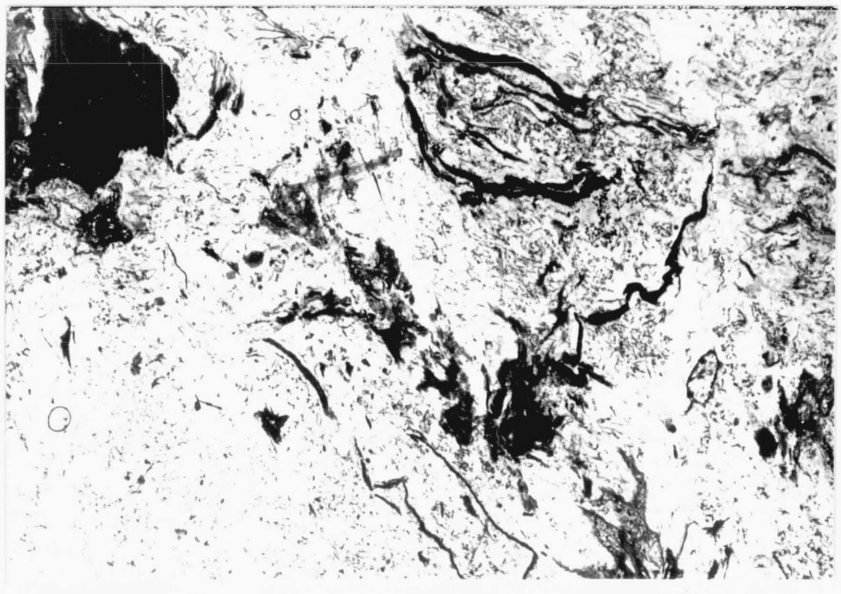
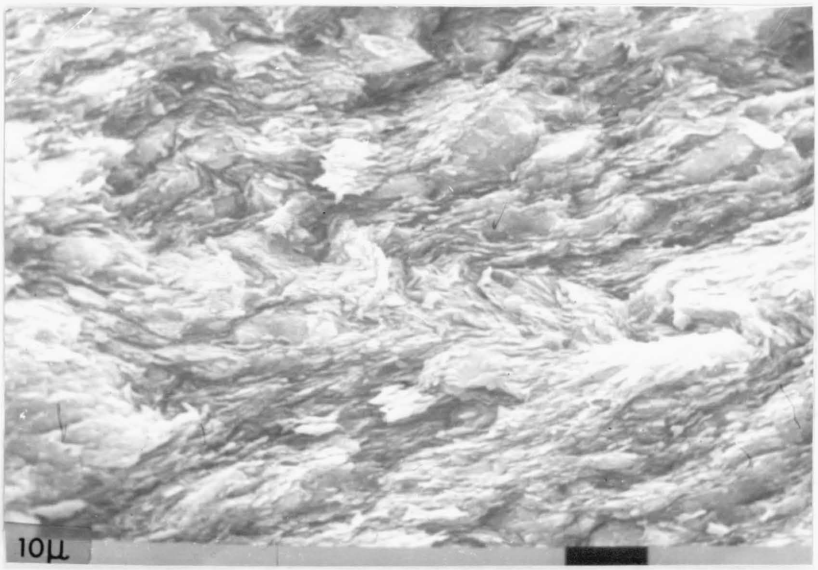
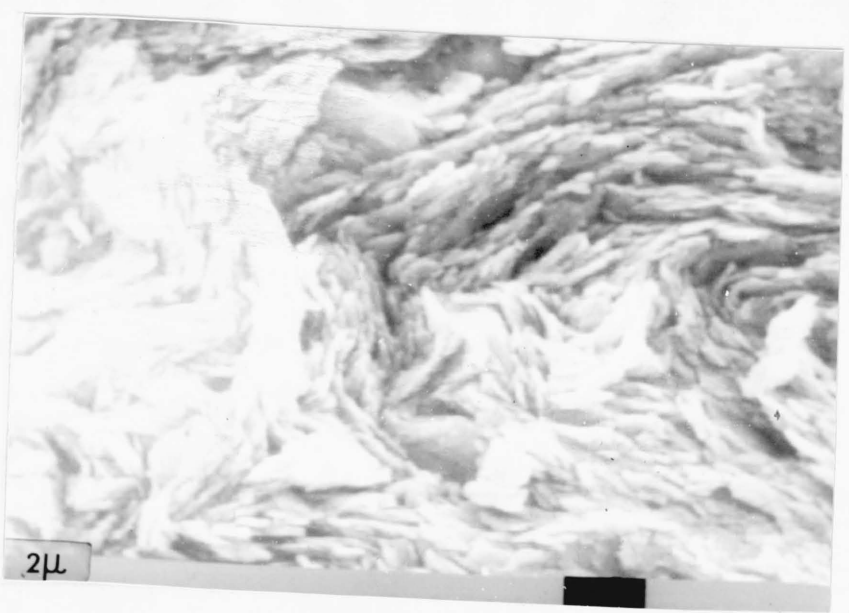


PLATE 9.32 Electron micrographs of stoneware ball clay showing heavily flow structured fabric;

(a) Magnification x 2,000 Tilt 80°
(b) Magnification x 5,000 Tilt 85°
(c) Magnification x 10,000 Tilt 85°


10μ


~μ


2μ

However, the absence of such may support the belief of Best and Fookes (1970) that during the process of burial the sediments retained the fabric acquired during the initial drying (see also discussion in section 9.11).

Plate 9.33 is a series of photographs showing the stages of fissility development on slaking (according to the experiments described in section 9.4) of the undisturbed Falmouth sediments and Petrockstow ball clay. Their performance is compared with that of BC.CHP.19. No emphasis is needed on the powerfulness of this test in showing the difference in the orientation degree, and conforming with the earlier observations.

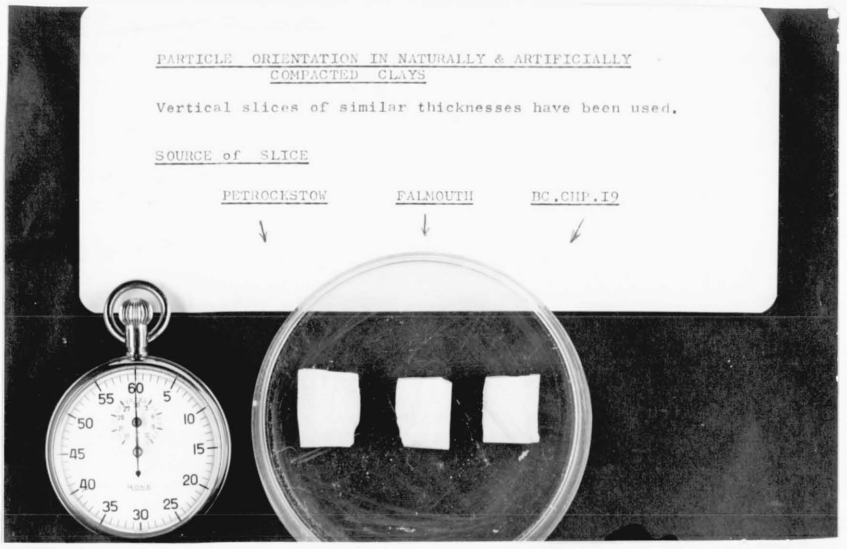
9.11 DEVELOPMENT OF FABRIC WITH CONSOLIDATION

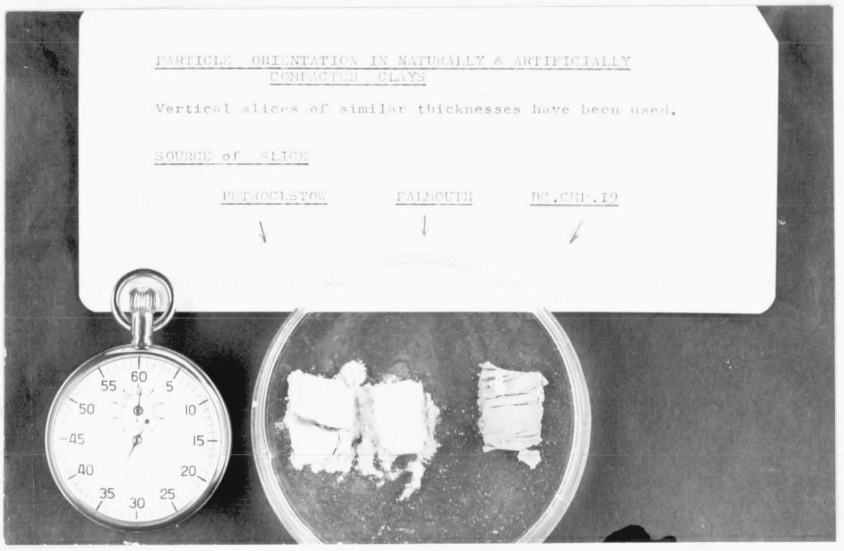
As discussed earlier, the fabric resulting from the processes of consolidation and subsequent rebound has been analysed quantitatively using X-ray diffraction and optical microscopy. Results of the optical microscopy are given in Table 9.I. The results of the X-ray analysis are shown in Tables 9.II, 9.III and 9.IV.

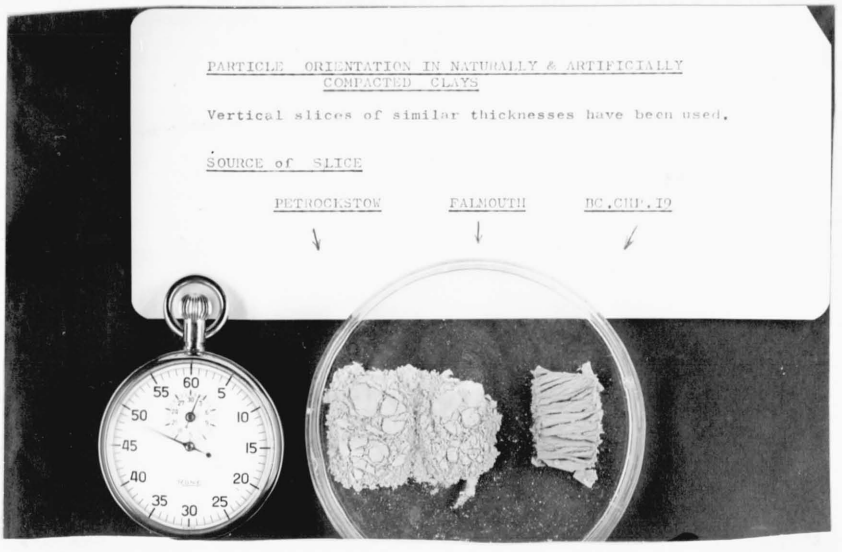
Following on from the discussion of the process of flow structuring, it is clear that equal resistance is offered by the fabric to develop a preferred orientation. The development of preferred orientation is best effected by consolidating samples of very high moisture content. Figure 9.6 shows the

PLATE 9.33 Comparison of the degree of particle orientation in undisturbed Ball Clay, Falmouth Clay and from test BC.CHP.19 using the fissility experiment:

a) before test;
b) 1.5 minutes after adding water;
c) 3 minutes after adding water.


PARTICLE ORIENTATION IN NATURALLY & ARTIFICIALLY COMPACTED CLAYS
Vertical slices of similar thicknesses have been used.
SOURCE of SLICE
PETROCKSTOW
FALMOUTH
BC.CHP.I9


PARTICLE ORIENTATION IN NATURALLY & ARTIFICIALLY COMPACTED CLAYS
Vertical slices of similar thicknesses have been used.
SOURCE of SLICE
PETROCKSTOW
FALMOUTH
BC.CHP.I9


PARTICLE ORIENTATION IN NATURALLY & ARTIFICIALLY COMPACTED CLAYS
Vertical slices of similar thicknesses have been used.
SOURCE of SLICE
PETROCKSTOW
FALMOUTH
BC.CHP.I9

Stress History	Sample from Test Number	Remarks	Overall Birefringence Ratio β_{av} $\Sigma I_{min}/\Sigma I_{max}$	Anisotropy Index $\frac{\Sigma I_{max} - \Sigma I_{min}}{\Sigma I_{max} + \Sigma I_{min}}$	Discrete Values β_1	β_2	β_3	β_4	Standard Deviation	Mean Birefringence Ratio $\bar{\beta}$
Low Pressure Consolidation										
62.2 lbf/sq.in	BC.CLP.1	General area	0.391	0.438	.379	.400	.389	.396	0.009	0.391
31.1 lbf/sq.in	BC.CLP.2	General area	0.452	0.382	.451	.442	.450	.466	0.01	0.452
15.55 lbf/sq.in	BC.CLP.3	General area	0.514	0.563	.563	.526	.468	.508	0.039	0.516
	BC.CLP.3	Area near loading cap edge (see Plate 9)	0.734	0.153	.652	.778	.857	.666	0.084	0.738
7.25 lbf/sq.in	BC.CLP.4	General area	0.674	0.194	.726	.688	.638	.648	0.04	0.675
	BC.CLP.4	near loading cap edge	0.714	0.164	.686	.672	.726	.790	0.053	0.715
High Pressure Consolidation - Remoulded Clays										
	BC.CHP.12	Drained end	0.434	0.394	.416	.426	.424	.471	0.025	0.434
	BC.CHP.12	Undrained end	0.551	0.269	.555	.564	.542	.538	0.012	0.55
	BC.CHP.14	Drained end Near scraper	0.64	0.23	.60	.78	.65	.57	0.09	0.65
	BC.CHP.14	blade of drained end	0.77	0.128	.75	.783	.803	.754	0.03	0.772
	BC.CHP.14	Undrained end	0.87	0.07	.875	.862	.862	.875	0.02	0.868
	BC.CHP.14	Near scraper blade - Undrained end	0.89	0.058	.787	.803	.82	.806	0.013	0.804
	BC.CHP.15	Drained end	0.362	0.471	.363	.339	.379	.365	0.016	0.361
	BC.CHP.15	Undrained end	0.378	0.450	.365	.387	.367	.394	0.014	0.378
	BC.CHP.17	Drained end	0.362	0.467	.376	.365	.375	.345	0.014	0.362
	BC.CHP.17	Undrained end	0.44	0.381	.439	.412	.446	.500	0.037	0.449
	BC.CHP.18	Drained end	0.48	0.354	.447	.483	.520	.570	0.029	0.482
	BC.CHP.18	Near scraper blade of drained end	0.342	0.489	.310	.352	.367	.343	0.023	0.343
	BC.CHP.18	Undrained end	0.530	0.307	.531	.560	.515	.515	0.02	0.530
	BC.CHP.18	Near scraper blade of undrained end	0.537	0.301	.495	.549	.568	.543	0.03	0.538
	BC.CHP.19	Drained end	0.379	0.435	.373	.366	.363	.418	0.025	0.380
	BC.CHP.19	Near scraper blade of drained end	0.359	0.471	.348	.345	.352	.393	0.022	0.359
	BC.CHP.19	Undrained end	0.51	0.33	.48	.49	.51	.54	0.03	0.51
	BC.CHP.20	Drained	0.543	0.295	.55	.577	.542	.506	0.029	0.545
	BC.CHP.20	Near scraper blade of drained end	0.523	0.313	.51	.532	.500	.555	0.024	0.524
	BC.CHP.20	Undrained end	0.570	0.277	.597	.551	.552	.561	0.021	0.565
	BC.CHP.20	Near scraper blade of undrained end	0.590	0.254	.600	.556	.588	.635	0.032	0.594
	BC.CHP.21	Drained end	0.290	0.55	.28	.29	.32	.24	0.017	0.295
	BC.CHP.21	Undrained end	0.680	0.19	.622	.670	.753	.702	0.06	0.686
	Falmouth Clay									
	Undisturbed	Vertical General	0.880	0.063	.91	.885	.865	.859	.022	.880
	N.FA.CHP.2		0.813	0.102	.839	.801	.785	.841	.027	.816
	Petrockstow Ball Clay									
	Undisturbed		0.977	0.001	.967	.98	.98	.987	.008	.978
	N.BC.CHP.1	Drained end	0.917	0.045	.907	.928	.933	.907	.013	.919
		Undrained end	0.967	0.002	.976	.991	.916	.929	.036	.953

SEE TABLE 7-11b

TABLE 9.I QUANTITATIVE OPTICAL MICROSCOPY

Test No. and Position of Specimen	Clay Mineral Lattice	Peak Height Method	Peak Area Method	Corrected Peak Height	Corrected Peak Area Method	Total Count Method	Average per Kg. mineral lattice	Average
BC.CHP.12 (Drained end)	001 K	0.30	0.33	0.35	0.30	0.32	0.32	)
	002 K	0.55	0.58	0.46	0.51	0.40	0.60	) 0.35
	060 K	0.18	0.12	0.23	0.06	0.14	0.14	)
	001 I	0.59	0.67	0.67	0.61	0.62	0.63	)
	002 I	0.55	0.88	0.46	0.71	0.40	0.60	) 0.615
	020K+020I	0.21	0.17	0.23	0.23	0.03	0.17	
BC.CHP.12 (Undrained end)	001 K	0.36	0.27	0.38	0.34	0.35	0.34	)
	002 K	0.19	0.28	0.24	0.30	0.18	0.23	) 0.27
	060 K	0.18	0.15	0.71	0.15	0.10	0.25	)
	001 I	0.81	0.56	0.91	0.53	0.70	0.70	)
	002 I	0.42	0.37	0.40	0.40	0.58	0.43	) 0.56
	020K+020I	0.36	0.42	0.34	0.42	0.63	0.43	
BC.CHP.14 (Drained end)	001 K	0.30	0.30	0.33	0.27	0.31	0.30	)
	002 K	0.15	0.12	0.18	0.17	0.13	0.15	) 0.25
	060 K	0.30	0.23	0.35	0.17	0.55	0.32	)
	001 I	0.57	0.53	0.56	0.66	0.52	0.56	)
	002 I	0.63	0.63	0.57	0.44	0.09	0.47	) 0.51
	020K+020I	0.46	0.36	0.59	0.31	0.10	0.36	
BC.CHP.14 (Undrained end)	001 K	0.37	0.29	0.37	0.35	0.33	0.34	)
	002 K	0.19	0.22	0.21	0.21	0.11	0.18	) 0.21
	060 K	0.15	0.12	0.17	0.13	0.09	0.13	)
	001 I	0.63	1.00	0.69	0.96	0.38	0.73	)
	002 I	0.38	0.44	0.44	0.36	0.22	0.37	) 0.55
	020K+020I	0.22	0.25	0.24	0.30	0.26	0.25	
BC.CHP.18 (Drained end)	001 K	0.35	0.30	0.37	0.30	0.34	0.33	)
	002 K	0.32	0.30	0.36	0.29	0.20	0.29	) 0.34
	060 K	0.29	0.58	0.40	0.33	0.38	0.41	)
	001 I	0.66	0.75	0.50	0.70	0.68	0.65	)
	002 I	0.62	0.43	0.56	0.50	0.50	0.52	) 0.59
	020K+020I	0.20	0.35	0.30	0.28	0.20	0.26	
BC.CHP.18 (Undrained end)	001 K	0.41	0.35	0.43	0.31	0.36	0.37	)
	002 K	0.38	0.32	0.43	0.35	0.22	0.34	) 0.37
	060 K	0.33	0.42	0.46	0.43	0.41	0.41	)
	001 I	0.70	0.87	0.57	0.76	0.72	0.72	)
	002 I	0.58	0.39	0.50	0.45	0.46	0.47	) 0.59
	020K+020I	0.29	0.31	0.33	0.33	0.21	0.29	
BC.CHP.19 (Drained end)	001 K	0.24	0.24	0.28	0.28	0.20	0.25	)
	002 K	0.13	0.13	0.16	0.16	0.32	0.18	) 0.20
	060 K	0.20	0.15	0.25	0.24	0.17	0.19	)
	001 I	0.42	0.42	0.43	0.29	0.42	0.40	)
	002 I	0.45	0.20	0.50	0.30	0.26	0.32	) 0.36
	020K+020I	0.26	0.26	0.29	0.22	0.23	0.25	
BC.CHP.19 (Undrained end)	001 K	0.41	0.41	0.47	0.47	0.41	0.43	)
	002 K	0.20	0.20	0.24	0.24	0.33	0 24	) 0.29
	060 K	0.21	0.13	0.26	0.24	0.17	0.20	)
	001 I	0.83	0.83	0.79	0.83	0.78	0.81	)
	002 I	0.40	0.37	0.50	0.30	0.26	0.37	) 0.59
	020K+020I	0.33	0.33	0.39	0.21	0.38	0.33	

TABLE 9.II

COMPARISON OF THE PEAK RATIOS FROM ORTHOGONAL SECTIONS TECHNIQUE

(CHP series; Investigation (b) of Table 7.I)

Test No.	Clay Mineral Lattice	Peak Height Method	Peak Area Method	Corrected Peak Height	Corrected Peak Area Method	Total Count Method	Average per Kg. mineral lattice	
BC.CHP.15 (centre)	001 K	.20	.20	.18	.19	.25	.20	)
	002 K	.23	.22	.24	.24	.36	.26	) .22
	060 K	.25	.19	.22	.21	.17	.20	)
	001 I	.50	.50	.71	.71	.70	.60	)
	002 I	.47	.47	.50	.25	.48	.43	) .53
	020K+020I	.31	.31	.38	.32	.35	.33	
BC.CHP.17 (centre)	001 K	.33	.33	.36	.36	.38	.35	)
	002 K	.18	.18	.18	.18	.26	.20	) .25
	060 K	.24	.24	.21	.20	.18	.21	)
	001 I	.90	.90	.90	.88	.78	.87	)
	002 I	.20	.19	.36	.24	.22	.24	) .50
	020K+020I	.25	.25	.29	.21	.12	.22	
BC.CHP.20 (centre)	001 K	.06	.06	.09	.06	.16	.09	)
	002 K	.25	.21	.25	.25	.40	.27	) .26
	060 K	.12	.06	.13	.09	.45	.17	)
	001 I	.14	.06	.13	.05	.13	.10	)
	002 I	.50	.23	.13	.05	.16	.21	) .16
	020K+020I	.22	.33	.27	.31	.23	.27	
BC.CHP.21 (centre)	001 K	.89	.89	.82	.82	.88	.86	)
	002 K	.44	.44	.45	.45	.50	.45	) .66
	060 K	.09	.06	.13	.07	.06	.10	)
	001 I	.90	.45	.57	.50	.50	.58	)
	002 I	.32	.22	.32	.22	.30	.28	) .43
	020K+020I	.26	.26	.31	.28	.10	.27	

TABLE 9.III

COMPARISON OF THE PEAK RATIOS FROM ORTHOGONAL SECTION TECHNIQUE

(CHP Series; Investigation (c) of Table 7.I)

TABLE 9.IV

XRD PEAK RATIOS FROM SINGLE SECTION TECHNIQUE

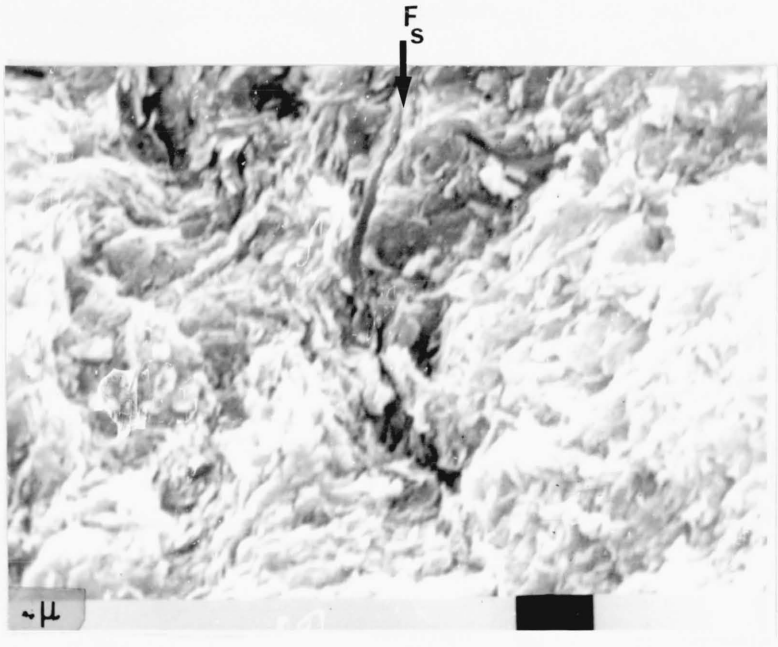
Section Analysed		$\frac{K(020)+I(020)}{K(001)}_V$	$\frac{K(020)+I(020)}{K(001)+I(001)}_V$
BC.CHP.12	Drained	0.317	0.279
	Undrained	0.098	0.089
BC.CHP.14	Drained	1.313	1.200
	Undrained	0.900	0.840
BC.CHP.19	Drained	1.494	1.344
	Undrained	0.433	0.393
BC.CHP.18	Centre	0.681	0.597
Falmouth	Undisturbed	0.278	0.249
N.FA.CHP.2	Centre	0.052	0.054
Ball Clay	Undisturbed	1.210	1.112
N.BC.CHP.1	Centre	0.033	0.032

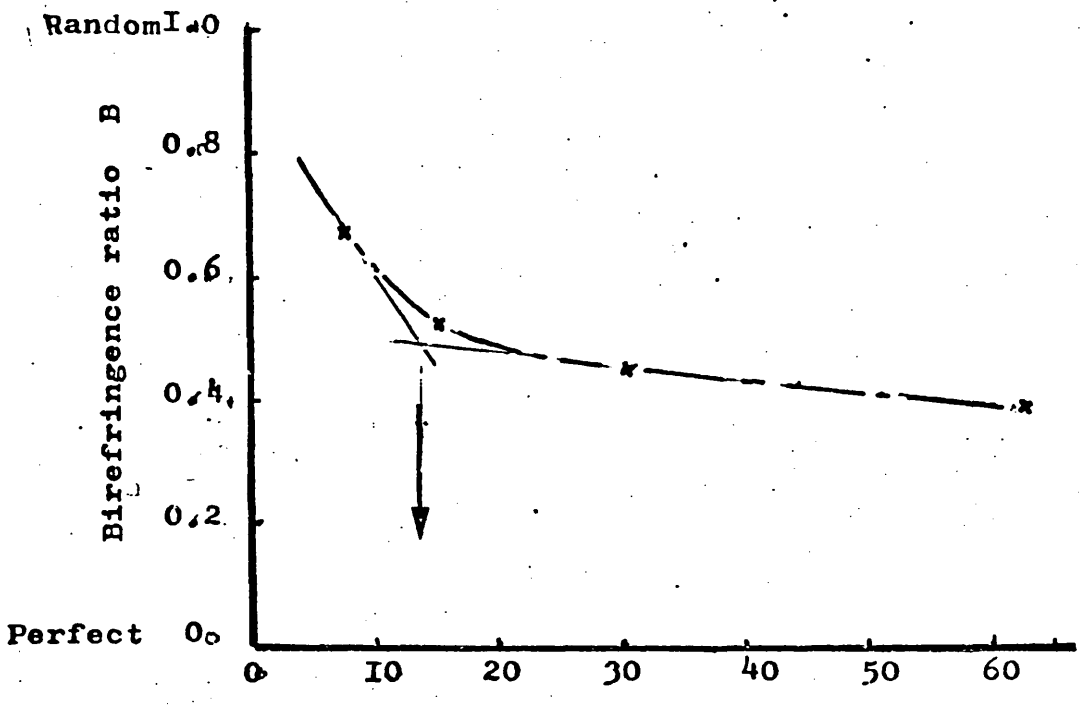
K - Kaolinite

I - Illite

V - Vertical Section

PLATE 9.34 A further micrograph of Whiteware Ball Clay showing a near vertical fissure, F_s.


F
S
~μ



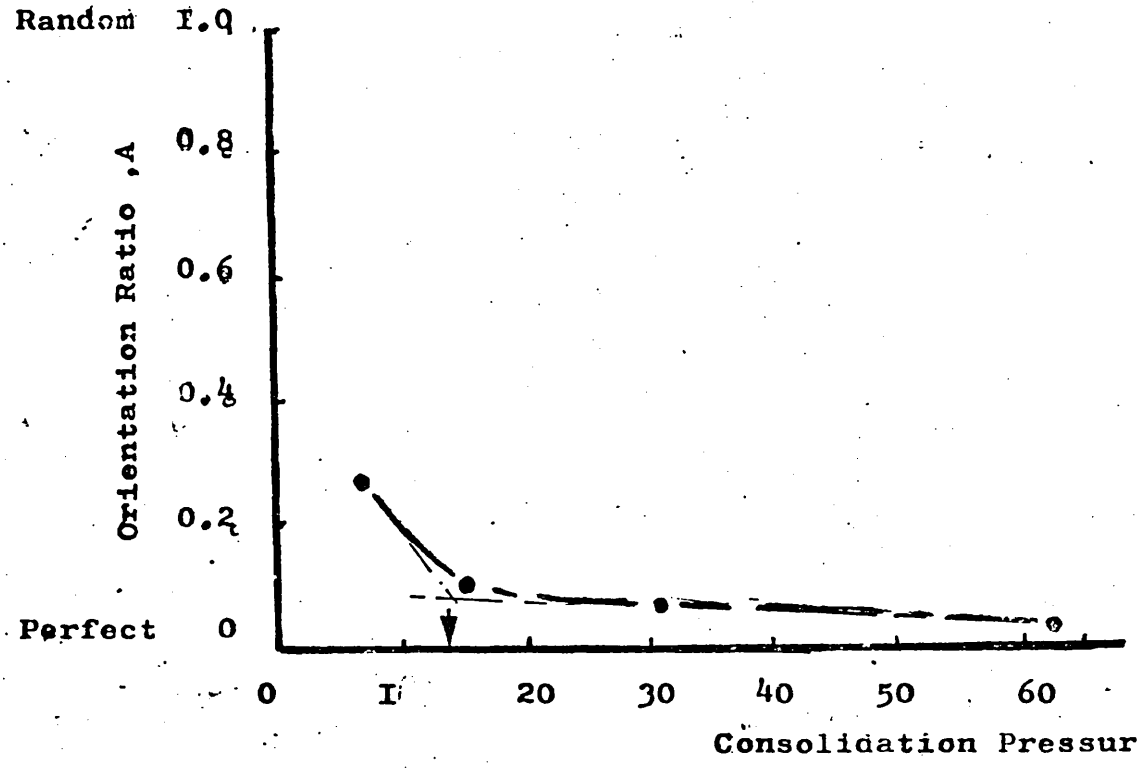


FIGURE 9.9 Plots of Birefringence ratio and Orientation ratio with consolidation pressure

plots of birefringence ratio with consolidation pressure and the orientation ratio with consolidation pressure. It appears from the figure that the major part of the orientation has already occurred at stress levels as low as 14 lbf/sq.in. Such results have also been consluded by Tchalenko (1967) who claims that at pressures in excess of 0.1 tons/sq.ft. (1.55 lbf/sq.in) the sediments attain a parallel particle configuration.

Further consolidation has little or no effect on reorientation of the particles. This has been well exemplified in the case of the natural samples (section 9.13) where even high pressure consolidation had little effect in causing a preferred orientation. Instead, the clay particles may be undergoing a process of filling the voids or crushing.

9.12 FABRICS PRODUCED IN THE DRAINED AND UNDRAINED ENDS

In extreme contrast to the preferred orientation produced in the very thin specimens described in section 9.9.1, the high pressure consolidation tests were on thick clay specimens. Accordingly, distinctly different pore fluid pressure environments are produced at the two ends of a thick specimen being consolidated with drainage occurring from one end only. Therefore it forms an ideal situation of comparing the fabrics produced at these two ends of the specimen, which had different pore fluid pressure.

9.12.1 Influence of rate of loading

Plate 9.35 compares the fabrics produced in the drained and undrained ends of the test specimen No. BC.CHP.12. Similarly, Plate 9.36 compares those of test No. BC.CHP.18. The rate of loading of test BC.CHP.18 was double that in test BC.CHP.12 and accordingly higher pore fluid pressures are developed in the undrained end of test BC.CHP.18. This is reflected in the fabrics too. A higher degree of flow structuring is seen in the undrained end of the test BC.CHP.18. The associated diffraction patterns presented with the respective micrographs aid in the above observation.

The quantitative fabrics data had been performed on both the drained and undrained end of most samples using optical microscopy and X-ray diffraction ratios.

Both types of observations (Tables 9.I and 9.II) show a reasonable difference of the ratios at the two ends. This further confirms the electron microscopic observation. Moreover, it emphasises the necessity of having low pore fluid pressures if preferred orientation is to be desired.

9.12.2 Influence of salinity

Plate 9.37 compares the fabrics produced at the drained and undrained ends from the test BC.CHP.17 in which

PLATE 9.35 Electron micrographs of vertical surfaces from specimen BC.CHP.12:

a) Drained end and its diffraction pattern.

b) Undrained end and its diffraction pattern.

Magnification x 2,000; tilt 87°.


10μ

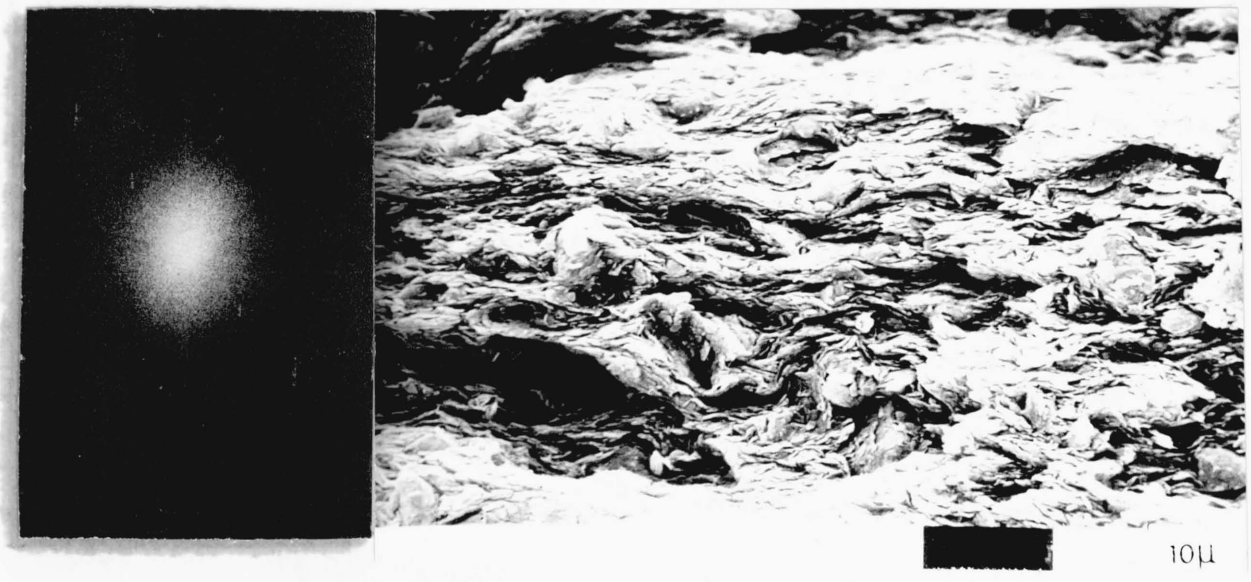
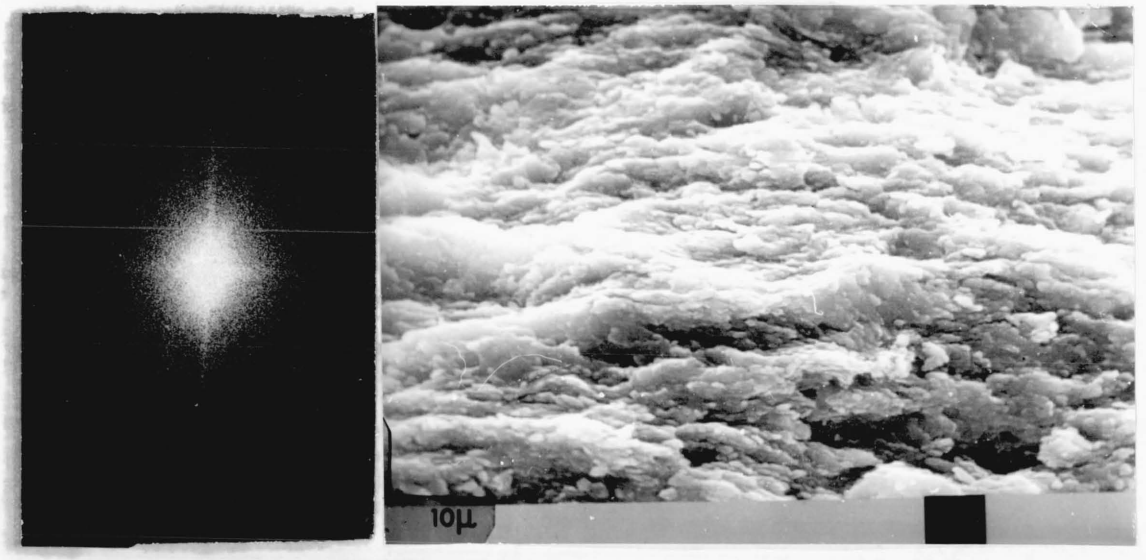

10μ

PLATE 9.36 Electron micrograph of vertical surfaces from specimen BC.CHP.18.

a) Drained end and its diffraction pattern.

b) Undrained end and its diffraction pattern.

Magnification x 2,000; tilt 80°.


10μ

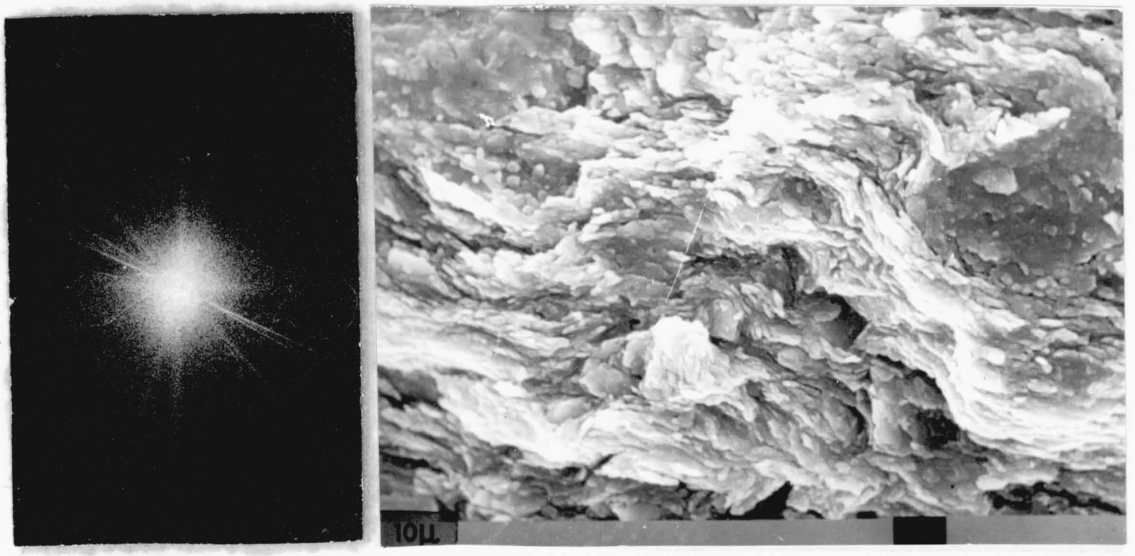
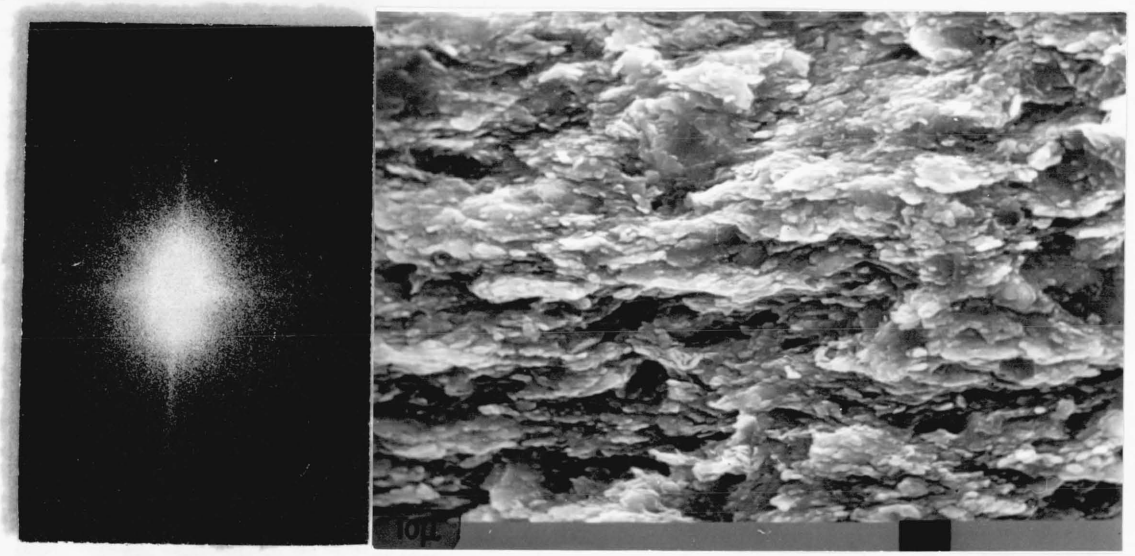

10μ

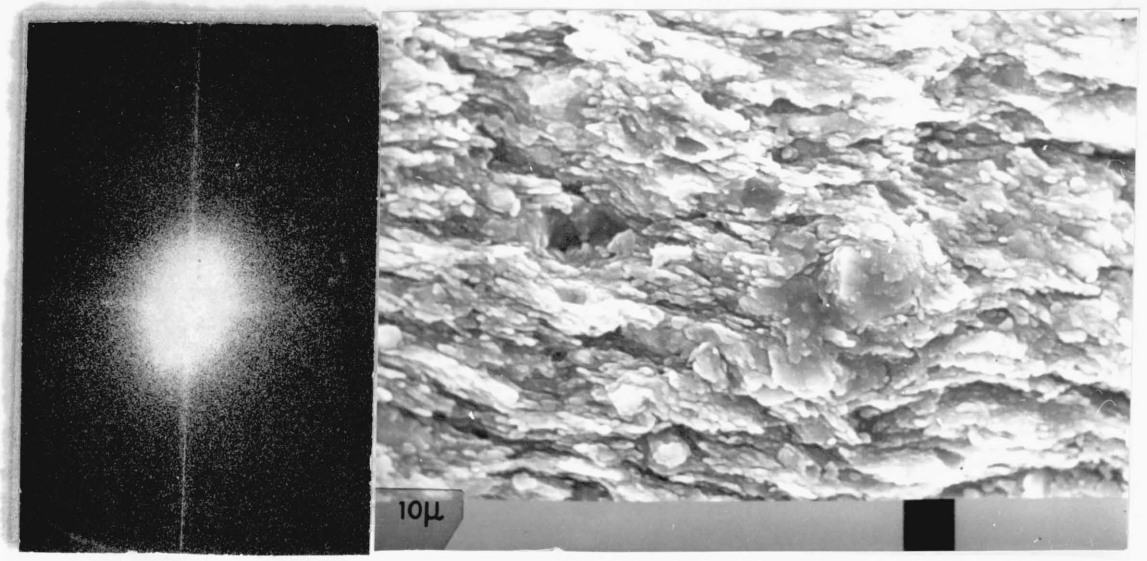
PLATE 9.37 Electron micrographs of vertical surface of sample from specimen BC.CHP.17.

a) Drained end and its diffraction pattern.

b) Undrained end and its diffraction pattern.

Magnification x 10,000; tilt 80°.


10μ


10μ

the clay was remoulded in hypersaline conditions.

The pore fluid pressure peak developed in this test was the least among the rest and accordingly the difference in the fabrics observed at the two ends was less marked. Quantitative X-ray analysis for the saline tests are given in Table 9.III.

Plate 9.38 shows the lack of development of a preferred fabric of the clay at increasing distances away from the drainage surface. The diffraction patterns for the micrographs aid in their comparison. It is noteworthy that similar observations have also been made by Tovey (1973).

9.13 FURTHER CONSOLIDATION OF UNDISTURBED SAMPLES

Plate 9.39 is a series of micrographs of different magnifications of an area of a specimen of Falmouth clay that was consolidated to a peak pressure of 29.0 lbf/sq.in. (N.FA.CLP.4). It is clear that the coarse particles hinder the parallel orientation of the fine grained particles. This is even evident in the high pressure consolidation tests. Figure 9.10 is a comparison of the rosettes of the intensity of the transmitted light and it serves to show that the orientation induced by the consolidation is slight.

A further interesting observation is the effect of the coarse mica particles on the rebound characteristics.

PLATE 9.38 Series of micrographs from the drainage end of test BC.CHP.14.

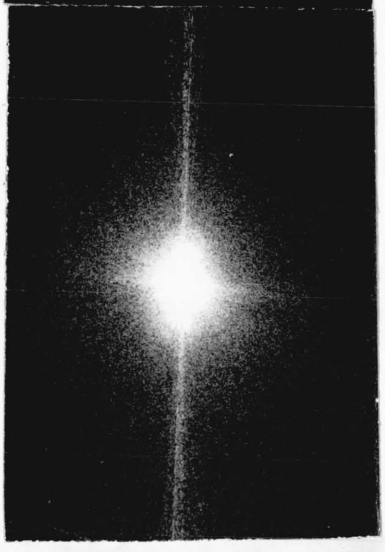
	Distance of centre of field from drainage end	Magnification	Tilt
a)	30μ	x 2,000	80°
b)	60μ	x 2,000	80°
c)	90μ	x 2,000	80°
d)	140μ	x 2,000	80°

Picture width is equivalent to 60μ.

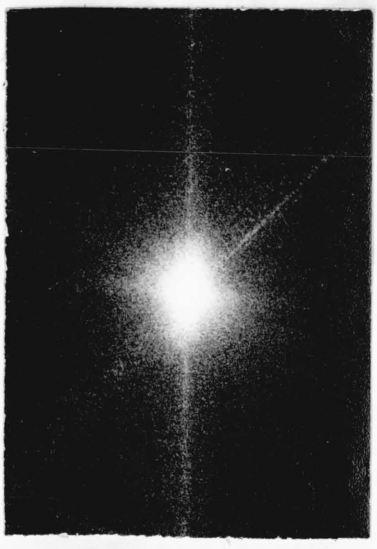












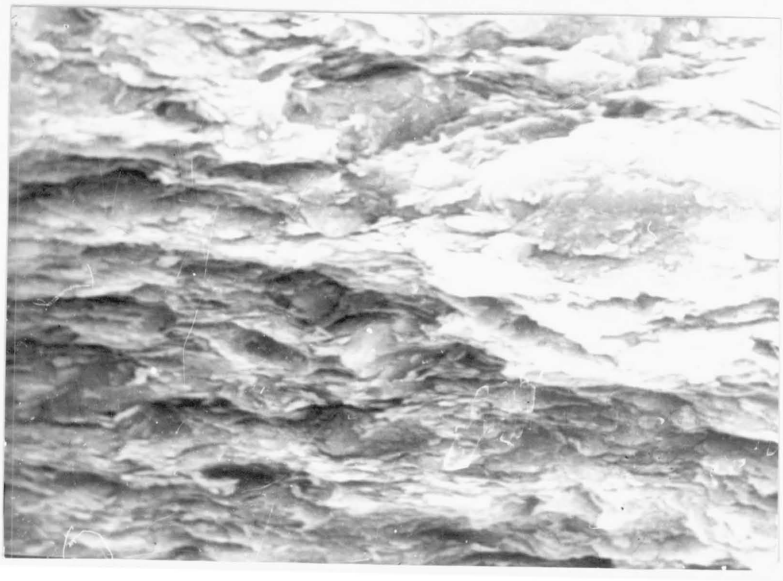


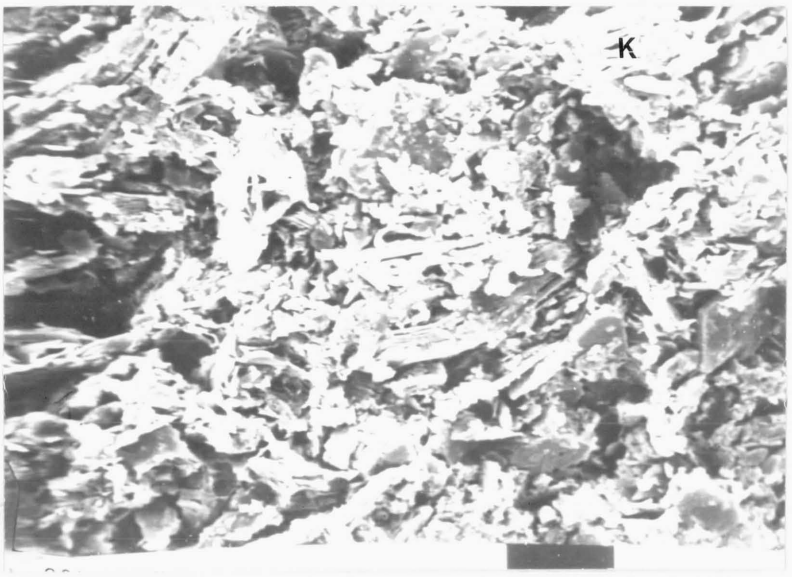


PLATE 9.39 Electron micrograph of consolidated Falmouth Clay (N.FA.CLP.4):

a) General view; magnification x 1,000 tilt 80.
K - Kaolinite; M - Muscovite Mica; Q - Quartz.

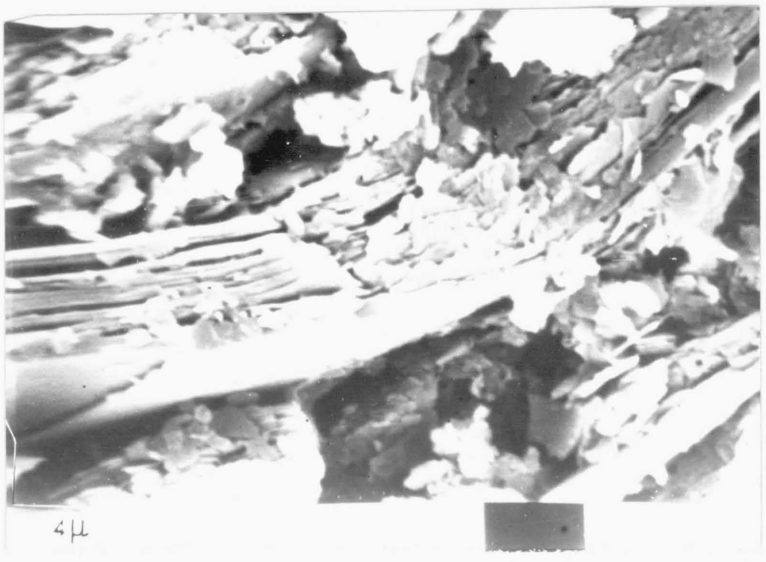
b) magnification x 2,000 tilt 80.

c) Muscovite Mica flake cleavage acting as a leaf spring; magnification x 5,000 tilt 80.





10μ



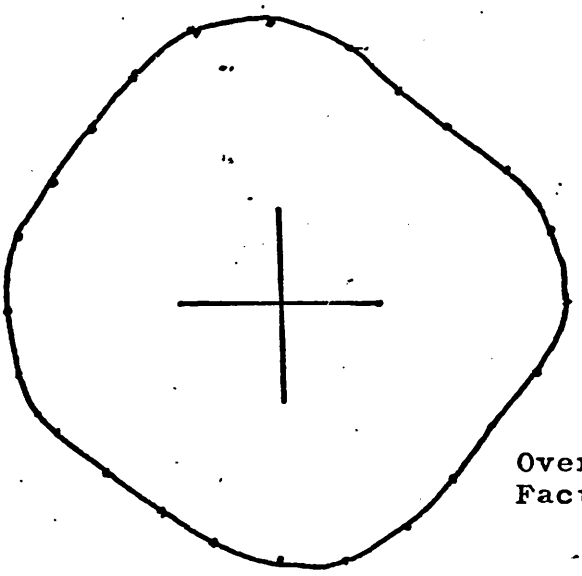
4μ

Meade (1964) suggested the increased rebound characteristics with increasing mica content. The ratio of the slopes of the rebound curves of the Falmouth clay to that of ball clay 661 is 2.5 - 3.0. The mechanism responsible for this enhanced rebound characters may be deduced from the morphology of the mica flakes as seen in Plate 9.39c. By virtue of the shape and weight of the mica flakes they have a natural tendency to settle into an approximately flat lying position. Its flexural properties impart to it a property comparable with that possessed by a mechanical "leaf spring" (see Plate 9.39c). Accordingly a stress release gives an enhanced rebound.

Figures 9.10 and 9.11 illustrate the change in the orientation of the particles in tests N.FA.CHP.2 and N.BC.CHP.1. In these instances the orientation is inhibited by both its initial disturbed fabric and by its low moisture content which restricts the degrees of freedom of the particles for preferred orientation. This is a further extension of the effect of the initial fabric resulting from drying that was imposed on the freshly deposited sediment as suggested by Best and Fookes (1970) in the case of the ball clays.

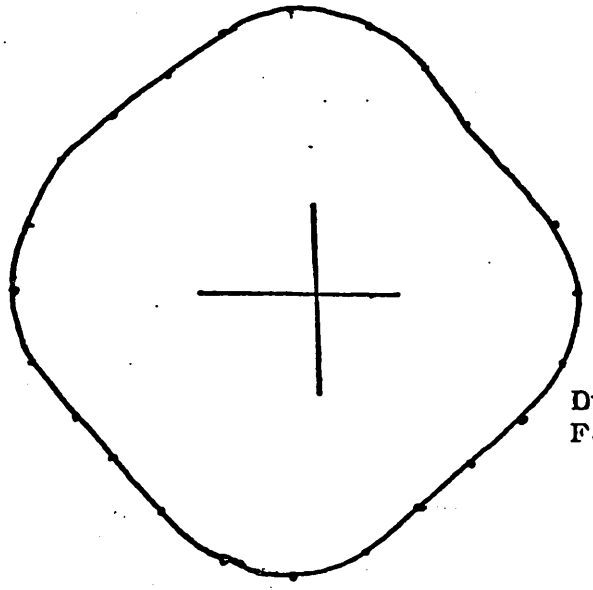
Plate 9.40 illustrates the results of a fissility test performed on both undisturbed and high pressure consolidated natural samples to support the observations described above.

a)



FALMOUTH UNDISTURBED
Overall Orientation
Factor = I.I85

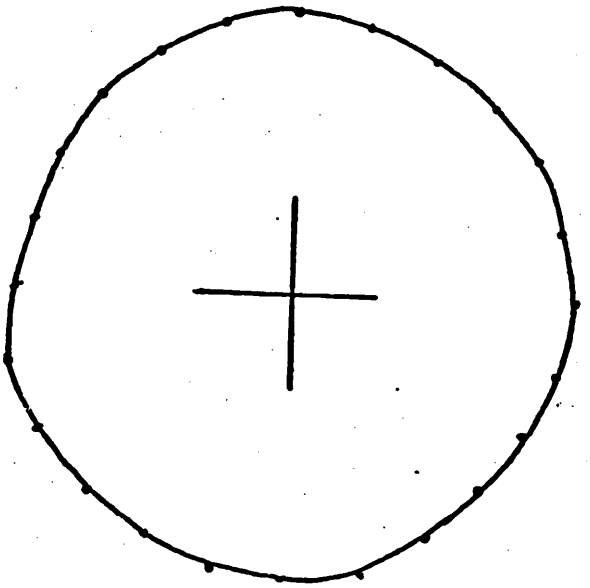
b)



TEST N.FA.CHP.2
Dverall Orientation
Factor = I.2003

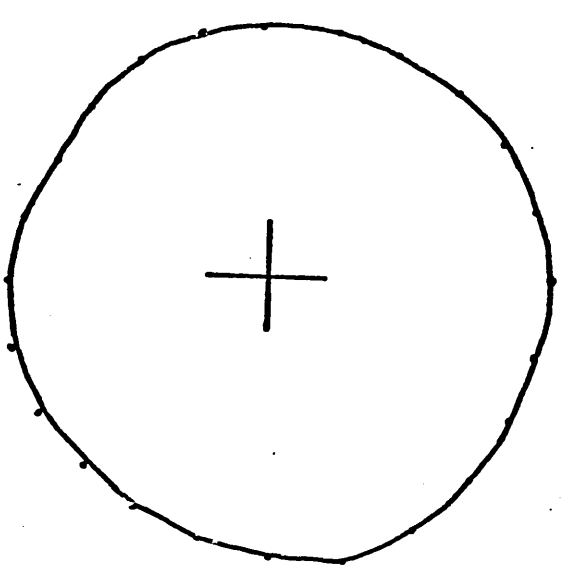
FIGURE 9.I0 Illumination rosettes for vertical sections of Falmouth Clay
a) Undisturbed clay
b) High pressure consolidated clay

a)



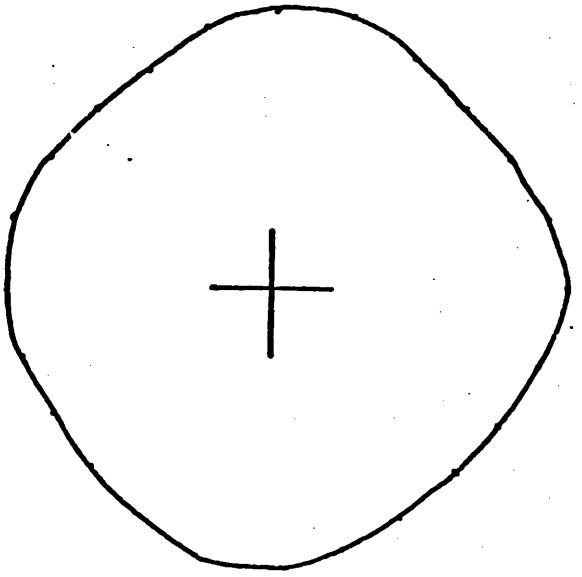
UNDISTURBED PETROCKSTOW BALL CLAY
Overall Orientation Factor =I.057

b)



UNDRAINED END

TEST. N.BC.CHP.I
O.O.F = I.I46



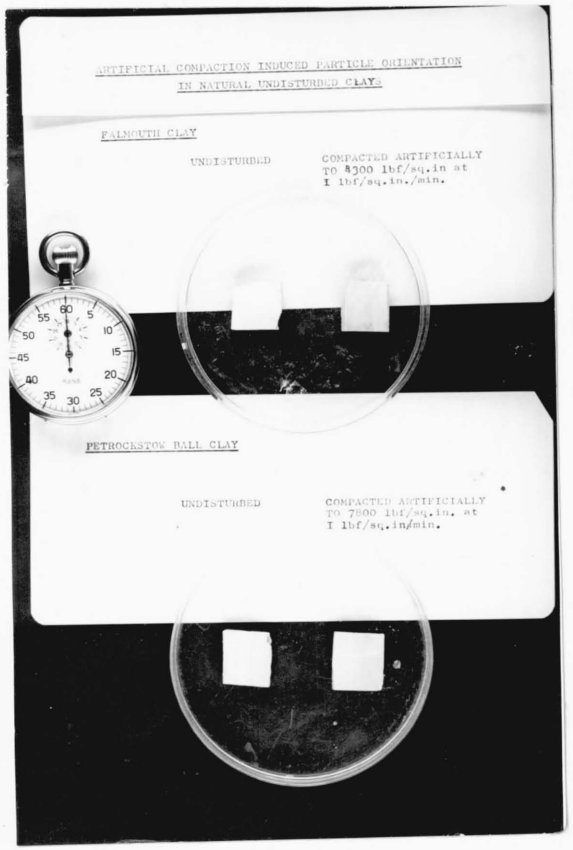
DRAINED END

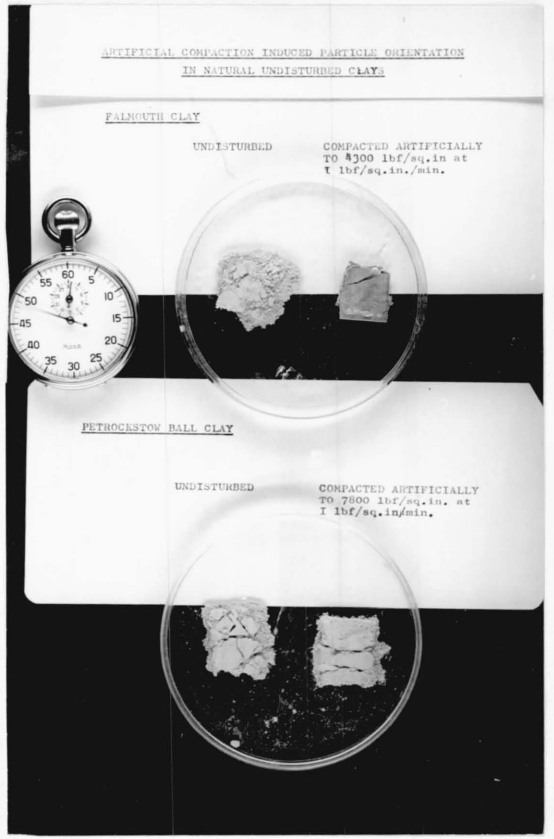
TEST. N.BC.CHP.I
O.O.F = I.I83

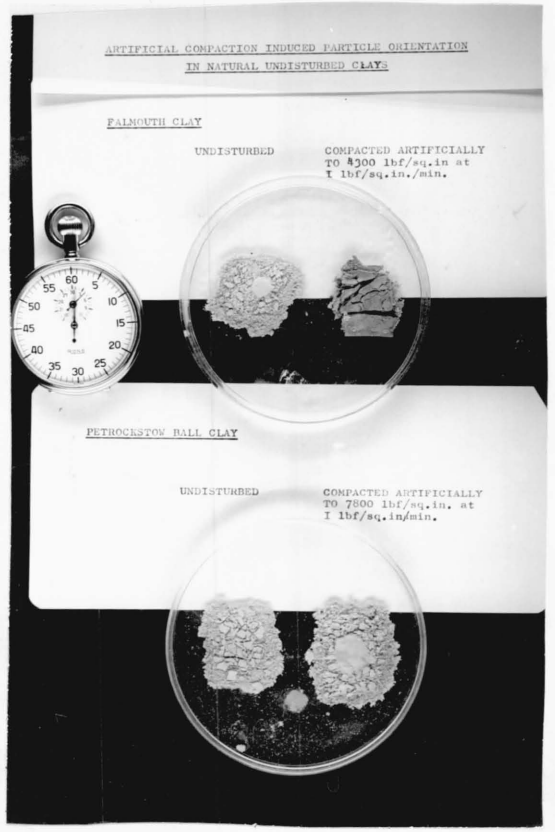
FIGURE 9.II Illumination rosettes for vertical sections off Undisturbed and High pressure consolidated Ball Clay

PLATE 9.40

Results of the fissility tests on vertical slices of undisturbed and consolidated samples.


ARTIFICIAL COMPACTION INDUCED PARTICLE ORIENTATION
IN NATURAL UNDISTURBED CLAYS
FALMOUTH CLAY
UNDISTURBED
COMPACTED ARTIFICIALLY
TO 4300 lbf/sq.in at
I lbf/sq.in./min.
PETROCKSTOW BALL CLAY
UNDISTURBED
COMPACTED ARTIFICIALLY
TO 7800 lbf/sq.in. at
I lbf/sq.in/min.


ARTIFICIAL COMPACTION INDUCED PARTICLE ORIENTATION
IN NATURAL UNDISTURBED CLAYS
FALMOUTH CLAY
UNDISTURBED
COMPACTED ARTIFICIALLY
TO 4300 lbf/sq.in at
I lbf/sq.in./min.
PETROCKSTOW BALL CLAY
UNDISTURBED
COMPACTED ARTIFICIALLY
TO 7800 lbf/sq.in. at
I lbf/sq.in/min.


ARTIFICIAL COMPACTION INDUCED PARTICLE ORIENTATION
IN NATURAL UNDISTURBED CLAYS
FALMOUTH CLAY
UNDISTURBED
COMPACTED ARTIFICIALLY
TO 4300 lbf/sq.in at
I lbf/sq.in./min.
PETROCKSTOW BALL CLAY
UNDISTURBED
COMPACTED ARTIFICIALLY
TO 7800 lbf/sq.in. at
I lbf/sq.in/min.

9.14 PREFERRED ORIENTATION INFLUENCED BY ORGANIC MATTER

The presence of lignite in the whiteware ball clay formed a suitable means of studying the influence of organic matter. Plate 9.41 shows the area in the vicinity of a lignite seam. The effect of drying is very marked in the lignite by the separation of the cells. Conversely the lignite seams possess a great affinity for water and can therefore act as localised drainage surfaces.

From the fabric observation cited in this chapter, it can be inferred that a high degree of preferred orientation will result in the periphery of the lignite seam. This is seen from the micrographs by the clay particles attaching themselves face on to the surfaces of the lignite seams. It must, however, be noted that this orientation is only tangential to the lignite seam and bears no relation to any sedimentological direction unless the lignite seams themselves bear such a relation.

9.15 MICROSCOPIC STUDY OF NATURAL AND ARTIFICIAL FISSURES

The genesis of some of the fissures produced in the specimens during laboratory consolidation and rebound has already been described. Their surface morphology is compared with those of natural fissures seen in the Bovey whiteware clay.

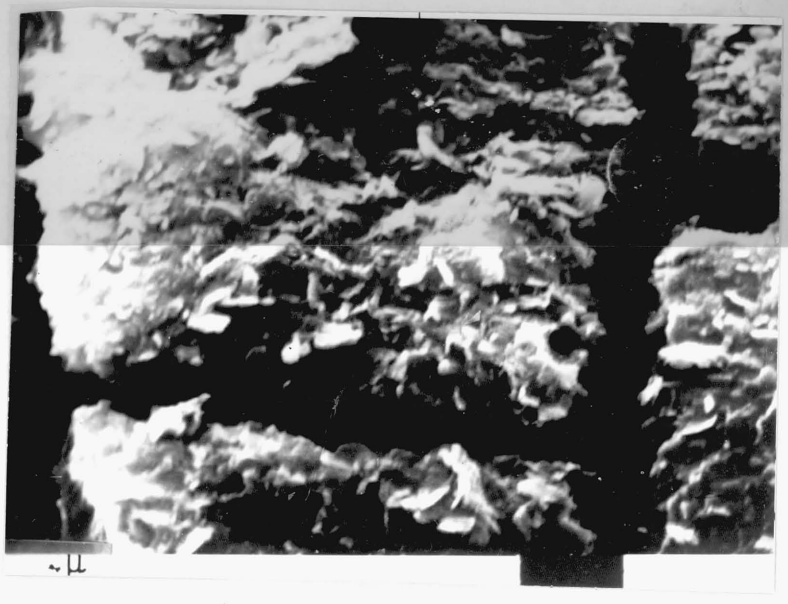
PLATE 9.41 Electron micrograph of Whiteware Ball Clay with lignite seam and associated clay particle orientation.

a) General View; magnification x 500 tilt 85°

b) Clay on face of lignite; magnification x 5,000 tilt 85°



×10




4011



Plate 9.42 is a view of a block of whiteware ball clay including a fissure surface and a lignite seam. The surface of the natural fissures appear slickensided and are highly polished as a result of the continued seepage of ground water flow. These fissures are potential planes of weakness, and Saldivar Sali (1974) has shown that the geotechnical properties of the clay are controlled by the attitude of these fissures.

One of the basic differences between the environment on these natural fissures and those artificial ones produced was the presence of the lignite seams in the former. As such, Plate 9.43 is a detailed photographic record of the five faces of a small block of whiteware clay bounded by a horizontal (F_h) and an inclined fissure (F_i). It is an aid to study the relation it bears to the associated lignite seam (L_1) also shown in the photograph.

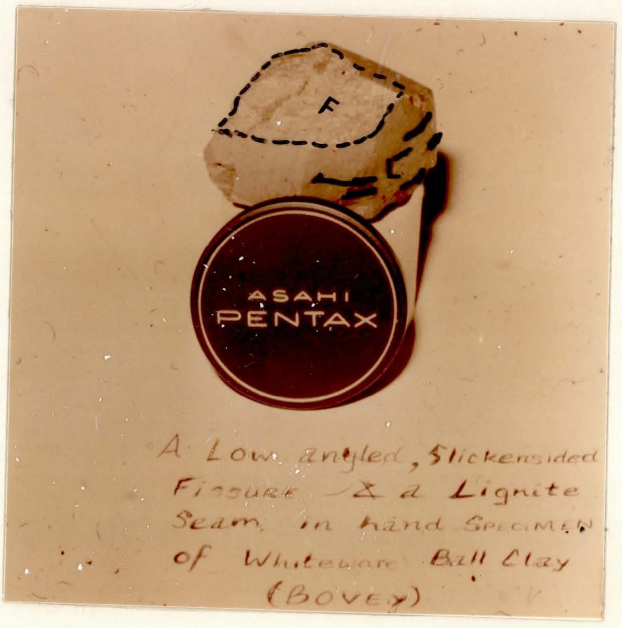
It appears that the surface of the inclined fissure (F_i) is approximately parallel to the lignite seam (L_1). As a consequence of the arguments presented in section 9.14, it may be deduced that a high degree of orientation of particles parallel to the surface of the seam must prevail near the lignite seam. Accordingly it is conceivable that the fissure F_i was a result of the orientation of particles induced by drainage of the pore fluid from its vicinity.



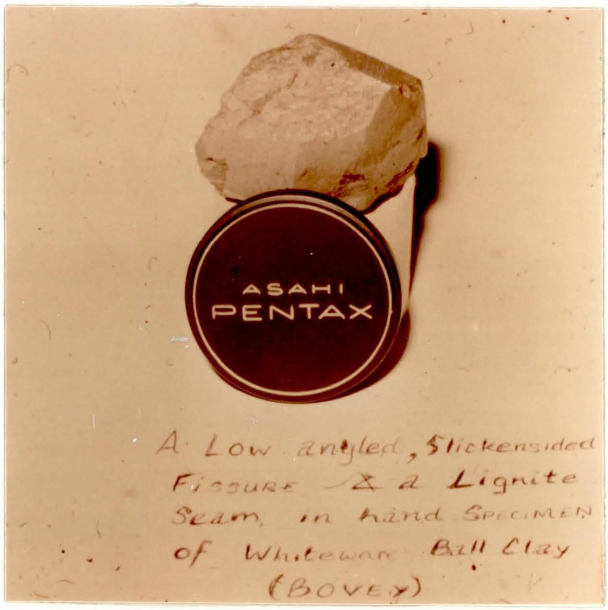
PLATE 9.42 A fissure in Whiteware Ball Clay:

F = fissure surface.
L = lignite seams.

Scale:
(Diameter of lens cap = 2.1")



A Low angled, Slickensided Fissure & a Lignite Seam in hand Specimen of Whiteware Ball Clay (Bovey)



A Low angled, Slickensided Fissure & a Lignite Seam in hand SPECIMEN of Whiteware Ball Clay (BOVEY)

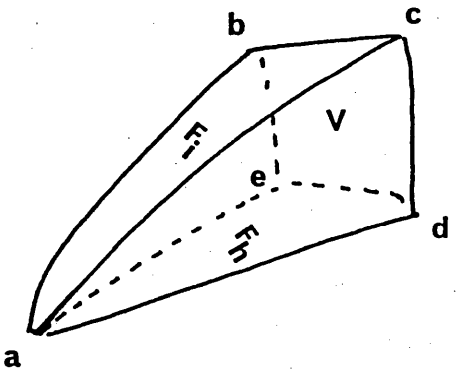


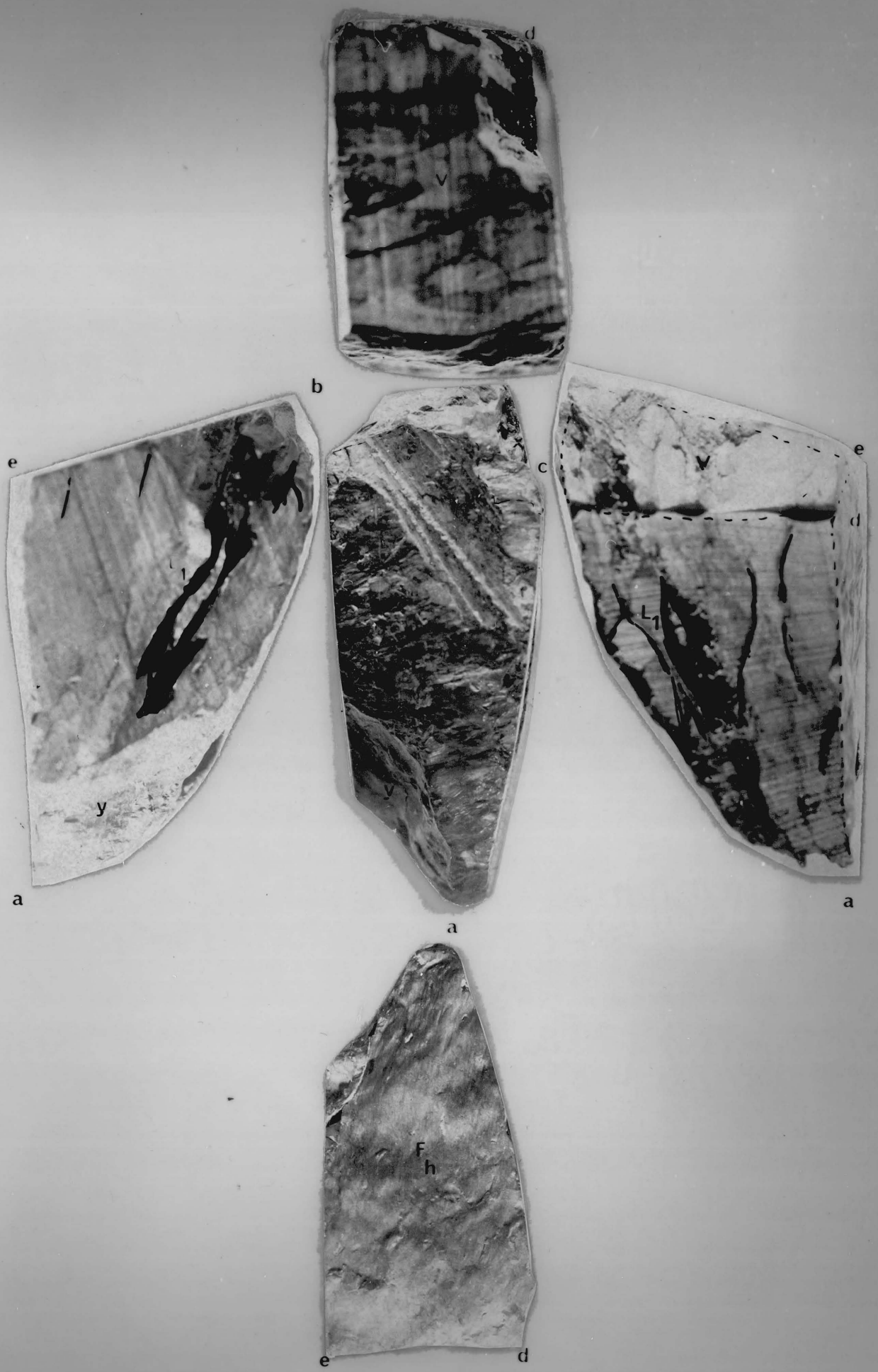
PLATE 9.43 A developed view of a block of Whiteware Ball Clay (from Bovey) contained between an inclined fissure and an horizontal fissure. (Magnification x3)

F_h = horizontal fissure.
F_i = inclined fissure.
V = vertical fracture.
L = lignite seam.



F i

F h


d
V
b
e
L1
y
a
c
V
V
a
e
d
L1
a
F
h
e
d



The probable genesis of fissures as a result of the progressive growth of the planes of weakness resulting from flow structuring (see fissure F_s in Plate 9.34) cannot also be ruled out. These two mechanisms are responsible for the development of the inclined fissures.

The genesis of the low angled fissures (F_h) has always been associated with the preferred orientation of the particles resulting from deep burial and their subsequent stress release on erosion of overburden. Saldivar Sali (1974) has supported this hypothesis with his observation that the spatial frequency of the low angled fissures increases with increasing degree of preconsolidation (see figure 3.25).

Plate 9.44 is a further illustration of a system of microfissures observed in a high pressure consolidated specimen. There is sufficient evidence from the magnified views that all fissures are associated with strong preferred orientation of the particle along the respective fissure surface, independent of the attitude of the particular fissure.

The micrographs in the Plate 9.45 are that of the surface morphology of the natural fissure. These must be compared with the micrographs in Plate 9.4. These emphasise the prime difference between the natural and the artificial fissure, as mentioned earlier, which is the high lustre on the

PLATE 9.44 Fabric details near different microfissures in a vertical sample from the drained end of the specimen from Test BC.CHP.12

Scale mark for detailed fabrics 40μ.

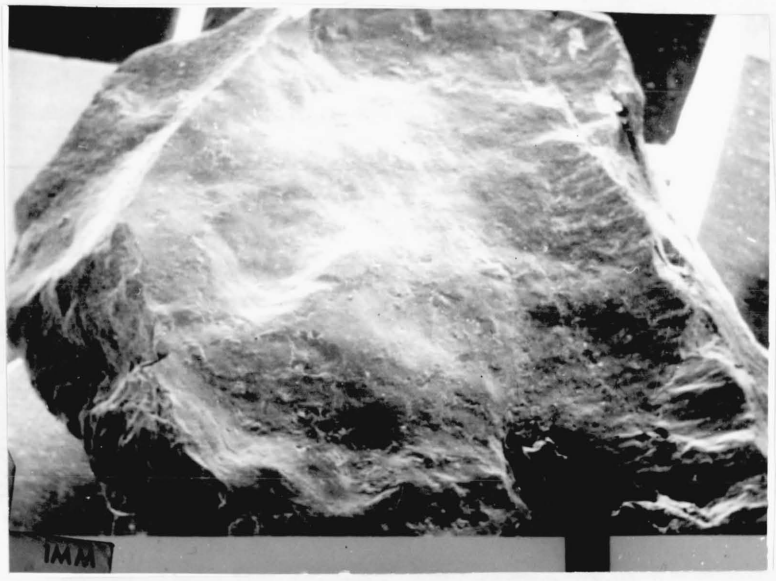
400µ


400μ

PLATE 9.45 Magnified view of surface of Bovey Whiteware fissure:

a) Magnification x 20
   Tilt 86°

b) Magnification x 2,000
   Tile 86°





surface of the natural fissure: the surface appears very smooth with almost all its particles lying 'flat', even at the high magnification of x2,000. Such a polished surface is more probably the result of consistent flow of water rather than due to shear slipping.

9.16 OBSERVATIONS OF MINERALISATION

Plate 9.46b is a micrograph of the horizontal surface of an area from near the drained end of a high pressure consolidated Falmouth sample. The prominent patterns are the traces of the growth of crystals.

Plates 9.46b and 9.46c are stereo pairs showing that the growth of these crystals is confined to the pore spaces between the flat lying plates. A spot chemical analysis using the X-ray attachment on the electron microscope suggests the crystals are one of the crystalline forms of calcite.

The concentration of the $[Ca^{++}]$ ion being expelled from the specimen near the end of the test was 0.15 gms/litre. From the solubility chart (figure 3.8) the concentration of Ca^{++} ion for saturation of $CaCO_3$ is 0.013 gms/litre.

9.17 P WAVE VELOCITY STUDY

Some anisotropy of the clay resulting from particle orientation was investigated by means of the P wave velocity

PLATE 9.46 Evidence of calcite mineralisation in the pores of the specimen N.FA.CHP.2 near its drained end;

i) isolated crystal growth - stereo

magnification x 20,000 Tilt angle difference 7°

ii) monoscopic view of the area showing distribution of mineralisation

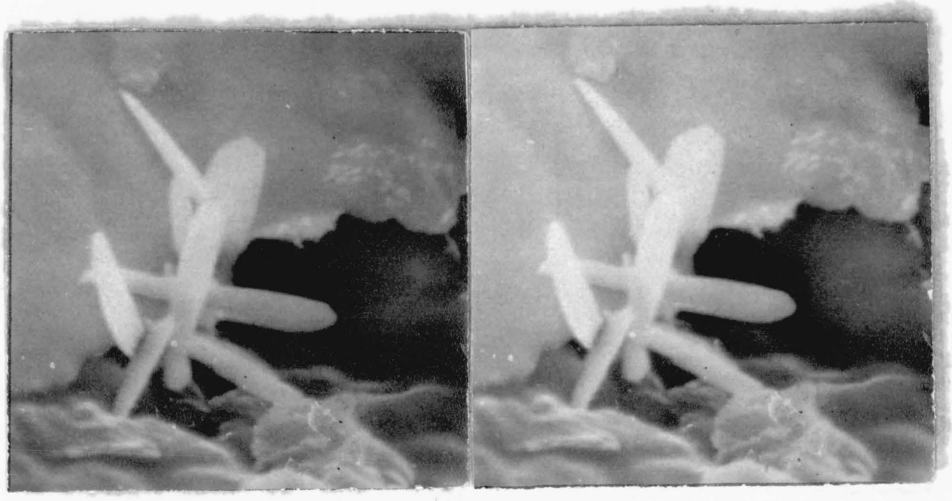
magnification x 2,000 tilt angle 84°

iii) multiple crystal growth - stereo

magnification x 20,000
tilt angle difference 6°







measurements on the artificial and natural samples. As shown in figure 9.1 four specimens were trimmed from the quadrant sections of each consolidated sample. As as illustrated the test specimens were prismatic, approximately 0.6 x 0.6 x 1.5 ins. with the long dimension representing the direction of the major consolidation stress.

P wave velocities were measured using an ultrasonic wave tester illustrated in Plate 9.47. It also shows the pick up and receiving transducer for the high frequency sound pulse kept in position on the ends of a cylindrical sample. The prismatic samples tested are also shown in the figure.

9.17.1 P wave velocity of air dried samples

Figure 9.12 is an attempt to correlate the vertical and horizontal velocities attained in the air dry state at different peak consolidation pressures. Attempts did not reveal any coherent pattern individually except for the increase in the axial velocity (in direction of maximum stress) with increase in consolidation. The velocity ratio showed a linear variation but the need for an understanding of its variation with moisture content was desired.

9.17.2 P wave velocity changes with water content

Following from the observations in section 9.17.1 directional wind P wave velocity measurements were made over a wide range

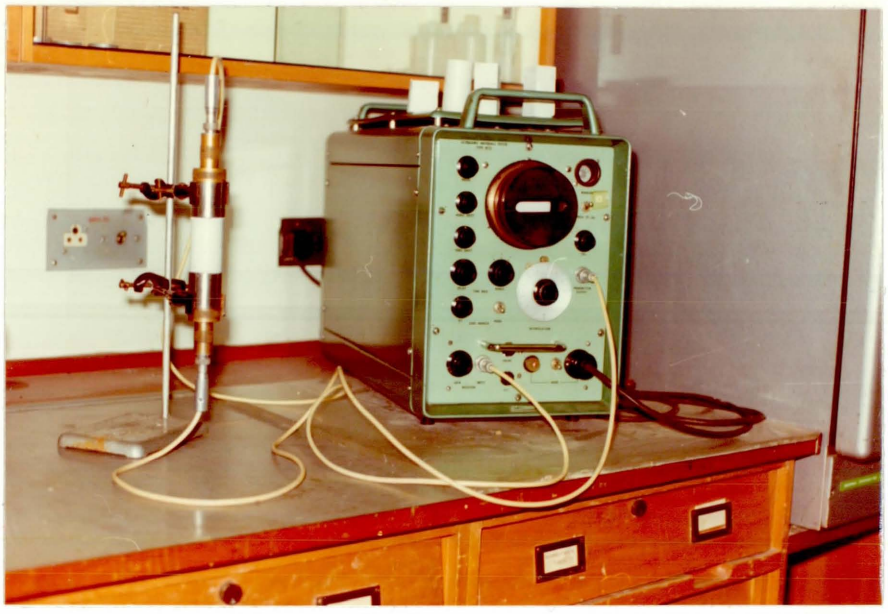
PLATE 9.47 A view of the ultrasonic materials tester used for the P wave velocity determination

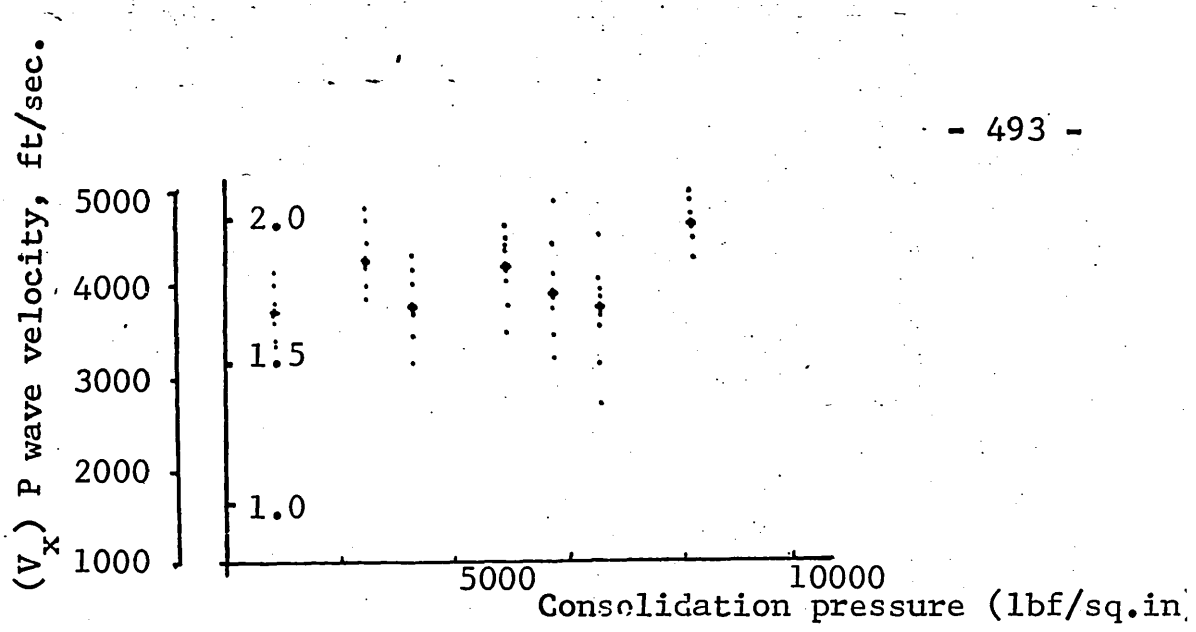
I & R - Input and Receiving Transducers

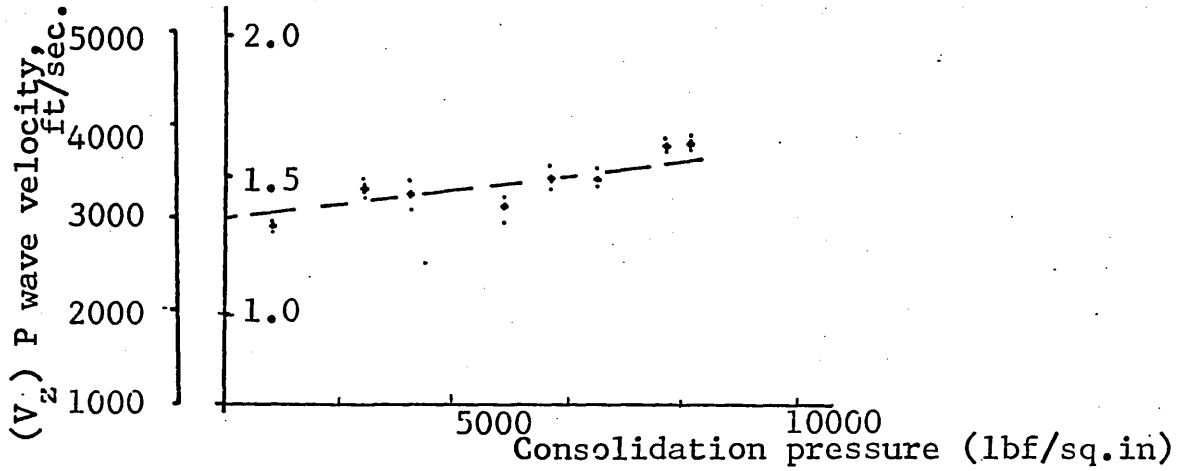
D - Signal Display

S - Prismatic Samples

C - Core Samples







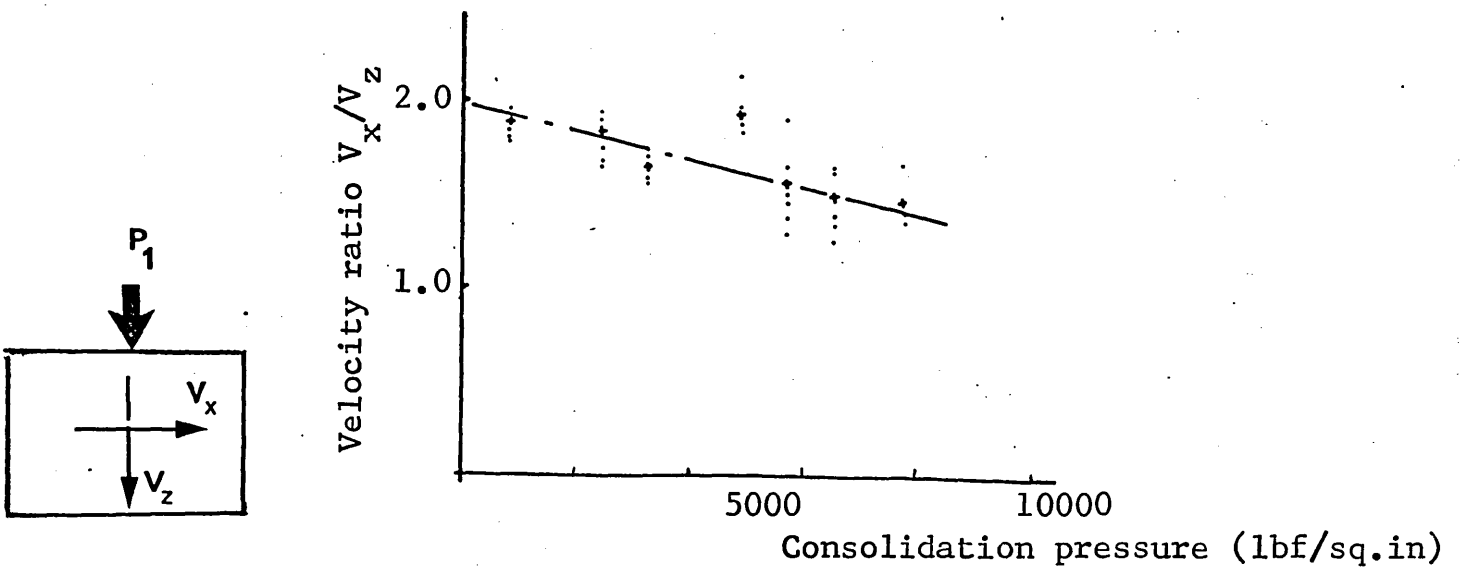
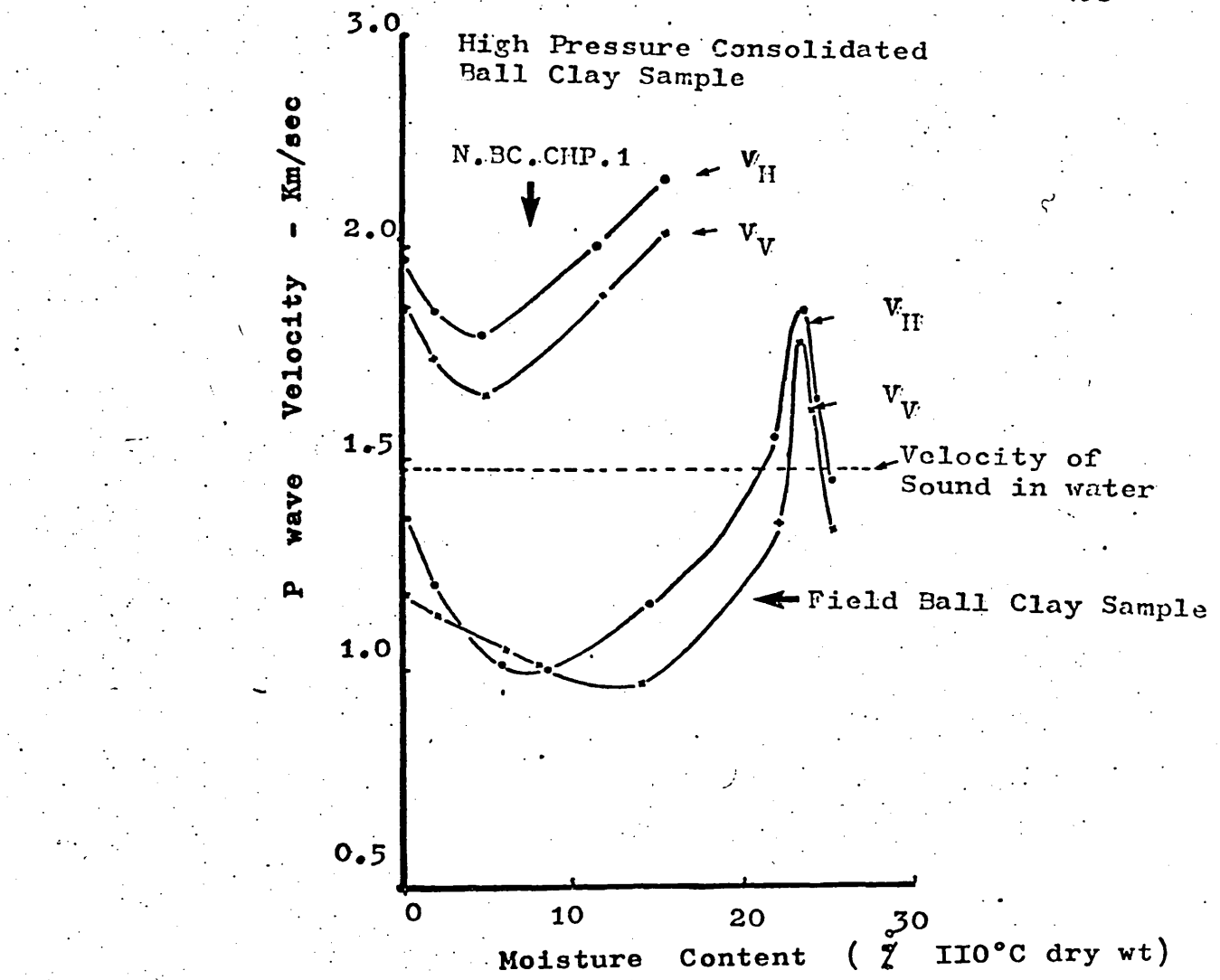


FIGURE 9.12 Results from the P wave velocity study

of water contents as saturated natural materials were allowed to air dry and subsequently oven dried. Figure 9.13 is the result of the observation.

It shows that P wave velocity of a saturated sample increases until its shrinkage limit and then decreases during its desaturation. The second increase is a result of the appearance of the shrinkage cracks.

The results of P wave velocity with drying for the consolidated specimens are also shown. By virtue of the compact structure attained in the process, an enhanced velocity is acquired.



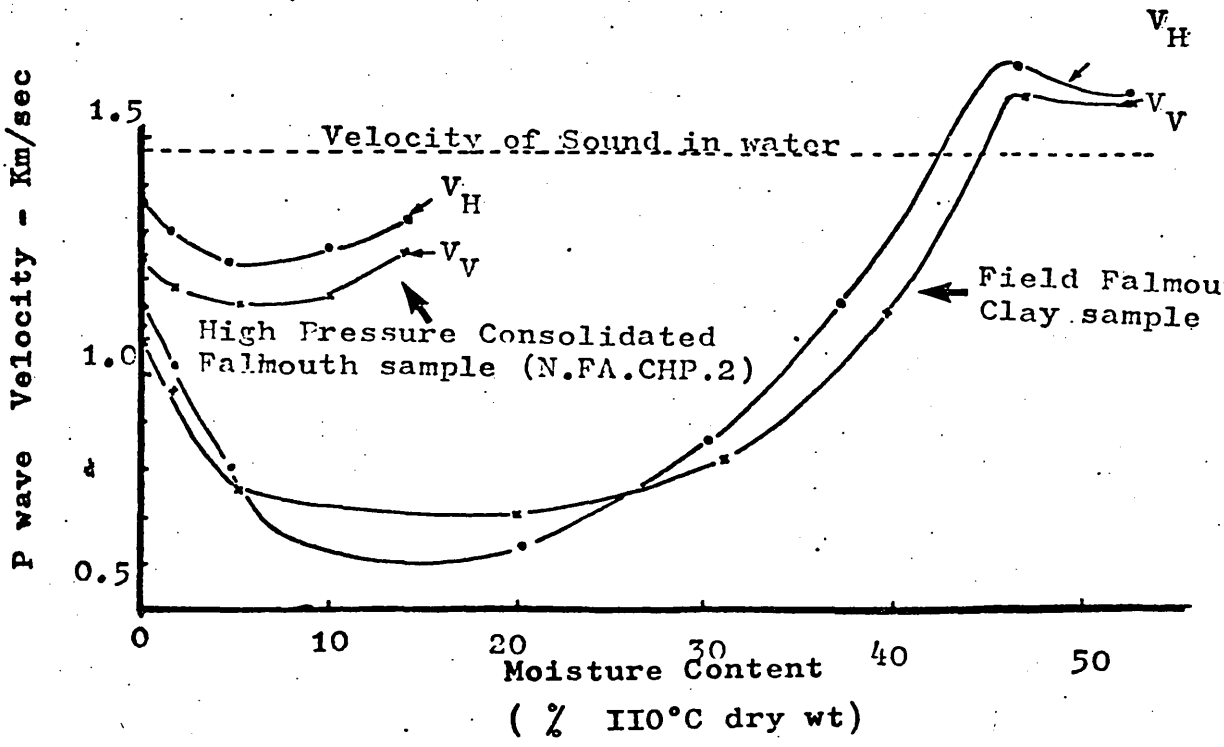


FIGURE 9.13 Observed changes in P wave velocity with moisture content on drying of samples

a) Ball Clay b) Falmouth Clay

CHAPTER TEN Concluding Discussion

10.1	Artificial Gravitational Compaction	497
10.2	Pore Fluid Chemistry Changes	499
10.3	Development of Fabric in Clays	503

CONCLUDING DISCUSSION

The results of the study have been described in the preceding chapters. In this chapter, the main observations are summarised and reviewed with their engineering-geological significance. Some aspects for further immediate research are outlined.

10.1 ARTIFICIAL GRAVITATIONAL COMPACTION

The versatility of the equipment described in simulating geological burial of sediments and thereby to study different associated processes is without question. However, the prime obstacle to hinder perfect simulation is the use of an unrepresentative time scale. This has been demonstrated by the study of the influence of the rate of loading on the compaction behaviour. Increased rates of loading give increased pore fluid pressure gradients within the specimen and therefore retard complete consolidation. Rates of loading in excess of 1.0 lbf/sq.in./min. are totally unreliable for Kaolinitic sediments of 4 inch initial thickness. Lower pore fluid pressure gradients can be achieved in using specimens of higher permeability and/or initially thinner specimens.

The observed variations in the response of the pore fluid pressure at the undrained end during laboratory compaction probably reflects different stages of gravitational compaction.

Such observations under similar dynamic stress conditions do not appear to be recorded elsewhere. It is suggested that the peak in the pore fluid pressure indicates the commencement of a marked change in the dewatering state of the pore fluid; perhaps the commencement of the mobilisation of the adsorbed water layers on the clay minerals, as a result of clay particles interacting with each other over short distances of separation, conducive to the removal of adsorbed water. This is the end of stage I of gravitational compaction as proposed by many workers (section 2.7) and specially by Hedberg (1936). This stage is further reflected on the plot of permeability with porosity (figure 7.13) where a sharp decline in permeability results at this porosity of about 40 per cent.

The persistence of a steady pore fluid pressure difference during further compaction and the dependence of both these on the rate of loading (figure 7.6) is indicative of a possible mechanism for the evolution of anomalous pore fluid pressures in the deep burial shales (confirming the conclusions of Smith (1971)). A definite correlation has been observed in the field of the dependence between clay content of the shale and the anomalous pressure and the distance to the drainage boundary and the anomalous pressure (figure 3.21). It will prove an interesting follow-up study to correlate the anomalous pressures in the field with areas subjected to different rates of geological burial.

It has also been observed in this study that this pore fluid pressure difference is also affected by the pore fluid chemistry, with lower orders of pressures resulting with higher salinities.

Pressure of overburden alone is not a sufficient agent to decrease the porosity of sediments below 15 per cent. The preliminary low temperature studies indicate a definite reduction in porosity with temperature suggesting the effect of geothermal gradient as another agent contributing to the production of shales of high bulk density. At these low temperature-pressure levels, the viscosity of the pore fluid has been shown to dominate the compaction process. These may not be true at high temperature-pressures. Further processes like clay mineral transformation are bound to occur, and whether all these processes are contributory to the reduction in porosity has to be investigated in the future. Powers (1969) however, believes that such clay mineral transformation, specially in montmorillonite, gives rise to an internal fluid release, which has been considered sometimes to be another cause of the occurrence of anomalous pore fluid pressures and low density shales.

10:2 PORE FLUID CHEMISTRY CHANGES

Consistent trends were observed of the depletion of the concentration of the Na^{+} and K^{+} ions with increasing compaction pressure. Slightly different variations were observed with the Ca^{++} and Mg^{++} ions which showed an initial depletion followed

by an enhancement of their concentration. It is unfortunate though, that these observations have been on the expelled pore fluid whose chemistry must be significantly different from the average chemistry of the pore fluid within the specimen. But it can be deduced from the observations that the clay minerals in the specimens have shown a consistent acceptance of cations and a markedly lower acceptance of anions. This is in correspondence with the relative available sites on the clay particles for ionic exchange. The observed decrease in the cation exchange capacity after compaction supports the above and in general the concept of the charged net theory.

The changes in pore fluid chemistry observed were susceptible to rates of loading. It can be comprehended that by virtue of the high pore fluid pressures created in rapidly loaded samples, the electrostatic equilibrium between the adsorbed ions and the clay face charges may be disturbed mechanically by the hydrodynamic forces of the fluid flow.

In a given volume of sediments there will be a fixed amount of available positions for ionis adsorption. This is reflected in the observations that the more dominant percentage variations were observed in more dilute pore fluid solutions (figure 8.10). Therefore, from this study it is apparent that rates of loading and the specimen size are important in order to have detectable variations in pore fluid chemistry. A

poorer control of the above two factors in the tests conducted by Chillingar et al (1968) have therefore failed, accordingly, to detect much change in the pore fluid chemistry in the compaction of Kaolinite clays.

A foresight into the behaviour of the montmorillonite when compacted indicates an expectance of more marked variations. The phenomenal transformation of montmorillonite to illite with deep burial can be the result of;

a) continued absorption of ions from the pore fluid which alters the structure of the clay, and

b) dehydration process of the montmorillonite.

These observations can be studied separately by conducting tests with and without heating. The alteration of Kaolinite to Dickite was not observed in the study and such alterations will require higher pressures and temperatures or may be a specific chemical environment.

It is easy for naturally buried sediments to lose all traces of the initial history of its pore fluid chemistry both as a result of its own ionic filtration characteristics and also as a result of the interference from the pore fluids expelled from neighbouring compacting sediments and groundwater. A noteworthy example is that of London Clay, which is well established to be a marine deposit but the pore fluids fail to show any trace of the chloride ion (Bishop, personal

communication). Such an effect is a clear indication of pore fluid "contamination" or a process of substitution of the original pore fluid with that of another. The London Clay, lying on the artesian chalk aquifer, is thereby continually subjected to an upward groundwater flow whereby the process of pore fluid substitution is even further activated. These cite the importance of the need for a more realistic geochemical environment to be simulated if gravitational compaction of a particular deposit is to be copied in the laboratory.

The preferential acceptance of cations and its consequent saturation in the pore fluid yield to mineralisation and electron micrographic evidence of such has been shown in this study (Plate 9.46). Mineralisation consequently forms a further process by which the volume of the pores is reduced, and the compacting shales made more dense. Such a process invariably causes a break down of equation (4.23) in the computation of the change in 'void ratio' as such a void ratio reduction is not accompanied by an equivalent reduction in thickness of the specimen. An alternative method of estimating the void ratio (or porosity) has to be sought, where, in this event the decrease in void ratio is proportional to the volume of pore fluid displaced and the extent of mineralisation.

10.3 DEVELOPMENT OF FABRIC IN CLAYS

The electron micrographs presented demonstrate the marked tendency for the clay particles to orient themselves preferentially in the directions and conditions of dewatering. Preferred orientation of clay particles in a horizontal direction is dependent on the initial fabric and the rate of burial of the sediments. A saturated clay acquires most of its horizontal preferred orientation at pressures as low as 14 lbf/sq.in. The reorientation of particles in consolidated specimens needs very high pressures and such orientations may be effected only by involuntary processes such as mechanical bending and crushing of the clay plates.

It has been shown in this study that the development of preferred orientation does not necessarily occur always parallel to the bedding. But preferred orientations can also result due to factors such as:

a) a plane of shear distortion,

b) a localised pore fluid pressure concentration,

c) presence of organic matter.

A localised concentration of pore fluid pressure will induce the fabric of the specimen at that point to attain a configuration conducive to its dissipation. This invariably becomes a progressive phenomenon which often produces a contorted pore fluid channel (a zone of localised weakness in

strength), which can perhaps further develop to a fissure. If continuous drainage of pore fluid occurs along this channel, it becomes a well established, polished, planar or curviplanar zone of weakness. The flow structured effects of localised pore fluid pressure have been exemplified in the comparison of micrographs from drained and undrained ends of each specimen. It is pertinent here to refer to the field observations of Odom (1967) who observed variations of preferred orientation of particles with distance from drainage surfaces and similar observations have been discussed in this study.

The most dominant mode of obtaining a plane of preferred orientation is that of a shear plane which has the double effect of both concentrating the pore fluid pressure and mechanically initiating a planar direction for the dissipation of its pressure. However, such planes of shear are associated with characteristic fabrics (kink band structures) near its plane.

Preferred orientations of clay particles near organic matter has been shown in a microscopic scale in this study. A macroscopic correlation between fissures in the lignite and the ball clay have been observed by Saldivar Sali (1974; figure 6.15). Thus in most types of fissures a preferred orientation of clay particles may be present, but its genesis may be different. The natural fissures of the stoneware

clay from Bovey Basin have a highly polished surface possibly due to persistent groundwater flow. Those showing striations on the surface may be a further result of the operation of a shear force in that plane, and the low angled fissures are invariably those resulting from the usual horizontal orientation of particles. A further set of fissures can also result parallel to lignite surfaces which, however, will therefore be controlled by the organic matter content of the clay.

Petrockstow ball clay gave a low preconsolidation value which was also reflected from the lack of horizontal particle orientation. Further consolidation did not improve significantly the degree of particle orientation.

The presence of coarse particles has been shown in this study to be a hindrance to the development of preferred orientation. These have also been observed in the field where shales with increasing clay content produce a greater fissility.

The development of preferred orientation in clays is essentially a stress-controlled process with much emphasis on the local pore fluid pressure and its mode of dissipation. The fabric, however, retains a memory of stress history, even on drying, and the fissility observed in the sections of the air-dried clays on slaking reflects this particle orientation.

APPENDICES

APPENDIX A	Notations and Conversion Factors	507
	A.1 Notations	507
	A.2 Conversion Factors	509
APPENDIX B	Terzaghi Theory of one-dimensional consolidation	510
APPENDIX C	Fourier Series Solution of the Diffusion Equation	512
APPENDIX D	Analytical Results from the High Pressure Consolidation Tests	514
APPENDIX E	Steady State Temperature Distribution within a test specimen	558
APPENDIX F	Results of the Chemical Analysis of the Pore Fluids	572

APPENDIX A

A.1 NOTATIONS

The following symbols have been used in the text of the thesis and any additional notations used have been defined where they appear:

$a_v = \frac{de}{dp}$; coefficient of compressibility of clay soil.

BC = Ball Clay; N.BC = Undisturbed Ball Clay.

b = Porosity decay factor as used in Athy's equation.

CC = China Clay.

CHP = High pressure consolidation.

CLP = Low pressure consolidation.

CLPT = Low pressure consolidation with heating.

CRS = Constant rate of strain consolidation.

C_c = Compressibility of the clay structure.

C_s = Compressibility of clay particles.

$C_v = \frac{k}{m_v \cdot \gamma_w}$ = Coefficient of consolidation.

C_w = Compressibility of water.

$D = \frac{1}{m_v}$ = Constrained modulus.

e = Void ratio.

FAL. = Falmouth Clay.

G_{s_d} = Specific gravity of soil.

H = Thickness of test specimen.

k = Coefficient of permeability.

m = Moisture content.

P, σ = Total pressure.

P_1 = Total overburden pressure or total axial compacting pressure.

p, σ' = Effective pressure.

p_1 = Effective overburden pressure or effective axial compacting pressure.

$\bar{p}_1$ = Average effective axial pressure.

r = Rate of loading.

t = Time elapsed from start of loading.

T = Dimensionless time factor.

u = Excess pore fluid pressure.

u_a = Pore air pressure.

V = Pore fluid flow rate.

Z, x = Measure of depth; of overburden or of a point in the test specimen.

γ_w = Unit weight of water.

ρ = Unit weight.

Δ = Difference function; Δu pore fluid pressure difference.

ε = Strain.

ϕ = Porosity.

A.2 CONVERSION FACTORS

	Unit used in text	Abbreviation	Conversion factor
Length	Inch	in.	2.54 cm.
	Foot	ft.	0.3048 m.
	Micron	μ	10^{-6} m.
	Angström	Å	10^{-8} cm.
Volume	Cubic Centimetre	cc.	0.06102 cu.cm.
Velocity	Metres per sec.	m/sec.	196.851 ft/sec.
Mass	Pounds	lb.	453.592 gms.
Stress	Pounds per sq. in.	lbf/sq.in.	6.8046×10^{-2} atmospheres
	Pounds per sq. in.	lbf/sq.in.	6.8947×10^{-2} bars
	Pounds per sq. in.	lbf/sq.in.	7.031×10^{-2} Kg/cm^2.
	Pounds per sq. in.	lbf/sq.in.	0.6895 kN/m^2.
Concentration	Grams per cubic centimetre	gms/cc.	3.6127×10^{-2} lb/cu.in.
Permeability	millidarcy	md	9.6×10^{-7} cm/sec.

TERZAGHI THEORY OF ONE-DIMENSIONAL

Consider an element, dx thick, and of cross-section area A in the clay sample as illustrated in Figure B.1.

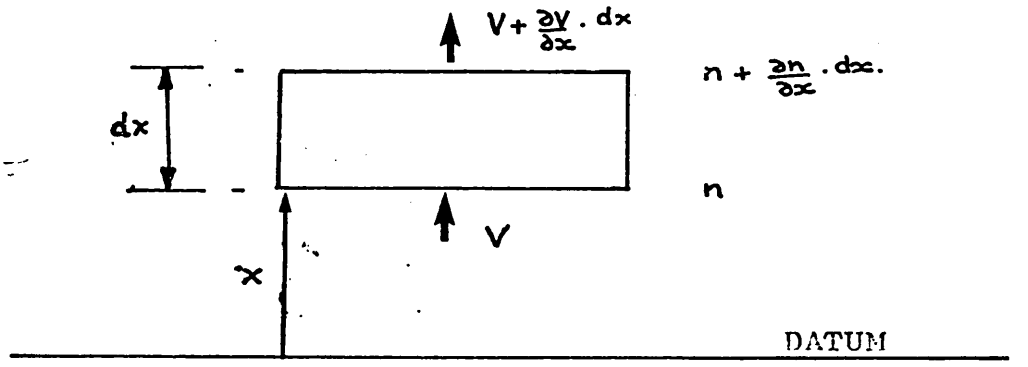


FIGURE B.1

Consolidation is a direct consequence of the dissipaticn of pore fluid pressure through drainage. If the vertical flow of water through the element is Q:

$$\text{The discharge velocity of flow} = V = \frac{Q}{A}$$

By definition of area porosity, n, of the soil:

$$n = \frac{\text{area of voids}}{\text{total area}} \quad \frac{(a)}{(A)}$$

The actual pore fluid velocity $V_w = \frac{Q}{a} = n_o V_o$

Rate of inflow to element = $V_w.a = n.V.a$

Rate of outflow from element = $(n_o V + \frac{\partial(nV)}{\partial x}.dx).a$

The rate of volume of pore fluid expelled from the element is therefore = $\left[n.V + \frac{\partial(nV)}{\partial x}.dx\right].da - Vna$

But rate of volume change of water in the element is = $-\frac{\partial}{\partial t}(V_w).a$

$= -V\frac{\partial n}{\partial t}$

Hence the condition for continuity of flow is:

$$\left[n.V + \frac{\partial(nV)}{\partial x}.dx\right], a - V.n.a = - V\frac{\partial n}{\partial t}$$

We know that: $V = A.dx$

$$n = \frac{e}{1 + e}$$

$$V_w = n.V$$

and we therefore.obtain:

$$\frac{\partial}{\partial x}(V_w) = - \frac{\partial}{\partial t}(\frac{e}{1+e})$$

but since $V_w = \frac{k}{\gamma_w} \frac{\partial u}{\partial x}$, it follows that:

$$\frac{\partial}{\partial x}(- \frac{k}{\gamma_w} \cdot \frac{\partial u}{\partial x}) = - \frac{\partial}{\partial t}(\frac{e}{1+e})$$

Therefore considering the constant volume of solids, we finally obtain the relationship between the excess pore water pressure and the void ratio:

$$\frac{k}{\gamma_w} \cdot \frac{\partial^2 u}{\partial x^2} = \frac{1}{1 + e} \cdot \frac{\partial e}{\partial t}$$

APPENDIX C

SOLUTION OF THE CONSOLIDATION EQUATION FOR THE CASE OF TIME DEPENDENT LOADING

When permeability is considered constant and the consolidation is unidimensional, the general time dependent loading consolidation is defined by the partial differential equation:

$$C_v \frac{\partial^2 u}{\partial x^2} + r(x,t) = \frac{\partial u}{\partial t} \qquad (C.1)$$

and the relevant boundary conditions for the analysis are:

$$u(0,t) = 0 \qquad 0 \leqslant t \leqslant \infty$$

$$u(2H,t) = 0 \qquad 0 \leqslant t \leqslant \infty$$

$$u(x,0) = \sigma(x) \qquad 0 \leqslant x \leqslant \infty$$

To solve equation (C.1), the method of Fourier transforms is conveniently adopted. Thus multiply both sides of it by $\mathrm{Sin}(\frac{n\pi x}{2H})$ and integrate from 0 to 2H with respect to x:

$$\int_0^{2H} \frac{\partial^2 u}{\partial x^2} \mathrm{Sin}(\frac{n\pi x}{2H})dx = -\frac{n^2\pi^2}{4H^2} \bar{U}_s$$

where: the Fourier transform, $\bar{U}_s(n,t) = \int_0^{2H} u(x,t)\mathrm{Sin}(\frac{n\pi x}{2H})dx$

This transformation satisfies the equation:

$$\frac{d}{dt}\bar{U}_s + \frac{C_v n^2\pi^2}{4H^2} \bar{U}_s = \bar{r}_s \qquad (C.2)$$

where: $\bar{r}_s$ = Fourier transform of r.

The inverse transform of the solution of (C.2) gives:

$$u(x,t) = \frac{1}{H}\sum_{n=1}^{\infty}\left[\int_0^{2H} \sigma(x)\ \mathrm{Sin}\frac{n\pi}{2H}x\,dx\right] \mathrm{Sin}\frac{n\pi}{2H}x\,e^{Mt} + \frac{1}{H}\sum_{n=1}^{\infty} \mathrm{Sin}\frac{n\pi}{2H}x\left\{\int_0^{t} r(x,t)\ \mathrm{Sin}\frac{n\pi}{2H}x\,dx\left[\ e^{M(t-r)}dr\right]\right\} \qquad (C.3)$$

in which $M = -\dfrac{C_v h^2 \pi^2}{4H^2}$

In the event of R being a constant for linear loading:

$$r = \frac{p_o}{t_o} = \frac{u_o}{t_o}$$

and also there being no initial excess pore pressure:

$$\sigma(x) = 0$$

Substituting these in equation (C.3) gives:

$$u(x,T) = \frac{16u_o}{T_o\pi^3}\sum_{n=1,3,5}\frac{1}{n^3}\mathrm{Sin}\frac{n\pi}{2H}x\left[1 - e^{-(n^2\pi^2/4)T}\right]$$

and T = time factor $= \dfrac{C_v t}{H^2}$

DETAILS OF CHR TESTS

This appendix presents a summary record of all the tests carried out in the research year, only omitting those for which no observations could be made due to early failure of equipment.

Contents

BC.CHP.12	Summary	515
BC.CHP.14	Summary	520
BC.CHP.15	Summary	525
BC.CHP.17	Summary	530
BC.CHP.18	Summary	535
BC.CHP.19	Summary	540
BC.CHP.20	Summary	545
BC.CHP.21	Summary	548
N.BC.CHP.1	Summary	550
N.BC.CHP.2	Summary	554

TEST NO. BC.CHP.12 Date: 15.2.73

Details of Test Material

Clay type; Ball clay; properties are in Table 6.II.
State of original sample; remoulded with distilled water.

Type of Test

Rate of loading; 1 psi per minute.
Salinity of the pore fluid initially; non-saline.
Maximum consolidating pressure; 2,500 psi.

Proposed Investigation

To investigate the influence of a time dependent increase in axial pressure on the consolidation behaviour of the clay.

Initial Condition of the Sample

Moisture content; 102.5 per cent.
Thickness; 3.780 inches.
Weight; 2.621 lbf.

Preconsolidation Stage

This specimen was not preconsolidated.

Loading Stage

Total decrease in thickness; 1.455 inches.
Equivalent change in Void Ratio; 1.155.

Unloading Stage

Rate of unloading; 2 psi per minute.
Total rebound of the sample= 0.179 inches.

Final Condition of the Sample

Moisture content; 20.7.
Thickness; 1.902 inches.
Weight; 2.183 lbf.

Further Comments

This test was the first to be performed with the semi-automatic loading system. The following points were noted:

(a) The initial condition of the specimen was too soft and proved inconvenient in the handling during assembly.

(b) Two peaks were observed in the pore water pressure variation as seen in the figure annexed; the second peak was associated with an abrupt change in the compaction behaviour. Furthermore, the pore fluids collected at this pressure showed traces of the hydraulic fluid probably due to a leak in the upper pore fluid connections.

(c) To load semi-automatically proved tedious as well as being not smooth; its effects are seen in the small scale variations superimposed on the main u_t variation.

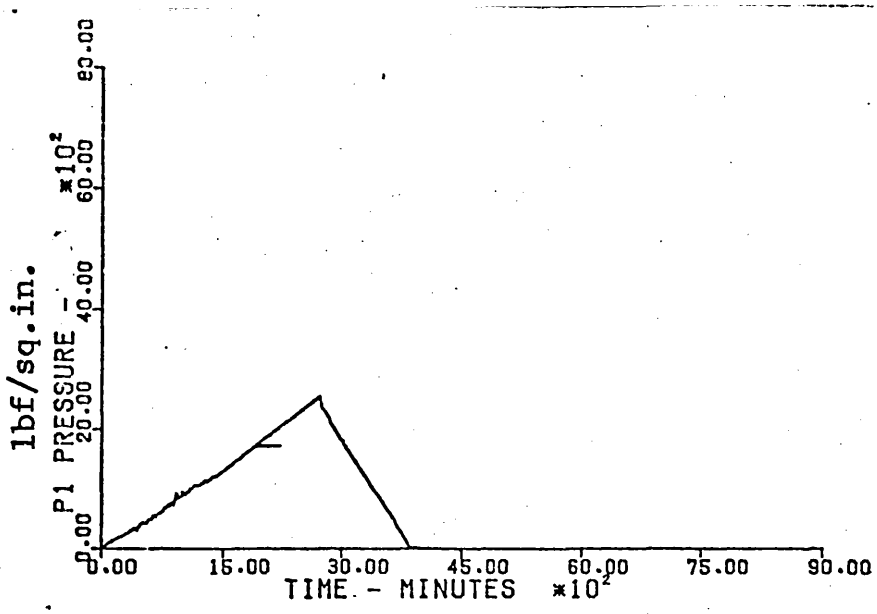


FIG.D.1a- PROGRAMMED (P1) PRESSURE TIME VARIATION

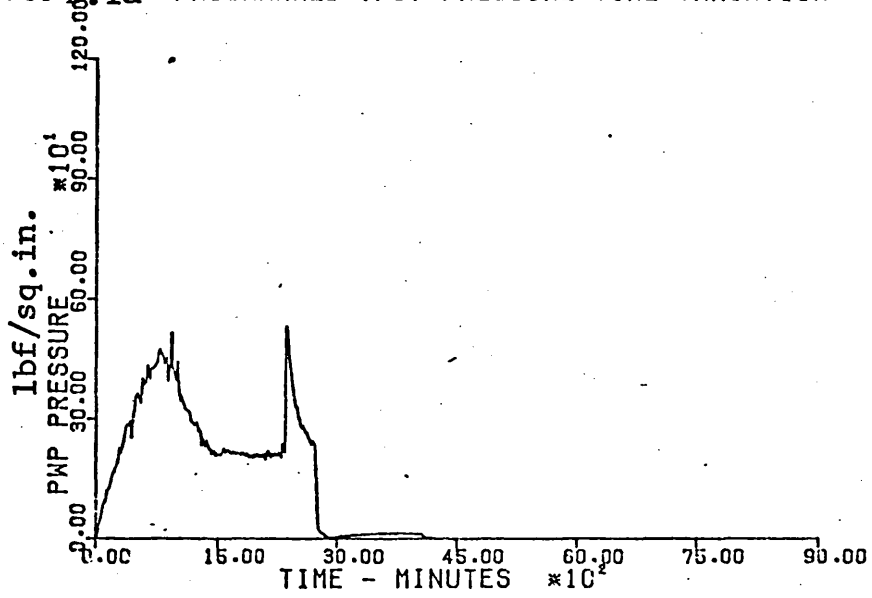


FIG.D.1b RESPONSE OF THE PORE WATER PRESSURE DIFFERENCE

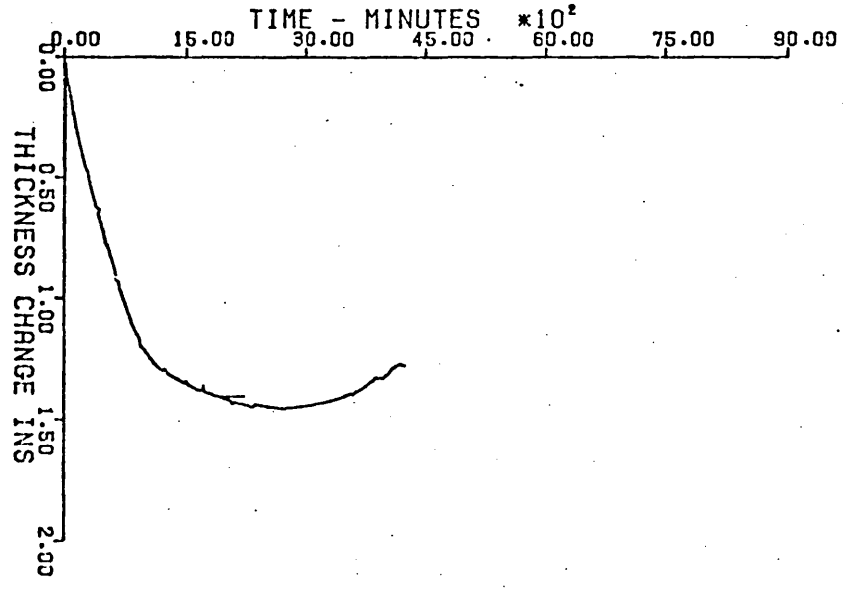
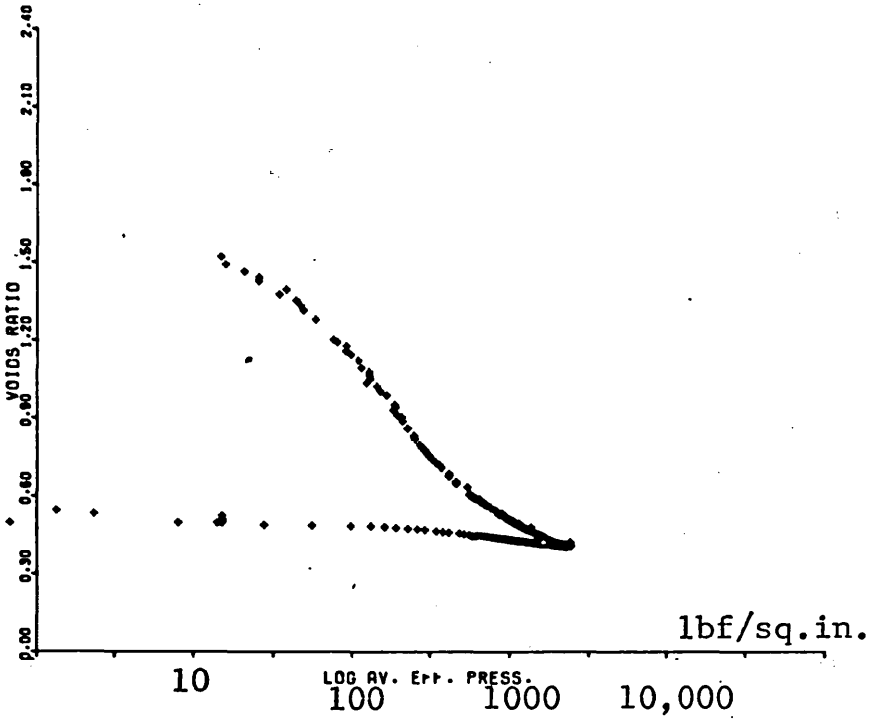
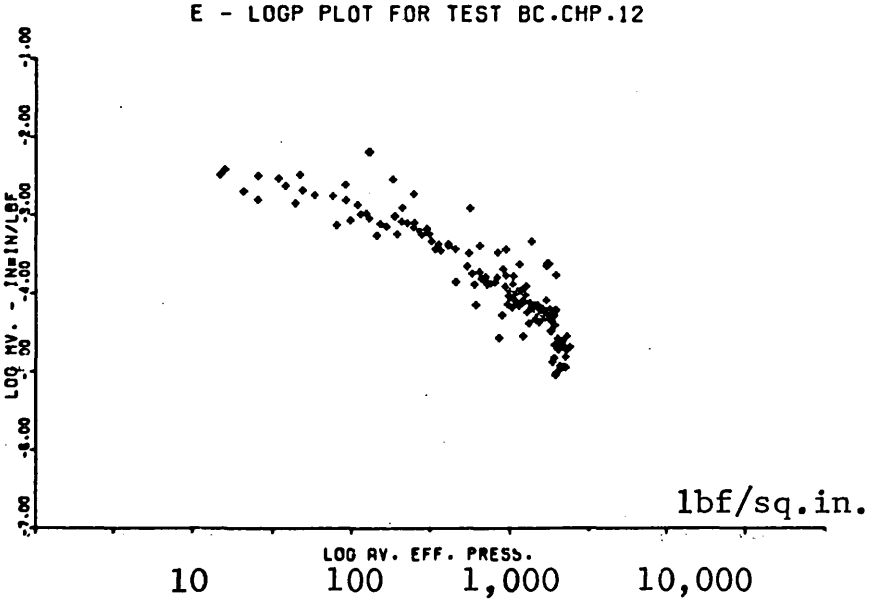


FIG.D.1c CHANGE IN THICKNESS OF THE SAMPLE

FIG.D.1 - VARIATION OF OBSERVED PARAMETERS IN TEST BC.CHP.12

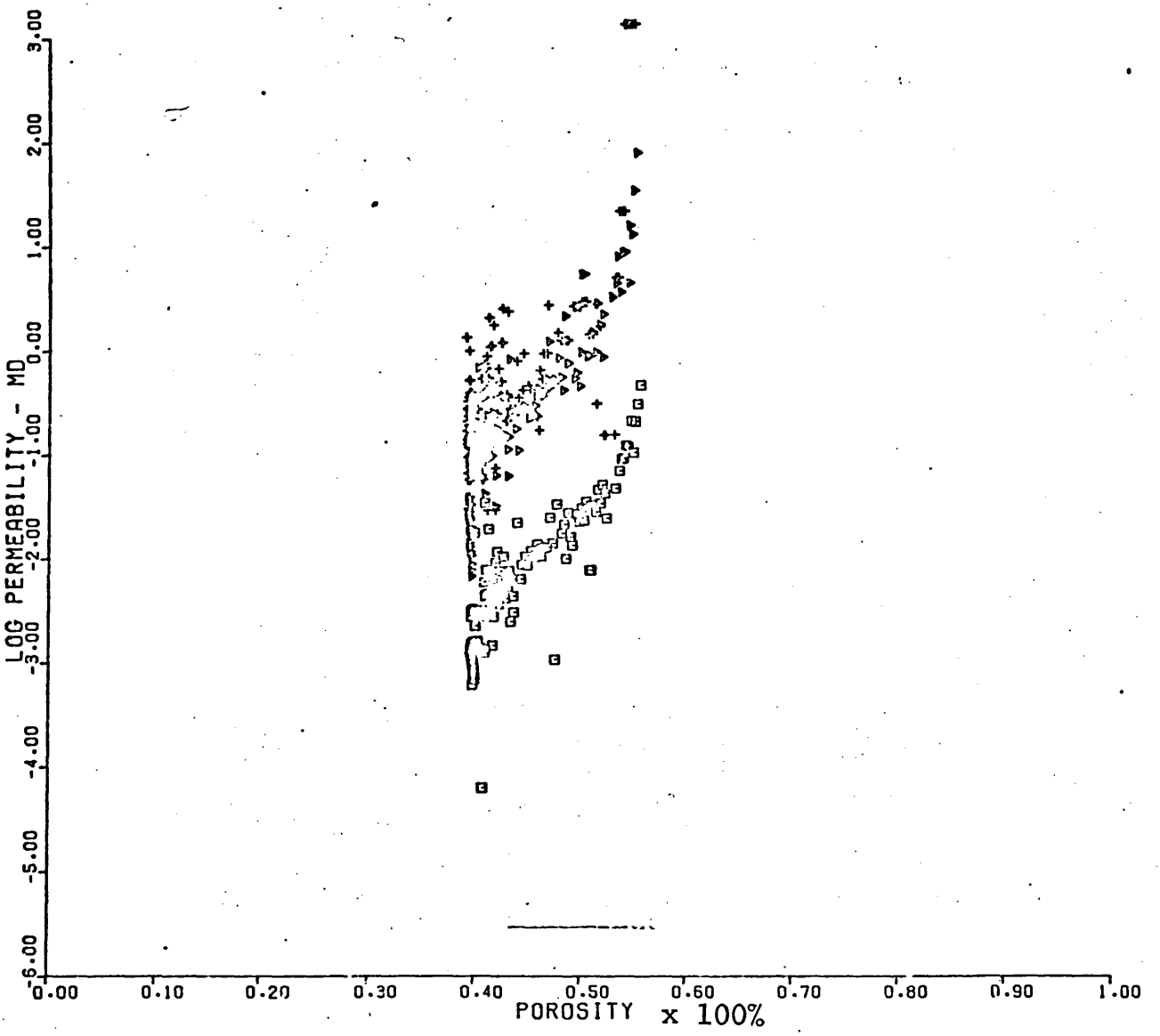


E - LOGP PLOT FOR TEST BC.CHP.12



COEFF. OF VOL. DECREASE - LOGP FOR TEST BC.CHP.12

FIG. D.2 Consolidation characters in test BC.CHP.12



PERMEABILITY - POROSITY PLOT FOR TEST BC.CHP.12

CROSS - CV CORRECTED

TRIANGLE - CV UNCORRECTED

SQUARE - LINEAR PH VARIATION ASSUMED

FIGURE D.3

TEST NO. BC.CHP.14 Date: 8.3.73

Details of the Test Material

Clay type; Ball clay; properties are in Table 6.II.
State of original sample; remoulded with distilled water.

Type of Test

Rate of loading; 1 psi/minute.
Salinity of the pore fluid initially; non saline.
Maximum consolidation pressure; 4653 psi.

Proposed Investigation

To study the repeatability of the experiment and also to observe the effects of preconsolidation.

Initial Condition of the Sample

Moisture content; 101.5%.
Thickness; 5.875 inches.
Weight; 3.918 lbf.

Preconsolidation Stage

Rate of strain; 0.0017 inches/min deformation.
Maximum preconsolidation stress; 84 psi.
Moisture content after preconsolidation; 56.70 (computed).
Thickness after preconsolidation; 3.970 inches.
Weight after preconsolidation; 3.021 lbf.

Loading Stage

Total decrease in thickness; 1.514 inches.
Equivalent change in void ratio; 1.005.

Unloading Stage

Rate of unloading; 2 psi/min.
Total rebound of the sample; 0.326 inches.

Final Condition of the Sample

Moisture content; 21.99%.

Thickness; 2.675 inches.

Weight; 2.485 lbf.

Further Comments

None.

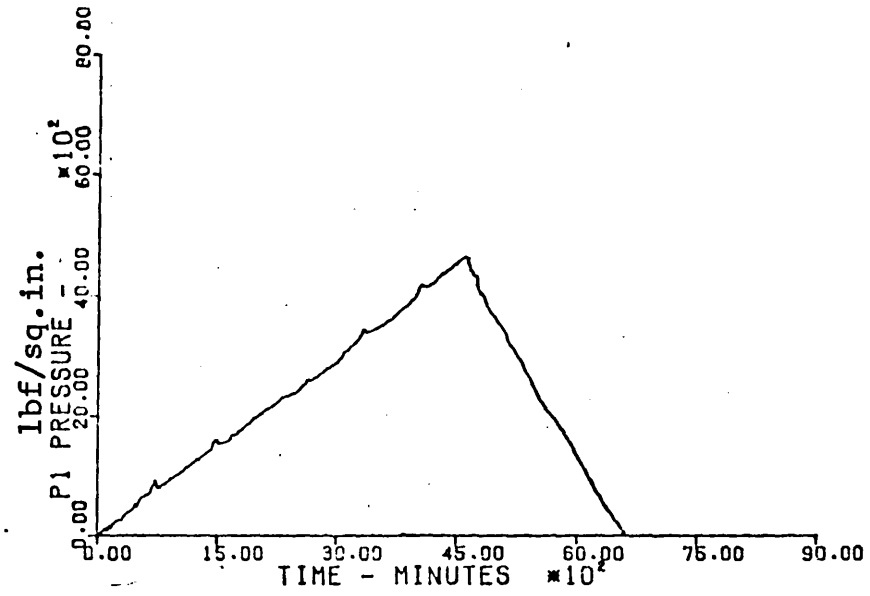


FIG.D.4a PROGRAMMED (P1) PRESSURE TIME VARIATION

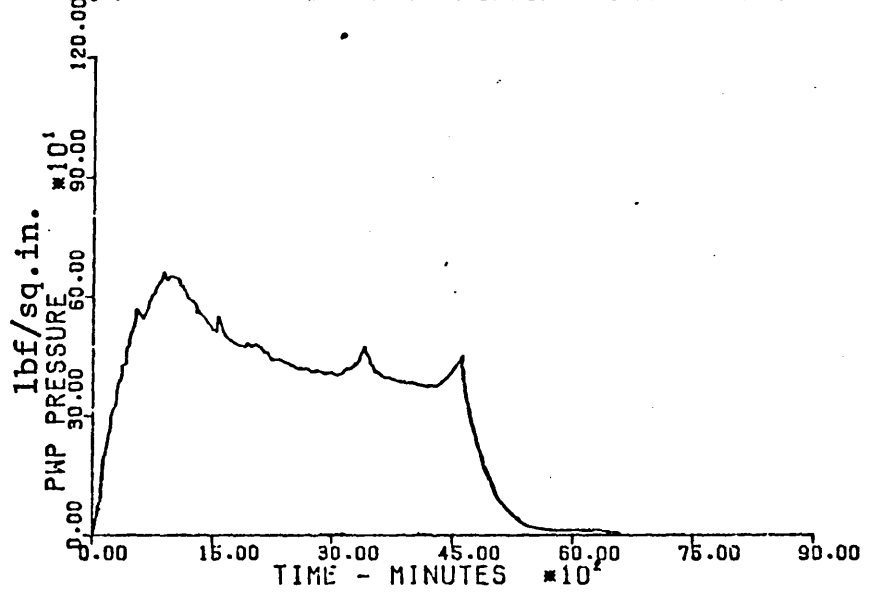


FIG.D.4b RESPONSE OF THE PORE WATER PRESSURE DIFFERENCE

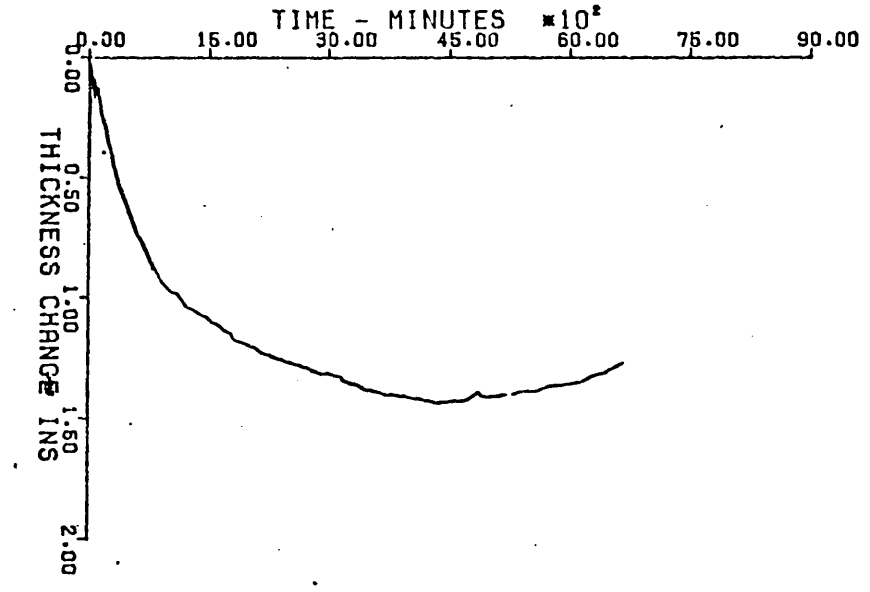
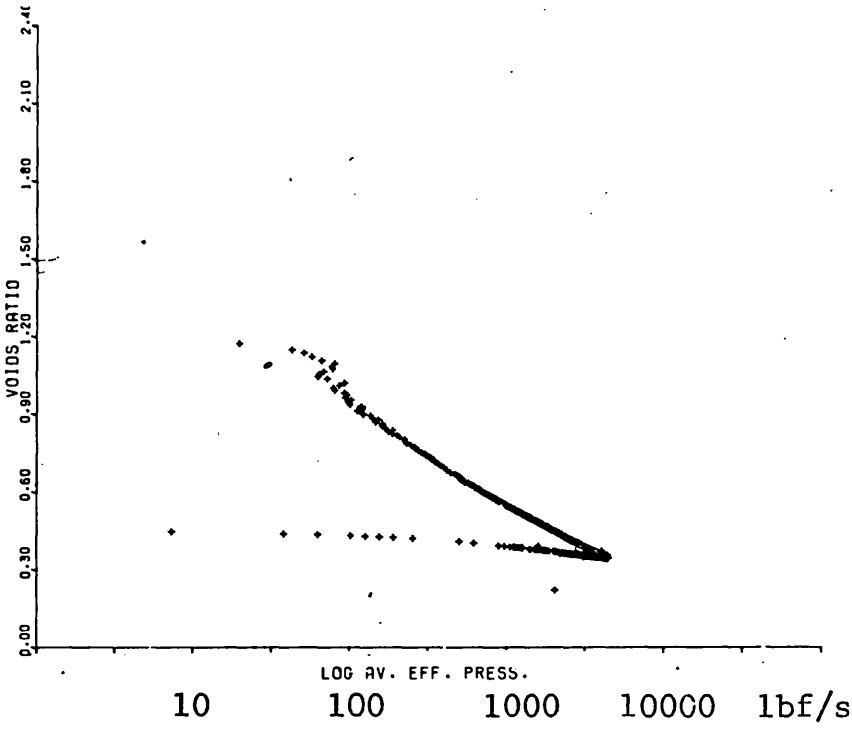
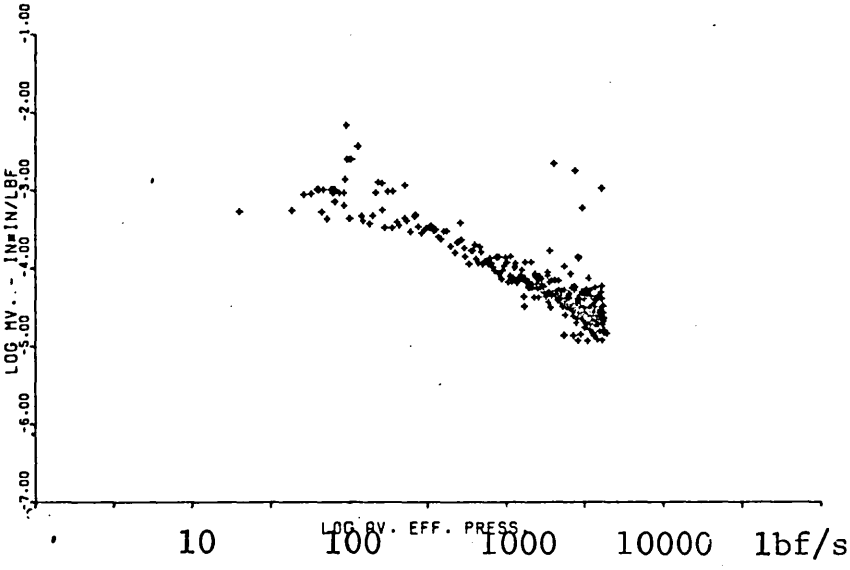


FIG.D.4c CHANGE IN THICKNESS OF THE SAMPLE

FIG. D.4 - VARIATION OF OBSERVED PARAMETERS IN TEST BC.CHP.14



E - LOGP PLOT FOR TEST BC.CHP.14



COEFF. OF VOL. DECREASE - LOGP FOR TEST BC.CHP.14

FIGURE D.5 Consolidation characters in Test BC.CHP.14.

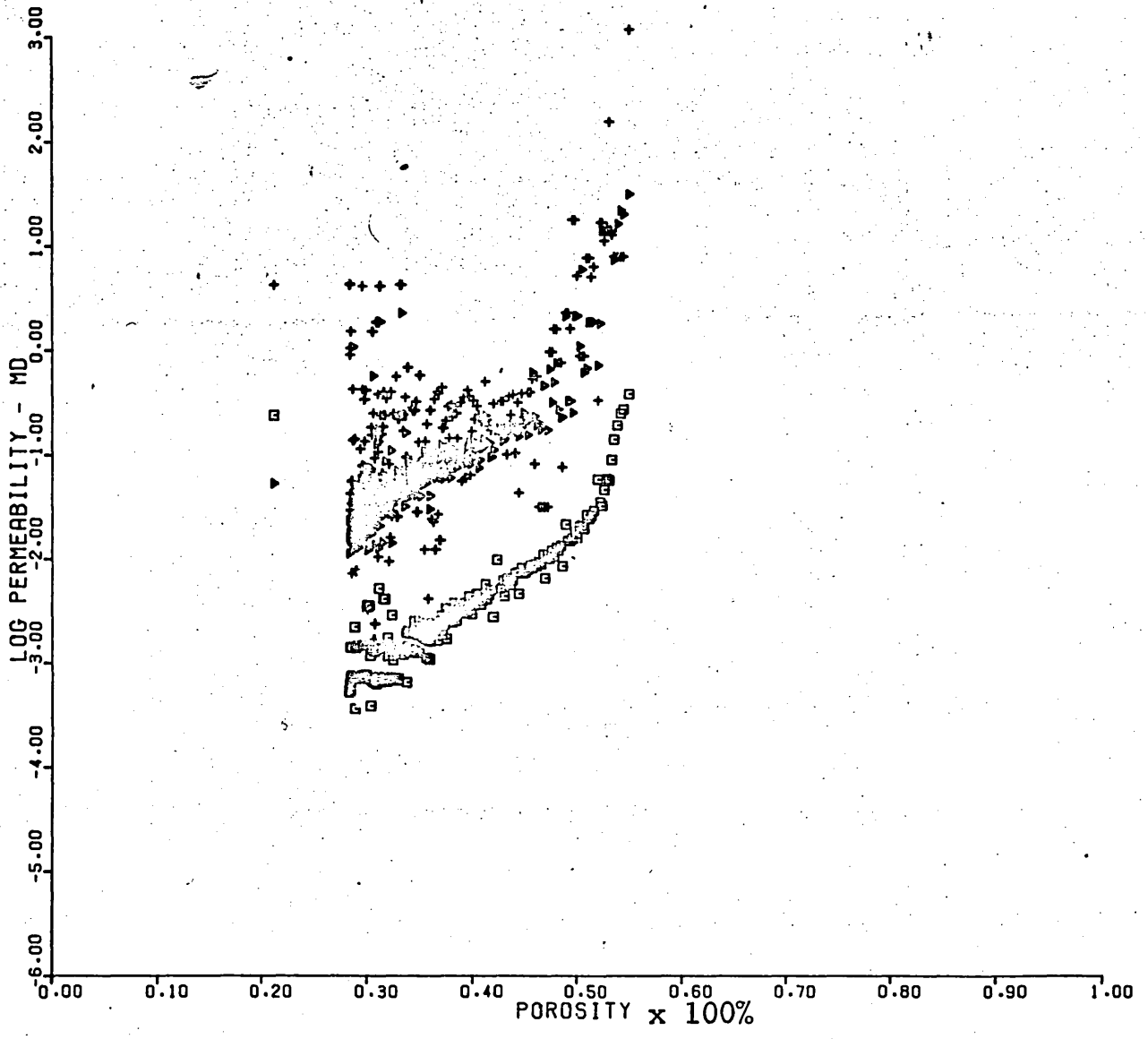


FIGURE D.6

PERMEABILITY - POROSITY PLOT FOR TEST BC.CHP.14

CROSS - CV CORRECTED

TRIANGLE - CV UNCORRECTED

SQUARE - LINEAR PW VARIATION ASSUMED

TEST NO. BC.CHP.15 Date: 22.5.73

Details of Test Material

Clay type; Ball clay properties in Table 6.II.
State of original sample; remoulded with half-normal saline water.

Type of Test

Rate of loading; 1 psi per minute.
Salinity of the pore fluid initially; half-normal saline.
Maximum consolidating pressure; 7000 psi.

Proposed Investigation

To investigate the influence of a saline pore fluid.

Initial Condition of the Sample

Moisture Content; 97.8 per cent.
Thickness; 5.45 inches.
Weight; 3.549 lbf.

Preconsolidation Stage

Rate of strain; 0.0017 inches per minute.
Maximum preconsolidation stress; 85 psi.
Moisture content after preconsolidation; 61.60 per cent.
Thickness after preconsolidation; 3.437 inches.
Weight after preconsolidation; 2.645 lbf.

Loading Stage

Total decrease in thickness; 1.58 inches.
Equivalent change in void ratio;

Unloading Stage

Total decrease in thickness; very rapid.
Total rebound of the sample; could not be monitored.

Final Condition of the Sample

Moisture content; 11.75 per cent.
Thickness; 2.210 inches.
Weight; 2.05 lbf.

Further Comments

In this test the pore fluid was saline and it was observed that (all other conditions remaining the same) the magnitude of the pore fluid pressure was less than in the earlier tests. But a second peak of very high intensity was observed (see Figure D.7); this too was associated with a peak in the consolidation curve. However, in this test the first one occurred as a result of an excessive build up of P_1' and its subsequent fall. With the rise in u_t the displacement monitor suddenly failed due to an earthing fault caused by the entry of pore fluid into the transducer housing. Therefore the unloading stage had to be rapidly executed so as to avoid the occurrence of unmonitored swelling.

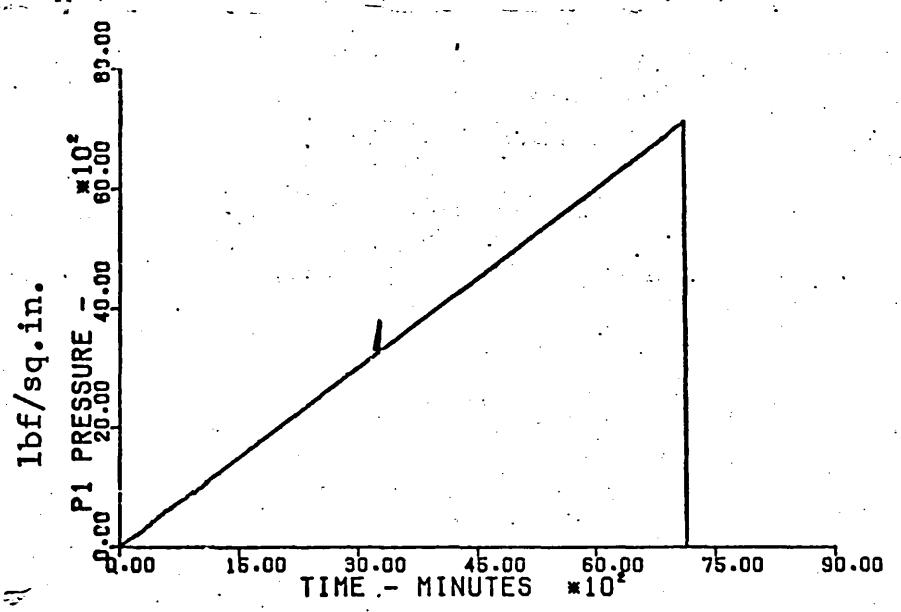


FIG.D.7a PROGRAMMED (P1) PRESSURE TIME VARIATION

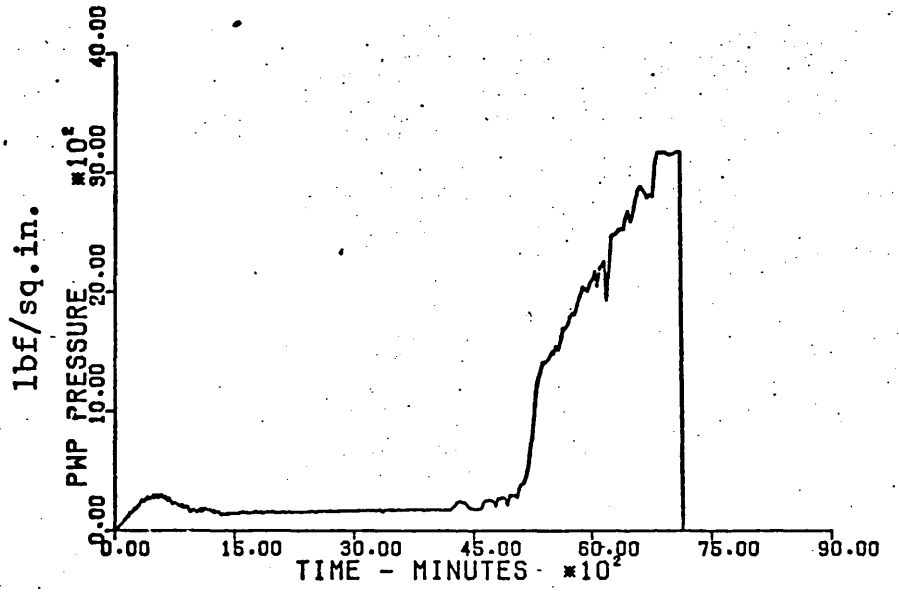


FIG.D.7b RESPONSE OF THE PORE WATER PRESSURE DIFFERENCE

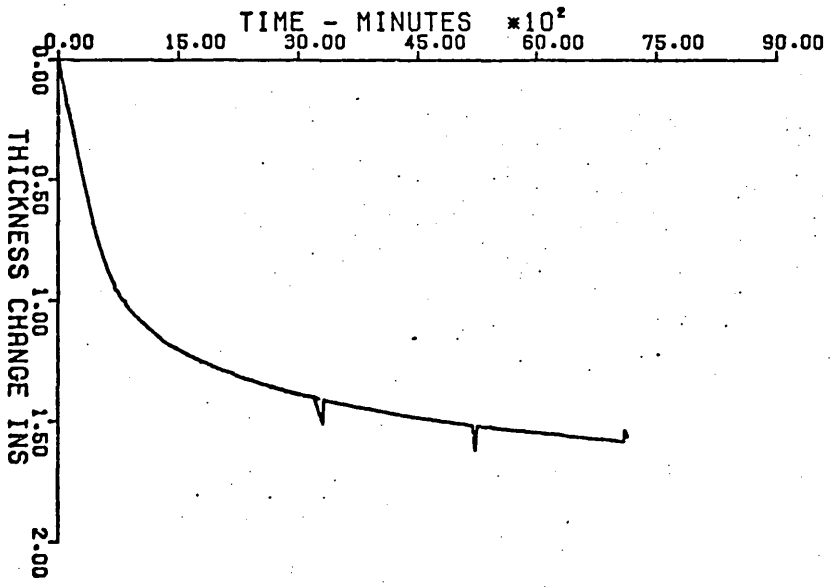
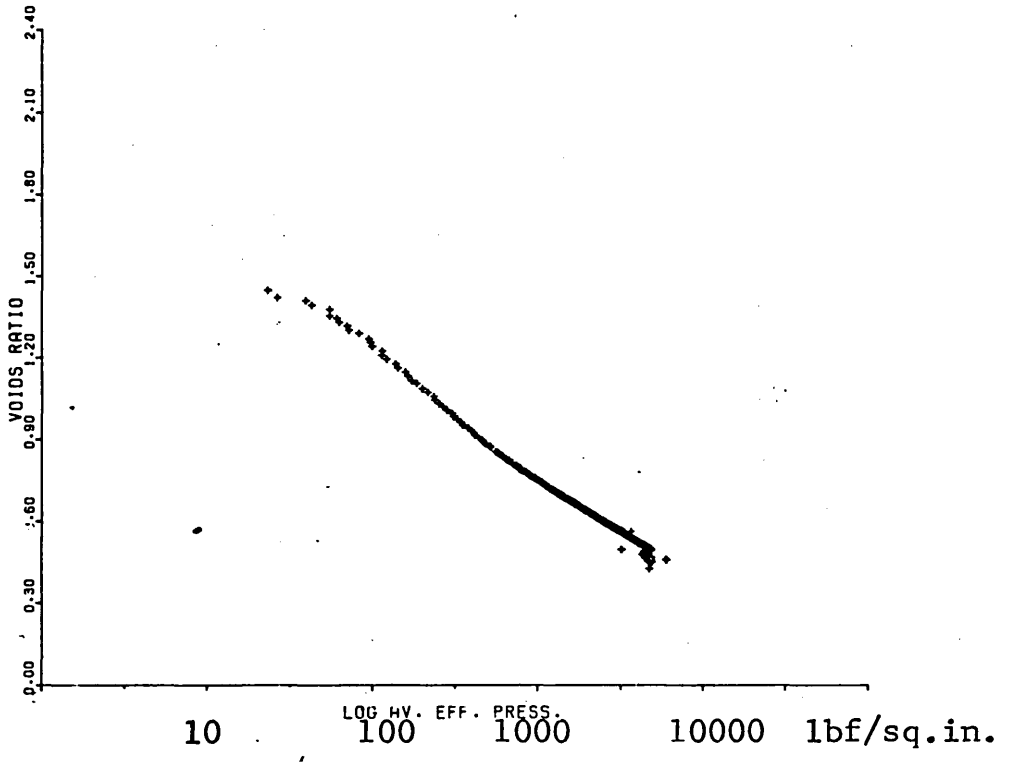
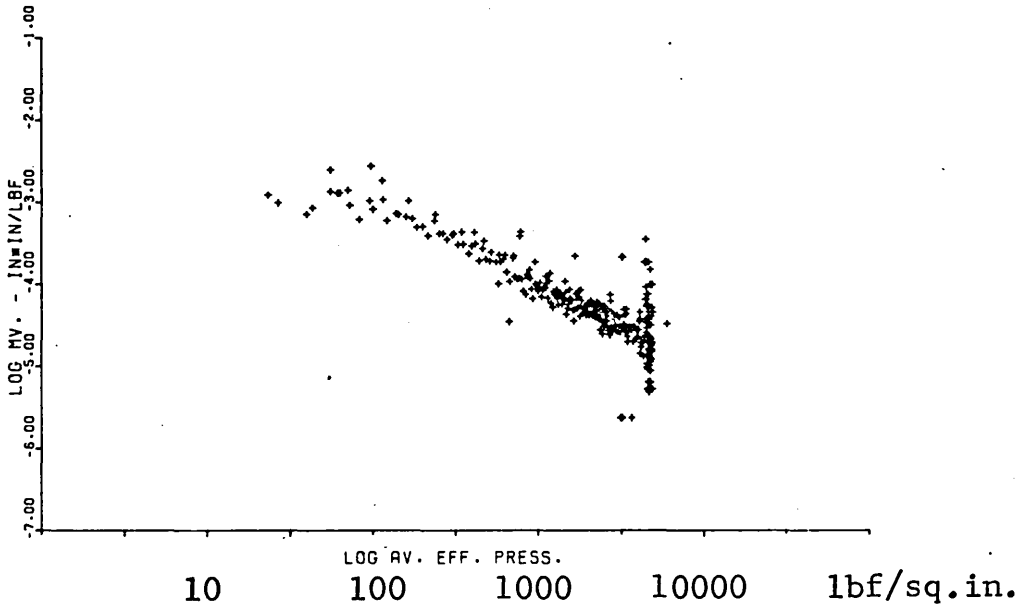


FIG.D.7c CHANGE IN THICKNESS OF THE SAMPLE

FIG. D.7 - VARIATION OF OBSERVED PARAMETERS IN TEST BC.CHP.1



E - LOGP PLOT FOR TEST BC.CHP.15



COEFF. OF VOL. DECREASE - LOGP FOR TEST BC.CHP.15

FIGURE D.8 Consolidation characters in Test BC.CHP.15.

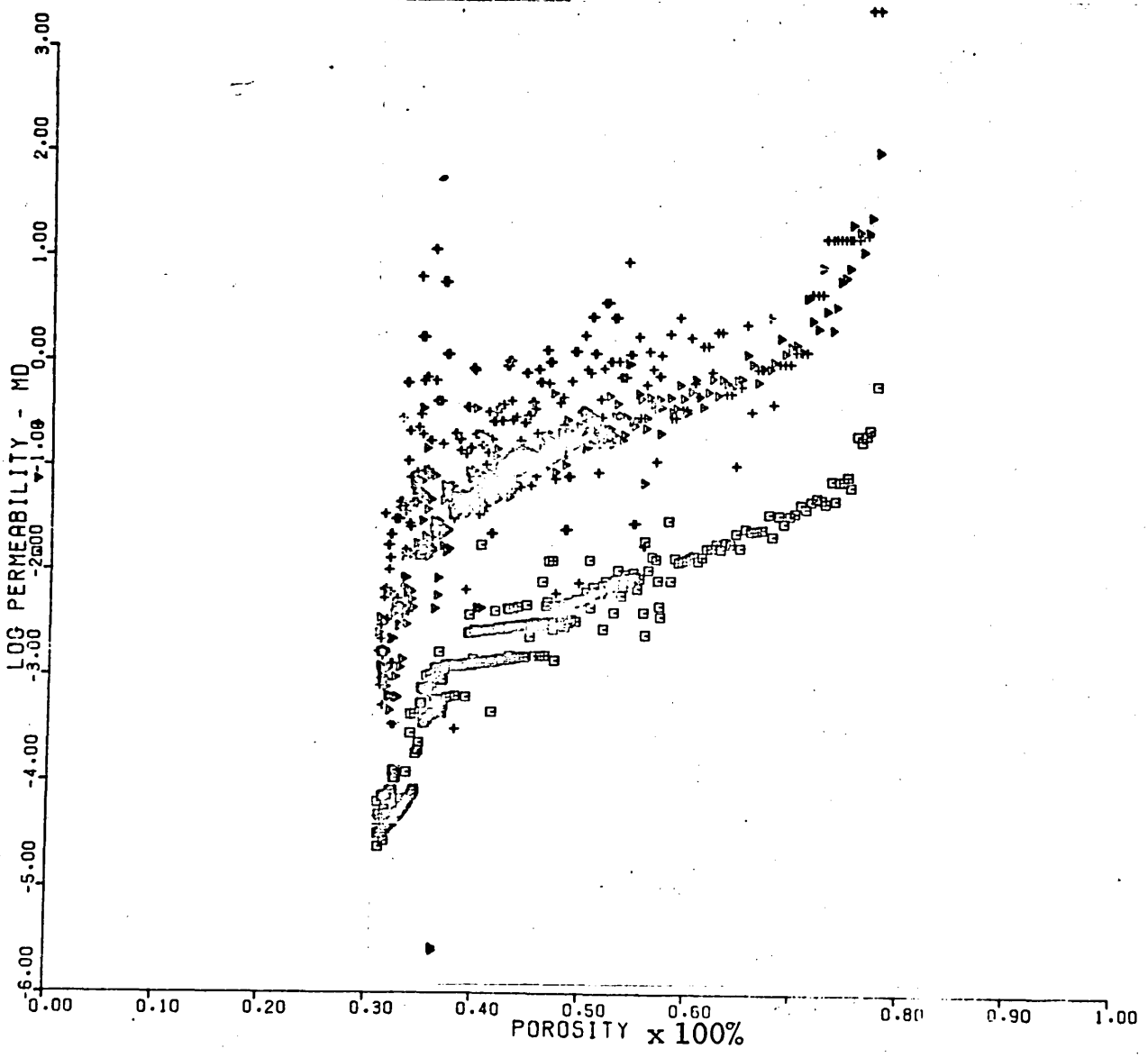


FIGURE D.9

PERMEABILITY - POROSITY PLOT FOR TEST BC.CHP.15

CROSS - CV CORRECTED

TRIANGLE - CV UNCORRECTED

SQUARE - LINEAR PK VARIATION ASSUMED

TEST NO. BC.CHP.17 Date: 2.7.73

Details of Test Material

Clay type; Ball clay; properties as in Table 6.II.
State of original sample; remoulded in saline water.

Type of Test

Rate of loading; 1 psi per minute.
Salinity of the pore fluid initially; unit salinity.
Maximum consolidation pressure; 5520 psi.

Proposed Investigation

The influence of an increased salinity on consolidation behaviour.

Initial Condition of the Sample

Moisture content; 94.0 per cent.
Thickness; 5.68 inches.
Weight; 3.527 lbf.

Preconsolidation Stage

Rate of strain; 0.0017 inch/min.
Maximum preconsolidation stress;
Moisture content after preconsolidation; 64.80 per cent.
Thickness after preconsolidation; 3.880 inches.
Weight after preconsolidation; 2.734 lbf.

Loading Stage

Total decrease in thickness; 1.335 inches.
Equivalent change in void ratio;

Unloading Stage

Rate of unloading; very rapid.
Total rebound of the sample; not monitored.

Final Condition of the Sample

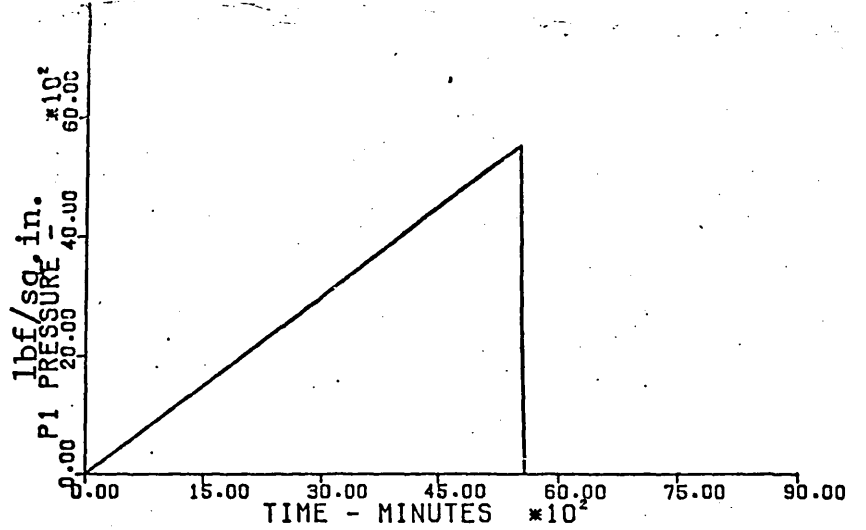
Moisture content; 16.36 per cent.
Thickness; 2.3125 inches.
Weight; 2.110 lbf.

Further Comments

This test showed that an increased salinity of the pore fluid further weakened the intensity of the first pore water pressure peak.

Around 1400 psi P_1' pressure, an instantaneous swell of the sample was noticed (see figure D.10). At the same time, the pore fluid pressure began to rise again and at about 5500 psi P_1' pressure, the displacement transducer did not read due to a short circuit. This resulted from a seepage of pore water near the bulkhead connector.

The specimen was quickly unloaded to avoid excessive unmonitored swelling.



FIGD 10a PROGRAMMED (P1) PRESSURE TIME VARIATION

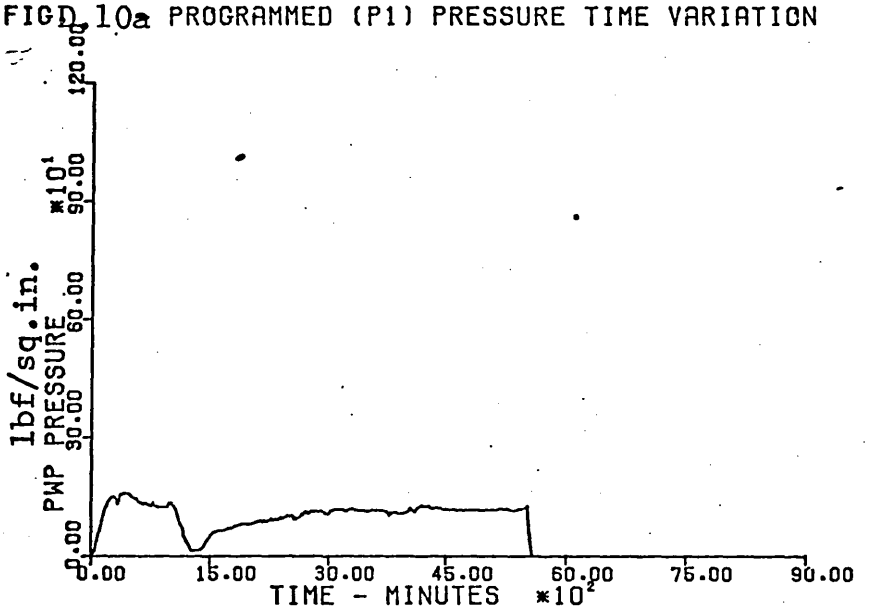


FIG.D.10b RESPONSE OF THE PORE WATER PRESSURE DIFFERENCE

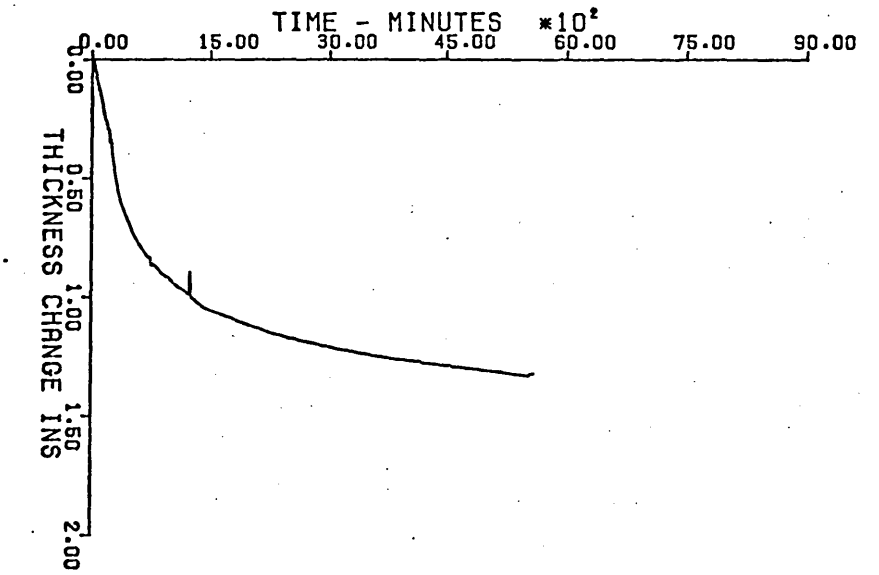
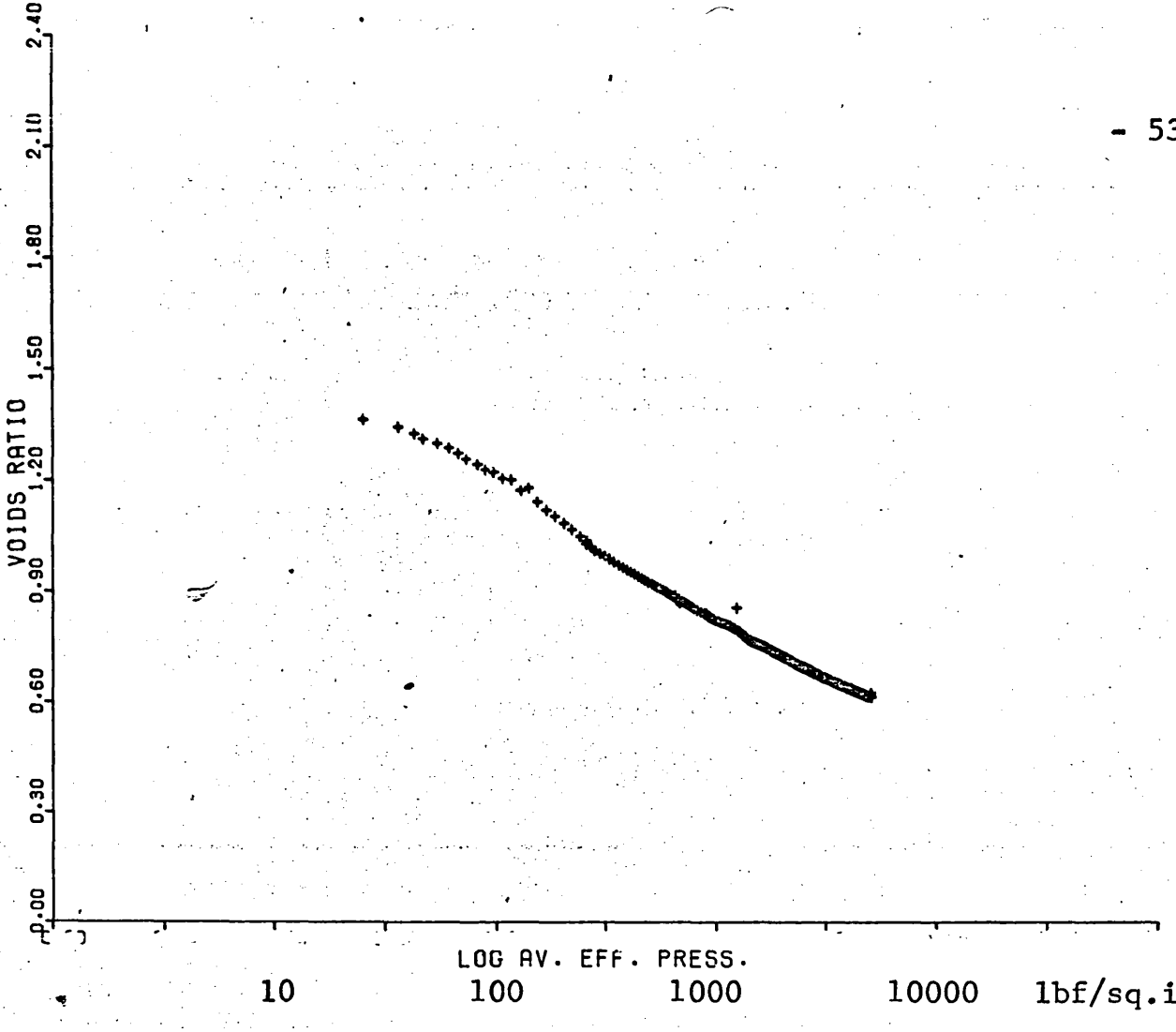
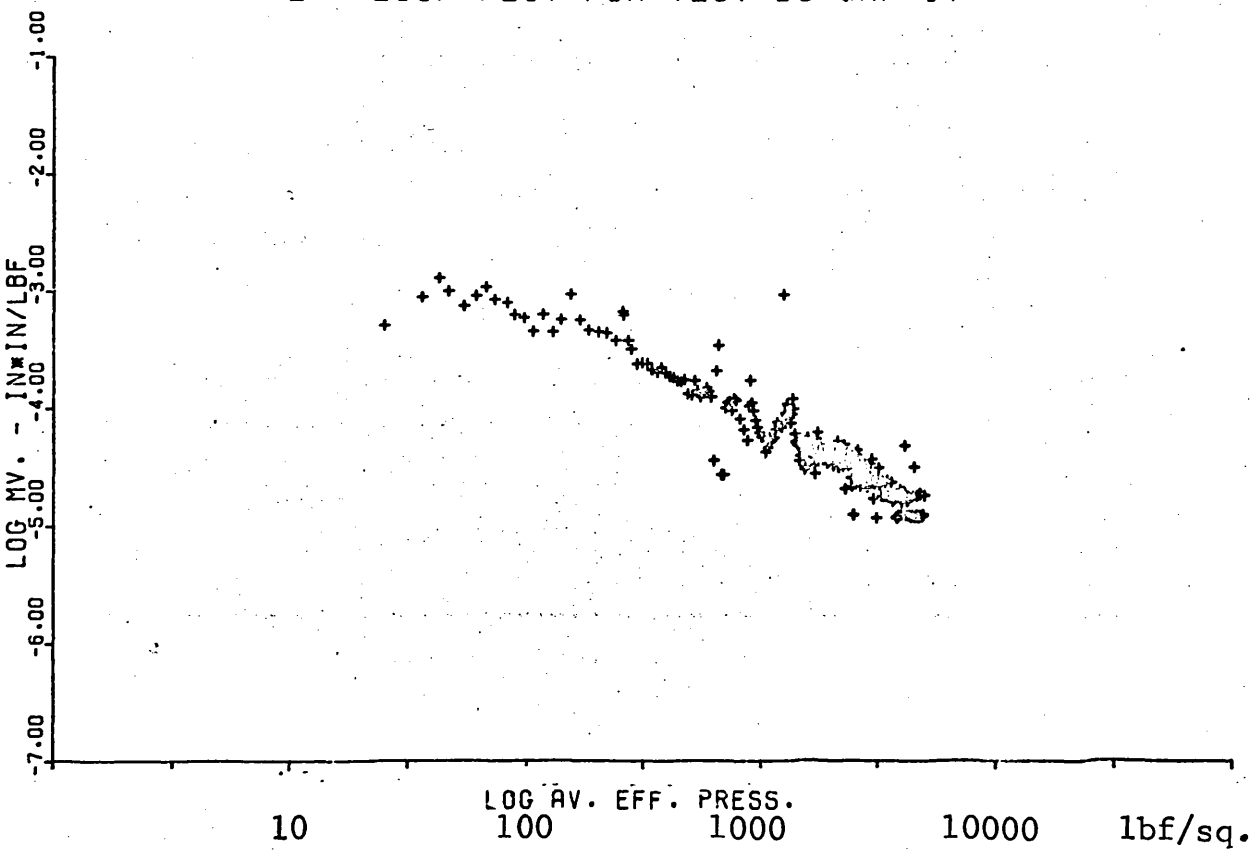


FIG.D.10c CHANGE IN THICKNESS OF THE SAMPLE

FIG. D.10 VARIATION OF OBSERVED PARAMETERS IN TEST BC.CHP.17



E - LOGP PLOT FOR TEST BC.CHP.17



COEFF. OF VOL. DECREASE - LOGP FOR TEST BC.CHP.17

FIGURE D.11 Consolidation characters in Test BC.CHP.17

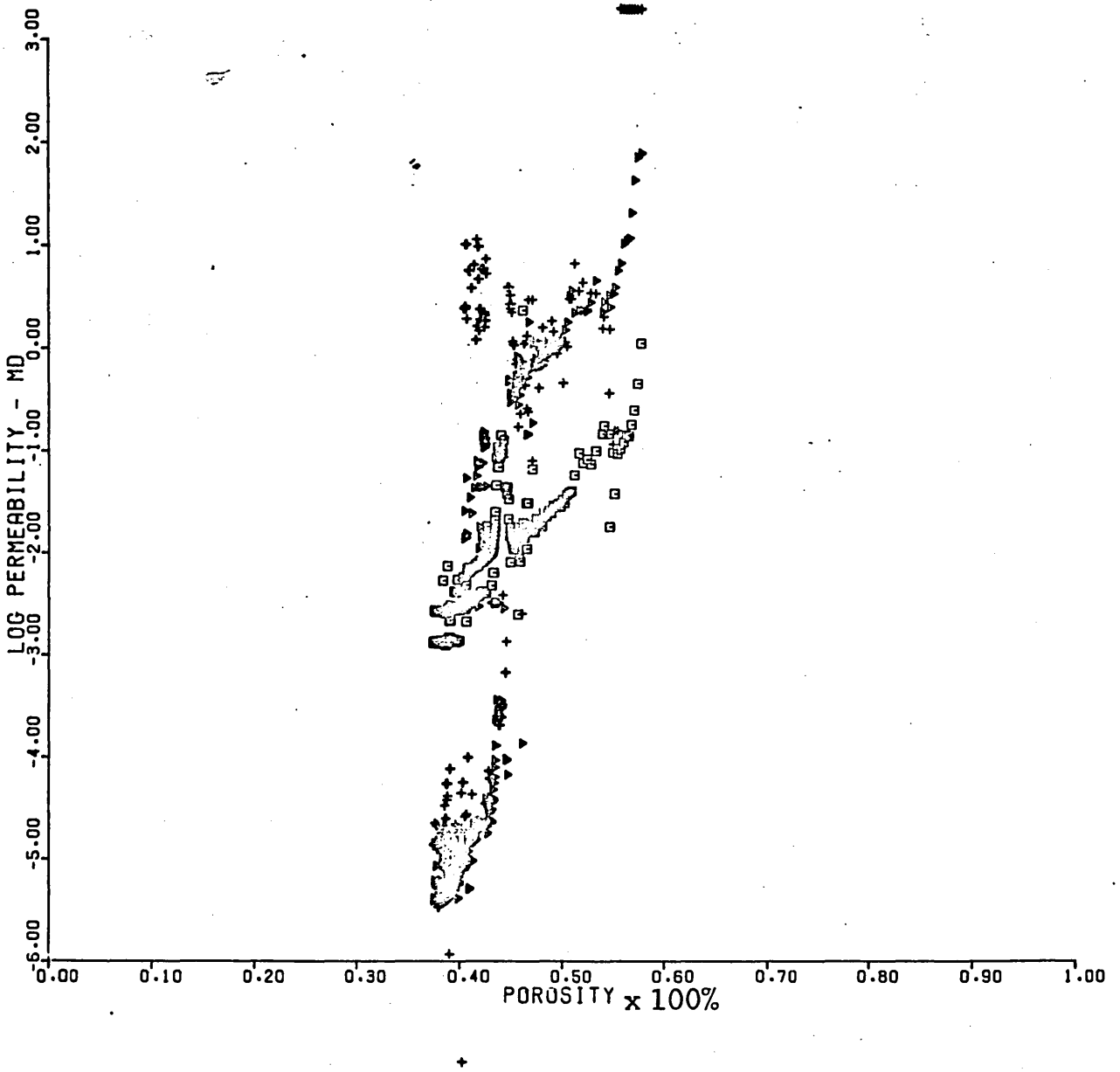


FIGURE D.12

PERMEABILITY - POROSITY PLOT FOR TEST BC.CHP.17

CROSS - CV CORRECTED

TRIANGLE - CV UNCORRECTED

SQUARE - LINEAR PW VARIATION ASSUMED

TEST NO. BC.CHP.18 Date: 5.10.73

Details of Test Material

Clay type; Ball clay; properties as in Table 6.II.
State of original sample; remoulded in distilled water.

Type of Test

Rate of loading; 2 psi per minute.
Salinity of the pore fluid initially; non saline.
Maximum consolidating pressure; 5015 psi.

Proposed Investigation

Second of a series of tests to investigate the effect of the rate of loading on the properties of the specimen.

Initial Condition of the Sample

Moisture content; 86.0 per cent.
Thickness; 5.775 inches.
Weight; 2.866 lbf.

Preconsolidation Stage

Rate of strain; 0.0017 inches/min.
Maximum preconsolidation stress; 80 psi.
Moisture content after preconsolidation; 61.0 per cent.
Thickness after preconsolidation; 3.955 inches.
Weight after preconsolidation; 2.381 lbf.

Loading Stage

Total decrease in thickness; 1.5548 inches.
Equivalent change in void ratio;

Unloading Stage

Rate of unloading; 2 psi per minute.
Total rebound of the sample; 0.0906 inches.

Final Condition of the Sample

Moisture content; 16.36 per cent.
Thickness; 2.3125 inches.
Weight; 2.110 lbf.

Further Comments

This was a fairly successful test except for times when the pressure pencil piston had been jammed on either increase or decrease (total number of occurrences = 4 times). The effects of such are clearly evident from the respective pore water pressure response curve (Figure D.13).

The obvious effect of the increased loading rate was to intensify the pore water pressure peak.

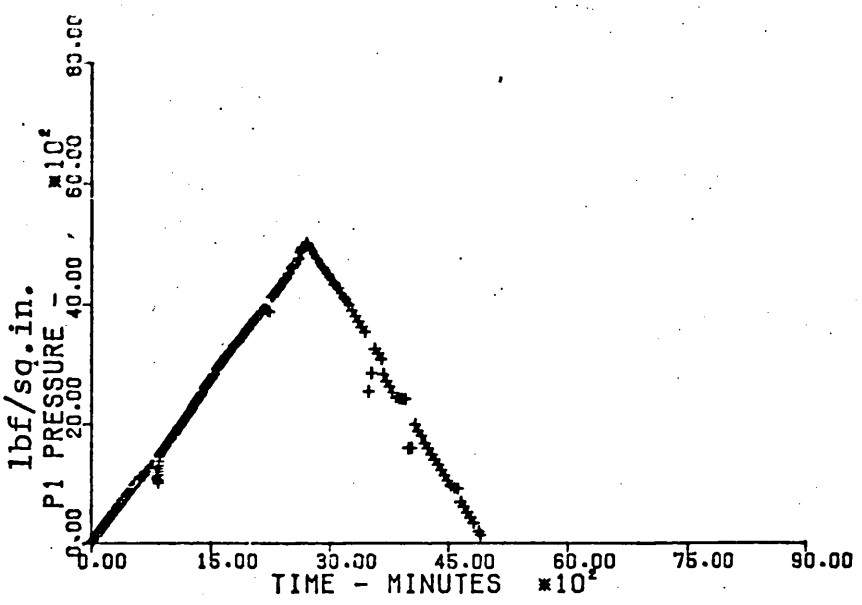


FIG D.13a PROGRAMMED (P1) PRESSURE TIME VARIATION

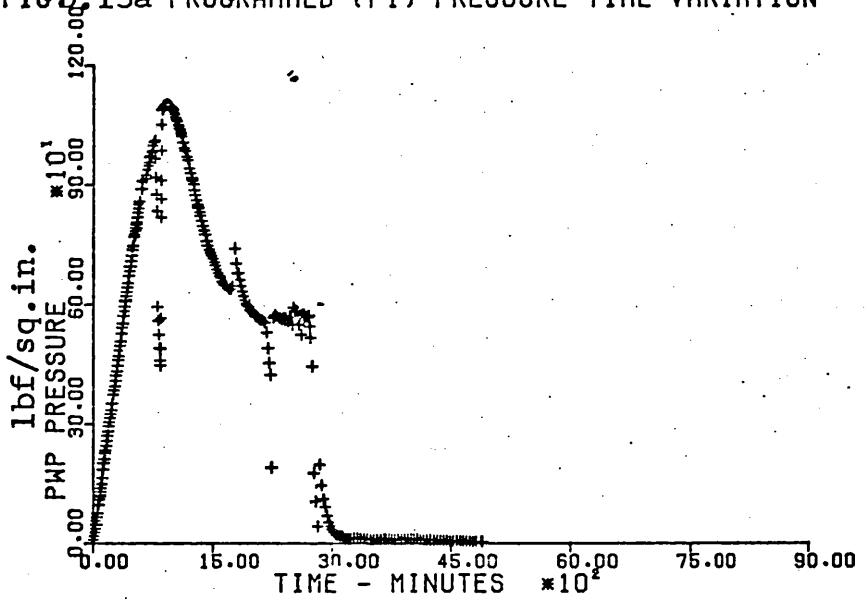


FIG D.13b RESPONSE OF THE PORE WATER PRESSURE DIFFERENCE

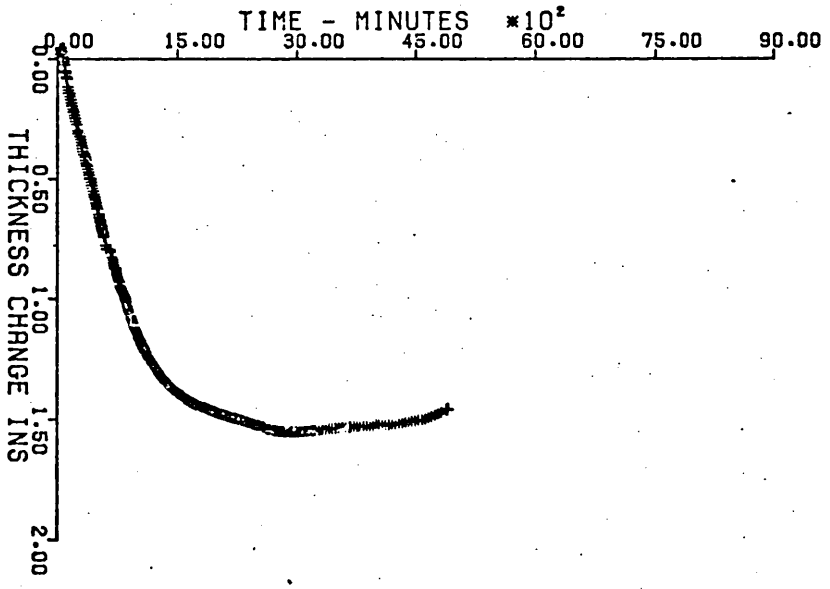
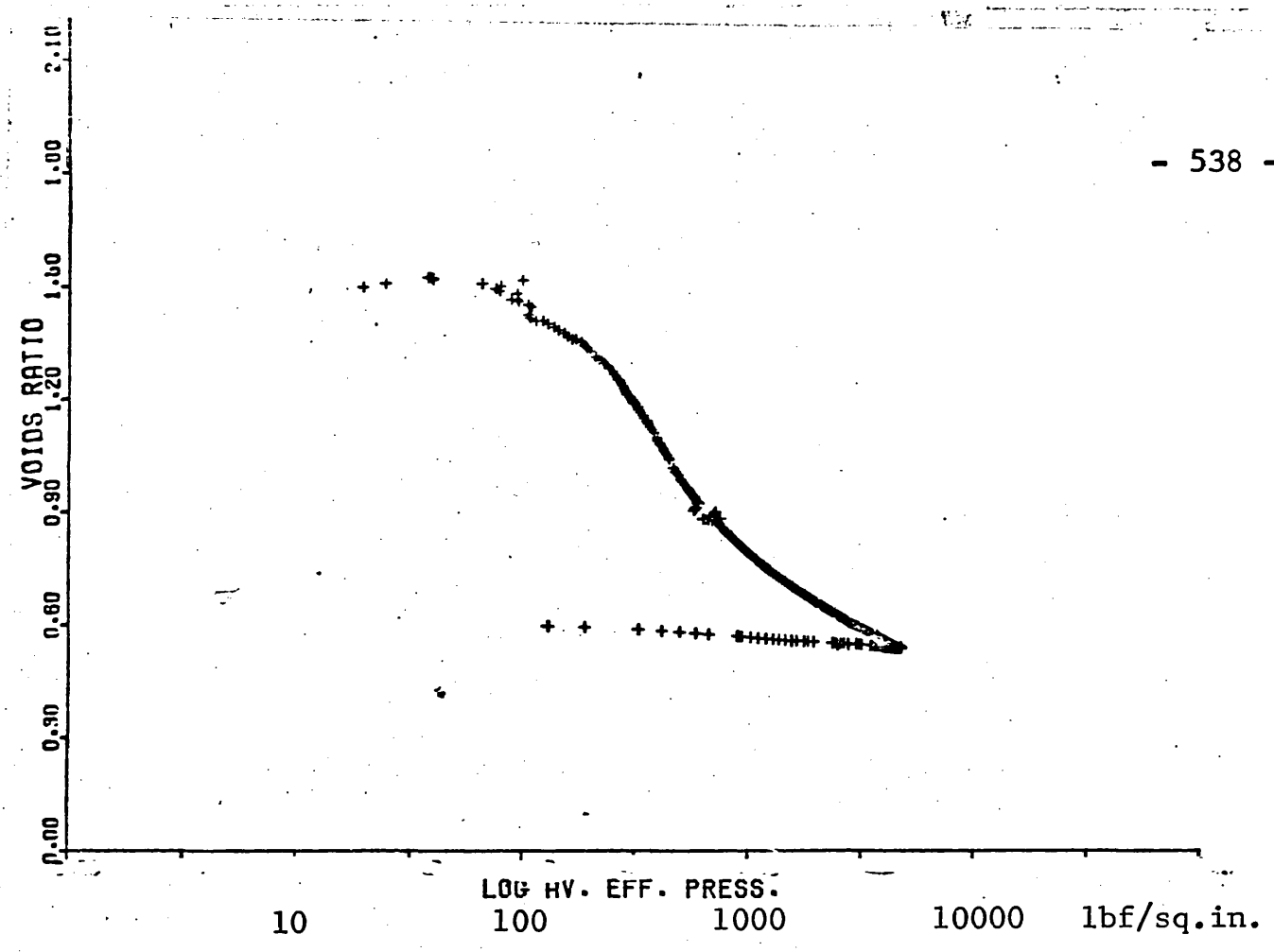
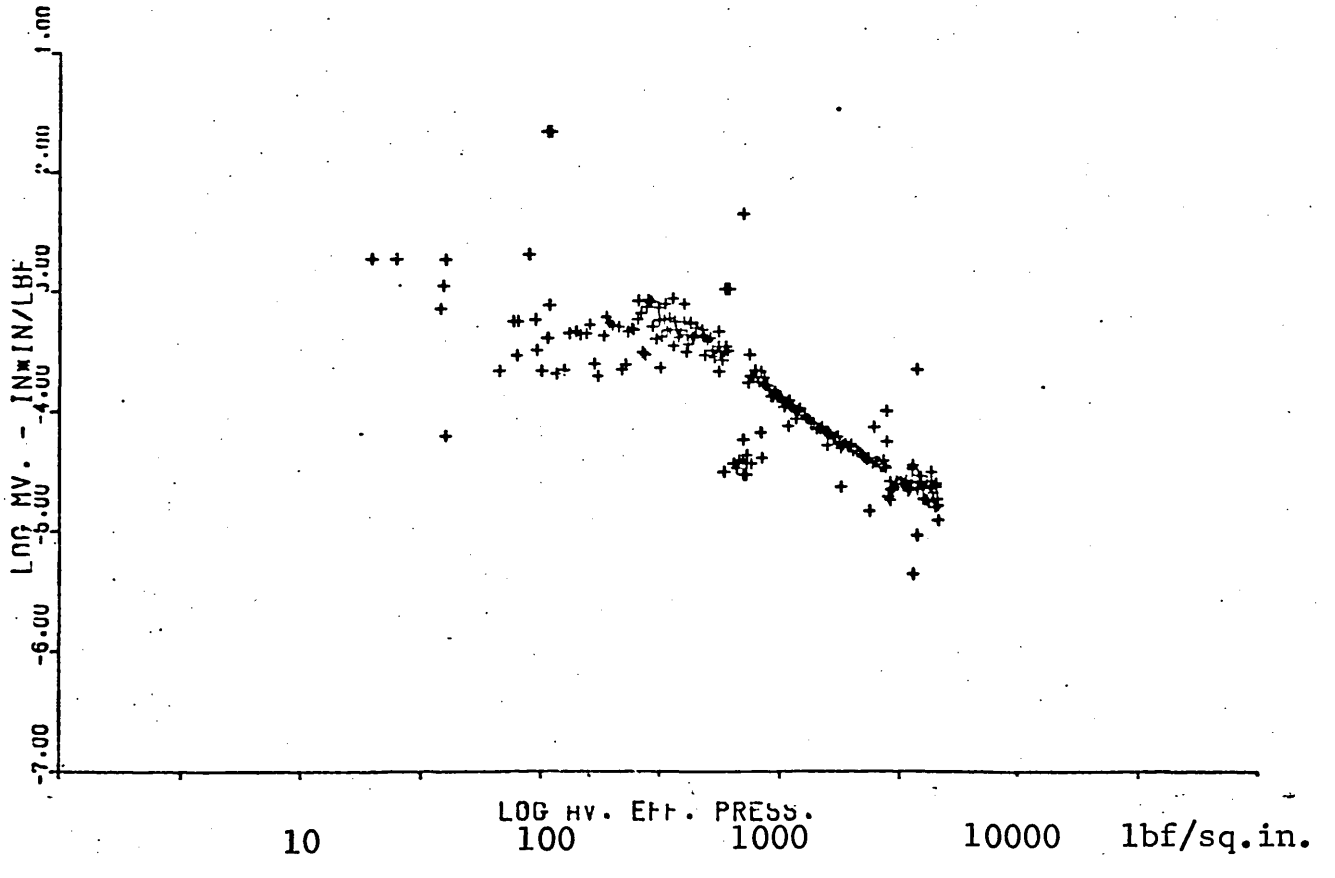


FIG D.13c CHANGE IN THICKNESS OF THE SAMPLE

FIG.D.13 - VARIATION OF OBSERVED PARAMETERS IN TEST BC.CHP.18



E - LOGP PLOT FOR TEST BC.CHP.18



COEFF. OF VOL. DECREASE - LOGP FOR TEST BC.CHP.18

FIGURE D.14 Consolidation characters in Test $BC_{CHP.18}$

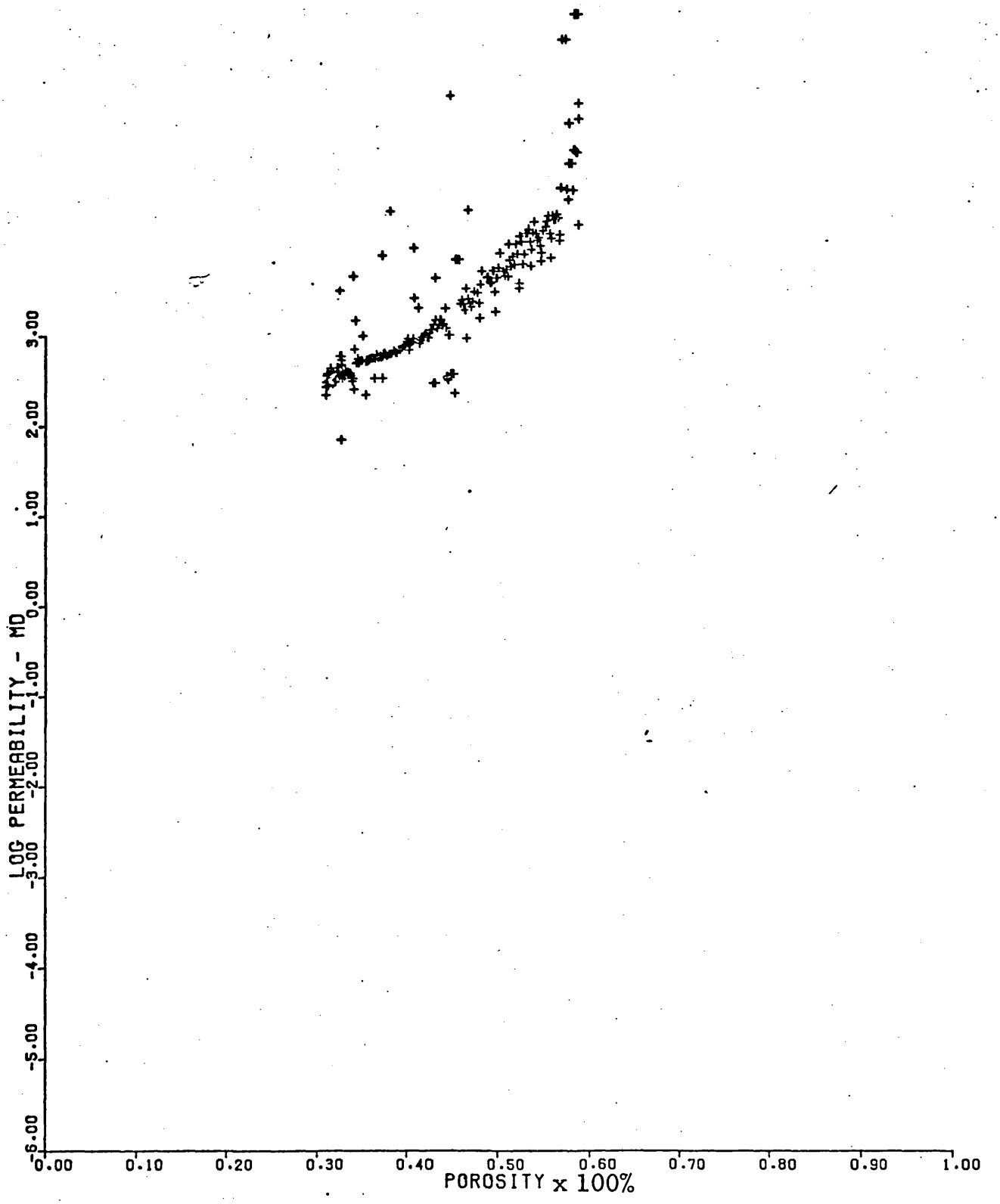


FIGURE D.15

PERMEABILITY - POROSITY PLOT FOR TEST BC.CHP.18

TEST NO. BC.CHP.19 Date: 26.10.73

Details of Test Material

Clay type; Ball clay; properties as in Table 6.II.
State of original sample; remoulded in distilled water.

Type of Test

Rate of loading; ½ psi per minute.
Salinity of the pore fluid initially; non saline.
Maximum consolidation pressure; 6504 psi.

Proposed Investigation

The third test of a series investigating the influence of rate of loading on the compaction behaviour.

Initial Condition of the Sample

Moisture content; 113.0 per cent.
Thickness; 5.405 inches.
Weight; 3.439 lbf.

Preconsolidation Stage

Rate of strain; 0.0017 inches per minute.
Maximum preconsolidation stress; 85 psi.
Moisture content after preconsolidation; 69.65.
Thickness after preconsolidation; 3.655 inches.
Weight after preconsolidation; 2.954 inches.

Loading Stage

Total decrease in thickness; 1.715 inches.
Equivalent change in void ratio;

Unloading Stage

Rate of unloading; 2 psi per minute.
Total rebound of the sample; 0.1278 inches.

Final Condition of the Sample

Moisture content; 13.13 per cent.
Thickness; 1.969 inches.
Weight; 1.825 lbf.

Further Comments

The instantaneous decay of pore fluid pressure response seen on Figure D.16 is a result of the pressure pencil piston sticking. The pore fluid pressure peak had a very low intensity associated with the slow rate of loading.

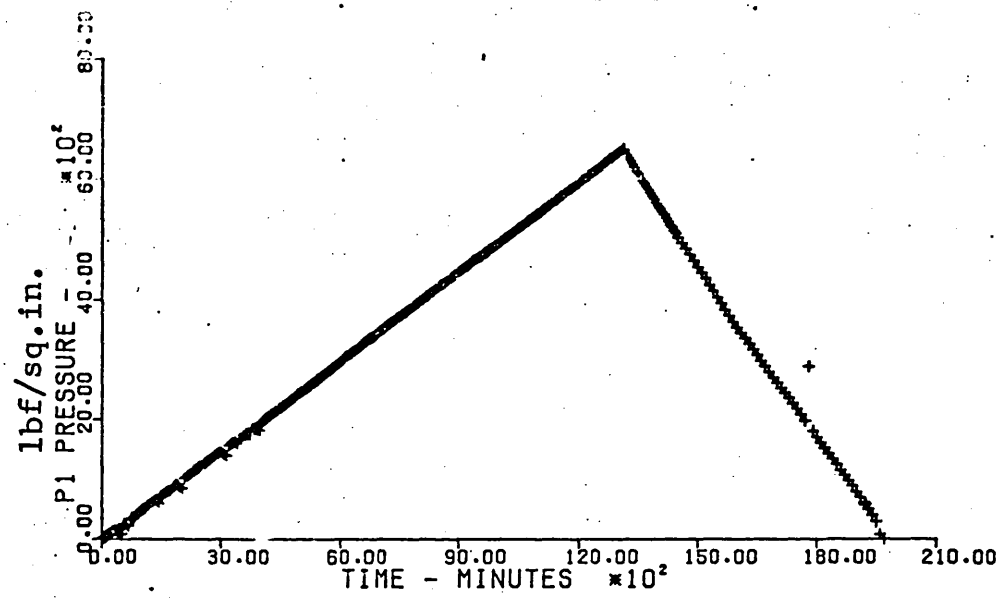


FIG D. 16a PROGRAMMED (P1) PRESSURE TIME VARIATION

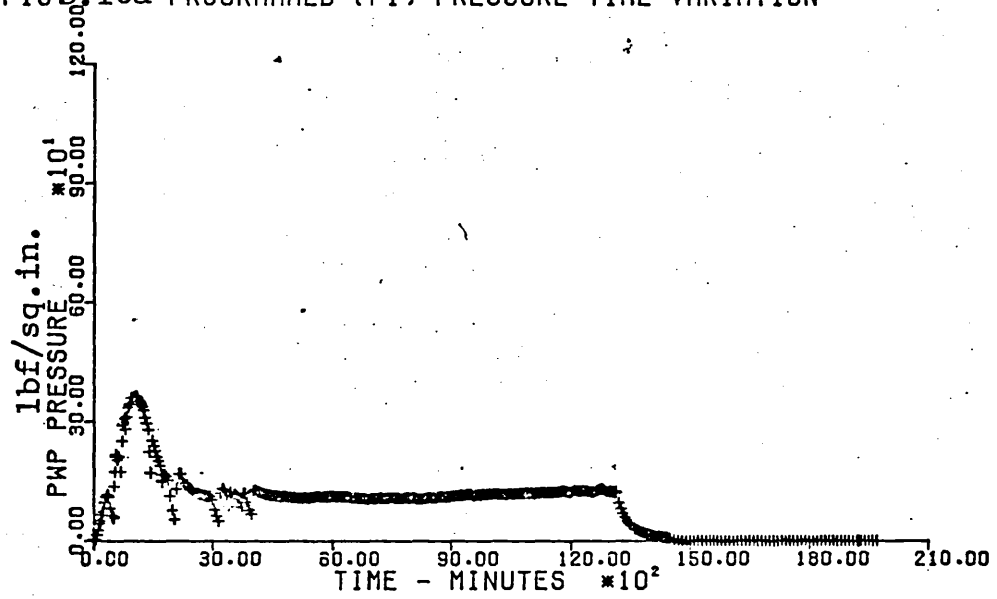


FIG D. 16b RESPONSE OF THE PORE WATER PRESSURE DIFFERENCE

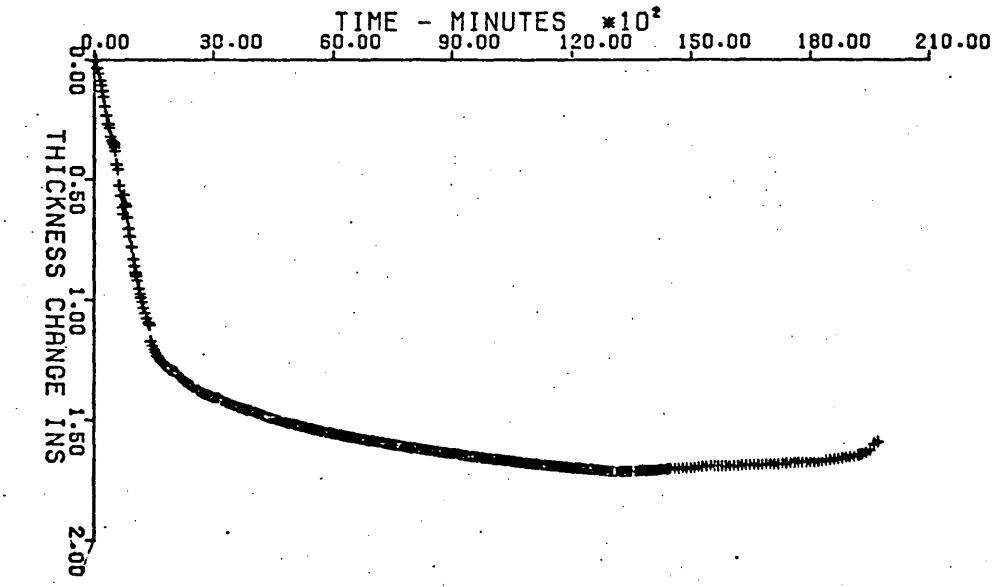
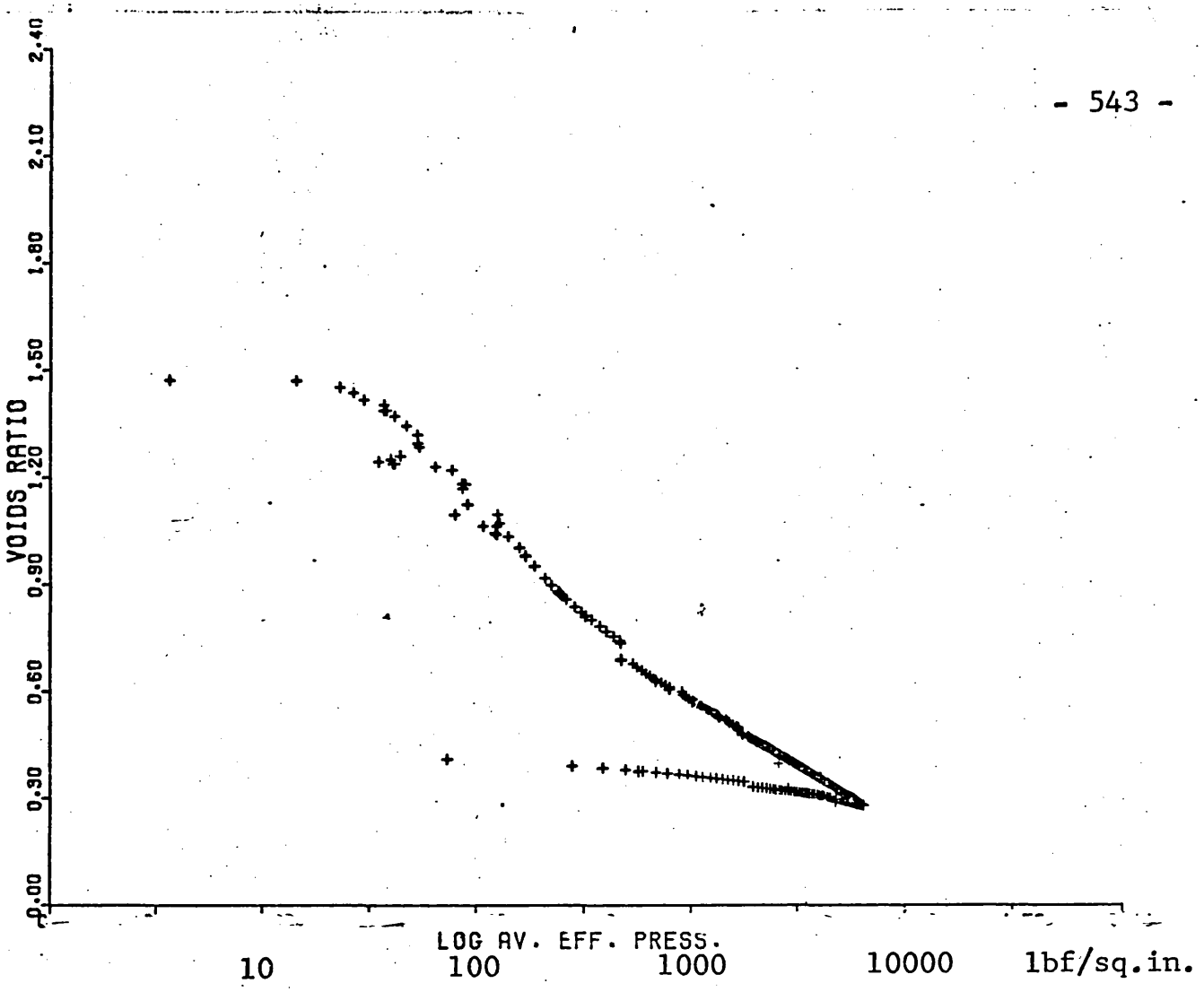
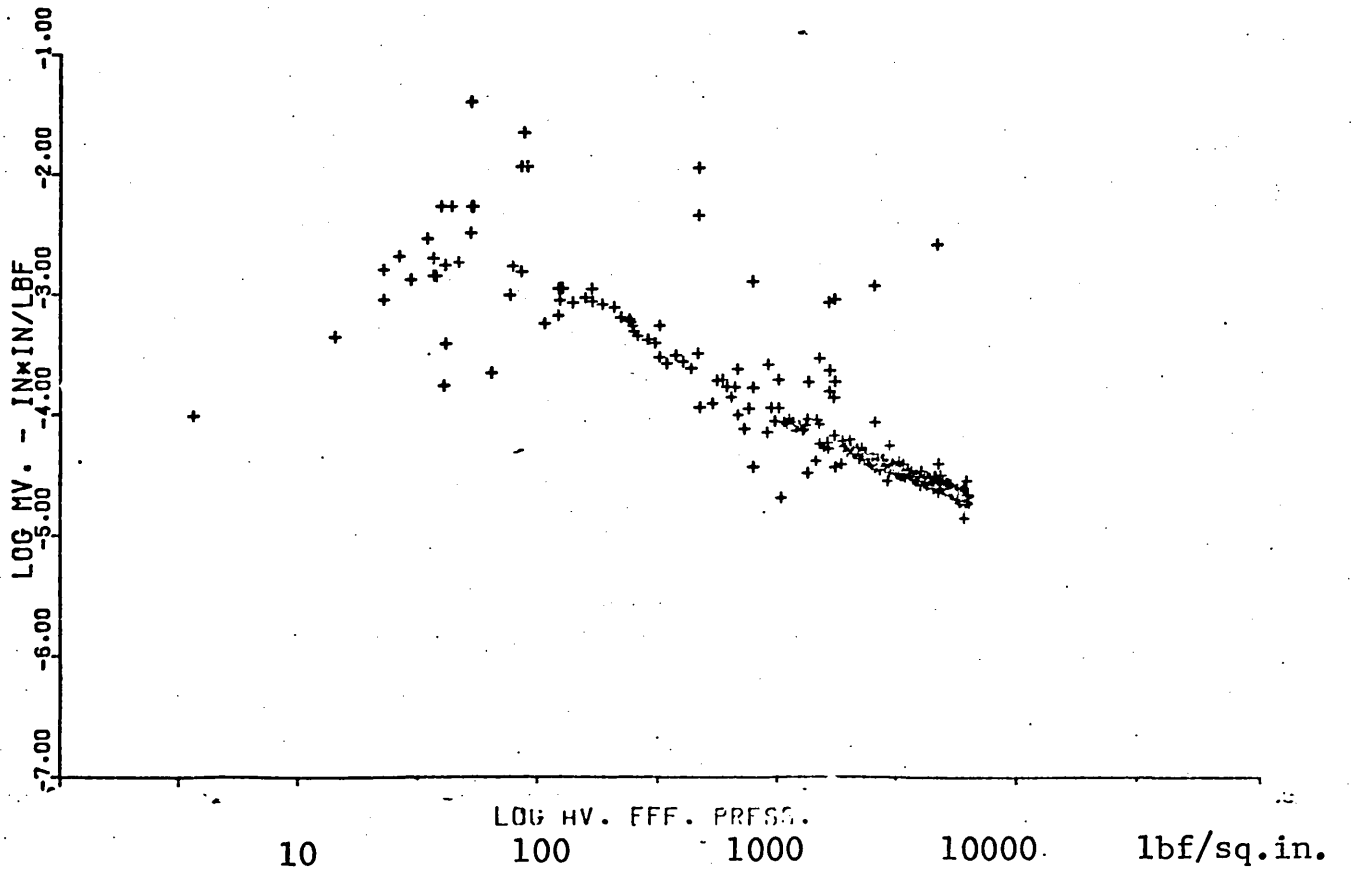


FIG D. 16c CHANGE IN THICKNESS OF THE SAMPLE

FIG. D.16 - VARIATION OF OBSERVED PARAMETERS IN TEST BC.CHP.19



c - LOGP PLOT FOR TEST BC.CHP.19



COEFF. OF VO . DECREASE LOOP FOR TEST BC.CHP.19

FIGURE D.17 Consolidation characters in test BC.CHP.19

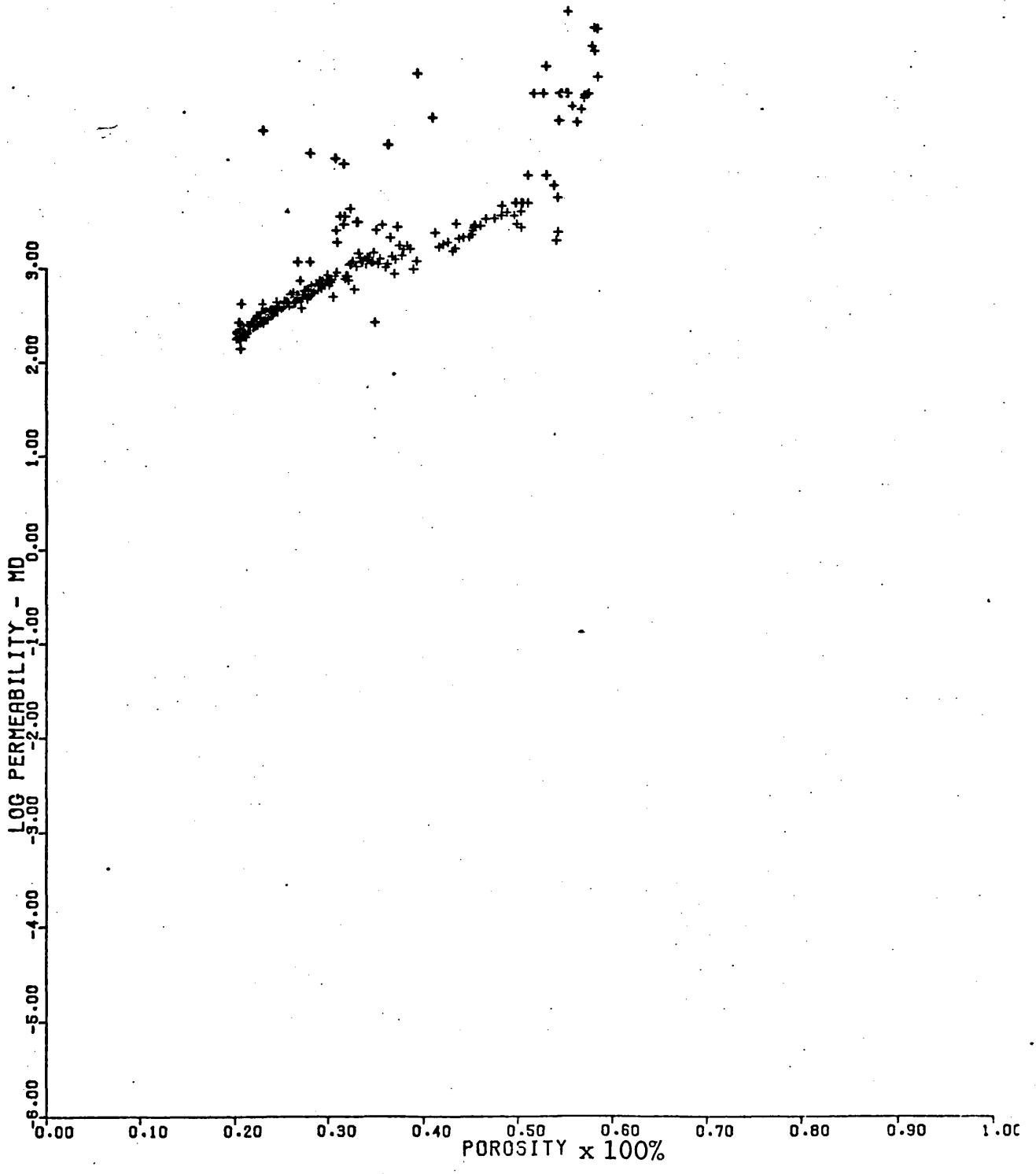


FIGURE D.18

PERMEABILITY - POROSITY PLOT FOR TEST BC.CHP.19

TEST NO. BC.CHP.20 Date: 15.12.73

Details of Test Material

Clay type; Ball clay; properties as in Table 6.II.
State of original sample; remoulded in hypersaline water.

Type of Test

Rate of loading; 2 psi per minute.
Salinity of the pore fluid initially; 2 x normal salinity.
Maximum consolidating pressure 6800 psi.

Proposed Investigation

To complete the series of tests investigating the influence of rate of loading and salinity on compaction behaviour.

Initial Condition of the Sample

Moisture content; 80.0 per cent.
Thickness; 5.80 inches.
Weight; 3.809 lbf.

Preconsolidation Stage

Rate of strain; 0.0017 inches/minute.
Maximum preconsolidation stress; 90 psi.
Moisture content after preconsolidation;
Thickness after preconsolidation; 3.822 inches.
Weight after preconsolidation; 2.921 lbf.

Loading Stage

Total decrease in thickness;
Equivalent change in void ratio;

Unloading Stage

Rate of unloading; 2 psi per minute.
Total rebound of the sample;

Final Condition of the Sample

Moisture content; 20.45 per cent.
Thickness; 2.850 inches.
Weight;

Further Comments

This test gave results that fell in line with the observations of the previous tests. There was, however, frequent difficulty with the sticking of pressure pencil piston.

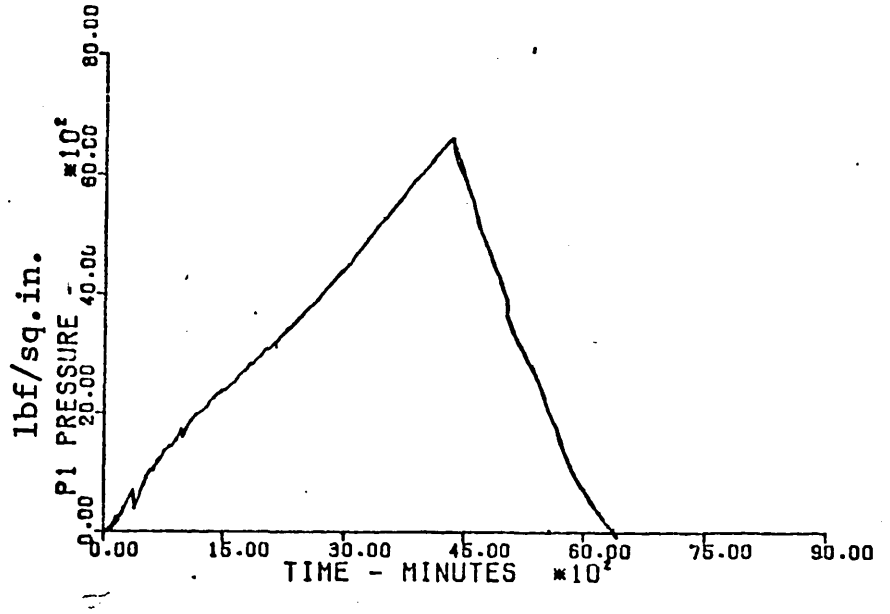


FIG D.19a PROGRAMMED (P1) PRESSURE TIME VARIATION

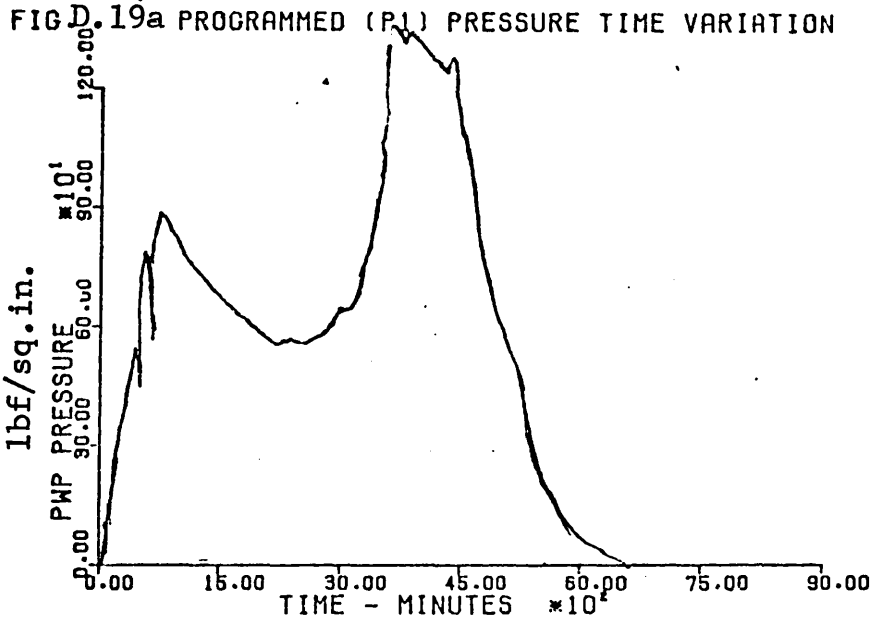


FIG D.19b RESPONSE OF THE PORE WATER PRESSURE DIFFERENCE

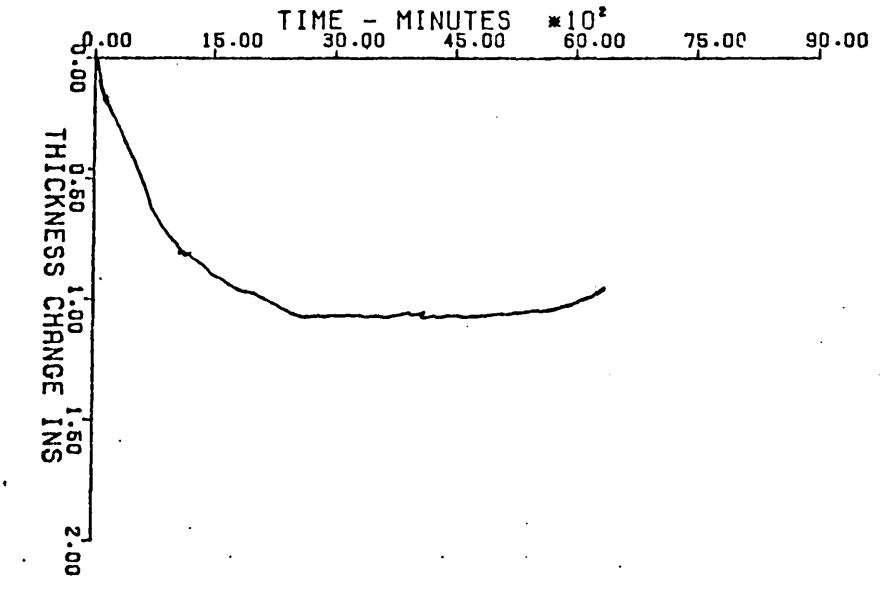


FIG D.19e CHANGE IN THICKNESS OF THE SAMPLE

FIG.D.19 - VARIATION OF OBSERVED PARAMETERS IN TEST BC.CHP.20.

TEST NO. BC.CHP.21 Date: 20.12.73

Details of Test Material

Clay Type; Ball Clay; properties in Table 6.II.
State of original sample; remoulded in hypersaline water (2).

Type of Test

Rate of loading: ½ lbf/sq.in./minute.
Salinity of the pore fluid initially; 2 x normal salinity.
Maximum consolidating pressure; 6825 lbf/sq.in.

Proposed Investigation

A further hypersaline test to investigate its influence on the observed parameters.

Initial Condition of the Sample

Moisture content; 120.0.
Thickness; 5.880.
Weight; 1713 gms.

Preconsolidation Stage

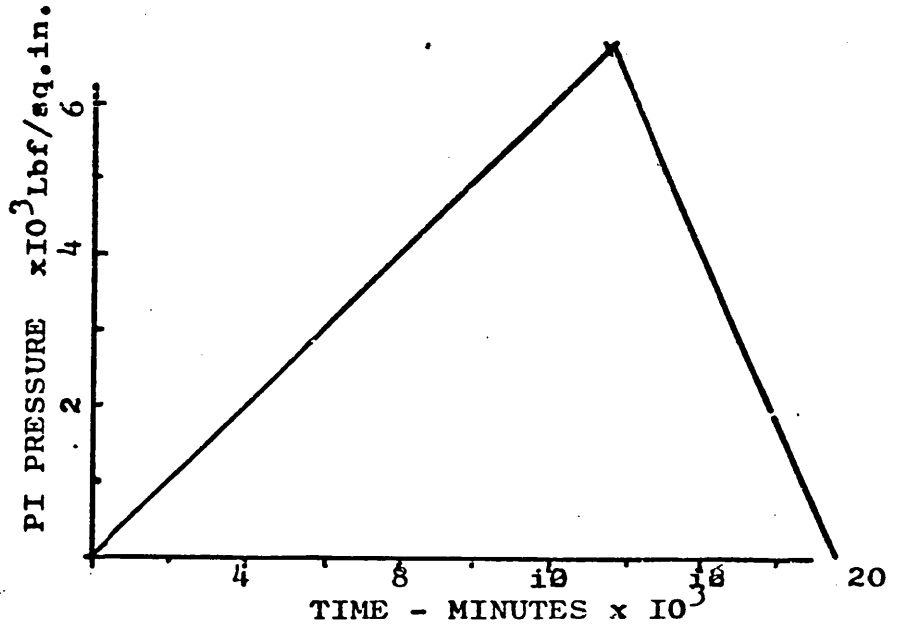
Rate of Strain; 0.00001 ins/minute.
Maximum consolidation stress; 50 lbf/sq.in.
Moisture content after preconsolidation; 67.92 per cent.
Thickness after preconsolidation; 3.138.
Weight after preconsolidation; 1268.00 gms.

Loading Stage

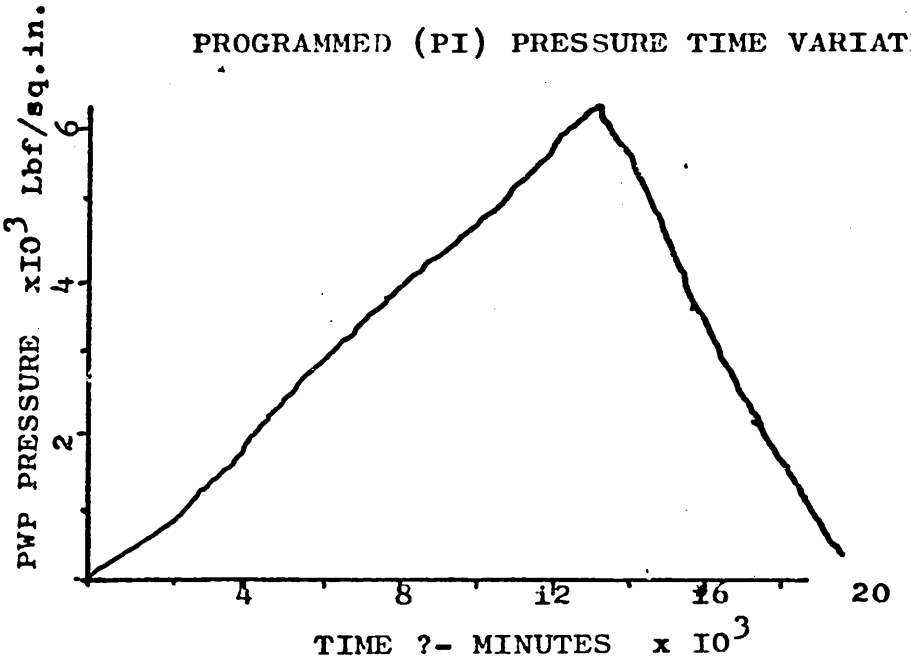
Total decrease in thickness; 1.061 ins.

Final Condition of Sample

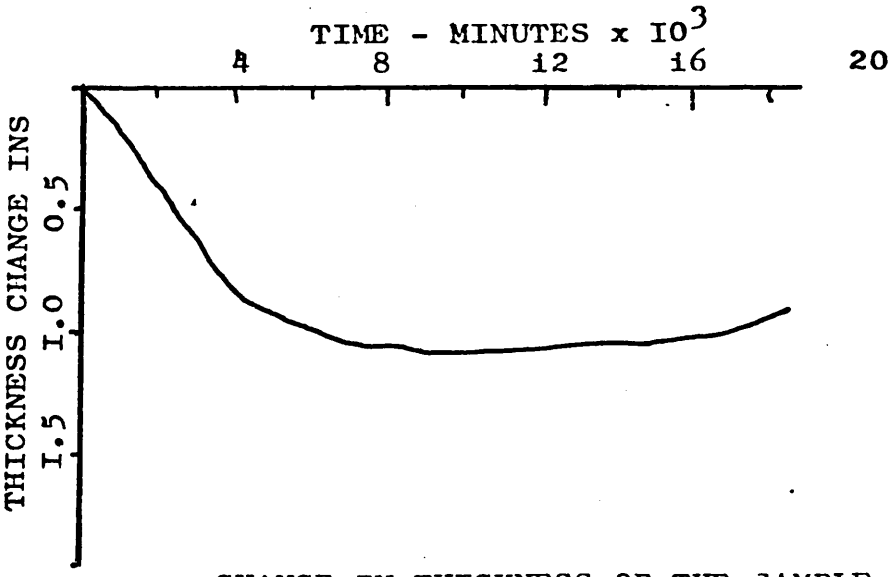
Moisture content; 20.45 per cent.
Thickness; 2.850 inches.
Weight; 847.09 gms.



PROGRAMMED (PI) PRESSURE TIME VARIATION



RESPONSE OF THE PORE WATER PRESSURE DIFFERENCE



CHANGE IN THICKNESS OF THE SAMPLE

FIG. D.20 VARIATION OF OBSERVED PARAMETERS IN TESTY BC.CHP.2I

TEST NO. N.BC.CHP.1 Date: 25.6.74

Details of Test Material

Clay type; Ball clay (Stoneware); properties in Table 6.II.
State of original sample; undisturbed trimmed from block.

Type of Test

Rate of loading; 1 lbf/sq.in./minute.
Maximum consolidating pressure; 7800 lbf/sq.in.

Proposed Investigation

To determine consolidation character of overconsolidated clay.
To estimate the preconsolidation load.

Initial Condition of Sample

Moisture content; 23.5 per cent.
Thickness; 3.09 inches.
Weight; 1248.00 gms.

Loading Stage

Total compaction; 1.38 inches.

Unloading Stage

Rate of unloading; 2 lbf/sq.in./minute.

Final Condition of Sample

Moisture content; 18.30 per cent.
Thickness; 2.710
Weight; 1164.00 gms.

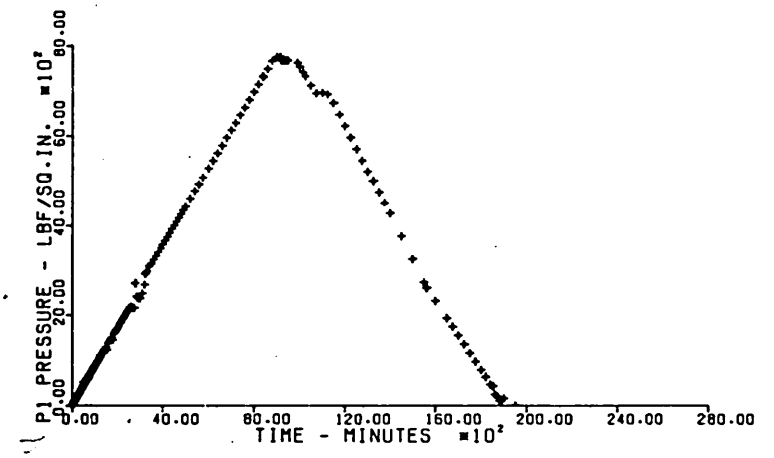


FIG D. 21 PROGRAMMED (P1) PRESSURE TIME VARIATION

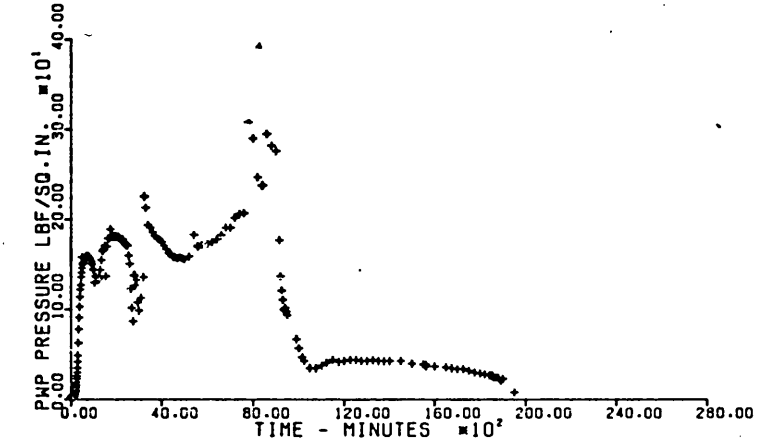


FIG. D. 21 RESPONSE OF THE PORE WATER PRESSURE DIFFERENCE

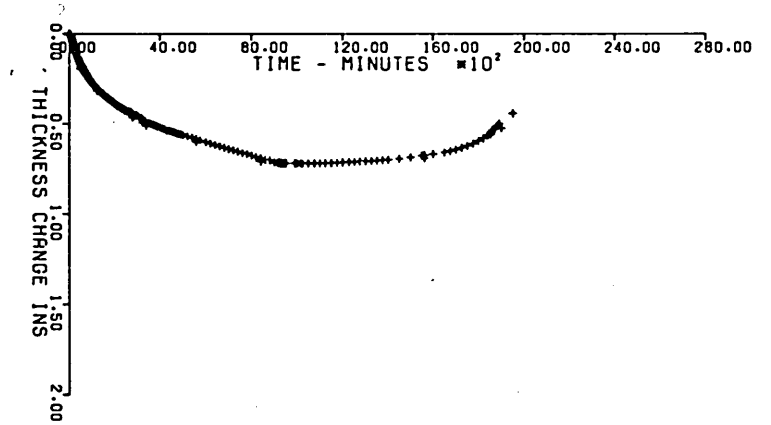
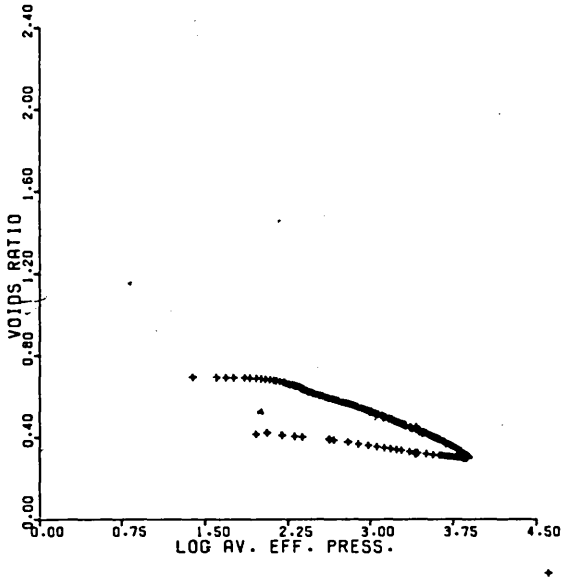
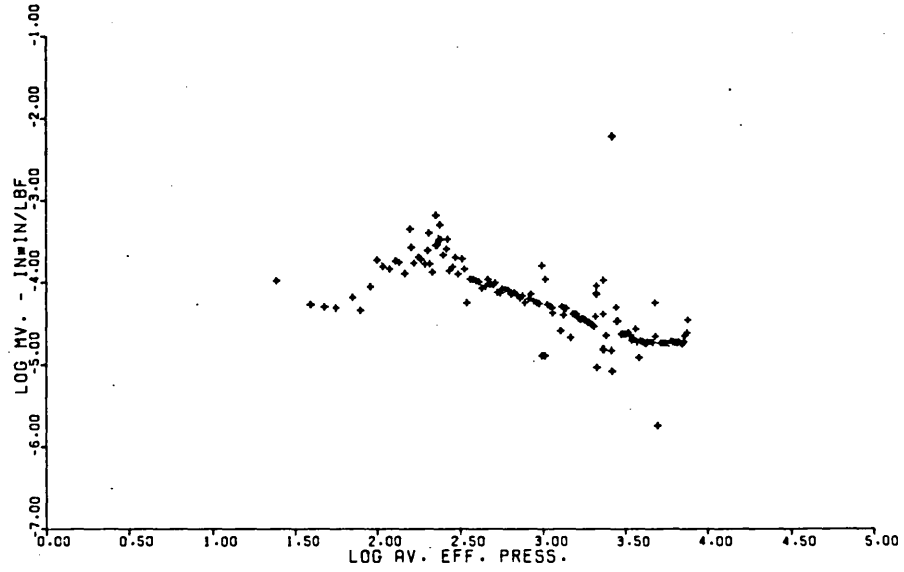


FIG. D. 21 CHANGE IN THICKNESS OF THE SAMPLE

FIG. D. 21 VARIATION OF OBSERVED PARAMETERS IN TEST N.BC.CHP.1



E - LOGP PLOT FOR TEST N.BC.CHP.1



COEFF. OF VOL. DECREASE - LOGP FOR TEST BGBCHBHP81

FIGURE D.22

Consolidation characters for Test N.BC.CHP.1

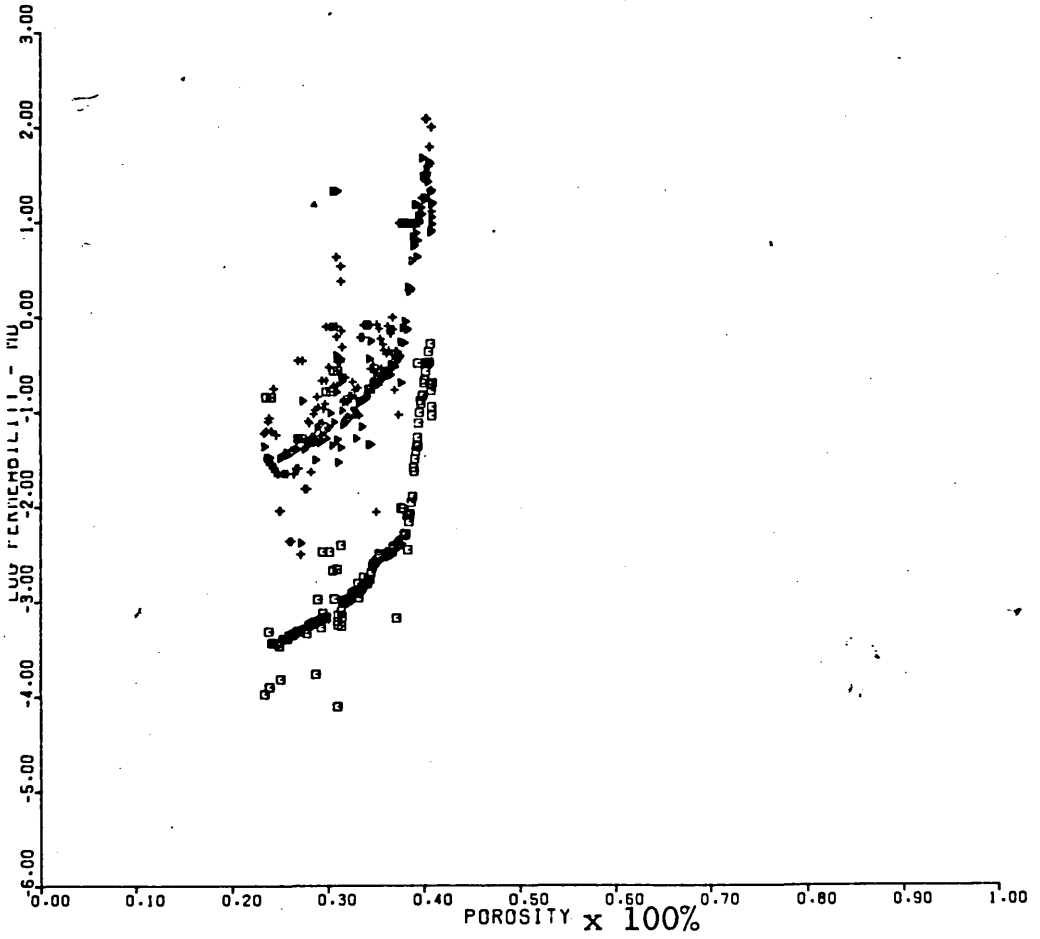


FIGURE D.23

PERMEABILITY - POROSITY PLOT FOR TEST N.BC.CHP.1

CROSS - CV CORRECTED

TRIANGLE - CV UNCORRECTED

SQUARE - LINEAR PW VARIATION ASSUMED

TEST NO. N.FA.CHP.2 Date: 10.9.74

Details of Test Material

Clay type; Kaolinitic sediments (Falmouth).
State of sample: undisturbed collected in required size from the field.

Type of Test

Rate of loading; 1 lbf/sq.in./minute.
Maximum consolidation pressure; 4300 lbf/sq.in.

Proposed Investigation

To determine consolidation of character (high pressure) of normally consolidated clay.

Initial Condition of Sample

Moisture content; 52.95 per cent.
Thickness; 3.685 inches.
Weight; 1300.0 gms.

Loading Stage

Total compaction; 1.365.

Unloading Stage

Rate of unloading; 2 lbf/sq.in./minute.

Final Condition of Sample

Moisture content; 17.92.
Thickness; 2.321.
Weight; 985.00.

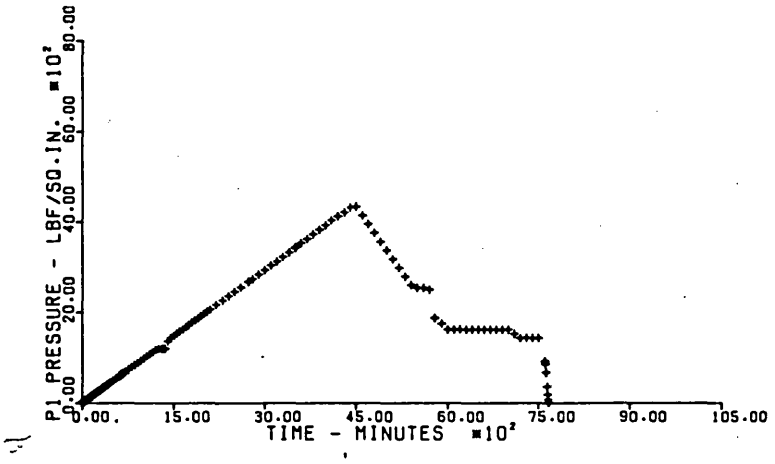


FIG. a - PROGRAMMED (P1) PRESSURE TIME VARIATION

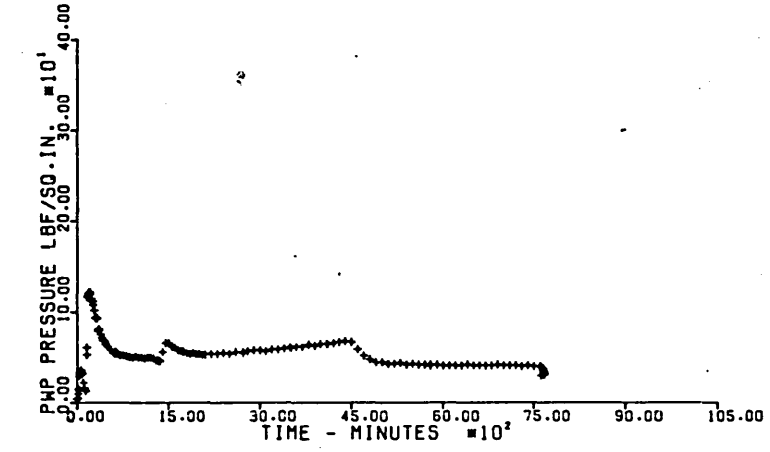


FIG. b - RESPONSE OF THE PORE WATER PRESSURE DIFFERENCE

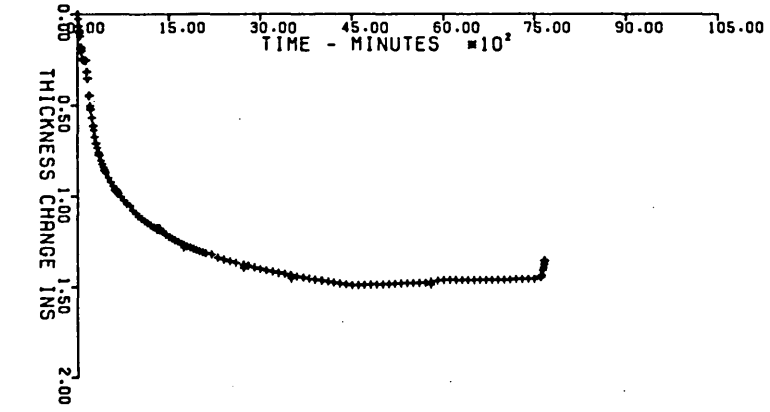
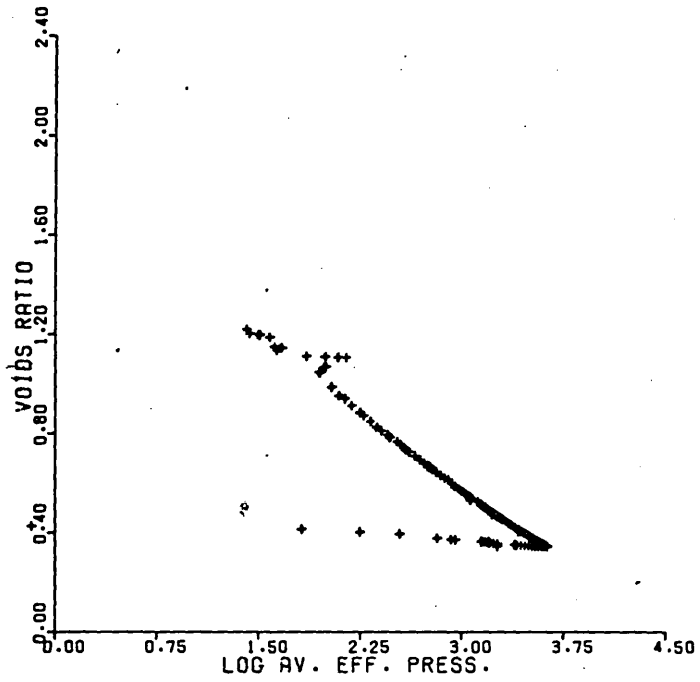
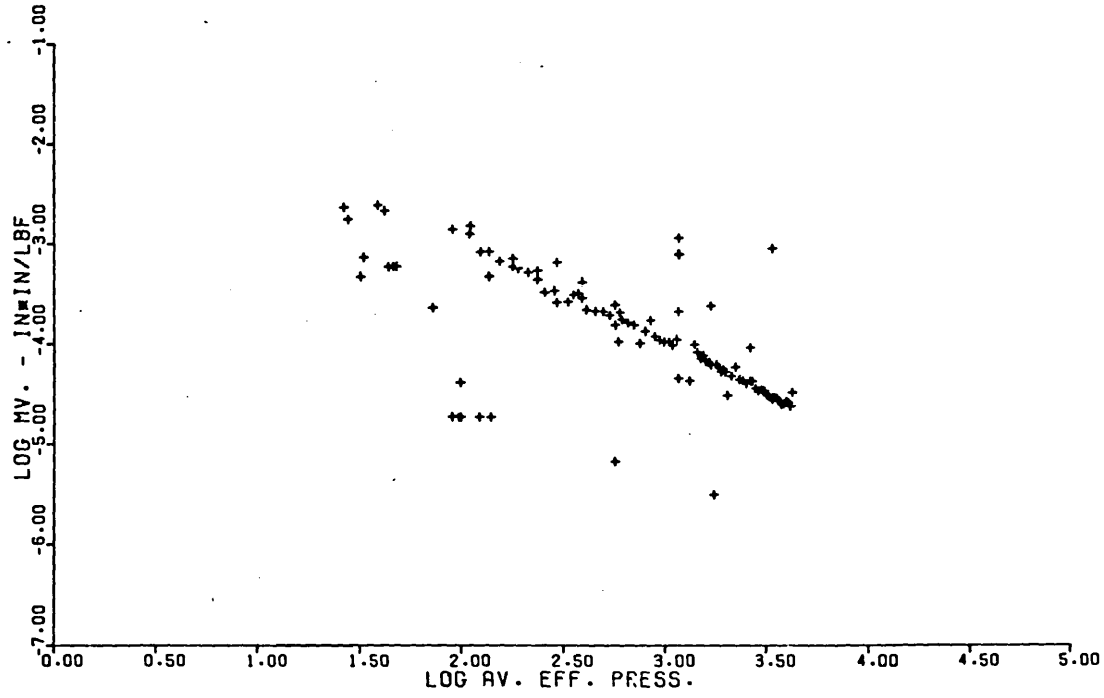


FIG. c - CHANGE IN THICKNESS OF THE SAMPLE

FIG.D.24- VARIATION OF OBSERVED PARAMETERS IN TEST N.FA.CHP.2



E - LOGP PLOT FOR TEST N.FA.CHP.2



COEFF. OF VOL. DECREASE - LOGP FOR TEST N.FA.CHP.2

FIGURE D.25 Consolidation characters for Test No. N.FA.CHP.2.

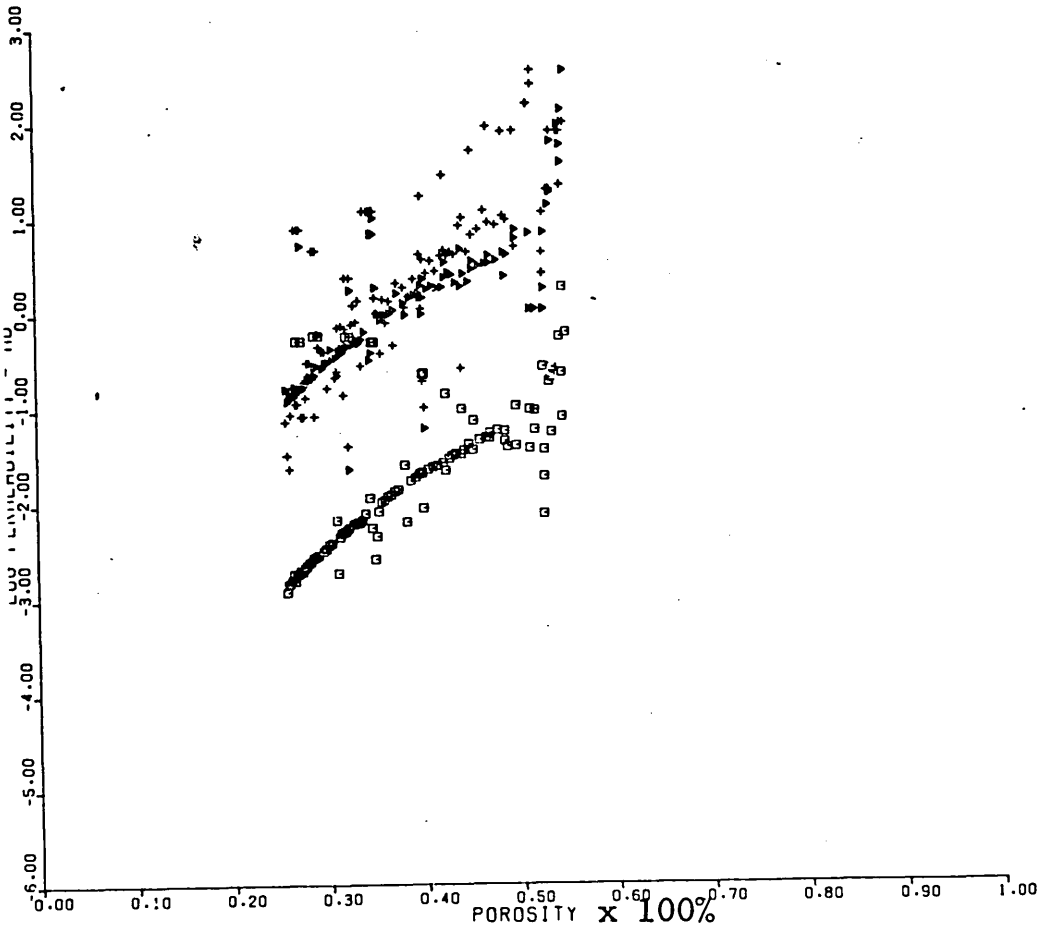


FIGURE D.26

PERMEABILITY - POROSITY PLOT FOR TEST N.FA.CHP.2

CROSS - CV CORRECTED

TRIANGLE - CV UNCORRECTED

SQUARE - LINEAR PW VARIATION ASSUMED

APPENDIX E

STEADY STATE TEMPERATURE DISTRIBUTIONS WITHIN THE TEST SPECIMEN

E.1 INTRODUCTION

A study of the 'pros and cons' of every possible technique of heating was necessarily made in order to select the most desirable method of heating. The sample being cylindrical in form, it is possible to adopt any of the following methods (figure E.1);

a) All round heating (i.e. wall heater and two end heaters).

b) Two heaters at the ends only.

c) Uniform wall heating only.

d) Variable wall heating with heat input proportional to source point.

e) Uniform wall heating and one end heater only.

f) One end heater only.

Whilst the electrical and mechanical aspects of the feasibility of the above alternatives were being sorted out, an insight into the respective steady state heat flow patterns within the sample was desired. Accordingly a finite element technique analysis was used to study the heat flow pattern.

E.2 COORDINATE SYSTEM AND FORMULATION OF THE PROBLEM

The sample being cylindrical in form, a system of cylindrical polar coordinates (r, θ, z) is appropriate for the analysis. Furthermore, the particular problem is axisymmetric by virtue of the symmetry of the heat source and the properties of the material about the axis of the specimen.

The general heat energy equation for the whole system is:

$$G\,Cp\,(U\frac{\partial T}{\partial r} + V\frac{\partial T}{\partial z}) = K(\frac{\partial^2 T}{\partial r^2} + \frac{\partial^2 T}{\partial z^2}) + 2\eta I_2$$

Convection Conduction Dissipation

However, in considering the closed system bounded by the walls and the ends of the sample, the convection and dissipation terms cease to exist. As such for the sample only:

$$K(\frac{\partial^2 T}{\partial r^2} + \frac{\partial^2 T}{\partial z^2}) = 0$$

where K = thermal conductivity,

and T = temperature.

which is a partial differential equation of the Laplace form.

A finite element technique was used for the solution of the above equation. The pertinent portion of any axial plane of the sample was represented by a rectangular net of 9 x 9 nodes, see Figure E.1.

The boundary conditions considered were mainly of two forms, viz:

a) Closed boundary value problem; with temperature being specified on all the boundaries.

b) Mixed boundary value problem, with temperature being specified at some surfaces, and the normal derivative of the temperature $(\frac{\partial T}{\partial n})$ being zero at the others.

E.3 MATERIAL PROPERTIES

The thermal conductivity of a typical piece of consolidated ball clay was determined using a Divided Bar apparatus. It was evaluated to be:

Conductivity of the non-porous rock $K_r = 8.4 \pm 0.7$ mcals/cm/sec/^oC,

and the conductivity at a desired porosity was obtained by assuming the equation (Saas, J.H. et al, 1971):

$$K_{pr} = K_w(\frac{K_r}{K_w})^{1-\phi_o}$$

where: ϕ_o = natural porosity,

K_w = thermal conductivity of liquid water at 25^oC,
= 1.46 mcals/cm/sec/^oC,

K_{pr} = conductivity of porous rock.

Accordingly the thermal conductivity changes during the consolidation process and for the analysis the variation took the form:

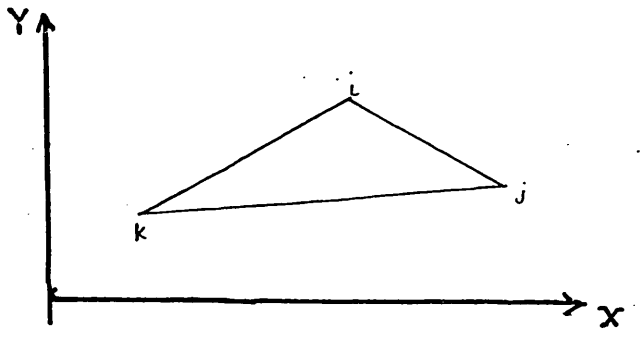
Specimen thickness (inches)	Thermal conductivity	
	mcals/cm/sec/^{o}C	BTU/ft/hr/^{o}F
4	5.91	2.32
2	7.10	2.80
1	7.70	3.04

E.4 OUTLINE OF ANALYSIS

The analysis is done using the techniques described in Zienkiewicz (1967, p. 154).

The functional to be minimised is:

$$x = \iint \frac{K}{2} \left\{ \left(\frac{\partial T}{\partial x}\right)^2 + \left(\frac{\partial T}{\partial y}\right)^2 \right\} dx\, dy$$



For an element:

$$\{T\}^e = \begin{Bmatrix} T_i \\ T_j \\ T_k \end{Bmatrix} \quad \text{and} \quad \frac{\partial x}{\partial T} = \begin{Bmatrix} \frac{\partial x}{\partial T_i} \\ \frac{\partial x}{\partial T_j} \\ \frac{\partial x}{\partial T_k} \end{Bmatrix}$$

Let us define: $T = T_i + c_1 x + c_2 y$

From the figure we can write: $T_j = T_i + c_1 a_j + c_a b_j$

$$T_k = T_i + c_1 a_k + c_2 b_k$$

$$\therefore \quad \frac{\partial T}{\partial x} = c_1, \qquad \frac{\partial T}{\partial y} = c_2.$$

$$\begin{Bmatrix} c_1 \\ c_2 \end{Bmatrix} = \frac{1}{2\Delta} \begin{bmatrix} b_j - b_k & b_k & -b_j \\ a_k - a_j & -a_k & a_j \end{bmatrix} \begin{Bmatrix} T_i \\ T_i^j \\ T_k \end{Bmatrix}$$

where: Δ = area of element.

Now:
$$\left\{\frac{\partial x}{\partial T}\right\}^e = \frac{\partial}{\partial T} \int\int \frac{1}{2} k \left\{ \left(\frac{\partial T}{\partial x}\right)^2 + \left(\frac{\partial T}{\partial y}\right)^2 \right\} dx\, dy$$

$$= \frac{1}{2} k \Delta \frac{\partial}{\partial T} \left[c_1^{\,2} + c_2^{\,2} \right]$$

$$= k\Delta \left[c_1 \frac{\partial c_1}{\partial T} + c_2 \frac{\partial c_2}{\partial T} \right]$$

$$\frac{\partial x}{\partial T_i} = k\Delta \left[c_1 \frac{\partial c_1}{\partial T_i} + c_2 \frac{\partial c_2}{\partial T_i} \right]$$

$$= \frac{k}{4\Delta} \Big[\left\{ (b_j - b_k)^2 + (a_k - a_k)^2 \right\} T_i + \left\{ b_k (b_j - b_k) - a_k (a_k - a_j) \right\} T_j$$

$$+ \left\{ -b_j (b_j - b_k) + a_j (a_k - a_j) \right\} T_k \Big]$$

$$\frac{\partial x}{\partial T_j} = k\Delta \left[c_1 \frac{\partial c_1}{\partial T_j} + c_2 \frac{\partial c_2}{\partial T_j} \right]$$

$$= \frac{k}{4\Delta} \Big[\left\{ b_k (b_j - b_k) - a_k (a_k - a_j) \right\} T_i + \left\{ b_k^2 + a_k^2 \right\} T_j$$

$$+ \left\{ b_k (-b_j) + (-a_k (a_j) \right\} T_k \Big]$$

$$\frac{\partial x}{\partial T_k} = k\Delta \left[c_1 \frac{\partial c_1}{\partial T_k} + c_2 \frac{\partial c_2}{\partial T_k} \right]$$

$$= \frac{k}{4\Delta}\left[\left\{-b_j(b_j-b_k)+a_j(a_k-a_j)\right\}T_i+\left\{-b_j(b_k)\right.\right.$$

$$\left.\left.+a_j(-a_k)\right\}T_j+\left\{b_j^2+a_i^2\right\}T_k\right]$$

$$\left\{\frac{\partial x}{\partial T}\right\}^e = \frac{k}{4\Delta}\begin{bmatrix} (b_j-b_k)^2 & b_k(b_j-b_k) & -b_j(b_j-b_x) \\ +(a_k-a_i)^2 & -a_k(a_k-a_j) & +a_j(a_k-a_j) \\ b_k(b_j-b_k) & b_k^2+a_k^2 & -b_j(b_k)-a_ja_k \\ -a_k(a_k-a_j) & & \\ -b_j(b_j-b_k) & -b_jb_k-a_ja_k & b_j^2+a_j^2 \\ +a_j(a_k-a_j) & & \end{bmatrix}\begin{Bmatrix} T_i \\ T_j \\ T_k \end{Bmatrix}$$

$$\left\{\frac{\partial x}{\partial T}\right\}^e = [h]\ \{T\}^e$$

The final equations become:

$$\frac{\partial x}{\partial T_i} = \sum \frac{\partial x^e}{\partial T_i} = 0$$

The boundary conditions are:

i) T specified on all the boundaries.

ii) $\frac{\partial T}{\partial n} = 0$ on the three screw surfaces and $T = T_B$ on the barred surface. T_B is the barred temperature.

The second type of boundary condition amounts to the true screw surfaces with the temperatures being unconstrained. To handle this type of boundary condition, all we do is to specify the

heater temperature along the top boundary only. Simply speaking, we consider the points lying on the top surfaces as the boundary points and all the remaining boundary points as free boundary points.

E.5 RESULTS

Figure E.1 illustrates the cases analysed and the details relevant to the area studied. The subsequent figures give the results. In each instance, the effect of consolidation has been investigated by considering different specimen thickness. The appropriate thermal conductivity values have been used in such cases.

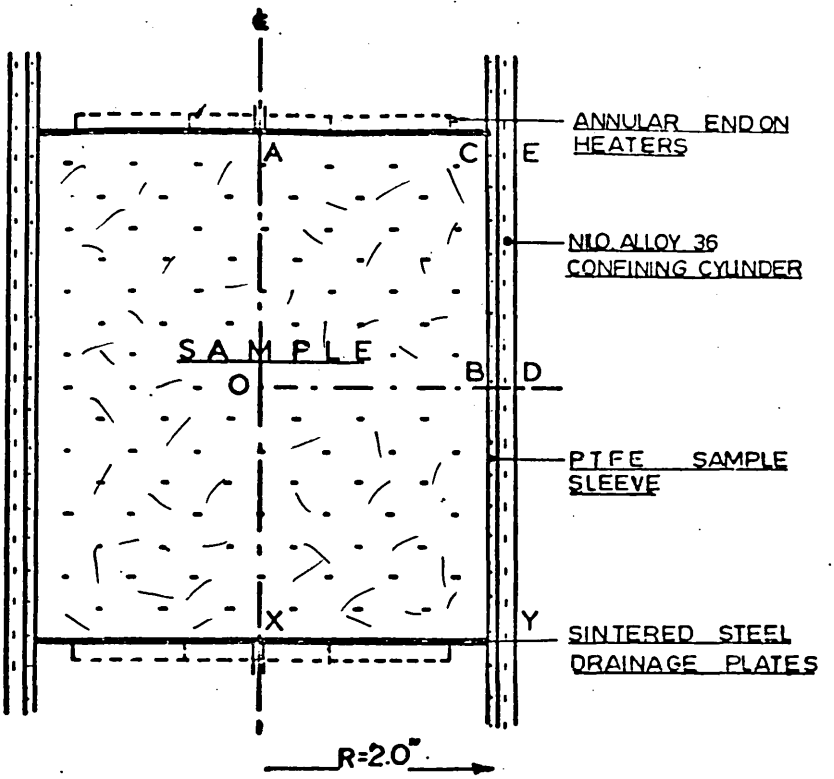


FIGURE E.I - GENERAL LAYOUT OF PROBLEM

CASES ANALYSED

NO.	TYPE OF HEATING CONSIDERED	SYMMETRY AXIS	SYMMETRY PLANE	PROBLEM BOUNDARY ANALYSED
1	END HEATING - assuming walls legged	AX	OBD	AOBC
2	END & WALL HEATING	AX	OBD	AODE
3	END HEATING ONLY	AX	OBD	AODE
4	UNIFORM WALL HEATING	AX	OBD	AODE
5	END HEATING - effects of layering considered	AX	OBD	AODE
6	WALL HEATING - effects of layering considered	AX	OBD	AODE
7	ONE END & UNIFORM WALL HEATING	AX		AXYE
8	LINEARLY VARYING WALL HEATING	AX		AXYE

NOTE - ALL DIAGRAMS ARE DRAWN TO FULL SIZE
ISOTHERMS ARE AS INDICATED AND IN °F

CASE 1 - END HEATING assuming walls well lagged

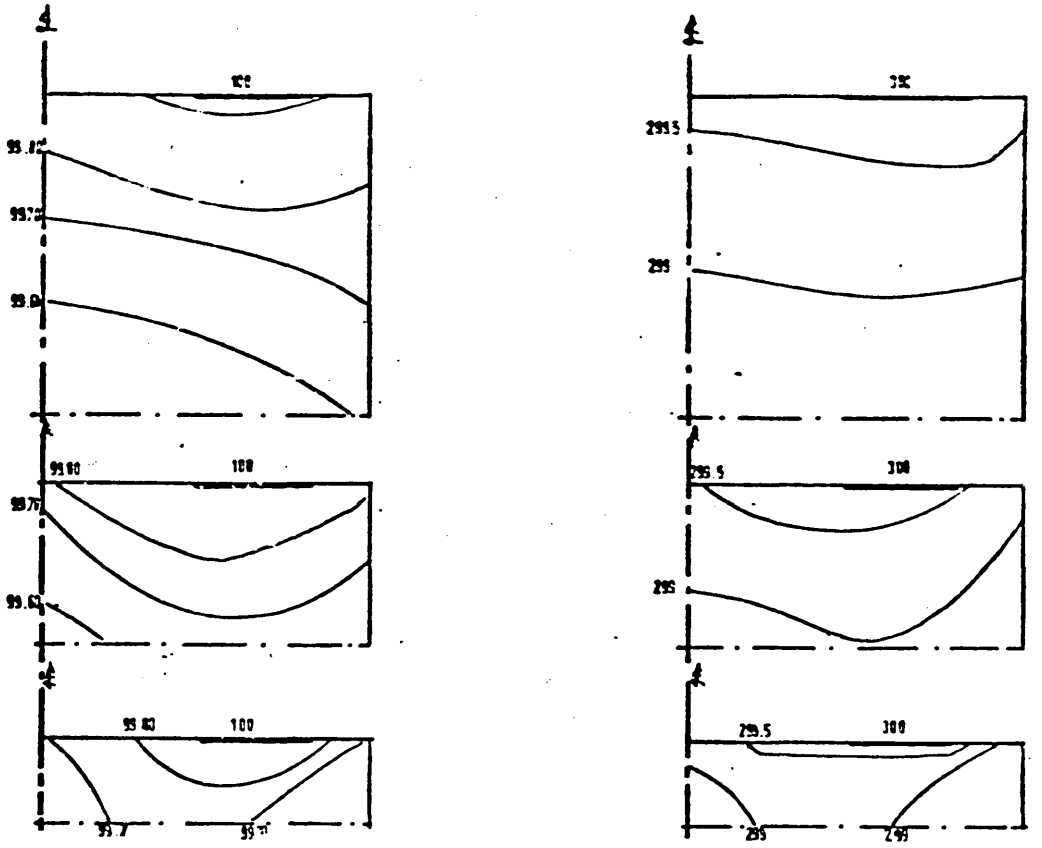


FIGURE E.2

CASE 2- END AND WALL HEATING

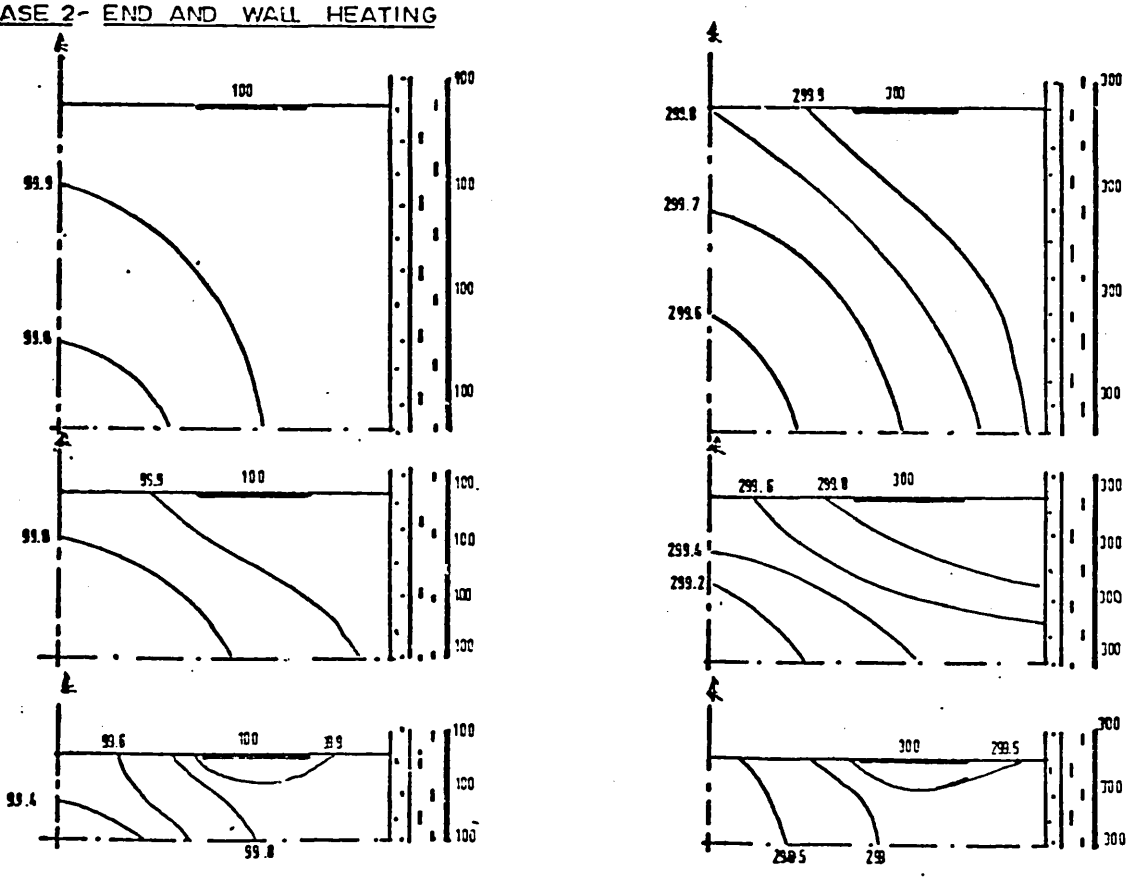


FIGURE E.3

CASE 3. - END HEATING ONLY

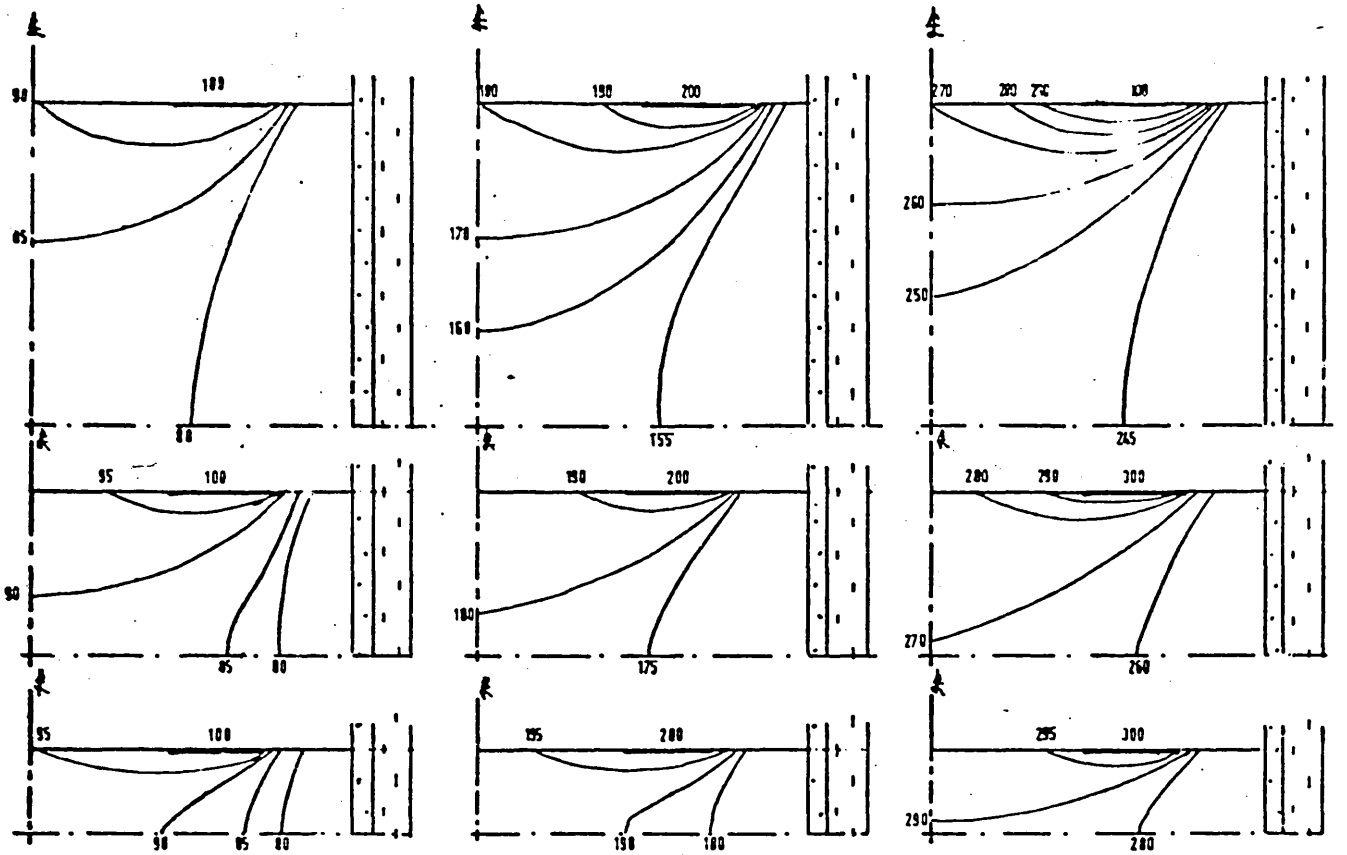


FIGURE E.4

CASE 4. - UNIFORM WALL HEATING

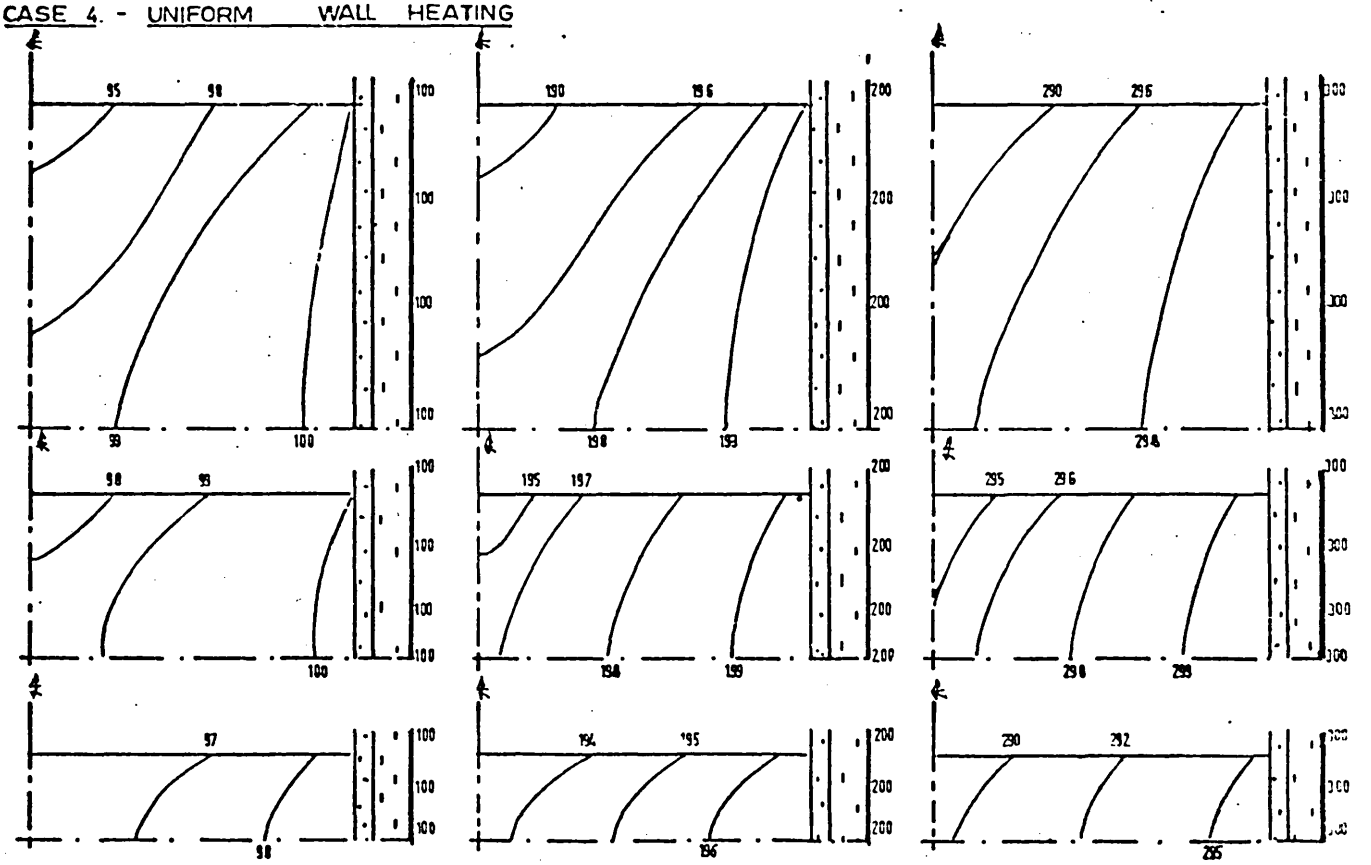


FIGURE E.5

CASE 5 - END HEATING - considering effects of layering

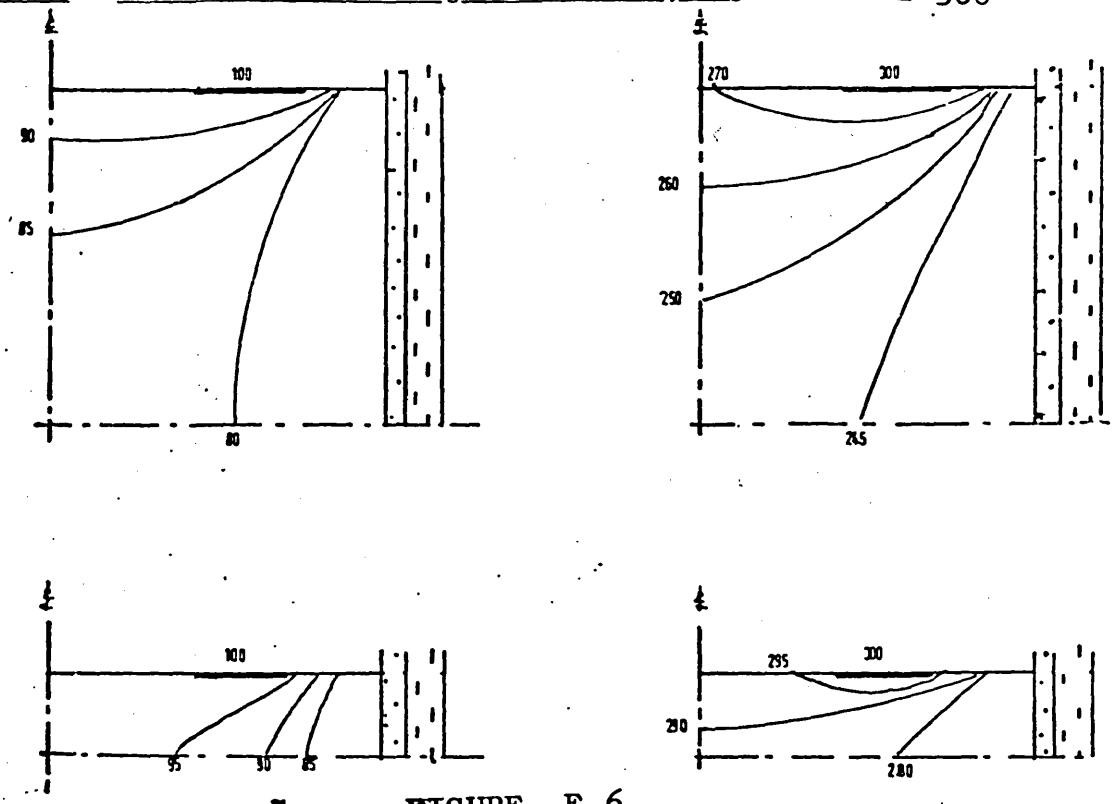


FIGURE E.6

CASE 6 - WALL HEATING - considering effects of layering

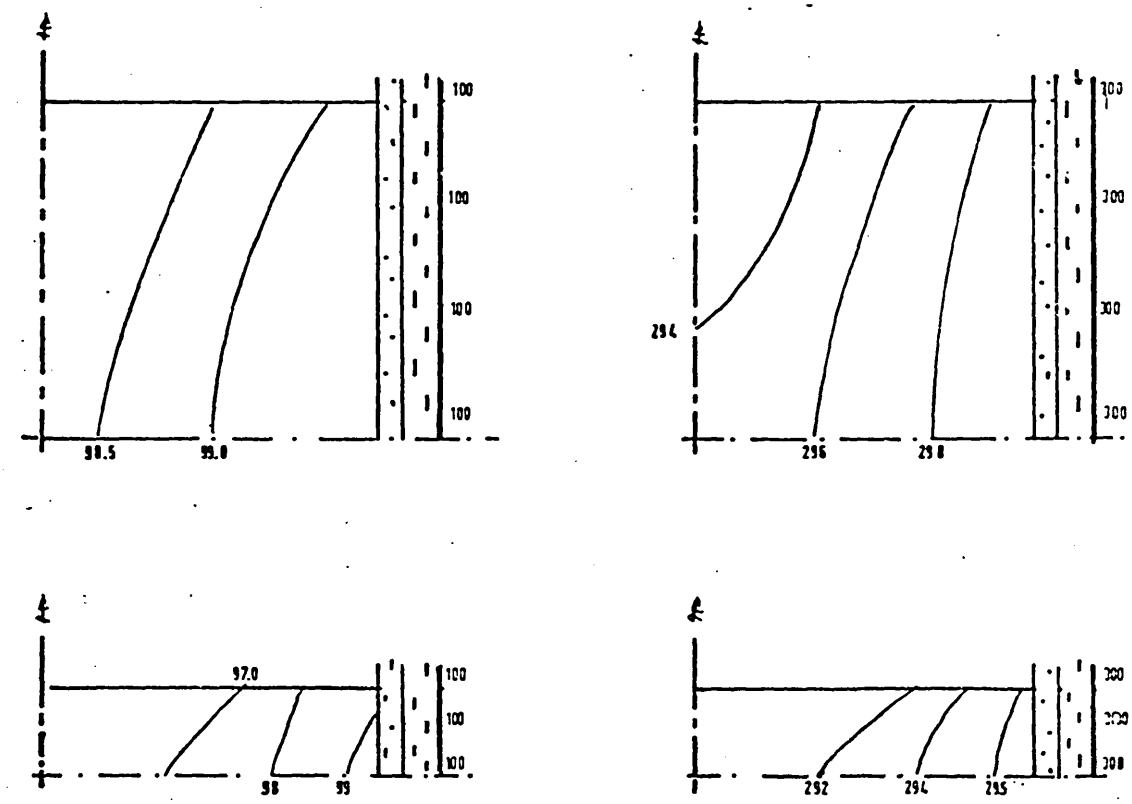


FIGURE E.7

CASE 7 - ONE END AND UNIFORM WALL HEATING

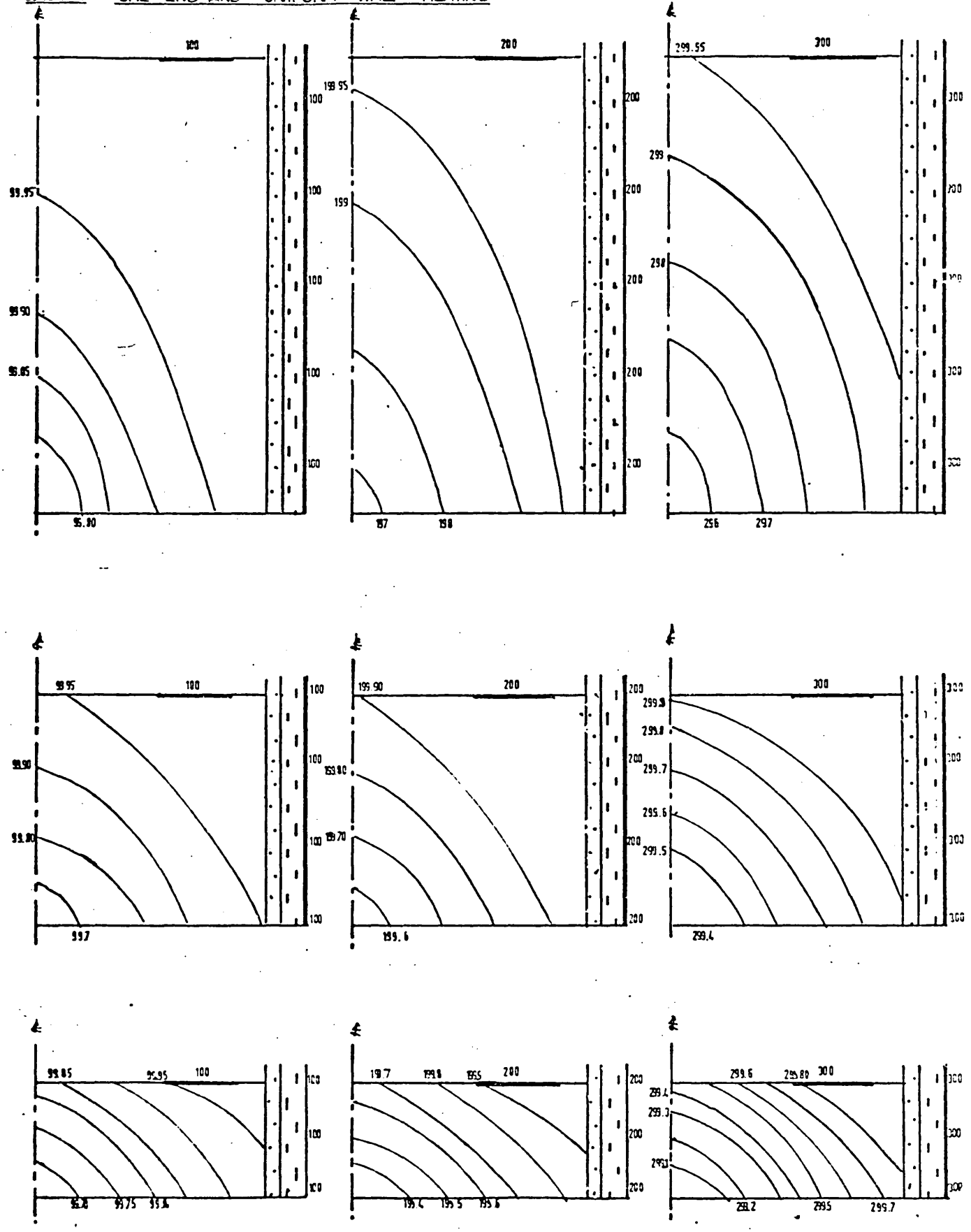


FIGURE E.8

CASE 8 - LINEARLY VARYING WALL HEATING

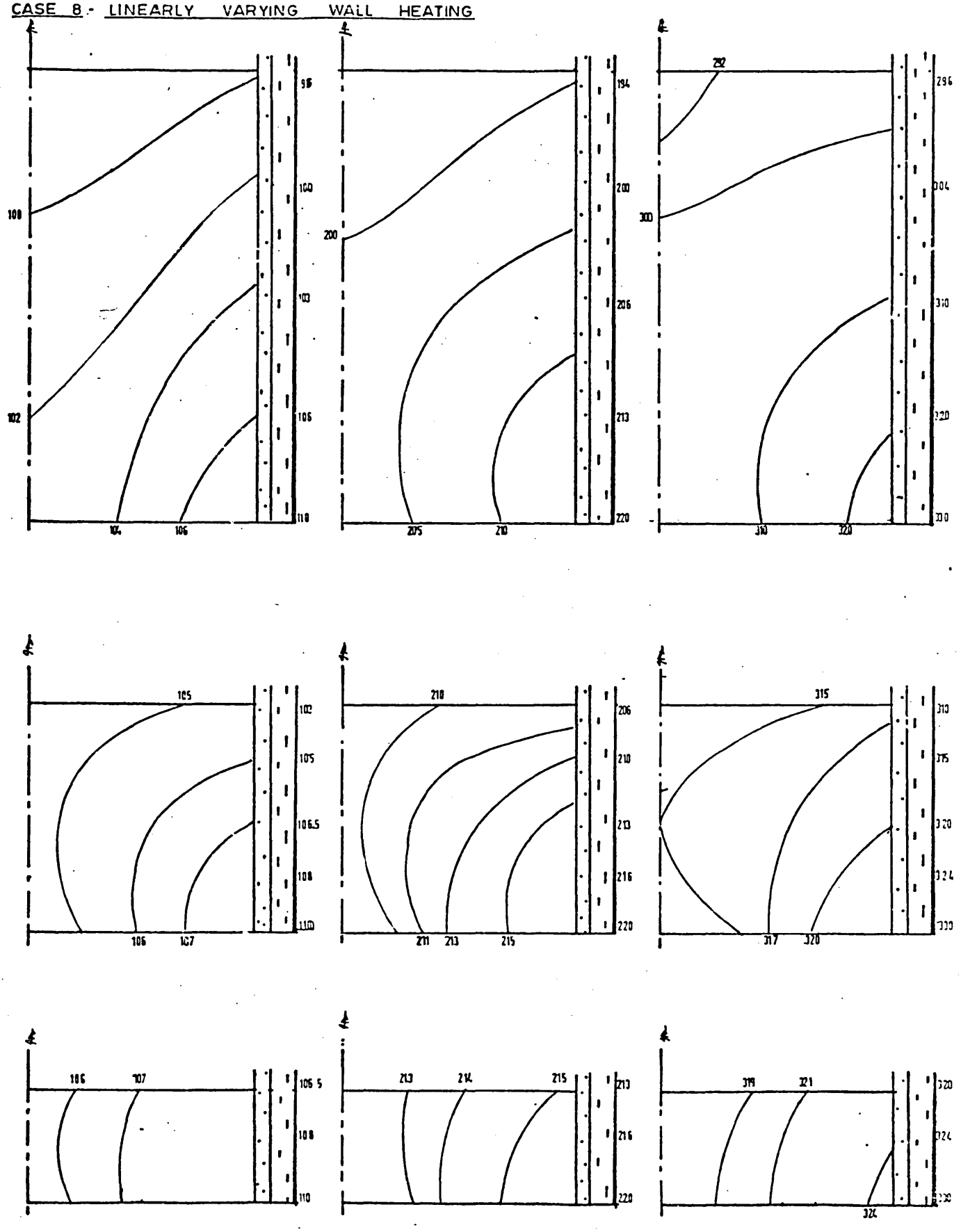


FIGURE E.9

CASE 9 - ONE END HEATER ONLY.

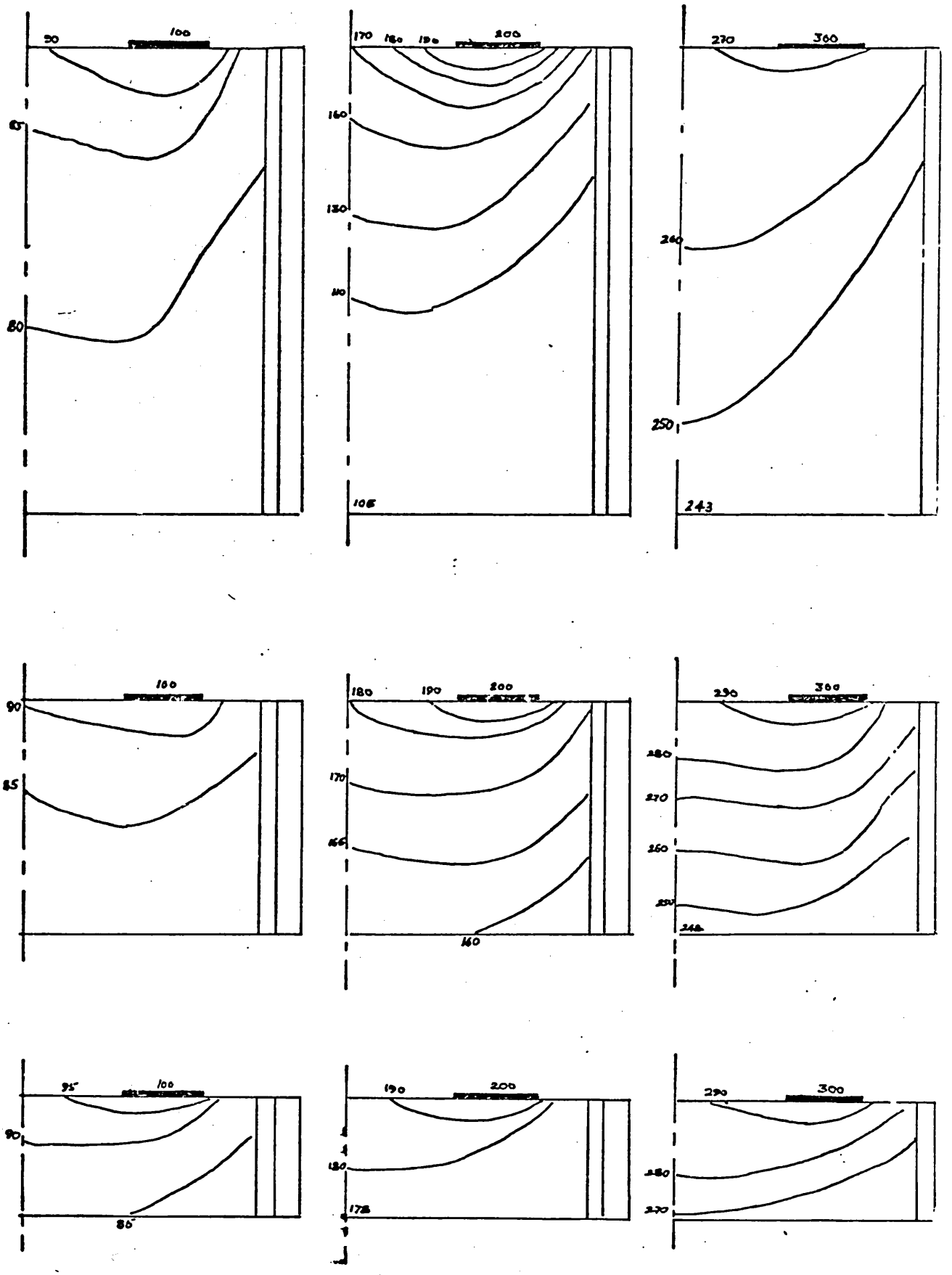


FIGURE E.10

APPENDIX F

RESULTS OF CHEMICAL ANALYSIS

As described in Section 8.4, the pore fluids expelled have been chemically analysed for the composition of the ions:

Na^+, K^+, Ca^{++}, Mg^{++}, Cl^-, SO_4^{--}.

The results from the tests are presented here.

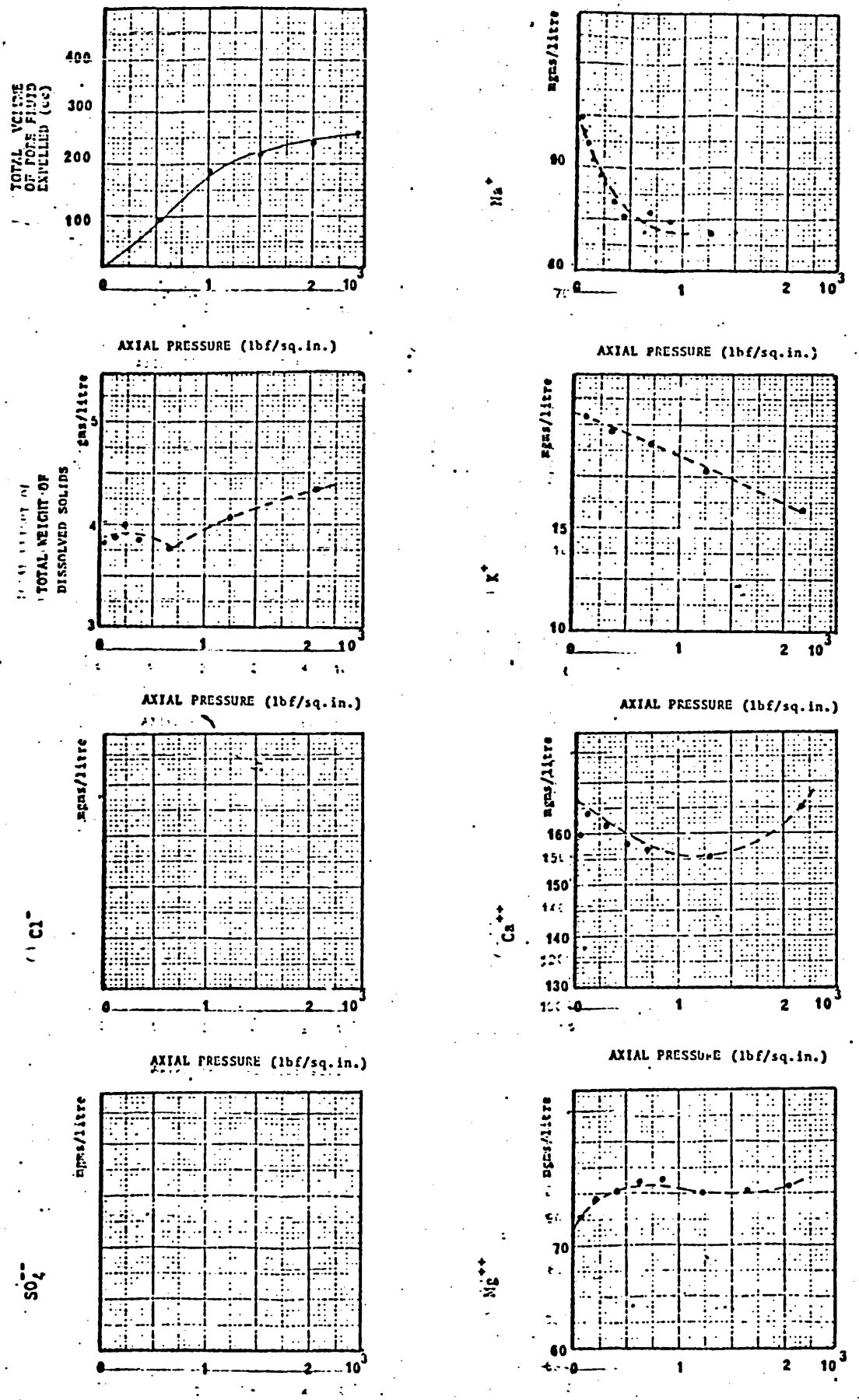


FIGURE F.1 Results of Chemical Analysis of Pore Fluid expelled during the Test No. BC.CHP.12

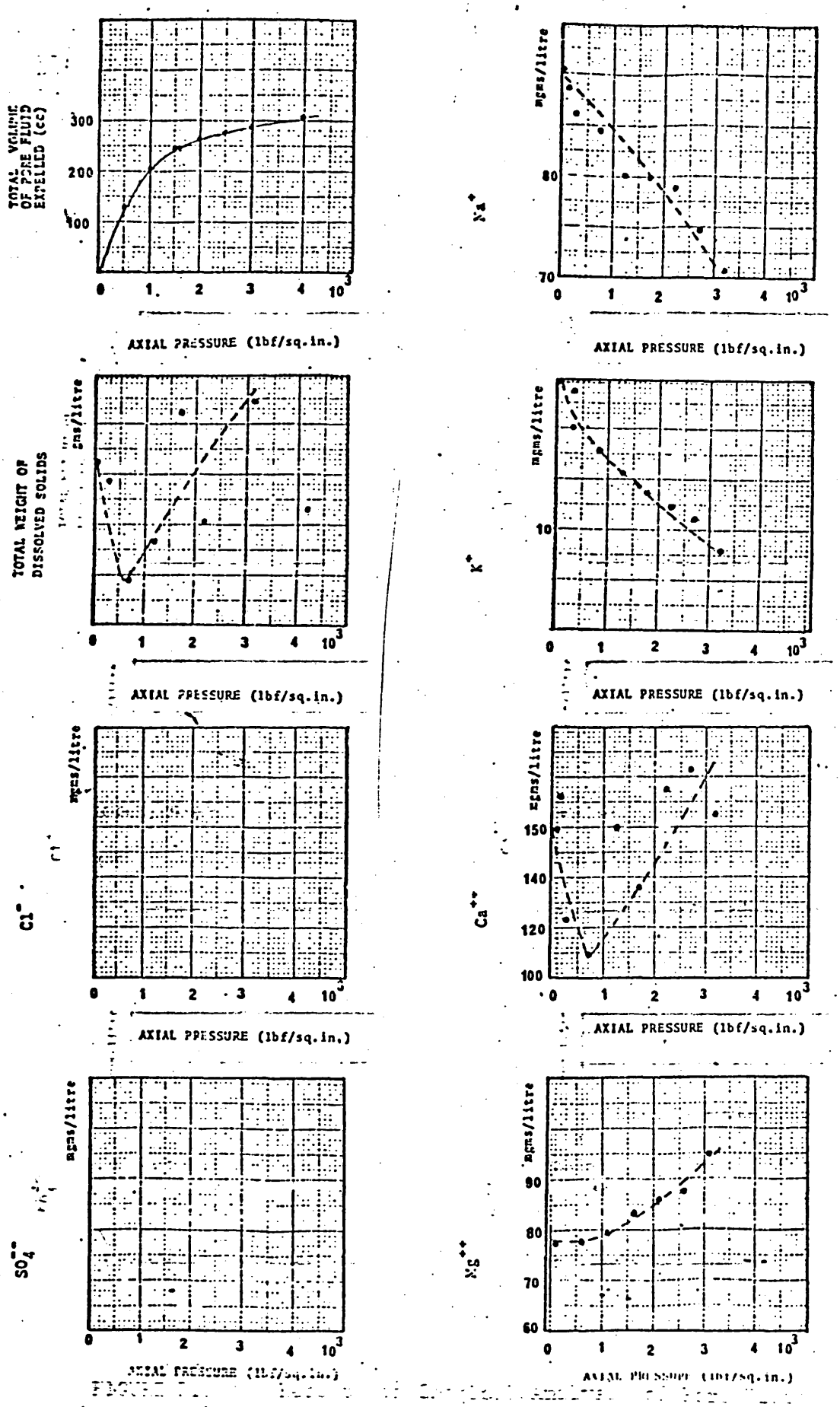


FIGURE F.2 Results of Chemical Analysis of Pore Fluid expelled during the Test No. BC.CHP.14

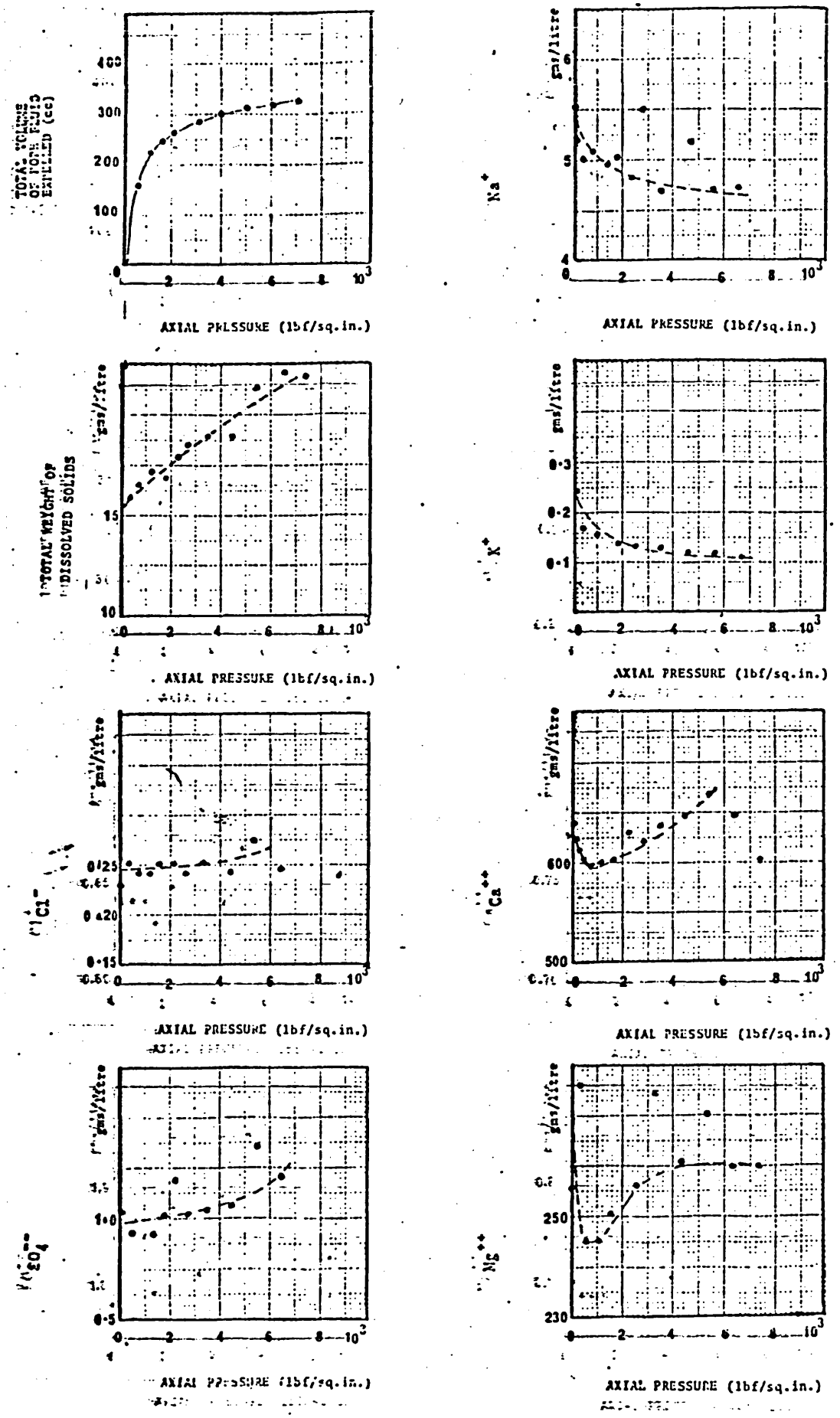


FIGURE F.3 Results of Chemical Analysis of Pore Fluid expelled during the Test No. BC.CHP.15

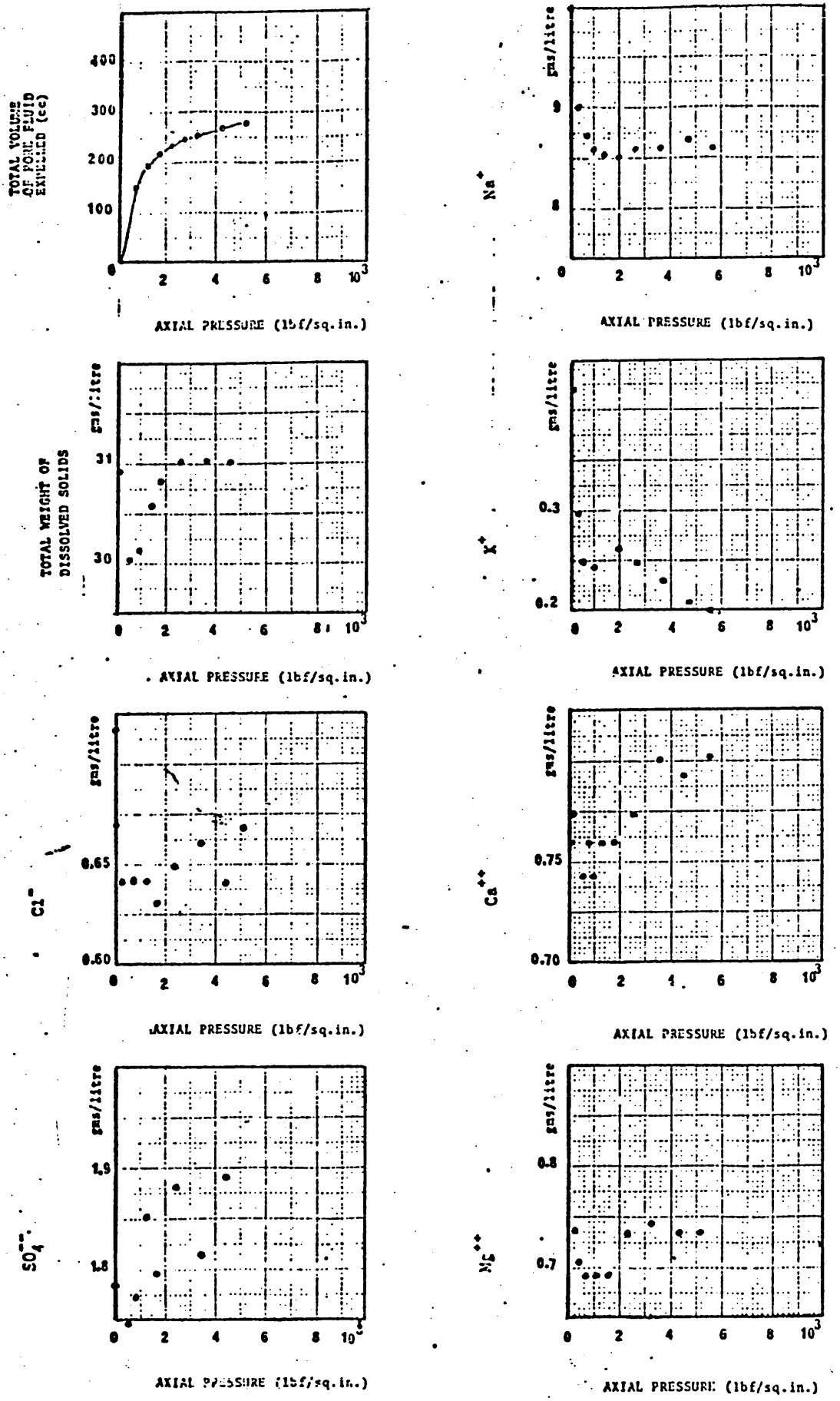


FIGURE F.4 Results of Chemical Analysis of Pore Fluid expelled during the Test No. BC.CHP.17

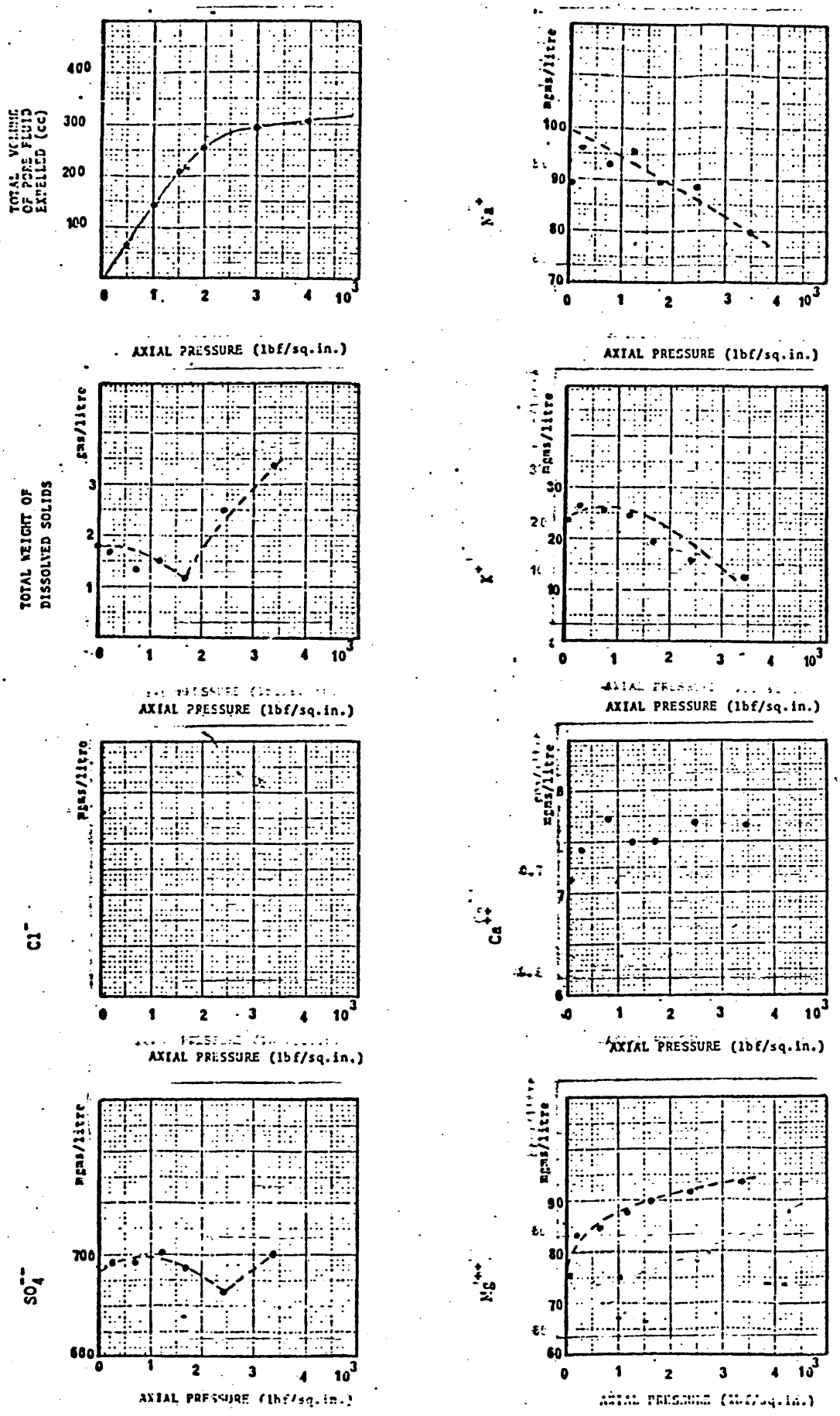
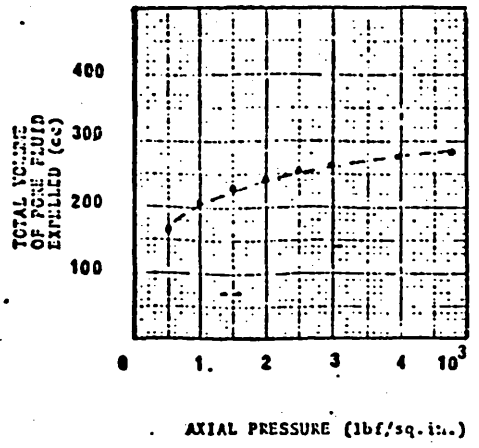
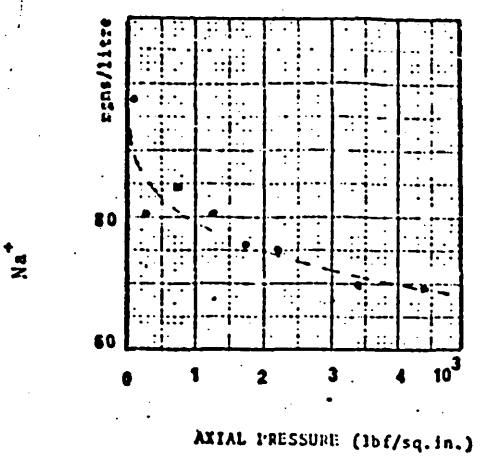
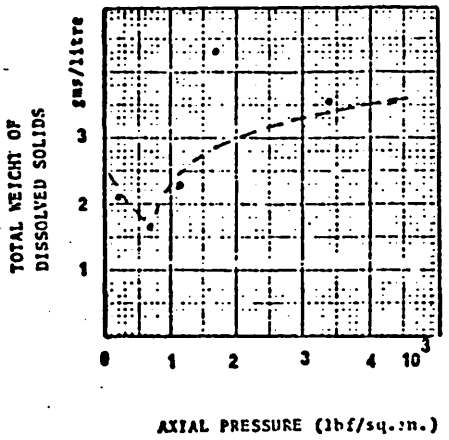
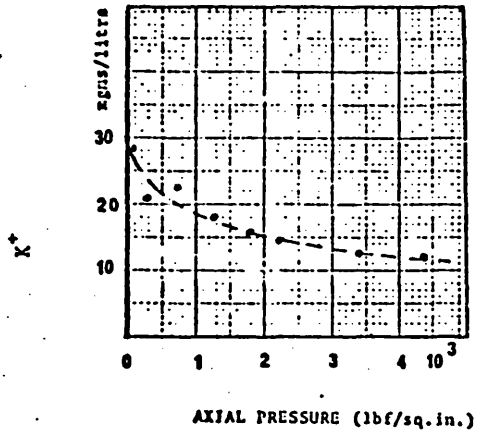


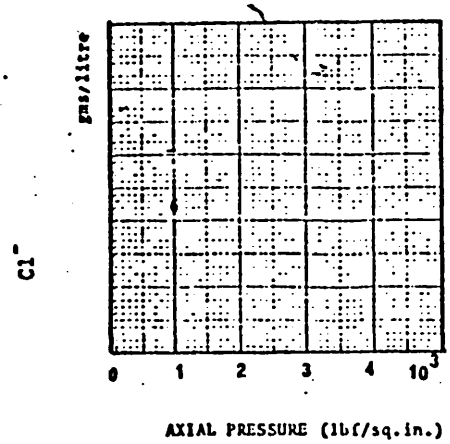
FIGURE F.5 Results of Chemical Analysis of Pore Fluid expelled during the Test No. BC.CHP.18

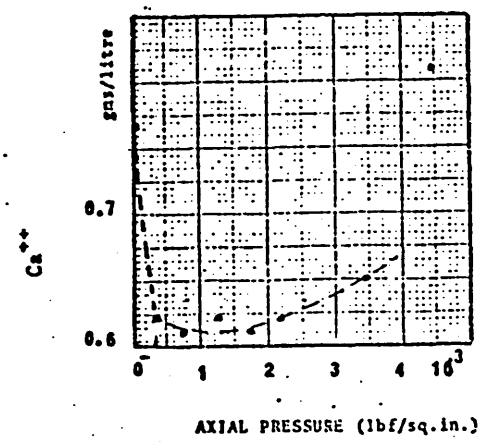


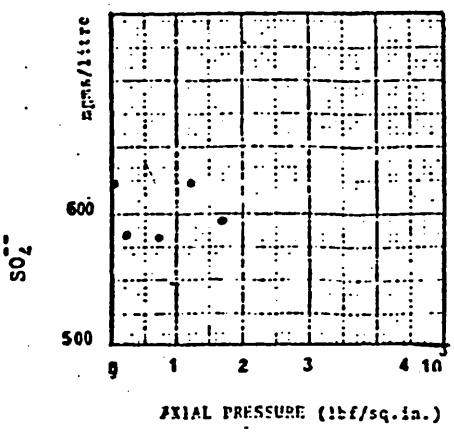












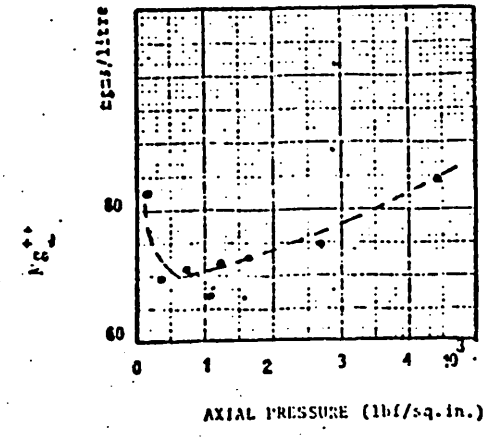


FIGURE F.6 Results of Chemical Analysis of Pore Fluid expelled during the Test No. BC.CHP.19

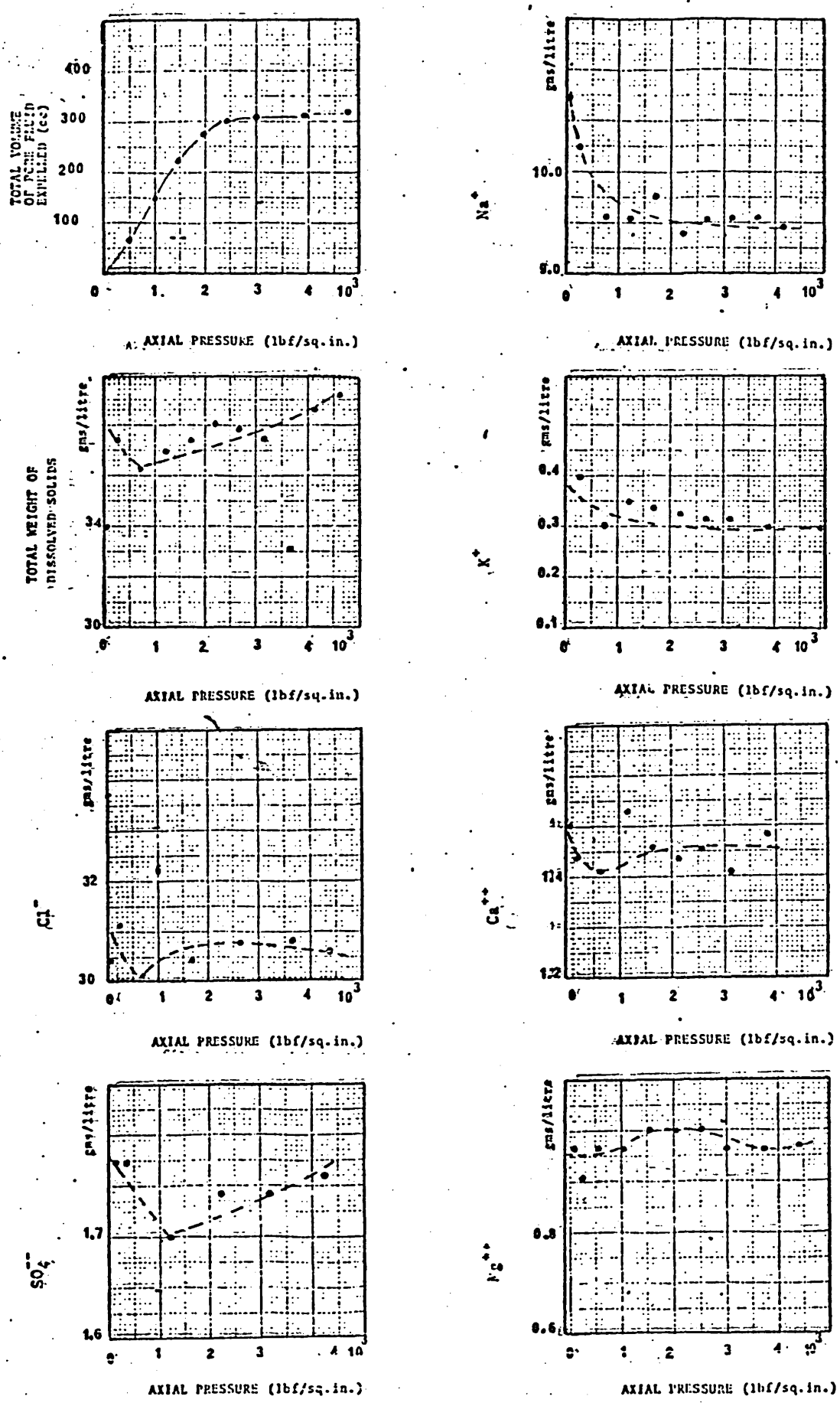


FIGURE F.7 Results of Chemical Analysis of Pore Fluid expelled during the Test No. BC.CHP.20.

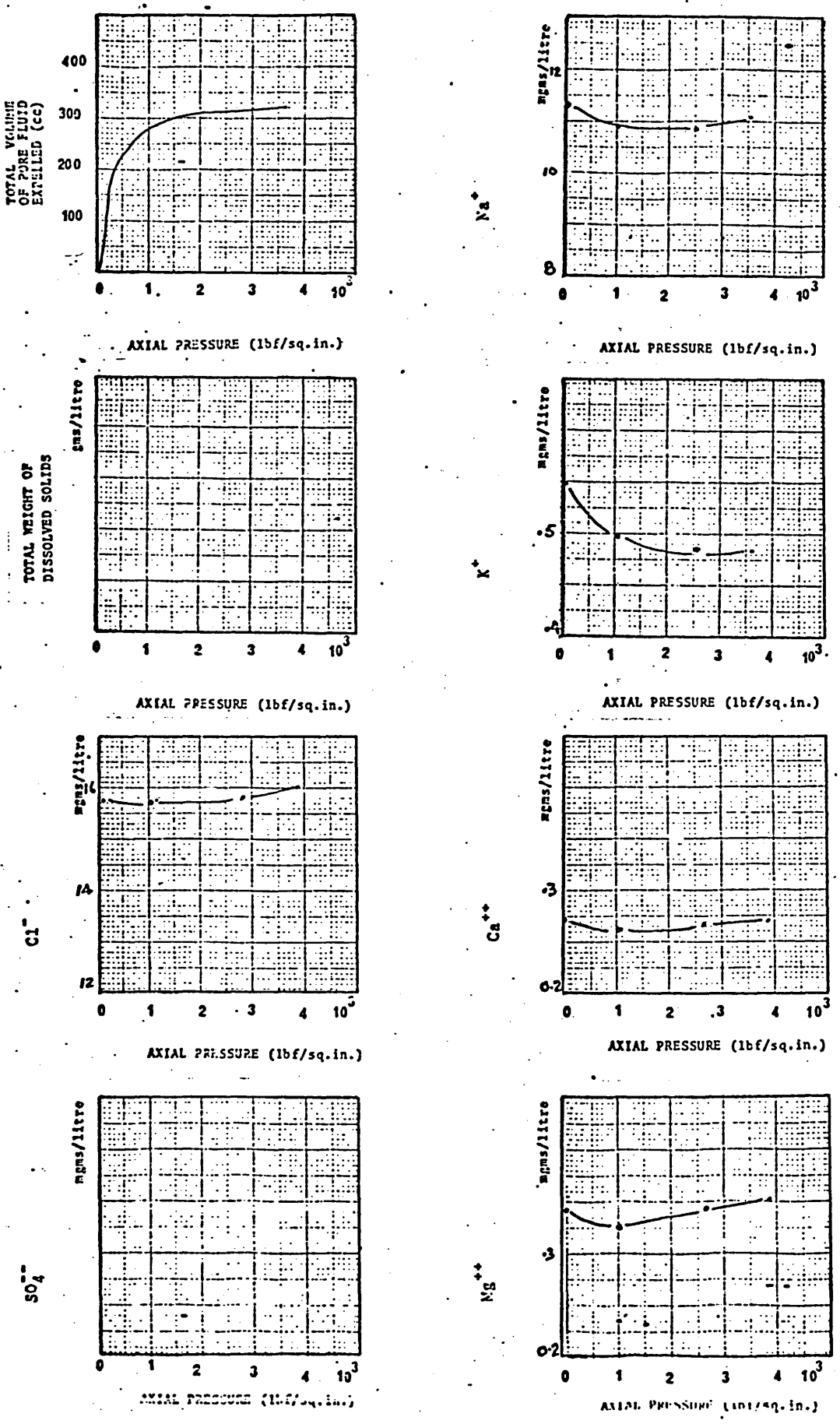
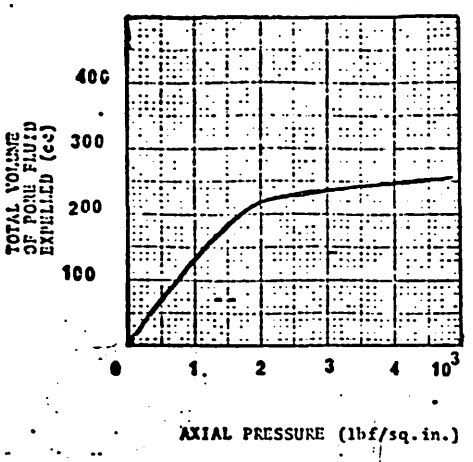
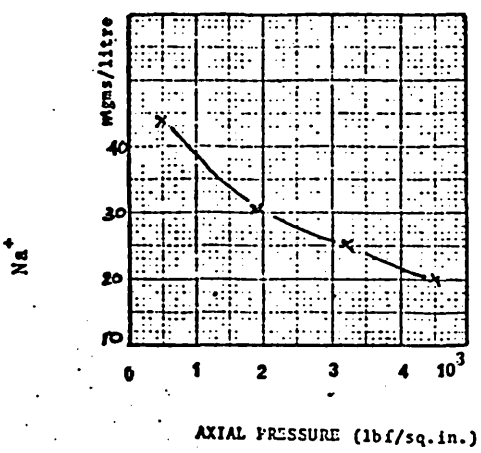
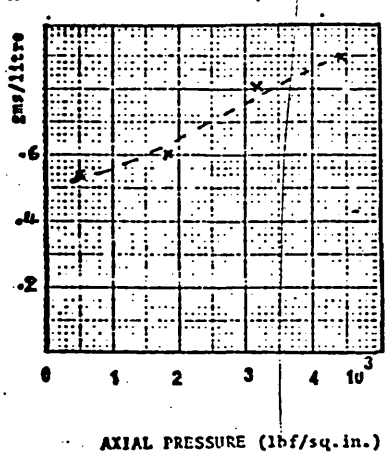
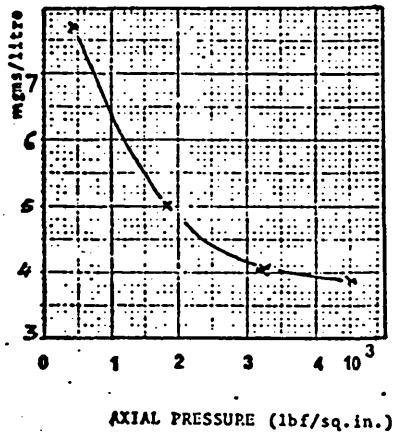


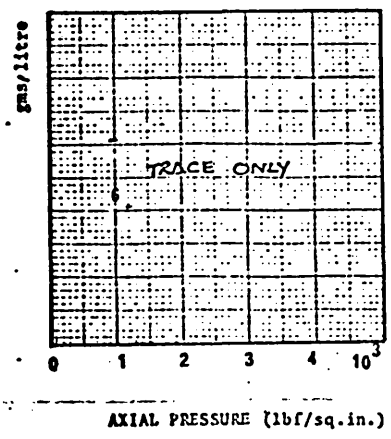
FIGURE F.8 The results of chemical analysis of pore fluid expelled from test BC.CHP.21

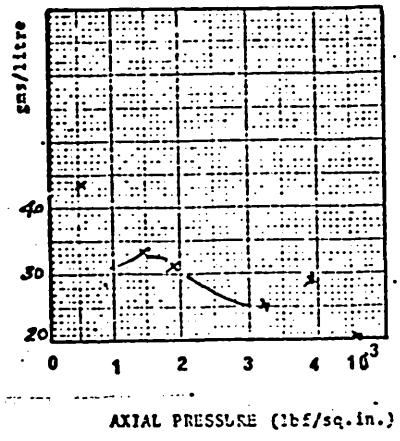


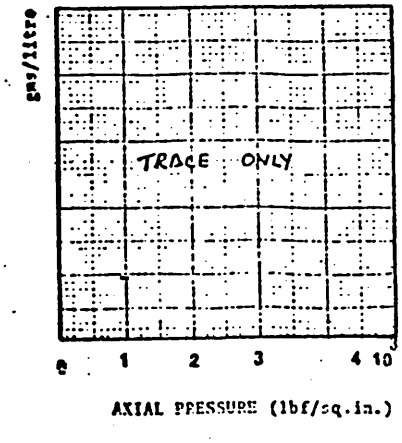












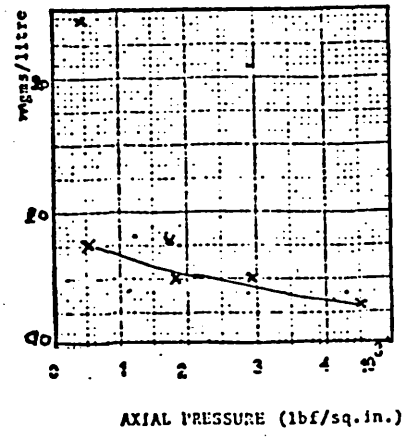
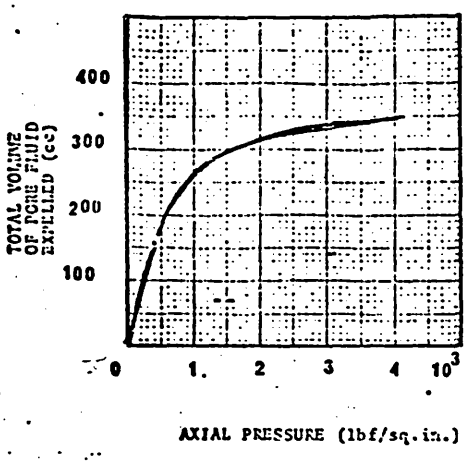
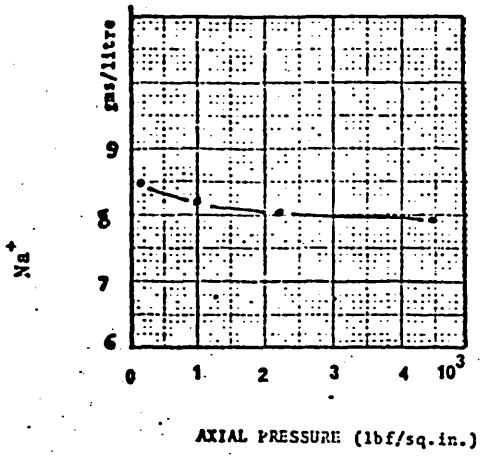
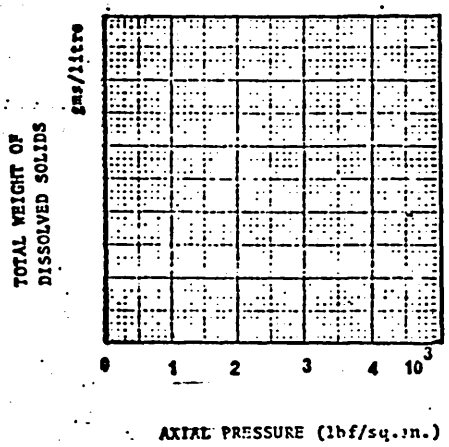
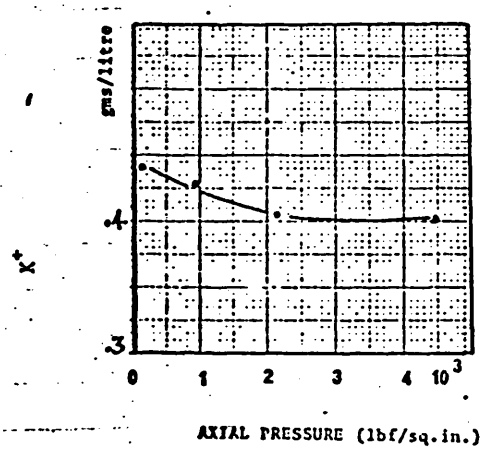


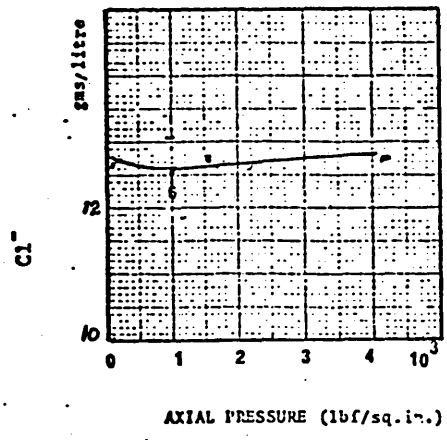
FIGURE F.9 The results of chemical analysis of pore fluid expelled from test N.BC.CHP.1

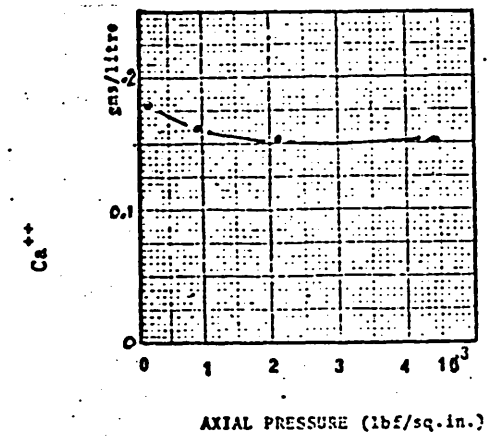


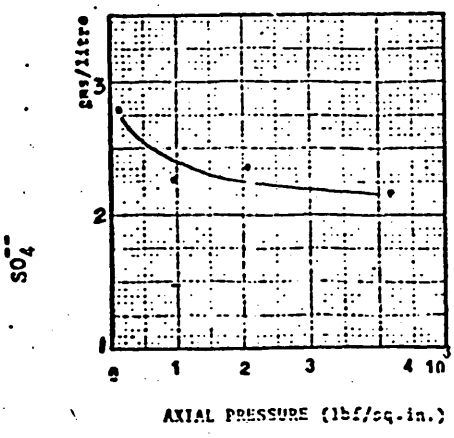












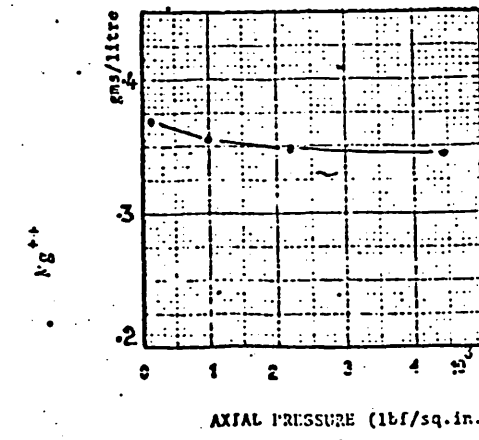


FIGURE F.10 The results of chemical analysis of pore fluid expelled from test N.FA.CHP.2

REFERENCES

AKHMEDORA, S.H.G. and GLYMANOV, A.A. (1970) "The influence of various factors on the therma conductivity of porous sedimentary rocks", Akad. Nauk. Azerbaydzhan SSR., IZV. Nauko. Zemle, Vol. 2 and p. 62-65.

AMERICAN GEOLOGICAL INSTITUTE (1957) "Dictionary of Geological Terms", Doubleday & Co. Inc., Garden City, New York.

AMERICAN GEOLOGICAL INSTITUTE (1972) "Glossary of Geology". Eds. M. Gary, R. McAfie Jr., C.L. Wolff.

AMERICAN SOCIETY OF CIVIL ENGINEERS (1958) "Glossary of terms and definitions in soil mechanics", Soil Mech. and Found. Div. Jour., A.S.C.E. Proc., V. 84, SM4. paper 1826, p. 43.

AMYX, J.W., BASS, D.M. Jr., & R.L. WHITING (1960) "Petroleum reservoir engineering: physica' properties", McGraw-Hill, New York, p. 610.

ANDERSON, D.M. and LOW, P.F. (1958) "Density of water absorbed by lithium-, sodium-potassium-bentonite", Soil Sci. Am. Proc., 22: p.99-10

ATHY, L.F. (1930a) "Density, porosity and compaction of sedimentary rocks", Am. Assoc. Petroleum Geologists' Bull., V. 14, p. 1-24.

ATHY, L.F. (1930b) "Compaction and oil migration", Am. Assoc. Geologists' Bull., V. 14, p. 25-35.

ATHY, L.F. (1934) "Compaction and its local effect on structure", in Problems of Petroleum Geology, Sidney Powers Memorial Vol., Eds. W.E. Wrather, F.H. Lahee., Am. Assoc. Petroleum Geologists, Tulsa, Oklahoma.

ATTEWELL, P.B. and TAYLOR, R.K. (1969) "A microtextural interpretation of a Welsh Slate", Int. J. Rock Mech. & Mining Sc., Vol. 6.

AYLMORE, L.A.G. and QUIRK, J.P. (1960) "Domain of turbostratic structure of clays", Nature, 187, p. 1046-1048.

BARDEN, L. and BERRY, P.L. (1965) "Consolidation of normally consolidated clay" Soil Mech. & Found. Div. Jour., A.S.C.E. Proc., Vol. 91, SM5, p. 15-35.

BARDEN, L. (1965a) "Consolidation of compacted and unsaturated clays", Geotechnique 15, p. 267-286.

BARDEN, L. (1965b) "Consolidation of clay with non-linear viscosity", Geotechnique 15, p. 345-362.

BARDEN, L. and SIDES, G. (1971) "Sample disturbance in the investigation of clay structure", Geotechnique 21, p. 211-223.

BARDEN, L. (1972) "Examples of clay structure and its influence on engineering behaviour", Proc. Roscoe Memorial Symp.

BATES, T.F. (1947) "Investigation of the micaceous minerals in slate", Am. Mineralogist, 32. p. 625-636.

BEALL, A.O. Jr. (1964) "Fabric and mineralogy of Woodbine sediments, east-central Texas", Stanford Univ., Ph.D. dissertation, p. 171.

BEALL, A.O. Jr. and FISHER, A.G. (1969) "Sedimentology", in M. Ewing et al (Eds.), Initial Reports of the Deep-Sea Drilling Project, U.S. Govt. Printing Office, Washington D.C., 1, p. 672

BEALL, A. (1974) Personal communication to Rieke, H.H. and Chillingarian, G.V., Compaction of Argillaceous sediments, Developments in Sedimentology, 16, Elsevier, Amsterdam.

BECK, A.E. & BECK, J.M. (1958) "On the measurement of the thermal conductivities of rocks by observations on a divided bar apparatus", Trans. Am. Geophys. Union, 30, p.1111-1213

BECKER, G.F. (1904) "Experiments on schistosity and slaty cleavage" U.S. Geol. Survey Bull., 241, p. 32.

BERRY, F.A.F. and HANSHAW, B.B. (1960) "Geological field evidence suggesting membrane properties of shales", International Geological Congress, 21st, Copenhagen Abstracts, p. 295-301.

BERRY, F.A. (1969) "Relative factors influencing membrane filtration effects in geologic environments", in Geochemistry of Subsurface brines, Chemical Geology, v. 4. p. 295-301.

BEST, R. and FOOKES, P.G. (1970) "Some geotechnical and sedimentary aspects of ball clays from Devon", Quart. Journal Engineering Geology, Vol. 3, p. 207-240.

BIOT, M.A. (1955) "Theory of elasticity and consolidation for a porous anisotropic solid", J. Appl. Phys., Vol. 26, p. 182-185.

BISHOP, A.W. and HENKEL, D.J. (1962) "The measurement of soil properties in the triaxial test", 2nd Ed., E. Arnold Ltd., London.

BISHOP, A.W. (1966) "The strength os soils as engineering materials Geotechnique 16.

BISHOP, A.W., WEBB, D.L. & LEWIN, P.I. (1965) "Undisturbed samples of London Clay from the Ashford Common Shaft: strength-effective stress relationships", Geotechnique, 15, p. 1-31.

BJERRUM, L. and KENNEY, T.C. (1967) "The effect of structures on the shear behaviour of normally consolidated quick clay", Proc. Geotech. Conf., Oslo, Vol. 11, p. 19-27.

BLACKMORE, A.V. and MILLER, R.D. (1961) "Tactoid size and osmotic swelling in calcium montmorillonite", Soil Sci. Soc. America Proc., v. 25, p. 169-173.

BLACKWELDER, E. (1920) "The origin of the central Kansas oil domes", Bull. Am. Assoc. Pet. Geologists, 4(10), p. 39-94.

BOATMAN, W.A.J. (1967) "Measuring and using shale density to aid on drilling wells in high pressure areas", Journal Petroleum Technology, vol. 19, no. 5, p. 1423-1429.

BOCHKO, R. (1973) "Types of microtextural elements and microporosity in clays (based on scanning electron microscopy studies)", Proc. Int. Symp. on Soil Structure, Gothenberg, p. 97-100.

BOLT, G.H. (1956) "Physico-chemical analysis of the compressibility of pure clays", Geotechnique (London), 6(1), p. 86-93.

BOSWELL, P.H.G. (1954) "The natural moisture content, voids (porosity) and compaction of unconsolidated clayey rocks", Liverpool and Manchester Geol. Jour, v. 1, p. 223-239.

BOSWELL, P.G.H. (1961) "Muddy sediments", Heffer & Sons.

BOWLES, F.A. BRYANT, W.R. and IRWIN, C. (1969) "Microstructure of unconsolidated and consolidated marine sediments", Journal of Sed. Pet., Vol. 39, 4, p. 1546.

BRADLEY, W.F. (1956) "The green compression strength of natural bentonites", Clays Clay Miner., Proc. Natl. Conf. Clays Clay Miner., 4th (1955), p. 41-44.

BREDEHOEFT, J.D., BLYTH, C.R., WHITE, W.A. and MAXEY, G.B. (1963) "Possible mechanism for concentration of brines in subsurface formations", Am. Assoc. Petroleum Geologists Bull., v. 47, p. 257-269.

BREDEHOEFT, J.D. and HANSHAW, B.B. (1968) "On the maintenance of anomalous fluid pressures: I. Thick sedimentary sequence", Geological Soc. Am. Bull, v. 79, p. 1097-1106.

BREWER, R. and HALDANE, A.D. (1957) "Preliminary experiments in the development of clay orientation in soils", J. of Soil Science, v. 84, p. 301.

BREWER, R. and SLEEMAN, J.R. (1960) "Soil structure and fabric: their definition and description", J. Soil. Sci., v. 11, p. 172.

BRISTOW, C.M. (1968) "The derivation of the Tertiary sediments in the Petrockstow Basin, North Devon", Proc. Ussher Soc., v. 2, p. 29-35.

BRITISH STANDARDS 1377 (1967) "Methods of testing soils by Civil Engineering" H.M.S.O.

BROWN, G. (1961) "The X-ray identification of crystals structure of clay minerals", Mineralogical Society, London.

BUESSEM, W.R. and NAGY, B. (1954) "The mechanism of the deformation of clays", Clays Clay Miner., Proc. Natl. Conf. Clays Clay Miner., 2 (1953), 327, p. 480-491.

BURST, J.F. (1958) "Post diagenetic clay mineral environmental relationships in the Gulf Coast Eocene", Clays and Clay Minerals, v. 6, p. 327-341.

BURST, J.F. (1969) "Diagenesis of Gulf Coast clayey sediments and its possible relation to petroleum migration". Am. Assoc. Petroleum Geologitst Bull., v. 53, p.73-93.

CAMPANELLS, R.G. and MITCHELL, J.K. (1968) "Influence of temperature variations on soil behaviour", Jour. Soil Mech. and Found, Div., A.S.C.E. Proc. paper 5958, v. 94, no. SM3, p. 709-734.

CASAGRANDE, A. (1932a) "The structure of clay and its importance in foundation engineering", J. Boston Soc. Civil Engrs., 19, p. 168-209.

CASAGRANDE, A. (1932b) "Research on the Atterberg limits of soils", Public Roads, 13, p.121-136.

CASAGRANDE, A. (1936) "The determination of the pre-consolidation load and its practical significance", Proc. 1st Int. Conf. on Soil Mechanics, Harvard, v. 3, p. 60-64.

CHANEY, P.E. (1949) "Abnormal pressures and lost circulation", in Drilling and Production Practice, Am. Petrol. Inst., New York, N.Y., pp. 145-148.

CHEPILOV, K.R., ERMOLOVA, E.R. and ORLOVA, N.A.	(1959) "Epigenetic minerals as indicators of lime arrival of petroleum into commercial sand reservoirs", Dokl. Akad. Nauk. S.S.S.R., Vol. 125, p. 1097-1099.
CHILLINGAR, G.V. and KNIGHT, L.	(1960) "Relationship between pressure and moisture content of kaolinite, illite and montmorillonite clays", Am. Assoc. Petroleum Geologists Bull., v. 44, p. 101-106.
CHILLINGARIAN, G.V. and RIEKE, H.H.	(1968) "Data on consolidation of finegrained sediments' Jour. Sedimentary Petrology, v. 38, p. 811-816.
CHILLINGARIAN, G.V., BEESON, C.M. and ERSHAGI, I.	(1971) "Porosity and permeability", in Rhodes. W. Fairbridge (Editor), Encyclopaedia of Earth Sciences, IV A, p. 964-970.
CLARK, B.R.	(1970) "Mechanical formation of preferred orientation in clays", Am. J. Sci., Vol. 269, No. 3.
COLLINS, A.G.	(1970) "Geochemistry of some petroleum-associated waters from Louisiana", U.S. Bureau Mines, Rep. Invest., 7326, p. 1-31.
CORDELL, R.J.	(1972) "Depths of oil origin and primary migration: a review and critique", Am. Assoc. Petroleum Geologists Bull., v. 56, p. 2029-2067.
CRAWFORD, C.B.	(1964) "Interpretation of the consolidation test", Soil Mech and Found Div. Jour., A.S.C.E., v. 90, SM1, p. 87-102.
DAS, A.S., ANANDAKRISHNAN, M. and GOKHALE, K.V.G.	(1969) "Shrinkage behaviour in clay-sand systems", International Clay Conference, Proc., p. 829-834.
DAVIS, L.E.	(1955) "Electrochemical properties of clays", in J.A. Park and M.D. Turner (Editors), Clays and Clay Technology, Proc. Natl. Conf. Clays Clay Technol., 1st. State of Calif., Div. Mines Bull, 169, p. 47-53.
DAVIS, E.H. and RAYMOND, G.P.	(1965) "A non-linear theory of consolidation", Geotechnique, vol. 15, p. 161-173.
DEGENS, E.T., HUNT, J.M., REUTER, J.H. and REED, W.E.	(1964) "Data on the distribution of amino-acids and oxygen isotopes in petroleum brine waters of various geologic ages", Sedimentology, 3, p. 199-225.
DE LORY, F.A. and LAI, H.W.	(1971) "Variations in undrained shearing strength by semiconfined tests", Canadian Geotechnical Journal, Vol. 8(4), p. 538-545.
DUNOYER DE SEGONZAC,G.	(1964) "Les argiles du Cretace superieur dans le basin de Douala (Cameroun); probleme de diagenese", Bull. Surv. Cart. Geol. Alsace Lorraine, v. 17. p. 287-310.
DUNOYER DE SEGONZAC,G.	(1970) "The transformation of clay minerals during diagenesis and low grade metamorphism: a review", Sedimentology, vol. 15, p. 281-346.
DE SITTER, L.E.	(1947) "Diagenesis of oil-field brines", Bull. Am. Assoc. Pet. Geologists, 31(11), p. 2030-2040.
DICKEY, P.A.	(1966) "Patterns of chemical composition in deep subsurface waters", Bull, Am. Assoc. Pet. Geologists, 50(11), p. 2472-2477.

DICKEY, P.A. (1969) "Increase in concentration of subsurface brines with depth", in, Geochemistry of Subsurface Brines: Chemical Geology, v. 4, p. 361-370.

DICKEY, P.A., SHIRAM, C.R. & PAINE, W.R. (1968) "Abnormal pressures in deep wells in southwestern Louisiana", Science, v. 160, p. 609-615.

DICKEY, P.A., COLLINS A.G. & FAJARDO, I. (1972) "Chemical composition of deep formation waters in southwestern Louisiana", Am. Assoc. Petroleum Geologists Bull., v. 37, p. 410-432.

DICKINSON, G. (1953) "Geological aspects of abnormal reservoir pressures in Gulf Coast Louisiana", Bull. Am. Assoc. Pet. Geologists, 37(2), p. 410-432.

DUNCAN, J.M. and SEED, H.B. (1966a) "Anisotropy and stress reorientation in clay", Proc. A.S.C.E., 92, SM5, p. 21-50.

DUNCAN, J.M. and SEED, H.B. (1966b) "Strength variation along failure surfaces in clay", Proc. A.S.C.E., 92, SM6, p. 81-104.

EMERY, K.O. and RITTENBERG, S.C. (1952) "Early diagenesis of California Basin sediments in relation to origin of oil", Bull. Am. Assoc. Pet. Geologists, 36(5), p. 735-806.

ENGELHARDT, W. von and GAIDA, K.H. (1963) "Concentration changes of pore solutions during the compaction of clay sediments", Jour. Sedimentary Petrology, v. 33, p. 919-930.

EVAN, G. (1974), personal communication.

FABUSS, B.M. and KOROSI, A. (1968) "Properties of sea water and solutions containing sodium chloride, potassium chloride, sodium sulfate and magnesium sulfate", Office of Saline Water R & D progress report no. 384, p. 143.

FAUST, G.T. (1940) "Staining of clay minerals as a rapid means of identification in natural and beneficiated products", Bur. Mines. Rept. Invest., 3522, p. 21.

FERTL, W.H. and TIMKO, D.J. (1970a) "Occurrence and significance of abnormal-pressure formations", Oil Gas J., January, 5, p.97-108

FERTL, W.H. and TIMKO, D.J. (1970b) "How abnormal-pressure-detection techniques are applied", Oil Gas J., January, 12, p. 62-71.

FERTL, W.H. and TIMKO, D.J. (1970c) "Occurrence of cemented roof rock and geopressure caprock and its implication in petroleum geology and geohydrology", Ann. Fall Meet. 45th, Soc. Pet. Engrs., Houston, Texas, SPE Paper No. 3085, p. 5.

FERTL, W.H. and TIMKO, D.J. (1971) "Application of well logs to geopressure problems in the search, drilling and production of hydrocarbons", Colloq. Assoc. Rech. Tech. Exploit. Pet. Commun., 4, p. 15.

FILATOV, K.V. (1958) "Silicate waters and their position in horizontal hydrochemical zonation", Dokl. Akad. Nauk. S.S.S.R., 138(3), p. 663-666.

FINCH, W.C. (1969) "Abnormal pressures in the Antelope Field, North Dakota", J. Pet. Technology, v. 21, 7, p.821-826

FOSTER, R.H. & DE,P.K. (1972) "Optical and electron microscopic investigation of shear induces structures in lightly-consolidated (soft) and heavily consolidated Kaolinite", Clays and Clay Minerals, 1971, vol. 19, p. 31-47.

FOSTER, R.H. and EVANS, J.S. (1971) "Image analysis of clay fabric by quantimet", Microscope, vol. 19, October, p. 377-399.

FRANKLIN, A.G. and MATTISON, P.A. (1972) "Directional variation of elastic wave velocities in oriented clay", Clays and Clay Minerals, vol. 20, p. 285-293.

FRIEDMAN, G.M., FABRIACAND, B.P., BREY, M.E. and SANDERS, J.E. (1968 "Chemical changes in interstitial waters from continental shelf sediments", J. Sediment. Petrol., 38(4), p. 1313-1319.

GARD, J.A. (1972) "The electron-optical investigation of clays", Mineralogical Society Monograph No. 3.

GIBSON, R.E. (1958) "The progress of consolidation in a clay layer, increasing in thickness with time", Geotechnique, v. 8 p. 171-182.

GIBSON, R.E. and LO (1961) "Theory of consolidation of saturated clays", Norwegian Geotechnical Institute Pub., No. 4.

GIBSON, R.E., ENGLAND, G.L. and HUSSEY, M.J.L. (1967) "The theory of one-dimensional consolidation of saturated clays, " Geotechnique 17, No. 3, p. 261-273

GIPSON, M. Jr. (1966) "A study of the relations with depth, porosity and clay mineral orientation in Pennsylvanian Shales", J. Sed. Petr., 36, p. 888-903.

GUPSON, M. Jr. (1965) "Application of the electron microscope to the study of particle orientation and fissility in shale", J. Sediment. Petrol., 35(2), p. 408-414.

GRIM, R.E. and CUTHBERT (1945) "Some clay-water properties of certain clay minerals", J. Amer. Ceram. Soc., V. 28, p. 90-95.

GRIM, R.E. (1953) "Clay mineralogy", McGraw-Hill, New York, p.384

GRIM, R.E. (1968) "Clay mineralogy", McGraw-Hill, New York, p.596

GRIM, R.E. and ALLEN, V.T. (1938) "Petrology of the Pennsylvanian underclay of Illinois", Bull. Geol. Soc. Am., 49, p. 1485-1513.

HAMILTON, E.L. (1959) "Thickness and consolidation of deep-sea sediments", Bull. Geol. Soc. Am., 70, p. 1399-1424.

HAMILTON, E.L. (1970a) "Sound velocity and related properties of marine sediments, North Pacific", J. Geophys. Res., 75(23), p. 4423-4446.

HAMILTON, E.L. (1970b) "Reflection coefficients and bottom losses at normal incidence computed from Pacific sediment properties", Geophysics, 35(6), p. 995-1004.

HAMILTON, E.L. (1971a) "Elastic properties of marine sediments", J. Geophys. Res., 76(2), p. 579-604.

HAMILTON, E.L. (1971b) "Prediction of in situ acoustic and elastic properties of marine sediments", Geophysics, 39(2), p. 266-284.

HANSBO, S. (1960) "Consolidation of clay with special reference t the influence of vertical sand drains", Swedish Geotech. Inst. Res. no. 18.

HANSEN, J.B. and GIBSON, R.E. (1949) "Undrained shear strength of anisotropically consolidated clays", Geotechnique, vol. 1, no. 3, p. 189-204.

HANSHAW, B.B. (1962) "Membrane properties of compacted clays" Thesis, Harvard Univ., Cambridge, Mass., p. 113.

HANSHAW, B.B. and BREDEHOEFT, J.D. (1968) "On the maintenance of anomalous fluid pressures; II, source layer at depth", Geological Soc. Am. Bull., v. 79, p. 1107-1122.

HANSHAW, B.B. (1964) "Cation-exchange constants for clays from electrochemical measurements", in Clays and Clay Minerals, v. 12, p. 397-421.

HANSHAW, B.B. and COPLEN, T.B. (1973) "Ultrafiltration by a compacted clay membrane; II, sodium ion exclusion at various ionic strengths", Geochemica et Cosmochemica Acta, vol. 37, no. 10, p. 2311-2328.

HARKINS, K.L. and BAUGHER, J.W. (1969) "Geological signifance of abnormal formation pressures", Jour. Petrol. Tech., vol. 21, no. 8, p. 961-966.

HEDBERG, H.D. (1926) "The effect of gravitational compaction on the structure of sedimentary rocks", Bull. Am. Assoc. Pet. Geologists, 10(10), p. 1035-1072.

HEDBERG, H.D. (1936) "Gravitational compaction of clays and shales", Am. J. Sci., 5th Ser., 31(184), p. 241-287.

HELING, D. (1970) "Microfabrics of shales and their rearrangement by composition", Sedimentology, v. 15, no. 3/4, p. 247-260.

HENDRICKS, S.B. and JEFFERSON, M.E. (1938) "Structure of Kaolin and Talc-Pyrophyllite Hydrates and their bearing on Water Sorption of Clays", Am. Miner. Vol. 23.

HILLIARD, J.E. (1971) "Quantitative analysis of scanning electron micrographs", 3rd Int. Congress for Stereology, Proc., Berne, Switzerland.

HILTRABRAND, R.R., FERRELL, R.E. and BILLINGS, G.K. (1973) "Experimental diagenesis of Gulf Coast argillaceous sediments", Am. Assoc. Petroleum Geologists Bull., v. 57, p. 338-348.

HOBSON, G.D. (1943) "Compaction and some oil field features", Jour. Inst. Petroleum, v. 29, p. 37-54.

HOBSON, G.D. (1954) "Some fundamentals of petroleum geology", Oxford Univ. Press, p. 139.

HORAI, K. and VYEDA, S. (1960) "Studies of thermal state of earth, 5, relation between thermal conductivity of sedimentary rocks and water content", Bull. Earthquake Res. Int., Tokyo University, 38, p. 199.

HOTTMAN, C.E. and JOHNSON, R.K. (1965) "Estimation of formation pressures from log-derived shale properties", J. Pet. Tech., p.717-722.

HSI, H.R. and CLIFTON, D.F. (1962) "Flocculation of selected clays by various electrolytes", p. 269-273, in, Swineford, Ada, and Franks, P.C., eds., Clays and clay minerals, New York, Pergamon Press, p. 614.

HUBBERT, M.K. (1953) "Entrapment of petroleum under hydrodynamic conditions", Am. Assoc. Petroleum Geologists, v. 37, p. 1954-2026.

HUBBERT, M.K. and RUBEY, W.W. (1959) "Role of fluid pressure in mechanics of overthrust faulting: I. Mechanics of fluid-filled porous solids and its application to overthrust faulting", Geological Soc. Am. Bull, v.70, p.115-166.

INGLES, O.G. and LEE, I.K. (1971) "The influence of grain shape and pore anisotropy on strength of brittle soils", Geotechnique, 21, no. 2, p. 143-153.

INGRAM, R.L. (1953) "Fissility of mudrocks", Bull. Geol. Soc. Am., 64, p. 869-878.

JACKSON, J.O. (1972) "Geotechnical properties of the Lower Oxford Clay related to deep burial", Ph.D. Thesis, University of London.

JANBU, N. (1965) "Consolidation of clay layers based on non-linear stress-strain", Proc. of the 6th Intl. Conf. on Soil Mech. and Found. Engg., vol. 2, Montreal, p. 83-87.

JIMENESZ SALAS, J.A. and SERRATOSA, J.N. (1953) "Compressibility of clays", 3rd Interntl. Conf. on Soil. Mech. and Found. Engg., Proc., v.15, p.192-

JONES, O.T. (1939) "The consolidation of muddy sediments", Geological Magazine, vol. 76, p. 170-172.

JONES, O.T. (1945) "The consolidation of muddy sediments", Quart, Journal Geological Soc., London, v.106, p.137-

KAARSBERG, E.A. (1959) "Introductory studies of natural and artificial argillaceous aggregates by sound-propagation and X-ray diffraction methods", J. Geol., 67, p. 447-472.

KAARSBERG, E.A. (1966) "Electron photomicrographs of some anisotropic sedimentary rocks", Trans. Soc. Min. Eng., 235, p. 123-126.

KAHN, H.L. (1968) "Principles and practice of atomic absorption in trace inorganics in water", Adv, Chem. Ser. 73. American Chemical Society, Washington, p. 183-229.

KEEP, C.E. and WARD, H.L. (1934) "Drilling against high rock pressures with particular reference to operations conducted in Khan Field, Punjab", J. Inst. Pet. Technologists, vol. 20, p. 990-1013.

KELLER, W.D. (1963) "Diagenesis in clay minerals - a review", Clays and clay minerals, v. 11, p. 136-157.

KELLER, W.D. (1968) "Flint-clay and flint-clay facies", Clays Clay Minerals. Proc. Natl. Conf. Clays Clay Minerals, 16th. vol. 2, p. 113-128.

KEMPER, W.D. (1960) "Water and ion movement in thin films as influenced by the electrostatic charge and diffuse layer of cations associated with the clay mineral surfaces", Soil Sci., Soc. Am. Proc., vol. 24, p.10-1

KHARAKA, Y.K. and BERRY, F.A. (1973) "Simultaneous flow of water and solutes through geological membranes: I. Experimental investigation", Geochimica et Cosmochimica Acta, v. 37, p. 2577-2603.

KHITAROV, N.I. and PUGIN, V.A. (1966) "Behaviour of montmorillomites under elevated temperatures and pressures", Geochem. Int., 3(4), p. 621-626.

KIDWELL, A.L. and HUNT, J.M. (1958) "Migration of oil in recent sediments of Pedernales, Venezuela", in, L.G. Weeks (Editor), Habitat of Oil, Am. Assoc. Pet. Geologists, Tulsa, Oklahomam p. 1384.

KITTRICK, (1961) "Smear-mounted and Disc-mounted clay specimens' Soil Science, vol. 92, p. 155.

KNILL, J.L., ARMSTRONG, M.K., CLARKE, B.A., DE FREITAS, M.H. and WIJEYESEKERA, D.C. (1974) "Artificially simulating the geological histor of clay", Internal Technical Report, European Researc Office, United States Army, London N.W.1.

KNILL, J.L. (1960) "A classification of cleavage with special reference to the Craiginish District of the Scottish Highlands", Rep. 21st Int. Geol. Cong., part 18, p. 317-325.

KONYUKHOV, A.I. and TEODOROVICH, G.I. (1969) "Optimum depth for the formation of oil in terrigenous Jurassic in Eastern Caucasia", Doklady, Akad. Nauk. SSSR, Vol. 188, p. 50-53.

KOTOVA, I.S. and PAVLOV, A.N. (1968) "About leaching of impervious rocks on increasing geostatic pressure", in; G.V. Bogomolov et al (Editors), Pore Solutions and Methods of their Study (A Symposium), Izd. Nauka i Technika, Minsk, p. 55-68.

KRASINTSEVA, V.V. and KORUNOVA, V.V. (1968) "Influence of pressure and temperature on composition of extruded solutions during mud compaction", in; G.V. Bogomolov et al (Editors), Pore Solutions and Methods of their Study (A Symposiu Izd, Mauka i Teckhnika, Minsk, p. 191-204.

KRYUKOV, P.A. (1961) "Toward procedures of squeezing out of solutions from sedimentary rocks", Gidrokhim. Inst. Novocherk., Gidrokhim Mater., 33, p. 191-197.

KRYUKOV, P.A. and KOMAROVA, N.A. (1954) "Concerning squeezing out of water from clays at very high pressures", Dokl. Akad. Nauk. S.S.S.R., 99(4), p. 617-619.

KRYUKOV, P.A. and ZHUCHKOVA, A.A. (1963) "Physical-chemical phenomena associated with driving out of solutions from rocks", in, Present Day concepts of bound water in rocks, Izd. Akad. Nauk. S.S.S.R., Laboratory of Hydrogeological Problems of F.P. Savarenskiy, Moscow, p. 95-105.

KRYUKOV, P.A., ZHUCHKOVA, A.A. and RENGARTEN, E.V. (1962) "Change in the composition of solutions pressed from clays and ion exchange resins", Dokl. Akad. Nauk. S.S.S.R., 144(4), p. 1363-1365.

LAFEBER, D. (1962) "Aspects of stress-induced differential movements of fabric elements in mineral soils", Proc. 1st Conf. Aust. Road. Res. Board, 1, p.1.059-067

LAFEBER, D. (1966) "Soil structural concepts", Engg. Geol. vol. 1, No. 4.

LAFEBER, D. (1967) "The optical determination of spatial (3-D) orientation of platy clay minerals in soil thin sections", Geoderma, Vol. 1, no. 3/4, p. 359-369.

LAFEBER, D. (1969) "Soil anisotropy and soil sampling", Proc. 7th Int. Conf. Soil Mech. Found. Eng. Speciality Session, No. 1, p. 32-39.

LAMBE, T.W. (1953) "The structure of inorganic soils", Proc. A.S.C.E. Separate No. 315.

LAMBE, T.W. (1958a)"The structure of compacted clay", J. Soil. Mech. Found. Div., Am. Soc. Civil Engrs, 84(SM2, Part 1), p. 1654-1711.

LAMBE, T.W. (1958b) "The engineering behaviour of compacted clay", J. Soil Mech. & Found. Div., Am. Soc. Civil Engrs., Proc., vol. 84, SM2.

LAMBE, T.W. and WHITMAN, R.V. (1969) "Soil Mechanics", John Wiley & Sons Inc.

LARSEN, T.J. (1967) "Purification of subsurface waters by reverse osmosis", J. Am. Water Works Assoc., 59(12),p.1527-15

LARSEN, G. and CHILLINGAR, G.V. (1967) (Editors) "Diagenesis in Sediments", Elsevier. Amsterdam, p. 524.

LAUGHTON, A.S. (1957) "Sound propagation in compacted ocean sediments Geophysics, 22, p. 233-260.

LEONARDS, G.A. and ALTSCHAFT, A.G. (1964) "Compressibility of clay", Journal Soil Mech. and Found. Div., ASCE, Vol.90, no.SM5, Proc. paper 4019, p. 143-155.

LEONARDS, G.A. and GIRAULT, P. (1962) "A study of the one-dimensional consolidation test", Proc. 5th Int. Conf. Soil Mech., Vol.1,p.213-21

LEVORSEN, A.I. (1967) "Geology of Petroleum", 2nd Edition, W.H. Freeman, p. 724.

LO, K.Y. (1966) "Stability of slope in anisotropic soils", Jour. of Soil Mech. and Found. Div., ASCE Proc., Vol. 94, SM4, p. 85-106.

LOW, P.F. (1961) "Physical chemistry of clay-water interaction", in, Normal, A.G. Ed., Advances in Agronomy, Vol. 13, New York, Academic Press, p. 269-327.

LYMAN, J. (1962) "Ocean and Oceanography", Encyclopaedia Britannica, Vol. 16, p. 686.

MAGARA, K. (1973) "Compaction and fluid migration in Cretaceous shales of western Canada", Geol. Surv. Canada, Paper 72-18, p. 81.

MANGELSDORF, P.C. Jr., MANHEIM, F.T. and GIESKES, J.M.T.M. (1970) "Role of gravity, temperature gradients and ion-exchange media in formation of fossil brines", Bull. Am. Assoc. Pet. Geologists 54(4), p. 617-626.

MANHEIM, F.T. (1966) "A hydraulic squeezer for obtaining interstitial water from consolidated and unconsolidated sediments", U.S. Geol. Surv. Profess. Paper, 550-C, p. 256-261.

MARTIN, R.T. (1962) "Adsorbed water on clay: a review", in, E. Ingerson (Editor), Clays Clay Miner., Proc. Natl. Conf. Clays Clay Miner., 9(1960), p. 28-70.

MARTIN, R.T. (1965) "Quantitative measurements of wet clay fabric" (abs.), in, E. Ingerson (Editor), Clays Clay Miner., Proc. Natl. Conf. Clays Clay Miner., 14(1964) p. 271-287.

MARTIN, R.T. (1966) "Quantitative fabric of wet kaolinite", Proc. 14th Nat. Conf. Clays and Clay Minerals, New York, Pergamon Press, p. 271-287.

McCLELLAND, B. (1967) "Progress of consolidation in delta front and prodelta clays of Mississippi River", in, A.F. Richards (Ed.), Marine Geotechnique Urbana (Univ. of Illinois Press), p. 22-40.

McKELVEY, J.G. and MILNE, I.H. (1962) "Flow of salt solutions through compacted clay", in, E. Ingerson (Ed.), Clays Clay Miner., Proc. Natl. Conf. Clays Clay Miner., 9(1960), p. 248-259.

MARCH, A. (1932) "Mathematische Theorie der Regelung nach der Korngestalt bei affiner Deformation", Zeitschrift Kristallographie, v. 81, p. 285-298.

MASON, S.G. and MANLY, R.St.J. (1956) "Particle motions in sheared suspensions orientation and interaction of rigid rocks", Proc. Roy. Soc. London, Series A, v.238, p.117-131.

MATSUO, S-I, and KAMON, M. (1973) "Microscopic research on the consolidated samples of clayey soils", Proc. Int. Symposium on Soil Structure, Gothenburg, 1973, p. 194.

MAXWELL, J.C. (1962) "Origin of slaty fracture cleavage in the Delaware water gap area, New Jersey and Pennsylvania", in, Engel, A.E.J, James, H.L. and Leonard G.F. (Eds.), Petrologic studies: a volume in honour of A.F. Buddington, Boulder Col., Geol. Soc. America, p.281-31

MEADE, R.H. (1961) "X-ray diffractometer method for measuring preferred orientation in claus", U.S. Geol. Surv., Profess. Paper, 424-B, B273-276.

MEADE, R.H. (1964) "Removal of water and rearrangement of particle during the compaction of clayey sediments - review", U.S. Geol. Surv., Profess. Paper., 497-B, p. 23.

MEADE, R.H. (1966) "Factors influencing the early stages of the compaction of clays and sands; a review", Jour. Sedimentary Petrology, v.36, p.1085-1101.

MEADE, R.H. (1968) "Compaction of sediments underlying areas of land subsidence in Central California", U.S. Geol. Surv. Profess. Paper, 497-D, p. 39.

MEANS, W.D. and PATTERSON, M.S. (1966) "Experiments on preferred orientation of platy minerals", Beitr. Mineralogie und Petrologie, v.13, p. 108-133.

MENARD, H.W. (1964) "Marine geology of the Pacific", McGraw-Hill Co., London.

MESRI, G. and OLSEN, R.E. (1971) "Mechanisms controlling the permeability of clays", Clays Clay Miner., 19(3), p. 151-158.

MIKASA, M. (1965) "The consolidation of soft clay", Civil Eng. in Japan, Jap. Soc. C.E.

MILLOT, G. (1970) "Geology of clays", Springer, New York, p.429.

MITCHELL, J.K. (1956) "The fabric of natural clays and its relation to engineering properties", Proc. Highway Res. Board, 35, p. 693.

MITCHELL, J.K. (1960) "The application of colloidal theory to the compressibility of clays", in; R.H. Parry (Ed.), Interparticle Forces in Clay-Water-Electrolyte Systems Commonwealth Sci. I. Res. Organisation, Melbourne, p. 2.92-2.97.

MITCHELL, J.K. and YOUNGER, J.S. (1967) "Abnormalities in hydraulic flow through fine-grained soils", in; Permeability and Capillarity of Soils, Am. Soc. Test. Mater., Spec. Tech. Publ., 417, p. 106-139.

MITCHELL, J.K. (1969) "Temperature affects on the engineering properties and behaviour of soils", Proc. Int. Conf. H.R.B. Special Report No. 103.

MORGAN, N.A. (1969) "Physical properties of marine sediments as related to seismic velocities", Geophysics, 34(4), p. 529-545.

MORGENSTERN, N.R. & TCHALENKO, J.S. (1967a) "The optical determination of preferred orientation in clays and its application to the study of microstructure in consolidated Kaolin", Proc. Roy. Soc. A-300.

MULLER, G. (1967) "Diagenesis in argillaceous sediments", in; G. Larsen and G.V. Chillingar (Eds.), Diagenesis in Sediments, Elsevier, Amsterdam, p. 127-177.

MURAYAMA, S. and SHIBATA, T. (1964) "Flow and stress relaxation of clays", Symposium on Rheology and Soil Mechanics, Grenoble, Proc., p. 19-29.

MYERS, R.I. and D.C. VAN SICLEN (1964) "Dynamic phenomena of sediment compaction in Matagorda County, Texas", Gulf Coast Assoc. Geol. Soc. Trans., v.14, p.241-252.

NEVINS, M.J. and WEINTRITT, D.J. (1967) "Determination of cation exchange capacity by Methylene Blue Adsorption", Bull. Am. Ceramic Soc., v.46, p.587-592.

NISHIDA, Y. and NAKAGAWA, S. (.969) "Water permeability and plastic index of soils" in; Land subsidence, IASH-UNESCO. Publ. No. 89, AIHS, 2, p. 573-578.

O'BRIEN, N.R. (1963) "A study of fissility in argillaceous rocks", Ph.D. Thesis, University of Illinois.

O'BRIEN, N.R. (1964) "Origin of Pennsylvanian underclays in the Illlinois Basin", Bull. Geol. Soc. Am., 75, p.823-832.

ODORM, I.E. (1967) "Clay fabric and its relation to structural properties in the mid-continent Pennsylvanian sediments", J. Sediment. Petrol., 37, p.610-623.

OLSEN, E.W. (1962) "Hydraulic flow through saturated clays", Clays and Clay Minerals, v.9, p.131-161.

OSMASTON, M.O., CLARKE, B.A., WIJEYESEKERA, D.C., DE FREITAS, M.H. and BAKER, P.H. (1974) "Apparatus for comprehensive experimental study of the deep burial and exhumation of sediments", (in preparation)

OLSEN, H.W. (1966) "Darcy's Law in saturated kaolinite", Water Resour., 2, p.287-294.

OLSEN, R.E. and MITRONOVAS, F. (1962) "Shear strength and consolidation characteristi of calcium and magnesium illite", Clays Clay Miner. Proc. Natl. Conf. Clays Clay. Miner., 9th, 1960, p.185-209.

OVERBEEK, J.Th.G. (1952) "The interaction between colloidal particles", in, Kruyt, H.R., Ed., Colloid Science, Amsterdam, Elsevier, v.1, p.245-277.

PAASWELL, R.E. (1967) "Temperature effects on clay and consolidation' Jour. Soil Mech. and Found. Div. ASCE Proc. Paper 522: V.93, No. SM3, p.9-22.

PERRY, E. and HOWER, J. (1970) "Burial diagenesis in Gulf Coast pelitic sediments", Clays and Clay Minerals, v.18, p.165-177.

PERRY, E. and HOWER, J. (1972) "Late stage dehydration in deeply buried pelitic sediments", Am. Assoc. Petroleum Geologists Bull., v.56, p. 2013-2021.

PETTIJOHN, F.J. (1957) "Sedimentary Rocks", Harper, New York, 2nd Ed., p. 718.

PHILLIPI, G.T. (1965) "On the depth, time and mechanism of petroleum generation", Geochimica et Cosmochimica Acta, v.29, p.1021-1050.

POL'STER, L.A., VISKOVSKIY, YU.A, GUSEVA, A.N., PARNOV, E.I. & PLASKOVA,A.G. (1967) "Physicochemical characteristics and hydrogeological factors of migration of natural solutions (in relation to study of oil- and gas-bearing basins)", Nedra, Leningrad, p. 172.

POPOV, I.V. (1944) "The cryptostructure of clays during their deformation", Acad. Sci. U.R.S.S. Comptes Rendus (Doklady), 45, p.162-164.

POSOKHOV, E.V. (1966) "Formation of chemical composition of underground waters (basic factors", Gidrometeorologischesko Izd., Leningrad, p.258.

POWERS, S. (1920) "The Sabine uplift, Louisians", Bull. Am. Assoc Petro. Geol., v.4, no.2, p.117-136.

POWERS, S. (1926) "Reflected buried hills in the oilfields of Persia, Egypt and Mescio"., Bull. Am. Assoc. Petrol. Geol., v.10, no.4, p.422-442.

POWERS, M.C. (1958) "Adjustment of clays to chemical change and the concept of equivalence value", Clays and Clay Minerals, v.6, p.309-326.

POWERS, M.C. (1967) "Fluid release mechanisms in compacting mudrocks and their importance in oil exploration", Am. Assoc. Petrol. Geol., Bull., v.51, p.1240-1253.

PUSCH, R. (1970) "Clay microstructure", Document D8, Swedish Geotechnical Institute, Gothenberg.

PUSCH, R. (1970) "Microstructural changes in soft quick clay at failure", Can. Geotech, j., 7(1), p.1-7.

QUIGLEY, R.M. and THOMPSON, C.D. (1966) "The fabric of anisotropically consolidated sensitive marine clay", Can. Geotech. J., 3(2), p.62-7

RAITBURD, Ts.M. (1958) "The study of deformation structures of the Kaolinite paste", Ivan Franko State University of Lvov, Conf. on Research and Uses of Clays Proc., p.779-794 (English summary, p.847-848).

RAITBURD, Ts.M. (1960) "Study of microstructure of clays by X-ray methods", in Reports to the Meeting of the Intl. Commission for the Study of Clays. Acad. Sci. USSR., Dept. Geol. Sci. Comm. for Study of Clays, p.108-118.

RAYMOND, G.P. (1965) "Rate of settlement and dissipation of pore water pressure during consolidation of clays", Ph.D. Thesis, University of London.

REED, P. (1946) "Trinidad leaseholds applies advanced methods in drilling and production", Oil Gas. J. Oct.5,p.44-46

REID, C. (1913) "The geology of the country around Newton Abbot", Mem. Geol. Surv. U.K., p.102-107.

REYNOLDS, R.J. (1971) "Atomic absorption spectroscopy - a practical view of the present state of the art", Lab. Equpt. Digest., vol.9, p.67.

RICHARDS, A.F. (1962) "Investigation of deep-sea sediment cores: II. mass physical properties", U.S. Navy Hydrog. Office Tech. Report 106, p.146.

RIEKE III, H.H., CHILLINGAR, G.V. and ROBERTSON JR. J.O. (1964) "High-pressure (up to 500,000 p.s.i.) compaction studies on various clays", Int. Geol. Congr., 22nd, New Delhi, 15, p.22-38.

RIEKE, H.H. III, and CHILLINGAR, G.V. (1973) "Compaction of argillaceous sediments", Developments in sedimentology, 16, Elsevier, Amsterdam, p.430.

ROBERTSON, E.C. (1967) "Laboratory consolidation of carbonate sediments", in; A.F. Richards (Ed.), Marine Geotechnic Univ. Illinois Press, Urbana, Illinois, p.327.

ROBERTSON, A. and ANON, B. (1962) "Dead Sea", Encyclopaedia Britannica, vol.7, p.99.

ROBERTSON, R.H.S. and PLESCH, P.H. (1948) "Adsorption to ionic surfaces", Nature, 616, p.1020-1021.

ROBERTSON, R.H.S. and WARD, R.M. (1951) "Assay of pharmaceutical clay", J. Pharm. Pharmacol., 3, p.27-35.

ROSENQVIST, I.Th. (1958) "Remarks to the mechanical properties of soil-water systems", Geol. Foren. Stockholm Forh. 80(4), p.435-457.

ROSENQVIST, I.Th. (1959) "Physicochemical properties of soils: soil-water systems", J. Soil Found. Div. Am. Soc. Civil Engrs., 85(SM2), p.31-53.

ROSENQVIST, I.Th. (1962) "The influence of physico-chemical factors upon the mechanical properties of clays", Proc. 9th Nat. Conf. Clays and Clay Minerals, New York, Pergamon Press, p.12-27.

ROSENQVIST, I.Th. (1955) "Investigations in the clay-electrolyte-water system", Norwegian Geotech. Inst. Publ. no. 9, p.125.

ROSHOLT, J.N., EMILANI, C., GEISS, J., KOCZY, F.F. & WANGERSKY, P.J. (1961) "Absolute dating of deep sea cores by the $^{231}Pa/^{230}Th$ method", Journal Geol., v.69, p.162-185.

ROWE, P.W. (1966) "The influence of geological features of a clay deposit on the design and performance of sand drains".

RUBEY, W.W. and HUBBERT, M.K. (1959) "Role of fluid pressure in mechanics of overthrust faulting: II. Overthrust belt in geosynclinal area of western Wyoming in light of fluid-pressure hypothesis", Geological Soc. Am. Bull, v.70, p.167-206.

ROWE, P.W. (1972) "The relevance of soil fabrics to site investigation practice", Geotechnique, vol.22, p.195-300.

SAAS, J.S., LACHENBRUCH, A.H., MUNROE, R.J. (1971) "Thermal conductivity of rocks from measurements on fragments and its application to heat flow determinations", J. Geophysics Res. v.76, no.14, p.3391-340

SAHABAD, T. (1962) "Caspian Sea", Encyclopaedia Britannica, 4, p.9

SANKARAN, K.S. and BHASKARAN, R. (1972) "Strength anisotropy in cohesive soils", Symp. on Modern Trends in Civ. Engg., Proc., v.11, p.27-31.

SALDIVAR SALI, A. (1974) "Influence of fissuring on the engineering behaviour of soft rocks", Ph.D. Thesis, Univ. of London.

SCHIFFMANN, R.L. (1958) "Consolidation of soil under time-dependent loading and varying permeability", Proc. Highways Res. Board, v.37, p.584-608.

SCHMERTMANN, J.H. (1966) "Discussion on stability of slopes in anisotropic soils by K.Y. Lo", J. of Soil Mech. and Found. Eng. Div. ASCE Proc., v.90, no.SM4, p.183-185.

SCHMIDT, G.W. (1971) "Interstitial water composition and geochemistr of deep Gulf Coast shales and sands", Masters Thesis, University of Tulsa.

SCHMIDT, G.W. (1973) "Interstitial water composition and geochemistr of Gulf Coast shales and sandstones", Am. Assoc. Petroleu, Geologists Bull., v.57, p.321-337.

SCHOFIELD, R.K. and SAMSON, H.R. (1953) "The deflocculation of kaolinite suspensions and the accompanying change-over from positive to negative chloride adsorption", Clay Minerals Bull., v.2, p.45-51.

SCHOFIELD, R.K. (1954) "Flocculation of kaolinite due to the attractic of oppositely charged crystal faces", Faraday Soc. (London), Discussions 18, p.135-145.

SCHULTZ, L.G. (1958) "Petrology of underclays", Bull. Geol. Soc. Am. 69, p.363.

SCHULTZ, L.G. (1949) "A direct method of determining preferred orientation of a flat reflection sample using a geiger counter X-ray spectrometer", J.App.Phys., v.12.

SCHULTZ, L.G. (1964) "Quantitative interpretation of mineralogical composition from X-ray and chemical data for the Pierre Shale", U.S. Geol. Surv. Prof. Paper 391-C.

SERRUYA, C.,PICARD,L. & CHILLINGARIAN,G.V. (1967) "Possible role of electrical currents and potentials during diagenesis (electrodiagenesis)", J. Sediment. Petrol, 37(2), p.695-698.

SERRUYA, C. (1969) "Problems of sedimentation in the Lake of Geneva", Verh. Int. Ver. Limnol. Stuttgart, 17,p.209-2

SHAW, H.F. (1972) "The preparation of oriented clay mineral specimens for X-ray diffraction analysis by a suction-onto-ceramic tile method", Clay Minerals, vol. 9, p.349-350.

SIEVER, R. (1966) "Mud into shale, when and how", Am. Assoc. Petroleum Geologists Bull., vol.50, p.635.

SKEMPTON, A.W. (1943) "Notes on the compressibility of clays", Geological Soc. London, v.100, p.119-135.

SKEMPTON, A.W. (1953) "Soil mechanics in relation to geology", Proc. Yorks. Geol. Soc., 29, p.33-62.

SKEMPTON, A.W. (1970) "The consolidation of clays by gravitational compaction", Q. J. Geol. Soc. London, 125(3),p.373-411

SKEMPTON, A.W. and HUTCHINSON, J. (1969) "Stability of natural slopes and embankments foundations", State of Art Report, State of Art Vol., 7th Int. Conf. on Soil Mech. and Found. Div. Mexico, p.308-332.

SLOANE, R.L. and KELL, T.R. (1966) "The fabric of mechanically compacted kaolin", Proc. 14th Nat. Conf. Clays and Clay Minerals, New York, Pergamon Press. p.289-295.

SMART, P. (1967) "Soil structure, mechanical properties and electron microscopy", Cambridge, Ph.D. Thesis.

SMITH, J.E. (1971) "The dynamics of shale compaction and evolution of pore-fluid pressures", J. Int. Assoc. Mathematical Geology, v.3, p.239-263.

SMITH, J.E., ERDMAN, J.G. & MORRIS, D.A. (1971) "Migration, accumulation and retention of petroleum in the earth", 8th World Petroleum Cong., v.2, p.13-26.

SMITH, J.E. (1973) "Shale Compaction", Soc. of Petrol. Engrs. J., vol.13, no.1, p.12-22.

SMITH, R.E. and WAHLS, H.E. (1969) "Consolidation under constant rate of strain", J. Soil Mech. and Found. Div., ASCE, v.95, no.SM2, Prof. paper 6452, p.519-539.

SNEDDON, I.N. (1951) "Fourier transform", McGraw-Hill, New York.

SORBY, H.C. (1908) "On the application of quantitative methods to the study of the structure and history of rocks", Q.J.Geol.Soc.London, 64, p.171-232.

SPOTTS McDOWELL, J. (1926) "Mineralogy of clay: I. the mineral constituent of clay", J. Am. Ceram. Soc., 9, p.55.

SRIDHARAN, A. and RAO, G.V. (1973) "Mechanisms controlling volume change of saturated clays and the role of effective stress concept", Geotechnique, v.23, p.359-382.

STEINER, A. (1967) "Clay minerals in hydrothermally altered rocks at Wairakei, New Zealand", Clay Miner. Conf. 16th, Abstr., p.31-33.

SUTHERLAND, H.B. and SINGH, R.B. (1971) "Resin impregnation of partially saturated clays for thin section studies", Can. Geotechn. J. Res. Notes, p.361-364.

SVERDRUP, H.V., FLEMING, R.H. and BARNES, C.A. "Encyclopaedia Britannica", vol. 12, p.629.

SAWABINI, C.T. and CHILLINGARIAN, G.V. (1972) "Changes in chemistry of interstitial solutions extruded of montmorillonite clay saturated in sea water with increasing overburden pressure". In preprtn

SAWABINI, C.T., CHILLINGAR, G.V. and ALLEN, D.R. (1971) "Design and operation of a triaxial temperature high-pressure compaction apparatus", J. Sediment. Petrol, 41(3), p.871-881.

TAN, T.K. (1958) "Discussion of soil properties and their measurement", Proc. 4th Int. Conf. Soil Mech., 3, p.87-89.

TAN, T.K. (1959) "Strucure mechanics of clays", Scientia Sinica, v.8, p.83-97.

TANNER, C.B. and JACKSON, M.L. (1947) "Nomographs of sedimentation times for soil particles under gravity or centrifugal acceleration", Soil. Sci. Am. Proc., vol.12, p.60-65.

TAYLOR, D.W. (1948) "Fundamentals of Soil Mechanics", Wiley, New York, p.700.

TCHALENKO, J.S. (1967) "The influence of shear and consolidation on the microstructure of some clays", Ph.D. Thesis (unpublished), Univ. of London.

TCHALENKO, J.S. (1968) "Microstructure of London Clay", Q.J.Eng.Geology, 1, p.155.

TCHALENKO, J.S., BURNETT, A.D. and HUNG, J.J. (1972) "The correspondence between optical and X-ray measurements of particle orientation in clays", Clay Minerals, vol.9, p.47-70.

TEAS, L.P. (1923) "Differential compacting the cause of certain Clairborne dips", Bull. Am. Assoc. Pet. Geologists, 9, p.370-373.

TEODOROVICH, G.I. and CHERNOV, A.A. (1968) "Character of changes with depth in productive deposits of Apsheron oil-gas-bearing region", Sov. Geol., 1968(4), p.83-93.

TEORELL, T. (1935) "An attempt to formulate a quantitative theory of membrane permeability", Proc. Soc. Exp. Biol. Med., 33, p.282-285.

TERZAGHI, K. (1923) "Die Berechnung der Durchlässigkeitsziffer des Tones aus den Verlauf der hydrodynamischen Spannungserscheinungen", Sitz. Akad.Wissen., Wien Math-Naturw., K.1.132, p.105-124.

TERZAGHI, K. (1925) "Principles of soil mechanics: II. Compressive strength of clays", Engineering News Record, v.95, p.796-800.

TERZAGHI, K. (1928) "The physical properties of clays", M.I.T. Tech. Eng.News, 9.

TERZAGHI, K. and FORLICH, O.K. (1936) "Theorie du tassement des concles argileuses", Dunod, Paris.

TERZAGHI, K. and FORLICH, O.K. (1936) "Theorie der Setzung von Tonschichten", Deuticke, Vienna.

TERZAGHI, K. (1943) "Theoretical soil mechanics", J. Wiley & Sons, New-York.

TERZAGHI, K. and PECK, R.B. (1948) "Soil mechanics in Engineering Practice", J. Wiley & Sons, New York, p.566.

TOVEY, (1970) "Electron microscopy of clays", Ph.D. Thesis, University of Cambridge.

URBAIN, P. (1937a) "Introduction a l'Etude Petrographique et Geotechnique des Roches Argileuses", Paris, Hermann, 2 volumes.

URBAIN, P. (1937b) "Texture microscopique des roches argileuses", Bull. Soc. Geol. Fr., 7, p.341-352.

VAN MOORT, J.C. (1971) "A comparative study of the diagenetic alteration of clay minerals in Mesozoic shales from Papua, New Guinea and in Tertiary shales from Louisians USA", Clays Clay Miner. 19(1), p.1-20.

VAN OLPHEN, H. (1963a) "An introduction to Clay Colloid chemistry", Wiley New York, p.301.

VAN OLPHEN, H. (1963b) "Compaction of clay sediments in the range of molecular particle distances", in: W.F. Bradley (Ed.). Clays and Clay Minerals, 11, p.178-187.

VASQUEZ, in PIRSON, S.J. (1963) "Handbook of Well Log Analysis", Prentice Hall Inc., Engelwood Cliffs, N.J.

VERWEY, E.J.W. and OVERBEEK, J.Th.G. (1948) "Theory of the Stability of Lyphobic Colloids - the interaction of soil particles having an electric double layer", Elsevier, Amsterdam, p.199.

WARD, W.H., SAMUELS, S.G. and BUTLER, M.E. (1959) "Further studies of the properties of London Clay", Geotechnique, 9, p.33-58.

WARKENTIN, B.P., BOLT, C.H. and MILLER, R.D. (1957) "Swelling pressures of montmorillonite". Proc. Soil Sci. Soc. Am., 21, p.495-497.

WARKENTON, B.P. and BOZOZUK, M. (1961) "Shrinking and swelling properties of two Canadian clays", Proc. 5th Int. Conf. Soil Mech, 3A, p.851.

WARNER, D.L. (1964) "An analysis of the influence of physical-chemical factors upon the consolidation of fine-graine elastic sediments", Thesis. California Univ., Berkeley, California, p.136.

WEAVER, C.E. (1958) "Geologic interpretation of argillaceous sediments", Bull. Am. Assoc. Petrol. Geol. v. 42.

WEAVER, C.E. (1960) "Possible uses of clay minerals in search for oil", Bull. Am. Assoc. Pet. Geologists, 44, p.1505-151

WEAVER, C.E. (1961) "Clay mineralogy of the late Cretaceous rocks of the Washakie Basin", Wyo. Geol. Assoc. Guideb., 16th Field Conf., p.148-154.

WEAVER, C.E. and BECK, K.C. (1969) "Changes in the clay-water system with depth, temperature and time", OWRR Proj. No. A-008-GA, Sch. Ceramic Eng., Georgia Inst. Tech., Atlanta, Ga.

WEAVER, C.E. (1967a) "The significance of clay minerals in sediments", in: B. Nagy and U. Colombo (Eds.), Fundamental aspects of petroleum geochemistry, Elsevier, Amsterdam, p.37-75.

WEAVER, C.E. (1967b) "Potassium, illite and the ocean", Geochem. et Cosmochem. Acta, v.31, p.2181-2196.

WEAVER, C.E. and BECK, K.C. (1971) "Clay-water diagenesis during burial: how mud becomes gneiss", Geological Soc. Am. Spec. Paper 134, p.96.

WEBB, D.L. (1966) "The mechanical properties of undisturbed samples of London Clay and Pierre Shale", Ph.D. Thesis, University of London.

WELLER, J.M. (1959) "Compaction of sediments", Am. Assoc. Petrol. Geologists Bull., v.43, p.273-310.

WEST, R. (1964) "The characteristics of filter pressed kaolinite-water pastes", Proc. 12th Nat. Conf. Clays and Clay Minerals, New York, Pergamon, p.209-222.

WEST, T.S. (1969) "Atomic flame spectroscopy in trace analysis, Part 1, Atomic absorption spectroscopy", Minerals Science Engineering. Vol.1, p.3-14.

WHITE, D.E. (1965) "Saline water of sedimentary rocks", in Fluids in subsurface environments, Ed. A. Young and J.E. Galley, Tulsa, Oklahoma, Am. Assoc. Petroleum Geologists Memoir 4, p.342-366.

WHITE, D.E. (1968) "Environments of generation of some base-metal ore deposits", Economic Geology, v.63, p.301-335.

WHITE, W.A. (1961) "Colloid phenomena and sedimentation of argillaceous rocks", J. Sediment. Petrol., 31(4), p.560-570.

WILLIAMSON, W.O. (1947) "The fabric, water distribution, drying-shrinkage and porosity of some shaped discs of clay", Am. J. Sci., 245, p.645-662.

WISSA, A.E.Z., CHRISTIAN, J.T., DAVIS, E.H. and HEIBERG, S. (1971) "Consolidation at constant rate of strain", Journal of Soil Mech. and Found. Div. ASCE, vol. 97, No. SM 10, paper 8447, p.1393-1413.

YAALON, D.H. (1962) "Mineral composition of the average shale", Clay Minerals Bulletin, v.5, p.31-36.

YOUNG, R.N. and WARKENTIN, B.P. (1966) "Introduction to Soil Behaviour", MacMillan & Co., New York.

ZIENKIEWICZ, O.C. (1967) "The finite element method in engineering aciences", McGraw-Hill, London.

ACKNOWLEDGEMENTS

The author is most grateful to his Supervisor, Professor J.L. Knill, for having suggested this topic of research, and is indebted to him for his help always, and patient guidance during the preparation of the thesis.

He is further indebted to Mr. M.H. de Freitas for his keen and helpful concern, which was an added impetus to the study.

The invaluable help received from Mr. B.A. Clarke in the mechanical development of the equipment and at all stages of testing is gratefully acknowledged. Thanks are also due to Mr. P.H. Baker for having developed the associated electronics and to Mr. K. Armstrong for the subsequent continuation of his work.

For their willingness to discuss problems and their help in numerous ways, the author is grateful to Miss. V. Boaden, Miss. M. McKinlay, Mr. R. Best, Mr. R. Chaplow, Dr. A.D. Burnett, Mr. T.W. Mellors, Dr. R.J. Watters, Mr. P. Kelsall, Dr. A. Saldivar Sali, Dr. S. Saket, Mr. E.A. Rogers, Mr. S. Hencher and Mr. M. Rosenbaum.

The author has been most fortunate in being able to call on and learn from the specialised skills and knowledge of numerous individuals in Imperial College and is accordingly

grateful to Mr. R. Curtis (X-ray diffraction), Mr. B. Hough and Dr. P.R. Bush (Geochemical analysis), Mr. P. Grant and Mr. M. Wicks (electron microscopy), Dr. J.S. Tchalenko (use of optical microscope), Dr. Barnett and Mr. P. Harrett (image analysis), and to the late Mr. J. Gee and Mrs. M. Richardson (photography).

Sincere thanks are expressed to Mr. M.F. Osmaston for the design study of the equipment and to all those who have been connected with the project. The development of the equipment was financed by several bodies; the Natural Environment Research Council; Central Research Fund of the University of London, and the European Research Office of the United States Army.

This research was primarily made possible by the study leave granted to the author from the University of Ceylon, Peradeniya, Sri Lanka, and for the consequent payment of tuition fees and subsistence received for which, though scanty, the author remains grateful. He is very thankful to his wife, Anoma, for having earned to supplement above in order to make ends meet. The author is grateful to the British Council for their kind payment of his fees for the year 1973-74. He is also very thankful to the Edwina Mountbatten Grant from the Sir Ernest Cassell Education Trust for the help in the preparation of the thesis.

The author is very grateful to Miss Shelagh Jenkins for her co-operation in prompt and accurate typing of the thesis.

The author is most grateful to the Lord, whose smile and guidance gave him constant release from the stress and strain of life. To his parents, he is grateful for their consistent concern of his well-being and for all those who may have upheld him in prayer.

He also acknowledges the consistent help and much valued fellowship from his faithful friend, Stanley Jeyaraj, and also thanks to Kumar and Mary Ponniah who jointly made living in a foreign country less difficult.

Finally, the author is deeply grateful to his wife, Anoma, and son, Devanath, for their patience and understanding during the final traumatic year. An apology is expressed to his son for any shortage of parental care during this time.